

IL NUOVO CIMENTO

ORGANO DELLA SOCIETÀ ITALIANA DI FISICA
SOTTO GLI AUSPICI DEL CONSIGLIO NAZIONALE DELLE RICERCHE

VOL. VI, N. 3

Serie decima

1º Settembre 1957

Mesure de l'énergie des paires d'électrons de plus de 1 GeV dans les émulsions nucléaires.

R. WEILL, M. GAILLOUD et PH. ROSSELET

Laboratoire de Recherches Nucléaires - Ecole Polytechnique de l'Université de Lausanne

(ricevuto il 20 Febbraio 1957)

Summary. — In order to measure the projected angle ω of an electron pair, we have established an absolute method which allows to diminish the uncertainties due to multiple scattering and grains dispersion. The measure of the tracks' separation on several points from the pairs' summit enables us to calculate $\Omega = \omega + Z$ where Z is a gaussian variable of zero mean value attributed to noise level (multiple scattering and grain dispersion). This method can be used for electron pairs up to 20 GeV if it is admitted that this measure has only sense when the probability P for $\omega > Z$ be greater than 0.68; while with the usual method where the tracks' separation is measured at only one point, energies up to 1.5 GeV can be determined. Ionization measurements on the initial tracks of high energy electron pairs give a relative measurement of their opening angles in space ω_e . We have determined g^* the gap density relative to the plateau on 6 electron pairs whose energies, greater than 10 GeV, have been measured by relative multiple scattering; g^* is a function of the distance to the summit and can be equated $g^* = 2 \cdot (1 - a \exp[-x/x_0])$. Two curves have been established, the one giving $1/x_0$ as function of ω_e , the other $\log(1 - 0.5g^*)$ as function of Y_e the tracks' separation. Given the above criterium ($P[\omega > Z] > 0.68$), energies over 10 GeV can be determined in this manner. The measured values of ionization agree qualitatively with those foreseen by the theory of Della Corte, taking into account dipole effect and geometrical considerations. We have measured the tracks' separation on 4 secondaries of a jet with an energy superior to 1000 GeV/nucleon and have noticed that the influence of spurious scattering is eliminated for horizontal separations and height differences not above 30 μm , and cell lengths up to 2 mm.

1. - Introduction.

Nos recherches sur les cascades électrophotoniques dans les émulsions nucléaires, notamment la détermination du libre parcours moyen de production de tridents.⁽¹⁾, nous ont conduits à étudier le problème de la détermination de l'énergie des paires d'électrons de plus de 1 GeV. La mesure de la diffusion multiple relative et celle de l'angle d'ouverture se heurtent, par application des techniques habituelles à diverses difficultés expérimentales qui limitent la valeur maximum de l'énergie mesurable. Celles-ci sont dues, dans le premier cas, à l'influence de la dispersion des grains d'argent autour des trajectoires, à laquelle s'ajoute dans le deuxième cas, l'effet de la diffusion coulombienne.

Nous nous sommes efforcés de reculer la limite des énergies mesurables, d'une part en améliorant les techniques en usage, d'autre part en établissant une méthode nouvelle basée sur la structure de la trace au voisinage de l'origine des paires. Nous avons également cherché à préciser, pour ce genre de mesure, l'influence de la diffusion parasite résultant des dislocations (« spurious scattering »).

2. - Détermination de l'angle d'ouverture projeté d'une paire à partir d'une mesure directe des distances séparant les traces des deux électrons.

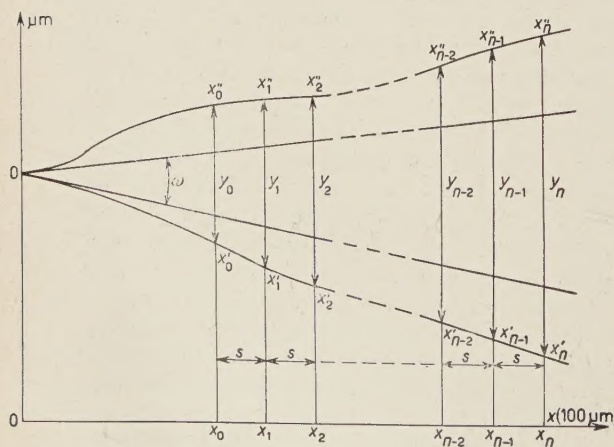


Fig. 1.

Considérons une paire d'électrons d'ouverture angulaire à l'origine donnée ω_e , soit ω (Fig. 1), l'angle projeté dans le plan de l'émulsion. Mesurons à intervalles réguliers s (longueur de cellule), les séparations projetées $Y_1, Y_0, \dots, Y_i, \dots, Y_n$ en μm des deux traces aux abscisses $x_0, x_1, \dots, x_i, \dots, x_n$ ^(*) (les grandeurs s et x_i étant toutes deux me-

(1) R. WEILL, M. GAILLOUD and PH. ROSSELET: *Helv. Phys. Acta*, **29**, 437 (1956).

(*) Dans le calcul suivant, nous admettons que $\omega/2 < 0,05$ et que $Y/(\cos \omega/2) \simeq Y$; nous nous limitons d'autre part à des distances x telles que la perte d'énergie des électrons soit négligeable.

surées en centaines de μm), on a:

$$Y_0 = \omega \cdot 10^2 S \cdot N + (\beta'_0 + \beta''_0) \cdot 10^2 S \cdot N + y'_0 + y''_0$$

$$Y_1 = Y_0 - y'_0 - y''_0 + \omega \cdot 10^2 S + (\beta'_1 + \beta''_1) \cdot 10^2 S + y'_1 + y''_1$$

$$Y_i = Y_{i-1} - y'_{i-1} - y''_{i-1} + \omega \cdot 10^2 S + (\beta'_i + \beta''_i) \cdot 10^2 S + y'_i + y''_i$$

où: $N = x_0/S$

$\beta'_i (\beta''_i)$ est $\left\{ \begin{array}{l} \text{pour } i = 0: \text{l'angle entre la corde } x'_0 O(x''_0) \text{ et la tangente à la} \\ \text{trajectoire correspondante en } O. \\ \text{pour } i \neq 0: \text{l'angle entre les cordes } x'_i, x'_{i-1} (x''_i, x''_{i-1}) \text{ et } x'_{i-1}, \\ x'_{i-2} (x''_{i-1}, x''_{i-2}). \end{array} \right.$

Le déplacement angulaire β'_i (β''_i) considéré ici est dû exclusivement à la diffusion multiple coulombienne. y'_i (y''_i) est le déplacement latéral de la trace résultant de la dispersion des grains autour de la trajectoire.

D'après notre expérience, la diffusion parasite provenant des dislocations de la gélatine est éliminée dans nos conditions lorsqu'on mesure la séparation de deux traces, ainsi que nous le montrons à la Sect. 4.

Sommons les valeurs Y_i mesurées, nous avons:

$$(1) \quad \sum_{i=0}^n Y_i = \frac{(n+1)(2N+n)10^2 S}{2} \cdot \Omega,$$

$$\text{où } \Omega = \omega + \{ [N(n+1)(\beta'_0 + \beta''_0) + n(\beta'_1 + \beta''_1) + \dots + (n-i+1)(\beta'_i + \beta''_i) + \dots + (\beta'_n + \beta''_n)] 10^2 S + + \sum_0^n (y'_i + y''_i) \} \frac{2}{(n+1)(2N+n)10^2 S}.$$

β'_i (β''_i) et y'_i (y''_i) étant des variables aléatoires indépendantes de moyenne nulle, que nous admettons distribuées selon une loi de Gauss, il résulte de l'expression (1) que Ω est également une variable gaussienne, de moyenne ω et de variance:

$$(2) \quad \Sigma^2 = \Sigma_d^2 + \Sigma_g^2,$$

où Σ_d^2 est la contribution de la diffusion multiple coulombienne, et Σ_g^2 celle de la dispersion des grains d'argent autour des trajectoires.

$$\Sigma_d^2 = \left(\frac{2}{(n+1)(2N+n)10^2 S} \right)^2 \cdot 10^4 \left(k \frac{\pi}{180} \sqrt{\frac{\pi}{2}} \right)^2 \left(\frac{1}{E'^2} + \frac{1}{E''^2} \right) S^3 \cdot \\ \cdot [0.5(n+1)^2 N^3 + n^2 + \dots + (n+1-i)^2 + \dots + 1]$$

$k \cong 27 \text{ MeV} \cdot \text{degré}/\sqrt{100\mu}$ est la constante de diffusion multiple utilisée dans les mesures sagittales,

$$\Sigma_g^2 = \left(\frac{2}{(n+1)(2N+n)10^2S} \right)^2 (n+1)2\bar{y}^2,$$

$$\bar{y}^2 = \left(\frac{0.17}{\sqrt{6}} \sqrt{\frac{\pi}{2}} \right)^2,$$

0.17 μm est la diffusion parasite due à la dispersion des grains dans les mesures sagittales.

Nous prendrons comme valeurs mesurées de l'angle d'ouverture ω celles calculées à l'aide de l'expression (1) en posant $\omega = \Omega$, cette valeur étant affectée d'une incertitude $\pm \Sigma$ (formule (2)), intervalle de confiance à 68% sur Ω . Le résultat obtenu n'a évidemment une signification que si $\omega > \Sigma$.

3. - Application de cette méthode à la détermination de l'angle d'ouverture projeté d'une paire d'électrons d'énergie donnée.

En pratique, les mesures de séparation ne sont faites que sur des paires d'électrons dont la bissectrice de l'angle d'ouverture des trajectoires à l'origine est faiblement inclinée; nous supposerons par la suite que pour toutes les paires considérées, la bissectrice est parallèle au plan de l'émulsion.

Soit tout d'abord un ensemble de paires d'électrons, de même énergie totale ($E = E' + E''$), dont le plan des tangentes à l'origine fait un angle θ avec le plan de l'émulsion.

La distribution (dans l'espace ou en projection) $B(\omega_e/\omega_a)$ du rapport de leur angle d'ouverture à l'angle d'ouverture le plus probable $\omega_a = 4m_ec^2/E$ a été calculé par BORSELLINO (2). L'une de ces paires étant prise au hasard et la mesure de Ω étant effectuée à l'aide de la méthode décrite précédemment, déterminons la probabilité P_θ pour que $\omega > |\Omega - \omega| = |Z|$ en admettant l'équpartition de l'énergie entre les deux électrons. $Z = \Omega - \omega$ satisfaisant à une distribution de Gauss, de moyenne nulle et de variance Σ^2 (formule (2)), on a:

$$P_\theta = \frac{2}{\sqrt{2\pi}\Sigma} \int_{Z=0}^{\infty} \exp\left[-\frac{Z^2}{2\Sigma^2}\right] dZ \int_{\omega/\omega_a = Z/\omega_a \cos \theta}^{\infty} B\left(\frac{\omega}{\omega_a}\right) \frac{d\omega}{\omega_a}.$$

Tenant compte de toutes les valeurs possibles de l'angle θ , on obtient:

$$P = \frac{1}{\pi} \int_{-\pi/2}^{\pi/2} P_\theta d\theta.$$

(2) A. BORSELLINO: *Phys. Rev.*, **89**, 1023 (1953).

Nous avons calculé P_θ par la méthode des trapèzes, l'intégration étant limitée à $\omega/\omega_a = 8.5$; les valeurs de P ont été déterminées ensuite à l'aide d'un planimètre. Les erreurs pouvant résulter des approximations ainsi faites et des méthodes d'intégration mises en œuvre n'excèdent pas 10 %. A la Fig. 2,

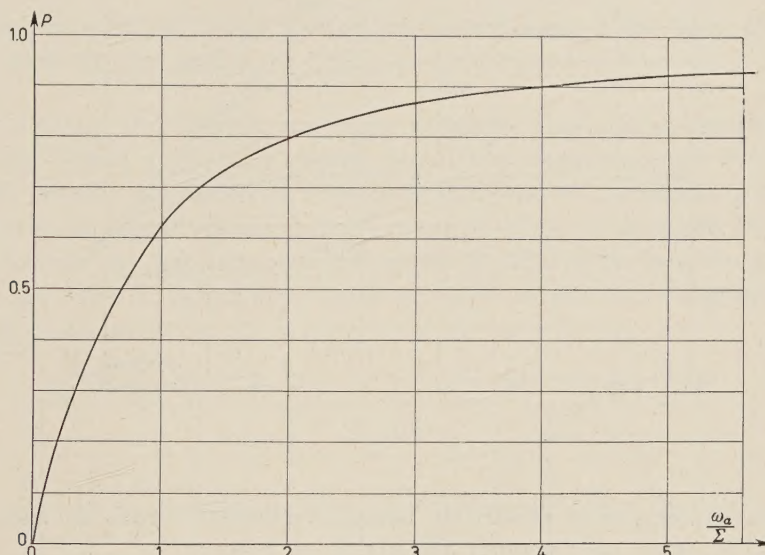


Fig. 2.

P est représenté en fonction de ω_a/Σ . A partir de ce graphique, diverses valeurs de P (Fig. 3) ont été calculées pour les conditions expérimentales suivantes:

$x_n = 100$ (en centaines de microns);

$Y_0 = 0.15 \mu\text{m}$, limite inférieure d' Y imposée par la dimension des grains de bromure d'argent. Les écartements compris entre $0.15 \mu\text{m}$ et $0.30 \mu\text{m}$ sont déterminés à partir du relevé du profil de la trace;

$0.1 < s < 20$ (en centaines de μm).

La valeur de Σ utilisée ici est celle correspondant à la moyenne de l'angle projeté le plus probable $(2/\pi)\omega_a$, ce qui, dans le domaine d'énergie considéré, n'affecte pas d'une manière appréciable les résultats obtenus.

A titre de comparaison, nous donnons à la Fig. 4 les valeurs de P calculées dans le cas où l'angle d'ouverture ω est déterminé à partir de l'écartement Y mesuré en un seul point d'abscisse x (c'est la méthode habituelle utilisée jusqu'ici; $n = 0$, Σ indépendant de ω). L'écartement minimum mesurable

est alors de $0.3 \mu\text{m}$ environ, auquel correspond une abscisse moyenne $x_{\min} \cong (0.3/\omega_a) \cdot 10^{-2}$ (centaines de microns).

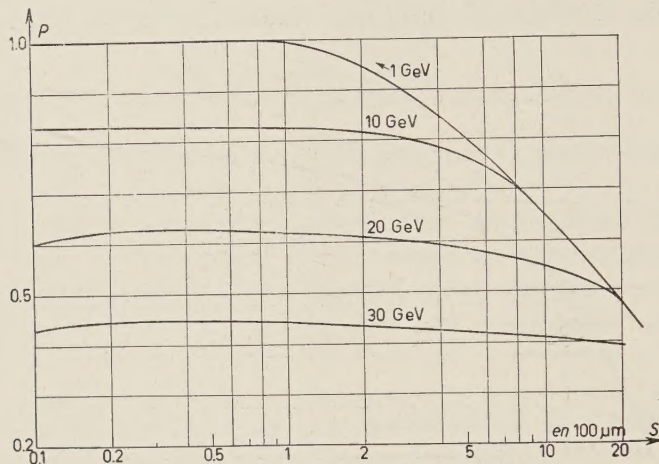


Fig. 3.

Si l'on admet que la mesure de l'angle d'ouverture ω n'a de sens que si $P > 0.68$, il ressort de l'examen des Fig. 3 et 4 que:

1) La méthode établie ci-dessus est utilisable dans le cas de paires d'électrons d'énergie allant jusqu'à 20 GeV environ, alors que la méthode habituelle est inapplicable au-delà de 1.5 GeV environ.

2) Cette dernière valeur (1.5 GeV) est légèrement supérieure à celle (0.5 GeV) indiqué par LOHRMANN (*) (3) et admise par divers auteurs.

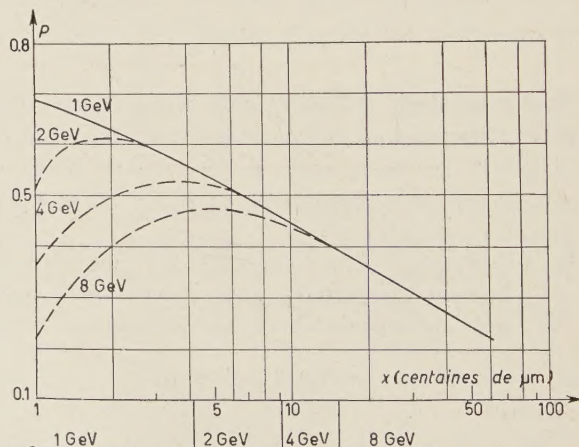


Fig. 4.

(*) Dans son calcul, Lohrmann néglige l'influence de la dispersion des grains; d'autre part il compare directement ω_a à Σ , ce qui nous paraît ne pas avoir de signification immédiate.

(3) E. LOHRMANN: *Nuovo Cimento*, **2**, 1029 (1955).

Dans l'application de cette méthode, il convient après avoir estimé grossièrement l'énergie de la paire d'électrons étudiée, d'adopter pour la mesure des écartements une longueur de cellules optimum qui peut être déterminée à partir du graphique de la Fig. 3.

4. — Détermination de l'angle d'ouverture dans l'espace d'une paire d'électrons à partir de l'ionisation.

Au voisinage de l'origine, une paire d'électrons de grande énergie se présente sous l'aspect d'une trace unique, tant que la séparation des deux trajectoires ne dépasse pas le rayon d'un grain d'argent de l'émulsion développée. Ainsi que l'ont signalé divers auteurs^(1,5) à la suite de PERKINS⁽⁴⁾ la densité de lacunes sur cette trace croît à partir du sommet de la paire pour n'atteindre deux fois la valeur au plateau qu'après un parcours de plusieurs centaines de microns.

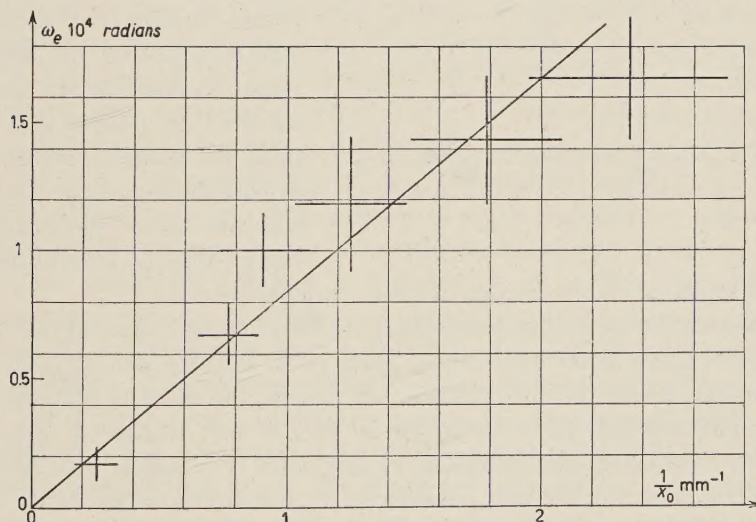


Fig. 5.

Utilisant des cellules de 200 à 300 μm , nous avons mesuré la densité de lacunes relative au plateau sur les traces initiales de 6 paires d'électrons dont les énergies, supérieures à 10 GeV, ont été déterminées par diffusion multiple relative; g^* peut être représentée en fonction de l'abscisse x par une relation du type: $g^* = 2(1 - a \exp[-x/x_0])$. A la Fig. 5, le paramètre $1/x_0$, déter-

⁽⁴⁾ D. H. PERKINS: *Phil. Mag.*, **46**, 1146 (1955).

⁽⁵⁾ W. WOLTER and M. MIĘSOWICZ: *Nuovo Cimento*, **4**, 648 (1956).

miné par l'analyse des moindres carrés pour chacune des paires étudiées, a été représenté en fonction de l'angle ω_a de Borsellino. Mais la droite tracée sur le graphique, résultant d'une moyenne, donne en fait la variation de $1/x_0$ avec l'angle ω_e dans l'espace. Elle indique que la densité de lacunes en un point de la trace considérée ne dépend que de la séparation des trajectoires en ce point, ce qui apparaît également à la Fig. 6 où nous avons reporté le $\log(1 - 0.5g^*)$ en fonction de l'écartement (dans l'espace) le plus probable $Y_e = \omega_e \cdot 10^2 \cdot x$ (courbe 1). De même que ci-dessus la valeur moyenne de Y_e se confond avec Y_a . La dispersion relativement grande des points autour des droites moyennes provient de divers facteurs: incertitude sur les valeurs admises de l'angle ω_a , fluctuations de nature statistique de la densité de lacunes et fluctuations liées aux inhomogénéités de développement, contribution de la

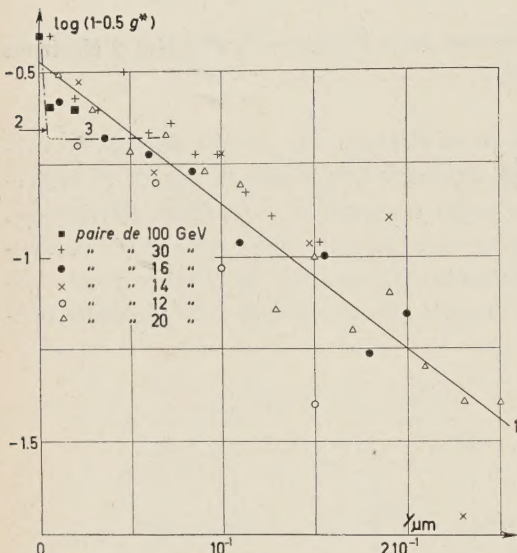


Fig. 6.

diffusion multiple à l'écartement des trajectoires.

Les graphiques ci-dessus permettent de déterminer l'angle d'ouverture ω_e dans l'espace d'une paire d'électrons, après avoir effectué des mesures de densité de lacunes g^* sur sa trace initiale. On pourra, soit calculer d'abord le paramètre x_0 pour obtenir ω_e à l'aide de la Fig. 5, soit utiliser la Fig. 6 pour trouver les séparations dans l'espace Y_{e_i} des deux trajectoires aux abscisses x_i des points milieux des cellules considérées et calculer ω_e à l'aide de l'expression (1) (page 415) en faisant $\Omega = \omega_e$; $N = \frac{1}{2}$. Nous avons calculé la probabilité P pour que la mesure ainsi effectuée ait une signification $P[\omega_e > |\Omega - \omega_e|]$ à l'aide de la relation (3'):

$$(3') \quad P = \frac{2}{\sqrt{2\pi}\sqrt{2\Sigma}} \int_{Z=0}^{\infty} \exp\left[-\frac{Z^2}{4\Sigma^2}\right] dZ \int_{\omega/\omega_a = Z/\omega_a}^{\infty} B\left(\frac{\omega}{\omega_a}\right) \frac{d\omega}{\omega_a}.$$

La variance considérée ici est $2\Sigma^2$ où Σ est donné par la formule (2) avec $\Sigma_g = 0$. P a été reporté à la Fig. 7 en fonction du nombre de cellules de mesure de $200 \mu\text{m}$; le long de l'abscisse nous indiquons également pour diverses énergies le nombre de cellules ($200 \mu\text{m}$) utilisables.

Nous avons constaté que la longueur totale des lacunes L^* , mesurée pour des cellules de 200 à 300 μm , reste sensiblement constante. La méthode ci-dessus est donc applicable également si l'on détermine la longueur moyenne des lacunes, les valeurs du paramètre x_0 à utiliser dans ce cas étant celles données à la Fig. 5.

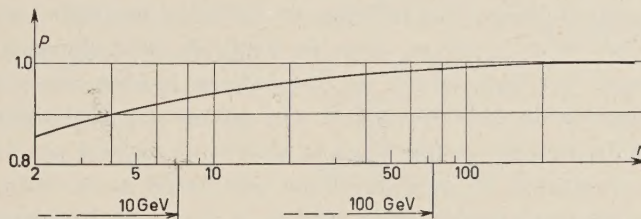


Fig. 7.

La densité de lacunes g^* de la trace initiale d'une paire d'électrons peut être calculée sur la base de la théorie de Della Corte (⁶). Lorsque les trajectoires sont distantes de moins du double du paramètre d'impact maximum correspondant à l'impression du grain d'AgBr, les deux électrons constituent un dipôle dont la perte d'énergie spécifique dE/dx a été donnée par ČUDAKOV (⁸) pour des écartements inférieurs à $3 \cdot 10^{-3} \mu\text{m}$. La probabilité $\pi(Y_e)$ pour un grain de bromure d'argent d'être rendu développable lorsqu'il est traversé par la paire d'électrons, peut être calculée à partir de celle (π) mesurée dans le cas d'un grain traversé par une particule de charge unité au plateau ($\pi \approx 0.05$), en admettant (d'après la formule (1) et la Fig. 2 de (⁷)) que π varie proportionnellement à dE/dx . La valeur de $\pi(Y_e)$ obtenue croît avec l'écartement Y_e , et la densité de lacunes $g^* = \pi((Y_e)/\pi) \{(1 - \pi(Y_e))/(1 - \pi)\}^k$ (formule (7) de (⁶), dans nos émulsions: $k \approx 4$) croît également avec Y_e pour atteindre 1.60 à $3 \cdot 10^{-3} \mu\text{m}$. Au-delà de $3 \cdot 10^{-3} \mu\text{m}$, les électrons agissent indépendamment, et il faut faire appel à des considérations géométriques pour rendre compte de l'augmentation de g^* . Tant que les trajectoires sont suffisamment rapprochées ($y_e < 5 \cdot 10^{-2} \mu\text{m}$) pour qu'on puisse considérer qu'elles passent au travers des mêmes grains, la probabilité pour un de ceux-ci d'être rendu développable est constante et égale à environ $2\pi - \pi^2$. Le calcul donne: $g^* = 1.60$. Ainsi qu'on peut le constater à la Fig. 6, les valeurs calculées de g^* sont d'un ordre de grandeur compatible avec celles résultant de nos expériences. Pour des écartements supérieurs à $5 \cdot 10^{-2} \mu\text{m}$, le modèle unidimensionnel de Della Corte n'est plus valable, et doit être remplacé par un modèle bidimensionnel. Nous poursuivons le calcul sur cette nouvelle base.

(⁶) M. DELLA CORTE, M. RAMAT et L. RONCHI jr.: *Nuovo Cimento*, **10**, 509 (1953).

(⁷) M. DELLA CORTE, M. RAMAT et L. RONCHI jr.: *Nuovo Cimento*, **10**, 958 (1953).

(⁸) A. E. ČUDAKOV: *Compt. Rend. Acad. Sci. U.R.S.S.*, **19**, 651 (1955).

5. - Influence de la diffusion parasite de dislocation.

Plusieurs auteurs (⁹⁻¹²) ont récemment mis en évidence un facteur susceptible de fausser considérablement les mesures de diffusion multiple aux très hautes énergies. Il s'agit d'un nouveau type de bruit de fond (spurious scattering) qui s'expliquerait par l'apparition de dislocations locales dans la gélatine au cours des opérations de développement. On sait que la flèche moyenne $\langle D_{BF} \rangle$ due aux bruits de fond des grains et de la platine ne dépend pas de la longueur de cellule; au contraire, la caractéristique essentielle de la diffusion parasite de dislocation est son augmentation rapide (à peu près linéaire) en fonction de s , d'où la nécessité d'utiliser de très grandes cellules (plusieurs millimètres) pour la mesure des énergies élevées (> 1 GeV). Il ressort des résultats publiés que l'importance du « spurious scattering » varie d'un stack à l'autre et, probablement aussi, dans un même stack, selon l'orientation de la trace utilisée pour la mesure.

Pour l'application des techniques décrites précédemment, il importe avant tout de vérifier si le « spurious scattering » est éliminé lors des mesures de diffusion multiple relative, c'est-à-dire si les dislocations responsables du phénomène se répercutent, identiques à elles-mêmes, sur des distances supérieures à l'écartement maximum des traces étudiées. Une première indication dans ce sens paraît ressortir du travail de BISWAS *et al.* (⁹). Nous avons voulu déterminer avec plus de précision que ces auteurs la valeur de la diffusion de dislocation relative $D_{rel,ss}$ pour divers écartements des trajectoires. Dans ce but, nous avons utilisé un jet de grande énergie, parallèle au plan de l'éмульSION ($cotg \varphi > 300$) provenant de la fragmentation d'un noyau lourd ($Z = 13$; $E > 1000$ GeV/nucléon). Sur quatre secondaires de ce jet émis sous un angle inférieur à 10^{-3} radians, nous avons mesuré la diffusion multiple relative et calculé la valeur de la diffusion de dislocation $D_{rel,ss}$ d'après la méthode de Biswas et coll. (⁹). A la Fig. 8, $D_{rel,ss}^2$ est donné en fonction de l'écartement projeté Y en microns, pour des cellules de 500, 1000 et 2000 μm . Le « spurious scattering » D_{ss} calculé pour ces mêmes longueurs de cellules à partir des mesures effectuées sur l'une des traces précédentes est de: (0.07 ± 0.01) ; (0.10 ± 0.02) et (0.20 ± 0.04) μm .

(⁹) S. BISWAS, B. PETERS et RAMA: *Proc. Ind. Acad. Sci., A* **41**, 154 (1955).

(¹⁰) E. LOHRMANN et M. TEUCHER: *Nuovo Cimento*, **3**, 59 (1956).

(¹¹) F. A. BRISBOUT, C. DAHANAYAKE, A. ENGLER, P. H. FOWLER et P. B. JONES: *Nuovo Cimento*, **3**, 1400 (1956).

(¹²) A. DEBENEDETTI, C. M. GARELLI, L. TALLONE et M. VIGONE: *Nuovo Cimento*, **4**, 1142 (1956).

Nos résultats montrent qu'à la précision des mesures près, l'influence de la diffusion de dislocation est éliminée dans les mesures de diffusion relative, pour des écartements horizontaux et des différences de cote n'excédant pas $30 \mu\text{m}$ et pour des longueurs de cellule allant jusqu'à 2 mm.

6. – Conclusions.

La méthode consistant à mesurer la séparation projetée des deux traces d'une paire d'électrons en plusieurs points au voisinage du sommet permet de réduire la variance résultant de la diffusion multiple et de la dispersion des grains, et par conséquent l'erreur affectant la valeur mesurée de l'angle d'ouverture projeté. Nous avons montré que dans les conditions réalisées pour ces mesures, la diffusion de dislocation n'intervient pas. Le critère de validité adopté étant d'avoir une probabilité supérieure à 68% pour que la contribution du bruit de fond soit inférieure à celle de l'angle d'ouverture initial, le calcul montre que cette méthode est applicable pour des énergies allant jusqu'à 20 GeV alors que la méthode usuelle est limitée à 1.5 GeV.

Pour des énergies supérieures à 10 GeV, une détermination relative de l'angle d'ouverture dans l'espace peut être faite à partir de la mesure de la variation de l'ionisation sur la trace initiale de la paire d'électrons étudiée en utilisant des courbes d'étalonnage. L'application du même critère que ci-dessus montre que l'utilisation de cette méthode n'est limitée que par la longueur de trace disponible. Des considérations géométriques et l'effet dipolaire signalé par PERKINS permettent, sur la base de la théorie de Della Corte, de rendre compte qualitativement des valeurs mesurées de la densité des lacunes, tant que la séparation des trajectoires est petite vis-à-vis du diamètre d'un grain de bromure d'argent.

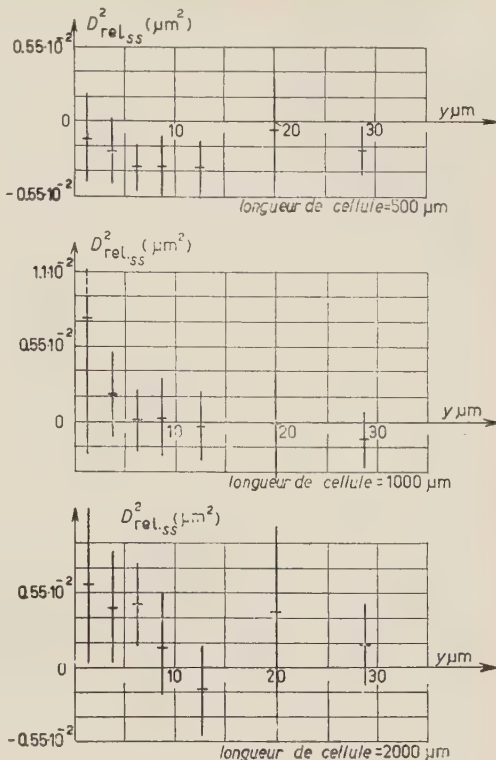


Fig. 8.

Nous exprimons notre reconnaissance à Monsieur le professeur CH. HAENNY pour l'intérêt qu'il a porté à notre travail, ainsi qu'au Fonds National Suisse pour la Recherche Scientifique dont les subsides nous ont permis ces recherches. Nous remercions le groupe de dépouillement de notre laboratoire pour sa précieuse collaboration.

RIASSUNTO (*)

Per misurare la proiezione dell'angolo ω di una coppia di elettroni abbiamo ideato un metodo assoluto che consente di diminuire le incertezze dovute allo scattering multiplo e alla dispersione granulare. La misura della separazione delle tracce in diversi punti a partire dal vertice della coppia ci mette in grado di calcolare $\Omega = \omega + Z$, dove Z è una variabile gaussiana di valor medio zero attribuita al disturbo (scattering multiplo e dispersione granulare). Questo metodo si può impiegare per coppie di elettroni fino a 20 GeV se si ammette che la misura indicata ha senso solo se la probabilità P per $\omega > Z$ sia superiore a 0.68; mentre col metodo consueto di misurare la separazione delle tracce solo in un punto si possono determinare solo energie fino a 1.5 GeV. Le misure di ionizzazione sulle tracce iniziali di coppie d'elettroni di grande energia danno una misura relativa dei loro angoli d'apertura nello spazio ω_e . Abbiamo determinato g^* , la densità di lacune relativa al plateau per 6 coppie d'elettroni le cui energie, maggiori di 10 GeV, sono state misurate per mezzo dello scattering multiplo relativo; g^* è funzione della distanza dal vertice e può essere espresso con $g^* = 2 \cdot (1 - a \exp[-x/x_0])$. Si sono costruite due curve, l'una che dà x/x_0 in funzione di ω_e , l'altra che dà $\log(1 - 0.5g^*)$ in funzione di Y_e , la separazione delle tracce. Dato il criterio espresso sopra ($P[\omega > Z] > 0.68$) si possono determinare così energie superiori a 10 GeV. I valori misurati della ionizzazione si accordano qualitativamente con quelli previsti dalla teoria di Della Corte, tenendo conto dell'effetto di dipolo e di considerazioni geometriche. Abbiamo misurato la separazione delle tracce su 4 secondari di un getto di energia superiore a 1000 GeV/nucleone e abbiamo notato che l'influenza dello scattering spurio risulta eliminata per separazioni orizzontali e differenze di altezza non superiori a 30 μm , e lunghezze di cella fino a 2 mm.

(*) Traduzione a cura della Relazione.

Non-Adiabatic Treatment of the Scattering of K^+ -Mesons by Nucleons.

C. CEOLIN and L. TAFFARA

Istituto di Fisica dell'Università - Padova

Istituto Nazionale di Fisica Nucleare - Sezione di Padova

(ricevuto il 28 Marzo 1957)

Summary. — The problem of the K^+ -nucleon scattering is treated with the method of Tamm-Dankoff in the two-meson approximation, both with scalar and pseudovector coupling. In both cases it turns out that the most important phase at low energy is $T=1$, which corresponds to an attractive potential. In the scalar case this phase does not lead to a resonance; in the pseudoscalar case there is, however, a resonant state whose position, is strongly dependent on the momentum cut-off K . At the end of the work there is a brief discussion of the results obtained, in relation to the few experimental data so far available.

1. — Introduction.

In a previous work ⁽¹⁾ the authors have treated the problem of the scattering of the K^+ -mesons by nucleons, using a perturbation method in relativistic approximation, and taking account of the possibility that both the Λ and Σ particles may take part in the intermediate state. The application of such a method has been justified by the fact that from the few experimental data at present available one may certainly deduce that the new K^+ -mesons interact in nuclear matter less strongly than the pions, and therefore one could perhaps expect that the interaction $K-Y-N$ would not lead to the formation of bound states and therefore to resonant phases.

At present, the slow increase with energy of the total cross-section in the K^+ -nucleon collision seems to exclude the existence of a resonance maximum

⁽¹⁾ C. CEOLIN and L. TAFFARA: *Nuovo Cimento*, 5, 435 (1957).

at least up to 200 MeV (the zone in which the resonance for the pion-nucleon scattering is situated). This however does not show that a resonant state cannot be formed at much higher energies, particularly if one assumes that, by extrapolation, an eventual resonance in the K^+ -nucleon scattering would be localized at an energy of the order of that of the rest mass energy of the K^+ -meson, namely at about 500 MeV. The existence of such a resonance would thus no longer allow the application of the perturbation method, especially at high energies.

For these reasons it would seem that an attempt might be made to resolve the problem of the K^+ -nucleon scattering by means of a non-perturbative method such as the method of Tamm-Dancoff. Although this is far from being an ideal method for solving scattering problems (the method has proved unsuitable for pion-nucleon scattering) it can at least give a better qualitative approximation than a perturbation theory, in the sense that it can show the existence of possible resonance states.

We have therefore attempted in the present work to apply this method of calculation, which seems more complete and general than the former in the two-mesons approximation with fixed source. The assumptions which have been made may be summarized in the following four points:

- a) It is assumed that the characteristics of the single interacting particles are those given by the Gell-Mann-Nishijima scheme (and so far not in contrast with the experimental facts) according to which the hyperons are fermions-isobosons (of isotopic spin 1 for the Σ and 0 for the Λ) and the K -mesons are bosons-isofermions (of isotopic spin $\frac{1}{2}$).
- b) For simplicity we will assume that the spin of hyperons is $\frac{1}{2}$ and the spin of the K 's is 0: this hypothesis, at least for the K 's, has been shown by various authors as being the most probable ⁽²⁾.
- c) We will suppose that charge independence is still valid for the K -Y-N forces.
- d) Finally we will suppose that the pions do not participate in the scattering process and so do not contribute to the formation of the intermediate states.

As far as the parity of the single interacting particles is concerned, the calculation has been made both with scalar and pseudovector coupling (in

⁽²⁾ M. RUDERMANN and R. KARPLUS: *Phys. Rev.*, **102**, 247 (1956); M. BALDO-CEOLIN, A. BONETTI, D. W. B. GREENING, S. LIMENTANI, M. MERLIN and G. VANDERHAEGHE: *Turin Conference*, September 1956 (in course of publication in the *Suppl. Nuovo Cimento*).

non-relativistic approximation), in order to consider the two possibilities that K-meson and hyperons have the same or opposite parity (3).

2. – Calculation of the constants of the motion.

The total hamiltonian of the system which has been adopted, and which satisfies conditions *a*), *b*), *c*) and *d*), has been suggested by d'ESPAGNAT and PRENTKI (4), i.e.:

$$(1) \quad H = H_0 + H_{\text{int}},$$

where the hamiltonian for the free fields H_0 is given by:

$$(2) \quad \begin{aligned} H_0 = & (m_N + \delta m_N) \sum_p \psi_N^*(p) \psi_N(p) + (m_\Sigma + \delta m_\Sigma) \sum_{ip} \psi_\Sigma^{*i}(p) \psi_\Sigma^i(p) + \\ & + (m_\Lambda + \delta m_\Lambda) \sum_p \psi_\Lambda^*(p) \psi_\Lambda(p) + \sum_k \omega(k) [a^*(k) a(k) + b^*(k) b(k)] = \\ = & (m_N + \delta m_N) \sum_p N(p) + (m_\Sigma + \delta m_\Sigma) \sum_{ip} N_\Sigma^i(p) + \\ & + (m_\Lambda + \delta m_\Lambda) \sum_p N_\Lambda(p) + \sum_k \omega(k) [N_K(k) + N_{\bar{K}}(k)], \end{aligned}$$

with obvious meaning for the N operators; and where the interaction hamiltonian H_{int} is:

$$(3) \quad \begin{aligned} H_{\text{int}} = & \sum_{i=1}^3 \sum_{pk} \frac{1}{\sqrt{2\omega(k)\Omega}} [\psi_\Sigma^{*i}(\mathbf{p} - \mathbf{k}) \Gamma_\Sigma(\mathbf{k}) a^*(\mathbf{k}) \tau_i \psi_N(\mathbf{p}) + \\ & + \psi_N^*(\mathbf{p} + \mathbf{k}) \tau_i \Gamma_\Sigma^*(\mathbf{k}) a(\mathbf{k}) \psi_\Sigma^i(\mathbf{p}) + \psi_\Sigma^{*i}(\mathbf{p} + \mathbf{k}) \Gamma_\Sigma(\mathbf{k}) b(\mathbf{k}) \tau_i \psi_N(\mathbf{p}) + \\ & + \psi_N^*(\mathbf{p} - \mathbf{k}) \tau_i \Gamma_\Sigma^*(\mathbf{k}) b^*(\mathbf{k}) \psi_\Sigma^i(\mathbf{p})] + \sum_{pk} \frac{1}{\sqrt{2\omega(k)\Omega}} [\psi_\Lambda^*(\mathbf{p} - \mathbf{k}) \Gamma_\Lambda(\mathbf{k}) a^*(\mathbf{k}) \psi_N(\mathbf{p}) + \\ & + \psi_N^*(\mathbf{p} + \mathbf{k}) \Gamma_\Lambda^*(\mathbf{k}) a(\mathbf{k}) \psi_\Lambda(\mathbf{p}) + \psi_\Lambda^*(\mathbf{p} + \mathbf{k}) \Gamma_\Lambda(\mathbf{k}) b(\mathbf{k}) \psi_N(\mathbf{p}) + \\ & + \psi_N^*(\mathbf{p} - \mathbf{k}) \Gamma_\Lambda^*(\mathbf{k}) b^*(\mathbf{k}) \psi_\Lambda^i(\mathbf{p})], \end{aligned}$$

with the following meaning of the symbols:

$\psi_\Sigma^{*i}, \psi_\Sigma^i$ = creation and destruction operators for Σ hyperons (spinor in ordinary space and vector in charge space);

(3) After this work was finished we received a preprint of a paper by D. AMATI and B. VITALE. These authors have obtained approximately the same results by treating the scalar case by means of the same model.

(4) B. d'ESPAGNAT and J. PRENTKI: *Nuclear Physics*, **1**, 33 (1956).

- $\psi_{\Lambda}^*, \psi_{\Lambda}$ = creation and destruction operators for Λ hyperons (spinor in ordinary space and scalar in charge space);
- ψ_{N}^*, ψ_N = creation and destruction operators for nucleons (spinor in both ordinary and charge space);
- $a^*(k), a(k)$ = creation and destruction operators for K-mesons (spinor in charge space and scalar in ordinary space);
- $b^*(k), b(k)$ = creation and destruction operators for \bar{K} -mesons (spinor in charge space and scalar in ordinary space);
- $\Gamma_Y(k)$ $\left\{ \begin{array}{l} = G_Y \text{ for the case of scalar coupling,} \\ = \frac{f_Y}{m_K} (i\sigma \times \mathbf{k}) \text{ for the case of pseudovector coupling.} \end{array} \right.$

The meaning of the other symbols is obvious.

The destruction and creation operators which appear in (2) and (3) satisfy the well-known rules of commutation and anticommutation:

$$(4) \quad \left\{ \begin{array}{l} \{\psi_{N\alpha}^*(\mathbf{P}), \psi_{N\beta}(\mathbf{P}')\} = \delta(\mathbf{P} - \mathbf{P}') \delta_{\alpha\beta} \{\psi_{\Lambda\alpha}^*(\mathbf{P}), \psi_{\Lambda\beta}(\mathbf{P}')\} = \delta(\mathbf{P} - \mathbf{P}') \delta_{\alpha\beta} \\ \{\psi_{\Sigma\alpha}^{*i}(\mathbf{P}), \psi_{\Sigma\beta}^i(\mathbf{P}')\} = \delta(\mathbf{P} - \mathbf{P}') \delta_{\alpha\beta} [a^*(\mathbf{k}), a(\mathbf{k}')] = \delta(\mathbf{k} - \mathbf{k}') \\ \{\psi_{\Sigma\alpha}^{*i}(\mathbf{P}), \psi_{\Sigma\beta}^j(\mathbf{P}')\} = 0 \quad \text{for } i \neq j [b^*(\mathbf{k}), b(\mathbf{k}')] = \delta(\mathbf{k} - \mathbf{k}') \\ [a^*(\mathbf{k}), a^*(\mathbf{k}')] = [a(\mathbf{k}), a(\mathbf{k}')] = [b^*(\mathbf{k}), b(\mathbf{k}')] = [b(\mathbf{k}), b(\mathbf{k}')] = 0 \end{array} \right.$$

It is easily seen that, with the operators for the numbers of particles defined in the usual way:

$$(5) \quad \left\{ \begin{array}{l} N_N = \sum_p N_N(p), \quad N_{\Lambda} = \sum_p N_{\Lambda}(p), \quad N_{\Sigma} = \sum_{ip} N_{\Sigma}^i(p) \\ N_K = \sum_k N_K(k), \quad N_{\bar{K}} = \sum_k N_{\bar{K}}(k) \end{array} \right.$$

and taking account of the rules (4), the hamiltonian (1) allows the following commutation rules:

$$(6) \quad \left\{ \begin{array}{l} [H, (N_N + N_{\Sigma} + N_{\Lambda})] = 0 \\ [H, (N_N + N_K - N_{\bar{K}})] = 0 \\ [H, (N_K - N_{\Lambda} - N_{\Sigma} - N_{\bar{K}})] = 0 \end{array} \right.$$

from which it follows that three numbers exist defined by:

$$(7) \quad \left\{ \begin{array}{l} s_1 = \pi_N + \pi_\Sigma + \pi_\Lambda \\ s_2 = \pi_N + \pi_K - \pi_{\bar{K}} \\ s_3 = \pi_K - \pi_\Lambda - \pi_\Sigma - \pi_{\bar{K}}, \end{array} \right.$$

which are conserved during the interaction, i.e. they are good quantum numbers.

The physical meaning of the three conservation theorems is obvious: s_1 is the number of baryons; s_2 the number of isofermions minus the number of anti-isofermions; s_3 the strangeness as defined in the theory of Gell-Mann and Nishijima (5). The values of s_1 , s_2 and s_3 for the various states of a single particle are reported in Table I.

TABLE I.

	N	Σ	Λ	K	\bar{K}
s_1	1	1	1	0	0
s_2	1	0	0	1	-1
s_3	0	-1	-1	1	-1

It is thus clear that, in treating a particular interaction problem, one must remember that transitions are only possible between states which have the same group of three quantum numbers s_1 , s_2 and s_3 .

3. – Self-energy of the nucleon.

The problem of the calculation of the self energy of the nucleon for absorption and emission of K-mesons must now be solved. For this purpose we consider the equation:

$$(8) \quad (E - H_0) |\bar{N}\rangle = H_{\text{int}} |\bar{N}\rangle,$$

where H_0 and H_{int} are given by (2) and (3) and where $|\bar{N}\rangle$ indicates the « real nucleon ». Because $|\bar{N}\rangle$ has a group of quantum numbers s_1 , s_2 and s_3 equal

(5) M. GELL-MANN and A. PAIS: *Proceedings of the 1954 Glasgow Conference on Nuclear and Meson Physics*, p. 342.

to 1, 1, 0 respectively, we obtain by expanding it in series of eigenstates of H_0 which possess the same s_1 , s_2 and s_3 :

$$(9) \quad |\bar{N}\rangle = c_0 |N\rangle + \sum_1^3 \sum_{\mathbf{k}_1} c_\Sigma^i(\mathbf{k}_1) |K\Sigma\rangle + \\ + \sum_{\mathbf{k}_1} c_\Lambda(\mathbf{k}_1) |K\Lambda\rangle + \sum_{\mathbf{k}_1 \mathbf{k}'_1} c_N(\mathbf{k}_1, \mathbf{k}'_1) |K\bar{K}N\rangle .$$

Introducing this into (8) one obtains in the one-meson approximation, the following equations:

$$[E - m_N - \delta m_N]c_0 = \frac{\Omega}{(2\pi)^3} \sum_{i=1}^3 \int d\mathbf{k} \frac{\tau_i \Gamma_\Sigma(\mathbf{k}) c_\Sigma^i(\mathbf{k})}{\sqrt{2\omega(\mathbf{k})\Omega}} + \frac{\Omega}{(2\pi)^3} \int d\mathbf{k} \frac{\Gamma_\Lambda(\mathbf{k}) c_\Lambda(\mathbf{k})}{\sqrt{2\omega(\mathbf{k})\Omega}}, \\ [E - m_\Sigma - \omega(\mathbf{k})]c_\Sigma^i(\mathbf{k}) = \frac{c_0 \tau_i \Gamma_\Sigma^*(\mathbf{k})}{\sqrt{2\omega(\mathbf{k})\Omega}}, \\ [E - m_\Lambda - \omega(\mathbf{k})]c_\Lambda(\mathbf{k}) = \frac{c_0 \Gamma_\Lambda^*(\mathbf{k})}{\sqrt{2\omega(\mathbf{k})\Omega}},$$

from which, by elimination of $c_\Sigma^i(\mathbf{k})$ and $c_\Lambda(\mathbf{k})$ and putting $E = m_N$, it results that:

$$(10) \quad -\delta m_N = \frac{3}{(2\pi)^3} \int d\mathbf{k} \frac{\Gamma_\Sigma(\mathbf{k}) \Gamma_\Sigma^*(\mathbf{k})}{2\omega(\mathbf{k})[m_N - m_\Sigma - \omega(\mathbf{k})]} + \\ + \frac{1}{(2\pi)^3} \int d\mathbf{k} \frac{\Gamma_\Lambda(\mathbf{k}) \Gamma_\Lambda^*(\mathbf{k})}{2\omega(\mathbf{k})[m_N - m_\Lambda - \omega(\mathbf{k})]},$$

again, by means of the normalization condition $\langle \bar{N} | N \rangle = 1$ one has:

$$(11) \quad c_0 = \frac{1}{(1+A)^{\frac{1}{2}}} = Z^{\frac{1}{2}},$$

where

$$(12) \quad A = \frac{3}{(2\pi)^3} \int \frac{d\mathbf{k} \Gamma_\Sigma(\mathbf{k}) \Gamma_\Sigma^*(\mathbf{k})}{2\omega(\mathbf{k})[m_\Sigma + \omega(\mathbf{k}) - m_N]^2} + \frac{1}{(2\pi)^3} \int \frac{d\mathbf{k} \Gamma_\Lambda(\mathbf{k}) \Gamma_\Lambda^*(\mathbf{k})}{2\omega(\mathbf{k})[m_\Lambda + \omega(\mathbf{k}) - m_N]^2}.$$

As is well known ⁽⁶⁾, Z_2 represents the renormalization factor of the coupling constant. Relations (10) with (12) are of the same form as those obtained by applying Lee's theory to the same problem.

⁽⁶⁾ T. D. LEE: *Phys. Rev.*, **95**, 1329 (1954).

4. - K^+ -nucleon scattering in the two-mesons approximations.

In order to treat this problem, the following equation must be solved:

$$(13) \quad (H_0 - E) |\overline{KN}\rangle = H_{\text{int}} |\overline{KN}\rangle .$$

Since the real state $|\overline{KN}\rangle$ has quantum numbers $s_1 = 1$, $s_2 = 2$ and $s_3 = 2$, it may be expanded in series of the eigenstates of H_0 which possess the same values of these numbers:

$$\begin{aligned} |\overline{KN}\rangle &= \sum_{\mathbf{k}_1} c_N(\mathbf{k}_1) |KN\rangle + \frac{1}{(2!)^{\frac{1}{2}}} \sum_{\mathbf{k}_1 \mathbf{k}_2 i} c^i(\mathbf{k}_1; \mathbf{k}_2) |KK\Sigma\rangle + \\ &+ \frac{1}{(2!)^{\frac{1}{2}}} \sum_{\mathbf{k}_1 \mathbf{k}_2} c(\mathbf{k}_1 \mathbf{k}_2) |KK\Lambda\rangle + \frac{1}{(2!)^{\frac{1}{2}}} \sum_{\mathbf{k}_1 \mathbf{k}_2 \mathbf{k}'_1} c_N(\mathbf{k}_1 \mathbf{k}_2; \mathbf{k}'_1) |KK\bar{N}\rangle + \dots . \end{aligned}$$

Substituting this in (13) together with the expressions (2) and (3) and following the usual procedure of the method, we obtain the following integral equation in the two-mesons approximations:

$$\begin{aligned} (13) \quad [\omega(\mathbf{k}) - \omega(\mathbf{k}_0)] c_N(\mathbf{k}) h(\omega) &= \\ &= \frac{1}{16\pi^3} \boldsymbol{\tau} \times \boldsymbol{\tau}' \int d\mathbf{k}' \Gamma_{\Sigma}^r(\mathbf{k}') \Gamma_{\Sigma}^{r*}(\mathbf{k}) K_{\Sigma}(\mathbf{k}; \mathbf{k}') c_N(\mathbf{k}') + \\ &+ \frac{1}{16\pi^3} \int d\mathbf{k}' \Gamma_{\Lambda}^r(\mathbf{k}') \Gamma_{\Lambda}^{r*}(\mathbf{k}) K_{\Lambda}(\mathbf{k}; \mathbf{k}') c_N(\mathbf{k}') , \end{aligned}$$

where

$$\begin{aligned} (14) \quad h(\omega) &= 1 - \\ &- \left\{ \frac{3}{16\pi^3} \int \frac{\Gamma_{\Sigma}^r(\mathbf{k}) \Gamma_{\Sigma}^{r*}(\mathbf{k}) [\omega(\mathbf{k}) - \omega(\mathbf{k}_0)] d\mathbf{k}'}{\omega(\mathbf{k}') [m_{\Sigma} + \omega(\mathbf{k}') - m_{\Sigma}]^2 [m_{\Sigma} + \omega(\mathbf{k}) + \omega(\mathbf{k}') - m_N - \omega(\mathbf{k}_0)]} + \right. \\ &\left. + \frac{1}{16\pi^3} \int \frac{\Gamma_{\Lambda}^r(\mathbf{k}) \Gamma_{\Lambda}^{r*}(\mathbf{k}) [\omega(\mathbf{k}) - \omega(\mathbf{k}_0)] d\mathbf{k}'}{\omega(\mathbf{k}') [m_{\Lambda} + \omega(\mathbf{k}') - m_N]^2 [m_{\Lambda} + \omega(\mathbf{k}) + \omega(\mathbf{k}') - m_N - \omega(\mathbf{k}_0)]} , \right. \end{aligned}$$

$$K_Y(\mathbf{k}; \mathbf{k}') = \frac{1}{\sqrt{\omega(\mathbf{k}) \omega(\mathbf{k}') [m_Y + \omega(\mathbf{k}) + \omega(\mathbf{k}') - m_N - \omega(\mathbf{k}_0)]}} ,$$

with $E = m_N + \omega(\mathbf{k}_0)$ and $\omega(\mathbf{k}_0)$ = energy of incoming meson. In (13) and (14) the interaction constants have been substituted by the renormalized constants $G_{rY}^2 = G_Y^2 \cdot Z_2$ and $f_{rY}^2 = f_Y^2 \cdot Z_2$ where Z_2 is given by (11).

5. – Solution of equation (13) for the scalar case.

In the approximation used here the only wave which contributes to the scattering process for the scalar case is the s -wave. There are therefore only two phases to be considered, namely ($l = 0$, $T = 1$) and ($l = 0$, $T = 0$). Equation (13) for the scalar case may easily be separated into its components $T = 0$ and $T = 1$, which leads to:

$$(16) \quad [\omega(\mathbf{k}) - \omega(\mathbf{k}_0)]c_N^1(\mathbf{k})h^s(\omega) = \frac{1}{16\pi^3} \int c_N^1(\mathbf{k}') d\mathbf{k}' [G_{r\Sigma}^2 K_\Sigma(\mathbf{k}; \mathbf{k}') + G_{r\Lambda}^2 K_\Lambda(\mathbf{k}; \mathbf{k}')],$$

$$(17) \quad [\omega(\mathbf{k}) - \omega(\mathbf{k}_0)]c_N^0(\mathbf{k})h^s(\omega) = \frac{1}{16\pi^3} \int c_N^0(\mathbf{k}') d\mathbf{k}' [G_{r\Lambda}^2 K_\Lambda(\mathbf{k}; \mathbf{k}') - 3G_{r\Sigma}^2 K_\Sigma(\mathbf{k}; \mathbf{k}')],$$

where $h^s(\omega)$ is given by (14) with $I_Y^*(\mathbf{k}) \cdot I_Y^{**}(\mathbf{k}) = G_{Yr}^2$. Expressions (16) and (17) can easily be transformed into:

$$(16') \quad f_1^s(\mathbf{k}) = f_{B1}^s(\mathbf{k}) + \frac{1}{4\pi^2} \int \frac{k'^2 f_1^s(k') dk'}{[\omega(\mathbf{k}') - \omega(\mathbf{k}_0)]h^s(\omega')} [G_{r\Lambda}^2 K_\Lambda(\mathbf{k}; \mathbf{k}') + G_{r\Sigma}^2 K_\Sigma(\mathbf{k}; \mathbf{k}')],$$

$$(17') \quad f_0^s(\mathbf{k}) = f_{B0}^s(\mathbf{k}) + \frac{1}{4\pi^2} \int \frac{k'^2 f_0^s(\mathbf{k}') dk'}{[\omega(\mathbf{k}') - \omega(\mathbf{k}_0)]h^s(\omega')} [G_{r\Lambda}^2 K_\Lambda(\mathbf{k}; \mathbf{k}') - 3G_{r\Sigma}^2 K_\Sigma(\mathbf{k}; \mathbf{k}')],$$

where $f^s(K)$ is related to $c_N(K)$ by:

$$c_N(k) = \delta(\mathbf{k} - \mathbf{k}_0) + \frac{f^s(k)}{[\omega(k) - \omega(k_0)]h^s(\omega)},$$

with $f_B^s(K)$ given by:

$$(18) \quad f_{B1}^s(k) = \frac{G_{r\Sigma}^2}{4\pi^2} k_0 \omega_0 K_\Sigma(k_0; k) + \frac{G_{r\Lambda}^2}{4\pi^2} k_0 \omega_0 K_\Lambda(k_0; k),$$

$$(18') \quad f_{B0}^s(k) = \frac{G_{r\Lambda}^2}{4\pi^2} k_0 \omega_0 K_\Lambda(k_0; k) - \frac{3G_{r\Sigma}^2}{4\pi^2} k_0 \omega_0 K_\Sigma(k_0; k).$$

The solution of equations (16') and (17') by means of Fredholm's method leads to the following expressions for the scattering amplitude $T = 0$ and $T = 1$:

$$(19) \quad f_1^s(k) = f_{B1}^s(k) \frac{1 + \Delta_1^1(k) - \Delta^1}{1 - \Delta^1},$$

$$(20) \quad f_0^s(k) = f_{B0}^s(k) \cdot \frac{1 + \Delta_1^0(k) - \Delta^0}{1 - \Delta^0},$$

where

$$(21) \quad A_1^1(k) = \frac{k_0}{16\pi^4 f_{B1}^2(k)} \int_{m_k}^{\omega_k} \frac{\sqrt{\omega^2 - 1} d\omega}{(\omega - \omega_0) h^s(\omega)} \left[\frac{G_{r\Sigma}^2}{m_\Sigma - m_N + \omega} + \frac{G_{r\Lambda}^2}{m_\Lambda - m_N + \omega} \right]^2,$$

$$(21') \quad A_1^0(k) = \frac{k_0}{16\pi^4 f_{B0}^2(k)} \int_{m_k}^{\omega_k} \frac{\sqrt{\omega^2 - 1} d\omega}{(\omega - \omega_0) h^s(\omega)} \left[\frac{G_{r\Lambda}^2}{m_\Lambda - m_N + \omega} - \frac{3G_{r\Sigma}^2}{m_\Sigma - m_N + \omega} \right]^2,$$

$$(22) \quad A' = \frac{1}{4\pi^2} \int_{m_k}^{\omega_k} \frac{\sqrt{\omega^2 - 1} d\omega}{(\omega - \omega_0) h^s(\omega)} \left[\frac{G_{r\Lambda}^2}{m_\Lambda - m_N + 2\omega - \omega_0} + \frac{G_{r\Sigma}^2}{m_\Sigma - m_N + 2\omega - \omega_0} \right],$$

$$(22') \quad A^0 = \frac{1}{4\pi^2} \int_{m_k}^{\omega_k} \frac{\sqrt{\omega^2 - 1} d\omega}{(\omega - \omega_0) h^s(\omega)} \left[\frac{G_{r\Lambda}^2}{m_\Lambda - m_N + 2\omega - \omega_0} - \frac{3G_{r\Sigma}^2}{m_\Sigma - m_N + 2\omega - \omega_0} \right].$$

From (19) and (20) one obtains for the phase shifts:

$$(23) \quad \delta_1^s = \operatorname{tg}^{-1} [\pi f_1^s(k_0)],$$

$$(23') \quad \delta_0^s = \operatorname{tg}^{-1} [\pi f_0^s(k_0)].$$

6. – Solution of equation (13) for the pseudovector case.

In the pseudovector case, however, the only wave which contributes to scattering is the p -wave. The phases to be found are therefore four in number and precisely ($T=1, J=\frac{3}{2}$); ($T=1, J=\frac{1}{2}$); ($T=0, J=\frac{3}{2}$) and ($T=0, J=\frac{1}{2}$), which will be indicated respectively with δ_{13} , δ_{11} , δ_{03} , and δ_{01} .

By means of the usual methods one may resolve equation (13) into its four components and one obtains:

$$(24) \quad f_{1i}^{pv}(k) = f_{B1i}^{pv}(k) + \alpha \frac{1}{m_k^2} \int_{m_k}^{\omega_k} \frac{k'^4 f_{1i}^{ps}(k')}{(\omega' - \omega_0) h^{ps}(\omega')} [f_{r\Lambda}^2 K_\Lambda(k; k') + f_{r\Sigma}^2 K_\Sigma(k; k')],$$

$$(25) \quad f_{0i}^{pv}(k) = f_{B0i}^{pv}(k) + \alpha \frac{1}{m_k^2} \int_{m_k}^{\omega_k} \frac{k'^4 f_{0i}^{ps}(k')}{(\omega' - \omega_0) h^{ps}(\omega')} [f_{r\Lambda}^2 K_\Lambda(k; k') - 3f_{r\Sigma}^2 K_\Sigma(k; k')],$$

where

$$(26) \quad f_{B1i}^{pv} = \frac{\alpha}{m_k^2} k_0^3 \omega_0 [f_{r\Sigma}^2 K_\Sigma(k_0; k) + f_{r\Lambda}^2 K_\Lambda(k_0; k)],$$

$$(27) \quad f_{B0i}^{pv} = \frac{\alpha}{m_k^2} k_0^3 \omega_0 [f_{r\Lambda}^2 K_\Lambda(k_0; k) - 3f_{r\Sigma}^2 K_\Sigma(k_0; k)],$$

and $h^{ps}(\omega')$ is given by (14) with $\Gamma_{Y_0}^r(k)\Gamma_{Y_0}^{r*}(k) = k^2(f_{rY}^2/m_k^2)$; $\alpha = -1/3\pi$ for $i=1$ and $2/3\pi$ for $i=3$.

The solution of equations (24) and (25) may be obtained with the usual method of Friedholm, which gives:

$$(28) \quad f_{1i}^{pv} = f_{B1i}^{pv} \frac{1 + A_1^{1i} - A^{1i}}{1 - A^{1i}},$$

$$(29) \quad f_{0i}^{pv} = f_{B0i}^{pv} \frac{1 + A_1^{0i} - A^{0i}}{1 - A^{0i}},$$

with:

$$(30) \quad A_1^{1i} = \frac{\alpha^2 k_0^3}{m_k^4 f_{E1i}^{ps}(k)} \int_{m_k}^{\omega_k} \frac{(\omega^2 - 1)^{\frac{3}{2}} d\omega}{(\omega - \omega_0) h^{ps}(\omega)} \left[\frac{f_{r\Sigma}^2}{m_\Sigma - m_N + \omega} + \frac{f_{r\Lambda}^2}{m_\Lambda - m_N + \omega} \right]^2,$$

$$(30') \quad A_1^{0i} = \frac{\alpha^2 k_0^3}{m_k^4 f_{B0i}^{ps}(k)} \int_{m_k}^{\omega_k} \frac{(\omega^2 - 1)^{\frac{3}{2}} d\omega}{(\omega - \omega_0) h^{ps}(\omega)} \left[\frac{f_{r\Lambda}^2}{m_\Lambda - m_N + \omega} - \frac{3f_{r\Sigma}^2}{m_\Sigma - m_N + \omega} \right]^2,$$

$$(31) \quad A^{1i} = \frac{\alpha}{m_k^2} \int_{m_k}^{\omega_k} \frac{(\omega^2 - 1)^{\frac{3}{2}} d\omega}{(\omega - \omega_0) h^{ps}(\omega)} \left[\frac{f_{r\Lambda}^2}{m_\Lambda - m_N + 2\omega - \omega_0} + \frac{f_{r\Sigma}^2}{m_\Sigma - m_N + 2\omega - \omega_0} \right],$$

$$(31') \quad A^{0i} = \frac{\alpha}{m_k^2} \int_{m_k}^{\omega_k} \frac{(\omega^2 - 1)^{\frac{3}{2}} d\omega}{(\omega - \omega_0) h^{ps}(\omega)} \left[\frac{f_{r\Lambda}^2}{m_\Lambda - m_N + 2\omega - \omega_0} - \frac{3f_{r\Sigma}^2}{m_\Sigma - m_N + 2\omega - \omega_0} \right].$$

from (28) and (29) one obtains the phase shifts:

$$(32) \quad \delta_{1i}^{pv} = \operatorname{tg}^{-1} [\pi f_{1i}^{pv}],$$

$$(32') \quad \delta_{0i}^{pv} = \operatorname{tg}^{-1} [\pi f_{0i}^{pv}].$$

7. – Numerical results.

7.1. Scalar case. – In Fig. 1 and 2 are shown the behaviours of δ_1^s and δ_0^s given by (23) as functions of the energy of the K-meson up to 280 MeV.

For simplicity it has been assumed that $G_\Lambda^2/4\pi = G_\Sigma^2/4\pi = g^2$ and, in addition, the term $h^s(\omega)$ (*), which takes into account the radiative correction,

(*) The term $1+h^s(\omega)$ turns out to be small and in practice may be ignored for small values of g^2 . For the case in which g^2 has been taken equal to one, a point has been calculated taking account of $1+h^s(\omega)$ at 120 MeV. This point is indicated in Fig. 1.

has been put equal to one. The curves refer to various values of the coupling constant g^2 and to two values of the cut-off momentum ($K = 3m_K$ and $4m_K$).

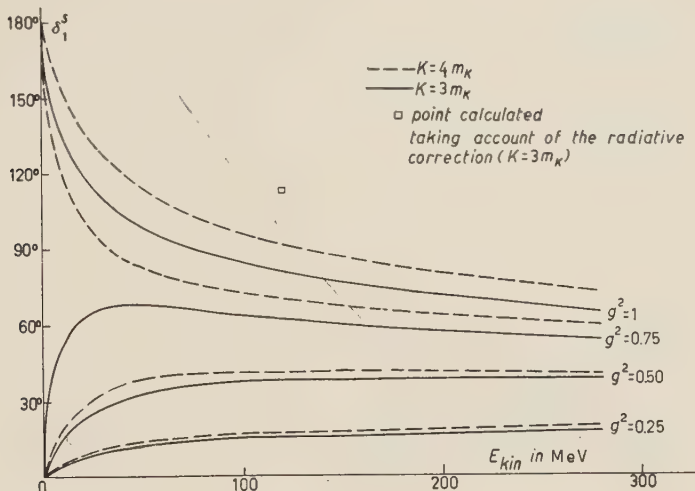


Fig. 1.

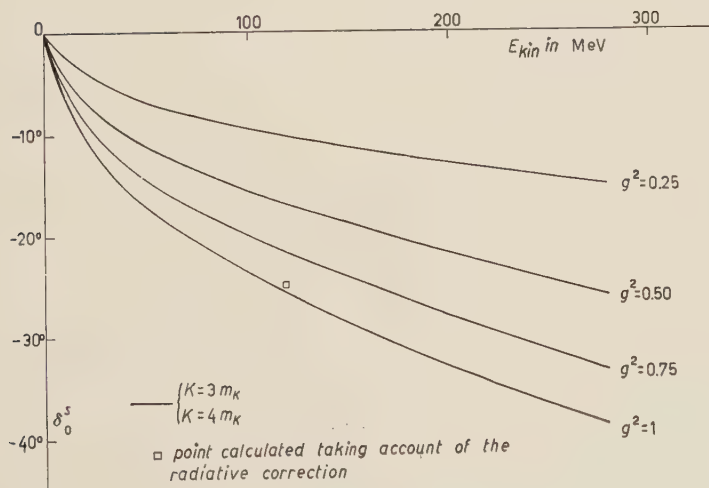


Fig. 2.

In Fig. 3 the shape of the total cross-section for the collision K^+ -proton is given as a function of g^2 for an incoming meson energy of 80 MeV. Supposing that at this energy the cross-section is ~ 10 mb, as appears from present experimental results, it follows that the corresponding value of the

coupling constant is $g^2 = 0.3$. Finally Fig. 4 gives the shape of the cross-section for K^+ -proton collision as a function of the kinetic energy of the K-meson.

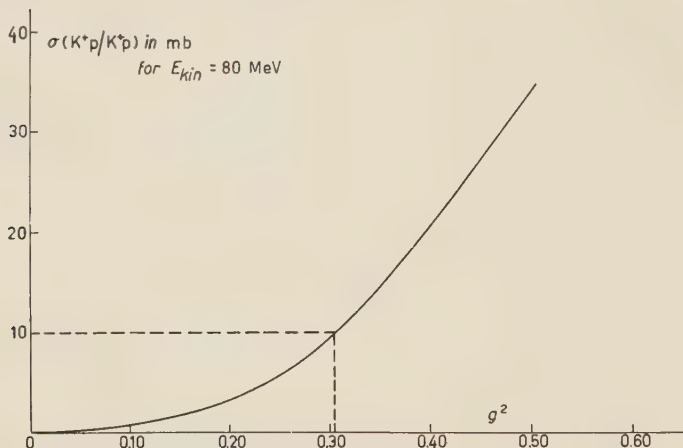


Fig. 3.

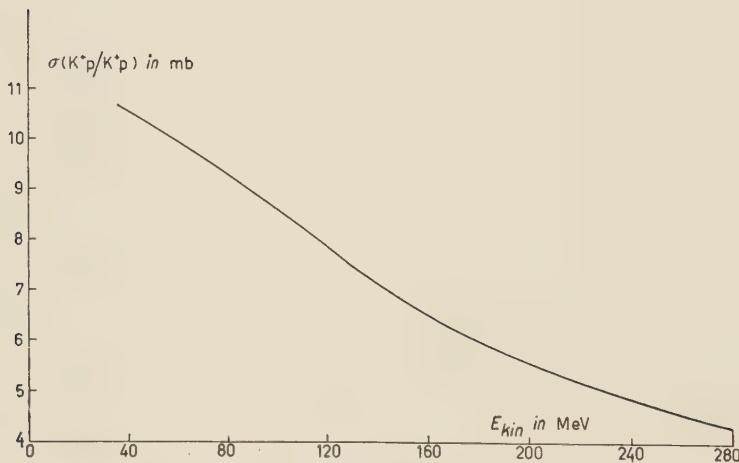


Fig. 4.

The conclusions which one may draw in this case are the following:

- a) The phase δ_1^s is positive (attractive potential) but does not lead to a resonant state. The phase δ_0^s instead, is repulsive and is smaller than δ_1^s in absolute value.
- b) The values of the phases are only little sensitive to the momentum cut-off in the integrals (21) and (22).

c) The phases, instead, are very sensitive to variations of the coupling constant. To an increase of this constant corresponds an increase in the value

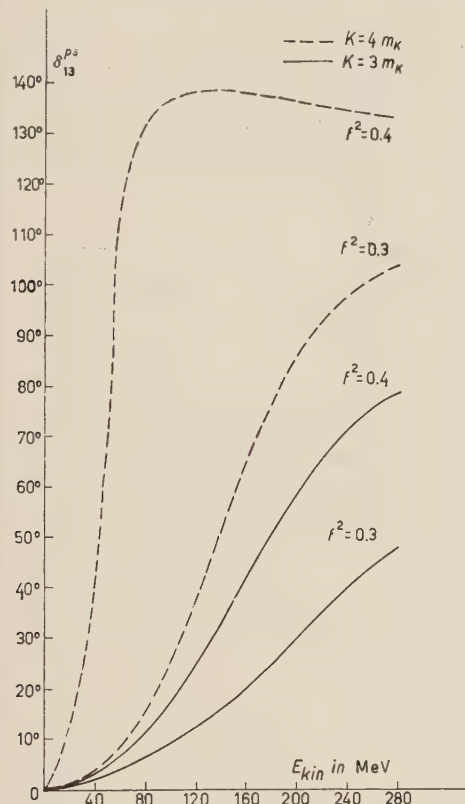


Fig. 5.

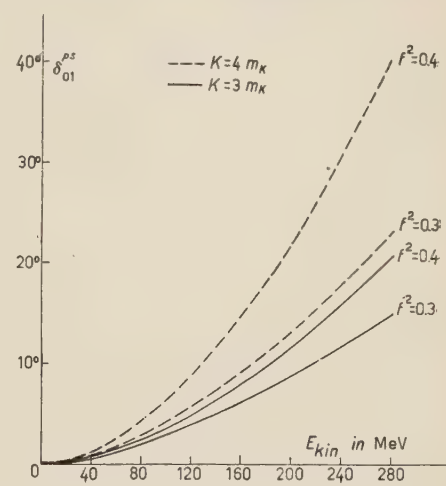


Fig. 6.

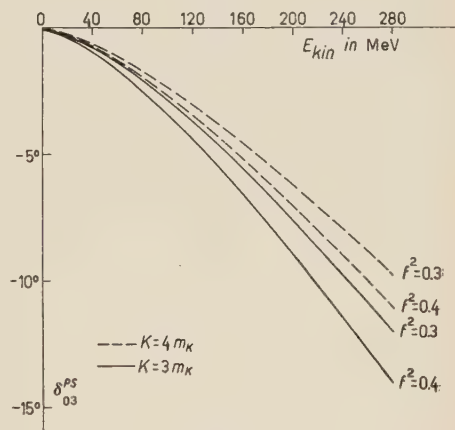


Fig. 7.

of the phase δ_1^s (for a fixed energy of the incident particle) and therefore the potential becomes more attractive. For values of g^2 greater than a certain value such that A^1 becomes equal to 1, the phase starts at 180° for zero energy, which corresponds to the formation of a bound state.

7.2. Pseudoscalar case. — In Fig. 5, 6, 7 and 8 are given the shapes of the phases δ_{13}^{ps} , δ_{01}^{ps} , δ_{03}^{ps} and δ_{11}^{ps} for various values of the coupling constant $f_\Sigma^2 = f_\Lambda^2 = f^2$ and of cut-off momentum K . Also in this case $h^{pv}(\omega)$ has been put equal to 1.

The conclusions which may be drawn are the following:

a) The δ_{13}^{ps} and δ_{01}^{ps} phases are positive (attractive potential) and lead to a resonance; moreover $\delta_{13}^{ps} > \delta_{01}^{ps}$.

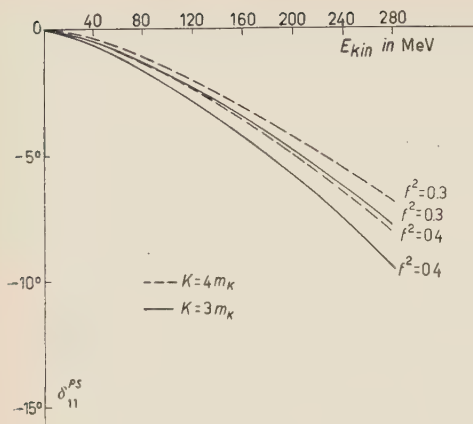


Fig. 8.

phases so far available, it is not yet possible to draw any definite conclusion about the validity of this theory and only a purely qualitative discussion of the results of this paper is possible. In fact, both the scalar and pseudovector coupling provide a large attractive potential for the $T=1$ state and a small repulsive potential for the $T=0$ state. That the $T=1$ state is the most important in the K^+ -proton scattering has been shown by various authors (⁷): the S wave with repulsive potential seems to predominate at least up to the energies which have been investigated.

If this evidence would be confirmed in the future, the interactions we have used should be considered inadequate to fit the experimental data and one might think that the K^+ -N-Y coupling is pseudoscalar. In fact the matrix element for the scattering of the K^+ mesons on protons in the hypothesis of pseudoscalar coupling and zero energy (S wave only) is, in the Born approximation,

$$M(T=1) = \frac{2\pi}{m_K} \left(\frac{g_\Lambda^2}{m_N - m_K + m_\Lambda} + \frac{g_\Sigma^2}{m_N - m_K + m_\Sigma} \right)$$

this is consistent with a repulsive potential in agreement with the experimental results.

(⁷) J. LANNUTTI, W. CHUPP, G. GOLDHABER, E. HELMY, E. ILOFF, A. PEVSNER and D. RITSON: *Phys. Rev.*, **101**, 1617 (1956); Communications of S. GOLDHABER and N. DALLAPORTA (results for several European Laboratories), *Proceedings of the Sixth Rochester Conference* (1956); Communications of the plate groups of Bologna, Bristol, Dublin and Padua laboratories, *Turin Conference*, September 1956; M. BALDO-CEOLIN, M. GRILLI, L. GUERRIERO, M. CRESTI, N. DALLAPORTA, M. MERLIN and G. ZAGO: *Nuovo Cimento*, **5**, 402 (1957).

The phases δ_{03}^{PV} and δ_{11}^{PV} are negative and further $|\delta_{03}^{PV}| > |\delta_{11}^{PV}|$.

b) The values of the single phases, and therefore the position in which the resonance should be situated, depend strongly on the momentum cut-off and on the coupling constant.

8. – Conclusions and comparison with experiment.

In view of the few experimental indications on the behaviour of the

Calculations on the cross-sections for the scattering of K^+ mesons on nucleons in the hypothesis of pseudoscalar coupling are in progress.

* * *

We are greateful to Prof. DALLAPORTA and Prof. CLEMENTEL for useful discussions.

RIASSUNTO

È stato trattato il problema dello scattering K -nucleone col metodo di Tamm-Dankoff in approssimazione di due mesoni, sia in accoppiamento scalare che in accoppiamento pseudoscalare in approssimazione non relativistica. Nei due casi risulta che la fase più importante a bassa energia è la $T=1$ la quale corrisponde ad un potenziale attrattivo. Mentre nel caso scalare tale fase non conduce a risonanza, nel caso pseudoscalare si ha uno stato risonante la posizione del quale dipende fortemente dal taglio nello spazio dei momenti K . Alla fine viene effettuata una breve discussione dei risultati ottenuti in relazione ai pochi risultati sperimentalni sino ad ora disponibili.

**The Interactions of Positive K-Mesons with Nuclei
in Photographic Emulsion at Energies in the Region 0÷130 MeV.**

B. BHOWMIK (*), D. EVANS, S. NILSSON (+) and D. J. PROWSE

H. H. Wills Physical Laboratory - Bristol

F. ANDERSON, D. KEEFE, A. KERNAN and J. LOSTY

University College - Dublin

(ricevuto il 12 Aprile 1957)

Summary. — 148 m of K^+ track have been followed in an unbiased way and 109 inelastic interactions with emulsion nuclei found. In addition 3 K^+ -proton scattering events have been found and numerous cases of elastic scattering from emulsion nuclei. The differential cross-section for the elastic scattering has been plotted for three energy intervals and the results compared with those predicted by the optical model for various nuclear well depths. The variation of cross-section with energy for the inelastic events is found to be consistent with isotropy if the Pauli Exclusion Principle is taken into account and the best fit for the experimental points is obtained for a repulsive potential well of 20 MeV. The inelastic events have been analysed on the basis of the statistical model of the nucleus and an attempt has also been made to obtain from the experimental data the angular distribution in the C.M. system of the K -nucleon cross-section. On any reasonable assumption this appears to be peaked backwards. These data also demand a repulsive potential of ~ 20 MeV. The value of the average K -nucleon cross-section within nuclear matter for meson energies between 40 and 120 MeV is 4 mb/nucleon; allowing for the events forbidden by the exclusion principle this implies a cross-section of 6 mb on a free nucleon. Taking $\sigma_p = (14 \pm 3)$ mb, it follows that $\sigma_p = (2 \pm 2)$ mb. The ratio of charge exchange events to non-charge exchange events is $.20 \pm .07$ — the value expected in the limit of a vanishingly small interaction in the $T = 0$ state.

(*) On leave from the University of Delhi.

(+) On leave from the University of Uppsala.

1. – Introduction.

The first observations that positive heavy mesons are effective in producing nuclear interactions and need not be annihilated in the process, were made in stacks of stripped photographic emulsion exposed to the cosmic radiation (^{1,2}). In tracing back the tracks of positive K-mesons observed to decay at rest, it was occasionally found that the heavy meson had suffered an inelastic collision with a nucleus of the emulsion between its creation and its decay. From the relative frequency of such occurrences, and what was known at the time about the production characteristics of K-particles (³), it was possible to estimate that the cross-section for the nuclear interaction of a positive heavy meson (followed by its emergence) was within an order of magnitude of the geometric value. This was in agreement with the observations on the tracks of heavy mesons followed out in an unbiassed way from their parent stars (³).

The availability of a focussed K⁺-beam at the Bevatron made a direct approach to the problem possible, by the exposure of stacks of emulsion to large numbers of mesons of known energy, and the scanning along their tracks for evidence of nuclear interactions, whether or not the K-particle emerged and decayed. In the first systematic experiment of this type (⁴) 38.5 m of K-meson track length were followed in emulsion for meson energies between 30 MeV and 120 MeV, yielding 33 elastic scatters, 25 inelastic scatters, 2 events interpreted as elastic scatters from hydrogen and 4 events in which the K-meson probably suffered charge exchange. In addition 18 decays in flight were observed. The mean free paths found for nuclear interactions and K-hydrogen collisions were 95 cm and 19 m respectively, compared with ~30 cm and 6 m for a particle interacting with a geometric cross-section. No event was found in which a hyperon was produced or in which the energy release was greater than the kinetic energy of the incoming meson, results which supported the law of conservation of strangeness demanded by many schemes for the classification of the unstable particles (^{5,6}). The statistics

(¹) R. R. DANIEL and D. LAL: *Proc. Ind. Acad. Sci.*, A **41**, 15 (1955).

(²) M. W. FRIEDLANDER, D. KEEFE and M. G. K. MENON: *Nuovo Cimento*, **1**, 694 (1955).

(³) C. DAHANAYAKE, P. E. FRANCOIS, Y. FUJIMOTO, P. IREDALE, C. J. WADDINGTON and M. YASIN: *Nuovo Cimento*, **1**, 889 (1955); P. H. FOWLER and D. H. PERKINS: *Pisa Conference* (mimeographed report), June 1955 and private communication.

(⁴) J. E. LANNUTTI, W. W. CHUPP, G. GOLDHABER, S. GOLDHABER, E. HELMY, E. L. ILOFF, A. PEVSNER and D. M. RITSON: *Phys. Rev.*, **101**, 1617 (1956).

(⁵) M. GELL-MANN and A. PAIS: *Proc. Int. Conf. Nuc. Phys.* (Glasgow, 1954); (Pergamon Press, 1955), p. 342.

(⁶) K. NISHIJIMA: *Progr. Theor. Phys.*, **13**, 285 (1955).

were insufficient to give any indication of an energy dependence of the cross-section and the scattering cross-section appeared to show isotropy above 40° .

The present experiment was designed to extend these earlier observations and, on the basis of larger statistics, to determine the behaviour of the interaction cross-section as a function of energy, to provide a qualitative description of the types of nuclear interactions involving K-mesons, and to obtain information about the K-nucleon interaction. Since the results of LANNUTTI *et al.* (4) showed the cross-section for K-hydrogen collisions to be small, it would seem plausible to obtain information on the K-meson nucleon interaction by analysing the nuclear interactions in terms of the collision of the meson within the nucleus with a single nucleon. Furthermore, given sufficient statistics on the K-hydrogen interaction, this analysis will then yield information on the K-neutron interaction and the validity of various nuclear models.

The present communication comprises results based on the combined measurements made at Bristol and Dublin. Preliminary reports of this work have been presented with those on the same topic from other laboratories, at the Rochester Conference (1956) and the Turin Conference (1956).

2. – Experimental details.

2.1. Exposure conditions. – A stack of stripped photographic emulsions, known as stack K₂, later divided among a number of European laboratories for the purpose of studying the properties of K⁺-particles, was exposed to the magnetically analysed positive heavy meson beam at the Bevatron, by courtesy of the members of the Berkeley group. Stack K₂ consisted of 300 plates 8 in. \times 10 in. \times 600 μm , and was exposed to the beam of positive particles produced in a copper target by the 6.2 GeV proton beam. The K-meson beam was at 90° with respect to the proton beam and the time of flight between the target and the stack was about $1.3 \cdot 10^{-8}$ s. The Bristol portion of the stack consisted of 100 plates which the K-particles entered with momenta between 379 and 425 MeV/c and the Dublin section comprised 50 plates exposed to particles of momenta between 402 and 425 MeV/c. The exposure density in this momentum region was ~ 300 K-particles per cm^2 . In addition to the heavy mesons, there was a much larger flux of π -mesons and protons of the same momentum; the K-meson tracks were easily distinguished from this large unwanted background since the protons were heavily ionizing, stopping after traversing about 3 cm of emulsion, and the π -mesons traversed the stack with an ionization corresponding to $g^* \sim 1$, whereas the K-mesons had a range of about 10 cm, corresponding to $g^* \sim 2$ just beyond the ends of the tracks produced by the proton beam.

2·2. Scanning procedure. — On all plates a line scan was made at right angles to the beam direction, about 3-5 mm away from the ends of the proton tracks. A track was selected for following if it lay within $\pm 5^\circ$ of the beam direction in either the vertical or the horizontal plane and if the grain density was within $\pm 15\%$ of the value expected for a K-meson track in that position in the stack. The decision whether to follow or not is thus based on inspection of only about 0.6 mm of the track and so does not introduce any bias into the selection of the events. About 90% of the tracks selected according to these criteria were due to K-mesons, the remainder being largely caused by protons of similar velocity. In slightly more than three-quarters of the cases, once a track had been selected for following, its identification was demanded whether or not it suffered a nuclear collision or left the stack. The nature of every track was determined by careful ionization measurements at a known range and in effect the mass spectrum of the particles investigated was obtained. In the later stages of the experiment, the results on the composition of a sample of tracks obeying the criteria were utilised and only the early portions of the track—corresponding to $E_K \gtrsim 60$ MeV—were followed, the relative proportion of K-meson and proton tracks scanned being estimated rather than directly measured.

A serious defect of the K_2 stack was the low value of the ionization minimum (7 grains per 50 μm) which made it difficult to see in all cases the secondary track associated with the end of a K-particle at rest. A meson which showed no evidence of a decay product at its end was labelled « K_0 » and the fraction of all K-particles so-called depended on the local development of the emulsion where they were brought to rest, and on the length of time spent in scrutinizing the ends of their tracks. The average proportion of K_0 tracks in this experiment was close to 20%, hence necessitating the mass analysis described above. Further details of the K_0 problem are treated in Appendix 1.

2·3. Classification of events. — Since the object of the experiment was to investigate the properties of both the elastic and inelastic interactions with nuclei, the following method of classifying events found during the track scanning was adopted with the idea of effecting a rough separation into the different physical categories. The events were later analysed as described in Sect. 2·4 to improve the separation of the elastic from the inelastic events. In every case, unless there was clear evidence of the emergence and decay of a heavy unstable particle, the primary particle of an interaction was identified and its energy at the collision deduced by the ionization-scattering method. Because of their higher cross-section for interaction the proton contamination in the interacting beam was about twice that in the tracks followed to rest.

(a) **Inelastic events.** — An event was recognized with certainty as being inelastic from the evidence of nuclear excitation leading to evaporation

prongs. In addition a special record was made of the events (70 in number) where a track was seen to stop in the emulsion whilst it was clear from the ionization that the particle had not come to rest. Most of these events (46) were at once recognized as being due to decays in flight by the presence of the lightly ionized associated track of the secondary product; the remainder were due either to charge exchange events or to decays in flight in which the poor development of the stack made the light track invisible. Of the 24 so-called stops 9 were reckoned to be due to charge exchange events in which no charged prongs were emitted. Details of the analysis of the stops have been fully set out elsewhere (7).

(b) Elastic events. — Any sharp scatters in a track being followed were recorded provisionally as elastic scatters if the following conditions were satisfied:

(i) The heavy meson had an expected residual range at the scatter of more than 1 cm corresponding to an energy of 40 MeV.

(ii) The projected angle deflection was $\geq 5^\circ$, irrespective of the dip. The Dublin group recorded, in addition, any scatter in which an observer judged there was an appreciable change in the dip angle, although the deflection in the emulsion plane was less than 5° . (The recording of such angles is subjective and biased for space angles $\leq 10^\circ$). They measured space angles of scatter for all events, while the Bristol group made projected angle measurements on all scatters and space angle measurements on only those angles $\geq 15^\circ$ in projected angle.

(iii) There was no sign of nuclear excitation in the form of evaporation prongs. Occasionally, the collision of a K-meson with a nucleus of C, N or O in which the angle of scatter was large, resulted in a nuclear recoil a few microns long. Such a recoil prong is easily recognized since it must be in the right direction and of the right range to conserve momentum (*).

(7) B. BHOWMIK, D. EVANS, S. NILSSON, D. J. PROWSE, F. ANDERSON, D. KEEFE, A. KERNAN, M. CECCARELLI, N. VARSHNEYA, P. WALOSCHEK, J. HOOPER, M. GRILLI and L. GUERRIERO: *Nuovo Cimento*, in press (1957).

(*) A diagram of prong length against angle of deflection of the K-meson has been plotted for these events and two correlation lines observed, corresponding to scattering off the light (C, N, O) and heavy nuclei (Ag, Br) respectively. A very small number of events had recoil prongs which were too long to have been due to the recoil of a light nucleus and were not coplanar with the K-meson tracks. It is possible that these were due to small angle scattering of bound protons. The large uncertainties in the measurements on the short recoils, however, and the impossibility of determining the low energy transfers involved, have precluded the direct inclusion of these events in the inelastic cross-section.

This category consists largely of events in which the K^+ -particle is elastically scattered in the nuclear and Coulomb field of a nucleus of an emulsion element other than hydrogen. Although « Elasticity » implies the conservation of energy in the centre of mass system, such events will also be nearly elastic in the laboratory system due to the high target to projectile mass ratio.

For an event to be included in the statistics, it was not demanded that the K-particle should stop within the stack, since this condition could introduce a bias against events of large scattering angles.

2.4. Analysis of events. — In the case of those inelastic events where the collision with the target nucleus was such as to result in the ejection of charged particles, both evaporation and knock-on, each of the black prongs was traced to rest and its range and direction of emission recorded. In addition some judgement was made on its nature—whether it had the appearance of a proton or α -particle track, etc, but because of the shortness of most of the prongs this information is highly subjective. In general, it was clear whether the K-particle emerged from the interaction, although in one case classified as a charge exchange interaction it is possible that a prong 800 μm long could have been due to the emergent K-particle since it ended very close to the glass boundary of the emulsion and evidence of decay might not have been noticed. (From the statistics of the other stars examined, this event is very probably correctly identified, since no K-particle has been seen to emerge from an interaction with a range less than 1.5 mm).

The so-called elastic scattering events which had any one of the following characteristics were examined for inelasticity:

- (i) The presence of an electron or a blob at the apex of the scatter;
- (ii) A total range shorter by more than one standard deviation (6 mm) than the average. This corresponds to an energy loss of about $7 \div 9$ MeV;
- (iii) An angle of scattering greater than 40° ;
- (iv) The escape before coming to rest of the emergent heavy meson from the part of the stack used.

Of the « elastic » events recorded, 107 obeyed at least one of these conditions and the energy loss or inelasticity was calculated for each. The energy of the K-particle before the scattering, was deduced in two independent ways: firstly by observing the co-ordinates of the event with respect to the entry point of the K-particles into the stack where their momentum is known; and secondly by direct measurement of the ionization of the track with a statistical precision of, at worst, 4%, the effect of the fluctuations between plates being eliminated by normalizing every plate by blob-counting the π -meson

tracks in the beam. The two results were in every case combined to give a weighted mean; since the first method is of increasing and the second of decreasing precision as the K-meson energy becomes greater, the error (*not* the percentage error) on the weighted mean energy remains remarkably constant (~ 5 MeV) over the whole range. In the great majority of cases the energy of the K-meson emerging from the collision could be found by direct measurement of its range, and in the remainder (e.g. where the particle left the stack or suffered a second scattering) further measurements of ionization had to be

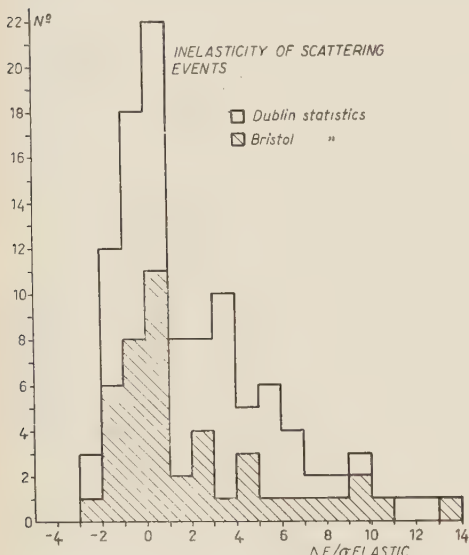
made. Thus the greater part of the error on the inelasticity, ΔE , arose from the estimation of the energy of the primary K-particle.

Fig. 1 shows a histogram of the quantity, $\Delta E/\sigma$, where $\Delta E \pm \sigma$ is the inelasticity of an individual event and σ is very close to 5 MeV. Had all the events examined been genuine elastic scatters then the histogram would have been symmetrical about a value very close to zero (corresponding to the energy gained by the recoil nucleus, ~ 0.2 MeV for Ag, Br, ~ 3 MeV for C, N, O). There is a very marked tail towards high values of inelasticity, however, which is extremely unlikely to have arisen by chance. It is clear that the greater proportion of the events with positive values of $\Delta E/\sigma$ occur at small values of the abscissa and are in fact elastic events in which statistical fluctuations have played a

Fig. 1. — $\Delta E/\sigma$ distribution for 0-prong scattering events satisfying the conditions given in Sect. 2.4. The distribution of inelastic events seems unambiguous for $\Delta E/\sigma \geq 3$. It is expected that 5 genuinely inelastic events lie in the interval $3 \geq \Delta E/\sigma \geq 2$.

part. The portion of the distribution corresponding to negative values of $\Delta E/\sigma$ is almost entirely due to similar fluctuations in an opposite sense, and so may be used as a guide to the true shape of the sampling distribution of the values of $\Delta E/\sigma$ arising from measurements on truly elastic events.

This distribution appears to be somewhat less peaked than a normal law. It will be seen that only 3 events have $-2 \geq \Delta E/\sigma \geq -3$ and none has $-3 \geq \Delta E/\sigma$; accordingly, all events with $\Delta E/\sigma \geq 3$ have been redefined as inelastic and of the 8 lying in $3 \geq \Delta E/\sigma \geq 2$, 5 have been called inelastic. Because one has no guide as to which 5 to choose, all 8 events were included in the individual analysis of events described in Sect. 5, in case their omission



should lead to bias. In the evaluation of the inelastic cross-section the 3 presumed elastic events have been omitted.

Of 13 events which appeared to have a low energy electron associated with the apex of the scatter, 3 were clearly inelastic, but for the remaining 10, the $\Delta E/\sigma$ distribution was symmetrical about zero. Some of the latter events might have been due to low energy excitation of the nucleus followed by β -decay, in which case the inelastic cross-section will have been underestimated. This small number of events, nevertheless, can all be explained by the chance association with the apex of the scatter, of a δ -ray occurring less than $2 \mu\text{m}$ away and cannot be taken as sufficient evidence that nuclear excitation has occurred. It is important to note, however, that events could not be detected by the above procedure in which there were small transfers of energy to the nucleus leading to the excitation of the nuclear energy levels. If such processes occurred frequently (cf. Sect. 3) the inelastic cross-section will be underestimated and the elastic cross-section correspondingly over-estimated. Subsequent results and discussions should be considered as subject to these reservations.

In the treatment of events defined as elastic by the above procedure, slightly different methods of analysis were used by the Dublin and Bristol groups because of their different methods of recording events. In the case of the Bristol sample, where a rigorous cut-off was imposed on the projected angle of scatter recorded, a geometric correction factor was used to allow for scatters taking place with planes steeply inclined to that of the emulsion. The experimental technique is simplified by this convention, with a loss of information at small angles since the geometric factors become large and the precision poor for space angles close to the chosen projected angle cut-off. In the sample recorded and analysed in Dublin an attempt has been made to ensure the recording of all events with space angles $\geq 12^\circ$. The subjective bias, if it existed should depend on the angle φ between the plane of the scatter and the plane of the emulsion, being absent for $\varphi = 0$ and a maximum for $\varphi = 90^\circ$. An analysis of the events for different intervals of φ showed no significant variation for space angles over 12° . Accordingly the two samples were combined and are believed to be unbiassed for space angles of $\geq 15^\circ$.

3. – Results and discussion on K-nucleus interactions.

3.1. General considerations. – In all, 148 m of heavy meson track have been scanned in an unbiassed way and a total of 109 inelastic nuclear events, (of which 2 were caused by mesons of < 40 MeV), 3 K-H scatters and over 1000 elastic scattering events were observed. (In the course of scanning, some 15 m of proton track were incidentally followed and 46 proton-induced stars

noted, in satisfactory agreement with the expected mean free path for star production by protons of these energies.) Details of the stars produced by

the K-particles are given in Table I together with the meson energies before and after the interaction and the mode of decay of the meson when this could be ascertained. The path length followed in metres is shown in Fig. 2.

No event has been observed in which a hyperon, a π -meson, a K^- -meson or a μ -meson was produced or in which the K-particle suffered annihilation giving rise to an exothermic reaction. No star was found to have an associated track at minimum ionization, an event which might

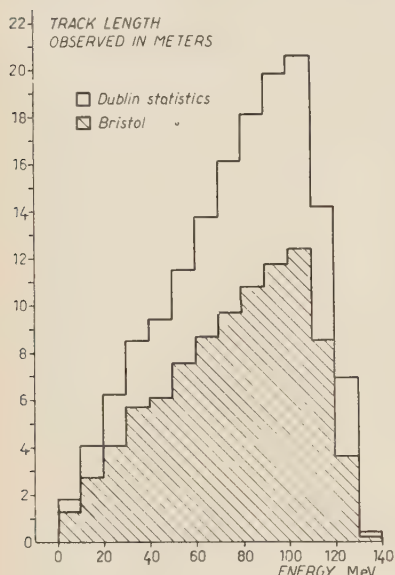


Fig. 2. — Distributions in K-meson path length followed as a function of the K-meson energy.

TABLE I. — Inelastic events.

Event No.	Primary Energy E_1 (MeV)	Emergent Energy E_2 (MeV)	K-angle of scatter θ^0	K-energy loss ΔE (MeV)	Decay Mode	Ranges of other prongs and remarks
1	127	97	55	30	K_L	Inelastic scatter
2	126	59	83	67	K_L	2.28 mm
3	125	25	41	100	K_L	Inelastic scatter
4	123	32	68	91	K_L	138 μm
5	120	103	5	17	K_L	806 μm , 3 μm
6	118	45	148	73	τ	248 μm , 1.0 μm
7	115	85	60	30	K_L	Inelastic scatter
8	115	59	50	56	K_0	Inelastic scatter
9	113	68	147	45	K_L	Recoil
10	112	73	89	39	K_L	3.05 mm
11	110	57	131	53	K_0	45 μm , 1.0 μm
12	109	49	80	60	K_L	5.0 μm
13	109	59	86	50	τ'	1 grain recoil
14	109	50	61	59	K_0	1.7 mm
15	108	37	119	71	K_L	Inelastic scatter
16	108	92	25	16	K_0	Inelastic scatter
17	108	81	47	27	—	Inelastic scatter
18	107					319 μm , 306 μm , blob charge exchange

TABLE I (continued).

Event No.	Primary Energy E_1 (MeV)	Emergent Energy E_2 MeV)	K-angle of scatter θ^0	K-energy loss ΔE (MeV)	Decay Mode	Ranges of other prongs and remarks
19	106	79	65	27	K_L	Inelastic scatter
20	106	59	46	47	K_L	Inelastic scatter
21	106	74	77	32	K_L	3 μm
22	106	54	70	52	K_L	1 grain recoil
23	106		charge exchange			758 μm , 1.0 μm
24	105	42	110	63	K_L	750 μm , 11.0 μm
25	104	46	85	58	K_L	3.9 mm
26	104	47	44	57	K_0	Inelastic scatter
27	104	83	27	21	K_L	Inelastic scatter
28	103	79	19	24	K_L	Inelastic scatter
29	102	64	106	38	K_0	Inelastic scatter
30	102	82	45	20	K_L	1 grain recoil
31	102	79	96	23	K_L	recoil
32	101	49	20	52	K_1	1.52 mm
33	100	52	107	48	K_0	Inelastic scatter
34	100	50	119	50	K_L	1.91 mm
35	100	66	69	34	τ	Inelastic scatter
36	100		charge exchange			867 μm , blob, β
37	98	68	127	30	K_L	recoil
38	97	79	41	18	K_0	3.5 μm
39	97	78	132	19	K_L	2 μm
40	97	72	150	25	K_L	Inelastic scatter
41	96	50	134	46	K_L	24 μm , 11.1 μm , 8.55 μm
42	96	61	17	35	K_L	930 μm
43	96	39	154	57	K_L	1.0 mm, 1.5 μm
44	95	61	134	34	K_L	120 μm , 13 μm
45	95	46	172	49	K_L	1 μm
46	94	48	68	46	K_L	250 μm
47	93	58	78	35	K_L	61 μm , 29.5 μm , 6.5 μm
48	93		charge exchange			284 μm , 133 μm
49	92	42	126	50	K_L	3.1 mm
50	92	75	14	17	K_L	Inelastic scatter
51	92	55	100	37	K_0	Inelastic scatter
52	90	14	72	76	K_0	14.8 mm, K bound P
53	90	41	85	49	K_L	32 μm , 3.5 μm , 3 μm
54	89	60	138	29	K_L	Inelastic scatter
55	89	45	63	44	K_L	3 μm recoil
56	89		charge exchange			9.7 mm, 0.5 mm, 0.5 mm
57	88	42	154	46	K_0	Inelastic scatter
58	88	51	47	37	K_L	4.93 mm, 22.2 μm
59	88	70	13	18	K_L	Recoil
60	87	51	111	36	K_0	5.0 mm
61	87	35	53	52	K_L	190 μm , β
62	86	54	26	32	K_L	Inelastic scatter

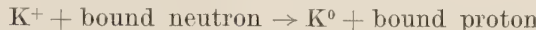
TABLE I (*continued*).

Event No.	Primary Energy E_1 (MeV)	Emergent Energy E_2 (MeV)	K-angle of scatter θ^0	K-energy loss ΔE (MeV)	Decay Mode	Ranges of other prongs and remarks
63	86	30	141	56	K_L	2 μm
64	85	63	93	22	—	$^{12}C(K^+, K^+)$ 3 4He
65	84	24	60	60	K_L	7.79 mm, 7 μm
66	83	63	91	20	—	30 μm , 33 μm
67	83	35	120	48	K_L	1.07 mm
68	82	70	155	12	K_0	Inelastic scatter
69	82	37	125	45	—	Recoil
70	80	60	73	20	K_L	5.0 μm
71	80	70	30	10	K_L	Inelastic scatter
72	80		charge exchange			7.94 mm, 71.8 μm , 6.5 μm , 2.2 μm
73	78	50	126	28	K_L	2.0 μm
74	77	66	40	11	K_L	Recoil
75	76	66	116	10	—	Inelastic scatter
76	76	31	131	35	K_L	Inelastic scatter
77	76	61	81	15	—	20 μm , 12 μm
78	75	50	137	25	K_0	9.0 μm
79	75	48	46	27	K_0	12 μm , 11 μm
80	74	25	96	49	K_0	180 μm
81	74	45	134	29	K_L	Inelastic scatter
82	74	54	62	20	K_L	Inelastic scatter
83	74		charge exchange			600 μm
84	72	45	70	27	K_L	35.4 μm , 4.0 μm
85	70	53	110	17	K_0	Recoil
86	69	34	136	35	K_L	2.1 μm
87	68	43	117	25	K_0	Inelastic scatter
88	66	58	12	8	K_L	38.6 μm
89	66		charge exchange			336 μm , 4.44 mm
90	65	32	140	33	K_0	Inelastic scatter
91	62	48	121	14	K_L	112 μm
92	59	40	152	19	τ	10 μm
93	59	44	31	14	τ	Inelastic scatter
94	57	43	129	14	K_L	Recoil
95	56	32	113	24	K_0	Inelastic scatter
96	55	41	46	15	K_L	Inelastic scatter
97	54	30	135	24	K_L	1 grain recoil
98	49	34	103	15	K_0	170 μm , 0.5 μm
99	43	28	148	15	K_L	603 μm , recoil
100	41	28	28	13	K_0	Inelastic scatter
101	41		charge exchange			110 μm
102	30	15	42	15	K_L	Recoil
103	29	15	103	14	τ	9 μm , 38 μm

In addition nine 0-prong charge-exchange events (see text).

be expected to arise if the outgoing K-particle underwent accelerated decay in the field of the nucleus or had a very short lifetime. The few events where the charged heavy meson did not emerge were all consistent with their being charge-exchange scatterings from a neutron in the emulsion nuclei.

Of the 24 «stops» observed (see Sect. 2.3) 9 were assumed to be due to charge-exchange reactions of the type:



leading to 0-prong stars. This number was estimated in two independent ways described in (7): firstly by reckoning the number of decays in flight included among the «stops» on the basis of the known efficiency of observation of the associated light tracks of the secondary particles; and secondly, from the proportion of 0-prong stars among the non-charge-exchange reactions. Both methods agree well in their answers, but unfortunately are only of

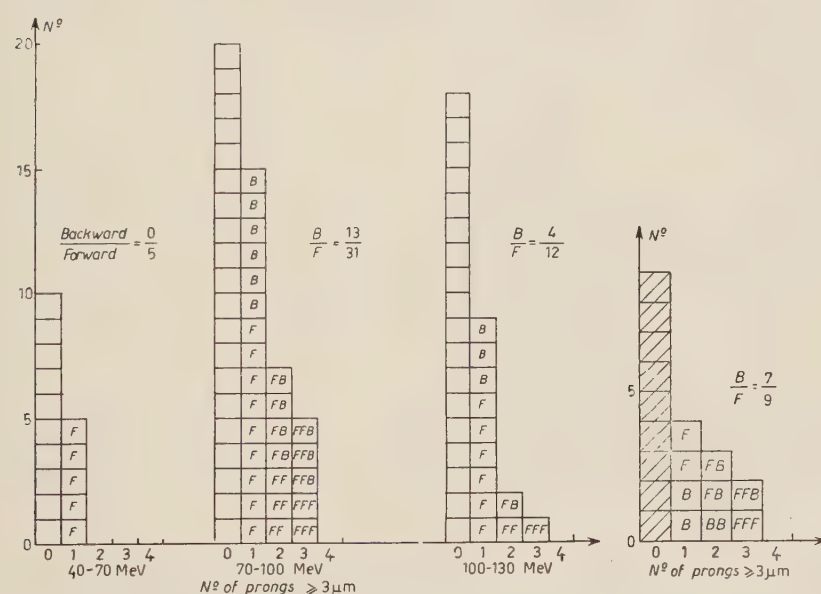


Fig. 3. – (a) The distribution of the number of nuclear fragments observed for events with different primary K-meson energies. In all cases the K-meson emerged from the star. (b) The prong number distribution for charge exchange events occurring at all energies. The number of 0-prong stars (hatched) is only approximately known.

statistical value in that they do not allow the classification of an individual event as either a decay or an interaction. It is therefore impossible to determine the energies at which the charge-exchange events occurred and so have direct information on the energy dependence of the K-neutron cross-section.

Fig. 3 shows the prong distribution of the stars produced at different K-meson energies. Also indicated for each energy is the ratio of the number of stable particles produced with a component of momentum in the same direction as the incident K-meson, to the number emitted in the opposite hemisphere. The number moving forward is clearly greater than that moving backward.

3.2. The elastic scattering of the heavy mesons. — The differential cross-section in the laboratory system for elastic scattering by the emulsion nuclei (other than hydrogen) is shown in Fig. 4. The data has been separated for

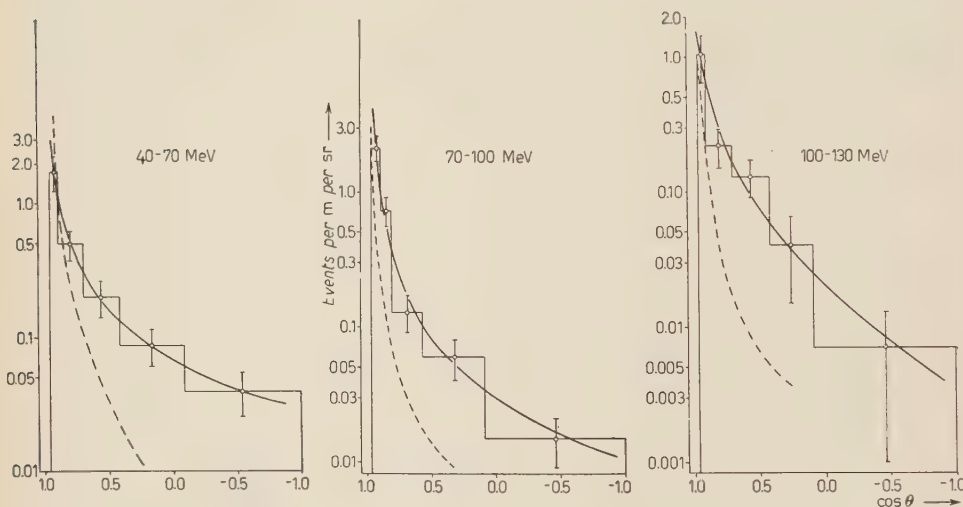


Fig. 4. — The differential cross-section for elastic scattering by emulsion nuclei other than hydrogen is shown for different K-meson energy intervals. The broken line represents the distribution for Coulomb scattering from a point charge.

the three energy intervals $40 \div 70$ MeV, $70 \div 100$ MeV and $100 \div 130$ MeV, since the shape of the angular distribution changes appreciably with energy. Also shown for the sake of comparison in each energy interval is the average distribution for Coulomb scattering assuming a nucleus to behave as a point charge, and it is clear that there is a substantial extra contribution from the nuclear potential scattering. In terms of the optical model (8) the scattering of a particle by a nucleus may be described by assuming a scattering potential of the type:

$$V_{\text{coulomb}}(r) + V_0 + iV_1,$$

(8) S. FERNBACH, R. SERBER and T. B. TAYLOR: *Phys. Rev.*, **75**, 1352 (1949).

where V_0 and V_1 are constant over the nuclear volume. In general the shape of the diffraction scattering distribution will depend quite sensitively on the choice of V_0 and V_1 , but in the present case of K-meson scattering a considerable simplification of the equations is possible. As described in Sect. 3.3 the nucleus is relatively transparent to K-particles and the mean free path, λ , within nuclear matter at 90 MeV is about twice the diameter of a silver nucleus. The imaginary potential iV_1 is determined by

$$V_1 = \frac{4.5(E_K + V_0)^{\frac{1}{2}}}{\lambda},$$

and becomes quite an unimportant term in the potential given above. Accordingly, if the optical model is applicable, both the magnitude and the shape of the differential scattering cross-section should be well described in terms of scattering from a Coulomb potential superimposed upon a square potential well. The solution of the appropriate wave equations using the Coulomb potential of an extended charge and for different values of V_0 have been given by COSTA and PATERGNANI (9) and by COCCONI *et al.* (10) for the collision of K-mesons with an average emulsion nucleus.

A convenient graph of the total elastic cross-section for angles $\geq 20^\circ$ is given by COSTA and PATERGNANI for different chosen values of V_0 , which allows an appropriate well-depth to be determined from the measured cross-section. The values of these cross-sections and the corresponding nuclear potentials for the present data are given in Table II.

TABLE II.

Energy Interval (MeV)	40 \div 70	70 \div 100	100 \div 130
Cross-section for angles $\geq 20^\circ$ (mb)	360 ± 70	290 ± 60	250 ± 50
Potential V_0 (MeV)	+12 or -22	+18 or -30	+20 or \sim -30

The general shape of the scattering distribution from the real potential is in agreement with the observations, a steep drop in $d\sigma/d\Omega$ for angles up to 60° , with no rapid change from a value of a few millibarns per steradian for larger angles. At large angles the form of $d\sigma/d\Omega$ is, of course very sensitive to the meson energy and the shape and depth of the potential well chosen. A detailed comparison in this region with the experimental results is thus not very meaningful.

(9) G. COSTA and G. PATERGNANI: *Nuovo Cimento*, **5**, 448 (1957).

(10) G. COCCONI, G. PUPPI, G. QUARENINI and A. STANGHELLINI: *Turin Conference Report* (September 1956). We are grateful to these two sets of authors (9,10) for prior knowledge of their results.

The measurement of the total cross-section is insufficient to fix the sign of V_0 ; the most direct way of deciding this is to observe constructive or destructive interference with the repulsive Coulomb field. The scattering angle where this effect can be most easily detected is small at these energies ($\sim 10^\circ$) and the present data do not allow a statistically significant comparison to be made with the predictions of the theoretical calculations. Experiments on small-angle elastic scattering (*) have unambiguously decided, however, in favour of a repulsive nuclear potential. That the sign of V_0 is indeed positive is confirmed by the analysis of the inelastic events, and the shape of the differential cross-section for K-H scattering discussed in Sect. 4. This is in contrast to an early report of the observation of destructive interference (11), in the differential elastic scattering cross-section.

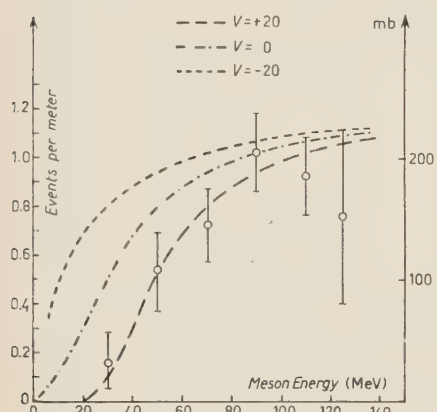


Fig. 5. — The total cross-section and mean free path for inelastic interactions including charge exchange, with emulsion nuclei other than hydrogen as a function of the meson energy. The approximate effect of the Coulomb field is included in the potential $V = V_c + V_0$.

seems too low for a maximum occurring at this energy to be explicable as a resonance phenomenon.

For meson energies between 40 MeV and 120 MeV the mean free path in emulsion is $(1.20 \pm .12)$ m implying a cross-section (4 ± 0.5) mb per nucleon within nuclear matter. Taking the nuclear radius to be $r_0 A^{\frac{1}{3}}$, the corresponding value for the mean free path in homogeneous nuclear matter is $(19 \pm 3)r_0$ or about twice the diameter of the silver nucleus. Because of the greater transparency of the smaller nuclei of carbon, nitrogen and oxygen, only about 19%

(*) Rochester and Padua groups: reported at the Turin Conference (Sept. 1956).

(11) L. OSBORNE: *Phys. Rev.*, **102**, 296 (1956).

of collisions involving transfers of energy to complex nuclei take place with light elements. (In the case of particles which interact with a geometrical cross-section, the figure is 26%).

In deducing the cross-section for an elementary collision with a single nucleon from the value of the mean free path in nuclear matter, account must be taken of the Pauli exclusion principle which greatly limits the number of small energy transfers to a bound nucleon. Thus the cross-section $\bar{\sigma}$ for interaction with a nucleon within a nucleus, will be less than that with a free nucleon by a factor $f(E)$, depending on the meson energy E . For interactions with an «average» bound nucleon:

$$\bar{\sigma} = f(E) \left(\frac{Z\sigma_p + (A - Z)\sigma_n}{A} \right),$$

where σ_p , σ_n are the cross-sections on a free proton and neutron respectively. Treating the nucleons within the nucleus as forming a degenerate Fermi-Dirac gas with a maximum Fermi energy of 24 MeV, and following the analysis of GOLDBERGER (12), the factor $f(E)$ has been calculated in the non-relativistic approximation for the case where the neutron and proton differential cross-sections are isotropic in the centre of mass system:

$$f(E) = 1 - \frac{2}{5} \frac{1}{P_0}; \quad P_0 \geq 1,$$

$$f(E) = -\frac{7}{10} P_0^3 + 4P_0 - 4 + \frac{3}{2} \frac{1}{P_0} - \frac{1}{5} \frac{1}{P_0^2}; \quad 1 \geq P_0 \geq \frac{1}{2},$$

and

$$f(E) = \frac{9}{10} P_0^3; \quad \frac{1}{2} \geq P_0 \geq 0,$$

where $P_{N_{\max}} = 215$ MeV/c is the maximum Fermi momentum, corresponding to a nucleon energy of 24 MeV, and P_0 = momentum of the K-particle within the nucleus in units of $P_{N_{\max}}$. (The effect of the exclusion principle is less for incident K-mesons than for incident nucleons of the same momentum (cf. GOLDBERGER, Eq. (14), op. cit) where the principle applies to both the projectile and target particles and not merely to the latter.)

It follows, therefore, that even if the K-p and K-n cross-sections are approximately constant, the cross-section on bound nucleons will increase quite rapidly with energy until P_0 substantially exceeds 1. The curves of Fig. 5

(12) M. GOLDBERGER: *Phys. Rev.*, **74**, 1269 (1948).

show the expected variation of the nuclear cross-section with energy for the simple case where both σ_p and σ_n are independent of energy, and where the corresponding differential cross-sections are isotropic, the average K-meson cross-section on a free nucleon being taken to be 6 mb. The curve for $V = +20$ MeV fits the measurements well, and the increasing cross-section experimentally observed in emulsion is therefore explicable in terms of the effects of the Pauli principle, and need not imply a strong energy dependence of σ_n and σ_p (*).

It will be seen in Sect. 4·1 that the assumption of energy independence is valid in the case of the K-p cross-section, although there is a considerable departure from isotropy at forward angles due to the effect of the Coulomb potential. Since the exclusion principle forbids most of the energy transfers involved in this forward angle scattering, the above analysis remains valid if for σ_p is taken the value of the total cross-section reduced by the contribution due to the Coulomb effects. There is no direct evidence yet available concerning the angular distribution of K-mesons scattered from neutrons, and the validity of the assumption about σ_n is unknown. In any case, it seems possible to explain reasonably well the energy dependence of the magnitude of the K-nucleus cross-section up to 120 MeV assuming a repulsive potential and without having to introduce other than S-wave interactions. The participation of higher angular momentum states in the scattering would result in a more rapid variation of the cross-section with energy.

3·4. Charge exchange interactions. — That the majority of K^+ -meson interactions at the energies of the present experiment result in the survival of the K-particle in the same charge state was first noted by LANNUTTI *et al.* (4) and now on the basis of much greater statistics would seem well established. Of the 109 inelastic events noted in the present experiment, only 18 are interpreted as involving the transition $K^+ \rightarrow K^0$. Of these, 9 result in 0-prong stars, and 9 in stars with one prong or more. The mean free path for charge-exchange in emulsion for energies between 40 and 130 MeV is $7.1^{+2.3}_{-1.4}$ m corresponding to a cross-section of 29 ± 7 mb. Unfortunately half these events are estimated by the statistical procedure described previously (Sect. 3·1 and (7)) and one is certain of the initial meson energy only in the cases where a star is associated. Since these events are biassed towards the higher K-meson energies, it is not possible to deduce reliably the variation of the charge-exchange cross-section as a function of energy, and so directly investigate the behaviour of the K-neutron interaction.

(*) The classical Coulomb factor $(1 + V_c/E_k)$ has not been included here and will change the shape of this curve only slightly, leaving the free nucleon cross-section of 6 mb unaltered. r_0 has been taken to be $1.33 \cdot 10^{-13}$ cm.

Using the isotopic spin assignment of $T=\frac{1}{2}$ proposed for the K-particle by GELL-MANN and PAIS (4) and NISHIJIMA (5), scattering can occur off a proton only in the $T=1$ state and off a neutron in both the $T=0$ and the $T=1$ states. Assuming the validity of charge independence, the possible reactions and their relative intensities may be written in the form:

<i>Reaction</i>	<i>Isotopic spin weight</i>
$K^+ + p \rightarrow K^+ + p$	R_1^2
$K^+ + n \rightarrow K^+ + n$	$\frac{1}{4} R_1 + R_0 ^2$
$\rightarrow K^0 + p$	$\frac{1}{4} R_1 - R_0 ^2$

where R_0 and R_1 are the amplitudes controlling the interactions in the $T=0$ and the $T=1$ states respectively, and will depend in general on the energy and angular momentum, etc. It follows that the ratio of the number of charge-exchange to the number of non-charge-exchange interactions will be (taking equal numbers of protons and neutrons):

$$F = \frac{|R_1 - R_0|^2}{4 |R_1|^2 + |R_1 + R_0|^2},$$

and F has the value $\frac{1}{5}$ if $R_1 \gg R_0$. A specific model of the meson-nucleon interaction is required in order to calculate F . MINAMI (13) and CEOLIN and TAFFARA (14) have obtained expressions for this parameter on the basis of a number of assumed models, but the presence of independently adjustable variables makes a comparison with experiment indeterminate. Since however, the experimental value of 0.2 ± 0.07 suggests that F is not very different from $\frac{1}{5}$, one might assume that the interaction in the $T=0$ state is small compared with that in the $T=1$ state, although $F=\frac{1}{5}$ could of course, arise from many different choices of R_1 and R_0 .

A measure of the relative strengths of the $T=0$ and the $T=1$ states is provided by a determination of the K-neutron and K-proton cross-sections, σ_n and σ_p . From the above, one has the following relations:

$$\frac{|R_0|^2}{|R_1|^2} = \frac{2\sigma_n}{\sigma_p} - 1, \quad \sigma_n \geq \frac{1}{2}\sigma_p.$$

In Sect. 4.1. the value of σ_p is given as 14 ± 3 mb, this is derived from the

(13) S. MINAMI: *Progr. Theor. Phys.*, **16**, 66 (1956).

(14) C. CEOLIN and L. TAFFARA: *Nuovo Cimento*, in press (1957).

available results on K-H scattering from all laboratories; the cross-section shows no apparent energy dependence. In the absence of the Coulomb field, $d\sigma_p/dQ$ would appear to be approximately isotropic, and have a value $(11 \pm 3)/4\pi$ mb/sr (allowing ~ 3 mb for the Coulomb effects.) Subject to the approximations and results of the previous Sect. 3·3, for $40 \text{ MeV} \ll E \leq 120 \text{ MeV}$:

$$\frac{\bar{\sigma}}{f(E)} = \frac{Z\sigma_p + (A - Z)\sigma_n}{A} = (6 \pm 1) \text{ mb.}$$

Hence:

$$\sigma_n = (2 \pm 2) \text{ mb.}$$

and,

$$\left| \frac{R_0}{R_1} \right|^2 = -0.5^{+0.6}_{-0.4}.$$

(The negative values are physically inadmissible, and arise because the condition $\sigma_n > \frac{1}{2}\sigma_p$ has not been imposed). The magnitudes of the cross-sections are quite consistent with a comparatively weak $T=0$ interaction at these energies though they by no means preclude interactions of the same order of strength in the two states.

It is important to note that this deduction of a K^+ -neutron cross-section close to its minimum value, $\frac{1}{2}\sigma_p$, depends quite sensitively on the measured cross-section within nuclear matter. Even if the assumptions and approximations of Sect. 3·3 were fully justified there remains the possibility that a large number of inelastic interactions leading to low-energy nuclear excitation ($\leq 6 \text{ MeV}$) has escaped detection and has led to an underestimate of $\bar{\sigma}$. The excitation of low-lying nuclear levels in ^{12}C is known to arise in the scattering of 90 MeV protons with a frequency corresponding to about 5% of the elastic cross-section (15). Whereas the methods already described would detect nuclear excitation of the light elements in emulsion, except for the 4.4 MeV level in carbon, most interactions in the present experiment take place with silver and bromine, the nuclear energy levels of which are known to be more low-lying and closer spaced than they are in light nuclei. In addition to the underestimation of the inelastic cross-section, failure to detect these near-elastic collisions can result in an over-estimation, and even a distortion of the elastic differential cross-section, the scattering involving excitation of a particular level leading to an angular distribution characteristic of that level. It has been generally assumed throughout this communication, in particular in

(1) K. STRAUCH and F. TITUS: *Phys. Rev.*, **103**, 200 (1956).

Sect. 5.3, that the proportion of such interactions producing low energy excitation is small, and in a first approximation will not affect the experimental data.

4. - Results on K-hydrogen scattering.

Three examples were observed during the course of the present work, of the scattering of K-particles by hydrogen nuclei in the emulsion. In each case all checks which could be applied were carried out to ensure that the event was not simply a star in which a single proton was ejected fortuitously in the correct direction; the tracks of the incoming and outgoing meson and that of the proton were checked for co-planarity, and the direction and the range of both the meson and the proton were examined for consistency with the curves of PEDRETTI (16). In all cases the balance of energy and momentum was within the errors of measurement and the probability of having included a spurious event is considered negligible. Details of the events are shown in Table III.

TABLE III.

K-meson energy (MeV)	Angle of scattering in laboratory-system (θ)	Range of proton (μm)	Angle of scattering in C.M.S. (χ)
12	15.2°	5.0	22°
88	33.0°	1130	50°
106	25.2°	650	41°

As there is a chance of missing events in which the scattering angle in the center of mass system is small, due to the very short range of the knock-on proton, interactions for which the angle of scatter, θ , of the K-meson is less than 10° in the laboratory system, have been excluded (*). The mean free path for a hydrogen collision ($\theta > 10^\circ$) is therefore 49 m and the corresponding cross-section (6 ± 4) mb. This is just consistent with the value of (14 ± 3) mb obtained from 27 events observed in emulsion in various laboratories as reported and summarized at the Turin Conference (17). The distribution in

(16) E. PEDRETTI: *Nuovo Cimento*, **3**, 956 (1956).

(*) A fourth event has been excluded by the requirements of these criteria: It had $E_K = 125$ MeV, $\theta = 4.7^\circ$, $\chi = 8^\circ$, $R_p = 1.2 \mu\text{m}$.

(17) Communications of the Bristol, Dublin U.C., Gottingen and Padova groups, Turin Conference (Sept. 1956). See also (1). We are grateful in particular to the Gottingen group who collected and distributed the data on K-hydrogen scattering. (See N. BISWAS *et al.*: *Nuovo Cimento*, **5**, 123 (1957); M. BALDO-C'EOLIN *et al.*: *Nuovo Cimento*, **5**, 402 (1957)).

angle of these events is shown in Fig. 6(a) and, as pointed out at the conference, is compatible with a superposition of Coulomb scattering upon *S*-wave repulsive nuclear scattering. The smooth and steep rise of $d\sigma_p/d\Omega$ at forward

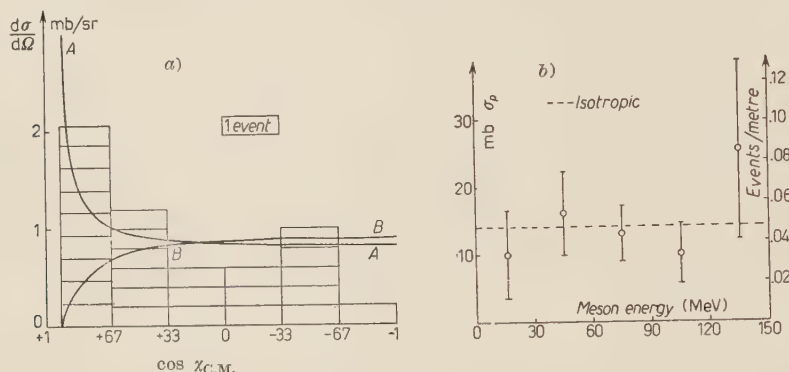


Fig. 6. — (a) The differential cross-section per unit solid angle for the scattering of K-particles from hydrogen. The curves indicated refer to isotropic (*A*) repulsive, (*B*) attractive nuclear scattering with superimposed point-charge Coulomb scattering.

(b) Cross-section for K-H scattering as a function of meson energy.

angles is incompatible with the destructive interference which would arise from an attractive nuclear potential. The smooth curves in Fig. 6(a) are drawn for combined Coulomb and *S*-wave nuclear scattering (18), and it can be seen that the curve for the repulsive interaction provides a reasonably good fit without the necessity of introducing higher angular momentum states. The magnitude of the scattering cross-section is consistent with the proton acting as a spherical potential barrier of $V \sim (20 : 40)$ MeV, depending on the radius assumed ($1.2 \div 1.4 \cdot 10^{-13}$ cm). Assuming the validity of the low-energy approximation, in the absence of any very strong interaction in higher angular momentum states the total cross-section will depart only slightly from the value expected at zero energy for an *S*-wave state. Fig. 6(b) shows the number of K-H scattering events as a function of K-meson energy and supports within the meagre statistics, the evidence from the angular distribution on the *S*-wave interaction.

5. — The K-nucleon cross-section and the scattering from nuclei.

5.1. *General considerations.* — It is known that the distributions in inelasticity and scattering angle for the inelastic interactions of 90 MeV neutrons

(18) See for example A. E. S. GREEN: *Nuclear Physics* (New York, 1955).

with heavy nuclei can be surprisingly well described in terms of a very simple model in which the nucleons within the nucleus are assumed to act as independent scattering centres, unaffected by their neighbours (12). The nucleus is considered as a degenerate Fermi-Dirac gas of neutrons and protons without mutual interaction, and the effect of the Pauli exclusion principle and the motion of the target nucleons on the scattering distributions analytically evaluated. *A fortiori*, the model should be applicable in the case of K⁺-nucleus interaction. The mean energy of the incident particles is 90 MeV, and the average energy lost in interaction is 35 MeV. Assuming the 20 MeV repulsive potential already suggested by the results, the mean energy of the K-meson after one collision within the nucleus will be 35 MeV. The corresponding mean free path in nuclear matter is $\sim 30 r_0$ (see Fig. 5). The fraction, f , of particles having a mean free path, λ , which on making one collision within a nucleus of radius R , will escape without further interaction is given by (19):

$$f = 3 \left(\frac{1}{2x} - \frac{1}{x^3} + \frac{1}{x^3} (1+x) \exp[-x] \right),$$

where

$$x = \frac{2R}{\lambda}.$$

Hence the fraction of K-mesons which undergo double scattering inside the nucleus is 7% and has been neglected. In addition, because it seems reasonable, the K-nucleon force is of shorter range than the nucleon-nucleon force, the smaller volume of interaction will be less likely to result in a many-body collision. Against these qualitative considerations the model has a similar defect for both K-meson and neutron collisions, in that the supposition of quasi-independent target particles must be an approximation at the low energies considered (~ 80 MeV), in view of the known density of nuclear matter and known range of nuclear forces. Nevertheless the consequences of the model have been pursued using the two different approaches described below.

If the model is found to be valid, the treatment of K-nucleus collisions can yield valuable information concerning the K-neutron interaction when the effects of the K-proton interaction have been allowed for. A maximum Fermi momentum of 215 MeV/c has been used for both protons and neutrons (assumed equal in number), corresponding to a nuclear radius of $1.4A^{1/3} \cdot 10^{-13}$ cm for both types of particle. The number of nucleons with momentum p_N is assumed to be proportional to $4\pi p_N^2 dp_N$ although, in fact, the distribution is now known to be exponential; the value of the exponent however, has not

(19) K. A. BRUECKNER, R. SERBER and K. M. WATSON: *Phys. Rev.*, **84**, 258 (1951).

been accurately determined (20,21). The assumption of an absolute maximum of 215 MeV/c does not seriously affect the following analysis although one might expect to observe a few events which demand a higher value of p_N .

The first procedure—see Sect. 5·2 below—is a direct adaptation of Goldberger's calculations to the case of a beam of K-mesons scattered by a nucleon gas—the elementary cross-sections being prescribed—and the main change is the relaxation of the exclusion principle in the case of the incident particle. The results of the correction to the mean free path inside the nucleus arising from this have been given in Sect. 3·3. The second method of approach—Sect. 5·3—involves a study of each individual event in an attempt to reconstruct from the angle of scattering and loss of energy in the laboratory frame of reference, the «most likely» circumstances in the centre of mass system of the meson and nucleon and to obtain information deduced *a posteriori* about the K⁺-nucleon collision.

5·2. *A comparison of the experimental results with the predictions of the statistical model.* — The inelasticity and the angle of scattering θ , in the laboratory system are related in a precise manner for the collision between a K-meson and a nucleon of given velocity. Since the nucleons in the nucleus have a variety of velocities, such a relationship is not known, but because their motion

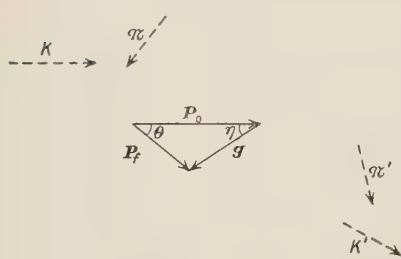


Fig. 7. — Diagram showing the relation between the initial K-meson momentum \mathbf{P}_0 , final momentum \mathbf{P}_f , momentum transfer \mathbf{g} and the angle η in the collision $K + N \rightarrow K' + N'$.

angle between \mathbf{g} and \mathbf{P}_0 (see Fig. 7). For the case of an isotropic K-nucleon cross section, $d\sigma_T/d\Omega = \sigma_T/4\pi$, where σ_T is the total cross-section on an average nucleon, then the relative probability of a momentum transfer between \mathbf{g}

falls within certain limits, there remains a correlation between inelasticity and angle, so that not all combinations are possible. If \mathbf{P}_0 is the initial momentum of the K-particle within the nucleus before the collision, \mathbf{P}_f its final momentum, then $\mathbf{P}_f - \mathbf{P}_0 = \mathbf{g}$ is the momentum transferred in the collision. All these quantities are measured within the nucleus where a potential may operate and they will depend on the value of this potential. The correlation between scattering angle and energy transferred, takes a particularly simple form when studied in terms of \mathbf{g} and the angle η , where $(180^\circ - \eta)$ is the angle between \mathbf{g} and \mathbf{P}_0 .

(20) W. SELOVE: *Phys. Rev.*, **101**, 231 (1956).

(21) J. G. McEWEN, W. M. GIBSON and P. J. DUKE: *Phil. Mag.*, **2**, 231 (1957).

and $\mathbf{g} + d\mathbf{g}$ takes the form $F(\mathbf{g}) d\mathbf{g}$, where

$$F(\mathbf{g}) d\mathbf{g} = \frac{27\pi}{2P_0^2} \left(\frac{\sigma_T}{4\pi} \right) (2P_0 \cos \eta - g) g^2 d\mathbf{g} d(\cos \eta),$$

for

$$g \leq 2P_0 \cos \eta \leq (1 + \frac{1}{2}g)$$

and

$$F(\mathbf{g}) d\mathbf{g} = \frac{27\pi}{4P_0^2} \left(\frac{\sigma_T}{4\pi} \right) \left(1 - 4P_0^2 \cos^2 \eta + 6gP_0 \cos \eta - \frac{9}{4}g^2 \right) g d\mathbf{g} d(\cos \eta),$$

for

$$(1 + \frac{1}{2}g) \leq 2P_0 \cos \eta \leq (1 + \frac{3}{2}g) \quad \text{and} \quad (\frac{3}{2}g - 1) \leq 2P_0 \cos \eta \leq (1 + \frac{3}{2}g).$$

The strong correlation between g and η is clear from Fig. 8 which shows the regions forbidden to certain pairs of g and $\cos \eta$ by the conservation laws and exclusion principle. (It will be seen that the relativistic corrections, as expected, alter only slightly the boundaries in Fig. 8). The experimental data are shown in the form of a scatter diagram for both $V=0$ and $V=+20$. The distribution of most of the points within the allowed area is in quite good agreement with that given by the form of $F(\mathbf{g}) d\mathbf{g}$ above. There remain about 4 events, represented by points lying well outside the allowed boundaries in the diagram, the dynamics of which are clearly inconsistent with the model—their number is however small enough to be accounted for by multiple nuclear scattering or many-body interactions. A few events have a large value of g coupled with very small scattering angles—such examples are explicable on the basis of double scattering (one expects about 7 such events; see Sect. 5.1). Other events have a small value of g coupled with

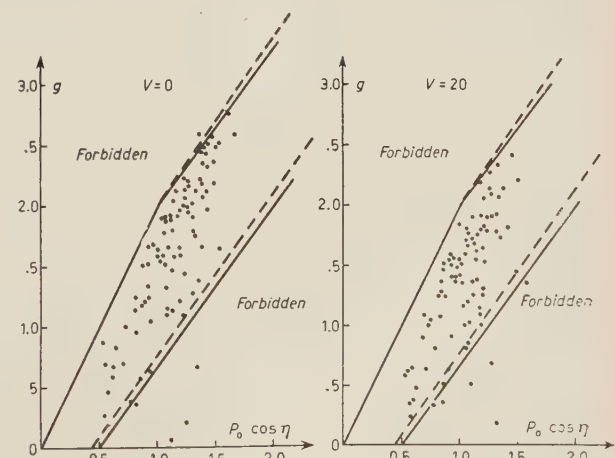


Fig. 8. — Diagram showing the allowed limits for g and $P_0 \cos \eta$ if the collision involves a single nucleon of a degenerate Fermi-Dirac gas with $P_N = 215$ MeV/c. The distribution in density of the points expected for an isotropic K-nucleon cross-section is given in the text.

large scattering angles—such examples are explicable if scattering took place off large nuclear agglomerates within the nucleus. Several of these events would be consistent with the model, however, if an exponential form were used for the nuclear momentum, instead of a sharp cut-off at 215 MeV/c.

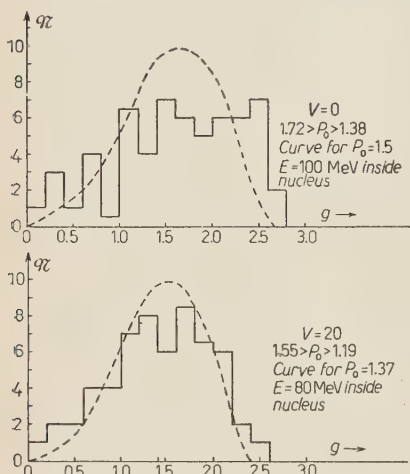


Fig. 9.—Distribution in momentum transfer expected on the Goldberger analysis for an isotropic K-nucleon cross-section for collisions with $E_K = 80 \div 120$ MeV and 2 values of the nuclear potential $V = 0$ and $V = 20$.

menta around P_0 , can be approximately taken to depend upon g alone (cf. discussion by GOLDBERGER, ref. (10), p. 1272), a comparison of the experimental histogram and curves calculated for various initial assumptions on the K-nucleon cross-section allows, in principle, the determination of the shape of $\sigma(g)$. In the present instance the «Isotropic» curve is in good accord with experiment within the rather large errors, the agreement is insensitive however to forward or backward asymmetries in the differential cross-section of less than a factor of two.

It is necessary to recall that the presence of a nuclear potential will cause both the reflection and refraction of particles, the former affecting the magnitude of the cross-section and the latter the angular relations. The reflection coefficient is negligible at all but the lowest energies and has been disregarded throughout. Refraction at the nuclear surface with a consequent change in the direction of both ingoing and outgoing particles, depends on the energy and direction of motion of the particles. Since in general the kinetic energy of the K-particles is many times greater than the probable value of the potential, the refractive index for most of our events will be 1 and so the effect has been considered to be small.

If a particular value of P_0 is chosen, corresponding to a monoenergetic beam of K-particles, then the distribution $F(g) dg$ may be integrated over all $\cos \eta$ to give an inelasticity diagram. Fig. 9 shows this distribution in g irrespective of η for $E_k = 100$ MeV and for an isotropic K-nucleon cross-section $\sigma_x / 4\pi$, and seems to represent well the experimental distribution found for events of about this initial K-energy. The figure shows the distributions for $V = 0$ and $V = + 20$, and there is little doubt that the fit is improved by the assumption of the repulsive potential. The assumption of an attractive potential will make the disagreement even more marked than for $V = 0$.

If the elementary K-nucleon differential cross-section over a small region of

5.3. The transformation to the centre of mass system.

(a) The reduction of each event to the center of mass system. In the laboratory system the K-particle is considered to enter the nucleus and, travelling with momentum \mathbf{P}_0 , to strike a moving nucleon, suffer a deflection, θ , in the laboratory system and emerge from the collision with a momentum \mathbf{P}_f . In the center of mass (C.M.) system let the momenta of the K-particle and nucleon be both equal to p^* and the angle of scattering of the K-particle be θ^* . The measurements made in the emulsion determine \mathbf{P}_0 , \mathbf{P}_f and θ for each event, but these parameters are not sufficient to define completely the initial nucleon momentum and to determine fully the kinematics of the collision. The prescribed energy and momentum lost by the K-particle do however impose a constraint on the allowed nucleon momenta; in effect, the collision can have occurred only with a nucleon which had a fixed component of momentum parallel to \mathbf{g} . Thus the end of the vector representing the target nucleon momentum, \mathbf{P}_N , is constrained to lie in a plane at right angles to \mathbf{g} , and since at the same time it must be within the Fermi sphere, it is confined to the discoid intersection of these two surfaces: see Appendix 2 for a more detailed treatment. The radius of this disc can vary between 0 and R , where $R = 215 \text{ MeV}/c$ is the radius of the Fermi sphere.

Since the momentum density within the sphere is a constant, the probability that a nucleon picked at random from the nucleus should have a momentum vector \mathbf{P}_N , ending within a certain area on the disc is proportional to that area. Corresponding to the various points in the disc are different nucleon momenta and correspondingly different values of θ^* . In general however, the partial kinematical restriction is sufficient to ensure upper and lower limits for θ^* . It can be shown that the locus of the end point of the vectors \mathbf{P}_N which correspond to a chosen value of θ^* , is an arc of a circle. All these arcs are concentric. The area enclosed on the disc between two arcs corresponding to θ_1^* and θ_2^* is directly proportional to the probability that θ^* lies within this interval ($\theta_1^* - \theta_2^*$), since the probability of \mathbf{P}_N ending within this region is proportional to the area. (In certain cases of low momentum transfer, the exclusion principle can forbid collisions involving the lower momentum nucleons and, as indicated in Fig. 10a, the disc has a forbidden central zone).

For each event, the radius of the disc (or annulus) was calculated from the experimentally determined \mathbf{P}_0 , \mathbf{P}_f and θ , and arcs drawn corresponding to equal intervals in $\cos \theta^*$ of 0.1. The areas between successive arcs were found graphically and plotted as in Fig. 10b to give an *a posteriori* probability distribution for the value $\cos \theta^*$ per unit interval arising in the scattering from a nucleon taken at random from the Fermi sphere. This distribution must be modified to take account of certain systematic effects. In an interaction the *a priori* probability of a collision depends on the orientation of the nucleon

momentum, the K-particle hitting more nucleons moving towards it than away from it. The relative probability of selection of a particular nucleon is thus obtained by multiplying by the factor V_{Rel}/V_K , where V_{Rel} = relative velocity of meson and nucleon and V_K = meson velocity in the laboratory

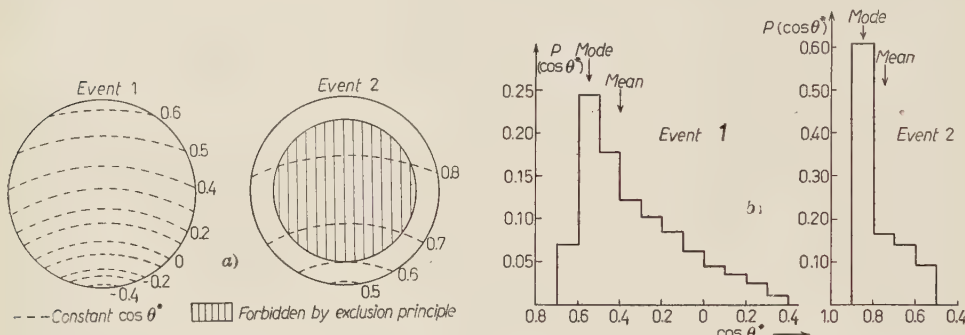


Fig. 10. – (a) Typical examples of discs and loci of constant $\cos \theta^*$ occurring in the graphical construction for the most likely value of $\cos \theta^*$. (b) The corresponding *a posteriori* probability $P(\cos \theta^*)$ distributions for the same 2 events, after weighting for the relative velocity factor.

system. Also the choice of a particular nucleon for a target can further depend on V_{Rel} if the total cross-section is energy dependent. Finally, once the meson has selected a collision partner certain values of $\cos \theta^*$ may, *a priori*, be more likely than others; for example, if the cross-section is other than isotropic. The relative probability of the various values of $\cos \theta^*$ must accordingly be weighted in proportion to the product of these three factors to obtain the correct *a posteriori* distribution.

In calculating the distribution, the first factor has always been included as a matter of course, although its effect is small and the results of introducing various energy and angular dependences separately studied. For example, an energy dependence proportional to the square root of the centre of mass energy left the modal or mean value of $\cos \theta^*$ unchanged for about two-thirds of the events, and caused an average positive shift of less than 0.2 for the others. The effect of introducing an *a priori* angular independence of $d\sigma/d\Omega$ results in an angular distribution of the observed modal values which is slightly closer to the assumed one; in general, because the individual distributions in $\cos \theta^*$ are fairly peaked the experimental distribution of the modal or mean values is not radically altered by any acceptable *a priori* form for $(d\sigma/d\Omega)$.

(b) The choice of $(\cos \theta^*)_{\text{M.L.}}$ as the «best estimate». When a probability distribution such as that shown in Fig. 10b has been obtained and the ordinates weighted as described according to the appropriate factors,

the next problem is to choose some parameter to measure the central tendency of the distribution to utilise in the subsequent analysis. In a typical case the total range of $\cos \theta^*$, i.e. between the maximum and minimum values allowed kinematically, was about 0.8, and the probability distribution skew and well-peaked. For half the events the difference between the mean $\langle \cos \theta^* \rangle$ and mode $(\cos \theta^*)_{M.L.}$ was not greater than ± 0.3 . (For the moderately skew distributions encountered the median value was always intermediate between the mean and mode).

When, however, one combines these estimates from separate events into a single distribution which is expected to represent the scattering angular distribution in the centre of mass system, the question arises as to whether the estimate chosen is a biased one or not. If it is, the angular distribution obtained will be spuriously enhanced in some places and depleted in others in a systematic way. Since $(\cos \theta^*)_{M.L.}$ and $\langle \cos \theta^* \rangle$ were very close in value for each event there was fortunately not a great deal of difference between their distributions. As can be seen from Fig. 11a and 11c, the backward peaking

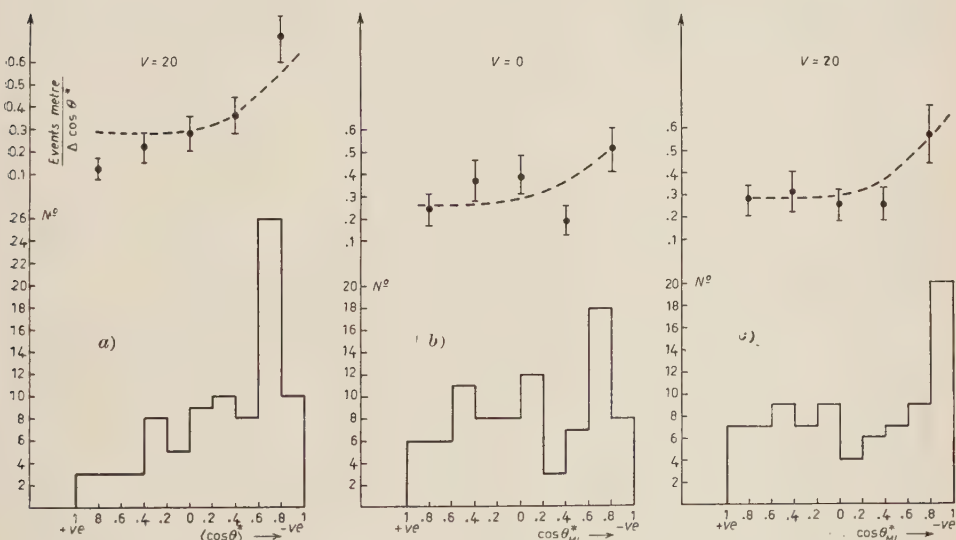


Fig. 11. — The distributions of: (a) $\langle \cos \theta^* \rangle$ for a repulsive nuclear potential $V = 20$. (b) $(\cos \theta^*)_{M.L.}$ for a nuclear potential $V = 0$. (c) $(\cos \theta^*)_{M.L.}$ for a repulsive nuclear potential $V = 20$.

of the cross-section is somewhat more enhanced for the distribution in $\langle \cos \theta^* \rangle$, although there is not a radical difference between the two distributions. For reasons to be described, it is believed that the distribution in $(\cos \theta^*)_{M.L.}$ represents more nearly the true distribution in the centre of mass system.

An attempt was made to study the extent to which the shape of the experimental cross-section (Fig. 11) was energy dependent. Assuming the estimate for the angle of scattering in the centre of mass system, the dynamical configuration of any event becomes determined and so too does the value of p^* the momentum in the centre of mass system, since

$$\cos \theta^* = 1 - g^{*2}/2p^{*2} \quad (\text{see Appendix II}).$$

We have then for each event an estimate of the centre of mass scattering angle and the centre of mass energy (proportional to p^{*2}). If, for example, the backward scattering in the centre of mass system arose largely from a P -wave contribution, then one expects the lowest values of $\cos \theta^*$ to be associated with the largest values of p^* —indicating the growth with energy of this contribution to the cross-section.

Here again arises the dilemma of whether to choose $\langle \cos \theta^* \rangle$ or $(\cos \theta^*)_{M.L.}$ to work with, and whereas before, it made not a great deal of difference, here the sensitivity of the results to the choice is both striking and unforeseeable. Fig. 12 shows the scatter diagrams of $\langle \cos \theta^* \rangle$ and $(\cos \theta^*)_{M.L.}$ plotted against the corresponding values of p^{*2} .

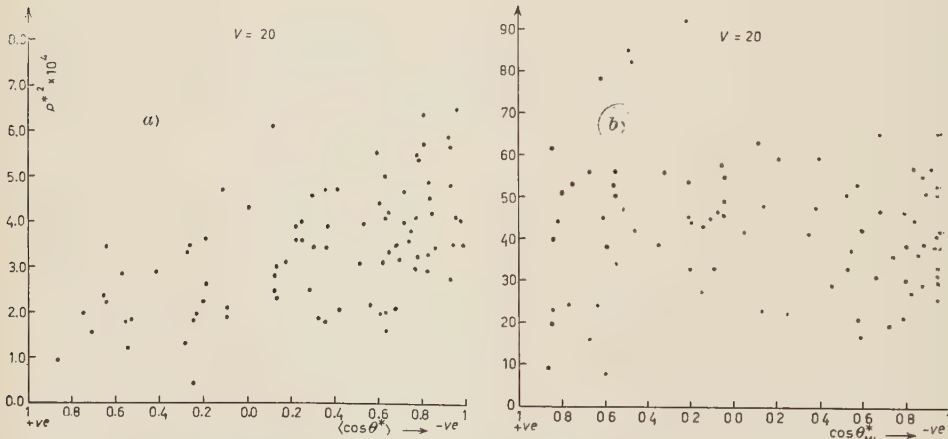


Fig. 12. — Scatter diagrams of (a) $\langle \cos \theta^* \rangle$ and (b) $(\cos \theta^*)_{M.L.}$ against their corresponding p^{*2} .

It is clear that the values of $\langle \cos \theta^* \rangle$ show a strong degree of correlation with the calculated p^{*2} —too strong to be interpreted as a p -wave contribution to the backward scattering. If such a correlation exists it should remain when the incident K-meson laboratory energy is plotted against $\langle \cos \theta^* \rangle$, this scatter diagram is shown in Fig. 13 and it is clear that the effect is absent. It seems

likely therefore that the choice of the mean as an estimate of $(\cos \theta^*)$ leads to a systematic under-estimation of p^* at forward angles. This correlation effect is not seriously altered by changing the value assumed for the nuclear potential. (See Sect. 5.3c).

We conclude therefore that because of the sensitivity of the deductions to small changes in the method of statistical estimation, no meaningful analysis of the variation in the shape of $(d\sigma_x/dQ)$ as a function of energy can be made by the method of *a posteriori* estimation, at least in this energy region. This is due to the diffi-

culty of estimating p^* reliably and does *not* imply a corresponding instability in the shape of the $\cos \theta^*$ distribution. Finally, it is believed that the mode provides a less biased estimate of $\cos \theta^*$ than does the mean.

In conclusion it must be recalled that in discussing the differential cross-section, the estimated distribution in angle shown in Fig. 11 applies only to collisions allowed by the exclusion principle; about one third as many events again should be added to correct for the effects of the principle, and these will be largely concentrated towards forward angles. The final form of cross-section will then look rather like the K-p cross section of Fig. 6a with a backward peak superimposed. The accumulation of large-angle events ($\cos \theta^* \sim -1$) seems statistically just significant, and if due to the K-neutron interaction implies a contribution from angular momentum states other than $l = 0$. Since the K-p cross-section shows no such effect at similar energies the occurrence of other than *S*-wave scattering would presumably be associated with the $T = 0$ state which occurs in the K-n and not the K-p interaction.

(c) The detection of a nuclear potential: The emulsion measurements serve only to fix the initial and final meson momenta outside the nucleus, and therefore yield \mathbf{P}_0 and \mathbf{P}_f , within the nucleus, when a choice of the nuclear potential V , is made. Thus from the collection of extra-nuclear measurements one derives for each event different sets $\mathbf{P}_0, \mathbf{P}_f, \mathbf{g}$ or $\mathbf{P}'_0, \mathbf{P}'_f, \mathbf{g}'$, etc., according to the value of V chosen, each leading to different probability distributions in $\cos \theta^*$ and so different values for the mode $(\cos \theta^*)_{M.L.}$ Thus the final distribution in $(\cos \theta^*)_{M.L.}$ for all events—which is to be taken as an estimate of the elementary K-nucleon cross-section—depends on the

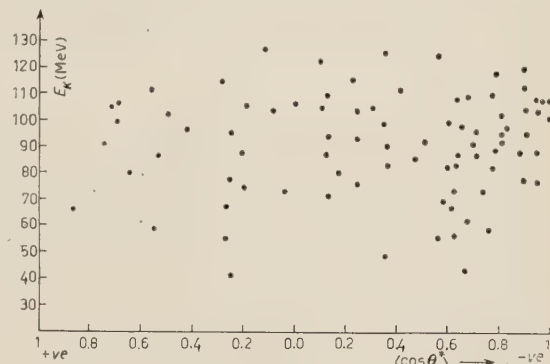


Fig. 13. — Scatter diagram of $\langle \cos \theta^* \rangle$ against the corresponding initial K-meson energy, E_K .

choice of the potential V . However, since this distribution is one of the things which is being sought, it is neither possible nor permissible to use these differences to decide a best value of V . The distributions of $(\cos \theta^*)_{ML}$ for $V = 0$ and $V = 20$ are shown in Fig. 11b,c. They are not strikingly different; in general the shape of the $(\cos \theta^*)_{ML}$ distribution is insensitive to variations in the choice of V .

However, from considerations which are independent of any variation with energy or intrinsic form of $(d\sigma_x/d\Omega)$, one can predict the distribution of certain parameters arising in the analysis and thus apply control tests to check for systematic errors. It happens that one such, viz. the distribution in disc size, is quite sensitive to the value of V . The relative frequency of occurrence of discs of a given size should be closely proportional to the disc size and independent of the centre of mass scattering angle. That this holds for $V = 20$, but not for $V = 0$ can be seen from Fig. 14. This shows a scatter diagram

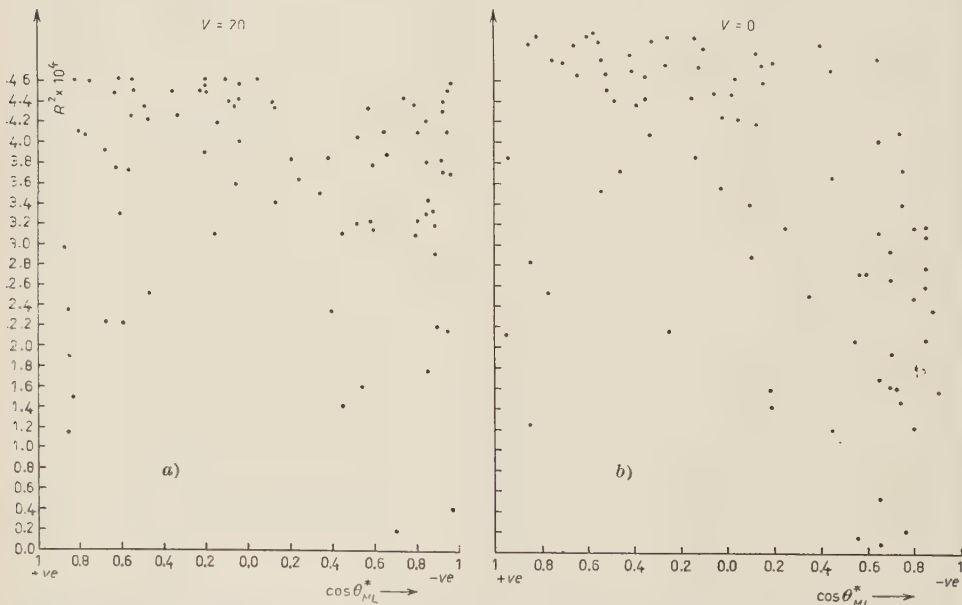


Fig. 14. – Scatter diagram of disc size R^2 against $(\cos \theta^*)_{ML}$ for (a) $V = 20$ and (b) $V = 0$.

of disc area versus $(\cos \theta^*)_{ML}$ for the two potentials. In the first the density of points increases linearly for any interval of $(\cos \theta^*)_{ML}$ as one proceeds from the bottom towards the top of the diagram, whereas in the second case there is an absence of events near $(\cos \theta^*)_{ML} = 0 \div 0.8$ and small and medium disc sizes, and near $(\cos \theta^*)_{ML} = -1$ and large disc sizes. The asymmetries in the latter distribution were taken to imply the existence of some

systematic effect, such as the proposed one (i.e. $V = 20$), which does not depend on the energy or angular dependence of the cross-section.

6. - Conclusions.

The present results show that the technique of using stripped photographic emulsions is capable of yielding useful information about the interactions of positive heavy mesons with nuclei and nucleons.

On the other hand the accumulation of very much greater statistics on many aspects of these problems would probably be less arduous by other techniques of nuclear physics. The results and conclusions based on events discovered in an unbiassed scan of 148 m of K-meson track for energies between 0 and 130 MeV may be summarized as follows:

(i) Failure to observe the slightest evidence of the annihilation of a K^+ -particle in a sample of over 100 nuclear interactions of heavy mesons supports the law of conservation of strangeness in strong interactions proposed to explain the properties of the heavy unstable particles.

(ii) The K^+ -particle predominantly emerges from nuclear interactions in the same charge state. The ratio of charge-exchange to non-charge-exchange interactions with emulsion nuclei is 0.2 ± 0.07 . Within the errors this is also the value expected in the limit of a vanishingly small interaction in the $T=0$ state. The mean free path for charge-exchange in emulsion is $7.1_{-1.4}^{+2.3}$ m.

(iii) In an examination of an estimated 18 stars where the K^+ -particle was not observed to emerge no evidence for the production of an excited fragment containing a bound K -particle was found. The metastability and decay of such θ -fragments has been discussed by PAIS and SERBER (22): the mean free path for their formation in emulsion must be very long ($\gtrsim 148$ m).

(iv) The value of the inelastic nuclear cross-section confirms that of LANNUTTI *et al.* (4); further it has been possible to plot its approximate energy dependence. The observed variation with energy of the cross-section on nuclei has been shown to be compatible with an approximately constant cross-section on nucleons. The collected information on K-H scattering does not indicate an increase in σ_p with meson energy.

(v) The cross-section for elastic scattering from emulsion nuclei for angles $\geq 20^\circ$ is found to be one to two times greater than the inelastic cross-section and to decrease with energy largely because of the diminished Coulomb

(22) A. PAIS and R. SERBER: *Phys. Rev.*, **99**, 1551 (1955).

effect. Comparison with the calculations of COSTA and PATERGNANI on the elastic scattering show that if the K-nucleus interaction may be approximated by a spherical well V_0 , with a superimposed Coulomb potential, then $V_0 = +15 \div +20$ MeV or $-20 \div -30$ MeV. Several independent pieces of evidence favour the repulsive potential.

(vi) Most but not all the nuclear interactions may be well described in terms of the statistical model. The approximation of the nucleon motion by a degenerate Fermi-Dirac gas, the neglect of many-body interactions and multiple scattering, forbid the possibility of complete agreement. The possibility of compound nucleus formation, the direct excitation of nuclear levels and the occurrence of small transfers of energy making a substantial contribution to the inelastic cross-section cannot be neglected; the experimental resolution is too poor to allow their detection.

(vii) It is shown that it is possible to extract meaningful information on the K-nucleon interaction by examining the relative probabilities of various dynamical configurations in the centre of mass system of the meson and target nucleon. The method requires the introduction of a repulsive potential inside the nucleus of about 20 MeV to ensure internal consistency; it predicts an angular distribution in the centre of mass system of the K-nucleon scattering which is reasonably stable against changes in the nuclear potential or the method of estimating $\cos \theta^*$. The behaviour of the cross-section with energy seems inaccessible by this method. Analysis indicates that the mode is the most reliable parameter to use for estimation in the circumstances.

(viii) The center of mass angular distribution obtained by the *a posteriori* method is deficient at forward angles and if it is to be compared with the cross-section on a free nucleon it must be corrected for the effects of the Pauli principle. Qualitatively this would appear to result in a forward peaking not unlike $d\sigma_p/d\Omega$ coupled with a less pronounced backward peak. This latter could be interpreted as arising in the K-neutron interaction, in which case it would be most likely to involve the $T=0$ state.

(ix) The value of the average K-nucleon cross-section within nuclear matter for meson energies between $40 \div 120$ MeV is (4 ± 0.5) mb/nucleon; allowing for the events forbidden by the exclusion principle this implies a cross-section of (6 ± 1) mb on a free nucleon. Taking $\sigma_p = (14 \pm 3)$ mb it follows that $\sigma_n \approx (2 \pm 2)$ mb.

* * *

For their care and attention in successfully exposing the stack to the K-beam at the Bevatron, we are particularly grateful to Dr. E. J. LOFGREN and his colleague, Dr. R. W. BIRGE. For the preparation of the stack we are

grateful to Mr. C. WALLER, Ilford Ltd. Our thanks are due to Professor C. F. POWELL, F.R.S., and to Professor T. E. NEVIN for their interest and encouragement; to the Misses JOAN BYRNE, MARIANNE PEARCE, Mrs. D. EVANS and Mrs. ANNE BOULT at Bristol, and to the Misses BRIGID MAHER, DENISE O'BRIEN and MARY SMITH at Dublin U.C. for their assistance in the scanning and analysis of events, and to Mrs. IRIS POBJOY who prepared the diagrams.

We would like to thank Dr. R. H. DALITZ for many informative and illuminating discussions.

Finally, we wish to acknowledge the cordial exchange of information with other laboratories working on the same problem, at Bologna, Göttingen and Padua, and to the members of the last named laboratory D.K. is grateful for many discussions.

D.E. is grateful to the University of Bristol for a graduate scholarship, S.N. wishes to thank the Swedish Atomic Energy Commission for a grant and the University of Uppsala for leave of absence. B.B. thanks the Colombo plan authorities for financial assistance and the University of Delhi for leave of absence.

APPENDIX I

The identification of the tracks followed and the related K_0 problem.

About 25% of all tracks which were found beyond the stopping points of the protons at the ionization expected for K-mesons (see text) ended without any visible associated product. The nature of the particles producing a number of these tracks was investigated by careful measurements of the normalized coefficient, g^* , of the exponent of the gap length distribution ⁽²³⁾ at a known residual range, R , and it was found that the greater number of these tracks were due to K-mesons (K_0). On a sample of 400 μ -e decays, it was found that in 18% of the cases no positron secondary could be associated with the μ -meson. This figure remained fairly constant with the depth of the end of the μ -meson track in the emulsion when the 30 μm nearest either interface were disregarded, but appeared to vary somewhat with the angle of dip of the secondary. It was therefore concluded that the occurrence of the K_0 -mesons was due to the low sensitivity of the emulsion which resulted in a blob density of about 7/50 μm for a track of minimum ionization. In order that a large error should not be made in the estimation of the cross-sections for the various K-meson interactions, it was necessary to find the contamination of protons in the tracks which had an ionization expected for the K-particles. To estimate g^* on each track observed for the large statistics obtained in the present expe-

⁽²³⁾ P. H. FOWLER and D. H. PERKINS: *Phil. Mag.*, **7**, 587 (1955).

periment would have been too tedious; the ionization was therefore estimated by measuring the blob density, b , at the pick up point for each track. Since $\log b$ varies linearly with $\log R$ for the values of b and R occurring in the present experiment, bR^n will have a different constant value for each particle. (n is the slope of the straight line obtained by plotting $\log b$ against $\log R$ and in the present case has the value of $\frac{1}{3}$ for both protons and K-mesons).

Due to the statistical errors involved in the estimation of ionization, a normal distribution is obtained for bR^n and a good discrimination between K-mesons and protons results when the blob density is known with a statistical uncertainty of about 7%.

APPENDIX II

Kinematical relations for collision with a moving nucleon, and the evaluation of $\langle \cos \theta^* \rangle$ for each event.

1) *General conditions.* — We adopt the following notation:

- θ = angle of scatter of K-meson;
- \mathbf{p}_0 = initial momentum of K-meson;
- \mathbf{p}_f = final momentum of K-meson;
- \mathbf{p}_0 = momentum of K-meson in C.M. system before collision;
- \mathbf{g} = momentum transferred;
- E_K = total energy of K-meson before collision;
- E_N = total energy of nucleon before collision;
- \mathbf{p}_N = momentum of nucleon before collision;
- M = mass of nucleon;
- m = mass of K-meson.

Except for \mathbf{p}_f quantities after the collision are primed. Quantities starred are referred to the centre of mass system.

From the general Lorentz transformation it follows that,

$$(1) \quad \mathbf{p}_0^* = \mathbf{p}_0 - E_K/(E_K + E_N) \cdot (\mathbf{p}_0 + \mathbf{p}_N) \quad \text{and} \quad \mathbf{p}_f^* = \mathbf{p}_f - E_K/(E_K + E_N) \cdot (\mathbf{p}_0 + \mathbf{p}_N).$$

In these equations terms in $\beta_{c.m.}^2$ are neglected where $\beta_{c.m.} = (\mathbf{p}_0 + \mathbf{p}_N)c/(E_K + E_N)$ the velocity of the centre of mass. Also $E_K\gamma_{c.m.}$ has been approximated by E_K ; The approximation is a good one since $\beta_{c.m.}$ is always less than 0.35. In fact it is possible to correct empirically for this approximation.

From (1) it follows that $\mathbf{g} = \mathbf{g}^*$ where

$$(2) \quad \mathbf{g} = \mathbf{p}_0 - \mathbf{p}_f \quad \text{and} \quad \mathbf{g}^* = \mathbf{p}_0^* - \mathbf{p}_f^*.$$

Since the total momentum is conserved during the reaction \mathbf{g}^* is independent of \mathbf{p}_N .

The angle θ^* between \mathbf{p}_0^* and \mathbf{p}_f^* is given by,

$$(3) \quad \cos \theta^* = 1 - g^2 / 2p_0^{*2}.$$

For each value of nucleon momentum \mathbf{p}_N , there exists a value of $\cos \theta^*$. The problem therefore, is to find the mean value of $\cos \theta^*$ for the whole range of \mathbf{p}_N . In the text the problem of whether to take $(\cos \theta^*)_{M.L.}$ or $\langle \cos \theta^* \rangle$ as the measure of the central tendency of the distribution is fully discussed.

We have the following kinematical restrictions on \mathbf{p}_N ,

$$(4) \quad E_K + E_N - E'_K = [(Mc^2)^2 + (\mathbf{p}_0 + \mathbf{p}_N - \mathbf{p}_f)^2 c^2]^{1/2}.$$

The nucleon can be treated non-relativistically so we have,

$$E_N = Mc^2 + p_N^2 / 2M.$$

Expanding the root in (4) as far as the second term (neglect of higher terms involves an error of only 3%) we have,

$$(5) \quad \mathbf{p}_N \cdot \mathbf{g} = -\frac{1}{2}g^2 + M\Delta E \quad \text{where} \quad \Delta E = E_K - E'_K.$$

It can be seen from this equation that the end point of \mathbf{p}_N lies on a plane perpendicular to the vector \mathbf{g} at a distance, $a = -\frac{1}{2}g + M\Delta E/g$, measured from $\mathbf{p}_N = 0$ in the direction of \mathbf{g} . We require p_N to be less than $p_{N \max}$ and also that a should be less than $p_{N \max}$ for the allowed plane to lie within the Fermi sphere.

2) *The exclusion principle.* — We assume a Fermi distribution for the initial nucleon momenta. The exclusion principle then requires that

$$(6) \quad E'_N > E_{N \max} \quad \text{if} \quad p_N > b = (p_{N \max}^2 - 2M\Delta E)^{1/2}.$$

The alternative condition $(\mathbf{p}_N + \mathbf{g})^2 > p_{N \max}^2$ is identical for points on the allowed plane since, for such points, the expressions $(\mathbf{p}_N + \mathbf{g})^2$ and $p_N^2 + 2M\Delta E$ are the same.

Two cases are possible, (1) $a > b$ and (2) $a < b$.

(1) The whole circle which is the intersection of the allowed plane and the momentum sphere is allowed.

(2) Only an annulus on the allowed circle can contribute to the event.

3) *The average value of $\cos \theta^*$.* — Equation (1) can be written as,

$$(7) \quad \mathbf{p}^* = E_K / (E_K + E_N) \cdot (E_N / E_K \cdot \mathbf{p}_0 - \mathbf{p}_f),$$

E_N can be considered a constant since the kinetic energy contributes less.

than 3 %. It is convenient to split $(E_N/E_K \cdot \mathbf{p}_0 - \mathbf{p}_f)$ into two components one parallel to \mathbf{g} and one perpendicular to \mathbf{g} . The parallel component does not vary with \mathbf{p}_N , the variation of the perpendicular component may therefore be taken alone.

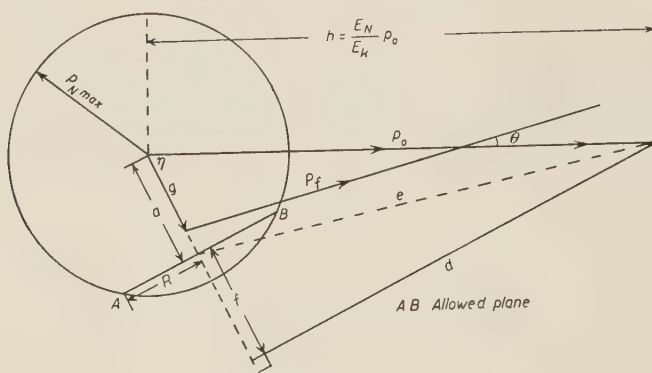


Fig. 15. — Diagram showing notation used in calculation of $\langle \cos \theta^* \rangle$.

With the notation of Fig. 15, introducing polar co-ordinates (r, φ) for the end point of the vector \mathbf{p}_N on the allowed plane AB , we have,

$$(8) \quad (E_N/E_K \cdot \mathbf{p}_0 - \mathbf{p}_f)^2 = f^2 + (r^2 + d^2 - 2dr \cos \varphi).$$

The number of nucleons with momentum \mathbf{p}_N with the co-ordinates (r, φ) is proportional to the surface element, $ds = r dr d\varphi$. If now the dependence of the cross-section on p^* and $\cos \theta^*$ is known, the average value of $\cos \theta^*$ over the permitted surface is:

$$(9) \quad \langle \cos \theta^* \rangle = \frac{\int \int \sigma(p^*, \cos \theta^*) \cos \theta^* ds}{\int \int \sigma(p^*, \cos \theta^*) ds}.$$

If $\cos \theta^*$ does not vary over wide limits on the allowed plane the mean value is little affected by the choice of cross-section variation either with p^{*2} or $\cos \theta^*$. Choosing an isotropic form in each case, the integration can be carried out explicitly using equations (3) for $\cos \theta^*$ and (7) and (8) for p^{*2} .

The result for case 1 ($a > b$) is:

$$\langle \cos \theta^* \rangle = 1 - g^2(E_K + E_N)^2 / 2E_K^2 R^2 \cdot \ln(R^2 + j^2 + (R^4 + 2j^2 R^2 + e^1)^{1/2} / 2f^2),$$

with $j^2 = f^2 - d^2$.

The result for case 2 ($a < b$) is:

$$\cos \theta^* = 1 - g^2(E_K + E_N)^2 / 2E_K^2(R^2 - S^2) \cdot \ln \left(\frac{R^2 + j^2 + (R^4 + 2j^2 R^2 + e^1)^{1/2}}{S^2 + j^2 + (S^4 + 2j^2 S^2 + e^1)^{1/2}} \right),$$

where S is the radius of the forbidden circle on the plane AB .

Thus for each inelastic event a mean, $\langle \cos \theta^* \rangle$ can be computed analytically from the above equations. The quantities a , b , and $E_N/E_K \cdot p_0$ are calculated and g , d , e , f , R and N are obtained very quickly from a drawing such as Fig. 15.

4) *Dependence on the value of $p_{N_{\max}}$.* — We have used a value of 215 MeV/e for the maximum Fermi momentum. This corresponds to a Fermi energy of 24 MeV and a mean nucleon energy of 15 MeV. It is known however that larger values certainly are possible. In view of this we have examined the effect on calculations of $\langle \cos \theta^* \rangle$ of changing $p_{N_{\max}}$ over wide limits. Fortunately the variation is very small and only changes the $\langle \cos \theta^* \rangle$ value when R is very small. For all normal events therefore the effect of arbitrarily choosing 215 MeV/e when the real momentum distribution extends beyond this figure is small.

RIASSUNTO (*)

Sono stati seguiti con tecnica atta ad evitare di influenzare i risultati 148 m di tracce di K^+ e furono trovate 109 interazioni anelastiche con nuclei dell'emulsione. Furono trovati inoltre 3 eventi di scattering K^- -protone e numerosi casi di scattering elastico sui nuclei dell'emulsione. La sezione d'urto differenziale per lo scattering elastico è stata messa in diagramma per tre intervalli di energia e si sono confrontati i risultati con quelli predetti dal modello ottico per varie profondità della buca nucleare. La variazione con l'energia della sezione d'urto degli eventi anelastici risulta compatibile con l'isotropia se si tien conto del principio d'esclusione di Pauli, e il miglior adattamento dei punti sperimentali si ottiene per un potenziale repulsivo di 20 MeV. Gli urti anelastici sono stati analizzati sulla base del modello statistico del nucleo ed è stato anche fatto il tentativo di ottenere dai dati sperimentali la distribuzione angolare nel sistema del C.M. della sezione d'urto K -nucleone. In base ad ogni ragionevole assunzione questa risulta presentare un picco all'indietro. Anche questi dati richiedono un potenziale repulsivo di ~ 20 MeV. Il valore della sezione d'urto K -nucleone media entro la materia nucleare per energie mesoniche tra 40 e 120 MeV è di 4 mb/nucleone; tenendo conto degli eventi proibiti dal principio d'esclusione, ciò richiede una sezione d'urto di 6 mb per nucleone libero. Prendendo $\sigma_p = (14 \pm 3)$ mb, ne segue che $\sigma_n = (2 \pm 2)$ mb. Il rapporto degli eventi con scambio di carica a quelli senza scambio è $.20 \pm .07$, coincidente col valore previsto per il limite di una interazione scomparientemente piccola nello stato $T=0$.

(*) Traduzione a cura della Redazione.

**The Relative Frequencies of the Decay Modes
of Positive K-Mesons and the Decay Spectra
of Modes $K_{\mu 3}$, τ' and K_β .**

G. ALEXANDER, R. H. W. JOHNSTON and C. O'CEALLAIGH
Dublin Institute for Advanced Studies, School of Cosmic Physics - Dublin

(ricevuto il 23 Aprile 1957)

Summary. — Some 3300 K-meson decay events have been studied in a large stack exposed to the positive K-beam at the Berkeley 6 GeV Bevatron. The events have been selected in an unbiassed way and have been used to yield preliminary information concerning the shape of the energy spectrum of the charged particle emitted in the rarer 3-body decay-modes τ' , $\chi(K_{\mu 3})$ and K_β . The relative abundance of the decay-modes has been estimated the results being summarized in the Table.

Mode	τ	τ'	$K_{\mu 2}$	$\chi(K_{\pi 2})$	$\chi(K_{\mu 3})$	K_β
Abundance (%)	6.77 ± 0.45	2.15 ± 0.42	57.0 ± 2.6	23.2 ± 2.2	5.9 ± 1.3	5.1 ± 1.3

The number of interactions observed over the first 4 cm from decay of the π -mesons secondary to χ -decay yields the surprisingly short estimate of the interaction M.F.P. of (11.1 ± 2.4) cm. This appears to be in significant disagreement with that found for artificial π^+ -mesons by other workers, namely 27 cm in the same energy region, $(109 \div 82)$ MeV.

1. — Aims of the investigation.

Some 3300 K-meson decay events have been examined in a large stack (K_2^+) of plates consisting of 300 pellicles each of dimensions $25 \text{ cm} \times 20 \text{ cm} \times 600 \mu\text{m}$ kindly exposed for the workers of the G-Stack Collaboration Group to the K-meson beam of the Berkeley Bevatron. The K-mesons produced in a target of copper were selected at constant momentum at 90° to the path

of the primary circulating 6.2 GeV proton beam by the the strong focussing spectrometer described by BIRGE *et al.* (1).

The aim of the experiments has been twofold. Firstly, it was desired to obtain evidence as to the relative frequencies of the decay modes of positive K-mesons, and secondly, it was hoped to obtain preliminary information concerning the experimental decay spectrum of the rarer three-body modes ($K_{\mu\eta}$), $\tau'(K_{\pi\eta})$ and K_β . In order to obtain information as quickly as possible, a method of scanning was adopted which, while avoiding the selection bias inherent in identifying secondary particles at the point of arrest of the K-mesons, at the same time did not suffer from the time-consuming disadvantages of the method «along the track scanning». A preliminary report on this work has already been given at the 6th Rochester Conference on High-Energy Nuclear Physics, 1956 (2). Since that time, the number of events has been doubled, and the present work involves the detailed study of about 360 examples of K-decay having secondary particles of small dip, and having a potential stack-length of ≥ 4 cm.

2. – Selection criteria and scanning bias.

The success of the two aims of the investigation, which clearly are inter-dependent, depends on achieving a negligible scanning bias. The method of selecting the preliminary sample of 3300 K-decays was as follows. For each plate being scanned, the position of the mean range of the decaying K-mesons was determined from the known variation in depth of the stack of the momentum of the beam particles. Rectangles of width ~ 1 mm were scanned in alternate strips at right angles to the direction of the beam. The area scrutinized was of width ± 1 cm centred on the line of mean K-meson range. During the scanning of each strip, those particles were noted which had values of apparent scattering and blob-density expected of particles of protonic mass or less having residual range 1 ± 2 mm. All primary tracks of which the ends fell within a distance $\leq 10 \mu\text{m}$ from glass or surface were automatically excluded from consideration. Each track so selected was followed to rest, and the end very carefully scrutinized to detect the association with a charged secondary particle. If none could be found, the track was traced back from the point of arrest, if necessary, by following into adjacent strips to allow of visual distinction between the track of a proton and that of a K-meson. If the appearance still favoured identification as the track of a K-meson a δ -ray

(1) R. W. BIRGE, R. P. HADDOCK, L. T. KEITH, J. R. PETERSON, J. SANDWEISS and M. N. WHITEHEAD: *Suppl. Nuovo Cimento*, **4**, 351 (1956).

(2) *Report on 6th Rochester Conference on High Energy Nuclear Physics* **5**, 18: 6, 31 (1956).

vs. residual range count was made. There remained however a residue of tracks 36 in number ($\sim 1\%$) which, judged by the above criteria were those of K-mesons, but of which the secondary tracks could not be seen.

The tracks of the secondary particles were classified as to dip (δ) and the three categories chosen, all per 100 μm in the processed emulsion, were as follows:

Class	Dip % (processed emulsion)
A	$0 < \delta < 6$
B	$6 < \delta < 20$
C	$20 < \delta$

In a preliminary investigation, only those in Class A, and with a potential track-length available for measurement in the Dublin portions of the stack $> 4\text{ cm}$ were selected for study, excluding from consideration any segment of track which lay in a strip of width 1 cm bounded by an uncut edge. It does not seem likely that the method described is affected by sensible scanning bias. Experimental evidence in support of this belief will be described in Appendix I.

3. - Methods of identification of the decay modes.

The identification of the tracks has been based (1) on blob-counts, (2) on estimates of the value of $p\beta c$ by scattering measurements. In the method adopted which will be referred to as the standard procedure (S.P.), two segments of the track were chosen each of length approximately 1 cm, the first lying as close as possible to the point of decay, the other as nearly as possible to coincide with the segment distant $3 \pm 4\text{ cm}$ from this point. Blob-counts (~ 1000 blobs) and estimates of $\bar{\alpha}_{100}$ using 100 observations in 100 μm cells, were made within the chosen segments. The depth gradient of development was found to be considerable, $(23 \pm 2)\%$ from 13 plates examined. This figure, assuming a linear gradient, has been used in what follows to correct the observed blob-count, to the mid-plane of the emulsion. The portions of secondary track lying within a distance $< 15\text{ }\mu\text{m}$ from glass or surface were excluded when making estimates of blob-density or of $p\beta c$. Since, in addition, variations in plateau blob-density occurred from plates from the stack processed in different batches, it became necessary to normalize the blob-densities. As a first step, the blob-counts were normalized to those corresponding to π -mesons in the beam. These were blob-counted in the region of the plates just beyond the extreme range of the protons, namely about 2 cm from the edge of entry

of the beam. Since the decay region of the K-mesons lay 8-12 cm from this edge, it might be thought preferable in order to avoid errors due to variations in sensitivity over the area of the plates to determine the blob-counts on the beam π -mesons in the region of decay of the K-mesons. However, the effects of scattering, elastic and inelastic, will tend to produce fluctuations in energy and inferior collimation of the beam π -mesons by the time that they have reached this region, and there will have been produced besides, an unwanted background of electrons from charge-exchange and knock-on processes. Accordingly, this method was abandoned in favour of the following. When a satisfactory number of well established cases of $K_{\mu 2}$, χ and K_{β} -decays had been obtained, an extensive calibration experiment was carried out. The secondary particles of the first two modes are of precisely known energy, and that of the latter is of constant and known velocity, and so the variation of blob density with velocity could be investigated. The results of this work, to which reference may be made, have been published separately (ALEXANDER and JOHNSTON (3)). In this way, we have been able to construct Table I which summarizes the criteria used for identification, the values of b^* for the various modes being normalized to the trough or minimum value of ionization.

TABLE I.

Decay-Mode	SEGMENT				Δb^*	$\Delta p\beta c$ (MeV)
	1st cm		4th cm			
	b^*	$p\beta c$ (MeV)	b^*	$p\beta c$ (MeV)		
$K_{\mu 2}$	1.040	214	1.060	194	0.020	20
$\chi(K_{\mu 3})$ [upper limit]	1.060	195	1.086	173	0.026	22
$\chi(K_{\mu 3})$ [critical]	1.17	134	1.28	105	0.11	29
$\chi(K_{\pi 2})$	1.205	165	1.286	138	0.081	27
K_{β}	1.123	—	1.123	—	0	Large
τ'	≥ 1.56	—	—	—	—	—

Apart from the absolute values of b^* and $p\beta c$, it will be seen that the changes in their values between the segments afford additional information which is

(3) G. ALEXANDER and R. H. W. JOHNSTON: *Nuovo Cimento*, 5, 363 (1957).

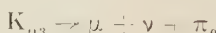
of value for identification. For the K_{μ^3} mode, two values are given, the first corresponding to the upper limit of the spectrum $K_{\mu^3} \rightarrow \mu + \nu + \pi_0$ (HOANG *et al.* (4)), and the other corresponding to an initial value of b^* such that there exists a possibility of confusion with the γ -mode when measurements are confined to the segment 0–4 cm from the point of decay. Table I therefore illustrates what we will call the Standard Procedure (S.P.). In certain cases where it does not suffice to identify the track, similar measurements may be carried out on longer track-lengths where available. This we may call the extended standard procedure (E.S.P.).

In the experimental estimation of $p\beta c$, 200 μm cells have been used for the cases of most frequent occurrence (K_{μ^2}) and γ , and the observed values of $p\beta c$ and of b^* have been corrected for ionization-loss back to the point of origin. The cut-off employed has in all cases been that of $4\bar{D}$ with replacement (developed by GOLDSACK (5)) and the values of the scattering constant obtained in a calibration in this laboratory (JOHNSTON (6)) have been used to estimate $p\beta c$.

For a given track, consideration of the set of measured values of the six critical parameters of which the values are listed in Table I, will in general be sufficient to identify the track. The results enable us to give estimates of the relative abundances of the various decay modes. Certain possibilities of ambiguity and difficulty may arise, however, and these will now be considered.

3.1. – K_{μ^2} and $K_{\pi^2}(\gamma)$. These constitute the most abundant decay mode of K-mesons. In general, it is a simple matter on the basis of the standardized measurements to distinguish between the two-body K_{μ^2} and γ modes. Contamination of the samples by misidentified cases of high decay of the comparatively rare mode K_{μ^3} may be neglected. On the other hand, the effect of such contamination must be taken into account in estimating the relative frequency of the K_{μ^3} mode itself. This point will now be discussed in detail.

3.2. – K_{μ^3} . Cases of the three-body decay-mode K_{μ^3} (4)



are the most difficult to identify, especially in the presence of a preponderating background of secondary particles from K_{μ^2} and γ -decay. We may consider first the energy region (~ 130 MeV) where there is confusion with the K_{μ^2} mode.

- (4) T. F. HOANG, M. F. KAPLON and G. YEKUTIELI: *Phys. Rev.*, **101**, 1834 (1956).
- (5) S. J. GOLDSACK: private communication.
- (6) R. H. W. JOHNSTON: *Suppl. Nuovo Cimento*, **4**, 456 (1956).

The end point energy of the secondary μ -meson corresponds to $p\beta c = 195$ MeV and range = 17.0 cm, and cannot be distinguished by the S.P. from the more abundant secondary particles from the $K_{\mu 2}$ -decay for which the corresponding values of the parameters $p\beta c = 219$ MeV and range = 21 cm. Because of statistical fluctuations, there will exist cases of $K_{\mu 2}$ -decay of which the estimates of $p\beta c$ are low while those of b^* are high. The S.P. does not suffice to distinguish such from cases of $K_{\mu 3}$ -decay with energy in the region of the end-point of the spectrum. This source of uncertainty is compensated for by those cases of $K_{\mu 3}$ decay which show statistical fluctuations in the opposite direction, but since the abundance ratio $K_{\mu 2}/K_{\mu 3} \approx 10$, the compensating effect is insignificant.

Since for such cases the S.P. is inadequate, we have adopted the extended procedure E.S.P. and have conducted measurements of $p\beta c$ and b^* over the available path-lengths. In our sample, a selection was made of ambiguous cases for which both the mean value of $p\beta c$ established by measurements on the 1st and 4th segments was lower by one standard deviation ($\sim 10\%$), and the mean estimated b^* higher by one standard deviation than that corresponding to the $K_{\mu 2}$ mode. Eight such particles were found, and estimates of b^* and $p\beta c$ were made as far as possible beyond a length of 4 cm. In 2 cases, the estimated range was significantly less than 21 cm the established range of the $K_{\mu 2}$ secondary particle, and these have been tentatively identified as cases of $K_{\mu 3}$. It is clear, however, since the basis of selection of the secondary tracks was on a basis of potential length ≥ 4 cm, that there exists a bias against the possibility of establishing the identification of any ambiguous case on the basis of extended measurements.

The hazard of confusion with cases of χ -decay becomes of importance at a lower energy of emission ((80 \div 100) MeV) of the μ -meson ($p\beta c$ (124 \div 151) MeV). In this region the S.P. fails as will be made clear by inspection of Fig. 1 taking into consideration the fact that the standard deviation of the estimates of the parameter $p\beta c$ is $\sim 14\%$.

The extended S.P. was used in this region, estimates of b^* and $p\beta c$ being

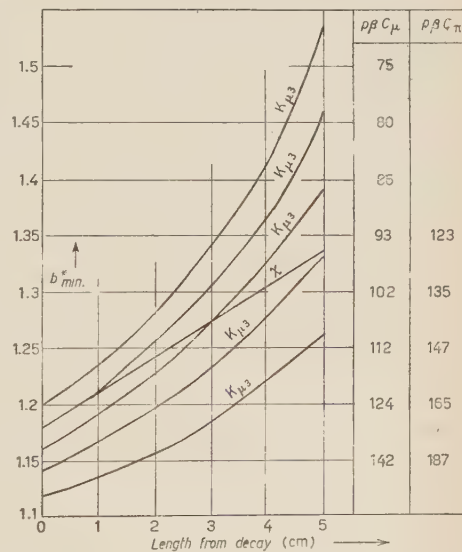


Fig. 1. — Ionization of secondaries as a function of length from decay.

made on all available portions of the track, and an attempt was made to trace the track to rest, unfortunately without success.

In addition, mass estimates were made on the basis of combined b^* and $p\beta e$ on all cases identified as χ -decay of which the secondary particle did not interact in flight (54 cases out of 78).

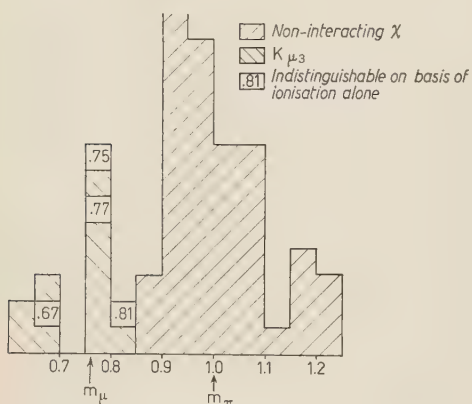


Fig. 2. — Mass estimates of non-interacting χ and $K_{\mu 3}$ secondaries.

fact that extended measurements have been made on those cases which were most liable to be mistaken for $K_{\mu 3}$. Since the abundance ratio of non-interacting χ to $K_{\mu 3}$ decay ~ 3 , the error of identification as $K_{\mu 3}$ of cases of χ -decay will tend to be compensated to some extent by the reverse process.

The cases of $K_{\mu 3}$ decay having energy within the range 60–80 MeV, may readily be identified using our standard method. For values of energy < 60 MeV

TABLE II.

Group	Kinetic Energy (MeV)	Range (cm)	Competitor	Method	Discrimination
1	0–60	0–5.5	τ'	T.R.	U
2	60–80	5.5–8.4	—	S.P.	U
3	80–100	8.4–11.5	χ	T.R. E.S.P.	U A
4	100–130	11.5–16.5	$\chi, K_{\mu 2}$	T.R. E.S.P.	U U
5	> 130	> 16.5	$K_{\mu 2}$	T.R. E.S.P.	U A

there is a possibility of confusion with τ' -decay. Consequently all tracks in this category were followed to rest, and identified by means of their decay products. This is not a very arduous procedure as the residual range of a μ -meson of energy 60 MeV is 5.5 cm.

Table II summarizes the procedure followed in respect of the $K_{\mu 3}$ decay-mode and will be referred to later when discussing the form of the decay spectrum. The mode competing for recognition is noted, and the quality of the discrimination is classified as U = unambiguous, or A = ambiguous, using the methods T.R. = traced to rest, S.P. = standard procedure or E.S.P. = extended S.P.

3.3. - $K_\beta(K_{e3})$. The identification of cases of K_β is more straightforward. In addition to evidence based on the values of the parameters in Table I, the occurrence of a large Bremsstrahlung loss is decisive. The computed radiation-length for G-5 emulsion is 2.93 cm. Since, for all tracks, the length followed is > 4 cm it will be seen from the following table which gives the probability of a fractional energy-loss after a path-length λ cm in G-5 emulsion.

This evidence, taken in conjunction with those from the observed b^* , is sufficient to identify all cases of K_β decay of $p\beta c$ comparable with those of the χ -value. For lower energies of emission it will be possible, in addition, to identify the particle as an electron from consideration of the combined values of $p\beta c$ and b^* (7).

TABLE III.

λ (cm)	Probability of Loss	
	40%	60%
1.0	0.3	0.17
2.0	0.6	0.37
3.0	0.8	0.58
4.0	0.9	0.75
5.0	0.95	0.86

3.4. - There remains the problem of identifying the cases of τ' -decay. The maximum energy of emission of a π -meson from the decay scheme $\tau' \rightarrow \pi^\pm + \pi^0 + \pi^0$ is $p\beta c = 93.0$ MeV, $b^* = 1.56$, and residual range 4.2 cm. All tracks

(7) R. H. W. JOHNSTON and C. O'CEALLAIGH: *Phil. Mag.*, **46**, 393 (1955).

with values of $b^* > 1.5$ are therefore followed to rest in the stack and thus identified unambiguously.

In order, however, to increase the statistical accuracy of the τ' decay-spectrum, we have also accepted Class B tracks. Such tracks as were « considered ionizing » when observed, were blob-counted over a segment of 1 mm by the scanner concerned. Most such were secondaries from γ -decay. If, however, the preliminary estimate of b^* exceeded 1.3 its value was carefully redetermined by a physicist. Such as then appeared to have $b > 1.5$ were traced to rest, and identified.

4. — Relative abundance of K-decay modes.

The problem of the relative abundance of the various decay modes has already been studied by several groups. The relative abundance of the decay modes of a sample of 55 identified K-mesons from stars produced by cosmic radiation has been made by the G-Stack Collaboration (⁸). An analogous experiment of much interest has been carried out by the École Polytechnique Group (⁹) using the decay of K-mesons produced in a stack of plates exposed to the direct proton beam of 6.2 GeV of the Berkeley Cosmotron. These experiments differ from all others in that the proper time of flight of the decaying K-mesons was $\sim 10^{-9}$ s. Other experiments have used K-mesons produced at 90° from targets of tantalum (M.I.T. Group (¹⁰)), of copper exposed to the proton beam of the Brookhaven Cosmotron (Rochester Group (¹¹)), or to the 6.3 GeV proton beam of the Bevatron. In all these experiments the proper time of flight was $\sim 10^{-8}$ s, and a significant difference in the partition ratios would have an important bearing on the problem of the identity of the particles producing the different established decay-modes.

There does not appear any evidence of a significant variation between the abundance ratios of the decay modes which may be correlated with a difference between the condition of production and detection. It must be noted, however, that the statistical weights of the G-stack and École Polytechnique result is not very large. A table summarizing results known up to the end of 1954 has been given by BIRGE *et al.* (¹²) and will be referred to in the discussion.

(⁸) G-STACK COLLABORATION: *Nuovo Cimento*, **2**, 1063 (1955).

(⁹) J. CRUSSARD, V. FOUCHÉ, J. HENNESSY, G. KAYAS, L. LEPRINCE-RINGUE, D. MORELLET and F. RENARD: *Nuovo Cimento*, **3**, 731 (1956); **4**, 1195 (1956).

(¹⁰) D. M. RITSON, A. PEVSNER, J. C. FUNG, M. WIDGOFF, G. T. ZORN, S. GOLDHABER and G. GOLDHABER: *Phys. Rev.*, **101**, 1085 (1956).

(¹¹) T. F. HOANG, M. F. KAPLON and G. YEKUTIELI: *Phys. Rev.*, **102**, 1185 (1956).

(¹²) R. W. BIRGE, D. H. PERKINS, J. R. PETERSON, D. H. STORK and M. M. WEINSTEIN: *Nuovo Cimento*, **4**, 834 (1956).

4.1. Results of the present experiment. — In the 33 plates scanned in the present work a total of 3336 K-endings was found. These include 226 cases of τ -decay and 67 cases in which no secondary particle could be found even after the most careful scrutiny by a number of observers. 408 cases fell into Class A (dip $\leq 6\%$) and of these 336 satisfied the additional criteria of (i) potential range 4 cm in the available portion of the stack and (ii) origin at distance $> 10 \mu\text{m}$ from surface or glass. On subsequent measurement, 308 secondaries could be traced and measured over the requisite 4 cm, but 29 could not be measured completely, having been lost between pellicles, having become too steep for measurement, or being of such geometry that they became undetectable against the background of beam particles. The identification of the particles by the procedures described and summarized in Table I is given in Table IV.

On general grounds, one would expect that there will be a bias in favour of losing the more lightly ionizing particles such as $K_{\mu 2}$, and the figures in the second row are not inconsistent with this view, although the observed difference is not statistically significant. Since, by the same argument, there will be a bias against being able to make complete measurements on cases of the faster particles, and also because the overall effect is small and difficult to calculate, it is felt that the most representative figures are based on the totals as given in the third row. No allowance has been made for cases of failure to observe a secondary particle, as it has been felt that this 1% effect is most likely to be of importance for secondary particles of unsatisfactory geometry.

TABLE IV.

Category	$K_{\mu 2}$		γ		$K_{\mu 3}$		K_β		τ'		Tot. K_l	Tot. K
	no.	%	no.	%	no.	%	no.	%	no.	%		
Complete	180	55.0	78	23.9	20	6.12	17	5.20	10	3.06	295	327
Incomplete	22.5 (*)	72.6	4.5 (*)	14.5	1	3.22	1	3.22	0	0	29	31
Total	202.5	56.3	82.5	22.9	21	5.84	18	5.00	10	3.06	324	358

(*) Two incomplete $K_{\mu 3}$ have been distributed as follows: 1, $\frac{1}{2}$, $\frac{1}{2}$, between $K_{\mu 3}$, $K_{\mu 2}$ and γ respectively.

It is convenient to separate the examples of the decay modes τ and τ' from the remaining categories $K_{\mu 2}$, γ , $K_{\mu 3}$ and K_β which we may for convenience describe as K_l since there is no possibility of experimental confusion between them. The relative abundance of the τ mode was found to be $\tau/K = 226/3336 = 6.77 \pm 0.43$. In the case of the τ' -mode, 10 cases of Class A

were traced to rest and identified among 327 cases of K. In addition, a further 16 examples in Class B were similarly identified. The total of K decays not τ or Class A+B was found to be 1129 (including an estimated 22 cases where no secondary particle could be detected). The estimated relative abundance $\tau'/K = 26/1211 = (2.15 \pm 0.42)\%$ and the ratio $\tau'/\tau = 26/82 = 0.317$.

The $\tau + \tau'$ modes are thus estimated to constitute $(8.92 \pm 0.47)\%$, and the K_i modes $(91.08 \pm 0.47)\%$ of all K-decays.

4.2. Discussion and comparison with results of other groups.

(a) τ -decay. In the case of the τ -mode the method of detection used by the various experimental groups have been similar and it appears profitable to combine their results. It is reasonable to assume that the efficiency of recognizing a τ -event is $\sim 100\%$, the only source of systematic difference between the results of the groups will be varying degrees of efficiency in detecting the K_i modes especially those of low ionization. This would lead to an underestimate of the total number of cases of K-decay other than τ in the sample. The figure for estimated loss given by the Berkeley Group is 15% and in the present work 2%. The effect does not appear to have been corrected for by all the other groups but probably does not exceed 15%. Table IV contains the principal available experimental results with estimated corrections (where stated by the authors). The present results $\tau/\text{all K} = (6.77 \pm 0.43)\%$ is in excellent agreement with the mean of the available numbers.

TABLE V.

Group	Total K-endings observed	No. observed	Assumed Effi- ciency (η)	Corrected Total Endings	Relative Abundance	
					$\eta = 1$	corrected
École Polytechnique	376	30	1	—	7.2 \pm 2.2	—
RITSON <i>et al.</i>	766	58	1	—	7.6 \pm 1.0	—
BIRGE <i>et al.</i>	2 613	171	0.85	3 075	6.54 \pm 0.4	5.56 \pm 0.39
Present work	3 269	226	0.98	3 336	6.91 \pm 0.44	6.77 \pm 0.43
Total	7 024	485	—	6 411	6.90 \pm 0.30	6.19 \pm 0.30

The present estimates of the τ' -abundance and of the ratio $\tau' / (\tau + \tau')$, are also in good agreement with those of other groups as may be seen by inspection of Table V (BIRGE *et al.* (12)).

There appear however to be certain significant discrepancies in the estimates of the relative abundance of the rarer K modes. Owing to differences between the experimental conditions and the manner of detection adopted by workers in the various laboratories, and also because of the smaller statistical weight of other work, it would appear most useful to compare in Table VI the present results only with those of the Berkeley Group.

In the Berkeley experiments the abundance of $K_{\mu 2}$ and χ were estimated by making blob-counts on a sample of K-secondaries of suitable dip and by tracing to rest of a smaller sample of tracks which had potential range < 21 cm. From the experimental abundance of $K_{\mu 2} + \chi$, the separate abundances were estimated by use of an experimental value for the ratio $K_{\mu 2}/K_{\pi 2}$ suitably corrected to take account of the estimate scanning efficiency (85%) for lightly ionizing tracks. As will be seen from Table VI, the estimated relative abundances of the mode $K_{\mu 2}$ is in good agreement with ours, while the difference between the estimates of the abundances of the χ -mode, taken by itself, cannot be regarded as significant.

TABLE VI.

Mode	Number	Class	% of all K-decay	
			Present experiment	Berkeley Group
$K_{\mu 2}$	202.5	A	56.9 ± 2.62	58.5 ± 3.0
$\chi (K_{\pi 2})$	82.5	A	23.2 ± 2.23	27.7 ± 2.7
$\chi (K_{\mu 3})$	21	A	5.90 ± 1.3	2.83 ± 0.95
$K_{\beta} (K_{e 3})$	18	A	5.06 ± 1.3	3.23 ± 1.30
Total K _i	324		91.06 ± 0.47	92.26 ± 1.50
τ	(24.1)	A+B+C	6.77 ± 0.43	5.56 ± 0.41
τ'	(7.6)	A+B	2.15 ± 0.42	2.15 ± 0.47
Total K	356		99.98	99.97

The abundances of the remaining modes were estimated by following systematically along a chosen sample of track for such distances that electrons and μ -mesons of certain selected energies could be identified. The numbers in the sample were corrected for scanning loss estimated as 15% for lightly-ionizing secondary particles, and assumed to be zero for cases of τ -decay and particles of $b > 1.3$ min. 6 cases of K_{β} decay were found among a corrected sample

of 186 tracks followed. No case of $K_{\mu 3}$ decay with secondary energy > 80 MeV was found, although 71 tracks were followed to such distance that a muon of energy (110 \pm 135) MeV should have been recognized. This result appears to be in disagreement with those of the present experiment as may be seen by inspection of Fig. 1 which shows a detailed analysis of our $K_{\mu 3}$ results. It will be seen that there are 12 cases of $K_{\mu 3}$ with secondary energy > 80 MeV corresponding to a partial abundance of $(3.7 \pm 0.96)\%$ a result in satisfactory agreement with the Berkeley estimate $(2.83 \pm 0.95)\%$. There remain, however 8 cases of energy > 80 MeV. Few of these are liable to be confused with cases of γ or $K_{\mu 2}$ decay as has already been shown by the detailed argument set out on p. 483. The values of the ratios $K_{\mu 3}/K_1$ and $(K_{\mu 3} + K_\beta)/K_1$ are insensitive to uncertainty in the estimated ratio $\gamma/K_{\mu 2}$. The comparative figures are

Abundance ratio	$K_{\mu 3}/K_1$ %	$(K_{\mu 3} + K_\beta)/K_1$ %
Berkeley experiment	3.07 ± 1.00	6.06 ± 1.41
Present experiment	6.48 ± 1.37	12.05 ± 1.8

This is a significant difference in the estimated abundance-ratios which it is only possible to remove by postulating that in the present experiment a certain number of cases of γ or $K_{\mu 2}$ decay have been incorrectly identified as being cases of $K_{\mu 3}$ or K_β . Alternatively, it may be removed by supposing that the reverse has occurred in the Berkeley experiment. The balance of the evidence appears as discussed on p. 483 and p. 484 to favour the latter hypothesis.

5. — Energy spectra of 3-body decay modes.

Since the K-meson decay events have been selected in a fashion which appears free from serious bias, much useful preliminary information has become available concerning the main features of the rarer three-body decay modes, τ , $K_{\mu 3}$ and K_β . Because the number of examples found in good geometry of each of these modes is ~ 20 , the present results can only be regarded as preliminary, but are of interest since the number of cases found hitherto in all other investigations is only of the same order of magnitude, and this information cannot usefully be combined in view of the many sources of bias involved in their selection. Furthermore, the results of the present measurements have given valuable indications that it is possible on the basis of less arduous measurements of b^* and $\gamma\beta\epsilon$ to separate cases of the rarer modes from the preponderating background of $K_{\mu 2}$ and γ -events. In this manner, it is hoped to assemble with reasonable speed a larger number of cases of interest

which should throw more light on the important problem of detailed structure of the spectra.

5.1. τ' decay. — As already described in Sect. 4, 26 cases of τ' -decay of Class A and Class B have been identified. 25 of these have been traced to

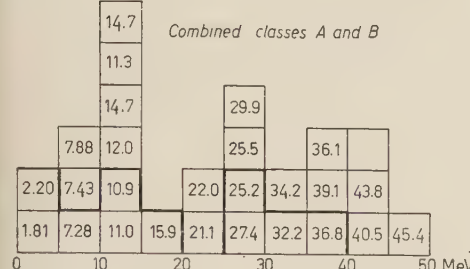


Fig. 3. — τ' energy spectrum. Class A secondary energies are shown under the heavy line.

range ($0 \div 25$) MeV and 13 in the range ($25 \div 50$) MeV. The general shape conforms to that expected from phase-space considerations, but clearly it is desirable to increase the statistics before more definite conclusions may be drawn.

5.2. $K_{\mu 3}$ spectrum. — As is clear from the discussion in Sect. 3, it is a difficult matter to obtain an unbiased spectrum of the μ -mesons secondary to $K_{\mu 3}$ decay, especially at higher energies where there are technical difficulties because of the possibility of confusion with cases of χ and $K_{\mu 2}$ decay. The results of the present experiment are shown in Fig. 4 in which the categories set out in Table II are indicated together with the estimated energies at emission for each case. Except in the case of Class 1 which represents those arrested in the stack, the energies at emission were estimated from the measurements of b^* and $p\beta e$. In the case of one track of Class 2 which could be traced to rest, the energy estimated in this manner was (72 ± 3) MeV which is in very satisfactory agree-

rest and their energies have been determined from their ranges. One case has been followed for a distance sufficient to distinguish it from cases of low energy $K_{\mu 3}$ and such that the residual range and hence the energy of emission could be estimated with precision. The results are shown in Fig. 3 both for the 10 cases of Class A and for the 26 cases of Class A and Class B combined. It will be seen that there is no evidence for asymmetry in the energy distribution, 13 cases being found in the energy

range ($0 \div 25$) MeV and 13 in the range ($25 \div 50$) MeV.

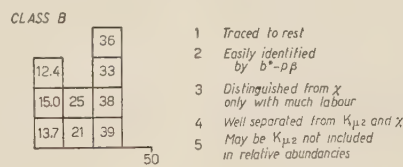
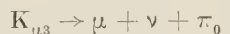


Fig. 4. — $K_{\mu 3}$ energy spectrum. Standard errors in all cases are $< 5\%$.

ement with that corresponding to the observed range namely 70 MeV. The status of the 4 cases in category 3 has been discussed in Sect. 3.2. The mass estimates shown in Fig. 2 would indicate that their identification as μ -mesons is well founded. In the case of the two tracks in Class 5, extended measurements yielded estimates of b^* consistently lower and of $p\beta c$ consistently higher than those of secondaries from $K_{\mu 2}$ decay. This lends colour to the belief that these also were μ -mesons emitted with energy near the maximum energy $p\beta c$ from the $K_{\mu 3}$ decay scheme



Unfortunately, however, it was not found possible to trace them to rest and so to determine their range, and thus some uncertainty remains as to the soundness of the above conclusion. For this reason, as already remarked in Sect. 4, these cases have been excluded in deriving the estimate of the relative abundance of the mode $K_{\mu 3}$. Using the known properties of the sampling distributions of the estimates of $p\beta c$ and of b^* , we calculate an expectation of 5 cases of $K_{\mu 2}$ showing an apparent value of $p\beta c < 200$ MeV estimated from the combination of both methods. The number of cases found was 8, and of these, only the two referred to above continued to yield consistently low estimates of $p\beta c$ when the measurements were extended over a range > 4 cm. Finally, as we have already observed there exists a bias against the possibility of extending measurements beyond 4 cm in such suspect cases. This leads to a tendency to underestimate their abundance. It is clear, however, that the only unambiguous evidence of the existence of μ -mesons in this energy region can be provided by examples which have been traced to rest. To obtain a satisfactory number of such, requires the use of very large stacks, and it is possible that the use of other techniques may prove more profitable in elucidating this point.

The form of the spectra expected for the decay modes $K_{\mu 3}$ and K_β have been investigated by the Hiroshima theoretical group ⁽¹³⁾ assuming that the decay involves the weak Fermi interaction, subject to the restriction of Lorentz invariance for the transition matrix. The theoretical energy spectra of the secondary μ -meson are given for a vector and also for a scalar K -meson, but the statistical weight, neither of the present experiment nor of previous work, which suffers from marked selection bias, is adequate to justify detailed comparison with the theoretical spectra. We may observe however that 9 cases of $K_{\mu 3}$ decay have been observed of energy < 68 MeV and 13 cases, including

⁽¹³⁾ S. FURUICHI, T. KODAMA, S. OGAWA, Y. SUGAHARA, A. WAKASA and M. YONEZAWA: *Progr. Theor. Phys.*, **17**, 189 (1957).

two doubtful, of energy > 68 MeV. This observation would seem to indicate that the spectrum is of approximately symmetrical form, or at least that emission of high energy μ -mesons occurs with comparable probability.

5.3. K_β spectrum. — In all, 19 examples (*) of the decay-mode K_β were found in the investigation. The criteria for selection have already been set out in Table III. The energy at emission has been estimated from scattering measurements carried out on the first cm of track from decay, using basic cell 50 μm and employing noise eliminations between 150 $\mu\text{m}/50 \mu\text{m}$ or 100 $\mu\text{m}/50 \mu\text{m}$ cells, according to the energy of emission. The estimated energies have been corrected for Bremsstrahlung loss by the methods described in Appendix II. The standard error of the estimate of energy is $\sim \pm 20\%$. The selection bias may be regarded as negligible for tracks of moderate and high energy. On the other hand, if emission at very low energies is probable, there will be a marked bias against establishing the existence of secondary electrons of energy > 15 MeV on account of the background of such tracks in the plates, and the difficulty of establishing the connection between the point of arrest of a K -meson and an electron of this energy.

The experimental spectrum is shown in Fig. 5. A feature, if statistically significant, is the appearance of 5 cases of secondary particles of energy > 200 MeV. This feature has already been noticed (14) and might be thought to provide evidence for the existence of a two-body decay mode.

$$K_{\beta 2} \rightarrow \beta + \nu.$$

However, the calculations of the Hiroshima Group already referred to (13) indicate a bimodal distribution for the case of scalar $K_{\beta 3}$ with tensor interaction, the smaller peak being centred around 100 MeV and the larger about 210 MeV. The statistical fluctuations in the experimental estimates of $p\beta c$ will tend to obscure somewhat the sharp separation of these peaks, if they exist. Nevertheless it must be observed that the present experimental observations are not in disagreement with such a theoretical spectrum.

(*) Including one kindly supplied by Dr. E. E. FAHY, University College, Cork.

(14) J. CRUSSARD on behalf of combined Dublin, Bristol, Berkeley, Rochester and École Polytechnique Groups. *Proceedings of the 6th Rochester Conference on High-Energy Nuclear Physics*, 5, 18 (1956).

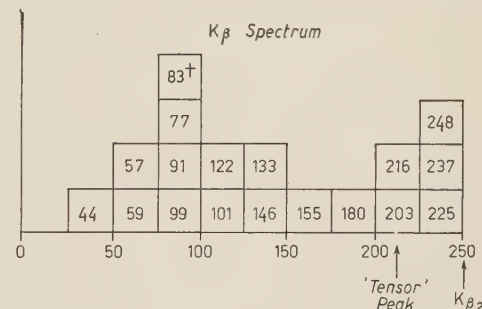


Fig. 5. — K_β spectrum. Standard errors $\sim 20\%$.

6. – Electron pairs associated with decay.

Five cases of decay accompanied by an electron pair were detected among the total of 3110 cases of K-decay. The secondary of one of these was of good geometry (Class *A*) and was identified as a case of χ -decay. The secondary of the remaining 4 cases could not be identified with certainty. Assuming for simplicity that a single π^0 secondary is produced in the decay of the modes χ , α , K_β and τ' , which together constitute 37% of the total or 1150 events, and that the probability of direct decay of the π^0 -meson to one γ -ray and one electron pair is 1/80⁽¹⁵⁾, one would expect to observe ~ 16 cases of decay accompanied by an electron pair. This expectation is 3 times that observed. Because of the methods of observation adopted in the present experiment, the efficiency of observing even lightly ionizing secondaries seems to be exceptionally high. The discrepancy may be due to unrecognized observational bias. If not, it is a difficult matter to put forward a satisfactory explanation especially on the basis of the accepted identification of the particles involved in the relevant decay schemes.

7. – Interaction length of the π -meson secondary to χ -decay.

In the course of systematic following of the secondary particle from the 82 cases of χ -decay scrutinized in the present investigation, a total of 24 cases of interaction was observed, 22 of which occur within a distance of 4 cm from the point of decay of the χ -meson. These interactions consisted of stars with black or grey prongs, or of «stops» in which the π -meson was arrested in flight without the further production of a visible charged particle. Cases of elastic scattering have not been included. The experimental mean free path in emulsion for such events was (11.1 ± 2.4) cm, a figure which is not due to an improbable statistical fluctuation, would correspond to a cross-section of $2 \div 3$ times the geometrical value. Since, as will be seen, there is no evidence from known work on the interactions of artificially produced π^+ -mesons in the energy range in question (~ 27 cm for G-5 emulsion), it was felt to be of interest to examine the information available from other work on the interaction mean free path for γ -meson secondaries. This information has been assembled in Table VII. The results appear to be consistent with our observation.

Taking these results as a whole, we find 39 interactions in a path length 543 cm corresponding to an interaction mean free path of (13.9 ± 2.9) cm.

⁽¹⁵⁾ R. H. DALITZ: *Proc. Phys. Soc.*, A 64, 667 (1951).

TABLE VII.

Author	Track-length observed (cm)	Number of Stars and Stops	Interaction M. F. P.
Berkeley Group (12)	118.5	4	29.6
M.I.T.-Brookhaven (10)	22.5	2	11.3
G-STACK (8)	86.5	4	21.6
École Polytechnique (9)	69.7	7	10.0
Present work	254.4	22	11.1
All work $0 \div 2$ cm	300.3	25	12.0
All work $2 \div 4$ cm	242.3	14	17.3

In the last two rows we have divided the range from decay into two segments $0 \div 2$ and $2 \div 4$ cm. Given sufficient statistics, it might be possible to establish a dependence on energy or on time of flight, but the present results are inconclusive.

A summary of available results on the π^+ interaction-length both in emulsion and other media is given in Table VIII.

TABLE VIII.

Author	Medium	Energy (MeV)	Interaction M.F.P. G.5 (cm)
BERNARDINI <i>et al.</i> (16)	Emulsion	75	31.2 ± 2.5
HOMA <i>et al.</i> (17)	Emulsion	151	32.7 ± 3.0
FERRARI <i>et al.</i> (18)	Emulsion	120	25.4 ± 2.0
ARONS <i>et al.</i> (19)	C, Cu, Al, Pb	110	Geometric $\pm 15\%$

(16) G. BERNARDINI and F. LEVY: *Phys. Rev.*, **84**, 610 (1951).

(17) G. HOMA, G. GOLDHABER and L. M. LEDERMAN: *Phys. Rev.*, **93**, 554 (1954).

(18) G. FERRARI, L. FERRETTI, R. GESSAROLI, E. MANARESI, E. PEDRETTI, G. PUPPI, G. QUAREN, A. RANZI, A. STANGHELLINI and S. STANTIC: *Suppl. Nuovo Cimento*, **4**, 914 (1956).

(19) M. ARONS, J. ASHKIN, F. FEINER, F. GARMAN and L. SMITH: *Phys. Rev.*, **90**, 342 (1953).

Taking the lowest experimental value from this Table namely 25.4 the expected number of interactions in the 543 cm of χ -secondary path observed, we would expect to find 21.4 interactions. 39 interactions appear to have been observed, a fluctuation of 3 standard deviations. On purely statistical grounds such a fluctuation, is very improbable. However, further observations are required in order to establish or reject the hypothesis. Such an investigation has been undertaken.

If the effect is not due to an improbable fluctuation, there may be grounds for entertaining the hypothesis that some unknown physical effect is involved. The supposition that a resonance effect exists in large nuclei is unsatisfactory, since such would be obliterated by the Fermi motion of the nucleons. It is not in evidence for Cu a nucleus of size comparable with Bromine or Silver. Further the π^+ -p resonance at 180 MeV is known to be completely smeared out in compound nuclei. There are, however, two obvious points of difference between pions secondary to χ -decay and pions artificially produced, namely (1) origin from K-decay and (2) shorter time of flight.

Although at the present moment such speculations may appear premature, there may well be some interest in examining the behaviour of secondary particles of K-mesons stopped in a bubble-chamber operating with condensed material, using the established abundance ratios to estimate the percentage of χ -decays in the mixed sample.

Further experiments might be envisaged, for example one in which secondary particles produced by the decay of K-mesons arrested in an absorber of small dimensions are selected with constant momentum by a vacuum spectrograph and are detected after suitably increased time of flight by a conveniently-disposed emulsion block or other detector.

Table IX gives the prong distributions of the observed interactions normalized to a total of 37 χ -secondary observations.

TABLE IX.

Author			PRONGS								Total
			0	1	2	3	4	5	6	7	
FERRARI <i>et al.</i>	120 MeV		0.9	2.9	7.9	10.2	8.4	4.1	2.6	0	37
χ -Secondaries	100 MeV		6	2	5	9	8	3	2	2	37
BERNARDINI, LEVY	75 MeV		0	3.5	10.3	10.0	5.8	4.8	2.0	0.6	37

* * *

As members of the G-Stack Collaboration Group we wish to thank Professor E. J. LOFGREN and the various members of the Bevatron Group for so generously arranging for the exposure of the stack. We wish also to thank all the members of the Bristol Group who took part in the arduous work of processing. We acknowledge with gratitude the excellent work of the members of our scanning team Mrs. MÁIRÍN JOHNSTON, Mrs. JOAN KEFFE, Miss PHYL LEAHY, Miss MOIRA O'BRIEN and Miss NORAH LEAHY, and desire also to thank Dr. E. F. FAHY for supplying some 20 analyzed events found by Miss M. M. O'HEA at University College Cork. Miss E. M. SMITH gave valuable assistance with the computations and Miss RÓISÍN RYAN drew the diagrams, our best thanks are due to them. The construction of the special microscope stages and various modifications of the instruments have been carried out by Mr. J. DALY and we have much pleasure in acknowledging his help.

One of us (R.H.W.J.) wishes to thank the Dublin Institute for Advanced Studies for a Studentship and the other, (G.A.), for a Research Scholarship.

APPENDIX I

Scanning bias. — Experimental evidence.

We have some experimental evidence which substantiates our belief that the method of scanning adopted does not introduce any appreciable selection bias. The 33 plates scanned were divided into two categories, 20 plates with the highest and 13 plates with the lowest mean value of b^* min. The information obtained by each scanner was analyzed on the basis of events found both for the «high» and «low» plates. If a selection bias on the basis of ionization were to exist, then we would expect that the number of $K_{\mu 2}$ particles referred to the number of cases of other modes, would show a significant variation between the «high» and «low» plates. No such evidence could be found and so we conclude, as would be expected, that there is no evidence for the existence of any significant scanning bias. A summary of these results is given in Table X.

The total number of cases of K-decay which occurred at distances from the surface or glass $\geq 10 \mu\text{m}$ was 36 and amounts to 1% of all cases of K-decay observed. This does not appear to be an unreasonable number having regard to the many factors which make it difficult to detect a secondary of unfavourable geometry even after the most rigorous scrutiny of the K-meson ending. It should be borne in mind however that some of these may be cases of K_β decay with emission of a low-energy electron which could not be established in the

TABLE X.

	« High » plates	« Low » plates
No. of plates	20	13
No. of K/plate	102	99
No. of τ /no. of K (total)	0.067	0.071
No. of $K_{\mu 2}$ /no. of K (measured)	0.557	0.552

presence of the rather large background of unassociated low energy background in the plates.

The total number of τ -decays found was 226 and of K-decays, other than τ was 3110 (*). The number found in various classes compared with the expected percentages calculated from dip and shrinkage factor is given in Table XI.

TABLE XI.

Class	Number	Experiment %	Calculated %
A	408	13.4 ± 0.5	12.9
A + B	1107	36.4 ± 0.9	37.9
C	1936	63.6 ± 0.9	62.8

There is a slight indication here of a systematic overestimate of the number of Class A tracks, although the agreement for Class A + B is satisfactory. Since we have had to use these figures in deriving our estimate of the ratio τ'/τ , we feel that the experimental values are the more reliable as systematic uncertainties in estimation of shrinkage factor and dip are difficult to avoid.

APPENDIX II

 K_β decay spectrum. – Correction for energy loss by bremsstrahlung.

As has been seen, the high probability that an electron will suffer a Bremsstrahlung loss in a path length ~ 4 cm in photographic emulsion, coupled with

(*) Includes 67 K_0 .

measured $b^* \sim 1.12$ over the first and fourth cm segments, affords a reliable means of identifying electron tracks in the presence of a background of other fast singly-ionizing particles such as K_{μ} , γ and $K_{\mu 2}$. Thus we may consider that our scheme of measurement will lead to an efficiency ~ 1 of identifying cases of even the highest energy ~ 240 MeV and that uncertainty in the experimental values quoted may be regarded as being entirely statistical.

The effect of radiation loss while essential for purposes of identification, is a hindrance to the estimation of the energy of emission ($p\beta c$) of the secondary track. Clearly, if very short lengths of track are used, the statistical fluctuations in the estimates of $p\beta c$ result in an experimental spectrum which is a distorted image of the true spectrum, the amount of this distortion decreasing as $N^{-\frac{1}{2}}$ where N = number of independent cells used in the measurements ⁽²⁰⁾. As however N , and hence the path length l is increased, so also is the probability of energy loss by radiation and ionization. While the latter fluctuates little, and its effect is readily allowed for, that due to Bremsstrahlung is subject to large straggling the degree of which increases with l ^(21,22). There exists therefore an optimum path-length say λ beyond which gain in statistical accuracy due to an increased N , is counterbalanced by a loss in accuracy due to the straggling of radiation losses. Approximate calculations suggest that the value of λ is ~ 1 cm. It is however necessary to correct the estimate of $p\beta c$ obtained by scattering over path length ~ 1 cm for ionization and radiation loss. Since the ionization is the lesser, and not subject to sensible straggling, it suffices to treat it as being independent of radiation loss.

Assuming that the electron is of sufficient energy and that the screening is complete, the following expression gives the average value of the energy E after a path length l cm of an electron initially of energy E_0

$$(1) \quad E = E_0 \exp [-l/X_0],$$

where X_0 is the value of the radiation length for G.5 emulsion ($= 2.93$ cm if $\beta = 1$). Treating the ionization loss as independent, and of value 6 MeV/cm we may have approximately, l being expressed in cm and the energy in Mev.

$$(2) \quad E_0 = E \exp [l/X_0] + \epsilon l.$$

Hence, if we divide the path of the track into successive segments of say 0.5 cm, we may obtain an estimate by scattering of the value of E corresponding to the mid point of each segment and then correct back to the origin using expression (2). In this way we obtain a series of estimates of E_0 the correction being based on the average value of the radiation loss. Owing however to the increasing fluctuation of the radiation loss, it was not thought advantageous to increase the length of segment corrected beyond 1 cm from the point of decay.

Another mode of correction may be employed. It is well known that the frequency function of the absolute values of second difference obtained by measurements using Fowler's method of constant cell is approximately normal. Considering any electron track of initial energy E_0 , and supposing that we

⁽²⁰⁾ C. O'CEALLAIGH: *Comm. Dublin Inst. Adv. Stud.*, A **10**, 139 (1952).

⁽²¹⁾ H. A. BETHE and H. HEITLER: *Proc. Roy. Soc. London*, **146**, 84 (1934).

⁽²²⁾ L. EYGES: *Phys. Rev.*, **76**, 264 (1949).

perform a series of scattering measurements along the length each of which yields a value of second difference. Then, because of the energy loss by radiation and ionization, the distribution of second difference will no longer be normal but will be less peaked with a longer tail. Using the expressions given by BETHE and HEITLER (21) for the distribution of energy loss by radiation, it is possible to obtain an expression which approximates well to the distribution of second difference for a track subject to Bremsstrahlung loss. It is also possible to compute the values of the mean absolute deviation say μ_0 of this expression for different values of cut-off and for various values of path-length from the point of origin of the electron track. The initial energy E_0 of the track may then be found by use of an expression of the type

$$(p\beta c)_0 = E_0 = K/\mu_0,$$

where K is understood to be the value of the scattering constant appropriate to the cut-off employed and the length of track measured.

A leading advantage of the second procedure, apart from the possibility of allowing for cut-off, is that we may estimate the sampling dispersion of the estimate of μ_0 by means of a simple Monte-Carlo experiment. Calculations are in progress (23) and it is intended to examine the distributions and to complete the values of the truncated moments for path-lengths $l = 0.5$ cm, 1.0 cm, 1.5 cm and 2 cm in order to decide upon the optimum value of l for experiments of this type.

(23) C. O'CEALLAIGH and M. J. O'CONNELL: in progress.

RIASSUNTO (*)

In un grande pacco di emulsioni esposto al fascio di K positivi del Bevatrone di Berkeley sono stati studiati circa 3300 decadimenti di mesoni K . Gli eventi sono stati scelti imparzialmente e sono stati usati per ottenerne informazioni preliminari sulla forma dello spettro d'energia della particella carica emessa nei meno frequenti decadimenti in 3 corpi τ' , χ ($K_{\mu 3}$) e K_β . Nella tabella sono riassunti i risultati della stima dell'abbondanza relativa dei modi di decadimento

Modo	τ	τ'	$K_{\mu 2}$	χ ($K_{\pi 2}$)	χ ($K_{\mu 3}$)	K_β
Abbondanza (%)	6.77 ± 0.45	2.15 ± 0.45	57.0 ± 2.6	23.2 ± 2.2	5.9 ± 1.3	5.1 ± 1.3

Il numero di interazioni, dovute al decadimento di mesoni π secondari a un decadimento χ , osservato dopo i primi 4 cm fornisce per il c.l.m. d'interazione la cifra sorprendentemente bassa di (11.1 ± 2.4) cm. Ciò appare in significativo disaccordo con quella trovata da altri sperimentatori pei mesoni π^+ artificiali e cioè 27 cm nella stessa regione d'energia $(109 \div 82)$ MeV.

(*) Traduzione a cura della Redazione.

Non Linear Effects in the Vacuum Polarization (II).

A. MINGUZZI

Istituto di Fisica dell'Università - Bologna

Istituto Nazionale di Fisica Nucleare - Sezione di Bologna

(ricevuto il 6 Maggio 1957)

Summary. — In this work we have studied the propagation of electromagnetic waves in a constant magnetic field region and it is concluded that the magnetic field region properties are summarized as in anisotropic media by a « dielectric tensor », whose imaginary part is connected with the creation of electron pairs. Some analytical properties of the « dielectric tensor » as function of the constant magnetic field are investigated.

1. — Introduction.

In a preceding paper ⁽¹⁾ (*), hereafter referred to as (I), we have investigated the current induced in the electron vacuum by the simultaneous presence of an arbitrarily varying electromagnetic field and a constant electromagnetic field, which reduces to a constant magnetic field in one frame. The polarization current can be exhibited as a finite, gauge invariant, covariant quantity, which, when the varying field is a radiation field, depends on the derivatives of the radiation field tensor $f_{\mu\nu}(x)$. The calculations have been performed using the exact Green function of the Dirac operator in the constant field and

(*) In the appendix of (I) one must correct a misprint. The b) formula must be read:

$$\lim_{x'' \rightarrow x'} \langle x'(s) | \exp [ik \cdot x^*(s')] \Pi_\mu(s') | x''(0) \rangle = \\ = - \exp [ik \cdot x'] \exp [-\frac{1}{2}N] R_{\mu t}(s') [1 - I(s') I^{-1}(s)]_{rt} k_r \lim_{x'' \rightarrow x'} \langle x'(s) | x''(0) \rangle ..$$

(1) A. MINGUZZI: *Nuovo Cimento*, **4**, 476 (1956).

taking into account only the first order contribution of the radiation field. The polarization current modifies the hamiltonian of the radiation field by adding to the free hamiltonian a term bilinear in the electromagnetic potentials. We shall see that the effective hamiltonian conserves energy-momentum and parity but will in general violate angular momentum conservation. The parity conservation is a feature of the used approximation and we expect that higher order contribution to the current will destroy this invariance.

The eigenvalues of the photon momentum referring to the modes of the propagation along and perpendicularly to the constant field have been calculated. The index of refraction of the « constant field region » is defined by

$$n(\omega) = \frac{k'}{k},$$

where k and k' are the eigenvalues of a one photon momentum with and without respectively the constant field, at equal energy. Owing to the anisotropy introduced by the constant field, $n(\omega)$ will depend on the direction of propagation, on the linear polarization as well as on the frequency ω of the photon.

A constant field of the type discussed above, and a radiation field, if acting separately do not polarize the matter vacuum and consequently do not create electron pairs. This will be no more the case when the two fields act simultaneously and we expect that pairs production becomes effective when the photon frequency exceeds twice the electron mass, if the radiation field interacts with the vacuum only once. Consequently $n(\omega)$ will become complex at this frequency. The role played by the constant field is to supply momentum, as one can argue from classical considerations.

If in this problem the perturbative procedure in respect to the constant field is meaningful, (1) represents the sum of all the graphs in which a single electron loop interacts once with the radiation field and even arbitrary times with the constant field. We will see that the radius of convergence of the power series of (1) in the constant field strength vanishes and this series represents only an asymptotic series of (1).

Energy-momentum conservation allows the splitting of a photon into two or more photons, and equally the inverse processes, if the photons are all correlated in one direction, because of the vanishing photon mass; only parity and angular momentum conservation forbid such processes. But in a constant magnetic field these processes are no more forbidden. Now the photons involved are at least three and in order to calculate the effect one must resort to the vacuum current at least in the second order in the radiation field. Incidentally we notice that due to the small but overall present magnetic field in the galactic spaces, the mechanism of « summing up of photons » could give contribution to the acceleration processes of the cosmic radiation.

2. – Propagation of photons in a constant magnetic field.

The vacuum polarization current, when the varying field is a radiation field is ⁽¹⁾ (*)

$$(1) \quad \langle J_\mu(x) \rangle = \frac{1}{(2\pi)^2} \int d^4k M_1 e^4 h_{\mu i} f_i(k) \exp[ik \cdot x] h_{\nu k} + \\ + \frac{1}{(2\pi)^2} \int d^4k M_2 i e^4 \tilde{h}_{\mu i} f_i(k) \exp[ik \cdot x] \tilde{h}_{\nu k},$$

$$(1') \quad M_1 = \frac{2}{(4\pi)^2} \int_0^1 dv \int_0^\infty ds \left\{ -\frac{1}{e^2 h^2 s} + \right. \\ \left. + \frac{v \sin ehs v \cotg ehs}{eh \sin ehs} + 2 \frac{\cos ehs v - \cos ehs}{eh \sin^3 ehs} \right\} \exp[R'],$$

$$(1'') \quad M_2 = \frac{2}{(4\pi)^2} \int_0^1 dv \int_0^\infty ds \left\{ \frac{1}{e^2 h^2 s} - \frac{\cotg ehs}{eh} \left(1 - v^2 + v \frac{\sin ehs v}{\sin ehs} \right) \right\} \exp[R'],$$

$$R' = -ism^2 - \frac{i}{2} [e^2 k_\mu h_\mu h_\nu k_\nu] \frac{1}{e^2 h^2} \left[\frac{1}{2} s(1 - v^2) - \frac{\cos ehs v - \cos ehs}{eh \sin ehs} \right],$$

where h is the positive definite invariant $\sqrt{\frac{1}{2} h_{\mu\nu} h_{\mu\nu}}$, built with the constant field tensor $h_{\mu\nu}$; $\tilde{h}_{\mu\nu}$ is the dual tensor of $h_{\mu\nu}$ ⁽¹⁾; $f_{\mu\nu}(k)$ is the radiation field tensor. The fact that (1) is finite without the separation of divergent quantities proves that the interaction between « radiation field photons » and « magnetic field photons » converges even if one does not use the perturbative approach, as it must be.

When $h \rightarrow 0$, $\langle J_\mu(x) \rangle \rightarrow 0$ as it must be.

The effective action integral is now

$$W_0 + W_1 = \int L_0(x) d^4x + \int L_1(x) d^4x,$$

where W_0 is the action of the free field and W_1 obeys the equation ⁽²⁾

$$\frac{\delta W_1}{\delta A_\mu(x)} = \langle J_\mu(x) \rangle.$$

(*) The expression (I.11) is obtainable from (1) when substitution $s \rightarrow -is$ and rotation of the integration path is performed. Whereas formula (1) is always valid, (I.11) is true only under the threshold of pair production.

(2) J. SCHWINGER: *Phys. Rev.*, **82**, 664 (1951).

The integration is easily performed and one gets the result

$$W_1 = \frac{1}{2} \int A_\mu(x) \langle J_\mu(x) \rangle d^4x.$$

The effective *c*-number hamiltonian is given by

$$(2) \quad H = H_0 - \frac{1}{2} \int A_\mu(x) \langle J_\mu(x) \rangle d^4x,$$

where H_0 is the free field hamiltonian. The effective *q*-number hamiltonian is obtained by taking the normal product of the r.h.s. of (2).

The effective *q*-number hamiltonian is hermitian as long as M_1 and M_2 are real functions. The invariance properties of this hamiltonian are easily investigated, observing that M_1 and M_2 depend on $k_\mu k_\nu k_\lambda k_\tau$ and $h_{\mu i} h_{\mu i}$ which are invariants in respect to the full Lorentz group. Apart the trivial invariance in respect to space and time translation, in performing space reflection A_μ transforms as x_μ ⁽³⁾ and H is consequently invariant.

In respect to time reversal (3)

$$A_i(x) \rightarrow A_i^\tau(x') = -A_i^\times(x) \quad l = 1, 2, 3$$

$$A_0(x) \rightarrow A_0^\tau(x') = A_0^\times(x),$$

where \times means complex coniugation; as long as H is hermitian it is even invariant in respect to time reversal; but this property is lost when M_1 and M_2 become complex and the irreversible processes of pair production become effective.

In order to test the property of H in respect to rotation, we choose the representation in which the linear momentum p , and the circular polarization, i.e. the spin angular momentum in the direction p of the propagation of the photon are diagonal. In the frame in which the constant field becomes a constant magnetic field pointing in the x_3 -direction, we will limit to the modes of the radiation field corresponding to propagation perpendicular and parallel to the constant magnetic field.

When the photon propagates in the direction of the magnetic field, the transversality condition assures that only $A_1(x_3, x_0)$ and $A_2(x_3, x_0)$ become effective; corresponding $\langle J_\mu(x) \rangle = 0$ and the free propagation go on undisturbed.

(3) JAUCH-ROHRLICH: *Theory of Photons and Electrons* (Cambridge Mass., 1955) p. 86.

On the contrary, when a photon propagates perpendicularly to the magnetic field, for instance along the x_1 -axis, only $A_2(x_1, x_0)$, $A_3(x_1, x_0)$ become effective and $\langle J_\mu((x)) \rangle$ no more vanishes. Now (4)

$$(3) \quad A(x_1, x_0) = (2V)^{-\frac{1}{2}} \sum_{k,\mu} \omega_k^{-\frac{1}{2}} g(k, \mu) \exp[i(kx_1 - \omega x_0)] \epsilon[\mu] + \text{Herm. conj.}$$

where for every k one must sum over the two opposite circular polarizations μ

$$\epsilon[+] = -\frac{1}{\sqrt{2}} [\epsilon_z + i\epsilon_y],$$

$$\epsilon[-] = \frac{1}{\sqrt{2}} [\epsilon_z - i\epsilon_y].$$

Substituting (3) into (2) and by taking the normal product, one gets

$$(4) \quad H - H_0 = -\frac{1}{8} \sum_k e^4 h^2 \omega_k (M_1 - M_2) [g^\dagger(k, +)g(k, -) + g^\dagger(k, -)g(k, +)] - \\ - \frac{1}{8} \sum_k e^4 h^2 \omega_k (M_1 + M_2) [g^\dagger(k, +)g(k, +) + g^\dagger(k, -)g(k, -)].$$

We note incidentally that the space reflection and charge conjugation invariance are tied by the fact that M_1 and M_2 have both even space and charge parity and in respect to the two transformations $g(k, \mu)$ transforms correspondingly (4)

$$g(k, \mu) \rightarrow -g(-k, \mu),$$

$$g(k, \mu) \rightarrow -g(k, \mu).$$

We expect that higher order contributions to the vacuum current will maintain charge conjugation invariance, but will destroy the invariance in respect to space reflection.

The first term on the r.h.s. of (4) shows that H possesses matrix elements between states of opposite circular polarization. It means that, if a right polarized wave enters the magnetic field region, it leaves it as a mixture of right and left polarization. Regarding the initial right polarized wave as the sum of two linearly polarized waves, we are forced to conclude that the two linear waves must propagate in the magnetic field region with different phase velocities. In fact, for propagation normal to the constant magnetic field, the

(4) S. WATANABE: *Rev. Mod. Phys.*, **27**, 40 (1955).

law of motion of $\mathbf{A}(x_1, x_0)$ (*c*-number) is now:

$$(5) \quad \left(\frac{\partial^2}{\partial x_1^2} - \frac{\partial^2}{\partial x_0^2} \right) A_2(x_1, x_0) = -e^4 h^2 M_1 \left(e^2 h^2 \frac{\partial^2}{\partial x_1^2}, e^2 h^2 \right) \frac{\partial^2 A_2(x_1, x_0)}{\partial x_1^2},$$

$$(5') \quad \left(\frac{\partial^2}{\partial x_1^2} - \frac{\partial^2}{\partial x_0^2} \right) A_3(x_1, x_0) = -e^4 h^2 M_2 \left(e^2 h^2 \frac{\partial^2}{\partial x_1^2}, e^2 h^2 \right) \frac{\partial^2 A_3(x_1, x_0)}{\partial x_0^2}.$$

Because the current terms in the r.h.s. of (5), (5'), are exact only in e^2 -approximation we substitute $\partial^2/\partial x_1^2 \rightarrow \partial^2/\partial x_0^2$.

The integration of (5), (5') gives

$$(6) \quad A_2(x_1, x_0) = \int_{-\infty}^{+\infty} A_2^{(P)}(\omega) \exp [i(k_1(\omega)x_1 - \omega x_0)] + \\ + \int_{-\infty}^{+\infty} A_2^{(R)}(\omega) \exp [-i(k_1(\omega)x_1 + \omega x_0)],$$

$$(6') \quad A_3(x_1, x_0) = \int_{-\infty}^{+\infty} A_3^{(P)} \exp [i(k_2(\omega)x_1 - \omega x_0)] + \\ + \int_{-\infty}^{+\infty} A_3^{(R)}(\omega) \exp [-i(k_2(\omega)x_1 + \omega x_0)],$$

where

$$k_1(\omega) = \omega [1 - \frac{1}{2} e^4 h^2 M_1(\omega)], \quad k_2(\omega) = \omega [1 - \frac{1}{2} e^4 h^2 M_2(\omega)]$$

and the two terms on the r.h.s. of (6), (6') represent progressive and regressive waves respectively.

In order to select the physically meaningful solutions we have used the information concerning the negative sign of the imaginary part of M_1 , M_2 , which follows from the unitary condition of the S -matrix; and we have defined the functions $M_1(\omega)$, $M_2(\omega)$, $A(\omega)$ for negative frequencies as:

$$M_1(-\omega) = M_1^*(\omega), \quad M_2(-\omega) = M_2^*(\omega), \quad \mathbf{A}(-\omega) = \mathbf{A}^*(\omega)$$

and $A^{(P)}(\omega)$, $A^{(R)}(\omega)$ are arbitrarily chosen.

Consequently

$$1 - \frac{1}{2} e^4 h^2 M_1(\omega), \quad 1 - \frac{1}{2} e^4 h^2 M_2(\omega)$$

are to be interpreted as « indexes of refraction of the magnetic field region » for waves propagating perpendicularly to the magnetic field, polarized per-

perpendicularly and parallelly respectively to the constant magnetic field. The magnetic field region through the dependence of M_1 and M_2 from the photon frequency, manifests dispersive properties.

For a wave travelling in the direction of the constant magnetic field, the index of refraction is one for every frequency.

As in dielectric media, we can write down the Maxwell-Lorentz equations, by introducing two tensors $f_{\mu\nu}(x)$ and $F_{\mu\nu}(x)$ obeying to:

$$\frac{\partial F_{\mu\nu}}{\partial x_\mu} = 0, \quad \frac{\partial f_{ik}}{\partial x_l} + \frac{\partial f_{kl}}{\partial x_i} + \frac{\partial f_{li}}{\partial x_k} = 0.$$

In the frame in which the constant field becomes a constant magnetic field, the relation between the two tensors is:

$$(7) \quad \left\{ \begin{array}{l} F_{12} = (1 + e^4 h^2 M_1) f_{12}, \\ F_{34} = (1 + e^4 h^2 M_2) f_{34} \end{array} \right.$$

all other components being equal.

When the varying field is generated by a current distribution $J_\mu(x)^{\text{ext}}$, one can again write down the Maxwell-Lorentz equations using the renormalized external current $J_\mu(x)^{\text{ren}}$. In this case the relation between the tensors $f_{\mu\nu}(x)$ and $F_{\mu\nu}(x)$ in respect to (7), involves another term which arises from the vacuum polarization current depending from $J_\mu(x)^{\text{ext}}$, and a generalization of the functions M_1 and M_2 (1).

3. - Properties of the M_1 and M_2 functions.

The M_1 and M_2 functions need some comment because the integrals over s which define them, possess essential singularities on the real s -axis at the points $s_n = n\pi/e\hbar$, with $n = 1, 2, 3, \dots$. We fix the indentation by requiring that as long as the photon frequency do not exceed two times the electron masses, the current $\langle J_\mu(x) \rangle$ and consequently M_1 and M_2 must be real quantities. In order to do so, we shift the singularities of the integrals upwards in the complex s -plane (Fig. 1) and we deform the integration path of v between 0 and 1 with a small detour under the real v -axis at the point $m^2 - (\omega^2/4) \cdot (1 - v^2) = 0$. This amounts to the substitution

$$m^2 \rightarrow m^2 - i\varepsilon$$

and

$$\operatorname{cosec} ehs \rightarrow \operatorname{cosec} ehs' = \operatorname{cosec} ehs(1 - ix)$$

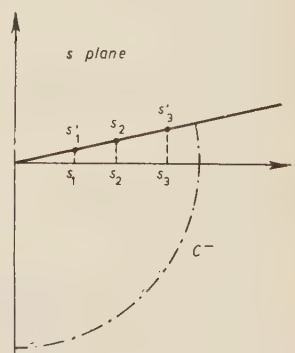


Fig. 1.

and the modifications which assure that the integral does not diverge at $s = 0$ and we take the limit for $\alpha, \varepsilon \rightarrow 0$. Now if $\omega < 2m$, $m^2 - (\omega^2/4)(1 - v^2)$ never vanishes and the path of integration of s can safely be continued to C^- (Fig. 1). Consequently it is allowed to rotate the integration path with the result:

$$(8) \quad M_1(\omega) = \frac{2}{(4\pi e h)^2} \int_0^1 dv \int_0^\infty ds \left\{ -\frac{1}{s} + \frac{e h v \sinh e h s v \operatorname{ctnh} e h s}{\sinh e h s} - \frac{2 e h}{\sinh^3 e h s} [\cosh e h s v - \cosh e h s] \right\} \exp [R],$$

$$M_2(\omega) = \frac{2}{(4\pi e h)^2} \int_0^1 dv \int_0^\infty ds \left\{ \frac{1}{s} - e h \operatorname{ctnh} e h s \left[1 - v^2 + v \frac{\sinh e h s v}{\sinh e h s} \right] \right\} \exp [R],$$

$$R = -s m^2 + \frac{s \omega^2}{4} (1 - v^2) + \frac{\omega^2}{2} \frac{\cosh e h s v - \cosh e h s}{e h \sinh e h s},$$

which show that M_1 and M_2 are real finite functions of ω .

If $\omega > 2m$, it is convenient to perform an integration by parts over s

$$(9) \quad M_2(\omega) = -\frac{2i}{(4\pi e h)^2} \lim_{\alpha, \varepsilon \rightarrow 0} \int_0^1 \frac{dv}{m^2 - i\varepsilon - (\omega^2/4)(1 - v^2)} \cdot$$

$$\cdot \int_0^\infty ds \exp \left[-is \left[m^2 - i\varepsilon - \frac{\omega^2}{4} (1 - v^2) \right] \right] \frac{d}{ds} \cdot$$

$$\cdot \left\{ \left[\frac{1}{s'} - e h \frac{\cos e h s}{\sin e h s} \left(1 - v^2 + \frac{v \sin e h s' v}{\sin e h s'} \right) \right] \exp \left[-\frac{i\omega^2}{2e h} \frac{\cos e h s v - \cos e h s}{\sin e h s'} \right] \right\},$$

The condition which assures that the integration over v in (9) is meaningful is that

$$(10) \quad \int_0^\infty ds \exp \left[-is \left[m^2 - \frac{\omega^2}{4} (1 - v^2) \right] \right] \frac{d}{ds} \cdot$$

$$\cdot \left\{ \left[\frac{1}{s'} - e h \frac{\cos e h s}{\sin e h s} \left(1 - v^2 + \frac{v \sin e h s' v}{\sin e h s'} \right) \right] \exp \left[-\frac{i\omega^2}{2e h} \frac{\cos e h s v - \cos e h s}{\sin e h s'} \right] \right\},$$

is a continuous function of $m^2 - (\omega^2/4)(1 - v^2)$. Using de la Vallée Poussin's test, one can show that (10) converges uniformly whichever is $m^2 - (\omega^2/4)(1 - v^2)$ and from this it is straightforward to conclude that (10) is continuous in $m^2 - (\omega^2/4)(1 - v^2)$.

Along the same lines one obtains

$$\begin{aligned}
 M_1(\omega) = \lim_{\alpha, \varepsilon \rightarrow 0} & -\frac{2i}{(4\pi e h)^2} \int_0^1 \frac{dv}{m^2 - (\omega^2/4)(1-v^2)} - \\
 & - i\varepsilon \int_0^\infty ds \exp \left[-is \left[m^2 - \frac{\omega^2}{4}(1-v^2) - i\varepsilon \right] \right] \frac{d}{ds} \left\{ \left[-\frac{1}{s'} + \frac{ehv \sin ehs' v \cos ehs}{\sin^2 ehs'} + \right. \right. \\
 & \left. \left. + \frac{2eh(\cos ehs' v - \cos ehs')}{\sin^3 ehs'} \right] \exp \left[-\frac{i\omega^2}{2eh} \frac{\cos ehs v - \cos ehs}{\sin ehs'} \right] \right\}. \quad (*)
 \end{aligned}$$

The number of electron pairs created per unit time and volume can be stated by exploiting the unitarity property of the S -matrix or more simply dividing the energy absorbed per unit time and volume by the photon energy.

By keeping coherently only the e^2 -approximation terms, one gets when the polarization of the radiation field is perpendicular to the constant magnetic field:

Number of pairs per unit time and volume = $-\int dk |E(k)|^2 \{I.P. e^{4h^2} M_2(k)\}$, where $E(k)$ is the electric field strength of the radiation field. It follows that the imaginary parts of M_1 , M_2 must be negative whichever is the frequency.

The calculations have been performed by assuming that the radiation field is small, and the perturbative approach is reliable at least in the sense of an asymptotic series. The problem arises to inspect the properties of M_1 and M_2 as functions of eh . Various authors (6) have investigated the analytical properties of the energy of the electron in a magnetic field and have concluded, that due to the vanishing photon mass, the Taylor series in eh of this energy has a vanishing radius of convergence. We will study the static index of refraction $M_2(\omega=0)$. If in (8) one puts $\omega=0$, integrates over v and performs the change of variable $s \rightarrow ehs$, one obtains:

$$(11) \quad M_2(\omega=0) = \frac{2}{(4\pi e h)^2} \int_0^\infty \exp[-ps] [\Phi(s) + \Psi(s)] ds,$$

(*) Work is in progress in order to test the two physical requirements which must be fulfilled by the index of refraction namely; a) is the imaginary part of the index of refraction a positive definite function of the frequency? b) Is the index of refraction almost everywhere the limit to the real ω -axis from above of a function analytic in the upper part of the complex ω -plane, i.e. is the causality requirement satisfied? (5).

(5) J. S. TOLL: *Phys. Rev.*, **104**, 1760 (1956).

(6) S. N. GUPTA: *Nature*, **163**, 686 (1949); M. DEMEUR: *Ac. Roy. Belg. Sci.*, **28**, fasc. 5 (1953); R. G. NEWTON: *Phys. Rev.*, **96**, 523 (1954).

where $p = m^2/e\hbar$ and

$$\Phi(s) = -\frac{L^2(s)}{s}; \quad \Psi(s) = -\frac{2}{3} L(s) - \frac{L(s)}{s^2} + \frac{1}{3s},$$

and $L(s)$ is the Langevin function $\cot g hs - 1/s$, whose power series around the point $s = 0$ converges uniformly when $|s| < \pi$. Performing in (8) successive integrations by parts one gets:

$$(12) \quad M_2(0) = \frac{2}{(4\pi m^2)^2} \left\{ \Phi^{(1)} + \Psi^{(1)} + \frac{\Phi^{(3)} + \Psi^{(3)}}{p^2} + \dots + \frac{\Phi^{(2n-1)} + \Psi^{(2n-1)}}{p^{2n-2}} + \right. \\ \left. + \frac{1}{p^{2n-1}} \int_0^\infty \exp[-ps] [(\Phi(s))^{(2n+1)} + (\Psi(s))^{(2n+1)}] ds, \right.$$

where $\Phi^{(k)} = (d^k \Phi(s)/ds^k)_{s=0}$ and observing that $\Phi^{(2n)} = \Psi^{(2n)} = 0$. Now

$$\Phi^{(2n-1)} = (-1)^n \left[\frac{2}{3} \frac{2^{2n}}{2n} B_n - \frac{2^{2n+2}}{2n(2n+1)(2n+2)} B_{n+1} \right], \\ \Psi^{(2n-1)} = (-1)^n 2^{2n+2} (2n-1)! \sum_1^n \frac{B_m B_{n+1-m}}{(2m)! [2(n+1-m)]!},$$

and B_r are the Bernouillian numbers:

$$B_r = \frac{(2r)!}{\pi^{2r} 2^{2r-1}} [1 + A_r], \quad A_r = \frac{1}{2^{2r}} + \frac{1}{3^{2r}} + \frac{1}{4^{2r}} + \dots.$$

The two power series in the square brackets of (12) are consequently two alternating series, whose coefficients corresponding to the same power of $1/p$ have the same sign. In fact

$$\frac{(2n-1)!}{\pi^{2n}} \left[\frac{2}{3} - \frac{1}{\pi^2} \right] [1 + A_n] < \left[\frac{2}{3} \frac{2^{2n}}{2n} B_n - \frac{2^{2n+2} B_{n+1}}{2n(2n+1)(2n+2)} \right] < \\ < \frac{(2n-1)!}{\pi^{2n}} \left[\frac{2}{3} - \frac{1}{\pi^2} \right] [1 + A_{n+1}].$$

The divergence of one of the two series assures the divergence of the full series. The Cauchy convergence test applied to the series with $\Phi^{(k)}$ coefficients

$$\left| \frac{\Phi^{(2n-1)}}{p^{2n-2}} \right| : \left| \frac{\Phi^{(2n-3)}}{p^{2n-4}} \right| > \frac{1}{p^2} \frac{(2n-1)!}{(2n-3)!} \frac{\pi^{2n+2}}{\pi^{2n}} \frac{1 + A_{n+1}}{1 + A_{n-1}},$$

is such that the

$$\lim_{n \rightarrow \infty} \left[\frac{1}{p^2} \pi^2 (2n-1)(2n-2) \frac{1+A_{n+1}}{1+A_{n-1}} \right] \rightarrow \infty,$$

whatever is p and the series diverges.

On the contrary the test of asymptotic convergence (7) is fulfilled by the whole series; in fact

$$\lim_{p \rightarrow \infty} \left[p^{2n-2} \frac{1}{p^{2n-1}} \int_0^\infty \exp[-ps] [\Phi(s)^{(2n+1)} + \Psi(s)^{(2n+1)}] ds \right] \rightarrow 0.$$

This means that corresponding to a magnetic field strength eh there is an optimum number of terms of the power series (12) which approximates M_2 and the corresponding unavoidable error can be made smaller the smaller is eh .

We note that if the integration over s instead of ranging between zero and infinity would have ranged between zero and some finite s_0 , which can be considered a device for introducing a finite photon mass, the corresponding power series would have been convergent, with a radius of convergence

$$R \propto \frac{\pi}{s_0},$$

where π enters being the radius of uniform convergence of the Taylor series of the Langevin function. This result shows again that the power series diverges because of the vanishing of the photon mass and of the finite range of uniform convergence of $L(s)$. Now $M_2(\omega)$ with arbitrary ω in respect to the static $M_2(0)$ contains additional expressions in which cosech ehs enters, and due to the fact that cosech x has the same finite radius of uniform convergence of $L(x)$, we expect that the conclusion drawn at $\omega = 0$ about the divergence of the power series in eh , is valid for arbitrary ω .

RIASSUNTO

In questo lavoro si è studiata la propagazione di onde elettromagnetiche in una regione in cui agisce un campo magnetico costante; come accade nei mezzi anisotropici, la regione del campo magnetico è descritta da un « tensore dielettrico », la cui parte immaginaria è connessa colla creazione di coppie di elettroni. Si sono esaminate alcune proprietà analitiche del « tensore dielettrico » in funzione del campo magnetico costante.

(7) E. T. WHITTAKER and G. N. WATSON: *Modern Analysis* (Cambridge 1952), p. 150.

High Sensitivity Transistor Pulse Trigger Circuit.

E. ZAGLIO

Istituto di Fisica Sperimentale del Politecnico - Milano

(ricevuto il 7 Maggio 1957)

Summary. — A high sensitivity current pulse discriminator is described. It is obtained by using a germanium diode and a differential negative resistance of high stability consisting of a transistor amplifier with a positive feedback. The threshold can be set in the range of 5 to 50 μA , its stability being of the order of 1%.

1. — Introduction.

Discriminators in the region of millivolts introduced by KANDIAH ⁽¹⁾ and developed in a successive work ⁽²⁾ have shown that it is possible to construct simple precision instruments for pulse integral counting.

Following this line, an instrument based on the same principle has been studied: a transistor amplifier has been used to obtain the negative differential resistance and a germanium diode to obtain the positive one.

As it is well known, the following equation stands for a germanium diode in a limited range of voltage:

$$I = I_0 \left(\exp \left[\frac{eV}{KT} \right] - 1 \right),$$

and consequently the differential conductance is

$$G = \frac{dI}{dV} = \frac{eI}{KT} \exp \left[\frac{eV}{KT} \right] = \frac{e}{KT} (I + I_0).$$

⁽¹⁾ K. KANDIAH: *Proc. Inst. Electr. Eng.* II, **101**, 239 (1954).

⁽²⁾ S. BARABASCHI, C. COTTINI and E. GATTI: *Nuovo Cimento*, **2**, 1042 (1955).

If a relatively high steady current I is made to flow through the diode, we may neglect I_0 with respect to I and say roughly that the differential conductance of the diode is defined provided the current I in the diode and the temperature is stabilized.

2. – Description of the instrument.

To obtain a stable negative differential resistance we have used a three stage transistor amplifier (Fig. 1) whose voltage gain from input E and output U is stabilized at 50 by voltage divider R_1, R_2 .

Input resistance is $50 \text{ k}\Omega$ and output resistance is 100Ω ; rise time is about $5 \cdot 10^{-7} \text{ s}$, while loop gain is about 100.

Starting from this amplifier, a stable negative differential resistance between the input terminals was obtained by means of a positive feedback from the output to the base of the first transistor.

This negative resistance is obviously given by

$$R_{\text{neg}} = \frac{R}{A-1},$$

where R is the positive feedback resistance and A the amplifier gain.

Germanium diode OA5 was connected in parallel to the input terminals; the signal pulse, injected into the same terminals, varied directly the steady current in the diode that was maintained at a fixed constant level by a high resistance from stabilized voltage supply.

The instrument is therefore a current threshold circuit, the threshold being dependent on the steady rest current. By varying this current it is possible to cover the range from 5 to 50 μ A. The instrument can work when directly connected to the output of a photomultiplier; the output pulse of the instrument is negative of about 12 V amplitude, and can be sent directly to a scaler.

The output signal, present even if the input signal level is below the threshold has to be maintained sufficiently low in order to obtain that the resistances R and R' were varied linearly and at the same time.

Moreover, a linear relationship between the steady rest current and the signal threshold level is obtained. The threshold was found nearly unvaried both in the short and long run, the percentage variation being better than 1%.

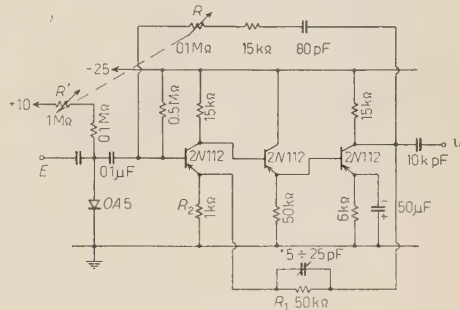


Fig. 1. — Discriminator scheme.

Drift of the threshold due to changes of temperature has been noted, though little, being about $0.1 \mu\text{A}$ per $^{\circ}\text{C}$.

The instrument was constantly tested by means of negative exponential current pulses, with a time constant of $2.5 \cdot 10^{-7} \text{ s}$, similar to those it would receive if connected to a photomultiplier with sodium-iodide scintillator. However the sensitivity of the instrument has shown to increase with the pulse duration, as reported in Fig. 2.

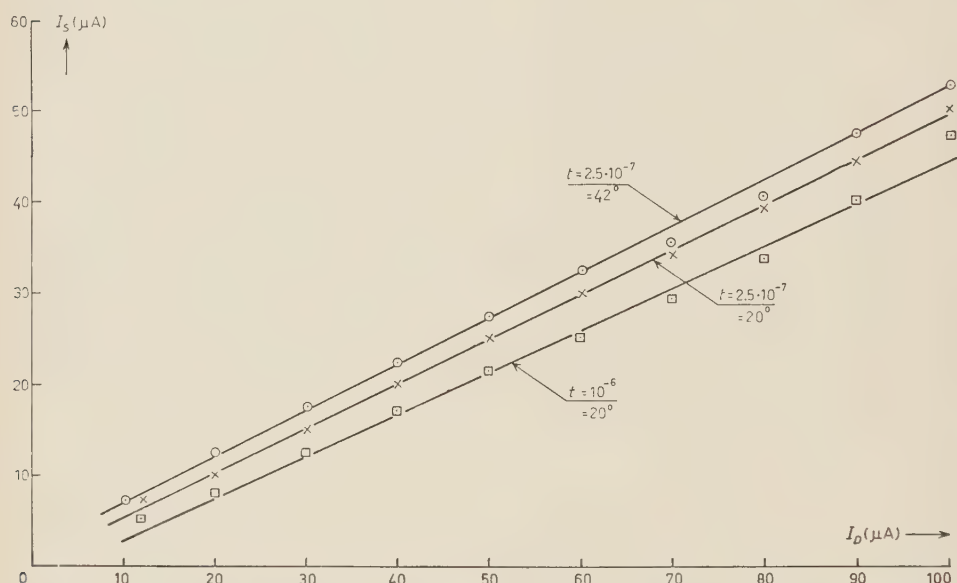


Fig. 2. — Experimental values of the threshold current as function of the steady rest current in the diode.

The noise of the transistors is quite effectiveless on the operation of the instrument; in fact, at a threshold value of $25 \mu\text{A}$, the uncertainty of threshold is held at about 1% of the level of input pulses, and it has not been found if this percentage was due to the noise in transistors or to disturbances in the power supply or superimposed to test signals.

In the circuit diagram shown in Fig. 1 it is noted that the transistor amplifier is a d.c. one, to obtain good recovering proprieties after a pulse; negative feedback is obtained by means of a compensated divider formed by resistors R_1 and R_2 ; positive feedback is due to resistor R , in series with a capacitor to obtain a given pulse duration.

Experimental values of the threshold current as function of steady rest current in the diode are given in Fig. 2; the rest current in the diode is in abscissa while the amplitude of the input current signal which caused trig-

gering is in ordinate. The measurements are with an error of a 1% in reading diode currents, and 2.5% in reading signal level.

Work temperature and the time constant of the exponential pulses used are indicated with each diagram.

* * *

I wish to express prof. BOLLA and prof. GATTI my thanks for their kind interest.

RIASSUNTO

Si descrive un discriminatore di impulsi di corrente di elevata sensibilità, ottenuto usando un diodo al germanio ed uno a resistenza differenziale negativa di grande stabilità, ottenuta mediante un amplificatore a transistors con reazione positiva. La soglia può essere variata nel campo tra 5 e 50 μ A e la sua stabilità è dell'ordine dell'1%.

The π - μ -e Asymmetry.

D. H. WILKINSON

Cavendish Laboratory - Cambridge

(ricevuto il 9 Maggio 1957)

Summary. — By comparing the apparent asymmetry of the μ -e decay observed for μ -mesons stopping in Ilford G5 nuclear emulsion in cyclotron experiments with that for « non-quenching » substances such as graphite it is possible to measure γ_{G5} , the probability that the μ -meson forgets its orientation on stopping in nuclear emulsion. This determination is independent of the degree of polarization of the μ -meson beam. This result may then be combined with the apparent asymmetry $1+A \cos \theta$ directly observed for π - μ -e events in nuclear emulsion to find the true asymmetry $1+\alpha \cos \theta$ for the fundamental π - μ -e process for all electrons observed without energy discrimination. A combination of results from the Columbia and Chicago cyclotron groups gives $\gamma_{G5}=0.55 \pm 0.03$. A combination of results from eight groups of emulsion workers gives $A=-0.129 \pm 0.015$. These yield $\alpha=-0.287 \pm 0.039$ which corresponds to the value of the parameter of the two-component neutrino theory $\xi=0.87 \pm 0.12$.

1. — Introduction.

It is now very well established by many experiments that parity conservation and charge conjugation both break down in both legs of the π - μ -e chain of decays. This was first demonstrated unequivocally in the experiments of GARWIN, LEDERMAN and WEINRICH ⁽¹⁾ with contemporaneous evidence coming from FRIEDMAN and TELELDI ⁽²⁾. It is now of importance to make this quantitative. Ideally we should measure the angular correlation $1+\alpha \cos \theta$, where θ

⁽¹⁾ R. L. GARWIN, L. M. LEDERMAN and M. WEINRICH: *Phys. Rev.*, **105**, 1415 (1957).

⁽²⁾ J. FRIEDMAN and V. L. TELELDI: *Phys. Rev.*, **105**, 1681 (1957) and private communication.

is the angle between the directions of emission of the μ -meson and the decay electron as a function of the energy of the decay electrons. Such measurements can and have been made (³) using moderated beams of μ -mesons derived from the decay in flight of π -mesons made by cyclotrons. Such measurements depend on the assumption that the moderated μ -mesons retain their initial spin orientation until they decay viz. that there is no « quenching » of the initial polarization by the moderating medium. It is assumed that such quenching would take place chiefly after the moderation (⁴). There exist many substances—graphite and several metals—which exhibit just the same apparent asymmetry in the cyclotron experiments and so it is very reasonable to suppose that for them the quenching is very small. However these measurements also depend on the assumption that the degree of polarization of the μ -meson beam from the cyclotron is whatever is given by the breakdown of parity and charge conjugation in the π - μ decay. This is equivalent to saying that all μ -mesons in the beam must have originated from *forward* emission in the rest system of the π -meson, viz. in the direction of the beam. At the moment the polarization of the cyclotron μ -meson beams has not been measured directly and the hope that it is high derives solely from ideas about the π -meson production at the target and the kinematics of the decay process. This means that even if the delicate questions of the energy sensitivity of the electron detector and the « folding-out » of its (considerable) angular acceptance are satisfactorily resolved the asymmetries observed with the cyclotron beams still cannot be immediately interpreted. The problem would be solved if the π - μ -e process could be *wholly* observed inside one of the substances for which we can infer that the quenching is small. This is not possible. The only substances within which it is at the moment practicable to observe the whole π - μ -e chain are nuclear emulsions and fluids which operate in bubble chambers. In such detectors the geometry is precisely defined and all electrons are detected without regard for their energy. But the observed correlation $1 + A \cos \theta$ is not the desired fundamental correlation because it is known from the cyclotron experiments that nuclear emulsion and the bubble chamber hydrocarbons show considerable quenching of the μ -meson spin. However as was pointed out earlier (⁵) one may make use of the cyclotron experiments accurately to measure the quenching in a chosen substance irrespective of the unknown degree of polarization of the cyclotron μ -meson beam and of poor geometry and unknown energy response so long as the set-up is identical for the chosen substance and for the unquenching comparator such as graphite.

(³) L. M. LEDERMAN: *Report to the 1957 Rochester Conference*.

(⁴) L. WOLFENSTEIN: *Phys. Rev.*, **75**, 1664 (1949).

(⁵) G. B. CHADWICK, S. A. DURRANI, L. M. EISBERG, P. B. JONES, J. W. G. WIGNALL and D. H. WILKINSON: *Phil. Mag.*, **2**, 684 (1957).

So far no very accurate measurements of the correlation have been reported from bubble chambers. In any case it would not be very simple to use liquid hydrocarbons at high temperature and pressure in the cyclotron experiment to measure the quenching. Such quenching measurements are however easy to make with nuclear emulsion. Quite good values of A are also available from several laboratories for the $\pi\text{-}\mu\text{-}e$ asymmetry observed in emulsion. It is the object of this paper to gather together the relevant data and use them to find the best present value of the true fundamental correlation $1 + \alpha \cos \theta$.

2. – The quenching in nuclear emulsion.

It seems that the quenching of Ilford G5 emulsion is a rather good constant. At least 16 different batches of such emulsion have been tested at the Columbia (^{1,3}) and Chicago (⁶) cyclotrons at temperatures from that of liquid air to room temperature and no departure from uniform behaviour has been found. It is also established that the quenching is rapid and does not seem to be a function of time after the arrest of the μ -meson. We therefore seek γ_{G5} as before (⁵) as the fraction of all polarised μ -mesons stopping in ordinary G5 emulsion which lose their memory of their initial spin direction.

From the published Columbia work (¹) and from further data supplied by Professor LEDERMAN we find the Columbia value using graphite as the comparator $\gamma_{G5} = 0.48 \pm 0.07$. The corresponding figure derived from the Chicago data (⁶) using graphite and certain metals as comparators is $\gamma_{G5} = 0.56 \pm 0.03$. We combine these data and use $\gamma_{G5} = 0.55 \pm 0.03$.

3. – The asymmetry in nuclear emulsion.

Many groups of workers, most of them stimulated by reports of the encouraging results being obtained by FRIEDMAN and TELELDI (²) have measured the asymmetry coefficient A found for the $\pi\text{-}\mu\text{-}e$ correlation in nuclear emulsion. Their results are shown in Table I.

The total number of events represented by this table is more than 16 000.

A word is necessary about the two Cambridge results. Cambridge I is that measured in ordinary G5 emulsion. Cambridge II is the result obtained

(⁶) N. P. CAMPBELL, E. L. GARWIN, J. C. SENS, R. A. SWANSON, V. L. TELELDI, S. C. WRIGHT and D. D. YOVANOVITCH: *Report to the 1957 Rochester Conference*. Also private communication from Dr. WRIGHT and Professor TELELDI.

in twice diluted emulsion which has been here corrected to its value in ordinary emulsion for purposes of inclusion in this table (*).

TABLE I.

Group	<i>A</i>
Bristol (7)	— 0.08 ± 0.05
Cambridge I (5)	— 0.149 ± 0.033
Cambridge II (5)	— 0.142 ± 0.035
Chicago (2)	— 0.174 ± 0.038
Copenhagen (8)	— 0.17 ± 0.07
Göttingen (3)	— 0.095 ± 0.044
Minnesota (10)	— 0.030 ± 0.038
Rochester (11)	— 0.19 ± 0.06
Rome (12)	— 0.222 ± 0.067

Before combining these results we must ask if they form a consistent set. This we do in the usual way finding $\chi^2 = 13.5$ which, with 8 degrees of freedom, corresponds to $P = 0.10$. Since this is better than the usual 5% level of

(*) To reduce the results found in twice diluted emulsion ($A = -0.190 \pm 0.033$) to ordinary G5 emulsion we must know the relative numbers of μ -mesons stopping in the halide and in the gelatine and the relative quenching powers of the two components. Earlier (5) it was assumed that the numbers of positive μ -mesons stopping in heavy and light elements stood in same ratio as for negative particles namely about 7:3. This is probably wrong as can be seen by examining the measured proton range-energy relations for protons at the lowest energies. The correct ratio is probably nearer 1:1 which we use here. (A discussion of this point with Dr. J. OREAR was very useful). The correction is very insensitive to this assumed ratio however. As to the quenching we may take it to be complete in the halide or about 90% as may be indicated by cyclotron asymmetry measurements on silver bromide (3). Again this correction is insensitive to the choice. Extreme variations in the assumptions lead to correction factors differing by only about 10%. We have quoted the value of A reduced from the twice diluted to ordinary emulsion using the stopping ratio 1:1 and complete quenching in the halide. The standard deviation of this corrected result would be ± 0.025 ; this has been increased to ± 0.035 which amply covers the uncertainty in evaluating the correction.

(7) B. BHOWMIK, D. EVANS and D. J. PROWSE: *Nuovo Cimento*, **5**, 1663 (1957).

(8) J. K. BOGGILD, K. HANSEN and M. SCHARFF: *Report to 1957 Rochester Conference*.

(9) N. N. BISWAS, M. CECCARELLI and J. CRUSSARD: *Nuovo Cimento*, **5**, 756 (1957).

(10) P. H. FOWLER, P. S. FREIER, C. M. G. LATTEES, E. P. NEY and S. J. ST. LORANT: *Report to the 1957 Rochester Conference*.

(11) D. DAVIS, A. ENGLER, C. GOEBEL, T. F. HOANG, M. F. KAPLON and J. KLARMANN: *Report to the 1957 Rochester Conference*.

(12) C. CASTAGNOLI, C. FRANZINETTI and A. MANFREDINI: *Nuovo Cimento*, **5**, 684 (1957).

significance we are not able to conclude that these results may not be combined. We may note in passing, however, that more than half this value of χ^2 is contributed by the low Minnesota result (*); had this been excluded we should have found $P = 0.6$. The value of $P = 0.1$ for all the results does not justify exclusion of the Minnesota point so we retain it and find the best mean value $A = -0.129 \pm 0.015$.

4. – The true asymmetry.

The above values for γ_{G5} and A are now combined to yield the true asymmetry coefficient for the fundamental process for all electrons without energy discrimination

$$\alpha = -0.287 \pm 0.039 .$$

The best values for the asymmetry coefficient observed directly with the cyclotron beams, corrected for the angular resolution and extrapolated to zero energy of the decay electrons, seem to run around $A \sim 0.26$ (3,6,13). This, taken in conjunction with the present value for α seems to indicate a polarization for the cyclotron μ -meson beams of about 90% although complete polarization is obviously not excluded.

We may also note that the above result for α is consistent with the two component neutrino theory (14,15) which allows (14) the extreme value $\alpha = -\frac{1}{3}$. The above result corresponds in the notation of LEE and YANG (14) to

$$\xi = (|f_A|^2 + |f_V|^2)^{-1} (f_V f_A^* + f_A f_V^*) = 0.87 \pm 0.12 .$$

These agree well with earlier (5) less accurate values.

It therefore seems quite possible that the extreme asymmetry allowed by the two component theory is not realized in this process although we must remark that if our assumption that there is no quenching in graphite and some metals is incorrect then α must be raised.

(*) A sample of the same emulsion as was used by the Minnesota group has been tested at the Chicago cyclotron (6) and found to show the same asymmetry as other samples.

(13) J. M. CASSELS, T. W. O'KEEFE, M. RIGBY, A. M. WETHERELL and J. R. WOERMAULD: *Proc. Phys. Soc. (London)*, A **70**, 543 (1957).

(14) T. D. LEE and C. N. YANG: *Phys. Rev.*, **105**, 1671 (1957).

(15) L. LANDAU: *Nuclear Physics*, **3**, 127 (1957); A. SALAM: *Nuovo Cimento*, **5** 299 (1957); B. F. TOUSCHEK: *Nuovo Cimento*, **5**, 754 (1957).

* * *

This paper draws from the work of about fifty people. Many people have been very generous in allowing the use of unpublished work which they had reported at the 1957 Rochester Conference: Dr. SCHARFF that of the Copenhagen group; Dr. P. H. FOWLER that of the Minnesota group; Professor M. F. KAPLON that of the Rochester group. I have also been very grateful for much information from Professor L. M. LEDERMAN about the Columbia cyclotron work and from Professor V. L. TELELDI and Dr. S. C. WRIGHT about the Chicago cyclotron work. Without the help of all these people this report could not have been put together at this time.

RIASSUNTO (*)

Confrontando l'apparente asimmetria del decadimento μ -e osservata nei mesoni μ arrestati in emulsioni nucleari Ilford G-5 negli esperimenti al ciclotrone con quella data da sostanze prive di smorzamento come la grafite, è possibile misurare γ_{G5} , la probabilità che il mesone μ dimentichi la sua orientazione arrestandosi nelle emulsioni nucleari. Tale determinazione è indipendente dal grado di polarizzazione del fascio di mesoni μ . Si può allora combinare questo risultato con l'asimmetria apparente $1 + A \cos \theta$ direttamente osservata negli eventi π - μ -e in emulsioni nucleari per trovare l'asimmetria vera $1 + \alpha \cos \theta$ per il processo π - μ -e fondamentale per tutti gli elettroni osservati senza discriminazione d'energia. La combinazione dei risultati dei gruppi dei ciclotroni di Columbia e di Chicago dà $\gamma_{G5} = 0.55 \pm 0.03$. La combinazione dei risultati di otto gruppi di sperimentatori con lastre dà $A = -0.129 \pm 0.015$. Ne risulta $\alpha = -0.287 \pm 0.039$, che corrisponde al valore del parametro della teoria del neutrino a due componenti $\xi = 0.087 \pm 0.12$.

(*) Traduzione a cura della Redazione.

Charge Conjugation and Angular Momentum.

C. B. VAN WYK

University of Orange Free State - Bloemfontein, South Africa

(ricevuto il 14 Maggio 1957)

Summary. — The formal correspondence between spin and charge as implied by the idea of isobaric spin, is explained by showing that rotations in three- and four-dimensional spaces can be expressed as generalized phase transformations. Reflections in three dimensions are also expressed as phase transformations, the eigenfunctions of which are linearly related to those of suitable rotations. It is shown that the Kramers-Pauli charge conjugation is the charge analogue of spin in four dimensions. Hence the charge conjugation formalism presents a spin angular momentum framework which is applicable to particles with two types of spin. The four-dimensional orbital angular momentum eigenfunctions are given as a generalization of spherical harmonics.

1. — Introduction.

According to the ideas underlying isobaric spin, mathematical formalisms that are suitable for the description of angular momentum states are also suitable for the description of certain charge states. For example, the spin states of a particle with spin unity and the three charge states of a pion can be described by the same formalism.

In the theory of the electron the relativistic description of a single charge state is impossible and the two pairs of charge and spin states are grouped together in a four-component wave function. This inter-relatedness of spin and charge and the resulting particle-antiparticle structure of the Dirac theory tends to obscure the correspondence between the spin and charge descriptions. However, closer examination shows that the Kramers-Pauli charge conjugation formalism describes both the spin and charge of the electron.

The first purpose of this paper is to show that the correspondence between

charge and spin as expressed by the isobaric spin formalism stems from the fact that three- and four-dimensional rotations can be expressed as generalized phase transformations. Thus the physical requirements of invariance under rotations and conservation of charge are both ensured by the single mathematical property of invariance under phase transformations.

Secondly, it will be shown that a representation of four-dimensional (Euclidean) rotations exists that has the structure of the charge conjugation formalism. Since angular momentum in four-dimensional space resolves into two sets of three-dimensional angular momenta, the angular momentum description that utilises all the freedom offered by the formalism of charge conjugation, can only be applied to the case of particles with two types of spin.

Thirdly, it will be pointed out that a reflection in three-dimensional space can also be represented by a phase transformation, the eigenstates of which have the charge self conjugate property.

In Sect. 2 a theorem about skew-symmetric hermitean matrices is proved. Applied to a three-dimensional rotation this theorem exhibits the basic properties of the spin states of a particle with spin unity. Sect. 3 shows how single- and double-valued, finite four-dimensional rotations can be expressed as phase transformations in terms of the same form for the infinitesimal rotation. The application of the theorem to the double-valued case shows that the various spin states are connected by the Kramers charge conjugation relation. In Sect. 4 the four-dimensional orbital angular momentum eigenfunctions Υ_{jmn} are defined and the charge self conjugate symmetry of $\Upsilon_{\frac{1}{2}mn}$ (the Cayley-Klein parameters) indicated. In Sect. 5 the spin-charge correspondence is discussed while Sect. 6 deals with the charge self conjugate symmetry of reflections in three dimensions.

2. — Rotations in three dimensions.

Theorem. If λ is an eigenvalue belonging to the normalized non-trivial eigenvector \mathbf{u}_λ of a skew-symmetric hermitean matrix then

- \mathbf{u}_λ is real only if $\lambda = 0$ while $\mathbf{u}_\lambda \cdot \mathbf{u}_\lambda = 0$ if $\lambda \neq 0$.
- $-\lambda$ is also an eigenvalue and belongs to the normalized eigenvector $\mathbf{u}_{-\lambda} = e^{i\alpha} \mathbf{u}_\lambda^*$. Here u^* denotes the complex conjugate of u and α is an arbitrary phase angle which we shall choose equal to zero.
- The real and imaginary parts of \mathbf{u}_λ , ($\lambda \neq 0$) are orthogonal vectors.

Part a) of the theorem follows from the skew symmetry. To prove part b) we need only note that if the matrix is a $n \times n$ matrix A then

$$\det(A - \lambda) = \det(A^T - \lambda) = (-1)^n \det(A + \lambda).$$

Hence if λ is a root of the characteristic equation of A then $-\lambda$ is also a root. By taking the complex conjugate of the eigenvalue equation of \mathbf{u}_λ , it follows that

$$\mathbf{u}_\lambda^* = \mathbf{u}_{-\lambda}.$$

Part e) viz. $(\mathbf{u}_\lambda + \mathbf{u}_{-\lambda}) \cdot (\mathbf{u}_\lambda - \mathbf{u}_{-\lambda}) = 0$ follows from a).

This theorem contains essential information about the eigenfunctions of finite rotations as will be pointed out below. A finite rotation can be generated from an infinitesimal rotation which is represented by a skew-symmetric matrix. In the infinitesimal three-dimensional rotation

$$(1) \quad x'_j = x_j + \varepsilon_{jk} x_k$$

the most general form for the skew-symmetric matrix (ε_{jk}) is given by A where

$$(2) \quad A = \begin{pmatrix} 0 & a_3 & -a_2 \\ -a_3 & 0 & a_1 \\ a_2 & -a_1 & 0 \end{pmatrix} = i\mathbf{s} \cdot \mathbf{a}.$$

The Hermitian matrices s_j satisfy the angular momentum commutation rules

$$(3) \quad [s_1, s_2] = is_3, \quad \text{etc.}$$

as well as the Duffin-Kemmer rules

$$(4) \quad s_j s_k s_m + s_m s_j s_k = s_j \delta_{km} + s_m \delta_{kj}.$$

From (4) follows that $(\mathbf{s} \cdot \mathbf{a})^3 = \mathbf{s} \cdot \mathbf{a}$ if \mathbf{a} is a unit vector.

The finite transformation T generated by (1) and (2) with $\varepsilon = A \delta\theta$, satisfies,

$$T(\theta + \delta\theta) = T(\theta) + A T(\theta) \delta\theta$$

whence

$$(5) \quad \left\{ \begin{array}{l} T(\theta) = \exp[i(\mathbf{s} \cdot \mathbf{a})\theta] \\ = 1 + i(\mathbf{s} \cdot \mathbf{a}) \sin \theta + (\mathbf{s} \cdot \mathbf{a})^2 (\cos \theta - 1) \\ = (C - i(\mathbf{s} \cdot \mathbf{a})S)^{-1} (C + i(\mathbf{s} \cdot \mathbf{a})S), \end{array} \right.$$

where $C = \cos(\theta/2)$ and $S = \sin(\theta/2)$.

It is obvious that the generalized phase transformation

$$(6) \quad \mathbf{x}' = T\mathbf{x}$$

represents a proper rotation through an angle θ about the direction of the unit vector \mathbf{a} . The characteristic equation of the matrix $\mathbf{s} \cdot \mathbf{a}$ is

$$\lambda^3 - \mathbf{a} \cdot \mathbf{a} \lambda = \lambda^3 - \lambda = 0.$$

Hence, for any unit vector \mathbf{a} , the matrix $\mathbf{s} \cdot \mathbf{a}$ has the eigenvalues $\lambda = 0, 1, -1$ and no representation of the three-dimensional rotation group other than (5) and (6) can be obtained from (2).

According to the theorem proved above, the eigenvalues 1, 0, -1 of $\mathbf{s} \cdot \mathbf{a}$ belong to the eigenvectors u_1, u_0, u_{-1} respectively, where

$$(7) \quad u_0 \text{ is real and } u_{-1} = u_1^*.$$

Because the matrices s_j have the angular momentum commutation properties (3), their eigenvectors (7) can be taken to represent the spin eigenstates of a particle with spin unity.

3. – Rotations in four dimensions.

Define the 4×4 skew-symmetric matrix

$$(8) \quad B = i \begin{pmatrix} 0 & -a_3 & a_2 & -b_1 \\ a_3 & 0 & -a_1 & -b_2 \\ -a_2 & a_1 & 0 & -b_3 \\ b_1 & b_2 & b_3 & 0 \end{pmatrix}$$

with a_k and b_k real. Define also B^D the dual matrix obtained from B by interchanging a_k and b_k . These two matrices have the same characteristic equation

$$(9) \quad \det(B - \lambda) = \det(B^D - \lambda) = \lambda^4 - (a^2 + b^2)\lambda^2 + (\mathbf{a} \cdot \mathbf{b})^2 = 0$$

and they commute

$$(10) \quad BB^D = B^DB = \mathbf{a} \cdot \mathbf{b}.$$

Since B and B^D satisfy (9) the operators $\exp[iB\alpha]$ and $\exp[iB^D\beta]$ will in general contain non-periodic functions of α and β . To obtain periodic functions and finite transformations that can be regarded as rotations, we have to impose

the conditions

$$(11) \quad \mathbf{a} \cdot \mathbf{b} = 0, \quad a^2 + b^2 = 1$$

on \mathbf{a} and \mathbf{b} .

Single-valued rotations. According to (9) and (11) the eigenvalues of B and B^D are $\lambda = 0, 0, 1, -1$ and as for A , or in virtue of the commutation rules of footnote (1) below, $B^3 = B$ and $(B^D)^3 = B^D$. Hence the finite operator generated by B is

$$\exp [iB\alpha] = 1 + iB \sin \alpha + B^2(\cos \alpha - 1).$$

This operator is orthogonal and represents a four-dimensional rotation that leaves invariant the two-space spanned by the eigenvectors of B belonging to the zero eigenvalues. Similarly for the operators $\exp [iB^D\beta]$.

By (11) the commutation rule (10) becomes $B\bar{B}^D = B^D\bar{B} = 0$ which means that the two-space which is affected by the transformation $\exp [iB\alpha]$, is left invariant by the transformation $\exp [iB^D\beta]$ and vice versa. The operator in (12) is orthogonal and contains six independent parameters. Hence the generalized phase transformation

$$(12) \quad x' = \exp [iB\alpha + iB^D\beta]x$$

can be regarded as the most general single-valued rotation in four-dimensional space. A Lorentz transformation relating to velocity in the direction \mathbf{a} and a rotation about the direction \mathbf{a} is represented by the operator $\exp [iB\alpha + B^D\beta]$ with $\mathbf{b} = 0$.

Double-valued rotations. Subject to (11) we find that

$$(13) \quad (B \pm B^D)^2 = B^2 + (B^D)^2 = 1.$$

Hence the matrices

$$(14) \quad B_+ = B + B^D, \quad B_- = B - B^D,$$

which are self-dual and anti-self-dual respectively, have the eigenvalues $\lambda = 1, 1, -1, -1$ and

$$\exp [iB_{\pm}\theta/2] = \cos (\theta/2) + iB_{\pm} \sin (\theta/2).$$

Operators of this type are encountered in the theory of quaternions and the Dirac theory of the electron. In four-dimensional space the general rotation

of a spinor has the form of a phase transformation

$$(15) \quad x' = \exp [(iB_+\theta + iB_-\varphi)/2]x.$$

The rotation operator contains six independent parameters and the half angles result from the double-valuedness of the spinor transformation.

In discussing the spin or double-valued representation of the rotation group, it is convenient to introduce

$$(16) \quad \begin{cases} 2^{\frac{1}{2}}z_1 = x_4 + ix_3, & 2^{\frac{1}{2}}z_3 = ix_1 + x_2, \\ 2^{\frac{1}{2}}z_2 = ix_1 - x_2, & 2^{\frac{1}{2}}z_4 = x_4 - ix_3. \end{cases}$$

The transformation (15) then takes the form

$$z' = \exp [(iD_+\theta + iD_-\varphi)/2]z,$$

where, in terms of the Dirac matrices

$$(17) \quad D_+ = \sigma \cdot (\mathbf{a} + \mathbf{b}), \quad D_- = \tau \cdot (\mathbf{a} - \mathbf{b})$$

are the transforms of B^+ and B^- respectively and

$$\tau_1 = -\gamma_5, \quad \tau_2 = -i\beta\gamma_5, \quad \tau_3 = -\beta, \quad \gamma_5 = -ix_1\alpha_2x_3.$$

Like σ , the matrices τ have the commutation properties of a three-dimensional spin vector. Hence rotations in four dimensions make provision for two spin angular momenta σ and τ . The former which is associated with the self-dual matrix B_+ occurs in the Dirac theory of the electron while the latter which is associated with the anti-self-dual matrix B_- does not appear in present-day physics.

Since σ and τ commute it is possible to determine four functions $v_{\sigma\tau}$, $(\sigma, \tau = 1, -1)$ that are eigenfunctions of the two angular momenta simultaneously. If (16) is written as

$$x = Ez \quad \text{and} \quad v = Eu$$

then the relationship $u_{-\lambda} = u_{\lambda}^*$ of the theorem of Sect. 2 is replaced by $v_{-\lambda} = E^{-1}E^*v_{\lambda}^*$. With the E of (16) we get

$$(18) \quad v_{-\sigma, -\tau} = i\beta\alpha_2v_{\sigma\tau}^*.$$

That (18) is indeed true follows from

$$(19) \quad X^T = -C^{-1}XC,$$

if $X = \sigma_j$, τ_k and $C = i\beta\alpha_2$. For the other ten Dirac matrices the minus sign in (19) is replaced by a plus sign.

4. Orbital angular momentum operators and eigenfunctions.

The four-dimensional orbital angular momentum operators corresponding to single-valued rotations are given by

$$\begin{aligned} K_{jk} &= -i\hbar(x_j \partial/\partial x_k - x_k \partial/\partial x_j) \\ &= \hbar x_\alpha (t_{jk})_{\alpha\beta} \partial/\partial x_\beta, \end{aligned}$$

with $j, k, \alpha, \beta = 1, \dots, 4$. The operators K_{jk} and the matrices t_{jk} satisfy the following commutation rules which are valid for angular momentum operators in n dimensions ⁽¹⁾

$$[t_{jk}, t_{\rho m}] = i(t_{j\rho}\delta_{km} + t_{km}\delta_{j\rho} - t_{jm}\delta_{kp} - t_{kp}\delta_{jm}).$$

Deriving the operators in the double-valued theory from those of the single-valued theory as in (14), we obtain the orbital angular momentum operators

$$L_k = \frac{1}{2}(K_{ij} + K_{k4}), \quad M_k = \frac{1}{2}(K_{ij} - K_{k4}),$$

with i, j, k in cyclic order, corresponding to the spins σ and τ . We introduce the transformation ⁽²⁾

$$(20) \quad \left\{ \begin{array}{ll} x_1 = \sin(\theta/2) \sin u, & x_3 = \cos(\theta/2) \sin v, \\ x_2 = \sin(\theta/2) \cos u, & x_4 = \cos(\theta/2) \cos v, \end{array} \right.$$

⁽¹⁾ These matrices also satisfy commutation rules that can be regarded as a generalization of the Duffin-Kemmer rules:

$$\begin{aligned} t_{ij}t_{kp}t_{mn} + t_{mn}t_{kp}t_{ij} &= t_{im}(\delta_{jk}\delta_{pn} - \delta_{jp}\delta_{kn}) + t_{in}(\delta_{jp}\delta_{km} - \delta_{jk}\delta_{pm}) + \\ &\quad + t_{jm}(\delta_{ip}\delta_{kn} - \delta_{ik}\delta_{pn}) + t_{jn}(\delta_{ik}\delta_{pm} - \delta_{ip}\delta_{km}). \end{aligned}$$

⁽²⁾ The method used here is taken from A. PAIS: *Proc. Nat. Acad. Sci.*, **40**, 835 (1954) but the presentation and the form of the solution (21) differs from that of Pais.

where $2u = \psi - \varphi$ and $2v = \psi + \varphi$. The simultaneous eigenfunctions Y_{jmn} of the commuting operators

$$L_3 = i\hbar \partial/\partial\psi, \quad M_3 = -i\hbar \partial/\partial\varphi, \quad K^2 = \frac{1}{2}K_{ik}^2$$

satisfy

$$K^2 Y_{jmn} = 4j(j+1) Y_{jmn}$$

and are given by

$$(21) \quad Y_{jmn} = N s^{m-n} c^{m+n} \exp [i(m\varphi + n\psi)] \frac{d^{j+m}}{(ds^2)^{j+m}} [s^{2(j+n)} c^{2(j-n)}],$$

where

$$s = \sin(\theta/2), \quad c = \cos(\theta/2)$$

$$j = 0, \frac{1}{2}, 1, \dots, \quad m, n = j, j-1, \dots, -j,$$

and

$$N = \left| \frac{2j+1}{4\pi} \frac{(j-m)!}{(j+m)!(j+n)!(j-n)!} \right|^{\frac{1}{2}},$$

is a normalization factor chosen in such a way that for $n = 0$ these functions reduce to the spherical harmonics

$$Y_{jm} = Y_{jmo}.$$

For fixed j the $(2j+1)^2$ functions Y_{jmn} can be arranged in a unitary matrix which constitutes a representation of the three-dimensional rotation group ⁽³⁾. The three angles θ, φ, ψ can in fact be interpreted as the Euler angles specifying the rotations of a rigid body. The four functions for which $j = \frac{1}{2}$ are

$$2^{\frac{1}{2}}z_1 = \cos(\theta/2) \exp[i(\varphi + \psi)/2], \quad 2^{\frac{1}{2}}z_3 = \sin(\theta/2) \exp[i(-\varphi + \psi)/2],$$

$$2^{\frac{1}{2}}z_2 = -\sin(\theta/2) \exp[i(\varphi - \psi)/2], \quad 2^{\frac{1}{2}}z_4 = \cos(\theta/2) \exp[-i(\varphi + \psi)/2],$$

with z_k as in (16) and (20). They are, apart from the normalization factor, the Cayley-Klein parameters. The fact that z_k can be arranged as a unitary 2×2 matrix, implies that the column matrix z satisfies

$$(22) \quad z' = i\beta z_2 z^* = z$$

(3) E. WIGNER: *Gruppentheorie und ihre Anwendung auf die Quantenmechanik der Atomspektren* (Akademie, 1944), p. 180.

in a notation to be explained below. In terms of this notation these four-dimensional angular momentum eigenfunctions have the symmetry property of charge self conjugate wave functions.

A consequence of (22) is that $z^*Fz = 0$ if $F = \sigma, \tau$. Nine of the ten remaining non-vanishing bilinear combinations of z_k are linear combinations of the Y_{lmn} and form the 3×3 rotation matrix of a rigid body

$$x'_k = S_{kj} x_j,$$

with $S_{k1} = z^* \alpha_k z$, $S_{k2} = iz^* \beta \alpha_k z$, $S_{k3} = z^* \beta \sigma_k z$. The tenth function is $z^*z = 1$ and represents the usual relation between the Cayley-Klein parameters.

5. – Discussion of spin-charge correspondence.

It is well-known that in the theory of charged particles, conservation of charge is ensured by the invariance of the theory under a phase transformation. Since rotations can be expressed in terms of such transformations, it follows that both conservation of charge and invariance under rotations are guaranteed by invariance under phase transformations. The formal correspondence between descriptions of charge and spin is therefore not surprising. It now follows that an uncharged particle with spin unity and a spin zero particle with three charge states are both described by three wave functions with the structure of (7).

In the case of the electron the Kramers-Pauli charge conjugation formalism introduces the relationship

$$(23) \quad \psi^\sigma = C\psi^*,$$

between the wave functions ψ and ψ^σ of the two charge states. The hermitean matrix C is symmetrical and the relation ⁽⁴⁾

$$(24) \quad X^T = \pm C^{-1}XC$$

holds with the minus sign for $X = \sigma$ and τ while the plus sign holds for the remaining ten Dirac matrices. In the usual representation for these matrices, $C = i\beta z_2$.

Comparison of (23) and (24) with (18) and (19) shows that the charge conjugation procedure for spin $\frac{1}{2}$ particles employs the same mathematical formalism as the double-valued representation of the four-dimensional ro-

⁽⁴⁾ C. B. VAN WYK: *Phys. Rev.*, **80**, 487 (1950).

tation group. This is also illustrated by the symmetry properties (22) of the $Y_{\frac{1}{2}mn}$ or the Cayley-Klein parameters.

Charge conjugation and four-dimensional rotations treat σ and τ on equal footing whereas in the rotation of a rigid body and the Dirac theory of the electron, τ -rotations appear to be «frozen». Since the Dirac theory can be regarded as a relativistic generalization of these restricted four-dimensional (rigid body) rotations, two possibilities suggest themselves. Particles might exist, in the relativistic theory of which *a*) the anti-self-dual τ -rotations are allowed while the self-dual σ -rotations are «frozen», *b*) the spin requires a description by means of the more comprehensive σ and τ angular momentum formalism.

These possibilities are perhaps strengthened by the fact that their descriptions would be partial or complete spin analogues of the charge conjugation formalism. Observations and further theoretical investigation would have to decide whether particles with these types of spin exist.

6. – Charge self conjugate functions and reflections.

A three-dimensional reflection in a plane having the unit normal vector \mathbf{a} , can be defined as a rotation through two right angles about \mathbf{a} together with the inversion represented by the negative unit matrix. Hence by (5) the reflection operator is given by

$$(25) \quad \left\{ \begin{array}{l} R_{jk} = -(\exp [i\pi \mathbf{s} \cdot \mathbf{a}])_{jk} = -(1 - 2(\mathbf{s} \cdot \mathbf{a})^2)_{jk} \\ \qquad \qquad \qquad = \delta_{jk} - 2a_j a_k . \end{array} \right.$$

The linear combinations

$$w_1 = u_1 + u_{-1}, \quad w_2 = i(u_1 - u_{-1}), \quad w_3 = u_0,$$

of the functions (7) satisfy

$$(\mathbf{s} \cdot \mathbf{a})w_1 = -iw_2, \quad (\mathbf{s} \cdot \mathbf{a})w_2 = iw_1, \quad (\mathbf{s} \cdot \mathbf{a})w_3 = 0.$$

Consequently we have

$$Rw_1 = w_1, \quad Rw_2 = w_2, \quad Rw_3 = -w_3$$

as is required of a reflection.

Hence in the three-dimensional case the real or charge self conjugate functions w_k constructed from the eigenvectors of the infinitesimal rotation operator $\mathbf{s} \cdot \alpha$, are the eigenstates of the operator R that represents a reflection in a plane normal to the vector α .

A reflection in four-dimensional space is also given by (25) with $j, k = 1, 2, 3, 4$. In both the three- and four-dimensional cases the infinitesimal rotation defines, according to part *c*) of the theorem of Sect. 2, a set of mutually orthogonal vectors which can be the eigenvectors of the symmetrical reflection matrix R . However, in four dimensions R cannot be expressed in terms of the infinitesimal rotation.

* * *

It is a pleasure to thank Dr. J. R. OPPENHEIMER for the hospitality of the Institute for Advanced Study, Princeton, N.J., which the author enjoyed for a few months and during which time a part of this work was completed

RIASSUNTO (*)

La corrispondenza formale tra spin e carica insita nel concetto di spin isobarico è spiegata mostrando che le rotazioni negli spazi tri- e quadridimensionale possono esprimersi come trasformazioni di fase generalizzate. Anche le riflessioni nello spazio tridimensionale sono espresse come trasformazioni di fase, le cui autofunzioni sono in relazione lineare con quelle di opportune rotazioni. Si dimostra che la coniugazione delle cariche di Kramers-Pauli è per la carica l'analogo dello spin in quattro dimensioni. Pertanto il formalismo della coniugazione delle cariche presenta un sistema spin-momento angolare applicabile a particelle con due tipi di spin. Le autofunzioni del momento angolare orbitale quadridimensionale si danno come generalizzazione di armoniche sferiche.

(*) Traduzione a cura della Redazione.

Angular Distribution of Neutrons from μ^- Absorption in Nuclei.

H. ÜBERALL

Nuclear Physics Research Laboratory - University of Liverpool

(ricevuto il 23 Maggio 1957)

Summary. — A general parity non-conserving absorption process of partly polarized μ^- -mesons by protons in a nucleus is considered. The Fermi gas model is used to estimate the effect of the motion of the protons inside the nucleus on the anisotropy of the emitted neutrons. It is found that the anisotropy of the neutron distribution in the fundamental interaction is mostly preserved, especially towards the upper end of the neutron spectrum: thus an experiment to observe the neutron asymmetry seems feasible.

1. — Introduction.

After the initial suggestion of parity non-conservation in weak interactions ⁽¹⁾, a wealth of experimental information has become available which all directly or indirectly confirms this property of nature. Parity non-conservation was proved to hold in β -decay by the experiment of WU *et al.* ⁽²⁾, and in muon decay by the experiment of GARWIN *et al.* ⁽³⁾. These and subsequent experimental results, which show that parity non-conserving effects reach the extreme values permitted by the coupling constants, are compatible with a special case of the parity non-conserving theory, i.e. Lee and Yang's two-component neutrino theory ⁽⁴⁾. There is no experiment reported which checks on parity non-conservation in the third weak interaction appearing in

⁽¹⁾ T. D. LEE and C. N. YANG: *Phys. Rev.*, **104**, 254 (1956).

⁽²⁾ C. S. WU, E. AMBLER, R. W. HAYWARD, D. D. HOPPES and R. P. HUDSON: *Phys. Rev.*, **105**, 1413 (1957).

⁽³⁾ R. L. GARWIN, L. M. LEDERMAN and M. WEINRICH: *Phys. Rev.*, **105**, 1415 (1957).

⁽⁴⁾ T. D. LEE and C. N. YANG: *Phys. Rev.*, **105**, 1671 (1957).

the Tiomno-Wheeler (4) triangle, namely μ^- absorption by a proton with emission of a neutron and a neutrino, for the simple reason that the elementary absorption process in hydrogen which is hard to realize experimentally because of its small probability, in fact has never been studied to date; and in the situation which is easier to investigate, absorption in complex nuclei, various factors are sure to affect the most obvious feature of parity non-conservation, namely the angular distribution of the neutrons with respect to the spin direction of the μ -meson. First, the meson may be partly depolarized during its passage through the material and subsequent orbital capture in the atom. Secondly, there is a reduction of angular asymmetry originating in the proton motion within the nucleus, which will be considered below. Finally, there is elastic scattering of the neutrons before they emerge from the nucleus, reducing the asymmetry further.

In order to estimate the role of the proton motion in the reduction of the neutron angular distribution, we use the Fermi gas model of Tiomno and Wheeler (5). The validity of the model for the total μ^- absorption probability was already discussed by these authors. Applicability to angular distributions is less clear. There are specific effects tending to influence the angular distribution, which are not incorporated in the model, e.g. absorption of the μ by a proton with high orbital angular momentum; this would be the case in a shell model treatment of the problem. It is also unknown to what extent a compound nucleus state will be established upon capture of the muon, with neutron evaporation a second step. Such a process would seriously reduce the neutron asymmetry.

2. - Evaluation.

The nucleons involved in the absorption process all have non-relativistic velocities, so we are allowed to use the non-relativistic approximation of the general parity non-conserving Hamiltonian:

$$(1) \quad H_{\text{int.}} = (\psi_N^\dagger \psi_P) \left(\psi_\nu^\dagger \gamma_4 \frac{C_s + C'_s \gamma_5}{2} \psi_\mu \right) + (\psi_N^\dagger \psi_P) \left(\psi_\nu^\dagger \frac{C_r + C'_r \gamma_5}{2} \psi_\mu \right) + \\ + (\psi_N^\dagger \sigma \psi_P) \left(\psi_\nu^\dagger \gamma_4 \sigma \frac{C_x + C'_x \gamma_5}{2} \psi_\mu \right) + (\psi_N^\dagger \sigma \psi_P) \left(\psi_\nu^\dagger \sigma \frac{C_A + C'_A \gamma_5}{2} \psi_\mu \right).$$

Calculating first the absorption probability of a μ^- by a proton at rest with

(5) J. TIOMNO and J. A. WHEELER: *Rev. Mod. Phys.*, **21**, 153 (1949).

a perturbation treatment using (1), we find

$$(2) \quad \begin{cases} w = (2\pi)^{-2}(\pi a_p^3)^{-1} |S|^2 d\Omega_N \int k^2 \delta\left(\mu + M_p - M_N - k - \frac{k^2}{2M_N}\right) dk, \\ |S|^2 = C(1 + \zeta P \cos \vartheta) = C(1 - \zeta P \cos \theta), \end{cases}$$

with the following notations:

\mathbf{k} = neutrino momentum = $-\mathbf{p}_N$ (\mathbf{p}_N = neutron momentum),

$\vartheta = \angle(\mathbf{s}_\mu, \mathbf{k}) = \pi + \theta, \theta = \angle(\mathbf{s}_\mu, \mathbf{p}_N);$

$d\Omega_N$ = neutron solid angle,

$$C = \frac{1}{8} \left\{ |C_s + C_v|^2 + |C'_s - C'_v|^2 + 3[|C_t + C_A|^2 + |C'_t - C'_A|^2] \right\},$$

$$\zeta = - \frac{2 \operatorname{Re} [(C_s + C_v)(C'_s - C'_v)^* - (C_t + C_A)(C'_t - C'_A)^*]}{|C_s + C_v|^2 + |C'_s - C'_v|^2 + 3[|C_t + C_A|^2 + |C'_t - C'_A|^2]}.$$

So, the factors of $\cos \theta$ may have values up to 1 for S, V , $\frac{1}{3}$ for T, A couplings. P is the degree of polarization of the μ^- at the moment of absorption, and a_p^3 the Bohr radius of the μ^- bound to the proton.

If we specialise to the two-component neutrino theory, $\gamma_5 \psi_\nu = -\psi_\nu$, the coupling constants satisfy $C_s = C_{s'}$, $C_v = -C_{v'}$, $C_t = C_{t'}$, $C_A = -C_{A'}$, and for real coupling constants, we find an asymmetry coefficient $\zeta = -1$ for S, V , $\zeta = \frac{1}{3}$ for T, A . These results were quoted by T. D. LEE at the 1957 Rochester Conference.

For muon absorption by a moving proton, momentum and energy conservation yield

$$(3) \quad \mathbf{p}_p = \mathbf{p}_N + \mathbf{k}, \quad \mu + E_p = E_N + k.$$

We shall split up the proton momentum into a parallel and a perpendicular component with respect to \mathbf{k} , and introduce the energy transfer to the nucleon, Δ :

$$(4) \quad \mathbf{p}_p = \mathbf{p}_N + \mathbf{p}_\perp, \quad \Delta = E_N - E_p = \mu - k.$$

Δ is a function of p_\parallel only:

$$2M\Delta = 2p_\parallel k + k^2.$$

The transition probability analogous to (2) must now be integrated over the distribution of the proton momenta permitted by the Pauli exclusion principle.

This situation is illustrated in Fig. 1. Neutrons and protons in the nucleus both occupy a sphere in momentum space with a radius P_F , which is determined by the number of states available and the number $(A/2)$ of neutrons or protons occupying them:

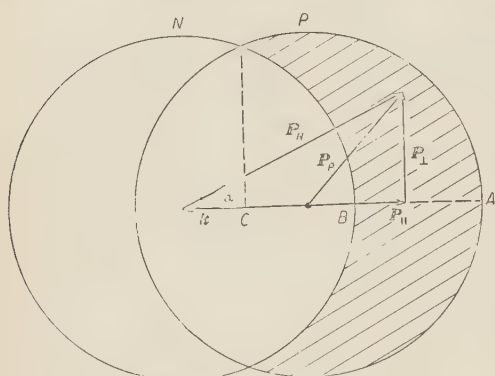


Fig. 1. — Vector diagram and Fermi spheres in momentum space.

$$2 \frac{4}{3} R^3 \pi \frac{4}{3} P_F^3 \pi = \frac{1}{2} A , \quad R = r_0 A^{\frac{1}{3}} ,$$

$$r_0 = 1.2 \cdot 10^{-13} \text{ cm} .$$

This leads to

$$P_F = \frac{1}{r_0} \left(\frac{3}{8\pi} \right)^{\frac{1}{3}} = 489 \text{ m}_e .$$

The absorption probability is, cf. (2):

$$(5) \quad w = \frac{C}{(2\pi)^2 \pi a_z^3} \frac{A}{2} \int (1 + \zeta P \cos \vartheta) k^2 dA 2\pi d\cos \vartheta \delta \left(\mu - k - \frac{k}{M} p_{\parallel} - \frac{k^2}{2M} \right) \frac{dV}{V} ;$$

it contains the new Bohr radius a_z and the Fermi momentum distribution volume $dV = dp_{\parallel} dp_{\perp} d\varphi$, $V = 3/16\pi r_0^3$. The same factor $|S|^2$ appears as in the case of the proton at rest, as in non-relativistic approximation, the slow proton motion does not change the angular distribution of the relativistic neutrino. We have to introduce the neutron emission angle $\theta \prec (\mathbf{s}_{\mu}, \mathbf{p}_N)$. With a moving proton, \mathbf{p}_N is no longer directed opposite to \mathbf{k} , and further angles must be used:

$$\begin{aligned} \pi - \vartheta &= \prec(\mathbf{s}_{\mu}, \mathbf{p}_{\parallel}), \\ \alpha &= \prec(\mathbf{p}_N, \mathbf{p}_{\parallel}), \\ \varphi &= \prec(\mathbf{s}_{\mu} \mathbf{p}_{\parallel} \text{ plane}, \mathbf{p}_N \mathbf{p}_{\parallel} \text{ plane}), \end{aligned}$$

and we shall call $\cos \vartheta = \omega$, $\cos \theta = W$. Then (5) becomes:

$$(6) \quad w = \frac{AC}{(2\pi)^2 a_z^3} \frac{16\pi r_0^3}{3} \int (1 + \zeta P\omega) k^2 \frac{\partial \omega}{\partial W} dW dA \left(\frac{dp_{\perp}}{dA} \right) p_{\perp} dp_{\perp} d\varphi ,$$

with $(dp/dA) = M/k$, expressing energy conservation. The following relations between the angles are easily deduced:

$$(7) \quad \operatorname{tg} \alpha = \frac{p_{\perp}}{p_{\parallel} + k} ,$$

$W = -\omega \cos \alpha + (1 - \omega^2)^{\frac{1}{2}} \sin \alpha \cos \varphi$ or

$$(8) \quad \omega = \frac{-W \cos \alpha + \sin \alpha \cos \varphi (1 - W^2 - \sin^2 \alpha \sin^2 \varphi)^{\frac{1}{2}}}{1 - \sin^2 \alpha \sin^2 \varphi},$$

Now let us take a closer look at the limits of integration. They are determined by the exclusion principle: p_p must lie within the proton sphere, and p_N outside of the occupied neutron sphere. Fig. 1 shows the allowed region (shaded portion of the figure); p can lie between C and B , corresponding to $p_{\parallel} = -\frac{1}{2}k$ and $P_F - k$, or

$$(9) \quad 0 \leq \Delta \leq \Delta^*, \quad P_F^2 - (p_{\parallel} + k^2) \leq p_{\perp}^2 \leq P_F^2 - p_{\parallel}^2,$$

or between B and A , ($P_F - k$ and P_F), or

$$(10) \quad \Delta^* \leq \Delta \leq \Delta_m, \quad 0 \leq p_{\perp}^2 \leq P_F^2 - p^2.$$

The corresponding values of Δ are given implicitly by

$$(11) \quad \frac{M\Delta^*}{k^*} + \frac{k^*}{2} = P_F, \quad \frac{M\Delta_m}{k_m} - \frac{k_m}{2} = P_F.$$

Now we perform the integration over φ , which goes from 0 to 2π , and obtain

$$(12) \quad w = M \frac{8AC}{3} \left(\frac{r_0}{a} \right)^3 dW \int_0^{A_m} k d\Delta \int_{\vec{p}_{\perp \min}}^{\vec{p}_{\perp \max}} dp_{\perp} (1 - \zeta PW \cos \alpha).$$

Our aim will now be to find the neutron angular distribution for any given neutron energy. Therefore we shall try to introduce E_N as one of the integration variables. We perform the integral transformation

$$(13) \quad \begin{cases} q = M + p_{\parallel} + k, \\ E_N = \frac{1}{2M} [p_{\perp}^2 + (p_{\parallel} + k)^2], \end{cases}$$

which gives the new limits:

$$(14) \quad \text{from (9):} \quad M + \frac{\mu}{2} \leq q \leq M + (2ME_F)^{\frac{1}{2}}, \quad E_F \leq E_N \leq E^*,$$

with $E_F = P_F^2/2M$ and $E^* = E_F + \mu - q + (q^2 - 2M\mu)^{\frac{1}{2}}$, and from (10):

$$(15) \quad M + (2ME_F)^{\frac{1}{2}} \leq q \leq [(M + (2ME_F)^{\frac{1}{2}})^2 + 2M\mu]^{\frac{1}{2}}, \quad \frac{1}{2M} (q - M)^2 \leq E_N \leq E^*.$$

For $\cos \alpha$, we find simply

$$(16) \quad \cos \alpha = \frac{q - M}{(2ME_N)^{\frac{1}{2}}}.$$

To obtain the neutron spectrum, we invert the order of integration, such that the integral over E_N is performed last. From (12) then follows:

$$(17) \quad w = M^2 \frac{8AC}{3} \left(\frac{r_0}{a_z}\right)^3 dW \int_{E_1}^{E_2} dE_N \int_{q_1}^{q_2} dq \cdot \\ \cdot \left((q^2 - 2M\mu)^{\frac{1}{2}} + \frac{q^2}{(q^2 - 2M\mu)^{\frac{1}{2}}} - 2q \right) \left(1 - \zeta PW \frac{q - M}{(2ME_N)^{\frac{1}{2}}} \right),$$

with the limits:

$$(18) \quad E_1 = E_F + E_B \quad (E_B = \text{binding energy of last neutron, 8 MeV}),$$

as we must have $E_N \geq E_F + E_B$, for the neutron to emerge,

$$E_2 = E_F + \mu + M + (2ME_F)^{\frac{1}{2}} - [(M + (2ME_F)^{\frac{1}{2}})^2 + 2M\mu]^{\frac{1}{2}}, \\ q_1 = \frac{(E_F + \mu - E_N)^2 + 2M\mu}{2(E_F + \mu - E_N)}, \\ q_2 = M + (2ME_N)^{\frac{1}{2}}.$$

The q integration is easily performed, and the neutron spectrum and angular distribution is finally:

$$(19) \quad \begin{cases} w = \bar{w}[J(E_N) - \zeta PWK(E_N)]dE_N dW, \\ \bar{w} = \frac{8}{3} m_e^2 M^2 A C \left(\frac{r_0}{a_z}\right)^3, \quad W = \cos \theta. \end{cases}$$

The functions $J(E_N)$ and $K(E_N)$ are found to be:

$$(20) \quad \begin{cases} J(E_N) = -[q(q - (q^2 - 2M\mu)^{\frac{1}{2}})]_{q_1}^{q_2}, \\ K(E_N) = -\frac{1}{(2ME_N)^{\frac{1}{2}}} [(\frac{2}{3}q - M)q(q - (q^2 - 2M\mu)^{\frac{1}{2}}) - \frac{2}{3}M\mu(q^2 - 2M\mu)^{\frac{1}{2}}]_{q_1}^{q_2}. \end{cases}$$

All masses and energies will be measured in units of the electron mass, m_e . Then we use the numerical values:

$$M = 1836, \quad \mu = 207, \quad E_F = 65, \quad E_B = 16,$$

and thus

$$E_1 = 81, \quad E_2 = 113.$$

Fig. 2 shows a plot of the functions $J(E_N)$, $K(E_N)$, and of their ratio. We see first of all that most neutrons emerge with low energies, but the spectrum decreases only linearly, up to the maximum energy of 16 MeV (outside the nucleus). The anisotropy is reduced by no more than a factor of 0.7 for the slowest neutrons, and not at all for the fastest ones. It is clear that K/J has to increase with E_N , as more energetic neutrons will be less influenced by the proton motion. Integrating J and K from E_1 to E_2 , we find

$$(21) \quad J = \int J(E_N) dE_N = 7.58 \cdot 10^2, \quad K = \int K(E_N) dE_N = 5.86 \cdot 10^2,$$

and

$$(22) \quad \frac{K}{J} = 0.773.$$

Thus, the angular distribution of neutrons is not substantially reduced by the motion of the protons inside the nucleus.

3. - Discussion.

As far as an experiment on the neutron asymmetry is concerned, this would appear not to be rendered unfeasible by the proton motion. We still have to look into the importance of the other reducing factors mentioned in I.

Limits on the polarization P of the μ^- -meson at the time that it has reached the lowest Bohr orbit may be set ⁽⁶⁾ by comparing the asymmetries observed in the distribution $1 - a_{\pm} \cos \theta$ of the integrated electron spectrum from

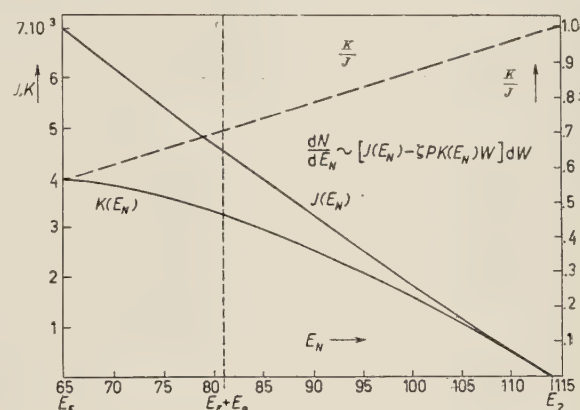


Fig. 2. - Neutron spectrum and asymmetry coefficient.

⁽⁶⁾ The following argument is due to Professor J. M. CASSELS.

μ^-e^+ and μ^-e^- decay. If invariance under CP is assumed, the observed asymmetries a_{\pm} are related to the polarizations P_{\pm} by

$$\frac{a_{+}}{P_{+}} = \frac{a_{-}}{P_{-}}.$$

Recent measurements give a maximum observed asymmetry coefficient (⁷) (for carbon), $a_{+} = \frac{1}{4}$, and a differential asymmetry coefficient (⁸) at the upper end of the electron spectrum, $a_{+}(E = \frac{1}{2}\mu) = \frac{2}{3}$. As the asymmetry coefficient has to be < 1 even for 100% polarization, the latter result implies $P_{+} \geq \frac{2}{3}$; thus

$$\frac{3}{8} > \frac{a_{+}}{P_{+}} > \frac{1}{4},$$

where the lower limit follows from $P_{+} \leq 1$. Using (23), we obtain the limits for P_{-} ,

$$(24) \quad \frac{3}{8} a_{-} \leq P_{-} \leq 4a_{-}.$$

From μ^- decay experiments, we have (⁹) $a_{-} = 0.065$ (for silicon), which leads to P_{-} values up to 0.25.

A similar analysis using two-component neutrino theory (⁴) and the fact that $\xi = 3a_{+}/P_{+} \leq 1$, produces the limits

$$(25) \quad 3a_{-} \leq P_{-} \leq 4a_{-}.$$

Scattering (or absorption) of the neutrons which emerge from the nucleus can be estimated from the mean free path of nucleons in nuclear matter. If we assume a cloudy crystal ball nuclear potential $V_0(1 + i\xi)$, the mean free path is given by (¹⁰)

$$(26) \quad \lambda = \frac{1}{(2M)^{\frac{1}{2}}} \frac{(E_0 + V_0)^{\frac{1}{2}}}{\xi V_0}, \quad V_0 = E_F - E_B,$$

where E_0 is the neutron energy measured outside of the nucleus, $E_0 = E_N - (E_F - E_B)$. These authors give an expression for the imaginary part of the

(⁷) J. M. CASSELS, T. W. O'KEEFFE, M. RIGBY, A. M. WETHERELL and J. R. WORMALD: *Proc. Phys. Soc.*, A **70**, 543 (1957).

(⁸) T. COFFIN, R. L. GARWIN, L. M. LEDERMAN, M. WEINRICH and D. BERLEY: *Bull. Am. Phys. Soc.*, **2**, 204 (1957); *Phys. Rev.*, **106**, 835 (1957).

(⁹) H. MUIRHEAD (unpublished).

(¹⁰) G. C. MORRISON, H. MUIRHEAD and P. A. B. MURDOCH: *Phil. Mag.*, **46**, 795 (1955).

potential for neutrons:

$$(27) \quad \xi V_0 = 6 + 0.35 E_0$$

(units: electron masses), leading to mean free paths of $\lambda = 9.5 \cdot 10^{-13}$ cm for neutrons with $E_N = E_1$, $\lambda = 3.9 \cdot 10^{-13}$ cm for $E_N = E_2$. Compared with nuclear radii $R = 2.58 \cdot 10^{-13}$ cm for $A = 10$, $R = 3.25 \cdot 10^{-13}$ cm for $A = 20$, it appears that an appreciable fraction of the neutrons will emerge without scattering. We can conclude that altogether the neutron asymmetry will not be reduced so much as to prevent experimental observation, provided that the Fermi gas model is applicable to the process considered.

* * *

My sincere thanks are due to Dr. CLAUDE ZANGER for help and discussions, and to Professor J. M. CASSELS and Dr. H. MUIRHEAD, for discussions and encouragement to carry out this investigation.

RIASSUNTO (*)

Si considera un processo generale, non conservante la parità, di assorbimento nei protoni in un nucleo di mesoni μ^- parzialmente polarizzati. Il modello del gas di Fermi è usato per stimare l'effetto del moto dei protoni entro il nucleo sull'anisotropia dei neutroni emessi. Si trova che l'anisotropia della distribuzione dei neutroni nell'interazione fondamentale è in gran parte conservata specialmente verso l'estremità superiore dello spettro neutronico; sembra pertanto attuabile un esperimento che permetta di osservare l'asimmetria dei neutroni.

(*) Traduzione a cura della Redazione.

Anomalous Magnetic Moment of the Nucleon.

S. OKUBO

University of Rochester

(ricevuto il 27 Maggio 1957)

Summary. — Miyazawa's method of calculation of the anomalous magnetic moment of the nucleon is given a covariant extension by using covariant dispersion relations. In this connection, some attention is paid to the difference between covariant and non-covariant definitions of magnetic moment from meson current contribution.

1. – Introduction.

Recently, MIYAZAWA (1) made an exact calculation of the anomalous magnetic moment of the nucleon, on the basis of Chew's static theory. He also showed that the contribution to this quantity from the pion current can be calculated by using dispersion relations only.

This paper treats the covariant generalization by using covariant dispersion relations. The final result is much simpler than the non-covariant one, and does not involve explicit divergence.

In this connection, some attention is paid to the difference between the covariant and non-covariant definition of the magnetic moment from the meson-current contribution.

Proceeding in this way, we have calculated parts of the anomalous magnetic moment of the nucleon, due to the meson current and the scalar part of the nucleon current. However, we did not succeed in obtaining by this method an expression for the vector part of the nucleon current.

(1) H. MIYAZAWA: *Phys. Rev.*, **101**, 1564 (1956); **104**, 1741 (1956).

2. – The meson current contribution to the anomalous magnetic moment of the nucleon.

Here, we consider the meson current part of the nucleon magnetic moment. The contribution to the S -matrix from the interaction of the nucleon with an external electromagnetic potential A_μ is given by

$$(1) \quad S = \frac{e}{(2\pi)^8} A_\mu(p' - p) \int \int d^4 k d^4 k' \frac{1}{(k^2 + \mu^2)} \frac{1}{(k'^2 + \mu^2)} (k_\mu + k'_\mu) \cdot \\ \cdot \frac{1}{2} [R_{21}(p, k, p', k') - R_{12}(p, k, p', k')] ,$$

where

$$(2) \quad R_{\beta\alpha}(p, k, p', k') = \int \int d^4 x d^4 y \exp[i k x - i k' y] \cdot \\ \cdot (\square_x - \mu^2)(\square_y - \mu^2)[\Psi^*(p') P(\varphi_\alpha(x) \varphi_\beta(y)) \Psi(p)] ,$$

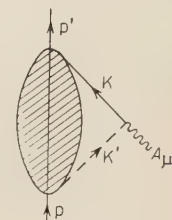


Fig. 1.

is the elastic scattering amplitude of a virtual meson by a real nucleon from an initial state with meson momentum k and nucleon momentum p to a final state with meson and nucleon momenta k' and p' respectively.

In (2), $\Psi(p)$ and $\Psi(p')$ are true one-nucleon states, whose momenta are p and p' , respectively, and $\varphi_\alpha(x)$ is the Heisenberg operator for the symmetrical meson field. Instead of the four dependent momenta p , p' , k and k' , it is more convenient to use the three independent momenta K , P , and Q , defined as follows:

$$(3) \quad \left\{ \begin{array}{l} Q = \frac{1}{2}(k + k') , \\ P = \frac{1}{2}(p + p') , \\ K = k - k' = p' - p . \end{array} \right.$$

The last identity for K follows from energy momentum conservation. Furthermore, from the Lorentz invariance of the theory, we can put:

$$(4) \quad R_{\beta\alpha}(pk, p'k') = 2\pi i \delta(p + k - p' - k') \left(\frac{m^2}{E_p E_{p'}} \right)^{\frac{1}{2}} (\bar{u}(p') U_{\beta\alpha}(P, Q, K) u(p)) ,$$

where the Dirac spinor u is normalized as follows:

$$\bar{u}(p) u(p) = 1 ,$$

so that U is relativistically invariant. From Dirac equations for $u(p)$ and

$u(p')$, and using Lorentz covariance and charge independence, we can rewrite U in (4) as follows:

$$(5) \quad U_{\beta\alpha}(P, Q, K) = -(\delta_{\beta\alpha}A^{(+)} + \frac{1}{2}[\tau_\beta, \tau_\alpha]A^{(-)}) + i\gamma Q(\delta_{\beta\alpha}B^{(+)} + \frac{1}{2}[\tau_\beta, \tau_\alpha]B^{(-)}).$$

Our notation is the same as Chew's ⁽²⁾ except for a factor 2 for K .

$A^{(\pm)}$ and $B^{(\pm)}$ are scalar quantities, which do not depend on the γ or τ matrices. From (2), it is easy to get the crossing symmetry relations:

$$(6) \quad \begin{cases} A^{(\pm)}(P, Q, K) = \pm A^{(\pm)}(P, -Q, K), \\ B^{(\pm)}(P, Q, K) = \mp B^{(\pm)}(P, -Q, K). \end{cases}$$

Furthermore, by using Wigner time reversal ⁽³⁾, we can derive

$$(7) \quad \begin{cases} A^{(\pm)}(P, Q, K) = A^{(\pm)}(P, Q, -K), \\ B^{(\pm)}(P, Q, K) = B^{(\pm)}(P, Q, -K), \end{cases}$$

Now, insert (4) and (5) into (1), and notice that

$$\begin{aligned} K_\mu A_\mu(K) &= 0, \quad u(p') i\gamma K u(p) = 0, \\ \bar{u}(p') i\gamma P u(p) &= -m \bar{u}(p') u(p). \end{aligned}$$

Hence, we may put

$$(8) \quad \int d\Omega \frac{1}{(Q + \frac{1}{2}K)^2 + \mu^2} \frac{1}{(Q - \frac{1}{2}K)^2 + \mu^2} Q_\mu (\bar{u}(p')[U_{21}(P, Q, K) - U_{12}(P, Q, K)]u(p)) = \\ = 2\bar{u}(p')(GP_\mu - iD\gamma_\mu)\tau_3 u(p),$$

where we have omitted terms proportional to K_μ , and G and D are suitable scalar functions. Therefore, (1) becomes

$$(9) \quad S = \frac{2e}{(2\pi)^7} A_\mu(K) \left(\frac{m^2}{E_p E_{p'}} \right)^{\frac{1}{2}} \bar{u}(p') [D\gamma_\mu + iGP_\mu]\tau_3 u(p).$$

Before an explicit calculation of D and G is made, it seems worthwhile to compare the covariant calculation of the magnetic moment with the non-covariant one in order to avoid some confusion.

⁽²⁾ G. CHEW: *Lecture Note at Institute for Advanced Study* (Princeton, 1956).

⁽³⁾ S. WATANABE: *Phys. Rev.*, **84**, 1008 (1951).

If we use the Dirac equation, we can rewrite (9) as follows:

$$(10) \quad S = \frac{2e}{(2\pi)^7} A_\mu(K) \left(\frac{m^2}{E_p E'_p} \right)^{\frac{1}{2}} \bar{u}(p') \left\{ [D - mG] \gamma_\mu + \frac{i}{4} [\gamma_\mu, \gamma K] G \right\} \tau_3 u(p) .$$

Now, $D - mG$ is divergent and its divergent term represents a renormalization effect and hence must be discarded. Then the 2nd term gives the anomalous magnetic moment,

$$(11) \quad \mu_e = \frac{e}{(2\pi)^4} G_0 ,$$

where G_0 is the value of G obtained by putting $K = 0$, $P = P_0 = (0, m)$. But non-covariantly, the situation is a little different, because in the non-relativistic limit, both $\gamma_\mu A_\mu$ and the anomalous term $-(i/4)[\gamma_\mu, \gamma_\nu] F_{\mu\nu}$ have the same form $(\sigma \cdot H)$ and so we can not distinguish between them, as was pointed out by YAMADA⁽⁴⁾. Hence, we can not discard the first term in (10). In this case, $i\gamma_\mu A_\mu \rightarrow (1/2m)(\sigma \cdot H)$ and we can see that the term containing G in the 1-st term of (10) cancels the 2-nd, and so: the non-covariant moment is given by

$$(12) \quad \mu_{n.c.} = \frac{e}{2m} \frac{2}{(2\pi)^4} D_0 ,$$

D_0 is the value of D , obtained by putting

$$K = 0 , \quad P = P_0 = (0, m) .$$

Alternatively, (12) can be derived more rigorously as follows. Take a reference system in which

$$p'_\mu = -p_\mu = \frac{1}{2} K_\mu \quad (\mu = 1, 2, 3)$$

and so

$$K_4 = 0 , \quad P_\mu = 0 \quad (\mu = 1, 2, 3)$$

and also choose the gauge so that $A_4 = 0$. Then, $P_\mu A_\mu = 0$, and using Dirac's equation, we have

$$\bar{u}(p') \gamma_\mu u(p) = -\frac{i}{4m} \bar{u}(p') [\gamma K, \gamma_\mu] u(p) ,$$

which gives formula (12) from (9). We therefore have the interesting fact

(4) E. YAMADA: private communication.

that the non-covariant calculation of the magnetic moment yields a value different from that obtained by means of the covariant method. For example, D_0 is divergent, at least in the 2-nd order perturbation calculation, but G_0 is not. However, this is not a real contradiction. It is due to the fact that we are calculating only the meson-contribution to the magnetic moment. If we take account of the contribution from the nucleon current, too, this discrepancy disappears. Hence, it will not be necessary to distinguish between μ_e and $\mu_{n.e.}$. To show this, add the contribution from the nucleon current to (10), then we know that the divergent term of the coefficient of γ_μ must vanish because of Ward's identity⁽⁵⁾ (in the approximation in which the photon interaction is considered only to the lowest order, namely when $z_3 = 1$). This means

$$D_0 - mG_0 + D_0^{(N)} - mG_0^{(N)} = 0,$$

where $D_0^{(N)}$ and $G_0^{(N)}$ are the contribution from the nucleon current. Therefore, formula (12) for the magnetic moment gives the same result as formula (11). Consequently, if we consider all contributions together, $\mu_{n.e.}$ is not different from μ_e . But part by part, the contribution to $\mu_{n.e.}$ and μ_e are different. Since we are calculating only the meson-current part, we can expect a difference between μ_e and $\mu_{n.e.}$. However, as we shall see later, this difference is small if we take a cut-off at the nucleon mass for high momentum. We shall discuss this point later.

Now, let us return to our original problem. As was mentioned at the beginning, $R_{\alpha\beta}$ in (2) is the scattering amplitude of a virtual meson scattered by a real nucleon. If the meson is real, namely if Q satisfies

$$(13) \quad (Q \pm \frac{1}{2}K)^2 + \mu^2 = 0,$$

we can use a relativistic dispersion relation for $A^{(\pm)}$ and $B^{(\pm)}$. In this case, according to CHEW⁽²⁾,

$$(14) \quad \left| \begin{array}{l} A^{(\pm)}(P, Q, K) = \int\limits_{(m+\mu)^2}^{\infty} dx \varrho_1^{(\pm)}(x) \left[\frac{1}{(P+Q)^2 + x - i\varepsilon} \pm \frac{1}{(P-Q)^2 + x - i\varepsilon} \right], \\ B^{(\pm)}(P, Q, K) = g^2 \left[\frac{1}{(P+Q)^2 + m^2 - i\varepsilon} \mp \frac{1}{(P-Q)^2 + m^2 - i\varepsilon} \right] + \\ \quad \mp \int\limits_{(m+\mu)^2}^{\infty} dx \varrho_2^{(\pm)}(x) \left[\frac{1}{(P+Q)^2 + x - i\varepsilon} \mp \frac{1}{(P-Q)^2 + x - i\varepsilon} \right], \end{array} \right.$$

⁽⁵⁾ J. WARD: *Phys. Rev.*, **78**, 182 (1950).

and

$$(15) \quad \left\{ \begin{array}{l} \varrho_1^{(\pm)}(x) = \frac{1}{\pi} \operatorname{Im} A^{(\pm)}(P, Q, K), \\ \varrho_2^{(\pm)}(x) = \frac{1}{\pi} \operatorname{Im} B^{(\pm)}(P, Q, K), \end{array} \right.$$

where, on the right hand side, Q must be replaced by

$$(16) \quad \left\{ \begin{array}{l} QK = 0, \quad -Q^2 = \mu^2 + \frac{1}{4}K^2 \\ QP = -\frac{1}{2}[x + P^2 - \frac{1}{4}K^2 - \mu^2]. \end{array} \right.$$

g^2 in (14) is the renormalized coupling constant, and ϱ_1 and ϱ_2 are independent of Q . Furthermore,

$$(17) \quad \left\{ \begin{array}{l} \operatorname{Im} A^{(\pm)} = \frac{w+m}{E+m} \sum_{i=0}^{\infty} q[P'_{i+1}(t)\sigma_{i+}^{(\pm)} - P'_{i-1}(t)\sigma_{i-}^{(\pm)}] - \\ \quad - \frac{w-m}{E-m} \sum_{i=0}^{\infty} q[\sigma_{i-}^{(\pm)} - \sigma_{i+}^{(\pm)}]P'_i(t), \\ \operatorname{Im} B^{(\pm)} = \frac{1}{E+m} \sum_{i=0}^{\infty} q[P'_{i+1}(t)\sigma_{i+}^{(\pm)} - P'_{i-1}(t)\sigma_{i-}^{(\pm)}] + \\ \quad + \frac{1}{E-m} \sum_{i=0}^{\infty} q[\sigma_{i-}^{(\pm)} - \sigma_{i+}^{(\pm)}]P'_i(t), \end{array} \right.$$

where q is the magnitude of the 3-momentum in the barycentric system, E is the energy of the nucleon alone, W is the total energy of the system, and

$$t = 1 - \frac{2K^2}{q^2}.$$

Now, our assumption is to use (14), even if Q does not satisfy the condition (13), which means that mesons are real. Justification for this is that the procedure is correct in the static limit as was exploited by MIYAZAWA (1). Namely, in the static limit, the matrix element for the emission or absorption of a pion depends linearly on the spatial momentum of the pion. Thus, processes involving the creation or annihilation of virtual mesons by nucleons can be interpreted in terms of real meson processes. Therefore, to use (14) for virtual meson scattering is correct in the lowest order of μ/m , if we neglect the pion-pion scattering diagram or pair creation graphs, which gives S -wave pions and so is expected to give small contribution to the magnetic moment. Actually, as we will see below, this procedure gives exactly the same result as MIYAZAWA's

in the non-relativistic limit. To better understand the nature of our approximation, consider the original idea by NAMBU⁽⁶⁾ on the representation of the Green function. According to NAMBU, $A^{(\pm)}$ and $B^{(\pm)}$ can be represented in the form

$$(18) \quad A^{(\pm)} \text{ or } B^{(\pm)} = \iiint dx dy dz \left[\frac{1}{(P+Q)^2 + x - i\varepsilon} \pm \frac{1}{(P-Q)^2 + \bar{x} - i\varepsilon} \right] \cdot \frac{(Q + \frac{1}{2}K)^2 + \mu^2}{(Q + \frac{1}{2}K)^2 + y - i\varepsilon} \frac{(Q - \frac{1}{2}K)^2 + \mu^2}{(Q - \frac{1}{2}K)^2 + z - i\varepsilon} \varrho_j^{(\pm)}(x, y, z),$$

where the integration range for x is the same as in (14), and for y and z it is the discrete point $y=\mu^2$ and the continuous range from $y, z \geq (3\mu)^2$. To use (14) means to neglect the continuous region $y, z \geq (3\mu)^2$ in the above. This corresponds to neglecting 3-pion production diagrams or pair creation graphs by incoming or outgoing virtual mesons. But unfortunately, the Nambu representation (18) seems incorrect.

A general representation⁽⁷⁾ of the Green function based upon a somewhat more rigorous basis gives an expression more complicated than (18), and unfortunately difficult to be applied here.

It is probable that (18) may be true, if we restrict ourselves only to the contributions from a special class of diagrams: (e.g. the ladder type). This possibility is being investigated⁽⁸⁾.

Returning to the beginning, the use of (14) is correct to the lowest order of μ/m , as was mentioned before. Now, the calculation of the magnetic moment is straightforward. To show that our method gives Miyazawa's result, we must calculate D_0 in accordance with the non-covariant formula (12). Inserting (5), and (14) into (8), integrating first with respect to the 4-th component Q_0 of the 4-momentum Q , neglecting terms of higher order than μ/m , and keeping only p -wave contribution in (17), we get the expression for the magnetic moment from (12):

$$(19) \quad \mu_{n.c.} = \left(\frac{e}{2m} \right) \left(\frac{8}{3\pi} \right) \frac{m}{\mu^2} \left(\frac{f^2}{4\pi} \right) \int_0^\infty dk \frac{k^4}{\omega_k^4} + \left(\frac{e}{2m} \right) \frac{m}{9\pi^2} \int_0^\infty dl l^4 \int_0^\infty dk \frac{1}{\omega_k} \left[\frac{1}{\omega_l^2(\omega_k + \omega_l)^2} + \frac{1}{\omega_l^3(\omega_k + \omega_l)} \right] \cdot [\sigma_{11}(k) - \sigma_{13}(k) - \sigma_{31}(k) + \sigma_{33}(k)],$$

⁽⁶⁾ Y. NAMBU: *Phys. Rev.*, **100**, 394 (1955).

⁽⁷⁾ Y. NAMBU: preprint; J. SCHWINGER: *Seventh Rochester Conference*.

⁽⁸⁾ This was suggested by Professor NAMBU. The author would like to express his thanks to Professor NAMBU for the comment.

where σ_{ij} is defined by

$$\sigma_{ij} = 4\pi \sin^2 \delta_{ij}/k^2$$

and we replaced g by $(2m/\mu)f$. If we notice that our definition of δ_{ij} differs by a factor 3 from Miyazawa's, we see that (19) gives exactly his formula.

Now, let us make a covariant calculation, using Feynman techniques: then we have

$$(20) \quad \left\{ \begin{array}{l} D_0 = -i \int dx \varrho_2^{(-)}(x) \int_0^1 dt (1-t) \int d^4 Q \frac{Q^2}{[Q^2 - m^2 t(1-t) + xt + \mu^2(1-t)]^3}, \\ G_0 = 2\pi^2 \int dx \int_0^1 dt \frac{t(1-t)[-\varrho_1^{(-)}(x) + mt\varrho_2^{(-)}(x)]}{[-m^2 t(1-t) + xt + \mu^2(1-t)]}. \end{array} \right.$$

Now, we again take the large mass limit, and neglect higher order waves than the P -wave. Then, from (15), (16) and (17), we get the covariant expression (11) for the magnetic moment:

$$(21) \quad \mu_c \doteq \frac{e}{2m} \left\{ \frac{2}{\pi} \left(\frac{m^2}{\mu^2} \right) \frac{f^2}{4\pi} + \frac{m^2}{6\pi^3} \int_0^\infty dk \frac{1}{\omega_k} [\sigma_{11}(k) - \sigma_{13}(k) - \sigma_{31}(k) + \sigma_{33}(k)] \right\}.$$

The 1-st term of (21) agrees with Case's ⁽⁹⁾ result; comparing (21) with (19), we see that the divergent integrals in (19) are replaced as follows:

$$\begin{aligned} & \int_0^\infty dk \frac{k^4}{\omega_k^4} \rightarrow \frac{3}{4} m, \\ & \int_0^\infty dl l^4 \left[\frac{1}{\omega_l^2(\omega_k + \omega_l)^2} + \frac{1}{\omega_l^3(\omega_k + \omega_l)} \right] \rightarrow \frac{3}{2} m. \end{aligned}$$

If the high moment cut-off is taken near the nucleon rest mass, this correspondence is almost statified. So, $\mu_{n.c.}$ gives almost the same value as μ_c . This circumstance means that the divergent term proportional to γ_μ in the nucleon current contribution is small if we use the same cut-off, as is clear from the argument presented earlier, in connection with the definition of μ_c and $\mu_{n.c.}$.

Let us investigate this point a little more carefully by making a covariant

⁽⁹⁾ K. CASE: *Phys. Rev.*, **76**, 1 (1949).

calculation of D_0 in (20). Separating the divergent term by first integrating partially with respect to t , and then taking the large mass limit after the Q -integration, we find

$$(22) \quad \mu_{n.c.} \doteqdot \left[1 + \frac{1}{3} \log \left(\frac{m^2 + L^2}{m^2} \right) - \frac{L^2(3L^2 + 2m^2)}{6(m^2 + L^2)^2} \right] \frac{3}{2} \mu_c,$$

where μ_c is given by (21); and L^2 is the cut-off momentum in the four dimensional Q -integral. Note that (22) is logarithmically divergent, whereas (19) diverges linearly. Hence (22) is rather insensitive to the cut-off, and if we take $L^2 \sim m^2$, we find that L^2 -dependent terms almost cancel each other and involve a correction of a few per cent only. Essentially, we have therefore

$$(22)' \quad \mu_{n.c.} \doteqdot \frac{3}{2} \mu_c.$$

The formula (21) does not contain explicit divergence, different from (19), and is in this respect superior to the non-covariant calculation (19). But actually the integral (21) may diverge at high momenta, as we show in the Appendix. However, our approximation is correct only for the low energy region, and so anyway it is necessary to cut-off the integral in (21) near the nucleon rest mass.

3. – The nucleon current contribution to the anomalous moment.

The magnetic moment operator arising from the nucleon-current is:

$$M_3^{(N)} = \frac{1}{2} ie \int dV \bar{\psi}(x_1 \gamma_2 - x_2 \gamma_1) \frac{1 + \tau_3}{2} \psi.$$

It is convenient to divide this expression into scalar and vector parts. The former is defined as the part which is independent of τ_3 and the latter as proportional to τ_3 .

In the static limit, MIYAZAWA⁽¹⁾ could calculate both parts in terms of the pion-nucleon scattering phase-shift. In the calculation of the scalar part, he utilized the fact that the physical nucleon state has total angular momentum $\frac{1}{2}$. As we shall see, for this part, we can extend his method, covariantly if we use the same approximation as was used in the previous calculation. For the vector part of the magnetic moment, Miyazawa's method was based upon the simple observation that in the static approximation, its matrix element has exactly the same form as that of the vertex operator of the static pseudo-vector interaction. Unfortunately, this connection only seems to hold in the static limit and the author has failed to obtain a covariant generalization of this result. It is quite probable that Miyazawa's success is dependent upon

the specific form of the interaction Hamiltonian, and hence is not derivable from dispersion relations and other general principles alone.

We therefore calculate only the scalar part, but we note that our method differs a little from Miyazawa's, in which the specific form of the interaction Hamiltonian was necessary, because the dispersion relation and other general principles are essential in our calculation. Now, let us consider the angular momentum (10):

$$(23) \quad \left\{ \begin{array}{l} J_3 = J_3^{(N)} + J_3^{(m)}, \\ J_3^{(N)} = -\frac{1}{4} i \int dV \left\{ \bar{\psi}(x_1\gamma_2 - x_2\gamma_1) \frac{\partial\psi}{\partial x_1} - \frac{\partial\bar{\psi}}{\partial x_1} (x_1\gamma_2 - x_2\gamma_1)\psi + \right. \right. \\ \left. \left. + \bar{\psi}\gamma_4 \left(x_1 \frac{\partial}{\partial x_2} - x_2 \frac{\partial}{\partial x_1} \right) \psi - \left(x_1 \frac{\partial}{\partial x_2} - x_2 \frac{\partial}{\partial x_1} \right) \bar{\psi} \cdot \gamma_4 \psi \right\}, \end{array} \right.$$

and

$$(24) \quad J_3^{(m)} = -i \int dV \left(x_1 \frac{\partial\varphi_\alpha}{\partial x_2} - x_2 \frac{\partial\varphi_\alpha}{\partial x_1} \right) \frac{\partial\varphi_\alpha}{\partial x_4}.$$

For the nucleon part, let us use the relation:

$$\frac{\partial}{\partial x_\mu} \psi = i[\psi, G_\mu],$$

where G_μ is the 4-momentum operator. Then,

$$(23') \quad J_3^{(N)} = \frac{1}{4} i \int dV \left\{ H\bar{\psi}(x_1\gamma_2 - x_2\gamma_1)\psi + \bar{\psi}(x_1\gamma_2 - x_2\gamma_1)\psi H \right\} + \\ + \frac{1}{4} \int dV \left\{ (G_2 x_1 - G_1 x_2) \bar{\psi} \gamma_4 \psi + \bar{\psi} \gamma_4 \psi (G_2 x_1 - G_1 x_2) \right\} - \\ - \frac{i}{2} \int dV \bar{\psi}(x_1\gamma_2 - x_2\gamma_1)H\psi - \frac{1}{2} \int dV \bar{\psi}(x_1 G_2 - x_2 G_1) \gamma_4 \psi,$$

where H is the total Hamiltonian of the system.

As we shall see later, the last two terms are smaller than the first two, in the static limit, and so we take only the first two terms. We therefore work in the approximation:

$$(25) \quad J_3^{(N)} \doteq \frac{1}{4} i \int dV \left\{ H\bar{\psi}(x_1\gamma_2 - x_2\gamma_1)\psi + \bar{\psi}(x_1\gamma_2 - x_2\gamma_1)\psi H \right\} + \\ + \frac{1}{4} \int dV \left\{ (x_1 G_2 - x_2 G_1) \bar{\psi} \gamma_4 \psi + \bar{\psi} \gamma_4 \psi (x_1 G_2 - x_2 G_1) \right\}.$$

(10) E.g. G. WENTZEL: *Quantum Theory of Fields* (New York, 1949).

In the large mass limit, we have for the expectation value of (25):

$$\langle J_3^{(N)} \rangle \doteqdot [\frac{1}{2} \sigma_3 + x_1 p_2 - x_2 p_1],$$

Thus (25) gives the usual expression for the angular momentum in the static limit.

Therefore, we can expect that the neglected terms in $J_3^{(N)}$ are of higher order in μ/m . For example, let us take the third term in (23)'. Taking the matrix element between real nucleon states:

$$\left\langle \int \bar{\psi}(x_1 \gamma_2 - x_2 \gamma_1) H \psi dV \right\rangle = \int dV (x_1 \gamma_2 - x_2 \gamma_1)_{\beta} \cdot \sum_n (\Psi^* \bar{\psi} \Psi_n) E_n (\Psi_n^* \psi_{\beta} \Psi). \quad (25)'$$

From the conservation of the Fermion number, Ψ_n must contain only mesons, or equal numbers of nucleons and anti-nucleons. Nucleon pair effects are probably small, because in this case, it will give the *S*-wave meson contribution. So assuming that the main contribution will come from intermediate states containing only one meson, we can say that $E_n \sim \mu$. This is smaller by a factor of μ/m , compared with the first term of (25)'. Thus our calculation is valid only to lowest order in μ/m .

Now, we know that the nucleon is an eigenstate of the angular momentum J_3 in its rest system. Therefore,

$$(\Psi^*(0) J_3 \Psi(p)) = \frac{1}{2} (u^*(0) \sigma_3 u(0)) \delta^{(3)}(\mathbf{p}),$$

where $u(0)$ is the usual Dirac spinor at zero momentum. Or more conveniently, if we note that J_3 commutes with the total Hamiltonian, we can rewrite it as:

$$(26) \quad \left(\Psi^*(0) \int_{-\infty}^{\infty} dt J_3 \Psi(p) \right) = \pi (u^*(0) \sigma_3 u(0)) \delta^{(4)}(K),$$

where $K = p' - p$, $p' = (0, m)$.

Inserting (26) into this expression, we get:

$$(27) \quad \begin{aligned} & \frac{i}{4} (E_p + m) \left(\Psi^*(0) \int d^4x \bar{\psi}(x_1 \gamma_2 - x_2 \gamma_1) \psi \Psi(p) \right) + \\ & + \frac{1}{4} \left(\Psi^*(0) \int d^4x \bar{\psi}(x_1 p_2 - x_2 p_1) \gamma_4 \psi \Psi(p) \right) + \left(\Psi^*(0) \int_{-\infty}^{\infty} dt J_3^{(m)} \Psi(p) \right) = \pi (u^*(0) \sigma_3 u(0)) \delta(K). \end{aligned}$$

We note that the first term of (27) is essentially the scalar part of the mag-

netic moment, namely:

$$(28) \quad \frac{i}{4} \left(\Psi^*(0) \int d^4x \bar{\psi}(x_1 \gamma_2 - x_2 \gamma_1) \psi \Psi(p) \right) \equiv \pi(\mu_s/e)(u^*(0) \sigma_3 u(0)) \delta(K),$$

where

$$(29) \quad \mu_s = \mu_p + \mu_N.$$

The second term of (27) gives zero as we prove below. Hence, if we write:

$$(30) \quad \left(\Psi^*(0) \int_{-\infty}^{\infty} dt J_3^{(m)} \Psi(p) \right) = A u^*(0) \sigma_3 u(0) \delta(K),$$

then, (27), (28), and (30) finally yield:

$$\mu_s = + \frac{e}{2m} \left(1 - \frac{1}{\pi} A \right).$$

By omitting the intrinsic Dirac moment, we have

$$(31) \quad \mu_s = - \frac{e}{2m} \frac{1}{\pi} A,$$

where this definition contains only the anomalous part.

Now, let us prove that the second term of (27) is zero. If we use:

$$(32) \quad \begin{cases} \psi(x) = \exp[-iGx] \psi(0) \exp[iGx], \\ \left(\Psi^*(0) \int d^4x \psi^*(x_1 p_2 - x_2 p_1) \psi \Psi(p) \right) = \\ = -(2\pi)^4 i \left(p_2 \frac{\partial \delta(p)}{\partial p_1} - p_1 \frac{\partial \delta(p)}{\partial p_2} \right) (\Psi^*(0) \psi^*(0) \psi(0) \Psi(p)), \end{cases}$$

and if we note:

$$\left(\Psi^*(0) \int \psi^*(x) \psi(x) dV \Psi(p) \right) = (\Psi^*(0) \Psi(p)) = \delta^{(2)}(\mathbf{p}),$$

because of Fermion number conservation, then

$$(\Psi^*(0) \psi^*(0) \psi(0) \Psi(0)) = \frac{1}{(2\pi)^3}$$

is finite. And finally if we remark that

$$(33) \quad p_\mu \frac{\partial \delta(p)}{\partial p_\nu} + \delta_{\mu\nu} \delta(p) = 0,$$

we see that (32) is zero. Thus (31) follows.

The next problem is the calculation of (30). We take the inverse Fourier transform of (2), and apply it to the explicit expression (24) for $J_3^{(M)}$. Using (33), we can put $K=0$ in the whole calculation, and we get next, taking account of (5) and (14), by using the same approximation as was used before

$$(34) \quad \left(\Psi^*(p') \int_{-\infty}^{\infty} dt J_3^{(m)} \Psi(p) \right) = \frac{1}{(2\pi)^3} \left(\frac{m^2}{E_p E'_p} \right)^{\frac{1}{2}} \bar{u}(p') M u(p),$$

where

$$(35) \quad M = \left\{ (i\gamma_4 P_2 + i\gamma_2 P_4) \frac{\partial \delta(K)}{\partial K_1} - (i\gamma_4 P_1 + i\gamma_1 P_4) \frac{\partial \delta(K)}{\partial K_2} \right\} S - \\ - P_4 \left(P_2 \frac{\partial \delta(K)}{\partial K_1} - P_1 \frac{\partial \delta(K)}{\partial K_2} \right) T, \\ (36) \quad \begin{cases} S = -3i \int dx \varrho_2^{(+)}(x) \int_0^1 dt t(1-t) \int d^4Q \frac{Q^2}{[Q^2 + P^2 t(1-t) + xt + \mu^2(1-t)]^3}, \\ T = 6\pi^2 \int dx \int_0^1 dt \frac{t^2(1-t)[\varrho_1^{(+)}(x) - m t \varrho_2^{(+)}(x)]}{P^2 t(1-t) + xt + \mu^2(1-t)}. \end{cases}$$

Now, put $p'_\mu = 0$ for $\mu = 1, 2, 3$, and so

$$\begin{aligned} P_\mu &= \frac{1}{2} p_\mu & (\mu = 1, 2, 3) & \quad P_4 = (i/\hbar)(E_p + m) \\ K_\mu &= -p_\mu & (\mu = 1, 2, 3) & \quad K_4 = i(m - E_p) \end{aligned}$$

and use the explicit form for $u(p)$:

$$u(p) = \left(\frac{1}{2m(E_p + m)} \right)^{\frac{1}{2}} (-i\gamma p + m) u(0).$$

Then, if we use (33) we have:

$$\left(\Psi^*(0) \int_{-\infty}^{\infty} dt J_3^{(m)} \Psi(p) \right) = \frac{1}{(2\pi)^3} S u^*(0) \sigma_3 u(0) \delta(K).$$

Comparing this with (30),

$$A = \frac{1}{(2\pi)^3} S,$$

and so from (31),

$$(37) \quad \mu_s = -\frac{e}{2m} \frac{1}{8\pi^4} S_0.$$

As we see from (36), S is logarithmically divergent.

The occurrence of the above divergence is probably due to our approximation (25), for $J_3^{(N)}$ because μ_s should be divergenceless. We note that in this case, because of Ward's identity for the scalar part, it is not necessary to make any distinction between μ_s and $\mu_{n.c.}$, which is different from the meson current case. In (36), we put $P^2 = -m^2$ and separate the divergence by partial integration on t , and after that, take the large mass limit. By using (15) and (17), and keeping only P -waves again, we have the following expression:

$$(38) \quad \mu_s \doteq -\frac{e}{2m} \left[\frac{5}{3} + \log \left(\frac{m^2 + L^2}{m^2} \right) - \frac{L^2(3L^2 + 2m^2)}{2(m^2 + L^2)^2} \right] \left(\frac{m^2}{\pi\mu^2} \right) \cdot \left| \frac{f^2}{4\pi} - \frac{\mu^2}{12\pi^2} \int_0^\infty dp \frac{1}{\omega_p} (2\sigma_{33}(p) + \sigma_{31}(p) - 2\sigma_{13}(p) - \sigma_{11}(p)) \right|,$$

where L^2 here is the cut-off momentum. If we take $L^2 \sim m^2$, then the L^2 -dependent terms can be seen to largely cancel each other, again. Therefore, we can neglect the L^2 -dependent terms and so

$$(38') \quad \mu_s \doteq -\frac{e}{2m} \left(\frac{3m^2}{\pi\mu^2} \right) \cdot \frac{5}{9} \left| \left(\frac{f^2}{4\pi} \right) - \frac{\mu^2}{12\pi^2} \int_0^\infty dp \frac{1}{\omega_p} (2\sigma_{33}(p) + \sigma_{31}(p) - 2\sigma_{13}(p) - \sigma_{11}(p)) \right|.$$

This is effectively divergenceless in the same sense as in the meson current case.

We can calculate μ_s completely non-covariantly, if we go back to the original definition of S , given by (35), and first integrate over the 4-th component of the 4-vector Q , and neglect terms of order μ/m . Then we get instead

of (38) or (38)':

$$(39) \quad \mu_s' = -\frac{e}{2m} \left\{ \frac{f^2}{4\pi} \frac{4}{\pi\mu^2} \int_0^\infty dk \frac{k^4}{\omega_k^3} - \right. \\ \left. - \frac{\mu^2}{3\pi^3} \int_0^\infty dk \int_0^\infty dp \frac{k^4}{\omega_p \omega_k (\omega_p + \omega_k)^2} [2\sigma_{33}(p) + \sigma_{31}(p) - 2\sigma_{13}(p) - \sigma_{11}(p)] \right\}.$$

This is essentially the same formula as given by MIYAZAWA (1), if we note that our μ_s differs by a factor 2 from his. Notice that (39) is quadratically divergent, and depends sensitively on the cut-off momentum. Thus, the covariant formula (38) or (38)' is much superior to the non-covariant formula (39).

If we compare (39) with (38)', we see that the divergent integrals of (39) are replaced in (38)' according to the scheme:

$$\int_0^\infty dk \frac{k^4}{\omega_k^3} \rightarrow \frac{5}{12} m^2, \\ \int_0^\infty dk \frac{k^4}{\omega_k(\omega_p + \omega_k)^2} \rightarrow \frac{5}{12} m^2.$$

If we take the cut-off momentum at $k \simeq m$, these conditions are almost satisfied. Therefore, in the non-covariant formula (39), we should take the cut-off at $k \simeq m$.

If one follows the above prescription in applying Miyazawa's result, the situation becomes less favourable because experimentally, $\mu_s = -0.12$, and the Born term of (38)' gives $\mu_s = -1.8$ for $f^2/4\pi = 0.08$. Of course, the contribution from the second term of (38)' reduces this number. However, this reduction is not sufficient to achieve the small experimental value. MIYAZAWA took the cut-off at $k \sim 5$ or $6 \mu\text{m}$, to obtain a small Born term for (39), although it is still not small enough to match the experimental value.

Finally we point out, that the terms neglected in the approximation of (25) tend to reduce (38)' slightly in the correct direction toward the experimental value, but this reduction is probably not sufficient, because it contains terms of higher order in μ/m .

* * *

The author would like to express his sincere thanks to Professor R. MARSHAK for suggesting this problem to him. He is also grateful to Drs. C. GOEBEL, G. SALZMAN, and Mr. G. SUDARSHAN for reading the original manuscript, and to Dr. K. TANAKA for useful comments.

APPENDIX

Let us divide the diagrams, which were considered in the calculation in 2 as follows:

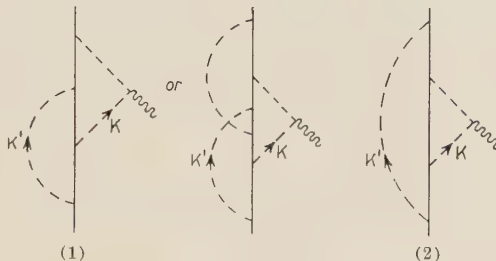


Fig. 2.

Let us consider diagrams of the type shown in Graph 1. We first integrate over the momentum k' of the inner lines and then absorb all divergences into charge and amplitude renormalization. After that, we integrate over the momentum k of the outer meson line, which interacts with the external electromagnetic field. In this case, we separate the divergent term $\gamma_\mu D_0$ and in the covariant calculation, we discard it. Thus, we have a finite contribution for μ_c : However, the situation is somewhat different for diagrams of the type shown in Graph 2. The order of our integration is different from the usual one in the renormalization theory. We fix k and integrate over k' first; then except for the renormalization for the meson field, no divergence appears. Next, we integrate over k and subtract the divergent term $\gamma_\mu D_0$. But in the usual renormalization procedure, the order of integration is reversed, namely we integrate over k first, and subtract the divergence, and after that integrate over k' . In the first k integration, the finite term gives, of course, a finite contribution to the magnetic moment, but the divergent term there has essentially the same form as the contribution from the nucleon current as in Fig. A3. Hence, our μ_c really has the form:

$$\mu_c = \mu_0 + A\mu_1$$

where μ_0 is finite, μ_1 is essentially the contribution to the anomalous magnetic moment from the τ_3 part of the nucleon current, and A is some divergent quantity. According to Ward's (5) identity, this divergence must be cancelled, if we add the contribution from the nucleon-current to it.



Fig. 3.

RIASSUNTO (*)

Si dà un'estensione covariante del metodo di Miyazawa per il calcolo del momento magnetico anomalo del nucleone usando relazioni di dispersione covarianti. Trattando l'argomento si considera la differenza tra le definizioni covarianti e non covarianti del momento magnetico dovuto al contributo della corrente mesonica.

(*) *Traduzione a cura della Redazione.*

Anomalous Heavy Primary Cascades Recorded on Viking 10 Rocket Flight (*).

H. YAGODA

National Institutes of Health - Bethesda, Md.

(ricevuto il 28 Maggio 1957)

Summary. — Emulsions flown to 136 miles on Viking 10 surrounded by only $2 \text{ g} \cdot \text{cm}^{-2}$ of superimposed metallic absorber have recorded two examples of heavy primaries which on collision with emulsion nuclei are not destroyed catastrophically. The heavily charged relativistic fragments emerging from the primary act produce secondary collisions after traversing distances that are small compared with the collision mean free path of the identified nuclei. The first event initiated by a particle of charge 14 ± 1 encompasses a total of 5 collisions which could originate by successive chance deviations from the geometric mean free path with a probability of $1.3 \cdot 10^{-6}$. The second cascade initiated by a carbon nucleus passes through two stages, and has its charge reduced to $Z = 3$ before the latter escapes from the detector. Considerations of the relative frequency of different modes of fragmentation and geometric escape further reduce the probability of these events originating by chance and being detected.

1. — Introduction.

On May 7, 1954 a 72.8 cm^3 block of Ilford G-5 pellicles measuring $9 \times 9 \text{ cm}^2$ composed of 6 sheets $1500 \mu\text{m}$ thick was flown to a peak altitude of 136 miles. The emulsions were mounted horizontally in the upper nosecone of Viking rocket no. 10 encased in a cylindrical shell of Dural aluminum alloy with a

(*) A brief description of cascade α was presented at the New York Meeting of the American Physical Society, *Bull. Am. Phys. Soc.*, ser. II, 1, 64 (1956). This event and cascade β were discussed at the 6th Annual Rochester Conference on High Energy Physics (April 1956), p. ix-30.

uniform wall thickness of 3.2 mm, as described in Fig. 1. The emulsions were recovered in excellent condition and developed satisfactorily (19 grains per 100 μm at minimum). Since the exposure was very exceptional in being conducted both in virtually complete absence of air and with only an average of $2 \text{ g} \cdot \text{cm}^{-2}$ of superimposed metallic absorber, the emulsions provided a unique opportunity for the study of the composition of the heavy primary flux incident on the top of the atmosphere. After a preliminary survey ⁽¹⁾ 48 particles of charge $6 < Z < 10$ and 24 particles of $Z > 10$ were observed in the stack corresponding to a total flux for heavy nuclei of $Z \geq 6$ of $(6.6 \pm 0.8) \text{ m}^{-2} \text{ s}^{-1} \text{ sr}^{-1}$ and M^0/H^0 ratio of 1.96 ± 0.5 at the top of the atmosphere for the medium and heavy groups of nuclei when corrected for fragmentation in condensed matter above the emulsions.

In following the heavy primary tracks through the horizontal stack we observed a total of 8 primary collisions initiated by particles of $Z \geq 6$, a description of which is given in Table I. Events α and β are noteworthy in that after the primary collision the heavy fragmentation products produce further secondary collisions after traversing comparatively short distances in the emulsion and these events will be referred to as anomalous cascades. Four additional units of emulsion of 63 cm^3 total volume were also recovered. These were located symmetrically with respect to position C of Fig. 1 in a vertical

plane facing the rocket skin. Radiation directed towards the back of the emulsions, however, encountered about 85 lbs. of instrumentation (chiefly aluminum). The average condensed matter absorption path for both faces is estimated at $(15 \pm 3) \text{ g} \cdot \text{cm}^{-2}$. Five additional heavy primary initiated interactions were observed in these less favorably exposed preparations, which are described in the lower half of Table I.

All charge determinations are based on δ -ray densities of 3 or more developed grains apparently associated with the trajectory. The primary charge stan-

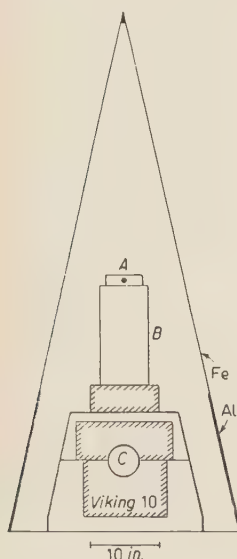


Fig. 1. - Nosecone instrument section of Viking 10, showing horizontal block of emulsion A supported on a thin walled aluminum cylinder B . The emulsion housing for A was uniformly $1/8$ in. thick and made of Dural. The rocket skin was made of stainless steel $1/32$ in. thick. Four additional units of emulsion were exposed vertically in a N-S-E-W position as shown at C .

⁽¹⁾ H. YAGODA: *Bull. Am. Phys. Soc.*, ser. II, **1**, 229 (1956).

dardization is based on the δ -ray density on relativistic α -particle tracks which were observed to be $0.32 \pm .02$ per $100 \mu\text{m}$. The emulsions aged only 29 days between manufacture and development. This circumstance together with the brevity of the high altitude cosmic ray exposure (411 s above 30 km) resulted in a very low random slow electron track density, and a correction for δ -ray noise was found to be unnecessary. Since the cut-off for heavy

TABLE I. — Description of heavy primary stars recorded on Viking 10 flight.

Position Event	Z	Fragments						N_π	N_h	ϵ_0 GeV
		M	Li	Be	B	He	H			
Horizontal α	14 ± 1	Si	—	—	—	—	—	1?	0	
	14	—	Li	—	B	He	0	0	1	18
	5						5	12	4	
	3						3	0	0?	11
	2						2	4	7	
Horizontal β	6	—	—	Be	—	—	2	0	4	4.7
	—	—	Li	—	—	—	1	7	3	6.4
Horizontal 177	7						7	2	0	2.0
Horizontal 174	7						7	18	3	40
Horizontal 175	6					2	2	8	8	1.1
Horizontal 175	8	N					1	1	2	
Horizontal 176	6					1	4	20	21	1.9
Horizontal 172	8	O						0	1	
Vertical 178	14						14	3	3	2.2
Vertical 183	16	S						0	1	
Vertical 183	8					4		38	18	1.6
Vertical 169	20	—	Li	—	—	1	15	0	4	
Vertical 179	12					2	8	0	4	

primary nuclei at White Sands (geomagnetic latitude 41° N) is 2.8 GeV, it can be assumed that the particles were entering the stack at near relativistic velocities and, hence the charge could be estimated from $Z = (12.6\delta)^{\frac{1}{2}}$. Owing to the large thickness of the individual pellicles and the ability to follow heavy tracks through all six layers slow particles ejected as heavy fragments from nuclear disruptions could be readily eliminated by inspection by either noting their characteristic track taper when at or near rest or by observation of their emission from the parent star.

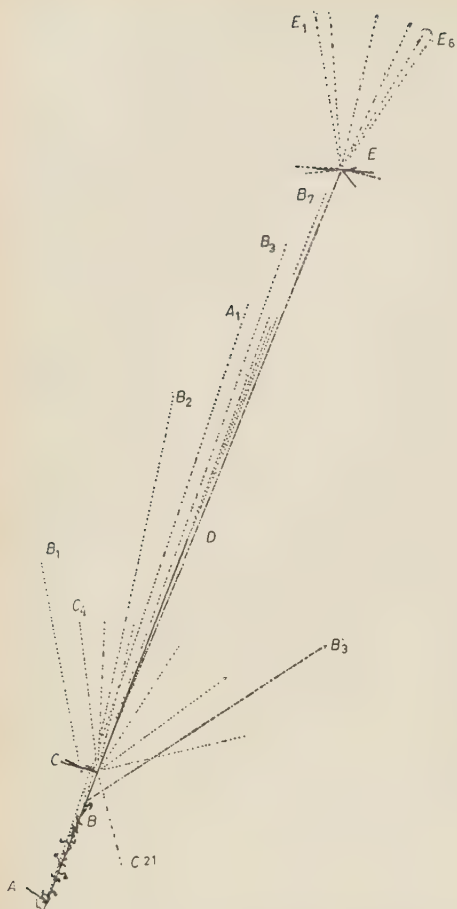


Fig. 2. — Projection drawing of cascade α .

13.7 ± 0.3 , consistent with the particle being a silicon nucleus. As shown in Fig. 4, eight particles emerge from point B , tracks $B1$ to 4 correspond to singly charged relativistic particles. Tracks $B5$ to 7 proceed in the same direction as the incident silicon nucleus and make an average angle of 0.0033 radians with the shower axis. In the region where these heavy tracks can be resolved (see insert of Fig. 4) δ -ray counts indicate that track $B5$ = lithium, track $B6$ = boron and track $B7$ = α -particle. Track $B8$ has a grain density $3.8 \times$ minimum and may represent the recoil of a target nucleon. With this assumption the collective 14 charges on tracks $B1$ to 7 confirm the δ -ray identification of the incident particle as a silicon nucleus. The small angle made by the lithium and β -particle tracks with the shower axis suggests that the incident silicon nucleus possessed a kinetic energy of 18 GeV per nucleon.

The boron nucleus makes a third collision at point C after traversing only

2. — Cascade alpha.

The first chain of rapid collisions is shown diagrammatically as a projection drawing in Fig. 2. A heavy particle enters at an apparent zenith angle of 76° with respect to the ground axis of the rocket and after traversing $310 \mu\text{m}$ makes a peripheral collision at point A . This path length is too small for a precise charge determination, but the δ -ray count is consistent with $Z=14 \pm 1$ for the parent particle. The residual nucleus and one singly charged particle ($A1$) emerge as shown in Fig. 3, at an angle 0.027 radians. Track $A1$ can be followed only in the first pellicle (23 grains per $100 \mu\text{m}$, or $1.2 \times$ min); its subsequent history in the stack is unknown, as it is impossible to follow it unambiguously owing to the swarms of similar minimum ionization tracks emerging in the nearby collision at points B , C , and D .

The residual heavy nucleus makes a second collision at point B separated by $3610 \mu\text{m}$ from point A . The δ -ray path along AB yields a charge of

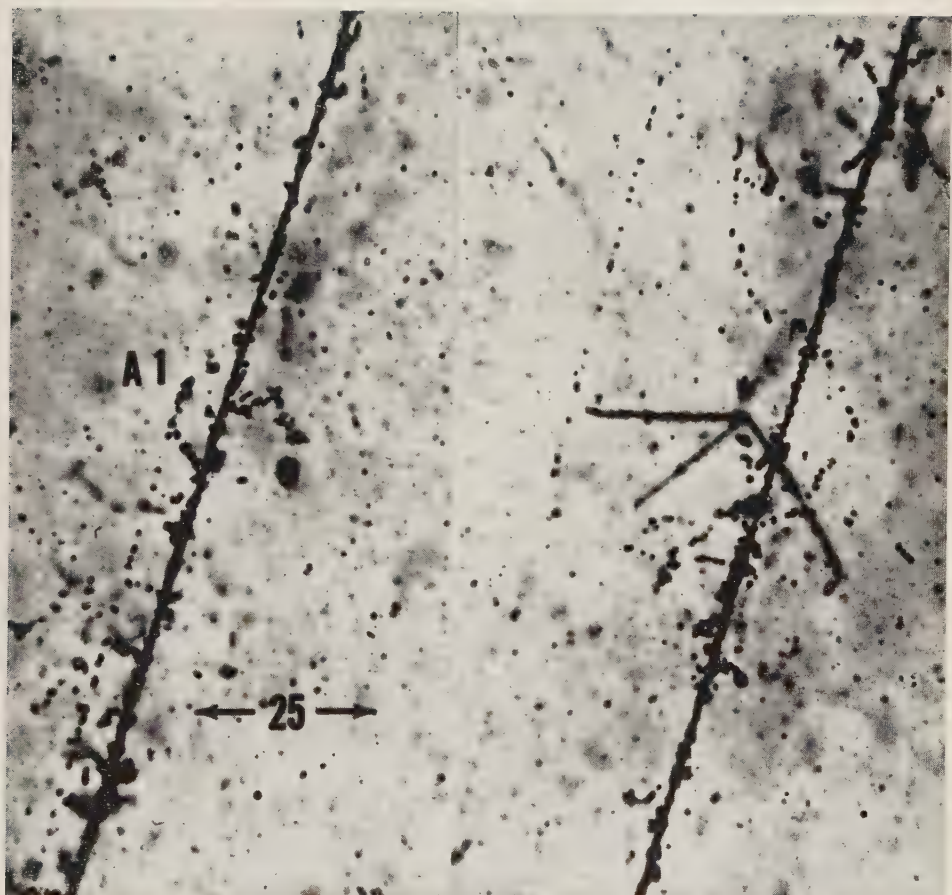


Fig. 3. — Photomicrographs of the silicon nucleus and its singly charged minimum ionization satellite track A_1 . The view on the left was taken $360 \mu\text{m}$ away from the point of interaction A , and the one at the right at a distance of $1185 \mu\text{m}$.

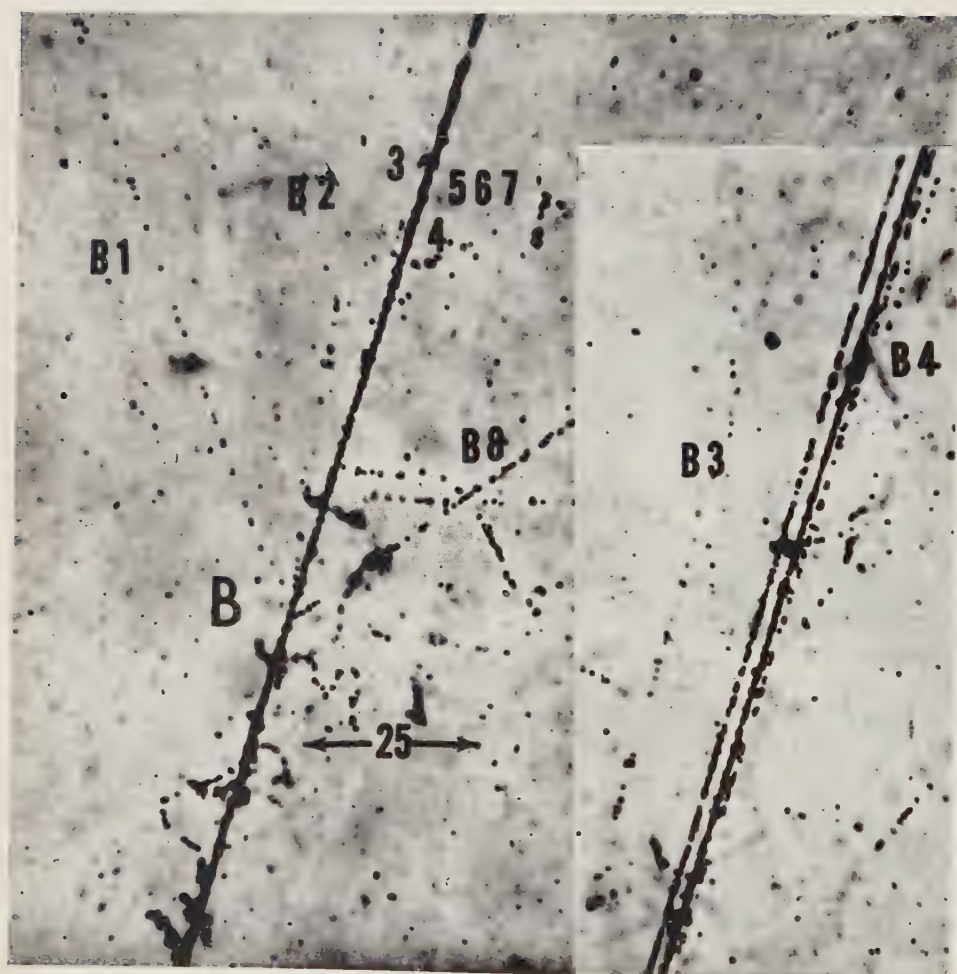


Fig. 4. — Photomicrograph of interaction *B*. The insert shows the 3 heavy fragments, tracks 5-6-7, resolved at a distance of $535 \mu\text{m}$ from point *B*. It also shows tracks *B*3 and *B*4 which also make very small angles with the shower axis.

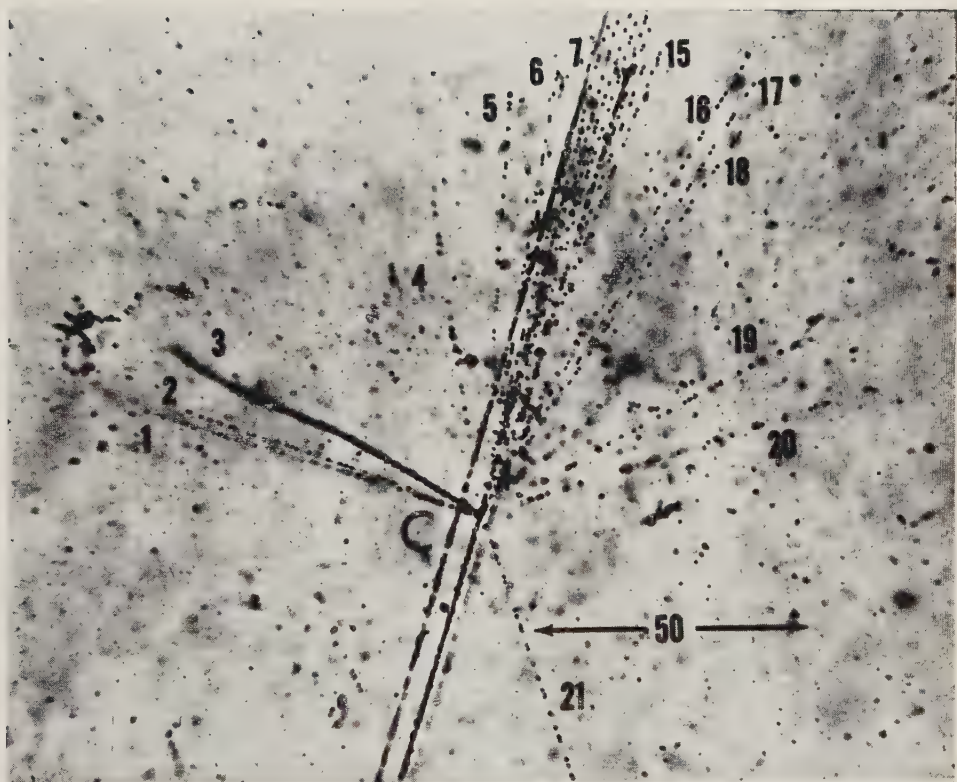


Fig. 5. — Photodrawing of interaction *C* produced by the boron nucleus originating at point *B*. Nine of the shower tracks (7-15) are emitted as a jet within a polar angle of 0.056 rad.

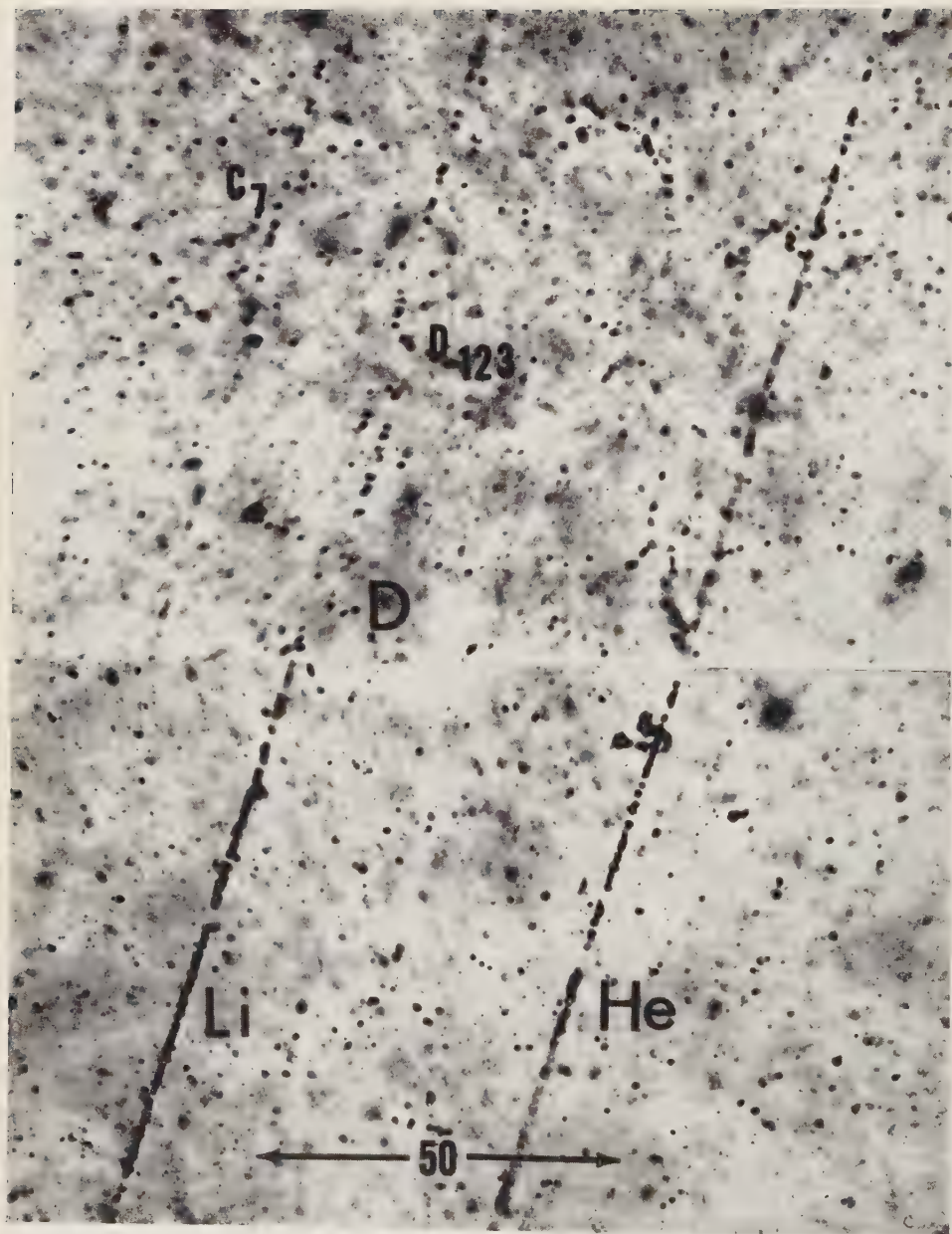


Fig. 6. Composite photomicrographs of adjoining pellicle interfaces showing the breakup of the lithium fragment created at point *B* into 3 singly charged minimum ionization tracks *D* 1-2-3. These tracks make an average angle with the initial line of flight of 0.01 rad. Tracks *D* 2-3 are superimposed near the point of interaction *D* and are not resolved in this focal setting. The particular focal setting also reveals track *C*7 and the satellite α particle fragment (*He*).

1030 μm of emulsion. As shown in Fig. 5 this collision is composed of 21 tracks only 4 of which are black or grey, the remainder corresponding to singly charged relativistic particles. Twelve of the latter are probably π or K-mesons. The ranges, grain-density and angular distribution of the shower particles are shown in Table II.

TABLE II. — *Track characteristics in interaction C of cascade α .*

Track no.	Ionization G/G Plateau	Angle with Shower Axis
1	2.8	90°
2	2.9	88°
3	> 6	77°
4	1.15	0.5 rad
5	1.20	0.32
6	(*)	0.108
7	(*)	0.049
8	(*)	0.031
9	(*)	0.026
9	1.45	0.020
11	(*)	0.016
12	(*)	0.0075
13	(*)	0.0038
14	(*)	0.019
15	1.25	0.048
16	1.05	0.202
17	1.00	0.229
18	1.15	0.243
19	(*)	45°
20	1.65	56°
21	1.15	154°

(*) These tracks are too close together for individual grain counting. They appear to be close to minimum of ionization for singly charged particles.

The lithium particle originating at point *B* traverses 7950 μm of emulsion and produces a collision in the tissue paper separating the 2nd and 3rd pellicle layers. As shown in Fig. 6 a narrow angle beam of 3 singly charged minimum ionization tracks appears at the interface of the third pellicle exactly in the position where the lithium track would have been in the absence of a collision. The satellite α -particle track, also emerging from point *B*, helps define the precise position of the interface collision. Owing to the location of collision *D* little can be said about the nature of any black or grey prongs associated with the event. Their number, however, must have been small

as no low energy tracks were observed to enter the adjoining faces of the emulsion layers. It would thus appear that the lithium fragment broke up into 3 protons as a result of a collision with a light element nucleus of the tissue paper. The 3 relativistic protons emerge with a mean angle of 0.011 radians with respect to the line of direction of the lithium fragment suggesting that the latter possessed a kinetic energy of 11 GeV per nucleon.

The α -particle originating in collision B traverses 4 pellicles and produces a star in the 5th layer after a total length of 22 mm. This collision, point E , is shown in the lower half of Fig. 7. The star consists of 7 black and gray tracks and a shower of 6 singly charged minimum tracks. A noteworthy feature of interaction E is that the 7 slow tracks are emitted largely at right angles to the incident α -particle (Table III). A similar orientation was observed by

TABLE III. — *Track characteristics of interaction E of cascade α .*

Track no.	Space angle with shower axis	Range (μm)	$(G/G)_{\text{plat.}}$	Identity	Kinetic energy, MeV
1	84.7°	13 900	—	p	63.5
2	63.4	375	—	α	32.2
3	90.0	609	—	p	10.7
4	99.8	109	—	p	3.8
5	82.8	7 100	—	p	43.2
6	87.2	630	—	p	10.9
7	77.2	escapes	3.1	p	~ 100
s 1	31.5		1.60		
s 2	27.0		1.07		
s 3	10.5		1.54		
s 4	1.5		1.08		
s 5	7.5		1.14		
s 6	10.5	17 000 (*)	1.13		

(*) Track s 6 produces a star of type 6 + 0p.

HILL⁽²⁾ in a star produced by a fast antiproton, the large transverse momentum being attributed to an annihilation process. Of the six shower particles track $E6$ produces a small star of type 6 + 0p at F after traversing 17.7 mm of emulsion. While path EF represents only a small fraction of the mean free path for protons in emulsion (~ 300 mm) we do not consider collision F as an anomaly in the cascade as a whole because the total length of all singly charged tracks associated with collisions A to F is large and the occurrence

(2) R. D. HILL, S. D. JOHANSSON and F. T. GARDNER: *Phys. Rev.*, **101**, 907 (1956); **103**, 250 (1956).

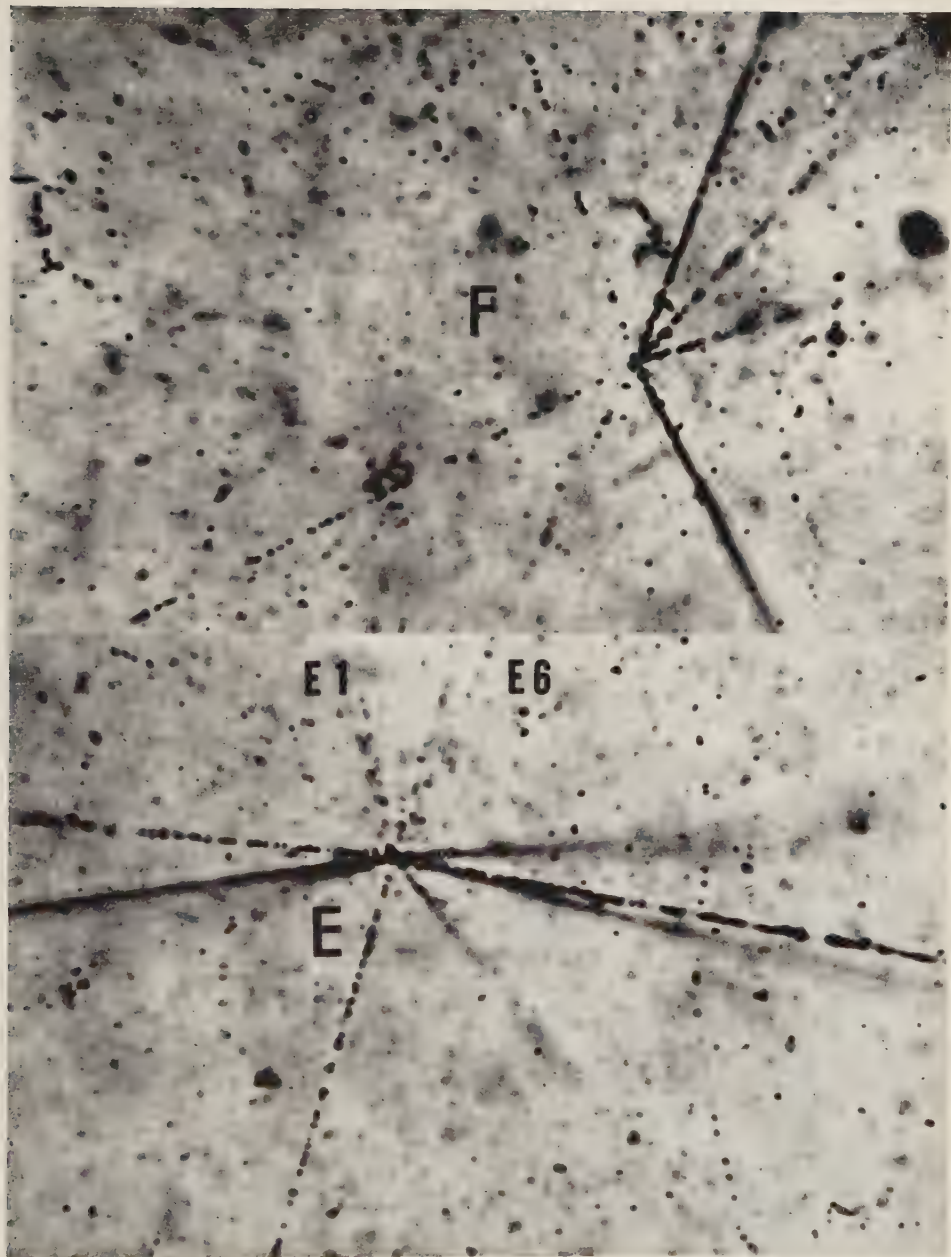


Fig. 7. - Photomicrograph of interaction *E* initiated by α particle generated at point *B* showing star of type 7-6 He. One of the shower particle tracks *E6* produces a 6 prong star *F* after traversing 17.7 mm of emulsion.

of one proton initiated star can be anticipated. It is perhaps noteworthy that in the cascade reported by MILONE⁽³⁾ one of the shower particles also interacts after traversing 18 mm of emulsion yielding a star of type 1+4p.

The 5 collisions initiated by the parent heavy primary occur over a total path of 3.49 cm of emulsion. The average collision path is 0.698 cm or $2.66 \text{ g} \cdot \text{cm}^{-2}$ on the basis of the measured density of the emulsion $3.8 \text{ g} \cdot \text{cm}^{-3}$. The average interaction path in cascade α is thus about 20 times smaller than the geometric mean free path λ for particles of $Z \geq 2$.

3. – Cascade beta.

Further scanning of the same block of emulsions has revealed a 2-stage cascade initiated by a relativistic carbon nucleus (Fig. 8). The incident particle enters the first pellicle and after traversing $340 \mu\text{m}$ breaks up into a fast Be-nucleus, 2 singly charged minimum ionization tracks and a 4-prong star. The Be-fragment travels undeviated for 43.3 mm and produces a star in the last pellicle composed of 3 evaporation tracks, 8 shower particles and a lithium fragment colinear with the Be-parent. The lithium fragment leaves the stack after 2.2 mm of recorded range. The average emulsion path length of the carbon and beryllium in these two collisions is 2.18 cm, which is about 6 times smaller than the geometric mean free path.

The kinetic energy of the incident carbon nucleus is estimated at 4.7 GeV per nucleon basis the root mean square angle of 0.026 radians made by the 2 relativistic protons associated with fragmentation A . The angular distri-

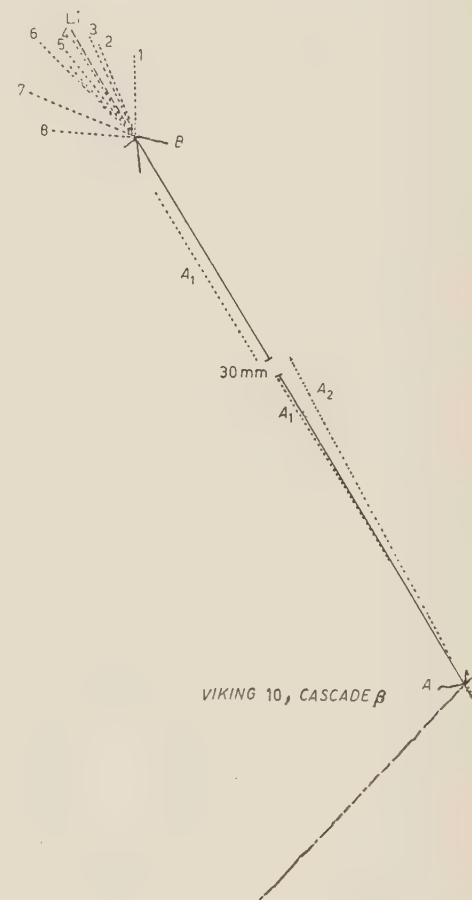


Fig. 8. – Horizontal projection of cascade β .

⁽³⁾ A. MILONE: *Suppl. Nuovo Cimento*, **2**, 353 (1954).

bution of the tracks in the meson shower initiated by the secondary beryllium fragment at point *B* provides an independent estimate of 6.4 GeV per nucleon.

It is noteworthy that the vertically oriented emulsions exposed on the same flight in the presence of $15 \text{ g} \cdot \text{cm}^{-2}$ of condensed matter did not show evidence for the cascading process. Likewise, in the examination ⁽⁴⁾ of 91 cm³ of emulsion flown on Viking no. 9, 10 interactions by heavy primary nuclei were observed, none of which initiated a cascade. Here again the emulsions were exposed in the presence of large amounts of absorber. Also, the use of individual sheets of emulsion, rather than stacks, provided a less favorable geometry for the detection of cascades. The horizontal stack of emulsion flown on Viking 10 is very exceptional in that for the first time the flux of cosmic radiation could be studied from all directions of the upper hemisphere. In particular, heavy primary nuclei could reach the detector at very large zenith angles. Cascades α and β were initiated by particles making apparent zenith angles of 76° and 79° respectively.

4. – Probability of a cascade originating as a chance fluctuation.

Consider a heavy primary of charge Z entering an emulsion unit and producing an initial collision at point *A* (such events will be referred to as *A*-stars). In order that a cascade follow, one or more heavy fragments of reduced charge $Z-n$ must be produced. This will have a probability p_f , dependent on Z , which can be estimated for L, M and H-nuclei from the data in the literature ^(5,6) (see Appendix A). A dual cascade is established when one of the secondary fragments produces an interaction at point *B*, the distance $AB=x_i$ defining a potential anomaly when x_i is a very small fraction of the mean free path λ for particle $Z-n$. The probability p_x that collision *B* occur over length AB assuming an exponential collision process is $p_x = 1 - \exp[-x/\lambda]$ which is closely approximated by x/λ for very small values of x . The geometric mean free path $\lambda = 1/\sum n_i \tau_i$ in emulsion for a particle of charge $Z = A/2$ was computed from the relationship $\sigma_i = \pi(R_i + R_p - 2\Delta R)^2$ with the nuclear radius on the projectile R_p taken as $1.45 \cdot 10^{-13} A^{1/3}$ cm, and the overlap for a collision to take place $\Delta R = 0.85 \cdot 10^{-13}$ cm. The resultant values of λ as a function of A , based on a recent chemical analysis of G-5 emulsion, supplied by the Ilford Company ⁽⁷⁾ are shown in Fig. 9.

⁽⁴⁾ H. YAGODA: *Canad. Journ. Phys.*, **34**, 122 (1956).

⁽⁵⁾ K. GOTTSSTEIN: *Phil. Mag.*, **45**, 352 (1954).

⁽⁶⁾ J. H. NOON and M. F. KAPLON: *Phys. Rev.*, **97**, 769 (1955).

⁽⁷⁾ Ilford Research Laboratory, Circular of August 10, 1956.

In order that events $A-B$ be observed in an emulsion of thickness t it must be favorably oriented with respect to the faces and edges of the detector, and a total track length of $x+2k$ must be considered where k is a distance of about 100 μm allowing for the detection of track Z and the observation of the tertiary tracks originating in event B . The probability p_g of meeting these geometric escape requirements neglecting edge effects are:

$$(1) \quad p_g = \left[1 - \frac{(x+2k)}{2t} \right] \text{ when } x+2k < t.$$

$$(2) \quad p_g = \frac{t}{2(x+2k)} \text{ when } x+2k > t.$$

The overall probability P_{calc} for a 2-stage cascade being produced and observed in a large block of emulsion is thus:

$$(4) \quad P_{\text{calc}} = p_f p_x p_g \quad \text{per } A\text{-star.}$$

The term p_g diminishes rapidly with increasing distance between collisions and is in general an important factor in the detection of the chain. However, since we are dealing at present with individual events occurring in detectors of variable geometry it is best to assume $p_g = 1$ in order to avoid biasing the major term of interest p_x . In a more complex chain of n -stages the overall probability of its formation by successive chance fluctuations in the individual mean free paths is:

$$(5) \quad \sum P = [p(f_1 x_1) \cdot p(f_2 x_2) \dots p(f_n x_n)] p_g,$$

where again p_g will tentatively be assigned a value of unity.

Application of these considerations to cascade α shows that it could originate as a chance fluctuation with a $\sum p_x = 1.32 \cdot 10^{-6}$ or $2 \cdot 10^{-7}$ if we also consider its particular mode of fragmentation. The 2-stage cascade β observed in the same rocket flight can originate by chance with a probability $p_f p_x = 0.01$. These events are compared in Table IV with 4-stage cascades observed on balloon flights by MILONE (3) and TOKUNAGA (8). In the absence of a tally of the total number of A -stars observed by all cosmic ray workers it is dif-

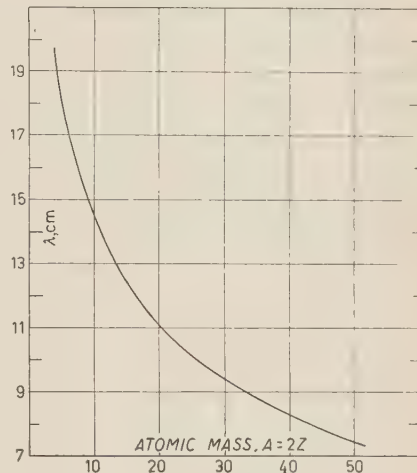


Fig. 9. – Computed collision mean free path for nuclei of mass number A in Ilford G5 emulsion of density $3.827 \text{ g} \cdot \text{cm}^{-3}$ conditioned to air at 58% R.H. at room temperature.

(8) S. TOKUNAGA, T. ISHII and K. NISHIKAWA: *Nuovo Cimento*, 5, 517 (1957).

ficult to properly assess these probabilities, but it would seem intuitively that the number of observations of cascades with ≥ 4 stages is too great to be attributed to chance.

The three large cascades have certain common features worth noting, although at present their significance is obscure:

1) No black or grey tracks are associated with the *A*-stage, the interactions consisting in the production of 1 or 2 (Milone event) singly charged relativistic particles. TOKUNAGA (8) has suggested that these might be high energy knock-on electrons. An alternative possibility is that these initial interactions may represent the decay in flight of hyperfragments.

TABLE IV. — Comparison of rocket and balloon cascades.

Event	Alpha	Beta	Tokunaga	Milone
Geomagnetic latitude	41° N	41° N	23° N	—
Total emulsion thickness, cm	0.90	0.90	2.88	—
Area of emulsion block, cm^{-2}	81	81	155	—
Vertical air mass, $\text{g} \cdot \text{cm}^{-2}$	none	none	≥ 8	—
Condensed matter, $\text{g} \cdot \text{cm}^{-2}$	$\ll 2$	$\ll 2$	—	—
Zenith angle of primary	76°	79°	37°	—
Energy per nucleon, GeV	18	6	500	9
Charge of incident particle	14 ± 1	6	11	13 ± 1
N_h of 1st stage	0	4	0	0
N_s of 1st stage	1	2	1	2
$\sum p_x$	$1.32 \cdot 10^{-6}$	0.25	$1.1 \cdot 10^{-4}$	$6.7 \cdot 10^{-4}$
$\sum p_f$	0.150	.039	.172	.055
$\sum P = \sum p_x \cdot \sum p_f$ per <i>A</i> star	$2 \cdot 10^{-7}$.01	$1.9 \cdot 10^{-5}$	$3.7 \cdot 10^{-5}$
Total number of stages	5	2	4	4
Collision mean free path within cascade, $\bar{\lambda}$ cm	0.698	2.33	.791	1.89
Average geometric mean free path for particles of $Z \geq 2$ involved in cascade, λ geom. cm	13.8	14.3	14.3	13.1
Ratio of λ geom./ $\bar{\lambda}$	19.8	6.1	18.1	6.9

2) The kinematics indicate that all three events are of very high energy ≥ 9 GeV per nucleon. There is the possibility that the collision cross-section of heavy nuclei increases appreciably in this velocity range.

3) The particles initiating the cascades are all of similar charge $Z=11$, 13 and 14. On the basis of fragmentation probabilities a cascade is more readily promulgated starting with more complex nuclei of $Z \geq 20$. It is possible that the particles seen to enter the emulsion are themselves secondaries formed by the interaction of more complex units with the upper atmosphere or the rocket skin.

If these occurrence be attributed to a new cosmic ray phenomenon characterized by a very small collision mean free path its elucidation will necessitate further observations near the top of the atmosphere employing thin-walled detectors. We are now studying a 300 cm³ block of G5 emulsion flown for 7 hours below (4.9 ± 0.04) g·cm⁻² of air in the presence of only 0.4 g·cm⁻² of wrapping material to secure further information on the frequency of the heavy primary cascade process. Likewise, two small stacks of emulsions flown to a peak elevation of 158 miles on Viking no. 11 are being scanned for heavy primary tracks. A new rocket exposure has been made in which the emulsions are exposed outside of the rocket skin in aluminum housings having a vertical absorber path of only 0.2 g·cm⁻²; the instrument section, however, has not been recovered from this first attempt.

* * *

This experiment was made possible by the co-operation of the Naval Research Test Facility at White Sands, New Mexico. Appreciation is expressed to M. W. ROSEN for providing choice space for the emulsions in the rocket tip. Thanks are due to HOMER E. NEWELL, Jr. for personally conveying the emulsions to the launching area, and to VIRGIL GOBLIRSCH for effecting their recovery after the flight.

APPENDIX

In order that a cascade be promulgated the heavy primary initiating stage *A* must avoid catastrophic destruction in the primary act and must fragment so that at least one α particle emerge from the *A*-star. In computing fragmentation probabilities in emulsion, p_f , we have employed the combined data presented by NOON and KAPLON⁽⁶⁾ in their Table I and the data listed by GOTTSSTEIN⁽⁵⁾:

Type of Interaction	NOON and KAPLON	GOTTSSTEIN	p_f
$H \rightarrow H'$ or M or L or He	83/86	21/21	0.97
$M \rightarrow M'$ or L or He	117/129	40/55	0.85
$L \rightarrow L'$ or He	—	18/29	0.62
$H \rightarrow H'$ or M or $> 1 L$	56/86	10/21	0.53
$H \rightarrow H'$ or M	33/86	7/21	0.37
$H \rightarrow H'$ or $M + > 1 He$	31/86	5/21	0.34
$M \rightarrow L$	41/129	11/55	0.28
$M \rightarrow L + > 1 He$	27/129	4/55	0.17
$H \rightarrow H'$	14/86	3/21	0.16
$H \rightarrow 2 L + > 1 He$	7/86	2/21	0.084
$L \rightarrow L'$	—	4/29	0.14
$L \rightarrow L' + > 1 He$	—	1/29	0.03

The subdivision of incident particles into L, M and H groups is based on the Rochester convention and the primed symbols refer to secondaries of reduced charge but still residing within the charge subdivision of L = Li, Be, B; M = C, N, O, F and Ne; and H representing all nuclei of charge greater than 10.

RIASSUNTO (*)

Emulsioni trasportate da un Viking 10 a 136 miglia d'altezza circondate da solo $2 \text{ g} \cdot \text{cm}^2$ di assorbitore metallico sovrapposto hanno registrato esempi di primari pesanti che nella collisione coi nuclei dell'emulsione non sono stati distrutti catastroficamente. I frammenti relativistici dotati di carica elevata che emergono dall'evento primario producono collisioni secondarie dopo aver percorso distanze piccole rispetto al cammino libero medio di collisione dei nuclei identificati. Il primo evento iniziato da una particella di carica 14 ± 1 comprende un totale di 5 collisioni che potrebbero aver avuto origine per successive deviazioni fortuite dal cammino libero medio geometrico con una probabilità di $1.1 \cdot 10^{-6}$. La seconda cascata iniziata da un nucleo di carbonio passa attraverso due stadi e la sua carica si riduce a $Z=3$ prima di uscire dal rivelatore. Considerazioni sulla frequenza relativa dei differenti modi di frammentazione e di cammino geometrico riducono ulteriormente la probabilità che questi eventi abbiano origine fortuita e siano rivelati.

(*) Traduzione a cura della Redazione.

Nuclear Collisions of Negative K-Mesons.

W. ALLES, N. N. BISWAS, M. CECCARELLI (*) and J. CRUSSARD (+)

Max-Planck-Institut für Physik - Göttingen

(ricevuto il 29 Maggio 1957)

Summary. — See Sect. 1 and Conclusion.

1. — Introduction.

This paper concerns an experiment on the collisions of negative heavy mesons of energies ranging from ~ 5 to 90 MeV with nuclei of photoemulsion. The events were found by track scanning in a $15 \text{ cm} \times 17.5 \text{ cm} \times 9 \text{ cm}$ stack which had been exposed to the enriched K^- -beam of the Berkeley Bevatron.

2. — Collisions on free protons.

2.1. *Scattering.* — In the scanning of 75 m of track, 18 cases of elastic scattering of K^- -meson on a hydrogen nucleus were found. In each of these cases the kinematics of the event fit very closely with those expected for such a scattering. In another case, the coplanarity is excellent but the energy and momentum balances are somewhat uncertain because the K^- suffers probably a second collision in flight.

Out of our data there are only 3 examples of inelastic scattering on complex nuclei in which only the K^- and another heavy track are emitted; therefore the above mentioned 18 cases are not accompanied by a large background and their attribution to $K^- + p$ events seems very safe. For the same reason the last event is probably also due to a collision on a free proton and is counted as such.

(*) On leave from the Padua University.

(+) On leave from the Laboratoire de l'Ecole Polytechnique - Paris.

In Table I are listed, for each event, the energy of the K^- at the point of collision and the angle of scattering in the center of mass system.

TABLE I. - K^- -p collisions in flight.

$E_{K^-} < 30 \text{ MeV}$			
$K^- + p \rightarrow K^- + p$			
E	χ	E	χ
29	52	24	53
8	70	10	103
29	106	—	—
$K^- + p \rightarrow \Sigma + \pi$			
E	χ		
29	107		

$30 < E_{K^-} < 60 \text{ MeV}$			
$K^- + p \rightarrow K^- + p$			
E	χ	E	χ
44	31	48	56
35	80	50	85
55	100	59	100
45	115	46	150

$K^- + p \rightarrow \Sigma + \pi$			
E	χ		
35	161		

$E_{K^-} > 60 \text{ MeV}$			
$K^- + p \rightarrow K^- + p$			
E	χ	E	χ
75	29	73	57
75	62	74	107
66	112	75	135

$K^- + p \rightarrow \Sigma + \pi$			
E	χ		
63	127		

SOCIETÀ ITALIANA DI FISICA

Rendiconti della III Conferenza Internazionale sui fenomeni di ionizzazione nei gas, tenutasi a Venezia dall'11 al 15 Giugno 1957.

Il Volume dei *Rendiconti della III Conferenza Internazionale sui fenomeni di ionizzazione nei gas*, sarà ultimato entro il mese di ottobre 1957: esso, è costituito di circa 1500 pagine ciclostilate e contiene la quasi totalità dei 130 lavori presentati alla Conferenza. Le bozze in ciclostile sono state rivedute dagli Autori e molte figure sono state tipograficamente riprodotte. Il volume è stato apprestato con molta cura.

Non si prevede di pubblicare i *Rendiconti* in edizione tipografica: il Volume ciclostilato, di cui sopra si è fatta parola, costituirà quindi l'edizione definitiva dei *Rendiconti*. Esso verrà preparato solo in 400 esemplari.

La mole del Volume assai maggiore di quanto si era previsto, e il notevole costo di esso, obbligano ad aumentare il prezzo inizialmente annunciato: il Volume verrà posto in vendita a \$ 12 o equivalentemente a L. 7.500 la copia: nel prezzo sono comprese le spese postali di spedizione raccomandata.

Chi desidera acquistare il Volume è pregato di inviare la somma suddetta a mezzo assegno bancario o vaglia postale al seguente indirizzo: prof. Ugo Facchini presso la Società Italiana di Fisica, Milano, Via Saldini, 50: indicando chiaramente a quale indirizzo va spedito il volume.

ITALIAN PHYSICAL SOCIETY

Proceedings of the Third International Conference on Ionization Phenomena in Gases, held in Venice from June 11 to 15, 1957.

The Volume containing the *Proceedings of the Third International Conference on Ionization Phenomena in Gases* will be ready within October 1957: it will consist of 1500 cyclostyle pages containing a total of almost 130 papers presented at the Conference. The cyclostyle proofs have been revised by the Authors and many figures were reproduced in print. The volume has been prepared with great care.

No printed edition of the *Proceedings* has been planned: the afore mentioned cyclostyle volume will therefore be the definite edition of the *Proceedings* and only 400 copies will be edited thereof.

The far larger size of the volume than originally expected and the considerable costs of editing it have necessitated an increase in the previously announced price: the volume will be on sale at \$ 12 or equivalently L. 7.500 per copy: mail charges by registered book-post included.

Please place your order and send the above quoted amount by check or postal order to the following address: prof. Ugo Faechini, c/o Società Italiana di Fisica, Milano, Via Saldini, 50: indicating clearly to which address Volume should be mailed.

2.2. *Capture in flight.* — On the same length of track along which the 19 K^- -p elastic scattering were found, 3 cases of K^- capture by free protons, leading to the emission of a charged Σ particle and an oppositely charged pion, where also observed. The energies and the angles χ between the light and the heavy meson in center of mass system are also tabulated in Table I (*).

2.3. *Comparison with other experimental data.* — Other recent emulsion data (1) show similar proportions: 39 scatterings and 8 captures, on free protons, with emission of charged particles. In contrast, the observation in the hydrogen bubble chamber at Berkeley (2) shows 6 elastic scattering events and 16 captures in flight, also leading to charged particles, at energies smaller than 30 MeV. Taking only events with K^- -energy ≤ 30 MeV, the emulsion data are 10 scatterings and 3 captures (3). This discrepancy between emulsion and bubble chamber results induced us to take all possible care to avoid biases against the detection of capture reactions. First of all, in those cases in which the recorded « K^- -end » could also have been that of a Σ^\pm -hyperon (4), a careful re-examination of all angles in the last ten millimeters of the « K^- track » ($E < 40$ MeV) was made, in order to find $K^- + p \rightarrow \Sigma^\pm + \pi^\mp$ events in which the π would have escaped detection and which would have been

(*) *Added in the proof:* By completing the scanning of the stack another five K^- -p events have been found on an additional track length of 26 m. The energies and angles are: *Scatterings:* $E = 6$ MeV, $\chi = 110^\circ$; $E = 65$ MeV, $\chi = 76^\circ$; $E = 73$ MeV, $\chi = 147^\circ$; *Captures:* $E = 34$ MeV, $\chi = 50^\circ$; $E = 52$ MeV, $\chi = 57^\circ$.

(1) The results of other groups which are mentioned in this paper are mostly unpublished; they will appear in the *Proc. of the 7th Rochester Conference* (1957).

(2) L. W. ALVAREZ, H. BRADNER, P. FALK-VAIRANT, J. D. GOW, A. H. ROSENFIELD, F. T. SOLMITZ and R. D. TRIPP: *Nuovo Cimento*, **5** 1026 (1957). See also *Proc. of the 7th Rochester Conference* (1957).

These include the following data, collected at the time of the *7th Rochester Conference* (1957)

Brookhaven	2 events
Berkeley { Barkas' group	13 events
Goldhaber's group	2 events
European collaboration experiment . .	12 events
Livermore	11 events
Rochester	7 events.

(3) It should be remembered that the primary energy spectrum is rather different for the two experiments. For the bubble chamber data we have estimated the average energy, in the $0 \div 30$ MeV region to be 14 MeV, whereas for the emulsions we have estimated the average energy to be 22 MeV. In case of a very rapid variation of σ_{abs} , with E the evaluation of this average energy plays a critical role.

(4) This is the case for: zero prong capture stars; stars with small energy release; emission of a fast pion alone; decays in flight.

taken for K^- scatterings. Additional checks were made on the possibility of a misinterpretation of a capture in flight by a free proton, at a range of less than 2 mm ($E < \sim 15$ MeV), as a capture at rest by a complex nucleus.

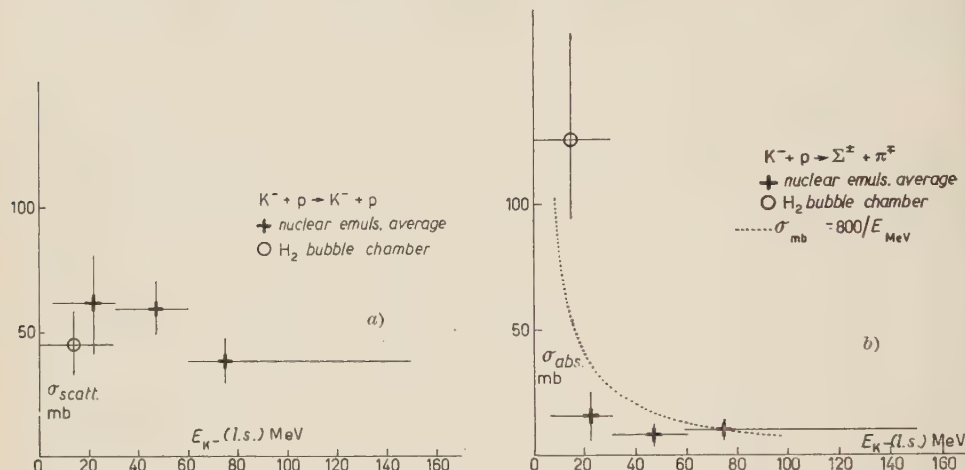


Fig. 1. - a-b) Cross-sections of K^- proton collision as a function of energy.

The negative result of these various checks enables us to exclude that a sample of K^- -p collisions obtained in a reasonably accurate track scanning

may be strongly biased, at least for energies greater than about 15 MeV. In Fig. 1 a and b are compiled the results on the cross-sections for scattering and for absorption as a function of energy, for K^- -p collisions observed both in nuclear emulsion and in bubble chamber. The data seem to favour a scattering cross-section fairly energy independent but an absorption cross-section decreasing with energy.

In Fig. 2 is given the distribution of angle χ for all emulsion events.

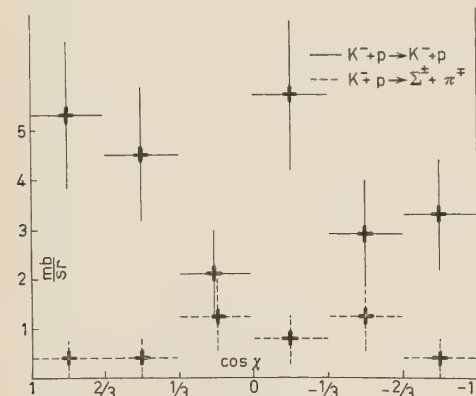


Fig. 2. - Angular distribution in c.m.s. of the K^- proton collisions.

3. - Scattering by complex nuclei.

All scattering angles larger than 5 degrees occurring on a K^- -track down to an energy of 30 MeV, and larger than 30 degrees down to the end were re-

corded, as well as all cases in which the primary track suffered a noticeable grain density variation or in which other prongs were emitted.

The K^- -meson energy loss at the point of scattering was determined by comparing the range of the scattered meson with that expected from the momentum dispersion curve of the beam. For the cases in which a significant energy loss appeared, grain density measurements were also made.

For the great majority of the scattering events (a few hundred), the experimental energy losses are small and symmetrically distributed around zero as expected for the case of elastic scattering. In particular there is no evidence of «slightly inelastic» events, a type of event which is frequently observed in proton and K^+ -meson scattering.

In order to establish in an unbiased way the percentage of inelastic scatterings among all nuclear collisions, only those events in which the inelastically scattered K^- ended in a more than one prong capture star were considered. This was done in order to eliminate the proton and the majority of the hyperon background. A correction to take into account this particular selection was introduced, using the prong distribution of the K^- capture stars (Fig. 5). No geometrical correction seemed necessary for mesons escaping the stack, because of its large dimensions.

Out of 302 nuclear interactions in flight, only 8 cases were inelastic scattering of a K^- from a nucleus, with the K^- ending in a capture star with more than one prong.

After correction, the inelastically scattered fraction of K^- -mesons turns out to be $(4.0 \pm 1.4)\%$, the remaining being captured or suffering charge-exchange.

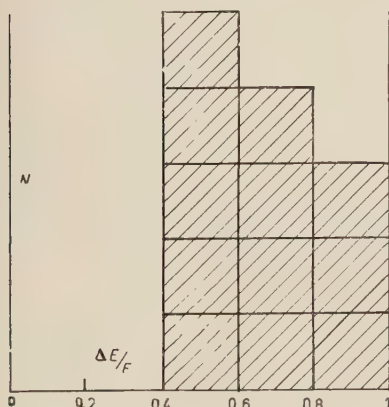


Fig. 3. — Relative energy loss in K^- inelastic scattering by complex nuclei.

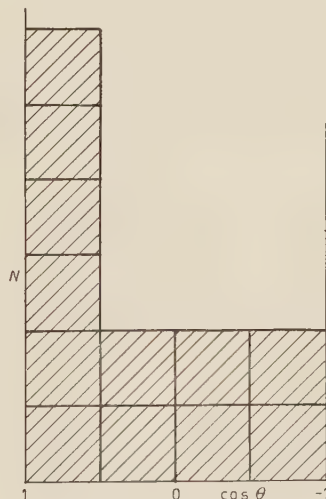


Fig. 4. — Angular distribution in laboratory system of the K^- inelastic scattering by complex nuclei.

For these 8 inelastic scattering events as well as for another 4 kindly communicated to us by S. GOLDHABER, the distribution of the relative energy loss and of the scattering angle in the laboratory system are shown in Fig. 3 and 4.

4. – Capture by complex nuclei.

The captures in flight of K^- -mesons by nuclei do not differ very much from those at rest, at the energies concerned here. This can be seen by comparing Fig. 5 and 6 in which are given the heavily ionizing prong distributions of captures in flight and at rest respectively. In each figure the two histograms correspond to events having or not a lightly ionizing particle among the capture products. Various average quantities for the two classes of events are presented in Table II.

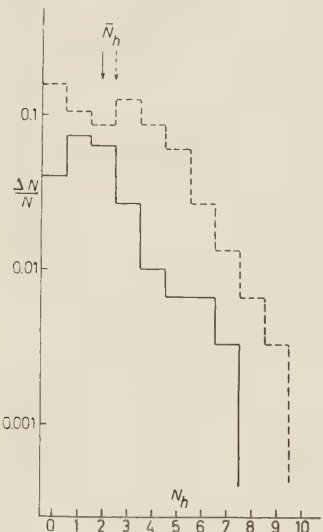


Fig. 5. – Prong distribution of K^- interaction stars in flight: — stars with a fast π -meson; --- stars without a fast π -meson.

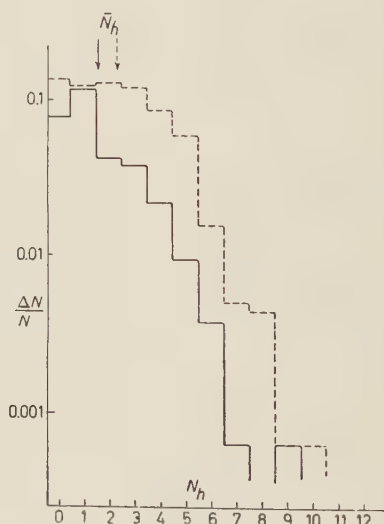


Fig. 6. – Prong distribution of K^- capture stars at rest: — stars with a fast π -meson; --- stars without a fast π -meson.

The mean values of the prong number in the captures in flight is slightly higher than in the captures at rest, which may well correspond to the fact that the total energy available in the collision is somewhat greater.

Since in the absorption in flight the actual capture process is likely to occur inside the nucleus at a distance from the nuclear surface of the order

TABLE II.

	collisions in flight	captures at rest
Average N_h (events with fast π)	1.93 ± 0.19	1.54 ± 0.07
Average N_h (events without fast π)	2.46 ± 0.17	2.27 ± 0.07
Events with fast π /Total	(27 ± 3)%	(31.7 ± 1.4)%
Events with only one heavily ionizing particle	(13.5 ± 2.1)%	(13.2 ± 0.9)%
Zero prong events, including those with a blob or a recoil	(18.5 ± 2.6)%	(14.0 ± 0.9)%
Zero prong events, excluding those with a blob or a recoil	(12.3 ± 2.3)%	(6.7 ± 0.6)%
$K^- + p \rightarrow K^- + p$	19	—
$K^- + p \rightarrow \Sigma^\pm + \pi^\mp$	3	4
Total number of events on hydrogen giving charged prongs	22 (6.8 ± 1.5)%	4 (0.19 ± 0.10)%
Total number of events	324	2019

of the K^- -meson mean free path, (probably $\approx 1 \cdot 10^{-13}$ cm), the close similarity existing between the captures at rest and in flight may indicate that the capture of a K^- at rest also occurs in this same region of the nucleus.

The angular distribution of the particles emitted from captures in flight is substantially isotropic. For fast pions a weak indication exists for an excess of backward emission in the laboratory system ($(N_{\text{for.}} - N_{\text{back.}}) / (N_{\text{for.}} + N_{\text{back.}}) = -0.15 \pm 0.11$). A little effect of this order may be expected as

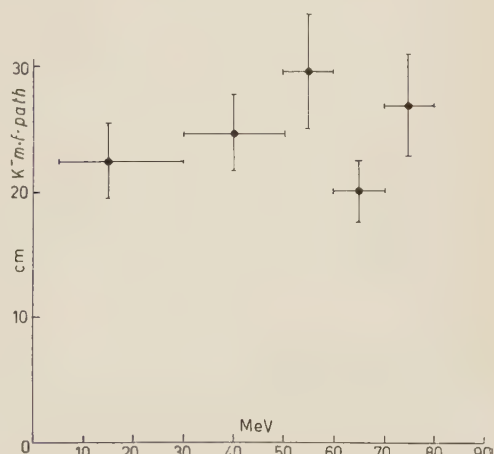


Fig. 7. — Interaction mean free path of K^- in emulsion as a function of energy.

a consequence of the fact that the majority of capture processes do probably occur in the backward hemisphere of the nucleus, with a resulting effect of shadow for pions emitted forwards.

Fig. 7 shows the K^- -interaction mean free path in emulsion as a function of the meson energy. The mean value is (25 ± 2) cm; the cross-section seems to be energy independent within the errors.

5. - Charge-exchange.

5.1. In nuclei. — Very little can be said about the number of cases in which a K^- -meson suffers a charge exchange in a nucleus and is re-emitted in a neutral state. If this process is assumed not to occur in the capture at rest, an indication that it is also rare in the interactions in flight comes from the fact that the percentage of stars with zero prongs, or one of low energy is only slightly greater for interactions in flight (32%) than at rest (27.2%). This sort of small stars would be frequent in the case of charge exchange and subsequent emission of the K^0 , since the nuclear excitation would then only be due to a neutron with an average energy of some 50 MeV.

From this rather tentative argument, and from the above given proportion of 4% for inelastic scattering, it would follow that in the collisions with complex nuclei the re-emission of the meson in either state of charge occurs in not more than about 10% of the cases, and possibly less because part of the zero prong events, as will be seen, can be due to collision on free protons.

5.2. On free protons. — Among the very small stars are 40 cases of disappearance in flight of the K^- track without any visible blob or recoil. Part of them are probably due to charge-exchange or absorption events on free protons and part to similar events in complex nuclei. A crude estimate of the latter fraction can be made by assuming that for events at rest and in flight the proportion of these zero prong stars due to interactions with complex nuclei is the same, and that, as can be seen from Table II, the interactions with hydrogen at rest are only in very small proportion. A correction must also be made for K^- decays in flight in which the secondary would escape observation (events near surfaces...) and which would have been counted in the 40 disappearances. This being done, the number of events which may be attributed to captures in flight or to charge exchange on free protons turns out to be ~ 15 . This is to be compared to 19 scattering events and 3 captures giving charged particles (see Sect. 2).

It can be assumed that the great majority of those estimated 15 «neutral» events on free protons is probably due to charge-exchange. This is because the captures by free protons giving neutral particles are probably still less

numerous than those giving charged particles (3 events), as suggested by the hydrogen bubble chamber results in which, for events at rest, the proportion of captures giving neutral hyperons does not seem to exceed 30%.

From this discussion and that of Sect. 2, the following tentative estimates of the cross-sections can be given, for K^- collisions on free protons at energies between 30 and 100 MeV.

Scattering	~ 50 mb
Charge-exchange	$\lesssim 50$ mb
Capture	~ 15 mb

The results of the hydrogen bubble chamber on charge exchange, still of very little statistical weight (2 events), seem to indicate a cross-section of ~ 35 mb for energies less than 30 MeV.

6. - Comparison between the collisions on free protons and on complex nuclei.

The striking features of the K^- -collisions is the very infrequent occurrence of inelastic scatterings on complex nuclei although in K^- -p collisions scattering seems to be as frequent as the total of all other reaction channels.

A possible way to bring in agreement the results of hydrogen and complex nuclei events is to assume that a strongly attractive nuclear potential prevents the K^- particle, which has suffered inside the nucleus a certain energy loss, from escaping.

In order to investigate more closely this point we have calculated, by the use of the Monte-Carlo method, a number of paths of a K^- -meson inside a nucleus. For these calculations we have assumed the K^- -nucleon scattering cross-section to be isotropic in the center of mass system, energy independent and with a total value of 50 mb. These assumptions, as can be seen from Fig. 1 a) and 2, are reasonable, at least for interactions on protons ⁽⁵⁾.

The value of the cross-section for the sum of absorption and charge exchange has been left as parameter, as well as the value of the nuclear potential acting on the meson. The distribution of the nucleons inside the nucleus has been assumed to be that of a completely degenerate Fermi gas.

400 K^- -particles have been followed through the nucleus using a three dimensional picture both for each elementary scattering process as well as

⁽⁵⁾ The results of the calculation are sensitive to the value of the $\sigma_{\text{scatt.}}/\sigma_{\text{total}}$ ratio, but rather insensitive to the absolute values of the cross-sections. As far as the scattering angular distribution is concerned, the results depend essentially on the forward/backward ratio, but much less on the detailed shape of the curve.

for the total development of the K^- -trajectory (⁶). The calculation has been restricted to three successive collisions since usually after this point the probability of a K^- -meson to survive capture or charge exchange is very small. We have however been able to estimate the little correction which results from this cut-off.

For the primary energy of the meson inside the nucleus various values have been taken so as to reproduce essentially the energy spectrum of our experiment for the different values of the nuclear potential used.

In the cases of repulsive potential, the K^- -meson was considered to be able to leave the nucleus if it reached the nuclear surface with an energy greater than the difference between attractive Coulomb and repulsive nuclear potentials. In the case of attractive nuclear potentials two extreme possibilities were considered: *a*) that at the nuclear surface the particle, irrespective of its energy, is reflected when it approaches the surface with an angle greater than that of the total reflection, and: *b*) that the particle can always traverse the nuclear surface provided its energy is greater than the sum of the nuclear and Coulomb potentials.

In Fig. 8 three groups of two curves, corresponding to the cases *a*) and *b*), are presented. Each group corresponds to a given ratio between the cross-section for scattering and for the total of charge-exchange and absorption by a nucleon.

The assumed values of this ratio are 2, 1 and $\frac{1}{2}$, which seem to cover all reasonable possibilities, according to the conclusions of the previous sections on K^- -proton events.

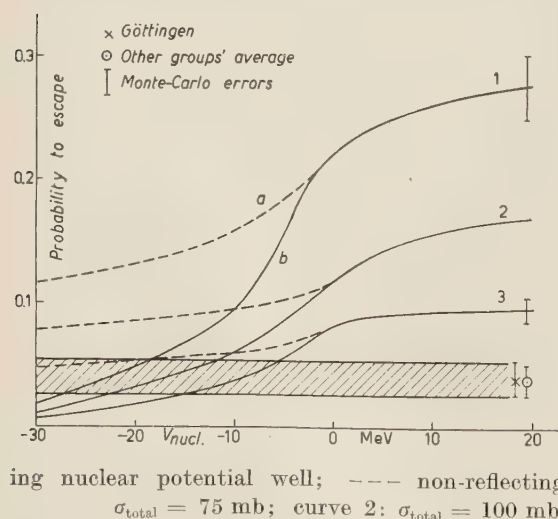


Fig. 8. – Results of a Monte-Carlo calculation on the escape probability of K^- -mesons: — reflecting nuclear potential well; --- non-reflecting nuclear potential well. Curve 1: $\sigma_{\text{total}} = 75 \text{ mb}$; curve 2: $\sigma_{\text{total}} = 100 \text{ mb}$; curve 3: $\sigma_{\text{total}} = 150 \text{ mb}$.

(⁶) In the construction of these 400 Monte-Carlo events, only elementary scattering processes have been considered and not absorption or charge exchange reactions. These latter reactions have been introduced both for obtaining the value of the mean free path in nuclear matter and, at the end of the calculation, for computing branching ratio coefficients at each step of the cascade. It was thus possible to obtain values of good statistical accuracy with a reasonable number of models.

This ratio has been considered to be energy independent down to 20 MeV; at lower energies the absorption cross-section has been taken to be infinite (7). For each value of the nuclear potential, the curves give the probability of observing a K^- -meson escaping after a collision with a complex nucleus. Our experimental value of this probability is given by the shaded area; for comparison an average value of the results of other laboratories is indicated; this value agrees very well with ours. It can be seen from Fig. 8 that, provided one does not want to assume for the ratio of the scattering to the total cross-section a value smaller than $\frac{1}{3}$, which would be hardly reconcilable with the present observations on K-p scattering, then the assumption of an attractive potential seems to be necessary.

The validity of this conclusions depends on the assumption that, in the collisions with neutrons the ratio of scattering to total cross-section is not much smaller than that for collisions on protons. In this respect it may be worthwhile to remember that since we are dealing with interactions with bound nucleons, small angle scatterings are more often forbidden by the Pauli principle than large angle scatterings, and consequently a difference in the scattering angular distributions would be, as far as scattering on bound nucleons is concerned, equivalent to a change in the value of the total cross-section. Our argument on the sign of the nuclear potential would not stand if the capture cross-section on neutrons were very much higher than that on protons, without a proportionate increase of the scattering cross-section. However, from the study of the interactions of K^- -mesons at rest on complex nuclei the events of the type $K^- + n \rightarrow \Sigma^0 + \pi^0$ do not, in fact, seem to be predominant over those of the type $K^- + p \rightarrow \Sigma^+ + \pi^-$.

In order to explain the very infrequent occurrence of inelastic scattering, possibilities other than the assumption of a strong attractive potential may be considered. Dr. QUAREN^I suggested that attention be payed to a possible contribution from K^- captures by two or more nucleons. From the fact that only two hyperons out of 12 have energy exceeding 50 MeV we may conclude that this process is probably rare. As another possibility, Dr. MITTELSTAEDT pointed out that, as an effect of the correlations between nucleons, the scattering/absorption ratio may be different for bound and for free nucleons.

An experimental determination of the $\sigma_{\text{scatt}}/\sigma_{\text{abs}}$ ratio inside a nucleus is very difficult. An indication that this ratio should not be very small is given

(7) This extreme hypothesis is suggested by the hydrogen bubble chamber results. If the absorption cross-section is instead supposed to be constant down to very low energies, the curves of Fig. 8 are slightly shifted upwards and the following conclusions remain unchanged.

by the presence, among the 12 previously reported inelastic scattering events, of several cases in which a large energy loss is associated to a small scattering angle. Such events turn out rather unlikely to be interpreted as single collisions with bound nucleons and they therefore supply an indication that the probability of a K^- -meson to survive to the first interaction is not negligible.

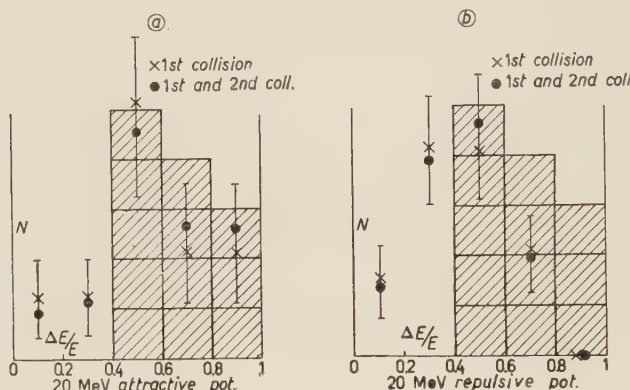


Fig. 9. - *a-b)* Comparison of the observed and calculated energy loss distribution in K^- inelastic scattering by nuclei. Histogram: experimental data. $\times \bullet$: results of the Monte-Carlo calculations. *a)* 20 MeV attractive potential; *b)* 20 MeV repulsive potential.

Another argument in favour to an attractive nuclear potential may be obtained by considering the distribution of the energy losses in inelastic scattering. In Fig. 9 *a* and *b*, this experimental distribution is compared with that expected from the previously described Monte Carlo calculations for two opposite values of the potential. In each figure, the points correspond to the results of two calculations, one assuming that only the first elementary collision contributes to the inelastic scattering (this occurs if $\sigma_{\text{scatt.}}/\sigma_{\text{total}}$ is very small), the other taking also successive collisions ($\sigma_{\text{scatt.}}/\sigma_{\text{total}} \sim \frac{1}{2}$). It can be seen from the figures, in spite of the small statistics, that here also the attractive potential is more satisfactory than the repulsive, because it explains the rather frequent occurrence of large energy losses. This is valid even in the first case ($\sigma_{\text{scatt.}}/\sigma_{\text{total}} \approx 0$) in which the other argument based on the low proportion of inelastic scattering events would not have any value.

7. - Conclusion.

From the collected experimental data the cross-section for scattering of K^- -mesons by protons should have a total value of about 50 mb, and at least

for energies between 10 and 100 MeV be substantially isotropic in the center of mass system and energy independent.

The total cross-section for absorption by protons leading to charged hyperons is about 10 mb in the region between 30 and 100 MeV. Below 30 MeV, as it can be seen from Fig. 1 b) a fair fit to the experimental points could be obtained by assuming a cross-section proportional to λ^2 . In the figure the dotted curve corresponds to $\sigma = 800/E$, where σ and E are respectively expressed in mb and in MeV. A rather strong discrepancy exists between the results of the nuclear emulsions and those of the bubble chamber experiment; the discrepancy may at present merely be attributed to a statistical fluctuation or possibly to some biases in the observation of very low energy capture events in nuclear emulsion.

For the charge exchange scattering on proton, the results, still incomplete, indicate that the cross-section is unlikely to be higher than the scattering cross-section.

The K^- -nucleon interaction should be dominated by rather strong attractive terms; this hypothesis explains the infrequent occurrence of inelastic scattering on complex nuclei and is also in agreement with observations of the very large energy losses in K^- inelastic scattering, which would not be expected for a repulsive potential.

* * *

It is a pleasure to thank Drs. W. H. BARKAS, G. GOLDHABER, K. GOTTSSTEIN and E. S. LOFGREN who very kindly arranged for us the exposure of the stack to the Berkeley Bevatron. For the very useful discussions we would like to thank Drs. W. H. BARKAS, G. and S. GOLDHABER, G. QUAREN, T. SALANDIN, F. T. SOLMITZ, P. WALOSCHEK, R. S. WHITE and G. T. ZORN, and again Drs. W. H. BARKAS, D. F. DAVIS, C. DILWORTH, F. C. GILBERT, G. and S. GOLDHABER, J. HORNBOSTEL, G. A. SNOW, F. T. SOLMITZ, R. D. TRIPP and R. S. WHITE for communicating us a number of unpublished results of their laboratories. We would finally like to thank Mr. C. WALLER for having manufactured the stack for us, Dr. G. KAYAS who has processed it and the scanners of the M.P.I. for their efficient work.

RIASSUNTO

Si descrive un esperimento sull'interazione nucleare di mesoni K^- d'energia compresa tra 5 e 90 MeV in emulsioni nucleari e si riportano anche dati raccolti da altri gruppi. La sezione d'urto per diffusione di mesoni K^- da protoni liberi ha un valore di circa 50 mb per energie tra 10 e 100 MeV, e sembra essere poco dipendente dal-

l'energia e con distribuzione angolare sostanzialmente isotropa nel centro di massa. La sezione d'urto per assorbimento con emissione d'iperoni carichi sembra di circa 10 mb per energie tra 30 e 100 MeV. Tra 0 e 30 MeV esiste apparentemente un grave disaccordo tra i dati delle emulsioni nucleari che indicherebbero un valore di circa 15 mb e quelli di un esperimento effettuato a Berkeley con la camera a bolle a idrogeno che darebbero un valore di circa 130 mb. L'apparente disaccordo potrebbe essere in parte dovuto ad una rapida variazione della sezione d'urto con l'energia. I dati sullo scambio di carica su protoni liberi, pur essendo ancora incompleti, sembrano indicare che la sezione d'urto di questo processo non supera la sezione d'urto per diffusione. La interazione tra mesoni K^- e nucleoni sembra dominata da forze attrattive; questa ipotesi spiega la rarità delle diffusioni anelastiche dei mesoni K^- su nuclei complessi ed è anche in accordo con l'osservazione delle molto forti perdite d'energia che spesso si producono in questi eventi.

Photoprottons from ^{100}Mo .

F. FERRERO, A. O. HANSON (*), R. MALVANO and C. TRIBUNO

Istituto di Fisica dell'Università - Torino

Istituto Nazionale di Fisica Nucleare - Sezione di Torino

(ricevuto il 29 Maggio 1957)

Summary. — The present work represents an extension of the measurements of the photoprotton yield from ^{100}Mo up to an energy of 30 MeV. It is found a rather large (γ, p) cross section at a higher energy than that for the (γ, n) reaction. A discussion is given of this evidence implying that the initial states of the protons involved in these transitions are different than those for the neutron or proton states responsible for the giant resonance in the (γ, n) reaction.

1. — Introduction.

The large yields of photoprottons from many elements have been noted for some time and a discussion of some aspects of these reactions has been given by WILKINSON (¹). A more complete study of photoprotton reactions should contribute to the understanding of the fundamental processes involved. ^{100}Mo is a particularly appropriate nucleus for study, since both the (γ, n) and (γ, p) reaction leads to radioactive nuclei and the (γ, p) activity is of the order of 100 times greater than one would expect on the basis of a statistical theory (²). The threshold for the (γ, n) and (γ, p) reactions were found to be 8.1 MeV and 10.5 MeV. The absolute yield and the angular and energy distribution of the photoprottons from ^{100}Mo irradiated by 22.5 MeV bremsstrahlung was determined by BUTLER and ALMY (³) using nuclear emulsions.

(*) University of Illinois.

(¹) D. H. WILKINSON: *Physica*, **22**, 1039 (1956).

(²) R. B. DUFFIELD, L. HSIAO and E. N. SLOTH: *Phys. Rev.*, **79**, 1011 (1950).

(³) W. A. BUTLER and G. M. ALMY: *Phys. Rev.*, **91**, 58 (1953).

The present work represents an extension of the measurements of the photoproton yield up to an energy of 30 MeV as detected by the 2.5 minutes ^{99}Nb . The fact that a rather large (γ, p) cross-section occurs at a higher energy than that for the (γ, n) reaction is of considerable interest and implies that the initial states of the protons involved in these transitions are distinctly different than those for the neutron or proton states responsible for the giant resonance in the (γ, n) cross-section.

2. - Method and results.

A 40 mg sample of ^{100}Mo was obtained from Oak Ridge as an oxide which consisted of 90.2% ^{100}Mo , and 2.85, 0.89, 1.33, 1.29, 1.82 and 0.85% of $^{98}, 97, 96, 95, 94$ and ^{92}Mo respectively. The sample was reduced to metal and deposited on an aluminum foil having a surface density 2 mg/cm^2 .

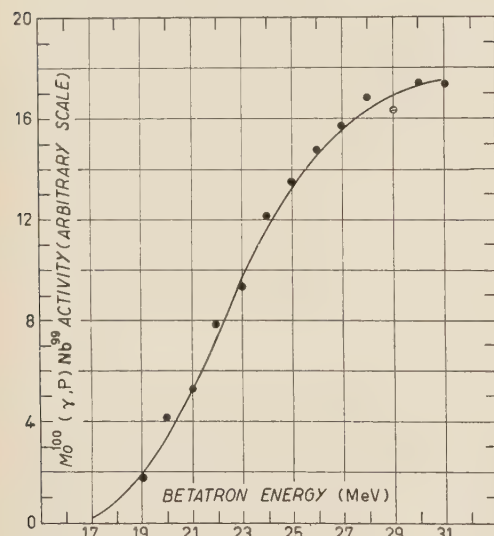
The sample was irradiated in the X-ray beam for periods of 2 min, and the 2.5 min activity from ^{99}Nb was counted by the use of an end window Geiger counter. Small backgrounds due to a 15 min activity which originated from neutron capture in ^{100}Mo and (γ, n) induced activity from ^{92}Mo , as well as the 67 hour (γ, n) induced activity from ^{100}Mo were subtracted. The background from the aluminum support was measured at the maximum energy and was found to be completely negligible.

Fig. 1.

The irradiations were monitored by a thick aluminum walled ionization chamber (⁴) which has a response which is nearly proportional to the total energy in the beam. The excitation curve is shown in Fig. 1. This excitation curve was renormalized to the monitor response used by KATZ and CAMERON (⁵) and the cross-section was calculated using the photon difference method of these authors. The resulting cross-section curve is shown in Fig. 2. The absolute value of the (γ, p) cross-section is obtained from the ratio of the

(⁴) F. FERRERO, R. MALVANO and C. TRIBUNO: *Nuovo Cimento*, **5**, 510 (1957).

(⁵) L. KATZ and A. G. CAMERON: *Can. Journ. of Physics*, **29**, 518 (1951).



observed counting rates for (γ, p) and (γ, n) activities in the sample after 15 min irradiation at 30 MeV. This ratio was 14.2 which gives a ratio of the two cross-sections averaged over a 30 MeV bremsstrahlung spectrum of 0.037.

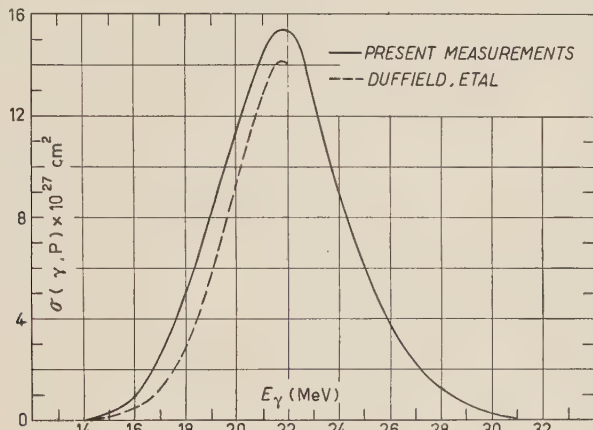


Fig. 2.

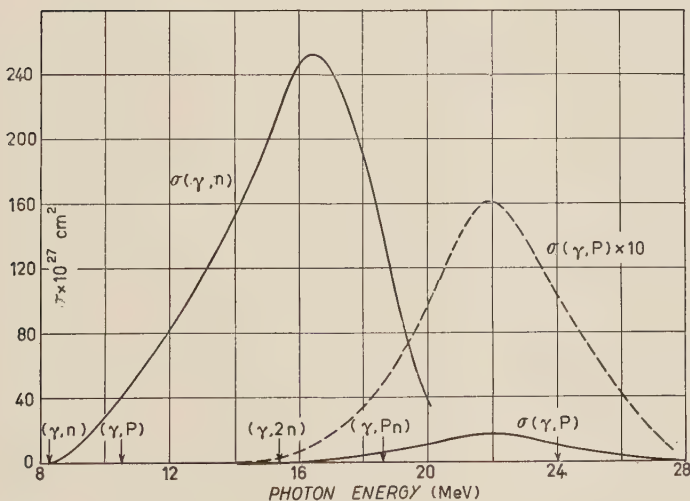


Fig. 3.

This ratio is used with the known value of $\sigma(\gamma, n)$ to determine the absolute value of $\sigma(\gamma, p)$ in Fig. 2 and, as can be seen, it is in good agreement with the scale obtained previously at lower energies. The (γ, n) cross-section as determined previously as well as the (γ, p) cross-section as measured in this work are shown in Fig. 3. The integrated cross-sections for the (γ, n) and the (γ, p) reactions are 1.5 ± 2 and $0.10 \pm .02$ MeV barns respectively.

3. – Discussion.

The present experiment clearly defines two separate peaks for the (γ, n) and (γ, p) cross-sections. Although it is possible to explain the fall off of the (γ, n) peak as arising from the increasing importance of the $(\gamma, 2n)$ reaction, the (γ, p) yields are too large to explain in terms of any usual statistical model. The observed integrated cross sections may be compared with a maximum of 2 MeV-barns obtained from other elements having about the same mass. The theoretical sum rule $\sigma_{int} = 0.06(NZ/A)(1+.8X)$ also gives about 2 MeV-barns for an exchange factor X equal to $\frac{1}{2}$. Thus there remains only 0.4 MeV-barns to be assigned to $(\gamma, 2n)$ and other reactions. It will be shown that this is more than accounted for by the 2n decay following direct proton transitions which are assumed to be responsible for the (γ, p) peak.

Although the spectrum of the emitted protons was not interpreted as a definite elastic group, we can attempt to estimate the fraction of the protons which are emitted before being absorbed as has been done by WILKINSON (1). As in a previous work (6) the width for absorption Γ_a which is twice the imaginary part of the complex potential, is taken as 10 MeV. The width for direct proton emission Γ_p is taken as the maximum width for a 10 MeV proton without a barrier (7.6 MeV) multiplied for the barrier penetration factor which for the smaller angular momenta can be obtained from the tables of BLOCK *et al.* (7).

A crude estimate of the contribution of various transitions is given in Table I, where the entire dipole strength is assumed to be distributed among those having the same number of nodes. One may note that in ^{100}Mo a large part of the strength of the neutron transitions can be identified with $1g \rightarrow 1h$ transitions and we would associate these with the 17 MeV maximum in the (γ, n) cross-section as measured by the ^{99}Mo activity.

The proton transitions on the other hand have their greatest strength in the $1f \rightarrow 1g$ transitions and it would be natural to associate these with the (γ, p) maximum at 22 MeV. It should be noted, however, that the $2p \rightarrow 2d$ transition would contribute appreciably to the fast proton yield if this transition has a maximum at the same energy since the barrier penetrability is appreciably higher. Only 8% of these transitions (or 4% of the total absorption cross-section) are estimated to lead to proton emission in agreement with the experimental results. This is also in approximate agreement with the general trend of the ratios of proton emission to the total absorption (1). It should

(6) F. FERRERO, A. O. HANSON, R. MALVANO and C. TRIBUNO: *Nuovo Cimento*, **4**, 418 (1956).

(7) I. BLOCK, M. H. HULL jr., A. A. BROYLES, W. G. BOURCIUS, B. E. FREEMAN and G. BREIT: *Rev. Mod. Phys.*, **23**, 147 (1951).

DOMUS GALILÆANA

PISA - VIA S. MARIA, 18

Ricorrendo il 19 Giugno scorso il tricentenario della prima riunione dell'Accademia del Cimento, la Domus Galilæana di Pisa e il Museo di Storia della Scienza di Firenze, giovandosi dell'aiuto finanziario, premurosamente porto dal Consiglio Nazionale delle Ricerche — al quale esprimono la loro gratitudine — hanno voluto celebrare la ricorrenza col pubblicare in un unico Volume di formato grande (27 cm × 36 cm) la ristampa fotolitografica dei *Saggi di Naturali Esperienze* (dedotta dalla editio princeps) e la presentazione, curata dalla dott. Maria Luisa Bonelli, degli strumenti e delle suppellettili dell'Accademia conservati presso sudetto Museo.

Il Volume in carta vergata simile all'originale, stampato in un numero ristretto di copie, è posto in vendita presso la Domus Galilæana (Via S. Maria, 18, Pisa) e presso il Museo di Storia della Scienza (Piazza dei Giudici, 1, Firenze) al prezzo di L. 14.000 la copia rilegata e di L. 12.000 la copia in brossura.

DOMUS GALILÆANA

PISA - VIA S. MARIA, 18

On June 19 last the tercentenary of the first reunion of the Accademia del Cimento took place and to celebrate this occasion the Domus Galilæana in Pisa and the Museo di Storia della Scienza in Florence, with the financial support of the National Council for Research — to which they are both much indebted — have published in a single large-sized volume (27 cm × 36 cm) the photo-lithographic reproduction of the *Saggi di Naturali Esperienze* (taken from the editio princeps) as well as the presentation written by Dr. Maria Luisa Bonelli of the instruments and fittings of the Accademia which are kept in the above mentioned Museum.

The Volume, in laid paper similar to the original one, has been printed in a limited number of copies and is on sale both at the Domus Galilæana (Via S. Maria, 18, Pisa) and at the Museo di Storia della Scienza (Piazza dei Giudici, 1, Florence) at the price of Lit. 14.000 for the bound edition and at Lit. 12.000 for the paper cover edition.

TABLE I. — *List of the strongest transitions in ^{100}Mo .*

The transition strengths S are based on the number of particles in shells which allow E^1 transitions multiplied by an enhancement factor to account for transition strengths transferred from the lower shells for which the E^1 transition is forbidden. For the proton transitions the barrier penetrability (P) for 10 MeV protons is estimated. The number of fast (10 MeV) protons emerging (N_F) are based on the relation

$$N_F = S_p \Gamma_p / (\Gamma_p + \Gamma_{\text{abs}}) \quad \text{where} \quad \Gamma_p = 7.6P \text{ MeV} \quad \text{and} \quad \Gamma_{\text{abs}} = 10 \text{ MeV.}$$

Transitions	Protons in initial shell	S_p	P	N_F	Neutrons in initial shell	S_N
$1g_{7/2} \rightarrow 1h_{9/2}$	0				8	21
$1g_{9/2} \rightarrow 1h_{11/2}$	2	6	0.01	0.05	10	29
$2p_{1/2} \rightarrow 2d_{3/2}$	2	3	0.24	0.47	2	3
$1f_{5/2} \rightarrow 1g_{7/2}$	6	13	0.11	1.01	6	0
$2p_{3/2} \rightarrow 2d_{5/2}$	4	5	0.24	0.78	4	5
$1f_{7/2} \rightarrow 1g_{9/2}$	8	15	0.11	1.17	8	0
lower shells	20	0			20	0
Total	42	42		3.48	58	58

be emphasized, however, that the estimates of the fast proton yields depend critically on the energies and widths assumed.

It is difficult to compare the energies of the observed maxima with what might be expected by a realistic shell model although some indication about the energy levels and transition energies can be obtained from the work of GREEN⁽⁸⁾, who has tried to use a realistic potential including spin orbit splitting. He finds the energy difference between the $1f_{7/2}$ and $1g_{9/2}$ states to be about 50% greater than that between the other states, although the transition energies are low by a factor of about two compared to those observed.

Even if a model could be found to explain the energies of the two observed maxima, an explanation of the results faces two difficulties. The first is the fact that the proton spectrum from 22.5 MeV bremsstrahlung fails to indicate any appreciable number of protons with the maximum available energy⁽³⁾.

⁽⁸⁾ A. E. S. GREEN: *Phys. Rev.*, **104**, 1617 (1956).

This could, perhaps, be explained by the fact that these protons come from an f state which is bound 3 or 4 MeV more than that of the least bound protons which are presumably in the $1g_{9/2}$ state. This assumption could be checked by measuring the proton energy distributions using bremsstrahlung at several higher energies to see if the maximum energy of the proton group increases in a way consistent with this assumption.

The second difficulty lies in the fact that if the entire proton transition strength is associated with the second resonance and one observes that only about 10% of the transition lead to fast protons, one must account for the remaining absorption of about 1 MeV-barn in some other manner. As mentioned previously, if this part of the transition strength leads to statistical excitation of the nucleus, it would lead predominantly to $(\gamma, 2n)$ reactions since the threshold of this reaction is expected to be about 15 MeV. Unfortunately, however, the $(\gamma, 2n)$ reaction leads to ^{98}Mo which is stable and cannot be detected by means of radioactivity. If larger samples of ^{100}Mo were available, the $(\gamma, 2n)$ yield could, of course, be measured by comparing the total neutron yield with that measured by the ^{99}Mo activity. In any case it is interesting to note that the total integrated cross-section as deduced above, would be 2.6 MeV-barns which is much above the 2 MeV-barns permitted by the electric dipole sum rule even if the $(\gamma, 2n)$ contribution of the 17 MeV resonance is neglected. It would be more satisfactory to assume that about one half of the proton transition strength is contained under the 17 MeV resonance and that the second resonance arises only from the strongest $1f_{7/2} \rightarrow 1g_{9/2}$ transition.

It is clearly desirable to get more detailed experimental data on these two maxima as well as similar second maxima in other nuclei⁽⁹⁾ to see if such resonances could be correlated with those expected in the shell model. It would, of course, be interesting to have more detailed calculations using some potential which is capable of giving the cross-sections as a function of energy as well as the energy and angular distributions of the particles in a manner which is more consistent than that attempted so far.

* * *

We would like to express our appreciation to Dr. P. BROVETTO for the chemical work in preparing the sample, to Dr. G. BUSSETTI for computational work on the photon difference method and Mr. G. MICHELETTA for assistance in the operation of the betatron.

⁽⁹⁾ L. KATZ, R. N. H. HASLAM, J. GOLDEMBERG and J. G. V. TAYLOR: *Can. Journ. of Phys.*, **32**, 580 (1954); B. M. SPICER: *Phys. Rev.*, **100**, 791 (1955); F. FERRERO, R. MALVANO and C. TRIBUNO: to be published.

RIASSUNTO

Il lavoro rappresenta una estensione fino a 30 MeV delle misure sull'emissione di fotoprotoni dal ^{100}Mo . Si riscontra che la sezione d'urto per reazione (γ, p) ha valori relativamente elevati per energie assai più grandi di quelle corrispondenti alla reazione (γ, n) . Questo fatto indicherebbe che gli stati iniziali dei protoni che danno luogo a queste transizioni dovrebbero essere assai diversi da quelli dei neutroni o dei protoni responsabili della risonanza gigante nella reazione (γ, n) .

Examples of K-Meson Production in 3 Gev π^- -Collisions (*).

T. BOWEN (†), D. M. HASKIN and M. SCHEIN

Department of Physics - University of Chicago, Illinois

(ricevuto il 31 Maggio 1957)

Summary. — The production of K-mesons by 3 GeV π^- -mesons has been studied in an emulsion stack by area scanning for stopped K-mesons and tracing to the originating interactions. Two examples of K-meson production are described which can be analyzed as due to pion-nucleon collisions. In one event a K^- -meson is produced as the only charged particle. In the other event, a K^+ -meson and a minimum ionization track are the only secondaries. This event can best be interpreted according to the scheme $\pi^- + P \rightarrow K^+ + \Sigma^0 + \pi^-$ assuming the collision to be with a free proton. Both of the events can be interpreted consistently with the Gell-Mann-Pais scheme.

The production of heavy mesons and hyperons in high energy accelerator beams has been studied by a number of groups (¹-⁵). While the associated production of hyperons and K-mesons according to the Pais-Gell-Mann (⁶) scheme has been demonstrated, it is still of considerable interest to identify

(*) Supported by a joint program of the U. S. Office of Naval Research and the U. S. Atomic Energy Commission.

(†) Now at Princeton University, Princeton, New Jersey.

(¹) R. D. HILL, E. O. SALANT, M. WIDGOFF, L. S. OSBORNE, A. PEVSNER, D. M. RITSON, J. CRUSSARD and W. D. WALKER: *Phys. Rev.*, **94**, 797 (1954).

(²) W. B. FOWLER, R. P. SHUTT, A. M. THORNDIKE and W. L. WHITTEMORE: *Phys. Rev.*, **93**, 861 (1954) and **98**, 121 (1955).

(³) W. D. WALKER: *Phys. Rev.*, **98**, 1407 (1955).

(⁴) G. MAENCHEN, W. M. POWELL, G. SAPHIR and R. W. WRIGHT: *Phys. Rev.*, **99**, 1619 (1955).

(⁵) R. BUDDE, M. CHRETIEN, J. LEITNER, N. P. SAMIOS, M. SCHWARTZ and J. STEINBERGER: *Phys. Rev.*, **103**, 1827 (1956).

(⁶) M. GELL-MANN and A. PAIS: *Proc. of the Glasgow Conference* (London, 1955).

the various production processes for these particles. The production of negative K-mesons is of particular interest, since, according to the rules for conservation of strangeness, they cannot be produced in association with any known hyperon, but, rather, must always be produced along with another K-meson. Only a few cases giving evidence of K-meson pair production have been reported (^{7,8}). The present study was undertaken for the purpose of identifying hyperon and K-meson production reactions by 3 GeV pions in an emulsion stack.

Generally, direct identification of the production of hyperons and K-mesons in emulsions is only possible when the particle is charged and is emitted at a low energy, coming to rest and decaying in the emulsion. At the high energies required for strange particle production it is unlikely that all the secondaries of an interaction will be directly identifiable. Therefore, we gave especially careful consideration to events which could be interpreted as pion-nucleon collisions, since the kinematical restrictions in such cases might assist in determining the production reactions. Events without low energy evaporation prongs were analyzed as pion-nucleon collisions, as the excitation of the nucleus was likely to be small.

A 10 cm × 15 cm × 5 cm stack of Ilford G-5 was exposed to a beam of 3.0 GeV π^- -mesons from the Bevatron. K-meson endings were found by area scanning, and the original interactions found by tracing back, in order to study the production of K-mesons by pions. Among 16 interactions where K-mesons or charged hyperons were produced, two interactions simple enough to allow analysis as pion-nucleon collisions are described here.

1. - Event 1.

Fig. 1 is a projection drawing of a K⁻-capture star and the originating interaction. An incoming track (K⁻) with grain density and scattering of a 1000 m_e particle came to rest and formed a four prong star (B). Tracks one and three were protons of 37 and 2.1 MeV respectively. Track two was identified as a pion of 50 MeV. Track four had a range of 19 μm and gave rise to the three prong disintegration (C) typical of a hyperfragment decay. This definitely identifies the incoming track as a K⁻-meson, captured according to the scheme $K^- + \text{nucleon} \rightarrow \text{hyperon} + \text{pion}$. The K⁻ was tracked back through 10 emulsions to the point of origin (A), consisting of an incident pion

(⁷) M. W. FRIEDLANDER, D. KEEFE and M. G. K. MENON: *Nuovo Cimento*, **2**, 666 (1955).

(⁸) M. CECCARELLI, M. GRILLI, M. MERLIN, A. SALANDIN and B. SECHI: *Nuovo Cimento*, **2**, 828 (1955).

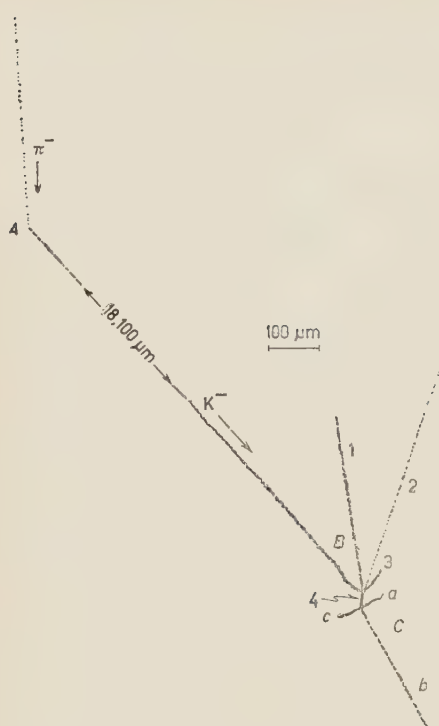
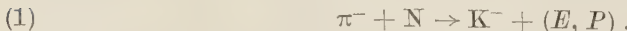


Fig. 1. — An incoming 3 GeV negative pion interacts at *A*. The only charged secondary is a negative K-meson which comes to rest and is captured at *B*. A hyperfragment from the capture star stops and disintegrates at *C*. (Observed by R. E. CAVANAUGH).

energy and momentum lost to the recoil nucleus is comparatively small, making an attempt to treat the event as a collision of a pion with a single neutron seems reasonable. Table I summarizes the data available on this event. The K⁻ was emitted backwards in the center of mass system at an angle of 158° with respect to the direction of motion of the incident pion. The figures given in the row labeled « Neutral Radiation » represent the energy, *E*, and momentum, *P*, which is unaccounted for in the reaction:



If the neutral radiation consists of a single particle, then its mass, *M*, is

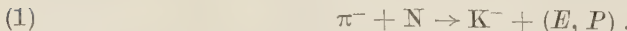
(⁹) W. F. FRY: *Phys. Rev.*, **93**, 845 (1954).

(¹⁰) G. TAKEDA: *Phys. Rev.*, **93**, 848 (1954).

and the K⁻ track only. The incident track was followed 3.5 cm in a single emulsion to the edge of the stack. The track is parallel with the beam and has the same grain density as other beam tracks, and so is quite certainly a 3 GeV pion. No clearly visible recoil is observed at *A*; however, a one grain recoil cannot be excluded.

Charge conservation excludes the possibility that the collision is with hydrogen in the emulsion, and so it is presumed to have occurred with a neutron in a nucleus. Since no recoil or evaporation prongs are visible, the maximum momentum transferred to a recoiling nucleus is estimated not to exceed in order of magnitude the particle momenta due to Fermi motion. Therefore, a momentum transfer greater than about 300 MeV/c is unlikely. Evidence supporting this conclusion is given by FRY (⁹) and TAKEDA (¹⁰), who investigated experimentally and theoretically 220 MeV π^- -collisions in emulsion where no recoil was observed.

Since the incident π^- brings in a total energy of 3140 MeV and a momentum of 3140 MeV/c, the amount of energy and momentum lost to the recoil nucleus is comparatively small, making an attempt to treat the event as a collision of a pion with a single neutron seems reasonable. Table I summarizes the data available on this event. The K⁻ was emitted backwards in the center of mass system at an angle of 158° with respect to the direction of motion of the incident pion. The figures given in the row labeled « Neutral Radiation » represent the energy, *E*, and momentum, *P*, which is unaccounted for in the reaction:



If the neutral radiation consists of a single particle, then its mass, *M*, is

(⁹) W. F. FRY: *Phys. Rev.*, **93**, 845 (1954).

(¹⁰) G. TAKEDA: *Phys. Rev.*, **93**, 848 (1954).

TABLE I.

Particle	Range	Kinetic Energy (MeV)	Total Energy	θ	φ	P_x	P_y	P_z	Total Momentum (MeV/c)	Angle of Emission in C.M.S. with respect to π^-	Kinetic Energy in C.M.S. (MeV)	Momentum in C.M.S.
π^-		3000	3140	0	0	3140	0	0	3140			
K ⁻	18000 μ m	55.5	549	37°	+11°	189	142	46	240.5	158°	142	400
Neutral Radiation			3511			2951	-142	-46	2955			

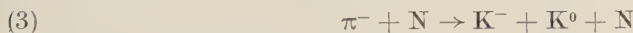
given by

$$(2) \quad M = \sqrt{E^2 - P^2},$$

M is found to be 1900 MeV or 3710 m_e . In taking into account the contribution of momentum from the neutron due to Fermi motion, only the x -component of momentum affects the uncertainty in M . We assume that the distribution of total momentum, P , in MeV/c of a nucleon can be represented (11) by a Gaussian distribution. The standard deviation, $(\langle p_x^2 \rangle)^{\frac{1}{2}}$ of the x -component of the nucleon momentum, is

$$\langle p_x^2 \rangle^{\frac{1}{2}} = (ME_0)^{\frac{1}{2}} \sim 137 \text{ MeV/c},$$

where M is the mass of the nucleon in MeV/c² and E_0 a constant which is about 20 MeV (11) for most nuclei. The standard error in the mass estimate is then, $\pm 420 m_e$. No particle is known in this mass range. Furthermore, if one is to follow the scheme of Gell-Mann, this particle would have to be a hyperon with a strangeness of +1, which seems improbable. Therefore, it seems natural to assume that two or more neutral particles were emitted. There is one restriction imposed by the kinematics of the event; the sum of the masses of the neutral particles must not exceed M , the mass of the above hypothetical particle. In other words, the total mass of the neutral particles must be less than about 4130 m_e . The production reaction,



predicted by the GELL-MANN assignments of strangeness, is completely con-

(11) J. M. WILCOX and B. J. MOYER: *Phys. Rev.*, **99**, 875 (1955).

sistent with this event. Hence, this event is best explained as an example of pair production of K-mesons.

2. - Event 2.

A projection drawing of a K^+ production event is shown in Fig. 2. A K-particle comes to rest at B and decays into a minimum ionizing steeply inclined secondary (track 2) too short for further measurements. The stopping track has grain densities and scattering typical of a 1000 m_e mass particle; hence the particle is identified as a K^+ meson. The K^+ has a range of 2185 μm , and originates in the same emulsion in a star (A) consisting of an incident pion and another secondary track, 1.

The incident track was traced back to the edge of the emulsion. It is parallel with the other beam tracks and has the same grain density, and so is quite certainly a 3 GeV π^- -meson. Secondary track 1 can be followed 7 mm in the same emulsion. The grain density was found to be $(0.98 \pm .05)$ times the density of 3 GeV π^- -tracks in the same emulsion. The multiple scattering indicated is $p\beta = (1000 \pm 300)$ MeV/c. No recoil track is observed; in fact, there are no grains within 0.94 μm of the point of intersection.

Charge conservation indicates that if the event is due to a pion-nucleon collision, the nucleon must be a proton. Following the same reasoning as in

Fig. 2. - A 3 GeV negative pion interacts at A , producing two charged secondaries. Secondary 1 is a minimum ionizing track. Secondary (K^+) is a positive K-meson which comes to rest at B and decays into a lightly ionizing secondary. (Observed by D. B. WILLIAMS).

Event 1, we may interpret the event as a collision with a proton in a light element or with a free proton. In experimental studies of 1.5 GeV π^- -nucleon interactions ⁽¹²⁾ and 3 GeV proton-nucleon interactions ⁽¹³⁾, it was found that of events with no visible recoil and otherwise consistent with collisions with protons, approximately one half are with free protons and one half with bound protons. Hence, there is at least an even chance that we are dealing with a collision with a free proton in this event.

⁽¹²⁾ W. D. WALKER and J. CRUSSARD: *Phys. Rev.*, **98**, 1416 (1955).

⁽¹³⁾ R. CESTER, T. F. HOANG and A. KERNAN: *Phys. Rev.*, **100**, 940 (1955).

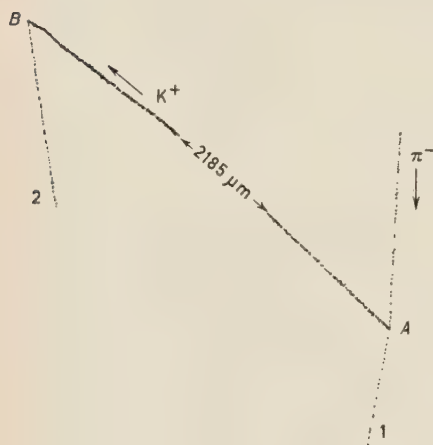


Table II summarizes the measurements on Event 2. The K^+ was emitted backwards in the center of mass system at an angle of 173° with respect to the direction of motion of the incident pion. Since the initial energy and momentum and the amounts carried away by the K^+ are known, we can calculate the maximum mass available for the other charged secondary (track 1) and the neutral radiation according to Equation (2). We find that the total mass of these secondaries may not exceed 1517 MeV or $2970 m_e$, which is sufficient for a hyperon and one or two pions or for another K -particle and a nucleon. If the track identified as a K^+ were assumed to be a Σ^+ , the square of the unbalanced momentum, P^2 , would be greater than the square of the remaining total energy E^2 , which is impossible, if the collision is indeed with a single proton. In fact, we can use the requirement that $E^2 - P^2 > 0$ to show that the mass of the particle K^+ is less than $1490 m_e$.

TABLE II.

Particle	Range	g/g_0	p (GeV)	Kinetic Energy (MeV)	Total Energy (MeV)	θ	φ	P_x	P_y	P_z	Total Momentum E (MeV/c)	Angle of Emission in C.M.S. with re- spect to π	Binetic Energy in C.M.S. (MeV)	Momen- tum in C.M.S. (MeV/c)
π^-			3.000	3.140	0	0	3.140	0	0	3.140				
K^+	2.185		16.7	510	$133^\circ + 4^\circ$	—	88	94	9	130	173°	410	757	
(?) ⁻	.98 ± ± 0.5	$1.1 \pm$ ± 0.3		3.568	$8^\circ - 2^\circ$	$1090 \pm$ ± 300	$153 \pm$ ± 30	$38 \pm$ ± 10	$1100 \pm$ ± 300					
Neutral Radiation							$2138 \pm$ ± 300	$247 \pm$ ± 30	$29 \pm$ ± 10	$2150 \pm$ ± 300				

In order to compute the apparent mass of the neutral radiation, the identity of track 1 must be known. The $p\beta$ and grain density require that the track have a mass of the order of 1000 m_e or less. By charge conservation, it must be negative. Of the known particles in this mass range, only the π^- and K^- are commonly emitted from nuclear collisions. If track 1 is a π^- , then the apparent mass, M , of the neutral radiation is $(2320 \pm 150) m_e$, assuming the target proton was hydrogen. If the target proton was found in a nucleus, then, as in event 1, the additional uncertainty in p_x is about ± 137 MeV/c, resulting in a standard error for M of $\pm 510 m_e$. An apparent mass of $2320 m_e$ is just the mass of the Σ^0 -particle ^(14,15) and the reaction would

⁽¹⁴⁾ W. ALVAREZ, H. BRADNER, P. FALK, J. D. GOW, A. H. ROSENFIELD, F. T. SOLMITZ and R. D. TRIPP: Rochester Conference.

⁽¹⁵⁾ R. PLANO, N. SAMIOS, M. SCHWARTZ and J. STEINBERGER: Rochester Conference.

be:



which is one of the reactions conserving strangeness. Due to the experimental uncertainty in the mass, the reaction:

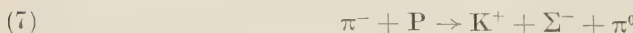


which also conserves strangeness is also possible. Reactions in which the neutral radiation consists of a neutron and one or two π^0 's cannot be excluded on the basis of the evidence in this event, but would violate the conservation of strangeness. If track 1 is assumed to be a K^- -meson, then the apparent mass of the neutral radiation is $(1900 \pm 30) m_e$, which could only be consistent with the emission of a single neutron according to:



which also conserves strangeness. The error in mass increases to $\pm 590 m_e$ if the proton is initially bound. While the errors in this event are too large to decide between reactions (4), (5) and (6), reaction (4) fits the data almost perfectly.

Since we are faced with the problem of choosing between several different reactions, all of which satisfy the known conservation laws, it is interesting to re-analyze the problem from another point of view, assuming that only the mass and direction of track 1 and the mass of the neutral particle are known. If we assign the masses according to reactions (4), (5) and (6), and use the known incident π^- and outgoing K^+ energies, we can calculate the energy, momentum and $p\beta$ which track 1 should have. The results of these calculations are shown in Table III. The energy, momentum, and direction of the neutral particle are, of course, also determined. The reaction:



was also tried, but was found to be excluded by the angles of the tracks in this event. In the case of reaction (6), the angles and energies allow two solutions. However, choice (b) is completely excluded by the measured grain density and scattering. It is evident from the table that no choice could ever be made between reactions (5) and (6a) on the basis of measurements of $p\beta$ on track 1. Grain density would be almost equally indecisive. One might scan the emulsion stack in the probable direction of the Λ^0 , hoping to find its decay. For this event, the chance of decaying in the stack is about 0.3,

TABLE III.

Reaction	Part- icle	Laboratory			Grain Density g/g_0	Center of Mass		
		Kinetic Energy (MeV)	Mo- mentum (MeV/e)	$p\beta$ (MeV/e)		Kinetic Energy (MeV)	Mo- mentum (MeV/e)	θ
$K^+ + \Sigma^+ + \pi^-$	Σ^0	1268	2150			83	454	33°
(4)	π^-	970	1100	1092	.910	384	400	23°
$K^+ + \Lambda^0 + \pi^-$	Λ^0	1070	1882			68	400	46°
(5)	π^-	1248	1382	1377	.913	385	506	23°
$K^+ + K^- + N$	K^-	1039	1452	1390	.897	177	454	27°
(6) (a)	N	1103	1813			102	449	47°
(6) (b)	K^-	316	641	508	1.145	9	94	78°
	N	1822	2600			260	748	14°
	K^+	17	128			410	757	173°

but the chance of finding the decay is considerably lower in this stack due to the high background. Reaction (4) can be singled out by an accurate measurement of $p\beta$, and, indeed, is favored by the experimental result.

3. - Conclusions.

It has been demonstrated that by tracing K-particles to their origins in an emulsion stack exposed to 3 GeV π^- -mesons, some apparently simple pion-nucleon collisions can be found. However, the analysis of these collisions is seriously restricted by the uncertainty in momentum caused by the Fermi motion in the nucleus. One might hope to avoid this difficulty by finding collisions with hydrogen nuclei in the emulsion. Previous workers (¹⁶⁻¹⁸) have used this technique, but they were studying reactions in which there were

(¹⁶) G. GOLDHABER: *Phys. Rev.*, **89**, 1187 (1953).

(¹⁷) J. OREAR: *Phys. Rev.*, **92**, 156 (1953).

(¹⁸) J. OREAR, J. J. LORD and A. B. WEAVER: *Phys. Rev.*, **93**, 575 (1954).

only two secondaries, so coplanarity and momentum balance could be used as criteria. However, when three or more secondary particles are present, one must rely solely on the lack of a star, recoil, or slow electron at the point of collision. It might be expected, that collisions with free protons form a reasonably large proportion (50%) of such cases.

In view of the uncertainties caused by Fermi momentum and the difficulties of identifying collisions with hydrogen, a higher yield of completely analyzable events might be found at energies nearer the production threshold. Lower energy secondaries could often be directly identified and the Fermi momentum uncertainty would cause less error in the estimate of the mass of the neutral secondaries.

No collision has been found which cannot be explained by the production reactions of strange particles proposed by GELL-MANN and PAIS. One event in which a negative K-meson is identified can be interpreted as a K^- - K^0 pair production. Another case has been found which is completely consistent with a collision between a pion and a free proton. With this interpretation, a Σ^0 -hyperon is very probably associated with an identified K^+ -meson.

* * *

The authors are indebted to Professors E. O. LAWRENCE and E. J. LOFGREN for making possible the exposures with the Bevatron.

RIASSUNTO (*)

Esplorando per area alla ricerca di mesoni K arrestati e rintracciando le interazioni che ne derivano si è studiata in un pacco di emulsioni la produzione di mesoni K da parte di mesoni π^- di 3 GeV. Si descrivono due esempi di produzione di mesoni K che si possono classificare come dovuti a collisioni piane-nucleone. In un evento un mesone K^- è prodotto come sola particella carica. Nell'altro evento un mesone K^+ e una traccia di ionizzazione minima sono gli unici secondari. Questo evento si interpreta nel miglior modo assumendo lo schema $\pi^- + P \rightarrow K^+ + \Sigma^0 + \pi^-$ e che la collisione sia avvenuta con un protone libero. Ambi gli eventi si accordano con lo schema di Gell-Mann-Pais.

(*) Traduzione a cura della Redazione.

Simple Treatment of Central Force Collisions with Particular Reference to Phase Shift Calculation.

S. FRANCHETTI

Istituto di Fisica dell'Università - Firenze

(ricevuto il 3 Giugno 1957)

Summary. — The problem of finding the positive energy solutions of the radial Schrödinger equation for a spherical potential behaving at infinity as r^{-n} , $n \geq 2$, is considered once again with particular reference to asymptotic phase shift determination. It is shown that by a proper choice of the unknown function, the Riccati equation of the problem transforms into a fairly simple 1-st order equation admittig an everywhere real, finite and single-valued solution (indeed, a very simple varying one and thus particularly suited to be computed by numerical integration) which leads directly to the asymptotic phase shift by given energy and momentum. If needed, the eigenfunction itself can be deduced, this step requiring only to perform ad additional quadrature. The numerical integration is restricted to a reasonable range. This and the nature of the solution make the computational work not unduly heavy, even by «hand» computation. Another valuable feature of the method is the ease with which the accuracy attained can be evaluated.

1. — Introduction.

In the course of an investigation on liquid helium, the author was led to study in a rigorous way the collision between two (neutral) helium atoms, that is to work out the positive energy solutions of a central-force (non-relativistic) Schrödinger equation, an obviously well known problem.

On that connection a numerical method was devised by which, if only a moderate accuracy is needed, the determination of the asymptotic phase shift under given values of energy E and momentum l , requires the not unduly

amount of some hours work with the aid of an ordinary desk calculating machine (1).

Although practically restricted to potentials decaying rapidly at large distances (say as r^{-n} , $n \geq 2$), it has been thought that the method could be of some general interest and it will therefore be described here, without any pretence to achieve full mathematical rigour or completeness.

2. – General outline of the phase shift calculation.

Let the radial part of the Schrödinger equation be

$$(1) \quad y'' + \varkappa \left[E - W(r) - \frac{1}{\varkappa} \frac{l(l+1)}{r^2} \right] y = 0$$

with

$$(1') \quad y = rR(r),$$

$$(1'') \quad \varkappa = \frac{8\pi^2\mu}{h^2},$$

where μ is the reduced mass and $R(r)$ is the radial part of the eigenfunction.

The usual position

$$(2) \quad u = \frac{d}{dr} \ln |y|$$

brings to the Riccati equation

$$(3) \quad u' + u^2 = f(r)$$

with

$$(3') \quad f(r) = -\varkappa \left[E - W(r) - \frac{1}{\varkappa} \frac{l(l+1)}{r^2} \right]$$

a known function of r .

(1) By moderate accuracy we mean an accuracy of, say, one or two units of the 2-nd decimal place. If very accurate values are to be obtained, one should of course resort to automatic computers. The method to be described should however prove advantageous even in this case.

We suppose $W(r)$ is sufficiently rapidly convergent to zero for $r \rightarrow \infty$ so that eq. (1) admits the asymptotic solution

$$(5) \quad y_\infty = \sin(k_0 r + \eta_\infty)$$

with

$$(5') \quad k_0 = (\varkappa E)^{\frac{1}{2}}$$

(a *real* constant).

According to the usual notation, (5) should be written

$$y_\infty = \sin(k_0 r + \eta_l - \frac{1}{2}\pi l),$$

so that one has

$$(5'') \quad \eta_l = \eta_\infty + \frac{1}{2}\pi l.$$

(The present notation has been chosen as the most natural one in relation to the method to be described).

The asymptotic expression for u is of course

$$(6) \quad u_\infty = k_0 \cot(k_0 r + \eta_\infty).$$

We may try to get the general solution $u(r)$ out of this formula by letting some of the parameters vary. Taking k_0 as a variable would evidently lead to some variety of the W.K.B. method. We shall not do so, however, putting instead

$$\eta = \eta(r),$$

that is

$$(6') \quad u(r) = k_0 \cot[k_0 r + \eta(r)]$$

from which the expression for the eigenfunction may be obtained ⁽²⁾ as

$$(6'') \quad R(r) = \frac{y}{r} = \pm \frac{1}{r} \exp \left[\int^r u dr \right] = \pm \frac{1}{r} \exp \left[k_0 \int^r \frac{dr}{\operatorname{tg}[k_0 r + \eta(r)]} \right].$$

The asymptotic phase shift will then be

$$(7) \quad \eta_\infty = \lim_{r \rightarrow \infty} \eta(r).$$

⁽²⁾ Concerning the double sign see Sect. 4.

As we shall presently see, the new unknown function shows some very valuable features, besides obeying a comparatively simple differential equation, namely (inserting (6') into (3))

$$(8) \quad \eta'(r) = -\mathcal{F}(r) \sin^2 [k_0 r + \eta(r)]$$

with

$$(8') \quad \mathcal{F}(r) = \frac{f(r)}{k_0} + k_0 = \frac{1}{k_0} \left[\varkappa W(r) + \frac{l(l+1)}{r^2} \right],$$

a known function of r .

Let us first discuss the behaviour of $\eta(r)$ near the origin. We recall that, concerning the behaviour of the eigenfunctions $R(r)$ near the origin, three cases may be considered.

Case 1) – The eigenfunction is finite but non-vanishing for $r = 0$.

Case 2) – The eigenfunction converges to zero as a power of r .

Case 3) – The eigenfunction converges to zero more rapidly than a power of r .

Case 1) corresponds to a « weakly » divergent (e.g. newtonian) or perhaps finite potential and $l = 0$. Referring to eq. (6'') one sees immediately that case 1) requires

$$\lim_{r \rightarrow 0} \int u dr = \ln r \quad (\text{Case 1}).$$

Case 2) corresponds to a weakly divergent potential and $l \neq 0$ (so that the coefficient of y in eq. (1) behaves as $-l(l+1)/r^2$ for $r \rightarrow 0$). The power law for $R(r)$ is then r^l and this requires

$$\lim_{r \rightarrow 0} \int u dr = (l+1) \ln r \quad (\text{Case 2}).$$

Case 3) corresponds to a strongly divergent (repulsive) potential Eq. (6'') shows that in this case one must have

$$\int u dr \text{ negatively divergent, more than logarithmically for } r \rightarrow 0. \quad (\text{Case 3}).$$

It follows from the above, expanding η in a power series (3), that the following conditions are to be fulfilled in the various cases.

Case 1) (Potential weakly divergent or finite at the origin, $l = 0$):

$$(9) \quad \begin{cases} \eta(r) = \sum_{n \geq n_0} a_n r^{n/q}, \\ \frac{n_0}{q} > 1 \end{cases} \quad (r \rightarrow 0, \text{ case 1}).$$

Case 2) (Potential as in 1), but $l \neq 0$:

$$(10) \quad \begin{cases} \eta(r) = \frac{-l}{l+1} k_0 r + \sum_{n \geq n_0} a_n r^{n/q}, \\ \frac{n_0}{q} > 1 \end{cases} \quad (r \rightarrow 0, \text{ case 2}).$$

Case 3) (Potential strongly divergent at the origin)

$$(11) \quad \begin{cases} \eta(r) = -k_0 r + \varepsilon, \\ \varepsilon = \sum_{n \geq n_0} a_n r^{n/q} > 0, \quad \frac{n_0}{q} > 1 \end{cases} \quad (r \rightarrow 0, \text{ case 3}).$$

Therefore, the coefficient of the term of first degree in the expansion of $\eta(r)$, that is $\eta'(0)$, is known in every case, thus providing an initial condition for the integration of (8).

Moreover, in every case

$$(12) \quad \eta(0) = 0$$

and also

$$(12') \quad \lim_{r \rightarrow \infty} (k_0 r + \eta) = 0.$$

As regards $\eta'(r)$, it follows from the above that it is finite at the origin. Since, moreover, the right hand side of (8) is visibly bounded everywhere outside the origin, it follows that $\eta'(r)$ is everywhere bounded. Moreover it

(3) The exponent in the power series will be written in the form n/q because sometimes a *fractionary* exponent is needed. (See example in the Appendix).

tends to zero (eq. (8)) as $r \rightarrow \infty$. Summing up:

$$(13) \quad \begin{cases} \eta'(r) \neq \infty \\ \eta'(\infty) = 0. \end{cases} \quad (0 \leq r \leq \infty)$$

It also follows from (8) and (8') that for $\eta'(r)$ to change sign, the condition

$$(14) \quad \varkappa W(r) + \frac{l(l+1)}{r^2} = 0$$

has to be fulfilled. Clearly, this can happen only rarely. For instance, the above expression is everywhere positive for a *repulsive* potential. It is everywhere negative for an *attractive* one and $l = 0$. For a power law, or exponential, attractive potential and $l \neq 0$ there can be only one (positive) root for (14), and so on ⁽⁴⁾.

All these features for $\eta(r)$ and $\eta'(r)$ characterize $\eta(r)$ as an everywhere finite and very « simply » varying function ⁽⁵⁾, that is one particularly suited for determination by numerical methods.

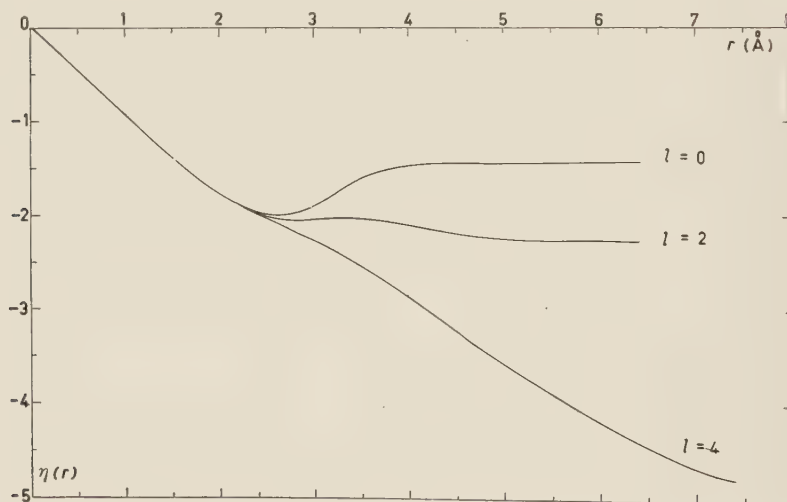


Fig. 1. – Examples of $\eta(r)$ curves. (Neutral Helium collision problem. Energy = $= 15 \cdot 10^{-16}$ erg, angular momentum as indicated). The curves stretch as far as the numerical integration has been extended (starting from $r = 1.5$). With an average of 30 calculated points each, these curves allow the corresponding asymptotic phase shifts $\eta(\infty)$ to be evaluated within about ± 0.01 . Note the linear behaviour near the origin, a feature common to every strongly divergent potential.

⁽⁴⁾ An example of repulsive-attractive potential is dealt with in the Appendix. It shows at most two inversion points for $\eta'(r)$.

⁽⁵⁾ As an example, Fig. 1 shows some $\eta(r)$ curves referring to the He-He problem.

To this aim, the following procedure suggests itself from what has been said.

1) One considers the differential equation (8) near the origin, where it lends itself to solution by series integration by means of formulae (9) to (11). (Remember that, because of (12'), the argument of \sin^2 in (8) tends to zero, allowing considerable simplification).

2) Starting with the value $\eta(r_0)$ obtained from the power series at a point r_0 where the approximation is still good (6), any standard method, as for instance the Runge-Kutta method, can be employed to extend the solution for $r > r_0$.

3) The above procedure is continued until $\eta(r)$ differs sufficiently little from $\eta(\infty)$ (7). To evaluate $|\eta_\infty - \eta(r)|$, a formula can immediately be derived from (8), that is

$$(15) \quad |\eta_\infty - \eta(r)| \approx \frac{1}{2} \int_r^\infty |\mathcal{F}(r)| dr$$

or else, more rigorously

$$(15') \quad |\eta_\infty - \eta(r)| < \int_r^\infty |\mathcal{F}(r)| dr .$$

(Note that the *sign* of $\eta_\infty - \eta(r)$ will in general be known). These formulae are very convenient ones, since, as a rule, there will be no difficulty in integrating $\mathcal{F}(r)$ especially for large r .

3. – Potential behaving as r^{-2} at infinity.

If $\mathcal{F}(r)$ (eq. (8')) is too slowly convergent to zero for $r \rightarrow \infty$, one has to compute $\eta(r)$ over a wide range to get an accurate value for η_∞ and the method ceases to be an useful one (at least for « hand » computation). However, even if the potential $W(r)$ decays sufficiently rapidly, in particular more rapidly than r^{-2} , the centrifugal term in the expression (8') for $\mathcal{F}(r)$ will make $\mathcal{F}(r)$ behave just as r^{-2} for $r \rightarrow \infty$ whenever we have $l \neq 0$. This case has therefore to be considered.

We take advantage of the fact that, after the potential $W(r)$ has died away,

(6) Obviously, a test of consistency can always be performed on (8) to check the accuracy of the solution.

(7) See however the next section for the case $l \neq 0$.

the Schrödinger equation (1) takes the form (recalling (5'))

$$(16) \quad y''_{\lim} + \left[k_0^2 - \frac{l(l+1)}{r^2} \right] y_{\lim} = 0,$$

whose general solution is (α and β constants)

$$(16') \quad y_{\lim} = r^{\frac{1}{2}} [\alpha J_{l+\frac{1}{2}}(k_0 r) + \beta J_{-l-\frac{1}{2}}(k_0 r)],$$

with the « extreme » limiting form

$$(16'') \quad y_{\infty} = \left(\frac{2}{\pi k_0} \right)^{\frac{1}{2}} \left\{ \alpha \sin \left[k_0 r - l \frac{\pi}{2} \right] + \beta \sin \left[k_0 r + (l+1) \frac{\pi}{2} \right] \right\}.$$

Comparing this with (5) one finds

$$(17) \quad \operatorname{tg} \eta_{\infty} = \varrho^{\cos(l+1)\pi}, \quad \varrho = \frac{\alpha}{\beta},$$

from which η_{∞} may be deduced (except for a multiple of π) if ϱ is known. The important point is that the limiting form (16') will be approached a good deal sooner than (5) (that is (16'')) and this allows ϱ and hence η_{∞} to be determined in a reasonable range (8).

Identifying y and y' with y'_{\lim} and y_{\lim} as deduced from (16'), the following formula for ϱ is easily found

$$(18) \quad \varrho = \frac{s J_{-l-\frac{1}{2}}(k_0 r) - J'_{-l-\frac{1}{2}}(k_0 r)}{J'_{l+\frac{1}{2}}(k_0 r) - s J_{l+\frac{1}{2}}(k_0 r)},$$

with

$$(18') \quad s = \cot [k_0 r + \eta(r)] - \frac{1}{2k_0 r}.$$

A simpler formula, namely

$$(18'') \quad \varrho = - \frac{J_{-l-\frac{1}{2}}(k_0 r)}{J_{l+\frac{1}{2}}(k_0 r)},$$

obtains from the general one, if r coincides with one of the zeros z for $y(r)$,

(8) Essentially the same idea, though developed somewhat differently, is to be found in J. E. KILPATRICK, E. F. HAMMEL and N. METROPOLIS: *Phys. Rev.*, **94**, 1103 (1954).

that is with one of the solutions of

$$(19) \quad k_0 z + \eta(z) = \pm m\pi, \quad m \text{ an integer.}$$

The value of ϱ obtained from (18) or (18'') at any point $r = r_n$ would be rigorous (i.e. coinciding with the value at $r = \infty$) and would therefore give the true value of η_∞ if

a) the potential $W(r)$ were rigorously nil beyond r_n ;

b) the value of $s(r_n)$ calculated by means of (18') were exact. Indeed, the fulfilment of these conditions would make ϱ rigorously constant for $r > r_n$ and rigorously «true».

We have therefore two sources of error from the necessarily imperfect fulfilment of a) and b).

The effect of neglecting $W(r)$ beyond r_n is readily evaluable by means of eq. (8). Indeed, the contribution to η_∞ coming from the W containing term is immediately seen to be

$$\Delta_a \eta_\infty = -\frac{\varkappa}{k_0} \int_{r_n}^{\infty} W(r) \sin^2 [k_0 r + \eta(r)] dr$$

from which

$$(20) \quad |\Delta_a \eta_\infty| < \frac{\varkappa}{k_0} \int_{r_n}^{\infty} |W(r)| dr.$$

(Notice, however, that the sign of $\Delta_a \eta_\infty$ will in general be known).

As regards point b), one can note that the value of s is affected by the incertitude in the value of $\eta(r_n)$ itself, which will depend on the accuracy with which the numerical integration has been performed. If $|\Delta\eta(r_n)|$ is the estimated error in $\eta(r_n)$, one finds easily by differentiating (18) and (17)

$$(18'') \quad |\Delta_b \eta_\infty| = \frac{|J_{-\ell-\frac{1}{2}} J'_{\ell+\frac{1}{2}} - J_{\ell+\frac{1}{2}} J'_{-\ell-\frac{1}{2}}|}{(J'_{-\ell-\frac{1}{2}} - s J_{\ell+\frac{1}{2}})^2 \sin^2(k_0 r_n + \eta)} \cdot \frac{|\Delta\eta(r_n)|}{1 + \varrho^2} \quad (^a).$$

(The argument in the J 's being everywhere $k_0 r_n$).

Summarizing, one may proceed as follows.

1) By the method described in Sect. 2 we determine $\eta(r)$ up to a point

(^a) Note that at points where $\sin(k_0 r + \eta)$ vanishes (and formula (18) has to be replaced by (18'')), the denominator of (18'') does not vanish. Indeed, at the points in question we have, because of (18') $s \sin(k_0 r + \eta) \pm 1$ and this makes the denominator simply equal to $J_{\ell+\frac{1}{2}}^2 \cdot (1 + \varrho^2)$. At the same points the (absolute) error $|\Delta\varrho|$ on ϱ may be comparatively large, without, however, affecting correspondingly the error $|\Delta\eta_\infty|$ on η_∞ .

r_n where the desired degree of accuracy—evaluated as explained above—has been attained.

As a rule, the condition

$$|\eta - \eta_\infty| < \pi .$$

with $|\eta - \eta_\infty|$ evaluated according to (15'), will by then be amply satisfied. (This condition is required to identify unambiguously η_∞ by means of eq (17)).

2) We evaluate $s(r_n)$ according to (18'). Then, through (18) (or (18'')) and (17), η_∞ may be calculated.

4. – The eigenfunctions.

Although particularly suited for phase shift calculations, the method was originally devised to find out the eigenfunctions themselves. This can be done through (6''), that is

$$(6'') \quad R(r) = \frac{y}{r} = \pm \frac{1}{r} \exp \left[k_0 \int^r \cot [k_0 r + \eta(r)] dr \right] .$$

Usually the integration will have to be performed numerically. To get $R(r)$ with an accuracy of, say, 1%, requires obviously to work out the value of the integral to within ± 0.01 , which is not particularly hard.

The sign in (6'') has to be reversed whenever r crosses one of the roots of eq. (19). At such points the integral in (6'') diverges and its computation would become difficult in the neighbourhood. However it becomes also superfluous, since $y(r)$ behave *linearly* at the points in question. It is therefore easy to find a suitable series (of a very few terms) in the powers of $r - z$, by means of which the zero z can be «crossed over» without difficulty.

To continue any eigenfunction beyond the point r_n reached by numerical integration, one proceeds as follows.

For $l = 0$, after having controlled, by means of eq. (15'), in the form

$$|\eta - \eta_\infty| < \frac{\pi}{k_0} \int_{r_n}^{\infty} |W(r)| dr ,$$

that η may be considered constant for $r > r_n$, one replaces $y(r)$ by the limiting form (5), with a suitable constant factor to make y continuous. (y' will also be continuous just because of $\eta'(r) \cong 0$ for $r > r_n$).

For $l = 0$, y is to be replaced by (16') for $r > r_n$. The value of $\varrho = \alpha/\beta$ calculated as explained in Sect. 3, together with the condition of continuity between y and y_{\lim} fix the constants α and β unambiguously. (Here also the continuity is ensured both for y and y').

APPENDIX

The method described in the preceding sections has been applied to the He-He collision problem.

The Slater-Kirkwood potential (10)

$$(A1) \quad W(r) = 7.7 \cdot 10^6 \exp[-4.59r] - 1.49 \cdot 10^4 r^{-6}$$

has been used. (Units are 10^{-16} erg for energies and 10^{-8} cm for lengths).

In the neighbourhood of $r = 1.5$ the above potential can be replaced by

$$(A2) \quad W(r) = 1.12 \cdot 10^5 r^{-7} \quad (r \approx 1.5)$$

so that eq. (8) for $l = 0$ takes the form

$$(A3) \quad \eta'(r) = -cr^{-7}(k_0r + \eta)^2 \quad (11) \quad (r \approx 1.5).$$

According to eq. (11) (« strongly » divergent potential), one puts

$$(A4) \quad \eta(r) = -k_0r + \sum_{n=3}^{\infty} a_n r^{n/2},$$

finding the following non-zero coefficients:

$$a_7 = +\left(\frac{k_0}{c}\right)^{\frac{1}{2}}, \quad a_{12} = -\frac{7}{4c}, \quad a_{17} = -a_{12} \frac{6 + ca_{12}}{2ca_7}, \quad a_{22} = -\left(\frac{4.25}{c} + a_{12}\right) \frac{a_{17}}{a_7}, \quad \dots.$$

The calculations have been performed for a value of $k_0 = 0.9471$ corresponding to an energy $E = 15$. (The value for c is $7.084 \cdot 10^3$). The series for η is then

$$\begin{aligned} \eta(r) = & -0.9471r + 1.156 \cdot 10^{-2}r^{3.5} - 2.470 \cdot 10^{-4}r^6 + \\ & + 6.411 \cdot 10^{+6}r^{8.5} - 1.956 \cdot 10^{-7}r^{11} \dots \quad (r \approx 1.5). \end{aligned}$$

from which the starting value for the numerical integration $\eta(1.5) = -1.375$ is found.

This result has been obtained for $l = 0$. Since, however, the centrifugal potential at $r = 1.5$ is negligible against $W(r)$ even for values of l up to 4,

(10) J. C. SLATER and J. G. KIRKWOOD: *Phys. Rev.*, **37**, 682 (1931).

(11) If desired, further terms in the expansion for $\sin^2(k_0r + \eta)$ could be added to the right hand side of (A3), but they are negligible in the present instance.

the same result has been employed also for $l = 2$ and $l = 4$ which were the values of interest.

The Runge-Kutta method has been employed (on the complete equation (8), with the true potential (A1)) to compute the solution from $r = 1.5$ up to $r = 6.4$. (Up to $r = 7.4$ for $l = 4$).

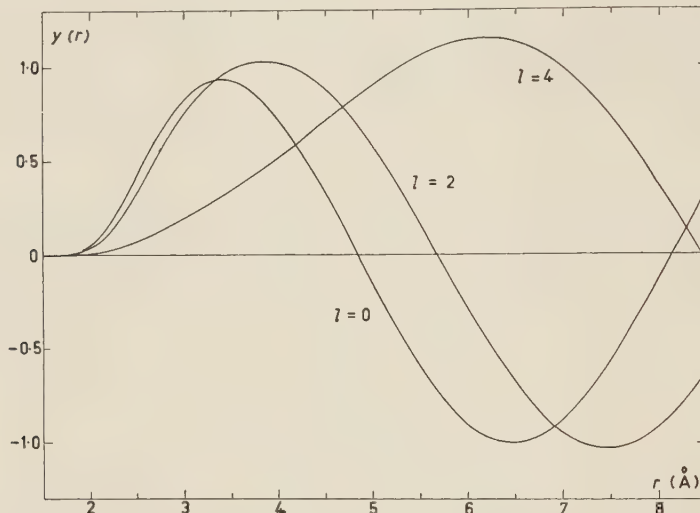


Fig. 2. – The functions $y(r) = rR(r)$, with $R(r)$ the radial part of the eigenfunction, for the same problem as in Fig. 1.

The η -curves are shown in Fig. 1 (12). Fig. 2 shows the results for the corresponding $y(r) = rR(r)$ functions (normalized to amplitude 1 at infinity). The accuracy is about 1% throughout.

For each η -curve an average of 30 points have been calculated, each point requiring rather less than about 10 minutes to be worked out (by hand computation).

* * *

The Author wishes to thank Miss. C. CIVIDALLI for help in performing the calculations for the He-He problem.

(12) The values for η_∞ are -1.42 , -2.80 , -6.124 for $l=0$, 2 , 4 respectively, corresponding (eq. (5'')) to $\eta_0 = -1.42$, $\eta_2 = 0.34$, $\eta_4 = 0.159$ in the usual notation.

RIASSUNTO

Si esamina una volta di più — e con particolare riguardo al calcolo delle fasi asintotiche — il problema della ricerca delle soluzioni à energia positiva dell'equazione di Schrödinger radiale, per potenziali che si comportano all'infinito come r^{-n} , $n \geq 2$. Si mostra che una scelta appropriata della funzione incognita permette di trasformare l'equazione di Riccati del problema in un'equazione del 1° ordine piuttosto semplice, la cui soluzione — che si presta particolarmente a essere ricavata con procedimenti di integrazione numerica — conduce direttamente alla fase asintotica per un dato valore dell'energia e del momento angolare. Ove occorra, la corrispondente autofunzione si può ricavare mediante un'ulteriore quadratura.

Theory of High-Energy Potential Scattering (*).

D. S. SAXON (†)

Universitetets Institut for Teoretisk Fysik - Copenhagen

L. I. SCHIFF (‡)

Laboratoire de Physique, École Normale Supérieure - Université de Paris

(ricevuto il 3 Giugno 1957)

Summary. — A new formulation for high-energy potential scattering, presented in a recent paper, is extended to provide explicit formulas for the scattering theory of the three-dimensional non-separable Schrödinger equation. An integral equation is derived, for which a single iteration gives the scattering when the potential energy is not too large and is slowly-varying compared to a wavelength. The result agrees with those obtained earlier for small and for large scattering angles, but applies as well to intermediate angles and improves the earlier accuracy. Further iterations can provide greater accuracy as well as an error estimate for the first approximation.

1. — Introduction.

In an earlier paper (¹), formulas for the Schrödinger scattered amplitude were obtained that are valid when the potential energy is small compared to the incident kinetic energy and slowly-varying compared to a wavelength, and the scattering angle is either small or large compared to $(kR)^{-\frac{1}{2}}$, where k is the wave number and R is the size of the potential. These results were obtained by iterating the usual integral equation an infinite number of times,

(*) Supported in part by the United States Air Force through the European Office, Air Research and Development Command.

(†) Fellow of the John Simon Guggenheim Memorial Foundation. Permanent address: University of California, Los Angeles, California, U.S.A.

(‡) Professeur d'échange, and Fellow of the John Simon Guggenheim Memorial Foundation. Permanent address: Stanford University, Stanford, California, U.S.A.

(¹) L. I. SCHIFF: *Phys. Rev.*, **103**, 443 (1956).

and summing the infinite Born series after approximating each term by the method of stationary phase. A more recent paper (2) develops a new formulation for high-energy scattering, in which a different integral equation is obtained with the help of a modified propagator in place of the usual free-particle Green's function. The formalism was applied there to the one dimensional problem, and to the radial wave equations that result from separation of the Schrödinger equation with a spherically symmetric potential. Some remarks were also made about the three-dimensional unseparated problem, and the resemblance to the results of reference (1) was pointed out.

The purpose of the present paper is to extend the formalism of reference (2) so as to obtain explicit formulas in the three-dimensional non-separable case. The emphasis is on methodology rather than on the attainment of practical results, so that only the Schrödinger equation is considered. The new integral equation is derived in Sect. 2, following the development of reference (2) with some repetition. From this, exact expressions for the scattered amplitude and for the differential and total cross-sections are obtained in Sect. 3. In Sect. 4, a more convenient form for the scattered amplitude is found, which is still exact. The first approximation to this exact result is obtained in Sect. 5, and an error estimate is made with the help of further iterations. In Sect. 6, simplified versions of the first approximation, valid for small and for large angles, are compared with earlier results. The notation follows that of reference (1) throughout.

2. – Derivation of the integral equation.

We wish to find a scattering solution of the Schrödinger wave equation

$$(1) \quad (\nabla^2 + k^2 - U)\psi = 0,$$

where $\hbar^2 k^2 / 2m$ is the kinetic energy of the incident particle and $\hbar^2 U / 2m = V$ is the scattering potential energy. In place of the usual free-particle Green's function

$$(2) \quad G(\varrho) = (-4\pi\varrho)^{-1} \exp[ik\varrho], \quad \varrho = \mathbf{r} - \mathbf{r}'$$

we define the modified propagator

$$(3) \quad F(\mathbf{r}, \mathbf{r}') = (-4\pi p)^{-1} \exp[iS(\mathbf{r}, \mathbf{r}')].$$

For the present we assume that $S(\mathbf{r}, \mathbf{r}') = S(\mathbf{r}', \mathbf{r})$ and $S(\mathbf{r}, \mathbf{r}) = 0$; also, for finite r' , with $\mathbf{r} = \hat{n} r$ as $r \rightarrow \infty$, we assume that $\nabla S \rightarrow \hat{n} k + O(r^{-1})$. Then F

(2) D. S. SAXON: *Formulation of High Energy Potential Scattering Problems* (submitted for publication to the *Phys. Rev.*).

satisfies the equation

$$(4) \quad (\nabla^2 + k^2 - U)F(\mathbf{r}, \mathbf{r}') = \delta(\mathbf{r} - \mathbf{r}') + (-|\nabla S|^2 + k^2 - U)F + i\varrho^2[\nabla \cdot (\varrho^{-2}\nabla S)]F.$$

We wish to obtain a solution of Eq. (1) that has the asymptotic form of a plane wave, $\exp[i\mathbf{k}_0 \cdot \mathbf{r}]$, plus an outgoing scattered wave. This can be accomplished by applying Green's identity to Eqs. (1) and (4) to obtain

$$(5) \quad \psi(\mathbf{r}) = \exp[i(\mathbf{k}_0 \cdot \mathbf{r} + \delta_0(\mathbf{r}))] - \int \left\{ -|\nabla' S|^2 + k^2 - U(\mathbf{r}') + i\varrho^2[\nabla' \cdot (\varrho^{-2}\nabla' S)] \right\} F(\mathbf{r}, \mathbf{r}') \psi(\mathbf{r}') d\tau',$$

where $\delta_0(r)$ is defined as

$$(6) \quad \delta_0(\mathbf{r}) = -\mathbf{k}_0 \cdot \mathbf{r} + \lim_{r' \rightarrow \infty} [S(\mathbf{r}, -\hat{\mathbf{k}}_0 r') - kr'] ,$$

and $\hat{\mathbf{k}}_0$ is a unit vector parallel to \mathbf{k}_0 .

Thus far, the choice of $S(\mathbf{r}, \mathbf{r}')$ has been left open. If it is taken to be $k\varrho$, then F becomes equal to G , and Eq. (5) reduces to the usual integral equation. It is natural at high energies to choose S to be proportional to the classical action function, so that the first three terms in the integrand of Eq. (5) add to zero; this was the intention in the work of reference (2). However, this leads to analytical complexity. A connection with the work of reference (1) is made most easily if we use for S a form that is equivalent to the approximation of the classical trajectories by straight lines. We therefore choose

$$(7) \quad \begin{cases} S(\mathbf{r}, \mathbf{r}') = k\varrho + \delta(\mathbf{r}, \mathbf{r}') , \\ \delta(\mathbf{r}, \mathbf{r}') = (-2k)^{-1} \int_0^\varrho U(\mathbf{r} - \hat{\mathbf{q}}s) ds = (-2k)^{-1} \int_0^\varrho U(\mathbf{r}' + \hat{\mathbf{q}}s) ds . \end{cases}$$

This also satisfies the requirements on S given below Eq. (3). Equations (5) and (6) then become

$$(8) \quad \begin{cases} \psi(\mathbf{r}) = \exp[i(\mathbf{k}_0 \cdot \mathbf{r} + \delta_0(\mathbf{r}))] - \int \left\{ (i/k\varrho) U(\mathbf{r}') \exp i\delta(\mathbf{r}, \mathbf{r}') \right. \\ \quad \left. + (\nabla'^2 \exp[i\delta(\mathbf{r}, \mathbf{r}')]) \right\} G(\varrho) \psi(\mathbf{r}') d\tau' , \\ \delta_0(\mathbf{r}) = (-2k)^{-1} \int_0^\infty U(\mathbf{r} - k_0 s) ds , \end{cases}$$

where G is given by Eq. (2). We shall work with the integral equation (8) throughout the remainder of this paper.

3. – Scattered amplitude and cross section.

In order to obtain the amplitude that corresponds to scattering from the initial wave vector \mathbf{k}_0 to the final wave vector \mathbf{k}_f , we must obtain the asymptotic form of $\psi(\mathbf{r})$ given by Eq. (8) for $\mathbf{r} = \hat{\mathbf{k}}_f r$ and $r \rightarrow \infty$. In doing this, we cannot make the usual assumption that r becomes large compared to r' in the integrand of Eq. (8); this assumption is valid for the first term of the integrand, since the domain of \mathbf{r}' is restricted by the presumed finite range of $U(\mathbf{r}')$. However, in the second term of the integrand, we note that for large r , $\delta(\mathbf{r}, \mathbf{r}')$ fails to vanish when \mathbf{r}' lies in the semi-infinite cylinder whose axis is in the direction $-\mathbf{k}_f$ and whose cross-section is the projected area of the scattering potential; we shall call this region C_f . Because of this, the parts of ∇'^2 that involve differentiation transverse to the cylinder axis give a finite contribution to the integrand no matter how large r' is.

This difficulty can be avoided by making use of the identity

$$(9) \quad \varrho = \mathbf{r} - \mathbf{r}' = \hat{\mathbf{k}}_f(r - \hat{\mathbf{k}}_f \cdot \mathbf{r}') - [\mathbf{r}' - \hat{\mathbf{k}}_f(\hat{\mathbf{k}}_f \cdot \mathbf{r}')].$$

The second term on the right side of Eq. (9) is the component of \mathbf{r}' perpendicular to \mathbf{k}_f , and is never larger than the size of the potential. Thus with $\mathbf{r} = \hat{\mathbf{k}}_f r$ and $r \rightarrow \infty$, we can put

$$(10) \quad \varrho = r - \hat{\mathbf{k}}_f \cdot \mathbf{r}' + O(r^{-1}),$$

and the asymptotic form of Eq. (8) becomes

$$(11) \quad \left\{ \begin{array}{l} \psi(\mathbf{r}) \rightarrow \exp[i(\mathbf{k}_0 \cdot \mathbf{r} + \delta_0(\mathbf{r}))] + (4\pi)^{-1} \exp[ikr] \cdot \\ \quad \cdot \int (r - \hat{\mathbf{k}}_f \cdot \mathbf{r}')^{-1} \exp[-i\mathbf{k}_f \cdot \mathbf{r}'] \psi(\mathbf{r}') [\nabla'^2 \exp i\delta_f(\mathbf{r}')] d\tau' + 0(r^{-2}), \\ \delta_f(\mathbf{r}') = (-2k)^{-1} \int_0^\infty U(\mathbf{r}' + \hat{\mathbf{k}}_f s) ds. \end{array} \right.$$

As written, the integral in Eq. (11) has a logarithmic divergence when the component of \mathbf{r}' parallel to \mathbf{k}_f is equal to r . If this domain of \mathbf{r}' were actually to appear in the evaluation of the integral, it would be necessary to keep the remainder terms in (10), which would then be of larger order than r^{-1} . However, it turns out that this difficulty does not arise.

We now define the scattered amplitude as

$$(12) \quad f(\mathbf{k}_f, \mathbf{k}_0) = (4\pi)^{-1} \lim_{r \rightarrow \infty} \left\{ r \int (r - \hat{\mathbf{k}}_f \cdot \mathbf{r}')^{-1} \exp[-i\mathbf{k}_f \cdot \mathbf{r}'] \psi(\mathbf{r}') (\nabla'^2 \exp[i\delta_f(\mathbf{r}')]) d\tau' \right\},$$

so that Eq. (11) becomes

$$(13) \quad \psi(\mathbf{r}) \rightarrow \exp[i(\mathbf{k}_0 \cdot \mathbf{r} + \delta_0(\mathbf{r}))] + r^{-1} \exp[ikr] f(\mathbf{k}_f, \mathbf{k}_0).$$

We recognize that the definition (12) omits the terms $\exp[i\mathbf{k}_0 \cdot \mathbf{r}] (\exp[i\delta_0(\mathbf{r})] - 1)$ from the scattered field. We must therefore show that in the asymptotic region, this term does not contribute to the scattering, and that the usual relations between the scattered amplitude and the differential and total cross-sections.

$$(14) \quad \begin{cases} \sigma(\mathbf{k}_f, \mathbf{k}_0) = |f(\mathbf{k}_f, \mathbf{k}_0)|^2, \\ \sigma = (4\pi/k) \operatorname{Im}[f(\mathbf{k}_0, \mathbf{k}_0)], \end{cases}$$

are not invalidated.

For large r , the additional phase $\delta_0(\mathbf{r})$ is zero except in nearly the forward direction, where it fails to vanish for angles $\theta \lesssim R/r$, where R is the size of the scattering potential. Thus $\partial\delta_0/\partial r$ can be neglected in computing the radially outgoing flux associated with Eq. (13) (3):

$$(15) \quad (\hbar/2im)\bar{\psi}(\partial\psi/\partial r) + \text{e. c.} \rightarrow (\hbar/2im)(\exp[-i(kr\mu + \delta_0)] + r^{-1} \exp[ikr]\bar{f}) \cdot \\ \cdot (ik\mu \exp[i(kr\mu + \delta_0)] + (ik/r) \exp[ikr]f) + \text{e. e.},$$

where μ is the cosine of the angle between \mathbf{r} and \mathbf{k}_0 . Further analysis along the lines of what follows shows that terms of the form $r^{-2} \exp[ikr]$, which arise both from differentiation of the f term in (13) and from neglected higher order terms in the asymptotic form of ψ , do not contribute to the scattering. We divide the flux (15) by the incident speed $v = \hbar k/m$, and multiply by r^2 , to obtain for the scattering per unit solid angle and per unit incident intensity:

$$(16) \quad r^2\mu + |f|^2 + \{ \frac{1}{2}rf(1+\mu) \exp[ikr(1-\mu) - i\delta_0] + \text{e. c.} \}.$$

(3) The analysis of the remainder of this section is a slight extension of that of E. FEENBERG: *Phys. Rev.*, **40**, 40 (1932), and L. I. SCHIFF: *Progr. Theor. Phys. (Kyoto)*, **11**, 288 (1954).

The first term of (16) arises from the plane wave, and integrates to zero over the sphere; it is not affected by the factor $\exp[i\delta_0]$. The second term is the usual differential scattering cross-section given by the first of Eqs. (14), and is also unaffected by $\exp[i\delta_0]$. The third term, in curly brackets, arises from interference between the two parts of (13); it is negligible except near the forward direction, because of the rapid oscillations of $\exp[ikr(1-\mu)]$. Thus the factor $\exp[i\delta_0]$ can at most affect the interference term, and hence the relation between total cross-section and forward scattered amplitude given by the second of Eqs. (14); we now show that there actually is no such effect.

Since ψ is a solution of Eq. (1) with a real potential, particles are conserved and the integral of (16) over the sphere is zero. If we define σ in the usual way as $\int |f|^2 d\Omega$ taken over the sphere, we obtain

$$(17) \quad \sigma = -\frac{1}{2}r \left\{ \int_0^{2\pi} d\varphi \int_{-1}^1 d\mu (1+\mu) f \exp[ikr(1-\mu) - i\delta_0] + \text{e.c.} \right\}.$$

The integral over μ in Eq. (17) can be rewritten as

$$\begin{aligned} \int_{-1}^1 d\mu (1+\mu) f \exp[i(kr(1-\mu) - \delta_0)] &= \int_{-1}^1 d\mu (1+\mu) f \exp[ikr(1-\mu)] + \\ &+ \int_{-1}^1 d\mu (1+\mu) f \exp[ikr(1-\mu)] (\exp[-i\delta_0] - 1). \end{aligned}$$

The first integral on the right side can be integrated by parts; the leading term for large r is $(2i/kr)f_0$, where $f_0 = f(\mathbf{k}_0, \mathbf{k}_0)$. The integrand of the second integral vanishes except for $\theta \lesssim R/r$, so that the integral is of order $(R/r)^2 f_0$. Thus on substitution into (17), we obtain in the limit of infinite r :

$$\sigma = -(2\pi i/k)f_0 + \text{e. c.},$$

which is the same as the second of Eqs. (14).

Thus the factor $\exp[i\delta_0]$ that multiplies the plane wave part of ψ has no effect on either the differential or total cross-section, and can be ignored so long as we deal with the asymptotic form of ψ .

4. – Reformulation of the scattered amplitude.

Equation (12) for the scattered amplitude is not in a convenient form, since the integrand fails to vanish when \mathbf{r}' lies in the semi-infinite cylinder C , defined in the preceding section. The integral converges in spite of this, be-

cause the use of Green's identity to obtain Eq. (8) requires that the point \mathbf{r}' be within the volume of integration of \mathbf{r}' . Thus the integration over \mathbf{r}' in Eq. (12), which extends to infinity, must be performed before the limit $r \rightarrow \infty$ is taken. Then the factor $(r - \hat{k}_f \cdot \mathbf{r}')$ in the denominator insures convergence. We emphasize that the order of the limit and integration operations in Eq. (12) is important, and must be preserved.

It is desirable to reformulate the expression for the scattered amplitude so that the potential appears explicitly as a factor in the integrand, thus limiting the domain of integration. As a first step in this direction, we rewrite Eq. (12) by replacing \mathbf{r}' by \mathbf{r} , and r by r_0 , and choose the positive z -axis along the direction of $-\mathbf{k}_f$:

$$f(\mathbf{k}_f, \mathbf{k}_0) = (4\pi)^{-1} \lim_{r_0 \rightarrow \infty} \int (1 + z/r_0)^{-1} \exp [ikz] \psi(\mathbf{r}) (\nabla^2 \exp [i\delta_f(\mathbf{r})]) d\tau .$$

Integrating by parts with respect to z , we obtain

$$\begin{aligned} f(\mathbf{k}_f, \mathbf{k}_0) &= (4\pi)^{-1} \lim_{r_0 \rightarrow \infty} \int_{-\infty}^{\infty} dx \int_{-\infty}^{\infty} dy \left\{ -(\nabla^2 \exp [i\delta_f(\mathbf{r})]) \int_z^{\infty} (1 + z'/r_0)^{-1} \exp [ikz'] \psi(\mathbf{r}') dz' \Big|_{-\infty}^{\infty} \right. \\ &\quad \left. - \int_{-\infty}^{\infty} dz (i/2k) \nabla^2 (U(\mathbf{r}) \exp [i\delta_f(\mathbf{r})]) \int_z^{\infty} (1 + z'/r_0)^{-1} \exp [ikz'] \psi(\mathbf{r}') dz' \right\}, \end{aligned}$$

where now $\mathbf{r}' = (x, y, z')$. The first term vanishes at the upper limit because of the integral, and at the lower limit because $\delta_f = 0$ at $z = -\infty$. Then since $U(\mathbf{r})$ is bounded in its spatial extent, the Laplacian can be transferred from operating on $(U \exp [i\delta_f])$ to operating on the remaining factors in the integrand of the second term. Finally, since the domain of \mathbf{r} is now bounded, the limit $r_0 \rightarrow \infty$ can be moved inside the first integral, to obtain

$$(18) \quad f(\mathbf{k}_f, \mathbf{k}_0) = (-i/8\pi k) \int U(\mathbf{r}) \exp [i\delta_f(\mathbf{r})] \lim_{r_0 \rightarrow \infty} \nabla^2 \int_z^{\infty} (1 + z'/r_0)^{-1} \cdot \exp [ikz'] \psi(\mathbf{r}') dz' d\tau .$$

The ψ that appears in the integrand of Eq. (18) can be written

$$(19) \quad \psi(\mathbf{r}) = \exp [i\mathbf{k}_0 \cdot \mathbf{r} + \psi_{sc}(\mathbf{r})].$$

We have chosen the scattered wave ψ_{sc} so that it contains a part $\exp [i\mathbf{k}_0 \cdot \mathbf{r}] \cdot (\exp [i\delta_0(\mathbf{r})] - 1)$, and a remainder that falls off like $(r^{-1} \exp [ikr])$ for large r ,

Since z is confined to a finite value by the appearance of $U(\mathbf{r})$ in the integrand, we need only consider the convergence of the z' integration at the upper limit. For the remainder part of ψ_{sc} this is assured by the factor r^{-1} even if the factor $(1+z'/r_0)^{-1}$ is omitted. Thus the limit $r_0 \rightarrow \infty$ can be taken at once for this part of ψ_{sc} . The first part of ψ_{sc} fails to vanish only in the semi-infinite cylinder whose axis is in the direction $+\mathbf{k}_0$ and whose cross-section is the projected area of the scattering potential; we shall call this region C_0 . However, since x , y and z are confined to finite values by the presence of $U(\mathbf{r})$, there are contributions to the z' integration only from the semi-infinite cylinder C_f . Unless the scattering angle is exactly 180° , the regions C_0 and C_f overlap only in the vicinity of the scattering potential, and there is no convergence difficulty even if the factor $(1+z'/r_0)^{-1}$ is omitted; directly backward scattering also causes no difficulty since it can be obtained as the limit scattering through the angle $180^\circ - \varepsilon$ as $\varepsilon \rightarrow 0$. Thus the limit $r_0 \rightarrow \infty$ can be taken at once for the entire ψ_{sc} .

We must now consider the contribution to the scattered amplitude from the plane wave part of ψ . This involves

$$\lim_{r_0 \rightarrow \infty} \nabla^2 \int_z^{\infty} (1 + z'/r_0)^{-1} \exp[i\mathbf{q} \cdot \mathbf{r}'] dz' , \quad \mathbf{q} = \mathbf{k}_0 - \mathbf{k}_f ,$$

since $kz' = -\mathbf{k}_f \cdot \mathbf{r}'$. Integrating by parts with respect to z' , we obtain

$$\lim_{r_0 \rightarrow \infty} \nabla^2 \left\{ (-i/q_z) (1 + z'/r_0)^{-1} \exp[i\mathbf{q} \cdot \mathbf{r}'] \Big|_z^{\infty} - (i/r_0 q_z) \int_z^{\infty} (1 + z'/r_0)^{-2} \exp[i\mathbf{q} \cdot \mathbf{r}'] dz' \right\} .$$

The first term is equal to $(-2ik \exp[i\mathbf{q} \cdot \mathbf{r}])$. The second term is bounded if q_z is finite, and hence vanishes in the limit $r_0 \rightarrow \infty$; since q_z must be finite, exactly zero scattering angle must be excluded, but can be arrived at without difficulty by a limiting process.

In this way, the expression (18) for the scattered amplitude becomes

$$(20) \quad f(\mathbf{k}_f, \mathbf{k}_0) = (-4\pi)^{-1} \int U(\mathbf{r}) \exp[i(\mathbf{q} \cdot \mathbf{r} + \delta_f(\mathbf{r}))] d\tau - \\ - (i/8\pi k) \int U(\mathbf{r}) \exp[i\delta_f(\mathbf{r})] \left[\nabla^2 \int_z^{\infty} \exp[ikz'] \psi_{sc}(\mathbf{r}') dz' \right] d\tau .$$

Equation (20) is exact when the ψ_{sc} that appears within the second integral is defined by (19), that is, with respect to the incident direction \mathbf{k}_0 . Since it is exact, we can use the reciprocity relation ⁽⁴⁾ $f(-\mathbf{k}_0, -\mathbf{k}_f) =$

$= f(\mathbf{k}_f, \mathbf{k}_0)$ to obtain an alternative expression for the scattered amplitude, which involves the wave function ψ^+ that corresponds to the incident direction $-\mathbf{k}_f$:

$$(21) \quad \psi^+(\mathbf{r}) = \exp[-i\mathbf{k}_f \cdot \mathbf{r}] + \psi_{sc}^+(\mathbf{r}).$$

It is easily shown that this expression is

$$(22) \quad f(\mathbf{k}_f, \mathbf{k}_0) = (4\pi)^{-1} \int U(\mathbf{r}) \exp[i(\mathbf{q} \cdot \mathbf{r} + \delta_0(\mathbf{r}))] d\tau - \\ - (i/8\pi k) \int U(\mathbf{r}) \exp[i\delta_0(\mathbf{r})] \left[\nabla^2 \int_z^\infty \exp[ikz'] \psi_{sc}^*(\mathbf{r}') dz' \right] d\tau,$$

where now the positive z -axis is along the direction of $+\mathbf{k}_0$.

5. — First approximation and error estimates.

We shall work for the remainder of the paper with Eq. (22). The integral equation satisfied by the ψ^+ of Eq. (21) is analogous to Eq. (8):

$$(23) \quad \psi^+(\mathbf{r}) = \exp[i(-\mathbf{k}_f \cdot \mathbf{r} + \delta_f(\mathbf{r}))] - \int \{ (i/k\varrho) U(\mathbf{r}') \exp[i\delta(\mathbf{r}, \mathbf{r}')] + \\ + [\nabla'^2 \exp[i\delta(\mathbf{r}, \mathbf{r}')]] \} G(\varrho) \psi^+(\mathbf{r}') d\tau'.$$

The first approximation to Eq. (22) is obtained by making use of the first approximation to ψ_{sc}^+ :

$$(24) \quad \psi_{sc}^{+(1)}(\mathbf{r}) = \exp[-i\mathbf{k}_f \cdot \mathbf{r}] (\exp[i\delta_f(\mathbf{r})] - 1).$$

Substitution of (24) into (22) yields

$$(25) \quad f^{(1)}(\mathbf{k}_f, \mathbf{k}_0) = (-4\pi)^{-1} \int U(\mathbf{r}) \exp[i(\mathbf{q} \cdot \mathbf{r} + \delta_0(\mathbf{r}))] d\tau - \\ - (i/8\pi k) \int U(\mathbf{r}) \exp[i\delta_0(\mathbf{r})] \left\{ \nabla^2 \int_z^\infty \exp[i\mathbf{q} \cdot \mathbf{r}'] (\exp[i\delta_f(\mathbf{r}')] - 1) dz' \right\} d\tau.$$

Equation (25) is our expression for the scattered amplitude.

(4) R. GLAUBER and V. SCHOMAKER: *Phys. Rev.*, **89**, 667 (1953).

In order to gauge the validity of (25), we first calculate the second approximation to ψ_{sc}^+ . This is obtained by substituting the first term on the right side of Eq. (23) into the integrand of the second term:

$$(26) \quad \psi_{sc}^{+(2)}(\mathbf{r}) = - \int \left\{ (i/k\varrho) U(\mathbf{r}') \exp [i\delta(\mathbf{r}, \mathbf{r}')] + (\nabla'^2 \exp [i\delta(\mathbf{r}, \mathbf{r}')] \right\} G(\varrho) \exp [i(-\mathbf{k}_f \cdot \mathbf{r}' + \delta_f(\mathbf{r}'))] d\tau' .$$

The difference between the first and second approximations to the scattered amplitude, Δf , is then found by substituting (26) into the integrand of the second term on the right side of Eq. (22). We shall regard Δf as a provisional estimate for the error of the first approximation (25), and consider further iterations in the last paragraph of this section.

Consider the integral

$$(27) \quad -(i/8\pi k) \int U(\mathbf{r}) \exp [i\delta_0(\mathbf{r})] \left[\nabla^2 \int_z^\infty \exp [(i\mathbf{q} \cdot \mathbf{r}') \Gamma(\mathbf{r}')] dz' \right] d\tau .$$

The second term of $f^{(1)}$ is given by (27) with Γ replaced by

$$(28) \quad \Gamma_1(\mathbf{r}) = \exp [i\delta_f(\mathbf{r})] - 1 ,$$

and Δf is given by (27) with Γ replaced by

$$(29) \quad \Gamma_2(\mathbf{r}) = - \int \left\{ (i/k\varrho) U(\mathbf{r}') \exp [i\delta(\mathbf{r}, \mathbf{r}')] + (\nabla'^2 \exp [i\delta(\mathbf{r}, \mathbf{r}')] \right\} \cdot G(\varrho) \exp [i(\mathbf{k}_f \cdot \mathbf{p} + \delta_f(\mathbf{r}'))] d\tau' .$$

The integrand of (29) is slowly-varying except for the factor $(G(\varrho) \exp [i\mathbf{k}_f \cdot \mathbf{p}])$. Thus we can change the variable of integration from \mathbf{r}' to \mathbf{p} , and use the stationary phase approximation ⁽¹⁾ to obtain

$$(30) \quad \Gamma_2(r) \simeq (i/2k) \int_0^\infty \{ \} \exp [i\delta_f(\mathbf{r} + \hat{\mathbf{k}}_f \varrho)] d\varrho ,$$

where $\{ \}$ is the curly bracket of (29) evaluated at $\mathbf{r}' = \mathbf{r} + \hat{\mathbf{k}}_f \varrho$.

We now compare Δf with the second term of $f^{(1)}$ by comparing Γ_2 with Γ_1 . Γ_1 is of order UR/k if $UR/k \lesssim 1$, and is of order unity if $UR/k > 1$. The first term in the curly bracket of (30) is of order U/kR , and the second is of

order U/kR or U^2/k^2 , whichever is the larger⁽⁵⁾; further, the effective range of the ϱ integration in (30) is of order R . Thus Γ_2 is of order U/k^2 if $UR/k \lesssim 1$, and is of order U^2R/k^3 if $UR/k > 1$. We conclude, therefore, that the ratio of the error in the scattered amplitude $f^{(1)}$ to the second term of $f^{(1)}$ is of order

$$(31) \quad \begin{cases} 1/kR, & \text{if } UR/k \lesssim 1; \\ (UR/k)^2/kR, & \text{if } UR/k > 1. \end{cases}$$

Since the stationary phase approximation requires that $kR \gg 1$, its use in passing from (29) to (30) is justified whenever (25) is a good approximation to the scattered amplitude.

The procedure described in the last three paragraphs can be continued with further iterations of the integral equation (23). The stationary phase approximation can be used for each integration, and successively higher powers of U/k^2 or U^2R/k^3 are obtained. Thus the fractional error in the first approximation to the scattered amplitude, given by Eq. (25), is of order (31) if this ratio is small compared to unity.

6. – Simplifications for large and small angles.

Equation (25) is the main result of this paper; it is valid for all scattering angles, and its accuracy is specified by (31). It can be simplified somewhat for large and small scattering angles, and this facilitates comparison with earlier results.

The z' integral in the second term of (25) can be integrated by parts repeatedly to obtain an asymptotic series in q_z^{-1} . This is expected to be a useful procedure only when $q_z = 2k \sin^2 \frac{1}{2}\theta$ is not too small, and hence for scattering angles θ that are not too small. The first two terms in this series are

$$(32) \quad \begin{aligned} \int_z^\infty \exp [i\mathbf{q} \cdot \mathbf{r}'] (\exp [i\delta_f(\mathbf{r}')] - 1) dz' &= \\ &= (i/q_z) \exp [i\mathbf{q} \cdot \mathbf{r}] \{ (\exp [i\delta_f(\mathbf{r})] - 1) - q_z^{-1} (\partial \delta_f / \partial z) \exp [i\delta_f(\mathbf{r}) + \dots] \}. \end{aligned}$$

(5) For simplicity, we assume that the distance over which the potential changes by an appreciable fraction of itself has the same order of magnitude as the size R of the potential.

The ratio of the second to the first term of (32) is of order

$$(33) \quad \begin{cases} 1/kR \sin^2 \frac{1}{2}\theta, & \text{if } UR/k \lesssim 1; \\ (UR/k)/kR \sin^2 \frac{1}{2}\theta, & \text{if } UR/k > 1. \end{cases}$$

We retain only the first term of (32) and substitute it into (25) to obtain

$$(34) \quad f^{(1)}(\mathbf{k}_f, \mathbf{k}_o) = (-4\pi)^{-1} \int U(\mathbf{r}) \exp [i(\mathbf{q} \cdot \mathbf{r} + \delta_o(\mathbf{r}) + \delta_f(\mathbf{r}))] d\tau,$$

which agrees with the large-angle result of reference (1). In applying the Laplacian to the first term of (32) to obtain (34), terms have been neglected that are of smaller fractional order than (33). Comparison of the ratios (31) and (33) then shows that the fractional error in Eq. (34) is of order

$$(35) \quad \begin{cases} 1/kR \sin^2 \frac{1}{2}\theta, & \text{if } UR/k \lesssim 1; \\ L\{(UR/k)^2/kR; (UR/k)/kR \sin^2 \frac{1}{2}\theta\}, & \text{if } UR/k \gtrsim 1. \end{cases}$$

Here, the symbol $L\{A; B; C; \dots\}$ denotes the largest of the quantities A, B, C, \dots

The small-angle result of reference (1) was obtained under the assumption that $q_z R \ll 1$, or $kR\theta^2 \ll 1$. Then only the leading terms in the expansion of $\exp[iq_z z']$ in powers of $q_z z'$ need be retained in the integrand of the second term of (25), and $\exp[iq_z z]$ can be replaced by unity in the first term. The first term of (25) then becomes

$$(36) \quad (ik/2\pi) \int_{-\infty}^{\infty} \int_{-\infty}^{\infty} \exp [i(q_x x + q_y y)] \left[1 - \exp [-i/2k] \int_{-\infty}^{\infty} U(\mathbf{r}) dz \right] dx dy.$$

The leading terms of the second part of (25) are

$$(37) \quad \begin{aligned} (4\pi)^{-1} \int & \exp [i(q_x x + q_y y)] \{ [i(\partial^2 \delta_f / \partial z^2) + (\partial \delta_f / \partial z)^2] \exp [i(\delta_o(\mathbf{r}) + \delta_f(\mathbf{r}))] + \\ & + [i(\partial^2 \delta_f / \partial x^2) + i(\partial^2 \delta_f / \partial y^2) - (\partial \delta_f / \partial x)^2 - (\partial \delta_f / \partial y)^2] \cdot \\ & \cdot (\exp [i\delta_o(\mathbf{r})] - 1) \exp [i\delta_f(\mathbf{r})] + \\ & + q_z (\partial \delta_o / \partial z) \exp [i\delta_o(\mathbf{r})] (\exp [i\delta_f(\mathbf{r})] - 1) - \\ & - 2[q_x (\partial \delta_f / \partial x) + q_y (\partial \delta_f / \partial y)] (\exp [i\delta_o(\mathbf{r})] - 1) \exp [i\delta_f(\mathbf{r})] - \\ & - (q_x^2 + q_y^2) (\exp [i\delta_o(\mathbf{r})] - 1) (\exp [i\delta_f(\mathbf{r})] - 1) \} d\tau. \end{aligned}$$

Study of the structure of (37) shows that the order of magnitude of the ratio of (37) to (36) is

$$(38) \quad \begin{cases} L\{U/k^2; \theta UR/k; \theta^2/kR; \theta^2 UR^2\}, & \text{if } UR/k \lesssim 1; \\ L\{U^2 R/k^3; \theta UR/k; \theta^2 kR\}, & \text{if } UR/k > 1. \end{cases}$$

Equation (36) is the small-angle scattered amplitude obtained in reference (1); (38) gives the error of this result without regard to (31), since (31) refers to the error relative to the second term of $f^{(1)}$, and this is much smaller than the first term of $f^{(1)}$ that is retained as (36).

For $\theta = 0$, \mathbf{q} is zero, and also the first term inside the curly bracket of (37) integrates to zero. The result is

$$(39) \quad \begin{aligned} f^{(1)}(\mathbf{k}_0, \mathbf{k}_0) = & (ik/2\pi) \int_{-\infty}^{\infty} \int_{-\infty}^{\infty} \left[1 - \exp \left[-i/2k \int_{-\infty}^{\infty} U(\mathbf{r}) dz \right] \right] dx dy + \\ & + (16\pi k^2)^{-1} \int U^2(\mathbf{r}) \exp \left[\left(-i/2k \int_{-\infty}^{\infty} U(\mathbf{r}') dz' \right) \right] d\tau - \\ & - (4\pi)^{-1} \int \left[1 - \exp \left[-i/2k \int_{-\infty}^z U(\mathbf{r}') dz' \right] \right] \nabla_t^2 \exp \left[\left(-i/2k \int_z^{\infty} U(\mathbf{r}') dz' \right) \right] d\tau, \end{aligned}$$

where $\nabla_t^2 = (\partial^2/\partial x^2) + (\partial^2/\partial y^2)$. Equation (39) was first obtained by WU (6). The order of magnitude of the first term of (39) is UR^3 if $UR/k \lesssim 1$, and kR^2 if $UR/k > 1$. The orders of magnitude of the second and third terms of (39) are each $U^2 R^3/k^2$, regardless of the magnitude of UR/k . Thus the error in (39) has the order of magnitude of the product of (31) and $U^2 R^3/k^2$, so that all terms in (39) may justifiably be retained.

7. – Conclusions.

We have obtained a closed expression for the scattered amplitude, Eq. (25) valid for all scattering angles, and possessing the accuracy given by (31). It reduces to the large and small angle results of reference (1), Eqs. (34) and (36), respectively, but is inherently superior to them in accuracy. For example, the asymptotic series of (32) could be employed to improve on (36). For the

(6) T. T. WU: ONR Technical Report No. 246, Cruft Laboratory, Harvard University, May 10, 1956 (unpublished). We wish to thank Dr. Wu for informing us of his result, which differs from ours through multiplication of the second term of Eq. (39) by 2.

forward scattering, Eq. (39) is the same as the corresponding result of reference (6). For intermediate angles, Eq. (25) is appreciably more complicated than the earlier results, but probably not much more difficult to handle by numerical methods than (34), for which numerical computation must be used in any event.

While error estimates were not given explicitly in reference (1), it was stated there that Eq. (34) should be valid for $kR \gg 1$, $U/k^2 \ll 1$, $\theta \gg (kR)^{-\frac{1}{2}}$, and UR/k unrestricted. These conditions are consistent with the error estimate (35) when $UR/k \lesssim 1$; however, they should be replaced by the more restrictive conditions $kR \gg (UR/k)^2$, $U/k^2 \ll (UR/k)^{-1}$, $\theta \gg (UR/k)^{\frac{1}{2}}(kR)^{-\frac{1}{2}}$, when $UR/k > 1$. Similarly, according to reference (1), Eq. (36) should be valid for $kR \gg 1$, $U/k^2 \ll 1$, $\theta \ll (kR)^{-\frac{1}{2}}$, and UR/k unrestricted. Again, these conditions are consistent with the error estimate (38) when $UR/k \lesssim 1$; however, they should be replaced by the more restrictive conditions $kR \gg (UR/k)^2$, $U/k^2 \ll (UR/k)^{-1}$, $\theta \ll (kR)^{-\frac{1}{2}}$, when $UR/k > 1$. The discrepancy between the validity conditions of reference (1) and the present error estimates, when $UR/k > 1$, may be due to an accumulation of remainders after the leading term of the stationary phase approximation in the infinite series of reference (1). The n -th term of this series becomes small when n is somewhat larger than UR/k , so that any such accumulation should be negligible for $UR/k \lesssim 1$, and should increase with UR/k when $UR/k > 1$. It appears now that this effect does not alter the leading terms obtained in reference (1), but does decrease their ranges of validity.

* * *

One of the authors (D. S. S.) wishes to thank the Universitetets Institut for Teoretisk Fysik, and the other (L. I. S.) the Laboratoire de Physique, de l'École Normale Supérieure, for hospitality extended during the 1956-57 academic year.

RIASSUNTO (*)

Si estende una nuova formulazione dello scattering per potenziali di alta energia presentata in un recente lavoro, per ricavare formole esplicite per la teoria dello scattering dell'equazione tridimensionale non separabile di Schrödinger. Si deriva un'equazione integrale per la quale una sola iterazione dà lo scattering se l'energia potenziale non è troppo grande e varia lentamente rispetto a una lunghezza d'onda. Il risultato si accorda con quelli ottenuti precedentemente per angoli di scattering piccoli e grandi, ma si può altrettanto bene applicare agli angoli medi e migliora la precedente esattezza. Ulteriori iterazioni possono dare maggior esattezza, come pure una stima dell'errore della prima approssimazione.

(*) Traduzione a cura della Redazione.

Theory of Scattering in the Quantized Field and Low-Chew-Wick's Formalism.

T. KANKI

Department of Physics, Osaka University - Osaka, Japan

(ricevuto il 4 Giugno 1957)

Summary. — The Lippmann-Schwinger equation is studied from the view point of the quantized field theory. The general prescription for separating the «incident physical state» is given by introducing the modified contraction technique. The Low-Chew-Wick formalism is derived from the L.S. equation by virtue of our contraction technique which makes the former more easy to understand.

Introduction.

In applying the Lippmann-Schwinger equation (*) (¹)

$$(1) \quad \Psi_q^{(\pm)} = \varphi_q + \frac{1}{E_q - H_0 \pm i\varepsilon} H_1 \cdot \Psi_q^{(\pm)},$$

to the scattering problems in the quantized field theory, there occur some cumbersome problems.

1) In the particle dynamics the validity of the L.S.-equation depends on the fact that the interaction-Hamiltonian H_1 induces only a negligibly small shift of the energy levels in the continuous spectrum. In the field theory, however, we encounter the difficulty of the infinite shifts of the energy levels which is usually overcome by the renormalization procedure (²). Namely, the

(*) Hereafter, this equation is referred to as L.S.-equation.

(¹) A. LIPPmann and J. SCHWINGER: *Phys. Rev.*, **79**, 469 (1950).

(²) For instance, J. PIRENE: *Phys. Rev.*, **86**, 395 (1952); M. GELL-MANN and M. GOLDBERGER: *Phys. Rev.*, **91**, 398 (1953).

unrenormalized Hamiltonian

$$H = H'_0 + H'_1$$

is replaced by the renormalized ones

$$(2a) \quad H_0 = H'_0 + \sum_a \varphi_a \rangle \Delta E_a \langle \varphi_a ,$$

and

$$(2b) \quad H_1 = H'_1 - \sum_a \varphi_a \rangle \Delta E_a \langle \varphi_a ,$$

where φ_a is the eigenfunction of the renormalized free Hamiltonian H_0 and ΔE_a is the level-shift of this state and is so determined as to make spectra of H and H_0 coincide with each other in the continuous region.

2) As DEWITT (3) pointed out, in the field theory, the state vector Ψ_q in (1) is not normalized to unity owing to the fact that the interaction H_1 is an integral over the whole space, even though φ_a has been normalized to unity.

3) Contrary to the scattering cases in the particle dynamics, the incident « physical state » is described not only by the φ_a but also by some parts of the second term of Eq. (1), because the former represents the incident « bare-state », while the latter the incident nucleons dressed with many virtual field quanta. For the calculation of the scattering cross-section the dressed states mentioned above should be separated from the second term in Eq. (1). It will be seen that this separation will allow us to normalize the Ψ_q in the field theory.

The main purpose of the present article is to give the general prescription for this kind of separation, by introducing some contraction-techniques which are similar to that devised by WICK (4) in the covariant field theory. In the present paper, for simplicity, the case of meson-nucleon scattering is exclusively studied, although our method is, of course, applicable to more complicated problems provided that the formation of nucleon-pairs is excluded.

In the case of the meson-nucleon scattering, we shall be able to give a field theoretical foundation to Wick's (5) formulation concerning Low-Chew theory (6) (*) from our view point. This is the second purpose of the present paper.

(3) B. S. DE WITT: *Phys. Rev.*, **100**, 905 (1955).

(4) G. C. WICK: *Phys. Rev.*, **80**, 268 (1950).

(5) G. C. WICK: *Rev. Mod. Phys.*, **27**, 339 (1955).

(6) F. E. LOW: *Phys. Rev.*, **97**, 1392 (1955); G. G. CHEW and F. E. LOW: *Phys. Rev.*, **101**, 1570 (1956).

(*) In what follows, the abbreviation L.C.W. is used.

1. – Contraction technique and separation of the incident « physical state ».

Let us consider a system of one nucleon and mesons with the interaction Hamiltonian

$$(1.1) \quad H'_1 = \sum_k (a_k V_k + a_k^* V_k^*) ,$$

where the same notations have been used as those in Wick's paper ⁽⁵⁾.

Since we shall deal with the rearrangements of the order of meson-operators appearing in the following types of products

$$(1.2) \quad A \dots B G_1(E_1) C \dots D G_2(E_2) E \dots ,$$

it is quite suitable for our present purpose to introduce the contraction-technique following Wick's line of thought in the covariant field theory. The symbols A, B, \dots , in (1.2) denote the creation or annihilation operators of mesons and $G(E)$ stands for

$$G(E) = \frac{1}{E - H_0 \pm i\epsilon} \times [\text{The operators being commutable with those of mesons}].$$

Definition 1. Our normal product (abbreviated as N -product) is defined as

$$(1.3) \quad N[A \dots B G_1(E_1) C G_2(E_2) D \dots G_n(E_n) E \dots K] \equiv \\ \equiv A C \dots E G_1(E_1 - \sum_{\alpha} \omega_{\alpha}) G_2(E_2 - \sum_{\beta} \omega_{\beta}) \dots G_n(E_n - \sum_{\gamma} \omega_{\gamma}) B D \dots K .$$

In the right-hand side of (1.3), all the meson-creation operators are transferred to the left side of all G 's and all the annihilation-operators to the right side, while the order of G 's are held as it was. $\sum \omega$ in the argument of G is the sum of energies corresponding to the meson-operators which have passed over the G concerned.

From the above definition, it is easily seen that our N -product is identical with that of WICK when G 's are absent from the product, and we have the following lemmas.

Lemma 1.

$$(1.4) \quad \begin{cases} N[G(E)a_p^*] = N[a_p^* G(E - \omega_p)] , \\ N[a_p G(E)] = N[G(E - \omega_p) \cdot a_p] . \end{cases}$$

These relations also hold for the case of the ordinary product as is easily seen.

Lemma 2.

$$(1.5) \quad G_0(E_0) \cdot N[AG_1(E_1) \dots] = N[G_0(E_0) \cdot AG_1(E_1) \dots].$$

Definition 2. The contraction of any couple of meson operators A and B is defined as

$$(1.6) \quad A \cdot B \equiv AB - N[AB],$$

For example, we see that

$$(1.7) \quad \begin{cases} a_p^* a_q^{**} = \delta_{pq}, \\ a_p^* a_q^* = a_p^{**} a_q^{**} = a_p^{**} a_q^* = 0. \end{cases}$$

Definition 3. The definition of the « mixed N -product » is given by

$$(1.8) \quad \begin{aligned} N[AG_1(E_1) \dots C \cdot D \cdot G_n(E_n)E] &= N[AG_1(E_1) \dots G_n(E_n)E](C \cdot D \cdot) \\ &= (C \cdot D \cdot)N[AG(E) \dots G(E)E]. \end{aligned}$$

All other cases are to be reduced to the above type by means of the lemma 1. If G 's do not appear, we can easily see that the present definition is identical with the current one.

Now let us state the most important theorem, proof of which will be given in the Appendix.

Theorem. Any product of operators can be expanded as a sum of N -products in the following way:

$$(1.9) \quad \left\{ \begin{array}{l} AG_1(E_1)B \dots CG_n(E_n)DF \\ = N[AG_1(E_1)B \dots CG_n(E_n)DF] \\ + N[AG_1(E_1)B \dots CG_n(E_n)D'F'] \\ + \dots \dots \dots \dots \dots \dots \\ + N[A''G_1(E_1)B'' \dots C'G_n(E_n)DF'] \\ + \dots \dots \dots \dots \dots \dots \end{array} \right.$$

where the summation on the right-hand side should be taken over all the possible sets of contractions of meson operators except for G 's.

We now return to the main problem stated in the introduction, namely,

the separation of the physical incident state. Let us consider the operator:

$$(1.10a) \quad Q^{(m)}(E) = \frac{1}{a(E)} H_1(1) \frac{1}{a(E)} H_1(2) \dots \frac{1}{a(E)} H_1(m),$$

where

$$(1.10b) \quad a(E) \equiv E - H_0 \pm i\varepsilon.$$

Thanks to the fact (*) that the meson-operators are commutable with V_k , V_k^* , and the ΔE -term, in H_1 , $Q^{(m)}(E)$ can be written as

$$Q^{(m)}(E) = \sum_{A \dots M} G_1(E) A G_2(E) B \dots G_m(E) M,$$

by inserting (1.1) into each H_1 of the above expression. By virtue of the theorem, a product $Q^{(m)}(E) a_q^*$ can be decomposed into a sum of N -products:

$$(1.11a) \quad Q^{(m)}(E) a_q^* = \sum_{A \dots M} \left\{ \begin{array}{l} N[G_1(E) A \cdot G_3(E) B \dots G_m(E) M \cdot a_q^*] + \\ + N[G_1(E) A \cdot G_1(E) B \cdot G_2(E) \dots G_m(E) M \cdot a_q^*] + \\ + \dots \dots \dots \dots \dots \dots \dots \dots + \\ + N[G_1(E) A \cdot G_2(E) B \dots G_m(E) M \cdot a_q^{**}] + \\ + N[G_1(E) A \cdot G_2(E) B \cdot G_3(E) \dots G_m(E) M \cdot a_q^{**}] + \\ + \dots \dots \dots \dots \dots \dots \dots \dots \dots \end{array} \right.$$

$$(1.11b) \quad = \bar{Q}^{(m)}(E) \bar{a}_q^* + Q^{(m)*}(E) q_q^{**},$$

where we have used the following abbreviations:

$$Q^{(m)*}(E) a_q^{**} = \left[\begin{array}{l} \text{a sum of } N\text{-products containing the «dotted» } a_q^* \\ \text{in the right-hand side of (1.11a)} \end{array} \right],$$

and

$$\bar{Q}^{(m)}(E) \bar{a}_q^* = [\text{a remaining part of the right-hand side of (1.11a)}].$$

(*) We may expect that the energy-renormalization ΔE of nucleons does not depend on the state of mesons but on the nucleon-states. If that is the case, the renormalization term can be expressed as a direct product

$$\Delta E \times \mathbf{1},$$

where ΔE is a matrix which works on the nucleon state-vector, while $\mathbf{1}$ a unit-matrix in the space of meson-states. Accordingly in the present paper we shall assume the commutability of the ΔE -term with meson operators.

Owing to the lemma 1, we have the following type of relations:

$$\begin{aligned} N[G_1(E) A \cdot G_2(E) B \cdot \dots G_m(E) M a_q^*] &= \\ = N[a_q^* G_1(E - \omega_q) A \cdot G_2(E - \omega_q) B \cdot \dots G_m(E - \omega_q) M] &= \\ = a_q^* N[G_1(E - \omega_q) A \cdot G_2(E - \omega_q) B \cdot \dots G_m(E - \omega_q) M], \text{ etc.,} \end{aligned}$$

from which we get the important relation:

$$(1.12) \quad \overline{\Omega^{(m)}(E) a_q^*} = a_q^* \overline{\Omega^{(m)}(E - \omega_q)} .$$

Let us introduce the operator $\Omega^{(\pm)}(E_q)$ defined by

$$(1.13) \quad \Omega^{(\pm)}(E_q) = 1 + \frac{1}{a(E_q)} H_1 \Omega^{(\pm)}(E_q) ,$$

the solution of which is given by means of the iteration method as an infinitive sum of terms of the type $\Omega^{(m)}(E_q)$. Accordingly we have

$$(1.14) \quad \Omega^{(\pm)}(E_q) a_q^* = \overline{\Omega^{(\pm)}(E_q) a_q^*} + \Omega^{(\pm)*}(E_q) a_q^{**} ,$$

and

$$(1.15) \quad \overline{\Omega^{(\pm)}(E_q) a_q^*} = a_q^* \cdot \Omega^{(\pm)}(E_q - \omega_q) .$$

By making both sides of (1.14) work on a (bare) one-nucleon state with no mesons, the first term of the right-hand side of (1.14) turns out to represent an incident « physical state », since the incident meson created by a_q^* is not destructed by $\Omega^{(\pm)}$ but comes out without being affected by the nucleon.

On the other hand, the left-hand side of (1.14) can be rewritten in the following way by virtue of (1.13),

$$\begin{aligned} (1.16) \quad \Omega^{(\pm)}(E_q) a_q^* &= \left\{ 1 + \frac{1}{a(E_q)} \cdot H_1 \cdot \Omega^{(\pm)}(E_q) \right\} a_q^* = \\ &= a_q^* + \frac{1}{a(E_q)} \cdot H_1 \cdot \left\{ \overline{\Omega^{(\pm)}(E_q) a_q^*} + \Omega^{(\pm)*}(E_q) a_q^{**} \right\} = \\ &= a_q^* + \frac{1}{a(E_q)} \cdot H_1 \cdot a_q^* \Omega^{(\pm)}(E_q - \omega_q) + \frac{1}{a(E_q)} \cdot H_1 \cdot \Omega^{(\pm)*}(E_q) a_q^{**} = \\ &= \left\{ a_q^* + \frac{1}{a(E_q)} \cdot H_1 \cdot \overline{a_q^* \Omega^{(\pm)}(E_q - \omega_q)} \right\} + \\ &\quad + \left\{ \frac{1}{a(E_q)} \cdot (H_1 a_q^*) \Omega^{(\pm)}(E_q - \omega_q) + \frac{1}{a(E_q)} \cdot H_1 \cdot \Omega^{(\pm)*}(E_q) a_q^{**} \right\} . \end{aligned}$$

From (1.14) and (1.16), we get an integral equation for $\Omega^{(\pm)*}(E_a)a_q^{**}$:

$$(1.17) \quad \Omega^{(\pm)*}(E_a)a_q^{**} = \frac{1}{a(E_a)}(H_1^*a_q^{**})\Omega^{(\pm)}(E_a - \omega_a) + \frac{1}{a(E_a)} \cdot H_1 \cdot \Omega^{(\pm)*}(E_a)a_q^{**}.$$

It can be easily proved by the iteration method that the expression

$$(1.18) \quad \Omega^{(\pm)*}(E_a)a_q^{**} = \frac{1}{a(E_a) - H_1} \cdot (H_1^* \cdot a_q^{**})\Omega^{(\pm)}(E_a - \omega_a),$$

satisfies the equation (1.17). Accordingly (1.14) becomes

$$(1.19) \quad \Omega^{(\pm)}(E_a)a_q^* = a_q^*\Omega^{(\pm)}(E_a - \omega_a) + \frac{1}{a(E_a) - H_1} \cdot (H_1^*a_q^{**})\Omega^{(\pm)}(E_a - \omega_a).$$

In a similar manner, we have also following equations:

$$(1.20) \quad a_p^*Q^{(\pm)*}(E) = \frac{1}{a(E - \omega_p) - H_1} (a_p^*H_1)\Omega^{(\pm)}(E),$$

and

$$(1.21) \quad a_p^*Q^{(-)*}(E) = Q^{(-)*}(E - \omega_p)(a_p^*H_1) \frac{1}{a_+(E) - H_1},$$

where $Q^{(-)*}$ is the operator defined by

$$(1.22) \quad Q^{(-)*}(E) = 1 + Q_{(E)}^{(-)*}H_1 \frac{1}{a_+(E)}.$$

The contractions appearing in (1.18)–(1.21) should be replaced by V or V^* according to

$$(1.23) \quad \begin{cases} (H_1^*a_q^{**}) = V_a, \\ (a_p^*H_1) = V_p^*. \end{cases}$$

2. – Renormalization.

Following DEWITT, the renormalized eigen-vector $\Psi_a^{(\pm)}$ of the total Hamiltonian is defined by

$$(2.1) \quad Z^\frac{1}{2}\cdot\Psi_a^{(\pm)} = \Psi_a^{(\pm)} \equiv \Omega^{(\pm)}(E_a)\varphi_a.$$

The renormalization factor Z_a is given by

$$(2.2) \quad Z_a = (\Psi_a^{(\pm)}, \Psi_a^{(\pm)}) = (\varphi_a, Z_a^{\dagger} \Psi_a^{(\pm)}) = \\ = (\varphi_a, \Omega^{(\pm)}(E_a) \varphi_a),$$

namely, Z_a is a diagonal element of the wave matrix $\langle \Omega^{(\pm)}(E_a) \rangle_{aa}$. DEWITT showed that Z_a is equal to the singular part of $\langle \Omega^{(\pm)}(E_a) \rangle_{aa}$ under the appropriate limit of $\varepsilon \rightarrow 0$, $V \rightarrow \infty$ (V is the volume of a box in which the system is enclosed), that is

$$(2.3) \quad \begin{cases} Z_a = \text{Sing } \langle \Omega^{(\pm)}(E_a) \rangle_{aa} \\ \langle \Omega^{(\pm)}(E_a) \rangle_{aa} = \text{Sing } \langle \Omega^{(\pm)}(E_a) \rangle_{aa} + \text{Rem } \langle \Omega^{(\pm)}(E_a) \rangle_{aa}. \end{cases}$$

From the view point of the Feynman diagram, the singular part of (2.3) corresponds to all the diagrams where the nucleon has no interactions with the incident mesons. The one-nucleon state without incident mesons belongs to the above singular part and has no remainder, namely

$$(2.4) \quad Z_0 = \langle \Omega^{(\pm)}(E_0) \rangle_{00} \equiv \text{Sing } \langle \Omega^{(\pm)}(E_0) \rangle_{00}.$$

It will be seen that Z_0 is independent of the sign (\pm) of $\Omega^{(\pm)}$, as $\Omega^{(\pm)}(E_0)\varphi_0$ does not depend on that sign (see appendix I) (*).

Next let us consider a state φ_a where one nucleon and one meson with a momentum q exist. The singular part of $\langle \Omega^{(\pm)}(E_a) \rangle_{aa}$ is in our formulation given by the first term of (1.19). By virtue of $E_a = E_0 + \omega_a$, Z_a becomes

$$(2.5) \quad Z_a = \text{Sing } \langle \Omega^{(\pm)}(E_a) \rangle_{aa} = (\varphi_a, a_q^* \Omega^{(\pm)}(E_a - \omega_a) \varphi_0) = \langle \Omega(E_0) \rangle_{00} \equiv Z_0.$$

By taking the diagonal element $(0, 0)$ of Eq. (1.13) and from (2.4), we have

$$(2.6) \quad \langle H_1 \cdot \Omega^{(\pm)}(E_0) \rangle_{00} = \pm i\varepsilon(Z_0 - 1).$$

The evaluation of the right-hand side of (2.5) will be given in the Appendix I.

3. – Derivation of L.C.W. formalism.

From (1.19), (1.23) and the definition (2.1), we have an equation of the following type

$$(3.1) \quad \Psi_a^{(\pm)} = a_q^* \Omega(E_0) \varphi_0 + \frac{1}{a(E_a) - H_1} V_a \cdot \Omega(E_0) \varphi_0,$$

(*) In what follows, the sign (\pm) of $\Omega^{(\pm)}$ will be omitted when φ_0 is concerned.

where the first term stands for the incident « physical state » as we desired. The renormalization of the state vector leads to Wick's equation in the L.C.W. theory (5):

$$(3.2) \quad \Psi_q^{(\pm)} = a_q^* \Psi_0 + \frac{1}{E_q - H \pm i\varepsilon} V_q \Psi_0 .$$

The expression for the R -matrix given by WICK can be also derived from the original definition of R -matrix proposed by MÖLLER from our view point. From (1.19), we have

$$\begin{aligned} \langle \Omega^{(+)}(E_q) \rangle_{pq} &\equiv \langle \Omega^{(+)}(E_q) a_q^* \rangle_{p0} = \\ &= \left\langle a_q^* \Omega(E_0) + \frac{1}{a_+(E_q) - H_1} \cdot V_q \Omega(E_0) \right\rangle_{p0} = \\ &= \delta_{pq} \langle \Omega(E_0) \rangle_{00} + \left\langle \frac{1}{a_+(E_q) - H_1} \cdot V_q \Omega(E_0) \right\rangle_{p0} . \end{aligned}$$

By inserting

$$\frac{1}{a_+(E_q) - H_1} = \frac{1}{a_+(E_q)} \Omega^{(-)*}(E_q) ,$$

and (2.5) into the above expression, it reads

$$= Z_0 \delta_{pq} + Z_0 \left\langle \frac{1}{a_+(E_q)} \cdot Z_0^{-1} \cdot \{ \Omega^{(-)*}(E_q) V_q \Omega(E_0) \} \right\rangle_{p0} ,$$

that is,

$$\langle \Omega^{(+)}(E_q) \rangle_{pq} = Z_0 \left\{ \delta_{pq} + \frac{1}{E_q - E_p + i\varepsilon} \mathbf{R}_{pq} \right\} ,$$

where the renormalized \mathbf{R} is defined by

$$(3.3) \quad \mathbf{R}_{pq} = \frac{1}{Z_0} \cdot (\varphi_p, \Omega^{(-)*}(E_q) V_q \Omega(E_0) \varphi_0) .$$

This is just the renormalized \mathbf{R} -matrix corresponding to that of MÖLLER. The S -matrix is easily derived from the above equation of $\langle \Omega^{(+)} \rangle$, by the usual manner,

$$\mathbf{S}_{pq} = \delta_{pq} - 2\pi i \delta(E_q - E_p) \mathbf{R}_{pq} .$$

The \mathbf{R} -matrix obtained above is a function of E_p and E_q , and has a physical correspondence only in the case of $E_p = E_q$. The \mathbf{T} -matrix introduced by

Low has a different dependence on energy, namely,

$$(3.4) \quad \begin{aligned} \mathbf{T}_{pq} &= \frac{1}{Z_0} (\varphi_p, \Omega^{(-)*}(E_p)V_q \Omega(E_0)\varphi_0), \\ &= \frac{1}{Z_0} (\Omega^{(-)}(E_p)\varphi_p, V_q \Omega(E_0)\varphi_0), \\ &= (\Psi_p^{(-)}, V_q \Psi_0). \end{aligned}$$

These two matrices agree with each other only on the energy-shell $E_p = E_q$. It is quite natural that these two satisfy the different types of equations which will be derived from our view point. It will be seen that our method of derivation seems more suitable for understanding the physical meaning of the equations obtained.

Consider an expression

$$(\varphi_p, \Omega^{(-)*}(E)V_q \Omega(E_0)\varphi_0) = (\varphi_0, a_p \Omega^{(-)*}(E)V_q \Omega(E_0)\varphi_0).$$

This expression becomes

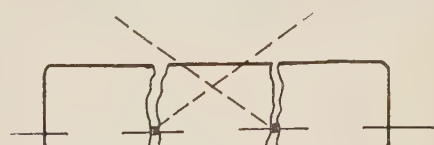
$$= (\varphi_0, \bar{a}_p \bar{\Omega}^{(-)*}(E)V_q \Omega(E_0)\varphi_0) + (\varphi_0, a_p^* \Omega^{(-)*}(E)V_q \Omega(E_0)\varphi_0),$$

by means of the contraction-technique, or by taking into account (1.15) and (1.21), it turns out to be

$$(3.5) \quad (\varphi_p, \Omega^{(-)*}(E)V_q \Omega(E_0)\varphi_0) = (\varphi_0, \Omega^{(-)*}(E - \omega_p)V_q a_p^* \Omega(E_0)\varphi_0) + \\ + \left(\varphi_0, \Omega^{(-)*}(E - \omega_p)V_p^* \frac{1}{a_{+}(E) - H_1} \cdot V_q \Omega(E_0)\varphi_0 \right).$$

This expression shows us that the \mathbf{R} or \mathbf{T} matrix can be represented by a sum of particular matrices which consist of three factors schematically shown in Fig. 1. The Low-Chew (L.C.) equation for \mathbf{T} can be derived automatically by this factorization.

Putting E in the above expression equal to E_p or E_q , we can derive the equations for \mathbf{T} or \mathbf{R} respectively.



(a) The first term.



(b) The second term.

Fig. 1. — The graph corresponding to Eq. (3.5).

(a) The equation for \mathbf{T}_{pq} .

By inserting (1.20) into (3.5), the latter becomes

$$(3.6) \quad (\varphi_p, \Omega^{(-)*}(E_p)V_q\Omega(E_0)\varphi_0) = \\ = \sum_n (\varphi_0, \Omega^{(-)*}(E_0)V_q\Psi_n^{(-)}) \frac{1}{E_0 - \omega_p - E_n + i\varepsilon} (\Psi_n^{(-)}, V_p^*\Omega(E_0)\varphi_0) + \\ + \sum_n (\varphi_0, \Omega^{(-)*}(E_0)V_p^*\Psi_n^{(-)}) \frac{1}{E_p - E_n + i\varepsilon} (\Psi_n^{(-)}, V_q\Omega(E_0)\varphi_0) ,$$

where the normalized complete set $\{\Psi_n^{(-)}\}$ has been used. The renormalization of (3.6) according to (2.1), (2.5) and (3.4) gives just the L.C. equation for \mathbf{T} . It is easily seen that the first term of the right-hand side in (3.6) is schematically illustrated by the Fig. 1a, that is, this term corresponds to the so-called « crossing-term ».

(b) The equation for \mathbf{R}_{pq} .

The relation

$$\frac{1}{a_+(E_q) - H_1} = \frac{1}{a_+(E_q)} \Omega^{(-)*}(E_q) ,$$

gives (3.5) a different form

$$(3.7) \quad (\varphi_p, \Omega^{(-)*}(E_q)V_q\Omega(E_0)\varphi_0) = (\varphi_0, \Omega^{(-)*}(E_q - \omega_p)V_qa_p \cdot \Psi_0) + \\ + \sum_n (\varphi_0, \Omega^{(-)*}(E_q - \omega_p)V_p^*\varphi_n) \frac{1}{E_q - E_n + i\varepsilon} (\varphi_n, \Omega^{(-)*}(E_q)V_q\Omega(E_0)\varphi_0) .$$

This complicated equation is that for \mathbf{R} .

* * *

The author wishes to express his gratitude to professor R. UTIYAMA for his continuous encouragement and valuable advice, and to Messrs. S. SUNAKAWA and T. IMAMURA for their kind discussions.

APPENDIX I

The determination of Z_0 and ΔE_0 .

Consider a projection operator η_a defined by

$$(A.1) \quad \begin{cases} \eta_a\varphi_a = \varphi_a , \\ \eta_a\varphi_n = 0 , \end{cases} \quad \text{for all } n \neq a .$$

by which $\Omega^{(\pm)}(E_a)\eta_a$ can be divided as follows;

$$(A.2) \quad \Omega^{(\pm)}(E_a)\eta_a = \eta_a\Omega^{(\pm)}(E_a)\eta_a + (1 - \eta_a)\Omega^{(\pm)}(E_a)\eta_a.$$

Using Eq. (1.13), we have an integral equation for $\{(1 - \eta_a)\Omega^{(\pm)}(E_a)\eta_a\}$:

$$\{(1 - \eta_a)\Omega^{(\pm)}(E_a)\eta_a\} = \frac{1}{a(E_a)} (1 - \eta_a)H_1\eta_a\Omega^{(\pm)}(E_a)\eta_a + \\ + \frac{1}{a(E_a)} (1 - \eta_a)H_1\{(1 - \eta_a)\Omega^{(\pm)}(E_a)\eta_a\},$$

with a formal solution:

$$(A.3) \quad \{(1 - \eta_a)\Omega^{(\pm)}(E_a)\eta_a\} = \frac{1}{a(E_a) - (1 - \eta_a)H_1} (1 - \eta_a) \cdot H_1(\eta_a\Omega^{(\pm)}(E_a)\eta_a).$$

By inserting (A.3) into (A.2), the latter becomes

$$(A.4) \quad \Omega^{(\pm)}(E_a)\eta_a = F^{(\pm)}(E_a) \cdot (\eta_a\Omega^{(\pm)}(E_a)\eta_a),$$

where

$$(A.5) \quad F^{(\pm)}(E_a) = \left\{ 1 + \frac{1}{a(E_a) - (1 - \eta_a)H_1} (1 - \eta_a)H_1\eta_a \right\}.$$

The definition of Z_0 is

$$Z_0^{(\pm)} = (\Psi_0^{(\pm)}, \Psi_0^{(\pm)}) = (\varphi_0, \Omega^{(\pm)*}(E_0)\Omega^{(\pm)}(E_0)\varphi_0),$$

which turns out to be

$$(A.6) \quad = |\langle \Omega^{(\pm)}(E_0) \rangle_{00}|^2 \cdot (\varphi_0, F^{(\pm)*}F^{(\pm)}\varphi_0) = \\ = |\langle \Omega^{(\pm)}(E_0) \rangle_{00}|^2 \cdot \left\{ 1 + \left\langle H_1(1 - \eta_0) \left| \frac{1}{a(E_0) - (1 - \eta_0)H_1} \right|^2 (1 - \eta_0)H_1 \right\rangle_{00} \right\}.$$

on account of (A.5). Since we have an alternative expression for Z_0 :

$$Z_0^{(\pm)} = \langle \Omega^{(\pm)}(E_0) \rangle_{00},$$

(A.6) leads to

$$(A.7) \quad Z_0 = \left[1 + \left\langle H_1(1 - \eta_0) \left| \frac{1}{a(E_0) - (1 - \eta_0)H_1} \right|^2 (1 - \eta_0)H_1 \right\rangle_{00} \right]^{-1}.$$

In order to evaluate Z_0 , let us expand the right-hand side of (A.7) into a power series in $(1 - \eta_0)H_1$. In this case, the propagator $1/a(E_0)$ gives rise to no singularities owing to the projection operator $(1 - \eta_0)$. Accordingly we see that Z_0 is independent of the sign (\pm) of $\Psi^{(\pm)}$, because the $\pm i\varepsilon$ in $a(E_0)$ can be omitted due to the fact mentioned above.

The equation (2.6) is now rewritten in the following way:

$$\begin{aligned} \pm ie(Z_0^{(\pm)} - 1) &= \langle H_1 \cdot Q^{(\pm)}(E_0) \rangle_{00} = \langle H_1 \cdot F^{(\pm)}(E_0) \rangle_{00} \cdot \langle Q^{(\pm)}(E_0) \rangle_{00} = \\ &= \{ \langle H_1' F^{(\pm)}(E_0) \rangle_{00} - \Delta E_0 \langle F^{(\pm)} \rangle_{00} \} \cdot \langle Q^{(\pm)}(E_0) \rangle_{00}. \end{aligned}$$

From (A.5), we see that $\langle F \rangle_{00} = 1$, and

$$(A.9) \quad \Delta E_0 = \mp ie(1 - Z_0^{(\pm)-1}) + \left\langle H_1' \frac{1}{a(E_0) - (1 - \eta_0)H_1} (1 - \eta_0)H_1 \right\rangle_{00},$$

which becomes in the limit $\varepsilon \rightarrow 0$

$$(A.10) \quad \Delta E_0 = \left\langle H_1(1 - \eta_0) \frac{1}{a(E_0) - (1 - \eta_0)H_1} (1 - \eta_0)H_1 \right\rangle_{00}.$$

Since ΔE_0 is contained in H_1 , this expression is a complicated non-linear equation for ΔE_0 , the solution of which may be obtained only when the perturbation will be used.

APPENDIX II

The proof of the theorem.

It is well-known that this theorem is valid when no G 's occur in the original product. Let us consider the product:

$$\begin{aligned} G_1(E_1)G_2(E_2) \dots G_n(E_n) \cdot A \cdot B \cdot C \dots E - \\ = G_1(E_1)G_2(E_2) \dots G_n(E_n)N[A \cdot B \cdot C \dots E] + \\ + G_1(E_1)G_2(E_2) \dots G_n(E_n)N[A \cdot B \cdot C \dots E] + \\ + \dots \dots \dots \dots \end{aligned}$$

which can be written by virtue of the « lemma 2 », in the following way:

$$\begin{aligned} &= N[G_1(E_1)G_2(E_2) \dots G_n(E_n) A \cdot B \cdot C \dots E] + \\ &+ N[G_1(E_1)G_2(E_2) \dots G_n(E_n) A \cdot B \cdot C \dots E] + \dots \end{aligned}$$

As it was already mentioned in the text that G 's and A 's obey the same commutation relations both in the cases of the usual products and of the N -products,

we have the following relation from the above result by transferring G 's

$$\begin{aligned} AG_1(E_1 \pm \omega_A)B \dots CG_n(E_n - \sum_{\gamma} \omega_{\gamma} \pm \sum_{\delta} \omega_{\delta}) \dots E = \\ = N[A G_1(E_1 \pm \omega_A)B \dots CG_n(E_n - \sum_{\gamma} \omega_{\gamma} + \sum_{\delta} \omega_{\delta}) \dots E] + \\ + N[A' G_1(E_1 \pm \omega_A)B \dots CG_n(E_n - \sum_{\gamma} \omega_{\gamma} + \sum_{\delta} \omega_{\delta}) \dots E] + \dots \end{aligned}$$

This final expression gives us the proof for the theorem provided the arguments $E_i - \sum_{\alpha} \omega_{\alpha} + \sum_{\delta} \omega_{\delta}$ of G 's are replaced by E'_i 's.

R I A S S U N T O (*)

Si studia l'equazione di Lippmann-Schwinger dal punto di vista della teoria di campo quantizzata. Si dà la regola generale per la separazione dello « stato fisico incidente » introducendo la tecnica di contrazione modificata. Si deriva il formalismo di Low-Chew-White dall'equazione di L.S. in virtù della nostra tecnica di contrazione che rende più comprensibile il suddetto formalismo.

(*) Traduzione a cura della Redazione

The Parity of Elementary Particles.

P. T. MATTHEWS

Department of Physics - University of Rochester ()*

(ricevuto il 6 Giugno 1957)

Summary. — In determining the intrinsic parities of elementary particles, the invariance of the interactions under gauge transformations makes the relative parity of certain groups of particles a matter of convention. On the other hand, charge independence puts definite restrictions on the relative parities of the members of isotopic multiplets. The interplay of these conventions and restrictions is analysed and the general considerations applied to the known particles.

1. — Introduction.

We discuss here in some detail the notion of the intrinsic parity of elementary particles, in the light of what is now generally accepted about the conservation laws of charge, baryon number and « strangeness » for strong interactions, and the breakdown of parity conservation in the weak interactions.

We shall be borrowing freely from the ideas expressed by WICK, WIGHTMAN and WIGNER⁽¹⁾ but will use the language of field theory, and state these notions in a more explicit form by assuming that the interactions of the elementary particles can be expressed in terms of a Lagrangian. In this way it is possible to show explicitly the extent to which the intrinsic parities are matters of convention, and how much they are of physical significance. However, it will be evident from the final results that they do not depend essentially on a lagrangian formulation.

The specific results, which we obtain may be gotten more directly by considering the particular physical processes, which we shall quote as illustrations;

(*) On leave of absence from the University of Birmingham, Birmingham, England

(¹) G. C. WICK, A. S. WIGHTMAN and E. P. WIGNER: *Phys. Rev.*, **88**, 101 (1952).

but we will set the theory up in a general form, which can be applied to any physical situation.

2. – Gauge invariance of the first kind.

Since it is essential to the argument we will first summarize the theory of gauge transformations.

We assume that a system of interacting particles, may be described by a Lagrangian

$$(2.1) \quad L[\Phi_i(x)],$$

where Φ_i is the field corresponding to particles of type i . If the Lagrangian and all the observable properties of the system are invariant under the simultaneous transformation

$$(2.2) \quad \begin{cases} \Phi_a \rightarrow \Phi'_a = \exp[i\chi]\Phi_a, \\ \Phi_a^\dagger \rightarrow \Phi'^\dagger_a = \exp[-i\chi]\Phi_a^\dagger, \end{cases}$$

(χ is an arbitrary real number) of a set of fields $\{\Phi_a\}$, we shall say that the fields $\{\Phi_a\}$ form a gauge group. The transformation (2.2) may be induced by a unitary transformation

$$(2.3) \quad U(\chi) = \exp[i\chi F],$$

where F is hermitian. From the invariance of L under U , it follows that

$$(2.4) \quad ULU^{-1} = L.$$

Hence

$$(2.5) \quad [U, L] = 0, \quad [F, L] = 0.$$

Thus, associated with any gauge group is an « observable », F , which is also a constant of the motion.

In the Schrödinger representation, using the canonical formalism, one has, for any interacting system,

$$(2.6) \quad \begin{cases} F = -i\int\{\pi_a\Phi_a - \pi_a^\dagger\Phi_a^\dagger\} d^3x, \\ = n_a - \bar{n}_a, \end{cases}$$

where n_a is the number of particles of the group a and \bar{n}_a is the number of

anti-particles (2). Since the value of F must be the same in the initial and final state of any process, the invariance of L under a gauge transformation, leads to a very simple type of selection rule, of which the conservation of electric charge is the most familiar example.

If a particular gauge invariance is a general property of all interactions, then the corresponding selection rule is a «super-selection rule», as defined by WICK, WIGHTMAN and WIGNER (1).

3. – Parity.

The space reflection operation is induced by a unitary operator P such that for (ps -) scalar Bose fields

$$(3.1) \quad P\Phi(\mathbf{x}, t)P^{-1} = \eta_B \Phi(-\mathbf{x}, t), \quad \eta_B = \pm 1,$$

the plus (minus) sign referring to scalar (pseudo-scalar) fields. For Bose fields particle and anti-particle have the same parity (2a). For fermions

$$(3.2) \quad P\psi(\mathbf{x}, t)P^{-1} = \eta_F \gamma_4 \psi(-\mathbf{x}, t),$$

(2) See for example G. WENTZEL: *Quantum Theory of Fields* (New York, 1949).

(2a) To show how the parities of the particles are related to the reflection properties of the corresponding field, expand the field in a suitable complete set of functions of definite parity.

$$(1) \quad \varphi(\mathbf{x}) = \sum_n a_n u_n(\mathbf{r}) \exp[-i\varepsilon_n t] + b_n^\dagger u_n^\dagger(\mathbf{r}) \exp[i\varepsilon_n t],$$

where

$$(2) \quad u_n(-\mathbf{r}) = (-1)^n u_n(\mathbf{r}).$$

Then by (3.1)

$$\sum_n P a_n P^{-1} u_n(\mathbf{r}) \exp[-i\varepsilon_n t] + \dots = \eta_B \sum_n a_n u_n(-\mathbf{r}) \exp[-i\varepsilon_n t] + \dots$$

Using (2)

$$P a_n P^{-1} = \eta_B (-1)^n a_n.$$

The state vector for a particle with wave function $u_n(\mathbf{r})$ is

$$a_n^\dagger \rangle,$$

where \rangle is the vacuum. The transformed state is

$$\begin{aligned} P a_n^\dagger \rangle &= P a_n^\dagger P^{-1} P \rangle \\ &= \eta_B (-1)^n a_n^\dagger \rangle. \end{aligned}$$

Thus the reflection properties of a particle associated with a pseudo-scalar field ($\eta_B = -1$) contain an extra minus compared to that to be expected from its orbital motion, implying negative intrinsic parity. The same argument applied to b_n shows that for Bose fields particle and anti-particle have the same parity.

where

$$(3.3) \quad \eta_F = \pm 1, \pm i.$$

For a particle spinor

$$(3.4) \quad \gamma_4 u_+(p) = u_+(-p).$$

However, for an antiparticle spinor

$$(3.5) \quad \gamma_4 u_-(p) = -u_-(-p).$$

Thus for fermions particle and anti-particle have opposite intrinsic parities.

The choice of signs for η_B rather than an arbitrary phase factor, is dictated by the condition that after double reflection an observable quantity should return to its original value. The four values of η_F arise because an observable must involve an even number of spinors, (since spinors change sign on rotation through one complete revolution). These lead to four possible parity types of Fermi particles ⁽³⁾.

Suppose the complete Lagrangian for the interacting particles is invariant for a certain parity operator, P , with a specific choice $\{\eta_i\}$, for the intrinsic parities of the particles. If the Lagrangian is also invariant under gauge transformations $U_a(\chi_a), \dots, U_b(\chi_b)$, then it is invariant under the transformation

$$(3.6) \quad P'(\chi_a, \dots, \chi_b) = P U_a(\chi_a) \dots U_b(\chi_b).$$

If the values of χ_a, \dots, χ_b are taken to be 0 or π , P' again satisfies (3.1) and (3.2). This provides an alternative, and physically indistinguishable, definition of the intrinsic parities, with the same possible values for the η 's. It is clear that the choice $\chi_a = \pi$ has the effect of inverting the parities of all members of the group a .

This is the essential point made by WICK, WIGHTMAN and WIGNER ⁽¹⁾. Expressed as a gauge invariance, it is physically rather trivial. Invariance of the interaction under (2.2) ensures that the particle of the group always occur in pairs in any interaction. It is then clear that only the relative parity of the particles within the group is physically observable. Only a particle which is not a member of any gauge group can be emitted or absorbed in an interaction in which all the other particles in the initial and final states occur twice. Only such particles have well defined parities independent of conventions, (apart from the natural convention that the vacuum has even parity).

⁽³⁾ C. N. YANG and J. TIOMNO: *Phys. Rev.*, **79**, 495 (1950).

The only remaining complication is the effect of several gauge groups whose members may overlap. Clearly one is at liberty to chose the phases $\chi_a \dots \chi_b$ in the definition of P' by convention. It is more convenient to chose the parities of certain particles by convention. To do this we make use of the fact that if we have two groups with members

$$(a_1 \dots a_n b_1 \dots b_m),$$

$$(b_1 \dots b_m c_1 \dots c_n),$$

for the purpose of defining parity, we may alternatively consider the groups

$$(a_1 \dots a_n b_1 \dots b_m),$$

$$(a_1 \dots a_n c_1 \dots c_n).$$

Using this extra freedom one may rearrange the groups thus,

$$(b_1 b_2 \dots c_1 c_2 \dots d_1 d_2 \dots),$$

$$(c_1 c_2 \dots d_1 \dots),$$

$$(d_1 \dots).$$

The parity of any one of the b particles may be chosen arbitrarily by convention; the parities of the other b particles may then, in principle, be determined by experiment. Fixing one c particle by convention then makes the other c particle parities observable, and so on. One particle parity in each group may be fixed by convention. The parities of the remaining particles, which do not occur in any subsequent group may then be measured. As mentioned above, there may also be some particles $x_1 \dots x_n$, which are not members of any group, whose parities are directly observable independent of any convention.

So far we have assumed that the neutral and charged particles are described by independent fields. However, if the particles are described as isotopic multiplets in a charge independent formalism, the charged and neutral particles are treated as different components of the same field. This implies that, for at least one choice of the phases $\chi_a \dots \chi_b$, each of the isotopic multiplets combines particles of the same intrinsic parity. Thus, whereas gauge invariance makes the relative parity of some particles purely conventional, the assumption of charge independence makes definite predictions about the relative parities within an isotopic multiplet.

Finally we remark that if one has both 1-type ($\eta_F = \pm 1$) and i -types ($\eta_F = \pm i$) fermions, then each type must appear in pairs in the interactions, for parity conservation. However, this is not equivalent to a new gauge group, since one can construct allowed interactions out of products of fields and charge-conjugate fields of the same type, which do not conserve the particle number of the type (3).

4. – The parities of the particles.

We will discuss the strong interactions of the particles

$$\Xi^{-,0}, \quad \Sigma^{+,-,0}, \quad \Lambda^0, \quad p, \quad n, \quad K^+, \quad K^0, \quad \pi^{+,0}.$$

We assume that parity is conserved in the strong interactions and, for the time being, that the weak interaction may be completely neglected.

The essential features of the Gell-Mann-Nishijima (4) scheme may be expressed, without introducing isotopic spin, as the invariance of the strong interactions under three-gauge transformations (5),

(i) Baryon number ($F = N$

$$(n, \Xi^0, p, \Xi^-, \Sigma^+, \Sigma^-, \Sigma^0, \Lambda^0),$$

(ii) Charge ($F = Q$

$$(p, \pi^+, (-)\Xi^-, K^+, \Sigma^+, (-)\Sigma^-),$$

(iii) Isofermion number (or Hypercharge (6)) ($F = U$ (or Y)

$$(n, p, (-)\Xi^0, (-)\Xi^-, K^+, K^0).$$

We have exhibited explicitly all the independent fields. The $(-)$ signs denote that the field appears with a negative phase factor in the gauge transformation. (It is easily checked that $U - N = S$, the more familiar « strangeness » number).

(4) M. GELL-MANN: *Phys. Rev.*, **92**, 833 (1953); T. NAKANO and K. NISHIJIMA: *Progr. Theor. Phys.*, **10**, 581 (1953).

(5) B. d'ESPAGNAT and J. PRENTKI: *Phys. Rev.*, **99**, 328 (1955).

(6) J. SCHWINGER: *Phys. Rev.*, **104**, 1164 (1956).

For the purpose of defining parity, we have π^0 which occurs in no gauge group and whose parity is well defined (e.g. by $\pi^0 \rightarrow 2\nu$). In place of (iii) one may take

$$(iv) \quad (\Lambda^0, \Sigma^+, \Sigma^-, \Sigma^0, K^+, K^0),$$

which is the combination of (i) and (iii). The groups (i), (ii) and (iv) then have the form described at the end of the last section. By (i), we can choose the parity of n by convention. It is then, in principle, possible to measure the parity of Ξ^0 (e.g. by $\pi^0 + n \rightarrow \Xi^0 + 2K^0$ (!)). If one then fixes p by convention, π^+ and Ξ^- are accessible to experiment, ($p + n + \pi^- \rightarrow n + n; \pi^- + n \rightarrow \Xi^- + 2K^0$). Finally fixing say Λ^0 , the parities of $\Sigma^{+,0}$ and $K^{+,0}$ may be determined. Since interactions occur which involve one nucleon and one Ξ , Σ or Λ particle, all the baryon parities are of the same type, say ($\eta_p = \pm 1$) (7).

The choice of n , p and Λ^0 parities to be fixed by convention is not unique, but a consistent choice is restricted by the gauge groups.

If one now includes the full content of the charge independent strong interaction formalism,

$$(p, n), \quad (\pi^{\pm,0}), \quad (K^{+,0}), \quad (\Sigma^{+,0}), \quad (\Xi^{0,-}),$$

are interpreted as isotopic multiplets. With the convention that p and n parities are the same, this implies that all the other parities within the multiplets are the same. These are specific predictions of the charge independence hypothesis of which the parity of the pion triplet seems to be well established by the analysis of charge exchange scattering and photo-production on this basis (8).

Of the remaining particles, the intrinsic parity of the photon is known to be negative since from classical physics the vector potential is a true vector. e^- and μ^- interact strongly only through the electromagnetic field. However, since baryons are conserved, electrons and muons must be conserved and their

(7) R. UTIYAMA and W. TOBOCMAN: *Phys. Rev.*, **98**, 780 (1955).

(8) To illustrate the freedom due to gauge groups and the restrictions imposed by charge independence, we can consider the pion-nucleon situation. The fact that the reaction $\pi^+ + d \rightarrow n + n$ is observed to go for (spin zero) pions in s -states, establishes only that, of the three particles p , n , π^+ , just one has negative intrinsic parity.

The gauge groups of charge and nucleon number allow two parities, (say p and n), to be chosen by convention. (The form of the interaction, $\psi_p \gamma_5 \psi_n \varphi + h.c.$ implied by this result is independent of the convention).

The assumption of charge independence now predicts that π^0 also has negative parity — a prediction which could be checked directly by observing the polarization of the γ -rays in the π^0 -decay. (See e.g. L. WOLFENSTEIN and D. G. RAVENAHLL: *Phys. Rev.*, **88**, 279 (1953)).

number must, in fact, be separately conserved in strong interactions to avoid strong $\mu \rightarrow e$ decay. Thus the parities of μ and e relative to each other and to the other particles is of no physical significance. (Of course e^+ and e^- (and μ^+ and μ^-), have opposite intrinsic parity).

Some of these remarks have to be modified, when one includes the effect of the weak (decay) interactions. Since parity is known to be violated in the $\mu \rightarrow e$ decay, (involving neutrinos), the previous paragraph stands unchanged. If parity is also violated in the other decay interactions, (not involving neutrinos), all the remarks above remain unchanged with the minor modification that the true « strange » particles will not be eigenstates of the parity operator, but will include very small, (10^{-12}), admixtures of states of the « wrong » parity. If, on the other hand, parity is conserved in the decay of the « strange » particles, the parity of Σ , Λ and K (group (iv)) relative to the nucleons and pions is determined by their decay modes, and is not a matter of convention. However it is still true that, insofar as the weak interactions may be neglected, the relative parity of this group is of no physical significance for the strong interactions.

* * *

The author would like to thank Prof. CHARLES GOEBEL for helpful discussions and the University of Rochester for kind hospitality.

R IASSUNTO (*)

Nella determinazione della gravità delle particelle elementari, l'invarianza delle interazioni rispetto alle trasformazioni di gauge, rende la parità relativa di determinati gruppi di particelle materia di convenzione. D'altro lato, l'indipendenza dalla carica pone definite restrizioni alle parità relative dei membri dei multipletti isotopici. Si analizzano la reciproca influenza di queste convenzioni e restrizioni e le considerazioni generali si applicano alle particelle conosciute.

(*) Traduzione a cura della Redazione.

Isotopic Spin Selection Rules and Parity Non-Conservation in the Decay of the Strange Particles (*).

B. T. FELD

*Department of Physics and Laboratory for Nuclear Science
Massachusetts Institute of Technology - Cambridge, Massachusetts*

(ricevuto l'8 Giugno 1957)

Summary. — The experimental situation is reviewed on the decay ratios of the θ -meson and hyperons from the point of view of testing the validity of the suggested $\Delta T = \pm \frac{1}{2}$ selection rule. Assuming charge-independence, it is shown that the observed decay ratios of the Σ -hyperons require a very large admixture of $\Delta T = \pm \frac{3}{2}$ decay, provided parity is conserved in the decay. However, if the requirement of parity conservation is discarded, the hyperon decay ratios can be accounted for, in a most natural fashion, while still preserving the $\Delta T = \pm \frac{1}{2}$ selection rule. This explanation leads to the prediction of large asymmetries in the angular distributions from the decay of polarized hyperons. Furthermore, these asymmetries are very sensitive to the degree of time-reversal invariance of the decay interaction. A table is given for the expected asymmetry parameters in parity non-conserving hyperon decays with and without time-reversal invariance.

Introduction.

In the scheme proposed by GELL-MANN and NISHIJIMA (¹) to account for the production and decay of the heavy mesons and hyperons, the decays are characterized by the isotopic spin selection rule $\Delta T_3 = \pm \frac{1}{2}$. It has been further suggested (²) that these decays exhibit the stronger selection rule

(*) This work was supported in part by the joint program of the U. S. Office of Naval Research and the U. S. Atomic Energy Commission.

(¹) M. GELL-MANN: *Phys. Rev.*, **92**, 833 (1953); T. NAKANO and K. NISHIJIMA: *Progr. Theor. Phys.*, **10**, 581 (1953).

(²) M. GELL-MANN and A. PAIS: *Proc. of the Glasgow Conference* (London, 1955).

$\Delta T = \pm \frac{1}{2}$. The consequences of this selection rule have been explored by a number of authors (3-7). The result of these investigations, when compared with the most recent observations (8), has been to cast serious doubt on the validity of the $\Delta T = \pm \frac{1}{2}$ selection rule.

In summary, the observations used in testing the selection rules are the following:

- 1) The branching ratio in the θ_1^0 decay:

$$(1) \quad \theta_1^0 \rightarrow \frac{\pi^+ + \pi^-}{2\pi^0}.$$

In this decay, the first mode is observed (9) to predominate; however, it is somewhat difficult to arrive at a firm value for the probability of the second decay mode

$$(2) \quad R_\theta = \frac{w(\theta_1^0 \rightarrow 2\pi^0)}{w(\theta_1^0)}.$$

Direct observation indicates (10) $R_\theta = 0.14 \pm .06$; however, owing to the difficulty of observing the $2\pi^0$ decays, it is perhaps more reasonable to take the result of the observation on the π^\pm decay mode (9), $1 - R_\theta = 0.84 \pm .10$, as giving an upper limit, $R_\theta < 0.26$. On the assumption of a scalar (spin 0) θ , the $\Delta T = \pm \frac{1}{2}$ selection rule predicts $R_\theta = \frac{1}{3}$. For a vector (spin 1) θ , on the other hand, $R_\theta = 0$ follows from the fact that the spin of the π^0 is 0, without further assumptions.

- 2) The decay of the charged θ^\pm ,

$$(3) \quad \theta^\pm \rightarrow \pi^\pm + \pi^0,$$

is much slower than that of the θ_1^0 . The observed lifetimes, together with the

(3) G. WENTZEL: *Phys. Rev.*, **101**, 1214 (1956).

(4) G. TAKEDA: *Phys. Rev.*, **101**, 1547 (1956).

(5) R. GATTO: *Nuovo Cimento*, **3**, 318 (1956).

(6) B. D'ESPAGNAT and J. PRENTKI: *Nuovo Cimento*, **3**, 1045 (1956).

(7) M. KAWAGUCHI and K. NISHIJIMA: *Progr. Theor. Phys.*, **15**, 180, 182 (1956).

(8) *Reports at the Seventh Annual Rochester Conference on High-Energy Physics* (1957).

(9) M. SCHWARTZ and J. STEINBERGER: *Report at the Rochester Conference* (1957) and private communications.

(10) This value is from the work of the Columbia bubble chamber group, cited above. The M.I.T. cloud chamber group, on the other hand, finds $R_\theta = 0.1^{+.06}_{-.1}$ (D. CALDWELL and YASH PAL: private communication).

branching ratio for the K_{π^2} decay mode of the K^\pm -meson, indicate (8)

$$(4) \quad R'_\theta \equiv \frac{w(\theta^\pm)}{w(\theta_1^0)} \cong 1$$

For a K -meson of even spin, the 0^\pm decay is forbidden by the $\Delta T = \pm \frac{1}{2}$ selection rule, and Eq. (4) merely indicates a weak violation of this rule. For an odd-spin K -meson, both 0^\pm and 0_1^0 decay with $\Delta T = \pm \frac{1}{2}$, and charge-independence would require comparable half-lives, in contradiction with the observed R'_θ (Eq. (4)).

3) In the decay of the Λ^0 ,

$$(5) \quad \begin{array}{c} \Lambda^0 \rightarrow p + \pi^- \\ \Lambda^0 \rightarrow n + \pi^0 \end{array},$$

the Columbia group (9) has observed

$$(6) \quad R_\Lambda \equiv \frac{w(\Lambda^0 \rightarrow p + \pi^-)}{w(\Lambda^0)} = 0.65 \pm .05.$$

Since the $\Delta T = \pm \frac{1}{2}$ selection rule predicts $R_\Lambda = \frac{2}{3}$, the agreement could hardly be better.

4) There are three observable modes in the decay of the charged Σ -hyperons,

$$(7) \quad \Sigma^- \rightarrow n + \pi^-$$

$$(8) \quad \Sigma^+ \rightarrow \begin{array}{c} p + \pi^0 \\ n + \pi^+ \end{array}.$$

Observations, mainly by the Berkeley bubble chamber group (11), yield

$$(9) \quad R'_\Sigma \equiv \frac{w(\Sigma^+)}{w(\Sigma^-)} \cong 2,$$

(from the ratio of the lifetimes of Σ^- and Σ^+), and

$$(10) \quad R_\Sigma \equiv \frac{w(\Sigma^+ \rightarrow p + \pi^0)}{w(\Sigma^+ \rightarrow n + \pi^+)} \cong 1.$$

As has been demonstrated by these authors (11), these ratios cannot be re-

(11) L. W. ALVAREZ, H. BRADNER, P. FALK-VAIRANT, J. D. GOW, A. H. ROSENFELD, F. T. SOLMITZ and R. D. TRIPP: *Nuovo Cimento*, 5, 1026 (1957).

conciled with the $\Delta T = \pm \frac{1}{2}$ selection rule (provided, as is implicitly assumed in all of the theoretical treatments⁽³⁻⁷⁾ that the usual invariance principles apply in the Σ -decays).

Now there are—*short of discarding the principle of « charge-independence »* in the decay of the strange particles—a number of alternatives available for reconciling the discrepancies outlined above. One is to allow a violation of the $\Delta T = \pm \frac{1}{2}$ selection rule, permitting decays to proceed partially with $\Delta T = \pm \frac{3}{2}$. Indeed, owing to the presence of electromagnetic interactions, we would expect such violations to occur, but with a probability not much greater than $\sim 1/137$. The possibility of this explanation for the observations on the θ -decay has been explored by DALITZ^(11a), by GELL-MANN⁽¹²⁾ and by ONEDA⁽¹³⁾. In the following Sect. 1, we consider the possibility of accounting for the hyperon decay ratios on the basis of a small $\Delta T = \pm \frac{3}{2}$ violation of the basic $\Delta T = \pm \frac{1}{2}$ selection rule.

However, another means of explaining the hyperon decay ratios, without giving up the $\Delta T = \pm \frac{1}{2}$ selection rule, arises if parity is not conserved in the hyperon decays. Although the hypothesis of parity non-conservation was first considered by LEE and YANG⁽¹⁴⁾ primarily as a means of explaining the « θ - τ paradox », the only processes in which parity non-conservation has thus far been experimentally established are β -decay processes; thus, the possibility remains that the non-conservation of parity is an exclusive feature of decays involving the emission of a neutrino⁽¹⁵⁾. While there is, nevertheless, a strong presumption that parity is not conserved in the K-meson decays, there is, if the K-meson has spin 0, no experimental means available for directly establishing the non-conservation of parity in the decay modes involving only pions. If, however, parity non-conservation should turn out to be a universal feature of « slow » decay processes, the decay of the hyperons provides an excellent means for its direct observation.

Thus, after considering, in Sect. 2, the effects of parity non-conservation on the hyperon decay ratios, some suggestions for observing its consequences in the angular distribution: from the decay of polarized hyperons will be discussed in Sect. 3.

Although the spins of the K-meson and hyperons are not yet established with any certainty, the available evidence⁽⁸⁾ favors spin 0 for the K and $\frac{1}{2}$ the Λ^0 - and Σ^\pm -hyperons. We shall, unless specifically stating otherwise, assume these spin values. We make no specific assumptions concerning the

^(11a) R. H. DALITZ: *Proc. Phys. Soc.*, A **69**, 527 (1956).

⁽¹²⁾ M. GELL-MANN: *Nuovo Cimento*, **5**, 758 (1957).

⁽¹³⁾ S. ONEDA: *Nucl. Phys.*, **3**, 97 (1957).

⁽¹⁴⁾ T. D. LEE and C. N. YANG: *Phys. Rev.*, **104**, 254 (1956).

⁽¹⁵⁾ T. D. LEE and C. N. YANG: *Phys. Rev.*, **105**, 1671 (1957); L. LANDAU: *Nucl. Phys.*, **3**, 127 (1957); A. SALAM: *Nuovo Cimento*, **5**, 299 (1957).

intrinsic parity of the Λ^0 and Σ^\pm , as the arguments to follow do not depend on a knowledge of this property. However, in Sect. 1, we assume that the decay processes are invariant with respect to both space- and time-reversal.

1. – Isotopic spin selection rules and the decay ratios.

The problem of the θ_1^0 decay ratio, R_0 (Eq. (2)), has been discussed in detail by GELL-MANN (12). In essence, provided that charge-independence applies in the θ -decays, the degree of violation of the $\Delta T = \pm \frac{1}{2}$ selection rule is measured by the $\theta^\pm \rightarrow \pi^\pm + \pi^0$ lifetime, since this decay requires $\Delta T \geq \frac{3}{2}$ (for a θ of even spin). Using the relative θ^\pm to θ_1^0 half-lives, R'_0 , as a measure of the relative amplitude for the decay with $\Delta T = \frac{3}{2}$, GELL-MANN obtains a lower limit for R_0 of 0.26. Since this is in the range of the current upper limit of the experiments (10), any firm conclusions concerning the validity of charge-independence in the K_{π^2} decays awaits further improvement of the experimental situation.

Most theoretical discussions of the hyperon decay ratios (3-7) have been based on possible models for the hyperon decay mechanism. In the following phenomenological treatment, we do not attempt to specify the nature of the decay interaction beyond the statement that it is «charge-independent». Let $Y_T^{T_3}$ represent a hyperon of isotopic spin T and charge T_3 ($Y_1^1 = \Sigma^+$, $Y_1^{-1} = \Sigma^-$, $Y_0^0 = \Lambda^0$). Then a decay in which the isotopic spin can change by either $\frac{1}{2}$ or $\frac{3}{2}$, but in which $\Delta T_3 = -\frac{1}{2}$, may be described by the expression (16)

$$(11) \quad \left\{ \begin{array}{l} Y_T^{T_3} \rightarrow a_1 C(T, T_3 | \frac{1}{2}, T_3 - \frac{1}{2}; \frac{1}{2}, \frac{1}{2}) \quad \chi_{\frac{1}{2}}^{T_3 - \frac{1}{2}} \\ \quad + a_3 C(T, T_3 | \frac{3}{2}, T_3 - \frac{1}{2}; \frac{1}{2}, \frac{1}{2}) \quad \chi_{\frac{3}{2}}^{T_3 - \frac{1}{2}} \\ \quad + a'_1 C(T, T_3 | \frac{1}{2}, T_3 - \frac{1}{2}; \frac{3}{2}, \frac{1}{2}) \quad \chi_{\frac{3}{2}}^{T_3 - \frac{1}{2}} \\ \quad + a'_3 C(T, T_3 | \frac{3}{2}, T_3 - \frac{1}{2}; \frac{3}{2}, \frac{1}{2}) \quad \chi_{\frac{1}{2}}^{T_3 - \frac{1}{2}}, \end{array} \right.$$

in which the a_{2t} 's represent the amplitudes corresponding to decay into the various possible final pion-nucleon states, $\chi_t^{t_3}$, with $\Delta T = \frac{1}{2}$ (a_1 and a_3) and $\Delta T = \frac{3}{2}$ (a'_1 and a'_3), the C 's are the appropriate Clebsch-Gordan coefficients (17).

(16) Equation (11) is an analytical representation of decay through the emission of Wentzel's «spurion», a «particle» whose sole property is that it carries away one unit of strangeness ($t_3 = \frac{1}{2}$); in our case, we require two «spurions», of isotopic spin $\frac{1}{2}$ and $\frac{3}{2}$.

(17) E. U. CONDON and G. H. SHORTLEY: *The Theory of Atomic Spectra* (Cambridge, 1935), p. 76.

connecting the Y 's and the χ 's, and the $\chi_i^{t_3}$ are the appropriate nucleon-pion combinations

$$(12) \quad \left\{ \begin{array}{l} \chi_{\frac{1}{2}}^{\frac{1}{2}} = -\sqrt{\frac{1}{3}} p\pi^0 + \sqrt{\frac{2}{3}} n\pi^+, \\ \chi_{\frac{1}{2}}^{-\frac{1}{2}} = -\sqrt{\frac{2}{3}} p\pi^- + \sqrt{\frac{1}{3}} n\pi^0, \\ \chi_{\frac{3}{2}}^{\frac{3}{2}} = p\pi^+, \quad \chi_{\frac{3}{2}}^{-\frac{3}{2}} = n\pi^-, \\ \chi_{\frac{3}{2}}^{\frac{1}{2}} = \sqrt{\frac{2}{3}} p\pi^0 + \sqrt{\frac{1}{3}} n\pi^+, \\ \chi_{\frac{3}{2}}^{-\frac{1}{2}} = \sqrt{\frac{1}{3}} p\pi^- + \sqrt{\frac{2}{3}} n\pi^0. \end{array} \right.$$

In terms of the amplitudes defined in Eq. (11), the decay probabilities of interest are, for the Λ^0 decay,

$$(13) \quad \left\{ \begin{array}{l} w(\Lambda^0 \rightarrow p\pi^-) = \frac{1}{3} |a_1 + \frac{1}{2}a'_3|^2 \\ w(\Lambda^0 \rightarrow n\pi^0) = \frac{1}{6} |-a_1 + a'_3|^2 \\ w(\Lambda^0) = \frac{1}{2} |a_1|^2 + \frac{1}{4} |a'_3|^2. \end{array} \right.$$

For the Σ decays, since the amplitudes need not be the same as in Eqs. (13), we use b_{2i} instead of a_{2i} ,

$$(14) \quad \left\{ \begin{array}{l} w(\Sigma^- \rightarrow n\pi^-) = \frac{3}{4} |b_3 - \sqrt{\frac{2}{5}} b'_3|^2 \\ w(\Sigma^+ \rightarrow p\pi^0) = \frac{1}{3} |(b_1 + \frac{1}{2}b'_1) + \sqrt{\frac{1}{2}}(b_3 + \sqrt{\frac{8}{5}} b'_3)|^2 \\ w(\Sigma^+ \rightarrow n\pi^+) = \frac{1}{3} |\sqrt{2}(b_1 + \frac{1}{2}b'_1) - \frac{1}{2}(b_3 + \sqrt{\frac{8}{5}} b'_3)|^2 \\ w(\Sigma^+) = |b_1 + \frac{1}{2}b'_1|^2 + \frac{1}{4} |b_3 + \sqrt{\frac{8}{5}} b'_3|^2. \end{array} \right.$$

Although the amplitudes in Eqs. (13) and (14) are, in general, complex, it has been shown by TAKEDA (4) that, provided that the decay interaction is invariant with respect to time-reversal, these amplitudes have the form,

$$(15) \quad a_{2i} := \alpha_{2i} \exp [i\delta_{2i,2j}],$$

where the α 's are real and the $\delta_{2i,2j}$ are the pion-nucleon scattering phase shifts in the final states. Whether the δ 's correspond to the s - or p -wave pion scattering phase shifts depends on whether the hyperon has relative parity — or +, with respect to that of the nucleon. In either event, assuming spin $\frac{1}{2}$ for both Λ^0 and Σ^\pm , the scattering phase shifts are small ($< 15^\circ$) at the energies cor-

responding to the decays, and can be neglected without appreciably altering the results (18).

For the Λ^0 decay, Eqs. (13) can be reconciled with the R_Λ of Eq. (6) only if $a'_3 \ll a_1$. For the Σ decays, however, Eqs. (9) and (10) are not compatible with $b'_1 \approx b'_3 \approx 0$ in Eqs. (14). Since we have, in Eqs. (14), three adjustable parameters (there are four constants, but only three independent ratios) to fit two experimental constants, R_Σ and R'_Σ , a multiplicity of solutions is possible. In Table I are exhibited the solutions which give $R_\Sigma = 1$, $R'_\Sigma = 2$.

TABLE I. — Properties of the decay constants for the Σ -decays, with $\Delta T = \pm \frac{1}{2}$ and $\pm \frac{3}{2}$, required for $R_\Sigma = 1$, $R'_\Sigma = 2$.

solution	b'_3/b_3	$(1 + b'_1/2b_1)$	b'_1/b_1 (assumed)	b_3/b_1	a'_3/a_1 (assumed)	R_Λ
1a	—0.38	$1.5b_3/b_1$	—0.38	0.54	—0.21	0.52
1b	—0.38	$1.5b_3/b_1$	0.38	0.79	—0.30	0.46
1c	—0.38	$1.5b_3/b_1$	—1.0	0.33	—0.12	0.58
2a	0.51	$-0.14b_3/b_1$	0.51	—8.9	—4.5	0.09
2b	0.51	$-0.14b_3/b_1$	—0.51	—5.3	—2.7	0.02

and, at the same time, permit $b'_3 < b_3$, $b'_1 < b_1$. It turns out that the combinations of constants appearing in R_Σ and R'_Σ allow of only two solutions for b'_3/b_3 , subject to the above conditions; these are shown in column 2, with the correspondingly unique solutions for the combination of the other constants given in column 3.

Columns 4-7 demonstrate the effect of the assumption that the Λ^0 decay exhibits the same degree of $\Delta T = \pm \frac{1}{2}$ violation as is required to account for the Σ -decay ratios (i.e., it is assumed that $a'_3/a_1 = b'_3/b_1$). All but solution 1c assume $b'_1/b_1 = +b'_3/b_3$; solution 1c represents an attempt to minimize a'_3/a_1 .

The significant conclusion from the results shown in Table I is that it is not possible to account for the Σ -decay ratios, within the framework of charge-independence and the usual invariance principles, without requiring a $\Delta T = \pm \frac{3}{2}$ decay probability of the same order of magnitude as that for $\Delta T = \pm \frac{1}{2}$. We are thus forced either to discard the $\Delta T = \pm \frac{1}{2}$ selection rule or to consider the possibility of relaxing the invariances. Since parity is now known not to be conserved in some weak interactions, it is natural to explore the consequences of its non-conservation in the hyperon decays.

(18) It is easily shown that the quantitative conclusions are very little affected by neglecting the phase shifts for spin $\frac{1}{2}$ hyperons. In the case of spin $\frac{3}{2}$, owing to the large δ_{33} scattering phase shift at the energy of the Σ -decay, this phase shift cannot be neglected in such considerations. However, the conclusions concerning the need for appreciable b'_1 and b'_3 are the same (11).

2. - Consequences of parity non-conservation for the decay ratios.

If parity is not conserved, a K-meson or hyperon can decay into a final state of mixed parity, irrespective of its initial intrinsic parity. For the K-meson, this would render possible the θ - and τ -decay modes from a single spin 0 particle. However, as far as the decay ratio R_0 (or the corresponding R_τ) is concerned, nothing is changed, since a final 2π (3π) state of spin 0 must have positive (negative) parity. Furthermore, since the 2π and 3π states cannot interfere, there is no other observable consequence of the parity non-conservation, and we can add nothing to the previous considerations on the K-mesons.

The situation is different for the hyperon decays. Here, the effect of parity non-conservation is to double the number of independent amplitudes describing the decay processes. Thus, it may be possible to satisfy the observed decay ratios and still maintain the strong selection rule $\Delta T = \pm \frac{1}{2}$ ($a' = b' = 0$ in eqs. (11), (13) and (14)).

We consider first the Σ decays: Let

$$(16) \quad \left\{ \begin{array}{l} b_{s_s} = \alpha \exp [i\delta_1] \\ \frac{1}{2} b_{3_s} = \beta \exp [i\delta_3] \\ b_{1_p} = \alpha \xi_1 \exp [i(\delta_{11} + \eta)] \\ \frac{1}{2} b_{3_p} = \beta \xi_3 \exp [i(\delta_{31} + \eta)], \end{array} \right.$$

in which α and β are arbitrary, real constants, the $\delta_{2t,l}$ are the pion-nucleon scattering phase shifts at the energy corresponding to the Σ decay, ξ_1 and ξ_3 are real constants which measure the degree of parity non-conservation in the decay to the final $t = \frac{1}{2}$ and $t = \frac{3}{2}$ states, respectively. η is a phase factor whose magnitude measures the degree of breakdown of time-reversal invariance in the decay.

The introduction of η is necessitated by the fact that ⁽¹⁹⁾, since the Schwinger-Lüders-Pauli Theorem requires the decay interaction to be invariant with respect to the combined operations of time-reversal, charge-conjugation, and space-inversion (TCP), the failure of P must be accompanied by non-invariance with respect to T or C or both. In particular ⁽⁴⁾, if (as appears to be the case in the β -decay) CP - and T -invariance are individually preserved, $\eta = 0$; for PT - and C -invariance, $\eta = \pi/2$; if only TCP remains, $0 < \eta < \pi/2$.

⁽¹⁹⁾ T. D. LEE, R. OEHME and C. N. YANG: *Phys. Rev.*, **106**, 340 (1957); G. LÜDERS and B. ZUMINO: *Phys. Rev.*, **106**, 385 (1957).

Now, in obtaining the decay rates, it is necessary to integrate the decay angular distribution over all angles. Under these circumstances, there remain no terms corresponding to interference between final s - and p -states, and the amplitudes of eq. (14) appear in the decay probabilities as independent amplitudes,

$$(17) \quad \left\{ \begin{array}{l} w(\Sigma^- \rightarrow n\pi^-) = 3\beta^2(1 + \xi_3^2) \\ w(\Sigma^+ \rightarrow p\pi^0) = \frac{1}{3}\alpha^2(1 + \xi_1^2) + \frac{2}{3}\beta(1 + \xi_3^2) + \\ \quad + (2\sqrt{2}/3)\alpha\beta[\cos(\delta_1 - \delta_3) + \xi_1\xi_3 \cos(\delta_{11} - \delta_{31})] \\ w(\Sigma^+ \rightarrow n\pi^+) = \frac{2}{3}\alpha^2(1 + \xi_1^2) + \frac{1}{3}\beta^2(1 + \xi_3^2) - \\ \quad - (2\sqrt{2}/3)\alpha\beta[\cos(\delta_1 - \delta_3) + \xi_1\xi_3 \cos(\delta_{11} - \delta_{31})] \\ w(\Sigma^+) = \alpha^2(1 + \xi_1^2) + \beta^2(1 + \xi_3^2). \end{array} \right.$$

(Note the independence on η .) In order to reduce the arbitrariness in fitting the observed decay ratios, R_Σ and R'_Σ , we make the natural assumption that the degree of parity non-conservation is independent of the isotopic spin in the final state,

$$(18) \quad \xi_1^2 = \xi_3^2 = \xi^2.$$

It turns out, then, that the decay ratios are obtained with

$$(19) \quad \left\{ \begin{array}{ll} \xi_1 = -\xi_3 = \pm 0.71, & (\xi^2 = 0.5) \\ \alpha/\beta = \sqrt{5.0}, & (|b_1|/|b_3| = 1.12). \end{array} \right.$$

What is most interesting about this solution is that the above value of ξ^2 is equal to the barrier-penetration factor for p -wave decay at the Σ -decay energy,

$$(20) \quad v_p = \frac{(kr_0)^2}{1 + (kr_0)^2},$$

for $r_0 = 0.72 \text{ } h/\mu c$, which is essentially the value of the pion-nucleon interaction range required in the interpretation of pion scattering and photoproduction experiments ⁽²⁰⁾. Thus, if we regard the above agreement ⁽²¹⁾ as more than

⁽²⁰⁾ E. FERMI: *Suppl. Nuovo Cimento*, **2**, 44 (1955).

⁽²¹⁾ The other features of the solution, that the p -wave decay amplitudes have opposite signs for the $t = \frac{1}{2}$ and $t = \frac{3}{2}$ final states and that the relative amplitudes (matrix elements) to these states are roughly equal, are consequences of the dynamics of the decay interaction about which a phenomenological theory can make no predictions.

fortunate, we may conclude that not only do the Σ -decay ratios provide an argument for the non-conservation of parity in the Σ -decays, but they indicate that, if this is indeed the explanation, the degree of parity non-conservation is (as in β -decay) close to the maximum possible (22),

It is important to note that this explanation of the Σ -decay ratios leaves unaltered the ratio $R_\Lambda = \frac{2}{3}$, eq. (6), since the absence of $s-p$ interference terms in the $w(\Lambda^0)$'s means that this ratio is entirely determined by the Clebsch-Gordan coefficients appropriate to the $\Delta T = \pm \frac{1}{2}$ decay into the $t = \frac{1}{2}$ state (eq. (13)).

3. - Angular distributions in the decay of polarized hyperons (23).

If, as is strongly suggested by the considerations of the last section, parity is not conserved in the hyperon decays, this may be detected by observations on the angular distributions of the decay products from polarized hyperons. Let θ be the angle between the direction of the polarized hyperon spin ($\frac{1}{2}$) and the direction of emission of the pion. Then, the decay angular distributions have the general form

$$(21) \quad W(\theta) = 1 - [\varepsilon A \cos(\eta + \delta_p - \delta_s)] \cos \theta,$$

where $\varepsilon = 2\langle m_s \rangle$ is the degree of polarization of the decaying hyperons,

$$(22) \quad A \cos(\eta + \delta_p - \delta_s) = \frac{2 \operatorname{Re} a_s^* a_p}{|a_s|^2 + |a_p|^2},$$

with the following a 's for the various Σ -decay processes of interest (ref. eqs. (13), (14) and (16)).

$$(23) \quad \begin{cases} a_{s,p}^0 = \sqrt{\frac{1}{3}} b_{1s,p} + \sqrt{\frac{2}{3}} b_{3s,p}/2, & (\Sigma^+ \rightarrow p\pi^0) \\ a_{s,p}^+ = \sqrt{\frac{2}{3}} b_{1s,p} - \sqrt{\frac{1}{3}} b_{3s,p}/2, & (\Sigma^+ \rightarrow n\pi^+) \\ a_{s,p}^- = \sqrt{3} b_{3s,p}/2, & (\Sigma^- \rightarrow n\pi^-). \end{cases}$$

(22) It would not be justified, however, to consider the foregoing also as an argument for spin $\frac{1}{2}$ for the Σ . The ratios $R_\Sigma = 1$, $R'_\Sigma = 2$ can also be fit on the assumption of spin $\frac{3}{2}$ ($s \rightarrow d$, $\delta_1 \cong \delta_3 \cong 0$, $\delta_{11} \rightarrow \delta_{13} \cong 0$, $\delta_{31} \rightarrow \delta_{33} = 44^\circ$ in Eqs. (16) with $\alpha/\beta = -\sqrt{5}$, $\xi_1 = -\xi_3$, $\xi^2 = 3.3$). The ratio of the angular momentum barriers is $v_g/v_d = 3.4$ for $r_0 = \hbar/\mu c$.

(23) Arguments, involving the considerations of this and the next section, were presented at the 1957 Rochester Conference by the author and by T. D. LEE, who reported on work by T. D. LEE, J. STEINBERGER, G. FEINBERG, P. K. KABIR and C. N. YANG: *Phys. Rev.*, **106**, 1367 (1957).

We have evaluated the asymmetry parameters on the assumption $\alpha/\beta = \sqrt{5}$, $\xi_1 = -\xi_3 = 0.71$, with the scattering phase shifts (24), at the Σ -decay energy ($Q = 114$ MeV), $\delta_1 = 13.1^\circ$, $\delta_3 = -8.2^\circ$, $\delta_{11} \simeq \delta_{31} \simeq -2.5^\circ$. The results are summarized in the first 7 rows of Table II, in which we use the symbols

$$(24) \quad \begin{cases} a_s = \gamma_s \exp [i\delta_s] \\ a_p = \gamma_p \exp [i\delta_p] \exp [i\eta] \\ B = A \cos (\eta + \delta_p - \delta_s). \end{cases}$$

(Note that the signs of all γ_p 's and A 's would be reversed if we reverse the signs of the ξ 's.)

TABLE II. — *Asymmetry parameters for parity non-conserving hyperon decay.*

	$\Sigma^+ \rightarrow p\pi^0$	$\Sigma^+ \rightarrow n\pi^+$	$\Sigma^- \rightarrow n\pi^-$	$\Lambda^0 \rightarrow p\pi^-$
γ_s/α	0.93	0.54	0.77	1.0
δ_s	4.9°	22.3°	-8.2°	6.7°
γ_p/α	0.15	0.76	-0.55	0.45
δ_p	-2.5°	-2.5°	-2.5°	0°
A	0.32	0.95	-0.94	0.75
B ($\eta = 0$)	0.31	0.86	-0.94	0.75
B ($\eta = \pi/2$)	0.04	0.40	0.09	0.09
$A_{\frac{1}{2}}$	0.26	1.00	-0.85	0.49
δ_p	17°	-16°	44°	0°
$B_{\frac{1}{2}}$ ($\eta = 0$)	0.25	0.96	-0.61	0.49
$B_{\frac{1}{2}}$ ($\eta = \pi/2$)	-0.08	0.27	0.59	0.00

Also shown in Table II are the parameters corresponding to the Λ^0 decays, for which we take

$$(25) \quad \begin{cases} a_{1s} = \alpha' \exp [i\delta'_1], \\ a_{1p} = \alpha' \xi'_1 \exp [i\delta'_{11}] \exp [i\eta], \\ B' = \frac{2\xi'_1}{1 + \xi'^2_1} \cos (\eta + \delta'_{11} - \delta'_1), \end{cases}$$

with $\delta'_1 = 6.7^\circ$, $\delta'_{11} \simeq 0$, and $\xi'^2_1 = 0.20 = v_p(kr_0)$ at the Λ^0 -decay energy (37 MeV) with $r_0 = 0.72 \hbar/\mu c$.

(24) Report of the Sixth Annual Rochester Conference on High Energy Physics (1956).

Table II shows that, provided the explanation for the hyperon decay ratios of the previous section is valid, large asymmetries are to be expected in the decay of polarized hyperons. Furthermore, these asymmetries differ both in magnitude and sign for the different decay modes. Thus, observation on the asymmetries in the two Σ^+ decays should enable a determination of both the degree of polarization, ϵ , and the degree of time-reversal non-invariance, η . It is also of interest that a large asymmetry is expected in the decay of polarized Λ^0 's, despite the small Q -value, provided that $\eta \approx 0$; this arises from the fact that the asymmetry parameter (eq. (25)) is very sensitive to small admixtures of final p -state.

The arguments of this section are easily repeated for the case of a (still possible but less probable) spin $\frac{3}{2}$ Σ or Λ . In this case, the decay angular distributions are

$$(26) \quad W(\theta) = f_m(\theta)(1 - B_{\frac{3}{2}} \cos \theta),$$

where $f_m(\theta)$ depends on the state of polarization of the hyperon,

$$(27) \quad \begin{cases} f_{\frac{3}{2}} = \frac{3}{2} \sin^2 \theta, \\ f_{\frac{1}{2}} = \frac{1}{2}(1 + 3 \cos^2 \theta), \end{cases}$$

while the B 's are computed from eq. (23), (24) and (25) with the substitutions previously defined (22). The corresponding asymmetry parameters are shown in the last four rows of Table II.

4. – Conclusions.

Although the foregoing cannot be considered as a proof of the non-conservation of parity in the hyperon decays, we believe that it represents a very strong suggestion that this may indeed be the case. Under these circumstances, observations of the type suggested in the previous section would be of extreme importance, for they would also serve in a straightforward fashion as a measure of the degree of time-reversal invariance of the decay interaction.

It might be argued that a sufficient number of hyperon decays (mostly Λ^0) have already been observed to render it unlikely that the asymmetries, if they exist, are as large as those indicated in the B ($\eta = 0$) rows of Table II. However, a brief examination of the present experimental situation (8) indicates that this is probably not the case. In the first place, in those observations (11) in which the hyperons were produced by K^- -capture we would not expect the hyperons to be polarized. If we confine ourselves to the bubble chamber

observations (mainly by the Michigan, Columbia, Bologna, and Pisa groups) of hyperons produced by pions on protons, there are available $\sim 150 \Lambda^0$ and $\sim 100 \Sigma^-$ events, produced by negative pions of energy ranging from 870 to 1300 MeV. As this presumably represents the complete sample, the net polarization is zero, since the target protons were unpolarized. An appreciably polarized sub-sample, if it could be extracted, would probably not contain a sufficient number of events to enable the observation of the decay asymmetry with reasonable statistical certainty.

Furthermore, it may be argued (23) that the polarization, ε in eq. (21), is probably not very large for any sample in the present observations. If we assume that the observations are sufficiently close to threshold that only s - and p -wave final K-Y states need be considered, the production angular distribution is

$$(28) \quad W(\theta) = |D|^2 + |E|^2 \sin^2 \theta,$$

where θ is the center of mass angle of emission of the hyperon with respect to the direction of the incident pion, and

$$(29) \quad \begin{cases} D = c(s_{\frac{1}{2}}) + [c(p_{\frac{1}{2}}) + 2c(p_{\frac{3}{2}})] \cos \theta \\ E = c(p_{\frac{1}{2}}) - c(p_{\frac{3}{2}}). \end{cases}$$

$c(s_{\frac{1}{2}})$, $c(p_{\frac{1}{2}})$, and $c(p_{\frac{3}{2}})$ are the amplitudes for associated production of a spin $\frac{1}{2}$ hyperon and spin 0 K-meson in the states indicated. The polarization, with respect to an axis perpendicular to the plane of production, is

$$(30) \quad \varepsilon = \frac{2 \operatorname{Im}(DE^*) \sin \theta \sin \varphi}{|D|^2 + |E|^2 \sin^2 \theta}.$$

The experimental indications, albeit as yet rather preliminary, are that the $\sin^2 \theta$ term in eq. (28) is small, in which case the polarization may be small at all angles of production. Whether this is true and, if true, represents an intrinsic feature of the production dynamics at all energies remains to be determined by further experimentation.

In any event, the problems raised by the possibility of parity non-conservation in the hyperon decays are of sufficient interest, and the observable consequences, as outlined in the foregoing, are sufficiently unique as to warrant the serious attention of investigators in this field.

RIASSUNTO (*)

Si passano in rassegna i risultati sperimentali sui rapporti di decadimento dei mesoni θ e degli iperoni allo scopo di saggiare la validità della proposta regola di selezione $\Delta T = \pm \frac{1}{2}$. Assumendo l'indipendenza dalla carica si dimostra che i rapporti di decadimento degli iperoni Σ osservati richiedono una assai abbondante presenza di decadimenti $\Delta T = \frac{3}{2}$, purchè nel decadimento sia conservata la parità. Tuttavia, se si rinuncia alla conservazione della parità, si può render conto in modo del tutto naturale dei rapporti di decadimento degli iperoni, pur conservando la regola di selezione $\Delta T = \frac{1}{2}$. Questa spiegazione porta alla predizione di grandi asimmetrie nella distribuzione angolare dei decadimenti degli iperoni polarizzati. Inoltre, tali asimmetrie sono molto sensibili al grado di invarianza dell'interazione di decadimento, rispetto all'inversione del tempo. Si dà una tabella dei parametri di asimmetria previsti nei decadimenti di iperoni senza conservazione della parità con o senza invarianza rispetto all'inversione del tempo.

(*) Traduzione a cura della Redazione.

Non-Static Effects on Individual Nucleons in a Spheroidal Potential.

W. E. FRAHN and R. H. LEMMER

*Nuclear Physics Division of the National Physical Research Laboratory, C.S.I.R.-
Pretoria, South Africa*

(ricevuto il 10 Giugno 1957)

Summary. — A generalized single-particle wave equation is derived in the effective mass approximation, starting from a non-local potential matrix for the nucleon-nucleus interaction as required by recent work on the nuclear many-body problem. The effective nucleon mass appearing in the kinetic energy operator of this equation depends on the shape of the local potential which is assumed as the static limit of the non-local interaction. The non-static effects on the motion of individual nucleons in non-spherical nuclei are illustrated using a spheroidal oscillator potential. By a perturbation treatment of the energy eigenvalue problem, it is shown that the non-static problem is approximately equivalent to a static one with a modified deformation parameter.

1. — Introduction.

The recent advances in the nuclear many-body problem ⁽¹⁾ have shown, that a self-consistent field method can be applied to determine the overall interaction of a nucleon with its partners in a nucleus. In contrast with the assumption of the usual Hartree method, however, the self-consistent interaction can no longer be represented by a local potential $V(\mathbf{r})$, but, for finite nuclei, must be non-local in both co-ordinate and momentum space and des-

⁽¹⁾ These advances are due to the work of K. A. BRUECKNER, K. M. WATSON, C. A. LEVINSON, H. M. MAHMOUD, R. J. EDEN and N. C. FRANCIS. Brueckner's method has been extended to finite nuclei by H. A. BETHE: *Phys. Rev.*, **103**, 1353 (1956). This paper also contains the references to the earlier literature.

cribed by a potential matrix $(\mathbf{r}|K|\mathbf{r}')$ or $(\mathbf{k}|K|\mathbf{k}')$. The determination of the self-consistent potential matrix is in general a difficult task and, moreover, requires the knowledge of the nucleon-nucleon interaction.

On the other hand, the successes of the single particle models with local potentials indicate, that the non-local effects cannot be too large. This suggests a phenomenological approach, which starts from the local potentials usually employed in shell model calculations and considers the non-locality as a correction.

In this approximation, the potential matrix $(\mathbf{r}|K|\mathbf{r}')$ can be separated in the variables $\frac{1}{2}(\mathbf{r} + \mathbf{r}')$ and $\mathbf{r} - \mathbf{r}'$. The functional dependence on these variables is determined by the requirements, that the local potential $V(\mathbf{r})$ should be the static limit of the interaction and that the non-locality must be translation-invariant in the case of infinitely extended nuclear matter. The potential matrix is then given by

$$(1) \quad (\mathbf{r}|K|\mathbf{r}') = V\left(\frac{\mathbf{r} + \mathbf{r}'}{2}\right)\delta_a(\mathbf{r} - \mathbf{r}'),$$

where δ_a denotes a normalized approximation function of $\delta(\mathbf{r} - \mathbf{r}')$ with the « range parameter » a , e.g. the Gaussian function $\delta_a(r) = \pi^{-\frac{3}{2}}a^{-3}\exp[-r^2/a^2]$.

With the further requirement, that (1) describes a small correction to the local potential $V(\mathbf{r})$, we can formally expand δ_a in powers of a and retain only the first order correction to δ , which is equivalent to a second-order velocity-dependent term in the interaction Hamiltonian.

It will be shown that this « effective mass approximation » leads to a generalized wave equation for a single nuclear particle, which takes the place of the individual nucleon of the static single particle models. The dynamical properties of these nuclear « particles » are formally characterized by a spatially variable effective mass, which is uniquely determined by the potential $V(\mathbf{r})$ and the non-local range parameter a . The latter again depends solely on the potential depth V_0 and the mass reduction M^*/M_0 characterizing infinitely extended nuclear matter. The numerical value of a will then be fixed by using the value of M^*/M_0 , which has been obtained by BRUECKNER (2) from a self-consistent calculation for infinite nuclei.

The potential matrix (1) describes the general case of a finite nucleus and contains as limiting cases

- 1) the local potential $V(\mathbf{r})$ for $a = 0$, and
- 2) the infinitely extended nucleus (« nuclear matter ») for

$$V\left(\frac{\mathbf{r} + \mathbf{r}'}{2}\right) = \text{const} = -V_0, \quad \text{or} \quad (\mathbf{k}|K|\mathbf{k}') = -V_0 \tilde{\delta}_a(k) \delta(\mathbf{k} - \mathbf{k}').$$

($\tilde{\delta}_a$ denotes the Fourier transform of δ_a).

(2) K. A. BRUECKNER: *Phys. Rev.*, **97**, 1353 (1955).

In a previous paper (3), the matrix (1) has been used with $V(\frac{1}{2}|\mathbf{r} + \mathbf{r}'|)$, leading to a spherically symmetric potential $V(r)$, and the energy eigenvalue problem has been studied in the particular case of the harmonic oscillator potential. With the general form (1) it is now possible to consider non-isotropic potentials.

The physical significance of anisotropic potentials has been disclosed by the large nuclear quadrupole moments in the regions of mass number $A = 155 \div 185$ and $A > 225$, which can be explained by strongly deformed nuclear equilibrium shapes (4). The investigation of the dynamical implications of this model has led Bohr and Mottelson to a unified picture of nuclear dynamics (5), which combines the single particle and collective aspects of nuclear motion. In the so-called strong coupling case, the single particle motion can be approximately separated from the collective motions and a simplified picture is obtained, in which individual nucleons move in a deformed static potential. Recently, NILSSON has given a detailed discussion of this case for a spheroidal oscillator potential (6).

In the present paper, we shall exemplify the non-static effects on the single-particle motion in anisotropic potentials by using the spheroidal oscillator potential as the static limit of the interaction, in order to have a convenient possibility of comparison with NILSSON's work.

2. - Derivation of the generalized single-particle equation.

The non-local wave equation is in co-ordinate space

$$(2) \quad \frac{\hbar^2}{2M_0} \Delta\psi(\mathbf{r}) + E\psi(\mathbf{r}) = \int (\mathbf{r} | K | \mathbf{r}') \psi(\mathbf{r}') d\mathbf{r}' .$$

In the interaction term, given by the right hand side of (2) with the kernel (1), we substitute $\mathbf{r}' = \mathbf{r} + a\boldsymbol{\rho}$ and expand the integrand in powers of a . Then we get up to the order a^2 :

$$\begin{aligned} \int (\mathbf{r} | K | \mathbf{r}') \psi(\mathbf{r}') d\mathbf{r}' &= \int V\left(\frac{\mathbf{r} + \mathbf{r}'}{2}\right) \delta_a(\mathbf{r} - \mathbf{r}') \psi(\mathbf{r}') d\mathbf{r}' = \\ &= \int V(\mathbf{r} + \frac{1}{2}a\boldsymbol{\rho}) \psi(\mathbf{r} + a\boldsymbol{\rho}) \delta_a(\boldsymbol{\rho}) a^3 d\boldsymbol{\rho} = \\ &= \int \left\{ V(\mathbf{r}) \psi(\mathbf{r}) + \frac{a^2 \varrho^2}{16} [\Delta V + 2\nabla V \nabla + V \Delta] \psi(\mathbf{r}) \right\} \delta_a(\boldsymbol{\rho}) a^3 d\boldsymbol{\rho} . \end{aligned}$$

(3) W. E. FRAHN and R. H. LEMMER: *Nuovo Cimento*, **5**, 1564 (1957).

(4) J. RAINWATER: *Phys. Rev.*, **79**, 432 (1950).

(5) A. BOHR: *Dan. Mat. Fys. Medd.*, **26**, No. 14 (1952). A. BOHR and B. R. MOTTELSON: *Dan. Mat. Fys. Medd.*, **27**, No. 16 (1953).

(6) S. G. NILSSON: *Dan. Mat. Fys. Medd.*, **29**, No. 16 (1955).

With the properties of δ_a given by

$$\int \delta_a(\varrho) a^3 d\varrho = 1; \quad \int \varrho^2 \delta_a(\varrho) a^3 d\varrho = \frac{3}{2},$$

we obtain

$$(3) \quad \int (\mathbf{r} | K | \mathbf{r}') \psi(\mathbf{r}') d\mathbf{r}' = V(\mathbf{r}) \psi(\mathbf{r}) + \frac{a^2}{16} [\Delta V(\mathbf{r}) + 2\nabla V(\mathbf{r}) \nabla + V(\mathbf{r}) A] \psi(\mathbf{r}).$$

Equation (2) can then be rewritten in the form

$$(4) \quad -\frac{\hbar^2}{8} \left[\Delta \frac{1}{M(\mathbf{r})} + \nabla \frac{2}{M(\mathbf{r})} \nabla + \frac{1}{M(\mathbf{r})} A \right] \psi(\mathbf{r}) + V(\mathbf{r}) \psi(\mathbf{r}) = E \psi(\mathbf{r}),$$

with

$$(5) \quad M(\mathbf{r}) = \frac{M_0}{1 - (a^2 M_0 / 2\hbar^2) V(\mathbf{r})}.$$

The single-particle wave equation (4) is seen to be a direct consequence of the two basic assumptions of (i) non-locality of the average nuclear field, as revealed by the many-body theory, and (ii) the approximate validity of the single-particle models with local potentials. Its general form is to a large extent independent of further assumptions on the interaction; in particular it is independent of the special type of the approximation function δ_a , of which the only property entering the result is the range a .

The expression (5) for $M(\mathbf{r})$, formally representing the « effective nucleon mass », describes the main effect of the non-static interaction, viz., that the inertial properties of the nuclear « particles » follow the spatial variations of the potential $V(\mathbf{r})$ everywhere, also with respect to its angular shape. Because the implications of (4) and (5) for the particular cases of infinitely extended nuclear matter and of spherically symmetric potentials $V(r)$ have been studied previously (3,7), we will at present consider the non-static effects on the angular variation of the static potential.

3. – The spheroidal oscillator potential.

Non-isotropic potentials have been investigated by several authors (6,8), mainly in connection with the strong-coupling case of the Bohr-Mottelson

(7) W. E. FRAHN: *Nuovo Cimento*, **4**, 313 (1956).

(8) E. FEENBERG and K. C. HAMMACK: *Phys. Rev.*, **81**, 285 (1951); S. GRANGER and R. D. SPENCE: *Phys. Rev.*, **83**, 460 (1951); S. GALLONE and C. SALVETTI: *Nuovo Cimento*, **8**, 970 (1951); **10**, 145 (1953); D. L. HILL and J. A. WHEELER: *Phys. Rev.*, **89**, 1102 (1953); D. PFIRSCH: *Zeits. f. Phys.*, **132**, 409 (1952); M. L. GURSKY: *Phys. Rev.*, **98**, 1205 (1955); S. A. MOSZKOWSKI: *Phys. Rev.*, **99**, 803 (1955); K. GOTTFRIED: *Phys. Rev.*, **103**, 1017 (1956).

theory. We will consider the particular case of the spheroidal oscillator potential. Although the oscillator shape is only a poor approximation for a heavy nucleus in a static model, it is deformed towards a more realistic shape by the non-static interaction (3). Moreover, the non-static effects on the angular dependence are to a large extent independent of the radial shape of the potential. The choice of the spheroidal oscillator allows a direct comparison with NILSSON's work (6), who has given a detailed discussion of the corresponding static case.

The single-particle Hamiltonian is given by

$$(6) \quad H = \frac{1}{8} \left[\mathbf{P}^2 \frac{1}{M(\mathbf{r})} + \mathbf{P} \frac{2}{M(\mathbf{r})} \mathbf{P} + \frac{1}{M(\mathbf{r})} \mathbf{P}^2 \right] + V(\mathbf{r}) + C(\mathbf{l}\mathbf{s}),$$

where a phenomenological spin-orbit interaction term has been included in order to obtain proper shell structure in the limit of spherical symmetry. $M(\mathbf{r})$ is given by (5) and $V(\mathbf{r})$ is the anisotropic oscillator potential

$$(7) \quad V(\mathbf{r}) = -V_0 + \frac{M_0}{2} (\omega_x^2 x^2 + \omega_y^2 y^2 + \omega_z^2 z^2).$$

The non-static Hamiltonian (6) reduces to that employed by NILSSON for $a = 0$ and $V_0 = 0$. Nilsson's Hamiltonian contains, however, an additional centrifugal term $D\mathbf{l}^2$, which serves to depress the higher angular momentum states and deforms the oscillator shape so that it gives slower raising of the oscillator walls at larger distances. The spectrum will then be intermediate between those of the harmonic oscillator and square well potentials. As will be shown below, an effect of this type and of the right magnitude is automatically included in the non-static part of the Hamiltonian (6), so that there is no need to introduce an extra centrifugal term.

Contrary to the static case, it is necessary in the non-static model to include a finite potential well depth V_0 , because the energy spectrum is then no longer invariant with respect to translations on the energy scale. The influence of V_0 represents generally the effect of the non-static interaction with infinitely extended nuclear matter and can in the effective mass approximation be described by a constant mass reduction (7) $M^*/M_0 = [1 + (a^2 M_0 / 2\hbar^2) V_0]^{-1}$. With the oscillator potential this is equivalent to an increase in the oscillator level spacing (3): $\omega^*/\omega = (M_0/M^*)^{1/2}$. Thus, the effect of V_0 can be represented by the replacement of M_0 by M^* or, equivalently, ω by ω^* .

With rotational symmetry about the z -axis, we have

$$(8) \quad \omega_x^2 = \omega_y^2 = \omega_0^2(1 + \varepsilon); \quad \omega_z^2 = \omega_0^2(1 - 2\varepsilon)$$

and

$$(9) \quad V(\mathbf{r}) = -V_0 + \frac{M_0 \omega_0^2}{2} [r^2 + \varepsilon(x^2 + y^2 - 2z^2)],$$

$$(10) \quad \frac{M_0}{M(\mathbf{r})} = 1 + \frac{a^2 M_0}{2\hbar^2} V_0 - \frac{a^2 M_0 \omega_0^2}{4\hbar^2} [r^2 + \varepsilon(x^2 + y^2 - 2z^2)].$$

With the substitution $\mathbf{p} = (\xi, \eta, \zeta) = (M^* \omega_0^* / \hbar)^{\frac{1}{2}} \mathbf{r}$ and $\varkappa^2 = \frac{1}{8} M_0 \omega_0^2 a^2$, we get

$$(11) \quad \frac{M^*}{M(\mathbf{r})} = 1 - \frac{2\varkappa^2}{\hbar \omega_0^*} [\varrho^2 + \varepsilon(\xi^2 + \eta^2 - 2\zeta^2)] = 1 - \frac{2\varkappa^2}{\hbar \omega_0^*} \varrho^2 \left[1 - \varepsilon 4 \sqrt{\frac{\pi}{5}} Y_{20} \right],$$

$$(12) \quad V(\mathbf{r}) = -V_0 + \frac{\hbar \omega_0^*}{2} [\varrho^2 + \varepsilon(\xi^2 + \eta^2 - 2\zeta^2)] = -V_0 + \frac{\hbar \omega_0^*}{2} \varrho^2 \left[1 - \varepsilon 4 \sqrt{\frac{\pi}{5}} Y_{20} \right].$$

The Hamiltonian becomes

$$(13) \quad H = -V_0 - \frac{\hbar \omega_0^*}{8} \left[\Delta \frac{M^*}{M(\mathbf{r})} + 2\nabla \frac{M^*}{M(\mathbf{r})} \nabla + \frac{M^*}{M(\mathbf{r})} \mathbf{J} \right] + \\ + \frac{\hbar \omega_0^*}{2} \varrho^2 \left(1 - \varepsilon 4 \sqrt{\frac{\pi}{5}} Y_{20} \right) + C(\mathbf{ls})$$

or

$$(14) \quad H = -V_0 + \frac{\hbar \omega_0^*}{2} [-\Delta + \varrho^2] + \frac{\varkappa^2}{4} [\Delta \varrho^2 + 2\nabla \varrho^2 \nabla + \varrho^2 \Delta] - \\ - 2\varepsilon \hbar \omega_0^* \sqrt{\frac{\pi}{5}} \varrho^2 Y_{20} - \varepsilon \varkappa^2 \sqrt{\frac{\pi}{5}} [\Delta \varrho^2 Y_{20} + 2\nabla \varrho^2 Y_{20} \nabla + \varrho^2 Y_{20} \Delta] + C(\mathbf{ls}).$$

The deformation parameter ε is approximately related to the β of Bohr and Mottelson by $\varepsilon \approx \sqrt{5/4\pi} \beta$ (*).

The Hamiltonian (14) reduces for $\varkappa^2 = 0$ to that of the static problem treated by NILSSON, and for $\varepsilon = 0$ to that of the non-static isotropic oscillator considered in reference (3). The characteristic feature of the present problem is the occurrence of the term $\sim \varepsilon \varkappa^2$, which describes a coupling between the non-static effects and the nuclear deformation.

4. – Reduction to an approximately equivalent static problem.

We now consider the eigenvalue problem of the Hamiltonian (14). The last four terms of (14) are treated as perturbations of the first two terms, which represent an isotropic harmonic oscillator. The unperturbed problem is

(*) The condition of constant nuclear volume required by nuclear incompressibility, $\omega_x \omega_y \omega_z = \text{const.}$, leads to an ε -dependence of ω_0 of the form $\omega_0(\varepsilon) = \dot{\omega}_0 [1 - 3\varepsilon^2 - 2\varepsilon^3]^{-\frac{1}{2}}$ and in the following ω_0 can, if necessary, always be understood to be $\omega_0(\varepsilon)$.

degenerate in $N = 2n+l$ and the eigenvalues have to be obtained by a diagonalization of the perturbation Hamiltonian. Like NILSSON, we choose a simultaneous diagonal representation, denoted by $|M\Lambda\Sigma\rangle$, of $\frac{1}{2}\hbar\omega_0^*(-\Delta + \varrho^2)$, \mathbf{k}^2 , l_z and s_z with quantum numbers N , l , Λ , Σ , respectively. In this representation, the matrix elements of the different parts of H are given by:-

$$(15) \quad \langle -\Delta + \varrho^2 \rangle = 2N + 3,$$

$$(16) \quad \langle \Delta \varrho^2 + 2\nabla \varrho^2 \nabla + \varrho^2 \Delta \rangle = -2[N(N+3) + l(l+1) + \frac{9}{2}],$$

$$(17) \quad \left\langle \sqrt{\frac{\pi}{5}} \varrho^2 Y_{20} \right\rangle = \begin{cases} \frac{1}{2} \frac{l(l+1) - 3\Lambda^2}{(2l-1)(2l+3)} \left(N + \frac{3}{2} \right); & (l' = l) \\ -\frac{3}{4(2l-1)} (N-l+2)^{\frac{1}{2}} (N+l+1)^{\frac{1}{2}} \cdot \\ \cdot \left[\frac{[(l-1)^2 - \Lambda^2][l^2 - \Lambda^2]}{(2l-3)(2l+1)} \right]^{\frac{1}{2}}; & (l' = l-2). \end{cases}$$

We further have

$$(18) \quad \langle \Delta \varrho^2 Y_{20} + 2\nabla \varrho^2 Y_{20} \nabla + \varrho^2 Y_{20} \Delta \rangle = 4 \langle \varrho^2 Y_{20} \Delta \rangle.$$

With

$$(19) \quad \langle \varrho^2 Y_{20} \Delta \rangle = \langle \varrho^4 Y_{20} \rangle - (2N+3) \langle \varrho^2 Y_{20} \rangle$$

and

$$(20) \quad \langle \varrho^4 Y_{20} \rangle = \frac{3}{2} \langle \varrho^2 Y_{20} \rangle \cdot \begin{cases} N + \frac{3}{2} - \frac{1}{3} \frac{l(l+1) - \frac{3}{4}}{N + \frac{3}{2}}; & (l' = l) \\ N + \frac{3}{2}; & (l' = l \pm 2) \end{cases}$$

we obtain

$$(21) \quad \langle \Delta \varrho^2 Y_{20} + 2\nabla \varrho^2 Y_{20} \nabla + \varrho^2 Y_{20} \Delta \rangle =$$

$$= -2 \langle \varrho^2 Y_{20} \rangle \begin{cases} N + \frac{3}{2} + \frac{l(l+1) - \frac{3}{4}}{N + \frac{3}{2}}; & (l' = l) \\ N + \frac{3}{2}; & (l' = l \pm 2). \end{cases}$$

Matrix elements between states with different N have been neglected. The

matrix elements of the total Hamiltonian are then given by

$$(22) \quad \langle H \rangle = -V_0 + C(\mathbf{ls}) + (N + \frac{3}{2})\hbar\omega_0^* +$$

$$+ \frac{3\hbar\omega_0}{2(2l+3)}(N-l)^{\frac{1}{2}}(N+l+3)^{\frac{1}{2}} \left[\frac{[(l+1)^2 - A^2][(l+2)^2 - A^2]}{(2l+1)(2l+5)} \right]^{\frac{1}{2}} \cdot \varepsilon \left[\frac{\omega_0^*}{\omega_0} - \frac{\varkappa^2}{\hbar\omega_0} \left(N + \frac{3}{2} \right) \right]; \quad (l' = l+2)$$

$$+ \left[-\frac{\varkappa^2}{2} \left[N(N+3) + l(l+1) + \frac{9}{2} \right] - \frac{l(l+1)-3A^2}{(2l-1)(2l+3)} \left(N + \frac{3}{2} \right) \hbar\omega_0 \right. \\ \left. + \varepsilon \left[\frac{\omega_0^*}{\omega_0} - \frac{\varkappa^2}{\hbar\omega_0} \left(N + \frac{3}{2} \right) \right] + \frac{\varepsilon\varkappa^2}{4} [l(l+1)-3A^2]; \quad (l' = l) \right]$$

$$+ \frac{3\hbar\omega_0}{2(2l-1)}(N-l+2)^{\frac{1}{2}}(N+l+1)^{\frac{1}{2}} \left[\frac{[(l-1)^2 - A^2][l^2 - A^2]}{(2l-3)(2l+1)} \right]^{\frac{1}{2}} \cdot \varepsilon \left[\frac{\omega_0^*}{\omega_0} - \frac{\varkappa^2}{\hbar\omega_0} \left(N + \frac{3}{2} \right) \right]; \quad (l' = l-2).$$

The exact diagonalization of the matrices (22) would be in most cases a very tedious task, which could only be carried out numerically. This has been done by NILSSON for the static problem. The non-static problem could thus be considered to be solved, if the non-static effects can be described in terms of a general modification of the static solution, which could be applied after the diagonalization of the static matrices has been carried out. This is indeed approximately the case:

When the coupling terms $\sim \varepsilon\varkappa^2$ are neglected, the problem reduces to a static one with a modified deformation parameter, $\varepsilon(\omega_0^*/\omega_0)$. This modification is entirely due to the increased level spacing in the non-static problem, or to the reduction M^*/M_0 of the nucleon mass.

When the coupling terms $\sim \varepsilon\varkappa^2$ are taken into account, the non-static problem cannot be exactly reduced to an equivalent static one. In a good approximation, however, the term $(\varepsilon\varkappa^2/4)[l(l+1)-3A^2]$, the mean value of which vanishes, can be neglected. Then the non-static effects can again be described by a modification of the deformation parameter, given by

$$(23) \quad \varepsilon^* = \varepsilon \left[\frac{\omega_0^*}{\omega_0} - \frac{\varkappa^2}{\hbar\omega_0} \left(N + \frac{3}{2} \right) \right].$$

If we further identify Nilsson's coefficient D by

$$(24) \quad D = -\frac{\varkappa^2}{2},$$

(see below), the non-static problem is in the approximation mentioned equivalent to the static problem, as treated by NILSSON, with the «effective deformation parameter» ε^* substituted for ε , and with a shift of the unperturbed oscillator levels by the amount

$$(25) \quad -V_0 + \left(N + \frac{3}{2} \right) \hbar\omega_0 \left(\frac{\omega_0^*}{\omega_0} - 1 \right) - \frac{\kappa^2}{2} \left[N(N+3) + \frac{9}{2} \right],$$

the effects of which have been discussed previously (3).

All numerical estimates of the parameter values will be based on the mass reduction $M^*/M_0 = 0.5$, which was obtained by Brueckner (2) from a self-consistent calculation for the infinite nucleus and is also supported by empirical evidence (*). Hence we obtain

$$(26) \quad \frac{\omega_0^*}{\omega_0} = \sqrt{2}; \quad \frac{\kappa^2 V_0}{(\hbar\omega_0)^2} = 0.25.$$

For the oscillator parameters, we use the values derived previously (9)

$$(27) \quad V_0 = 94 \text{ MeV}; \quad \hbar\omega_0^* = \frac{82 \text{ MeV}}{A^{1/3}},$$

The non-local range parameter becomes $a = 0.94 \cdot 10^{-13}$ cm. Finally, we assume $C = -\lambda(\hbar\omega_0)^2/4M_0c^2$, with $\lambda = 25$ (3). Using (24), we then obtain for Nilsson's parameters

$$(28) \quad \begin{cases} \kappa_{(N)} = -\frac{1}{2} \frac{C}{\hbar\omega_0} = \frac{\lambda}{8M_0c^2} \hbar\omega_0 \\ \mu = \frac{2D}{C} = \frac{4M_0c^2}{\lambda(\hbar\omega_0)^2} \kappa^2. \end{cases}$$

For $A = 100$, we have $\hbar\omega_0 = 12.5$ MeV and $\kappa^2 = 0.416$ MeV. Hence we get

$$\kappa_{(N)} = 0.04; \quad \mu = 0.40,$$

to be compared with Nilsson's values

$$\kappa_{(N)} = 0.05; \quad \mu = 0.35 \div 0.45.$$

This numerical agreement gives the possibility of an approximate quantitative derivation of the nucleon energy levels of the non-static problem from those given by NILSSON.

(*) Cf. the literature given in reference (3).

(9) W. E. FRAHN and R. H. LEMMER: *Nuovo Cimento* (in course of publication).

An estimate of the effective deformation parameter can be obtained with the approximate relation $(N+3/2)\hbar\omega_0^* \approx V_0 - E_b$ (E_b = binding energy). Then we get from (23):

$$(29) \quad \varepsilon^* = \varepsilon \frac{\omega_0^*}{\omega_0} \left[1 - \frac{\varepsilon^2}{(\hbar\omega_0^*)^2} (V_0 - E_b) \right] = \varepsilon \left(\frac{M_0}{M^*} \right)^{1/2} \left[1 - \frac{1}{4} \left(1 - \frac{M^*}{M_0} \right) \left(1 - \frac{E_b}{V_0} \right) \right].$$

The non-static modification of the deformation parameter is therefore a function of the mass reduction alone and it is always $\varepsilon^* \geq \varepsilon$ for $M^* \leq M_0$. With $M^*/M_0 = 0.5$ and $E_b = 10$ MeV, we obtain

$$(30) \quad \varepsilon^* = 1.26 \varepsilon.$$

5. – Conclusions.

The effects of a non-local interaction on the motion of individual nucleons in deformed nuclei have been studied in the effective mass approximation for the case of a spheroidal oscillator potential. It has been shown, that the main effect of the non-locality consists of a modification of the deformation parameter. The estimate (30) indicates, that for a given empirical measure of nuclear deformation (obtained for instance from the observed quadrupole moments) the «intrinsic» deformation ε of the potential required in the non-static model is about 20% smaller than that of the corresponding static case.

* * *

The authors are indebted to Dr. S. J. DU TOIT, head of the Nuclear Physics Division, for his interest and to the South African Council for Scientific and Industrial Research for permission of publication.

RIASSUNTO (*)

Un'equazione d'onda generalizzata per particelle singole si deriva nell'approssimazione della massa effettiva partendo da una matrice potenziale per l'interazione nucleone-nucleo come richiesto dai lavori recenti sul problema nucleare di più corpi. La massa nucleonica effettiva che compare nell'operatore dell'energia cinetica di questa equazione dipende dalla forma del potenziale locale che si ritiene essere il limite statico dell'interazione non locale. Gli effetti non statici sul moto dei singoli nucleoni nei nuclei non sferici sono illustrati ricorrendo a un potenziale oscillante sferoidale. Con un trattamento perturbativo del problema dell'autovalore dell'energia si dimostra che il problema non statico è approssimativamente equivalente a un problema statico con parametro di deformazione modificato.

(*) Traduzione a cura della Redazione.

Strange-Particle Effects in *S*-Wave Pion-Nucleon Scattering.

J. S. LANGER

Department of Mathematical Physics - University of Birmingham

(ricevuto il 10 Giugno 1957)

Summary. — An attempt is made to explain the isotopic-spin splitting of the *S*-wave phase shifts in pion-nucleon scattering in terms of virtual strange-particle effects. A very simple calculation is found to agree quite well with experiment.

Although pseudoscalar meson theory has achieved considerable success in reproducing the large *P*-wave phase shifts in meson-nucleon scattering, it has so far not been able to explain certain features of the *S*-wave data. In particular, the observed splitting of the two isotopic-spin states is not evident in any simple form of the present theory. It has been suggested that this discrepancy may be explained in terms of virtual strange-particle effects. The purpose of this paper is to investigate the possibility of including these effects in a scattering formalism, and to present a tentative and very simple solution which shows surprisingly good agreement with experiment.

The familiar form of the *S*-wave interaction resulting from a Foldy-Dyson transformation of the pseudoscalar Hamiltonian includes the terms $\lambda_0 \varphi^2 + \lambda_1 \boldsymbol{\tau} \cdot \boldsymbol{\varphi} \times \boldsymbol{\pi}$, where $\lambda_0 = g^2/2m$, $\lambda_1 = g/2m$ and g is the pseudoscalar coupling constant. Although the φ^2 term gives far too great a scattering in Born approximation, it is well understood that it actually corresponds to a strong but very short-ranged effective potential, and that a more exact treatment yields phase shifts of the correct order of magnitude. Nevertheless, a term of this size will still dominate the low-energy scattering and can never give the correct isotopic spin dependence. Unless the scattering matrix passes through zero or infinity at a total energy less than the meson rest mass, causing one of the phase shifts to change sign, it would seem that, for some reason, the φ^2 term plays almost no part in the interaction. DRELL, FRIEDMAN and

ZACHARIASEN⁽¹⁾ have used the above interaction in a Chew-Low type of calculation, treating the λ 's as completely adjustable parameters. They find that they can fit the data quite well by choosing the (renormalized) $\lambda_s^{(R)}$ to be only $\mu/2m$ times its original value relative to λ_1 . The hypothesis of this paper is that this reduction may be at least partly due to strange particle effects.

The interaction scheme that will be used here corresponds to the Lagrangian density:

$$(1) \quad \left\{ \begin{array}{l} \mathcal{L} = \mathcal{L}_0 - g_1 \bar{\psi}_N \gamma_5 \boldsymbol{\tau} \psi_N \cdot \boldsymbol{\varphi}_\pi + i g_2 \bar{\Psi}_\Sigma \gamma_5 \times \boldsymbol{\Psi}_\Sigma \cdot \boldsymbol{\varphi}_\pi - \\ - g_3 (\bar{\psi}_N \gamma_5 \boldsymbol{\tau} \varphi_K \cdot \boldsymbol{\Psi}_\Sigma + \bar{\Psi}_\Sigma \bar{\varphi}_K \gamma_5 \cdot \boldsymbol{\tau} \psi_N), \end{array} \right.$$

where \mathcal{L}_0 includes the usual expressions for the free fields. It has been assumed that the π -meson has no direct interaction with the K, that there is only one K-meson which has spin zero and negative parity relative to the Σ , that the Σ has spin $\frac{1}{2}$, and that Λ and Ξ particles may be neglected. The π - Σ interaction has been chosen in complete analogy to the π -N interaction with $g_1^2/4\pi = g_2^2/4\pi \approx 15$. Throughout this paper, g_3 , the coupling constant corresponding to production of strange particles, will be assumed to be considerably smaller than g_1 or g_2 . Except for the neglect of Λ and Ξ particles, which is in no way essential to the argument, all of the above assumptions are in accord with the scheme suggested by GELL-MANN and SCHWINGER at the 1957 Rochester Conference. Using the technique devised by SCHWINGER⁽²⁾ one can derive a formidable set of covariant, coupled, integral equations which relate the various scatterings that can take place between the four particles. An outline of this derivation is given in the Appendix. The first of these equations may be written symbolically in the form:

$$(2) \quad T^{rs}(N\pi|N\pi) = V^{rs}(N\pi|N\pi) + V^{rk}(N\pi|N\pi) \Delta(\pi) S(N) T^{ks}(N\pi|N\pi) + \\ + V^{sk}(N\pi|N\pi) \Delta(\pi) S(N) T^{kr}(N\pi|N\pi) + V^{rx}(N,\pi|\Sigma K) \Delta(K) S(\Sigma) T^{\alpha s}(\Sigma K|N\pi) + \\ + V^{s\alpha}(N\pi|\Sigma K) \Delta(K) S(\Sigma) T^{\alpha r}(\Sigma K|N\pi) + \dots$$

Here, the T 's are the usual covariant scattering matrices describing transitions between the sets of particles indicated inside the parentheses to the right and left of the vertical line. Δ and S are the Boson and Fermion propagators respectively. The superscripts are the Boson isotopic-spin indices. Several terms involving expressions of the form $\delta T / \delta \langle \varphi \rangle$ have not been written out explicitly, and are indicated by $+ \dots$. This equation, along with the definition

⁽¹⁾ S. D. DRELL, M. H. FRIEDMAN and F. ZACHARIASEN: *Phys. Rev.*, **104**, 236 (1956).

⁽²⁾ J. S. SCHWINGER: *Proc. Am. Acad. Sci.*, **37**, 452 (1951).

of the V 's, is written in terms of Feynman diagrams in Fig. 1. The next equation will be used to provide an expression for $T(\Sigma K | N\pi)$.

$$(3) \quad T^{\alpha\gamma}(\Sigma K | N\pi) = V^{\alpha r}(\Sigma K | N\pi) + V^{\alpha k}(\Sigma K | N\pi) A(\pi) S(N) T^{kr}(N\pi | N\pi) + \\ + V^{kr}(\Sigma\pi | \Sigma\pi) A(\pi) S(\Sigma) T^{sk}(\Sigma K | N\pi) + V^{\beta r}(\Sigma K | N\pi) A(K) S(N) T^{\alpha\beta}(NK | NK) + \\ + V^{\alpha\beta}(\Sigma K | \Sigma K) S(\Sigma) A(K) T^{\beta r}(\Sigma K | N\pi) + \dots.$$

The third equation for $T(NK | NK)$ will not be needed.

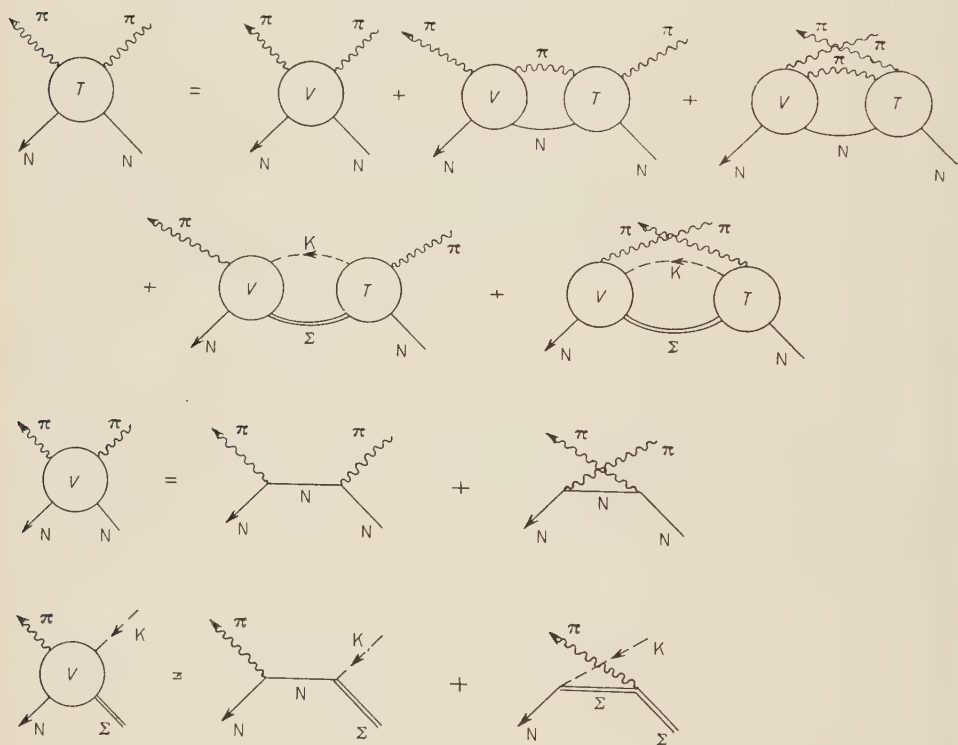


Fig. 1.

It is hardly necessary to say that is it impracticable to solve these equations as they stand. One might first note that the last two terms in (3) are smaller than the preceding ones by a factor $(g_3/g_1)^2$, and may perhaps be neglected. There remains an unrenormalized integral equation for $T(\Sigma K | N\pi)$. A no-recoil approximation is out of the question because the kernel corresponds to intermediate states with two π 's and a K in the field at the same time. In the following calculation, $T(\Sigma K | N\pi)$ will be approximated by the remaining

inhomogeneous terms in (3); that is:

$$(3') \quad T^{\alpha r}(\Sigma K | N\pi) \simeq V^{\alpha r}(\Sigma K | N\pi) + V^{\alpha k}(\Sigma K | N\pi) A(\pi) S(N) T^{kr}(N\pi | N\pi).$$

It is not at all clear to what extent this approximation is valid. If the reaction $\pi + N \rightarrow K + \Sigma$ goes through an effective δ -function potential in the S -wave as does $\pi + N \rightarrow \pi + N$, then the R.H.S. of (3') is probably too large. On the other hand, due to the assumed small value of g_3 relative to g_1 and the large mass of the K-meson, the two processes may not be strictly comparable. In any case, (3') can be expected to show the correct sign and isotopic spin behaviour.

On substituting (3') into (2), one arrives at the equation:

$$(4) \quad T^{rs}(N\pi | N\pi) = U^{rs}(N\pi | N\pi) + U^{rk}(N\pi | N\pi) S(N) A(\pi) T^{ks}(N\pi | N\pi) + \\ + U^{sk}(N\pi | N\pi) S(N) A(\pi) T^{kr}(N\pi | N\pi),$$

where

$$(5) \quad U^{rs}(N\pi | N\pi) = V^{rs}(N\pi | N\pi) + V^{r\alpha}(N\pi | \Sigma K) A(K) S(\Sigma) V^{\alpha s}(\Sigma K | N\pi) + \\ + V^{s\alpha}(N\pi | \Sigma K) A(K) S(\Sigma) V^{\alpha r}(\Sigma K | N\pi).$$

((Note that it is necessary to include some of the $\delta T \delta \varphi$ terms in order to derive (4) exactly). U is just the lowest order Born approximation to pion-nucleon scattering plus its first radiative corrections due to heavy mesons only.

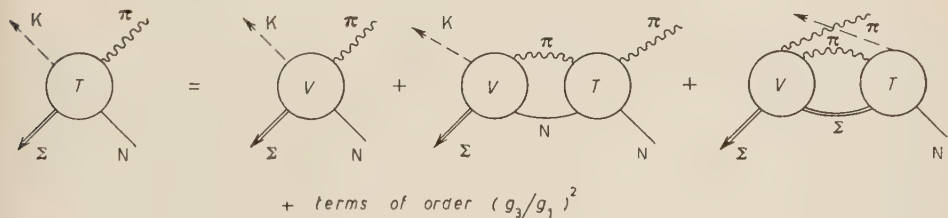


Fig. 2.

Since only pions occur in the intermediate states in equation (4), a no-recoil approximation for the nucleon should be reasonably accurate. Separating out the S -wave part, and assuming that the integration over meson momenta cuts off at some value Λ of the order of the nucleon mass, m , one gets the simple algebraic relationship:

$$(6) \quad T_s^{rs}(\omega) = U_s^{rs}(\omega) - U_s^{ri}(\omega) \int_{k^2 = \omega^2 - \mu^2}^{\Lambda^2} \frac{d^3 k}{i\varepsilon} T_s^{is}(\omega) + \text{crossed terms}, \quad \omega \ll m,$$

where ω is the total energy of the meson. $U^{rs}(\omega)$ has been evaluated from (5) by covariant integration and then, i.e. after renormalization, expanded in powers of ω . Renormalization of vertex parts has been performed in such a way that radiative corrections vanish at the unphysical point where the three particles satisfy $i\mathbf{p} + m = i\mathbf{p}' + m = 0$, $(p - p')^2 + \mu^2 = 0$. This is consistent with the definition of the P -wave coupling constant given by CHEW and LOW⁽³⁾.

The result of this calculation is:

$$(7) \quad U^{rs}(\omega) = \frac{g_s \delta_{rs}}{m(2\pi)^4} \left(\frac{1.76 g_s^2}{4\pi^2} - 1 \right) + \frac{g_s^2 [\tau_r, \tau_s]}{m^2 (2\pi)^4} \left(\frac{\mu^2}{4\omega} + \frac{0.52 g_s^2}{4\pi^2} \right).$$

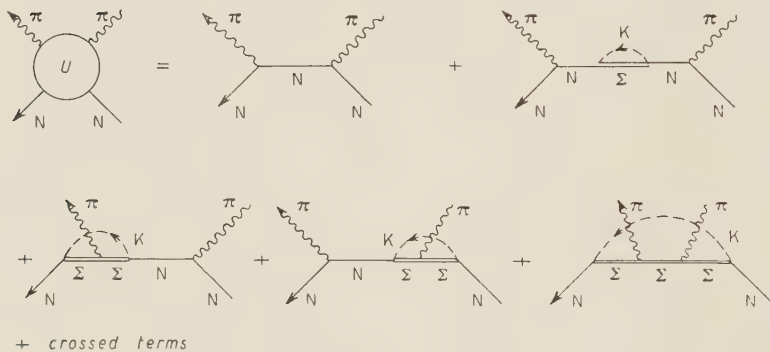


Fig. 3.

The numerical factors come from Feynman integrals involving masses of N, Σ , K, π . For the choice $g_s^2/4\pi = 1.8$, the term proportional to δ_{rs} vanishes. This cancellation is a direct result of the assumption that the K-meson has negative parity relative to the Σ particle. If the opposite parity is assumed, the cancellation does not occur. The remaining term is small and strongly isotopic-spin dependent. If it is inserted into (6), it is obvious that $T = U$ to a good approximation. The resulting expression for the phase shift,

$$(8) \quad \delta_T \cong \frac{g_s^2 \omega k n_T}{2(2\pi)^2 m^2} \cong 0.05 \frac{k}{\mu} n_T, \quad n_T = \begin{cases} +2 & \text{for } T = \frac{1}{2}, \\ -1 & \text{for } T = \frac{3}{2}, \end{cases}$$

shows the correct isotopic-spin splitting and is actually somewhat too small.

The essence of the above technique is the construction of an effective pion-nucleon potential $U_s^{rs}(\omega)$ which may be used in the Schrödinger equation (6). It seems fairly clear that a potential of the form derived here does produce the correct S -wave scattering at low energies. There remains the question of

⁽³⁾ G. F. CHEW and F. E. LOW: *Phys. Rev.*, **101**, 1570 (1956).

whether this treatment of strange-particle effects is consistent with the *P*-wave data. In view of the fact that the (3, 3) scattering is dominated by a pion resonance which cannot be expected to recur in the K-meson scattering at these energies, and that the other *P* phase shifts are so poorly known experimentally, it is felt that there are no real objections here. A more serious attempt at fitting the data must wait until more is known about the strange particles. Meanwhile, one must consider it possible that their effects are significant even at the lowest energies.

* * *

I should like to thank Professor R. E. PEIERLS, Dr. S. F. EDWARDS and Dr. P. T. MATTHEWS for suggesting this problem and for many helpful discussions. I should also like to acknowledge the award of a scholarship from the Marshall Aid Commemoration Commission.

APPENDIX

Derivation of the integral equations.

Following Schwinger's technique and notation, the «source» term, $\bar{\eta}\psi_N - \psi_N\eta - J\varphi_\pi + K\varphi_K + \bar{q}_K K$ are added to the Lagrangian (1). The equation for the true nucleon propagator, $S'_N(x, x')$, is

$$(A.1) \quad \left[S_N^{-1} + g_1\gamma_5\tau^j \left(\langle \varphi_\pi^j \rangle - i \frac{\delta}{\delta J^j} \right) \right] S'_N(x, x') = \delta(x - x') - g_3\tau^j\gamma_5 \frac{\delta}{\delta\eta(x')} \langle q_K\psi_\Sigma^j \rangle - \\ = \delta(x - x') - ig_3\tau^j\gamma_5 \langle (\varphi_K(x)\psi_\Sigma^j(x)\bar{\psi}_N(x'))_+ \rangle + ig_3\tau^j\gamma_5 \langle \varphi_K\psi_\Sigma^j \rangle \langle \bar{\psi}_N \rangle ,$$

where $S_N^{-1} = \gamma^\mu(\partial/\partial x_\mu) + m_N$, and all but isotopic-spin vector indices have been suppressed. The second term on the R.H.S. may be rewritten using the relationships:

$$\langle (\varphi_K(x)\psi_\Sigma^j(x)\bar{\psi}_N(x'))_+ \rangle = \langle \varphi_K(x) \rangle \langle (\psi_\Sigma^j(x)\bar{\psi}_N(x'))_+ \rangle - i \frac{\delta}{\delta K(x)} \langle (\psi_\Sigma^j(x)\bar{\psi}_N(x'))_+ \rangle , \\ \frac{\delta \langle \bar{\varphi}_K(x) \rangle}{\delta K(y)} = \Delta_K(x, y) ,$$

the K-meson propagator and the definition:

$$(A.2) \quad S'_{\Sigma N}^j(x, x') \equiv i \langle (\psi_\Sigma^j(x)\bar{\psi}_N(x'))_+ \rangle - i \langle \psi_\Sigma^j(x) \rangle \langle \bar{\psi}_N(x') \rangle .$$

Substituting these into (A.1) and dropping terms which vanish when $\eta \rightarrow 0$, $K \rightarrow 0$, we get:

$$(A.3) \quad \left[S_N^{-1} + g_1 \gamma_5 \tau^j \left(\langle \varphi_\pi^j \rangle - i \frac{\delta}{\delta J^j} \right) \right] S'_N(x, x') = \delta(x - x') + \\ + ig_3 \tau^j \gamma_5 \int \Delta_K(x, y) \frac{\delta S'_N(x, x')}{\delta \langle \varphi_K(y) \rangle} d^4y .$$

A similar equation may be derived for $S'_{\Sigma N}$.

$$(A.4) \quad S_{\Sigma N}^{-1} + ig_2 \epsilon_{ijk} \gamma_5 \left(\langle \varphi_\pi^i \rangle - i \frac{\delta}{\delta J^i} \right) S'_{\Sigma N}(x, x') = \\ = -g_3 \tau^j \gamma_5 \left[\langle \overline{\varphi}_K \rangle S'_N(x, x') - i \int \Delta_K(x, y) \frac{\delta S'_N(x, x')}{\delta \langle \varphi_K(y) \rangle} d^4y \right] .$$

Returning to the simplified notation used above (the particle subscripts go into parentheses), the relevant T matrices are expressed as follows

$$(A.5) \quad \begin{cases} T^{rs}(N\pi | N\pi) \equiv -i(S(N))^{-1} \frac{\delta^2 S^1(N)}{\delta \langle \varphi_\pi^r \rangle \delta \langle \varphi_\pi^s \rangle} (S'(N))^{-1}, \\ T^{\alpha s}(\Sigma K | N\pi) \equiv -i(S'(\Sigma))^{-1} \frac{\delta^2 S'(\Sigma N)}{\delta \langle \varphi_K^\alpha \rangle \delta \langle \varphi_\pi^s \rangle} (S'(N))^{-1}. \end{cases}$$

After operating to the left on (A.2) and (A.3) with $S(N)$ and $S(\Sigma)$ respectively, iterating once, applying (A.5), and combining terms, the resulting equation is:

$$(A.6) \quad T^{rs}(N\pi | N\pi) = (S'(N))^{-1} S(N) \{ V^{rs}(N\pi | N\pi) + \\ + V^{rk}(N\pi | N\pi) A'(\pi) S'(N) T^{ks}(N\pi | N\pi) + \\ + V^{rs}(N\pi | \Sigma K) A'(\Sigma) S'(\Sigma) T^{\alpha s}(\Sigma K | N\pi) + \text{crossed terms} + \\ + \Sigma_\pi S'(N) T^{rs}(N\pi | N\pi) + \Sigma_K S'(N) T^{rs}(N\pi | N\pi) + \dots \},$$

where

$$\Sigma_\pi = -ig_3^2 \gamma_5 \tau^j S(N) A'(\pi) \gamma_5 \tau^j ,$$

and

$$\Sigma_K = -ig_3^2 \gamma_5 \tau^j S(\Sigma) A'(\Sigma) \gamma_5 \tau^j ,$$

are self energy parts. The « $+ \dots$ » again stands for several terms involving $\delta T/\delta q$ which have been neglected. To the order of this approximation,

$$(A.7) \quad S'(N) \cong S(N) + (\Sigma_\pi + \Sigma_K) S'(N) .$$

A little algebra then shows that the factor $(S'(N))^{-1}S(N)$ exactly cancels the self energy terms in (A.6). Approximating S' and Γ' by S and Γ , one arrives at equation (2). Equation (3) may be derived in exactly the same manner.

RIASSUNTO (*)

Si cerca di spiegare la separazione degli spin isotopici degli sfasamenti dell'onda S nello scattering pion-nucleone in termini di effetti di particelle strane virtuali. Un calcolo semplicissimo si accorda assai bene con l'esperienza.

(*) Traduzione a cura della Redazione.

A Short Lived Isomeric State of ^{208}Bi .

S. DE BENEDETTI (*), U. FARINELLI, F. FERRERO, R. MALVANO,
G. PELLI and C. TRIBUNO

*Istituto di Fisica dell'Università - Torino
Istituto Nazionale di Fisica Nucleare - Sezione di Torino*

(ricevuto l'11 Giugno 1957)

Summary. — A previously known isomeric activity of 2.5 ms from irradiation of Bi has been assigned to ^{208}Bi . The method used was the observation of the excitation curve from betatron radiation on stable Bi: the shape of the curve and its threshold are characteristic of (γ, n) reactions. The problem of the ground state of ^{208}Bi is discussed.

An isomeric half life of 2.7 ms has been excited by VEGORS and AXEL (1) by bombardment of Bi with betatron radiation. An activity of about 2.3 ms was found by IAMPOL'SKII *et al.* (2) by neutron irradiation of Bi. The American authors make no isotopic assignement for their activity, and the Russian workers tentatively attribute theirs to ^{208}Bi since the cross section for its formation is of the proper order for an $(n, 2n)$ reaction. Considering that no information on ^{208}Bi is reported in nuclear tables, we considered of some interest to start the short-lived isomer program of the University of Turin with the assignement of the activity of Bi. This can be done by studying the excitation curve and its threshold, since these are markedly different for (γ, n) (3) and for (γ, γ') (4) reactions.

(*) Fulbright Scholar from Carnegie Institute of Technology, Pittsburgh, Pa.

(1) S. H. VEGORS and P. AXEL: *Phys. Rev.*, **101**, 1067 (1956); see also *Phys. Rev.*, **100**, 1238 (1955).

(2) P. A. IAMPOL'SKII, O. D. LEIPUNSKI, M. I. GEN and A. M. TIKHOMIROV: *Izvest. Akad. Nauk. Ser. Fiz. SSSR*, **19**, 338 (1955), as reported in NRC nuclear cards.

(3) See, for instance, the dotted line in Fig. 2, taken from: F. FERRERO, A. O. HANSON, R. MALVANO and C. TRIBUNO: *Nuovo Cimento*, **4**, 418 (1956).

(4) L. MEYER-SCHÜTZMEISTER and V. L. TELEDGI: *Phys. Rev.*, **104**, 185 (1956).

The activity was excited by the γ -ray beam of our BBC betatron (maximum energy 31 MeV). The method used to detect short lived activities between betatron pulses (20 ms apart) is similar to that of VEGERS and AXEL or of the Iowa group ().

Our instrumentation consisted of a NaI scintillation counter, connected to a flexible 5 channel time discriminator through a one channel differential pulse height selector. The electronics will be described in greater detail in a separate note by one of us (G.P.). The shielding against delayed background (mainly neutrons from the machine) is illustrated in Fig. 1, and consisted of a 60 cm H_2O wall covered with H_3BO_3 panels. The γ beam was caught in a water catcher; the counter was located near the beam and surrounded by organic material, H_3BO_3 and Pb.

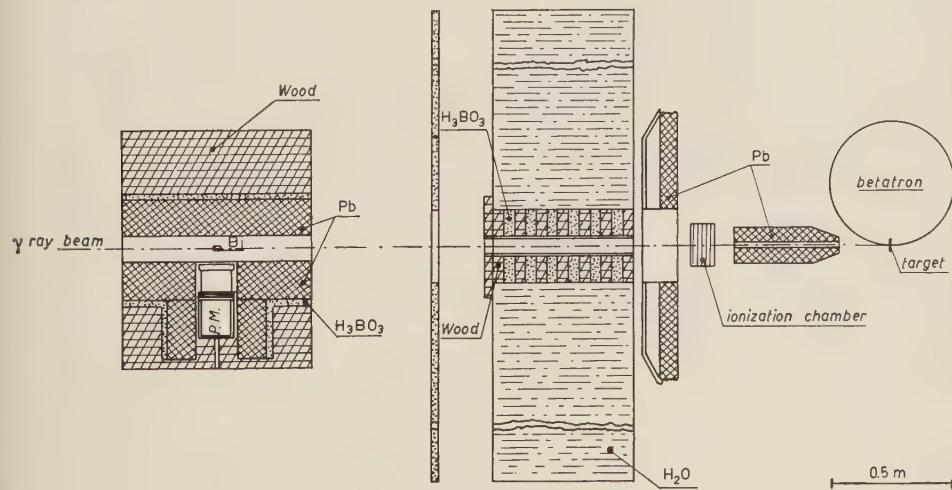


Fig. 1.

The half life discovered by VEGERS and AXEL was easily recognized but, despite the precaution, numerous sources of background were present. [Not negligible (and quite surprising, since unmentioned by previous workers) was the contribution of the 25 m activity of ^{128}I built up in the scintillator by the bombardment of neutrons from the target. In order to eliminate the short lived background (mostly due to neutrons delayed by time of flight) the counts were started 2.8 ms after the end of each betatron pulse. The counts were recorded on 5 successive channels, 2 ms in duration each, and starting immediately after one another. The long lived background was eliminated by

() A. J. BUREAN and C. L. HAMMER: *Phys. Rev.*, **105**, 1006 (1957).

subtracting either the counts in the last channel from these of the first one, or the counts in the last two channels from those in the first two; the results thus obtained (apart from a constant factor) were the same within statistical accuracy.

The γ -ray dose was measured by means of an ionization chamber, with a 5 cm thick Al converter, whose response has been discussed in a previous paper (⁶). When the counts recorded as described above were normalized to the γ -ray dose, and plotted against betatron energy, the points of Fig. 2 were obtained. The solid curve through these points has the characteristic appearance of a (γ, n) excitation curve, as clearly shown by a comparison with the total photoneutron cross-section for Bi (⁴) (dotted line in Fig. 2, multiplied by a convenient factor). The threshold appears to be shifted some 2 MeV upwards in the isomer excitation curve: this is in rough agreement with the fact that the metastable state is at ~ 1.43 MeV above the ground state of ²⁰⁸Bi, according to the γ' energies measured by VEGORS and AXEL (0.93 MeV and 0.5 MeV, presumably in cascade).

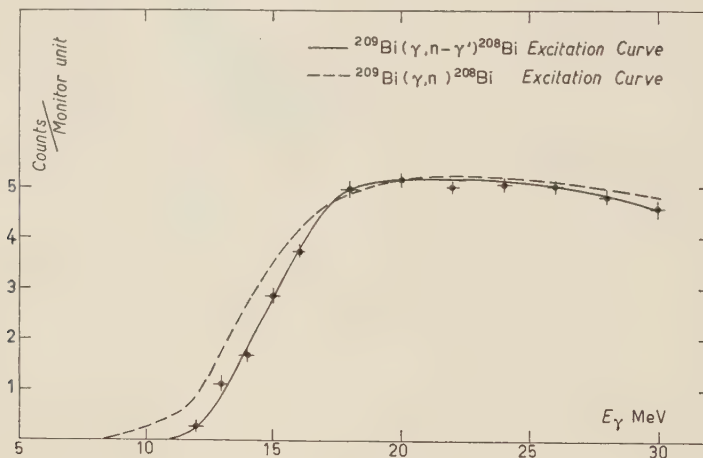


Fig. 2.

The cross-section for the production of the ²⁰⁸Bi isomer was evaluated by comparing the observed 0.5 MeV activity with that of a calibrated source of annihilation radiation (²²Na). The γ' yield at 25 MeV appears to be of the order of $4 \cdot 10^5 \text{ r}^{-1} \text{ mol}^{-1}$. Comparing this value with the corresponding neutron yield from ²⁰⁸Bi at the same energy, which is $2.7 \cdot 10^7 \text{ r}^{-1} \text{ mol}^{-1}$ according to

(⁶) F. FERRERO, R. MALVANO and C. TRIBUNO: *Nuovo Cimento*, **5**, 310 (1956).

MONTALBETTI *et al.* (⁷), the branching ratio for the formation of the isomeric state is found to be of the order of 1.5%.

Though it appears fairly certain that the 2.7 ms activity arises from an excited state of ^{208}Bi , the problems concerning the ground state of this nucleus remained still open. No activity corresponding to ^{208}Bi has ever been observed: the mean life of its ground state is reported to be either shorter than 30 s or much longer than 50 years (⁸).

We have looked for the activity of ^{208}Bi and our measurements rule out the possibility of an electron capture or positron emission of mean life in the range (5–30) s. Considering the energy available for this kind of decay (not more than 2.9 MeV for E.C.) the activity could not be shorter than ~ 10 s. It seems therefore probable that ^{208}Bi has a β life much longer than 50 years.

The energy available for α decay can be calculated from known values of atomic masses, and is of about 3.5 MeV: this corresponds to a mean life in the neighborhood of 10^{10} years. Since ^{208}Bi is not found in nature, it seems reasonable to assume that it decays by electron capture with a very long mean life. This is probably connected with a high value of spin of the ground state of ^{208}Bi , which has a single proton in the $h_{9/2}$ shell, and a single missing neutron in the $i_{13/2}$ shell.

(⁷) R. MONTALBETTI, L. KATZ and J. GOLDEMBERG: *Phys. Rev.*, **91**, 659 (1953).

(⁸) H. M. NEUMANN and I. PERLMAN: *Phys. Rev.*, **81**, 958 (1951).

RIASSUNTO

Un'attività isomerica di 2.5 ms precedentemente osservata nell'irradiazione del Bi è stata assegnata al ^{208}Bi . Il metodo seguito è stato quello di studiare la curva di eccitazione del Bi stabile irradiato con un betatrone: la forma della curva e la relativa soglia sono caratteristiche di reazioni (γ, n). Si discute il problema dello stato fondamentale del ^{208}Bi .

Charge Dependent Corrections to Dispersion Relations (II).

A. AGODI and M. CINI

Istituto di Fisica dell'Università - Catania

Centro Siciliano di Fisica Nucleare - Catania

(ricevuto il 12 Giugno 1957)

Summary. — The effect of the electromagnetic interactions on the dispersion relations for pion proton scattering is investigated. The correction, which can be interpreted as a difference between the coupling constants for positive and negative mesons, attains a maximum value of the order of 5% in the energy range between 50 and 150 MeV, and is therefore by far too small to account for recent experimental indications.

1. — Introduction.

Recent experimental results ⁽¹⁾ have given some indications that dispersion relations for forward scattering of pions on nucleons fail to be satisfied when amplitudes for positive and negative mesons are considered separately. In order to establish if a clear cut discrepancy exists between theory and experiment it seems necessary to examine the possible corrections which can be expected to arise from effects not considered explicitly in the conventional derivation of dispersion relations. Corrections due to the charged-neutral meson mass difference have been found to be negligible ⁽²⁾. Interactions of pions with hyperons have been considered, but the conventional form of dispersion relations is found not to be affected by their presence ⁽³⁾.

In this paper we will consider in detail the effects of electromagnetic interactions, which turn out to be also small, as already anticipated previously ⁽³⁾.

⁽¹⁾ G. PUPPI and A. STANGHELLINI: *Nuovo Cimento*, **5**, 1305 (1957).

⁽²⁾ A. AGODI and M. CINI: *Nuovo Cimento*, **5**, 1257 (1957).

⁽³⁾ A. AGODI, M. CINI and B. VITALE: *7-th Annual Rochester Conference*, 1957; *Phys. Rev.* (in press).

2. - Formal results.

We will follow closely the derivation of the dispersion relations given by GOLDBERGER (4), and introduce explicitly the electromagnetic interaction in the « current » $j_\alpha(x)$ defined by the Heisenberg equation of motion for the meson field $\varphi_\alpha(x)$:

$$(1) \quad (\square - \mu^2)\varphi_\alpha(x) = -j_\alpha(x) \quad (\alpha = 1, 2, 3).$$

It turns out therefore that we can write

$$(2) \quad j_\alpha(x) = j_\alpha^{(0)}(x) + eA_\nu\varepsilon_{\alpha\alpha'}\frac{\partial\varphi_{\alpha'}}{\partial x_\nu} \quad (\alpha, \alpha' = 1, 2, 3) \\ (\nu = 0, 1, 2, 3)$$

where summation over repeated indexes is understood.

Since we are only interested in the corrections to order e^2 , no contribution to $j_\alpha(x)$ from the term

$$e^2 A_\nu A_\nu \varphi^* \varphi$$

in the Lagrangian needs to be taken into account.

Although the current (2) contains also the time derivative of φ_α (which was excluded in G) it is easy to convince oneself that no change in the definitions G(2.13) and G(2.12) of $D_{\alpha\beta}(\omega; \lambda', \lambda)$ and $A_{\alpha\beta}(\omega; \lambda', \lambda)$ arises because

$$(3) \quad \left\{ \begin{array}{l} \delta(x_0)\langle p | [j_\alpha(x), \dot{\varphi}_\beta(0)] | p \rangle = \delta(x_0)\langle p | [\dot{j}_\alpha^{(0)}(x), \dot{\varphi}_\beta(0)] | p \rangle \\ \delta(x_0)\langle p | [j_\alpha(x), \varphi_\beta(0)] | p \rangle = 0 . \end{array} \right.$$

Eq. (3) hold since the states $|p\rangle$ are single nucleon states (with no photons). Therefore also the relations G(2.32) and G(2.33)

$$(4) \quad \left\{ \begin{array}{l} D_{\alpha\beta}^{(1)}(\omega; \lambda', \lambda) - D_{\alpha\beta}^{(1)}(\omega_0; \lambda', \lambda) = \frac{2(\omega^2 - \omega_0^2)}{\pi} \int_0^\infty d\omega' \frac{A_{\alpha\beta}^{(1)}(\omega'; \lambda', \lambda)\omega'}{(\omega'^2 - \omega_0^2)(\omega'^2 - \omega^2)} \\ D_{\alpha\beta}^{(2)}(\omega; \lambda', \lambda) - \frac{\omega}{\omega_0} D_{\alpha\beta}^{(2)}(\omega_0; \lambda', \lambda) = \frac{2\omega(\omega^2 - \omega_0^2)}{\pi} \int_0^\infty d\omega' \frac{A_{\alpha\beta}^{(2)}(\omega'; \lambda', \lambda)}{(\omega'^2 - \omega_0^2)(\omega'^2 - \omega^2)} \end{array} \right.$$

hold in our case.

(4) M. L. GOLDBERGER: *Phys. Rev.*, **99**, 979 (1957); (indicated by G. in the following).

At this stage rather than writing

$$T_{\alpha\beta}(\omega) = \delta_{\alpha\beta} T^{(1)}(\omega) + i\varepsilon_{\alpha\beta\gamma} \tau_\gamma T^{(2)}(\omega)$$

(a relation valid only for a charge independent theory) we use the property that, for charged mesons we can write

$$(5) \quad \begin{cases} D_m = \sum_{\alpha, \beta=1, 2} D_{\alpha\beta} \langle m | \alpha \rangle \langle \beta | m \rangle \\ A_m = \sum_{\alpha, \beta=1, 2} A_{\alpha\beta} \langle m | \alpha \rangle \langle \beta | m \rangle \end{cases} \quad (m = \pm)$$

with

$$(6) \quad \langle m | \alpha \rangle \langle \beta | m \rangle = \frac{1}{2} \delta_{\alpha\beta} + i \frac{m}{2} \varepsilon_{\alpha\beta\gamma} \quad (\alpha, \beta = 1, 2; m = \pm).$$

Then Eq. (5), (6) give immediately

$$(7) \quad D_+ + D_- = D_{11} + D_{22} \quad D_+ - D_- = i(D_{12} - D_{21})$$

and analogous relations for the A_{\pm} . Then Eqs. (2.5) and (2.6) of GMO (3) are obtained:

$$(8) \quad D_{\pm}(\omega) = \frac{1}{2} \left(1 + \frac{\omega}{\mu} \right) D_{\pm}(\mu) - \frac{1}{2} \left(1 - \frac{\omega}{\mu} \right) D_{\mp}(\mu) = \frac{q^2}{\pi} \int_0^{\infty} \frac{d\omega'}{q'^2} \left[\frac{A_+(\omega')}{\omega' \mp \omega} + \frac{A_-(\omega')}{\omega' \pm \omega} \right].$$

At this point we must discuss the behaviour of $A_{\pm}(\omega)$ in the unphysical region $0 < \omega < \mu$. The expression of $A_{\pm}(\omega)$ is again

$$(9) \quad A_{\pm}(\omega) = \pi \sum_n \left\{ |\langle n | j_{\pm}(0) | p \rangle|^2 \delta(M - E_n + \omega) - |\langle n | j_{\mp}(0) | p \rangle|^2 \delta(M - E_n - \omega) \right\} \quad (M = E_p).$$

When the state $|n\rangle$ is a single nucleon state, it is well known that $(M - E_n + \omega)$ can never vanish in the range $0 < \omega < \mu$, while $\delta(M - E_n - \omega)$ becomes $\delta(\omega - (\mu^2/2M))$.

(5) M. L. GOLDBERGER, H. MIYAZAWA and R. OEHME: *Phys. Rev.*, **99**, 986 (1955).

The contribution from this state exists, of course, also in the presence of electromagnetic interactions, and has the usual form

$$(10) \quad A_{\pm}^{(0)} = 0; \quad A_{+}^{(0)} = -2\pi \left(\frac{f}{\mu}\right)^2 q^2 \delta\left(\omega - \frac{\mu^2}{2M}\right)$$

if scattering on protons is considered.

However in our case states $|n\rangle$ with one nucleon and one photon (we work at order e^2) of total momentum \mathbf{q} can also have energies E_n in the range $M < E_n < M + \mu$.

For these two body states it is convenient to introduce the total mass M_n defined by

$$(11) \quad M_n = \sqrt{E_n^2 - q^2}.$$

It is clear that

$$(12) \quad M_n \geq M.$$

The first δ -function in eq. (9) can now vanish when

$$(13) \quad \omega = \frac{M_n^2 - M^2}{2M} - \frac{\mu^2}{2M}$$

while the second δ -function vanishes when

$$(14) \quad \omega = \frac{M^2 - M_n^2}{2M} + \frac{\mu^2}{2M}.$$

Clearly because of relation (12) a contribution to A_{\pm} from the term

$$(15) \quad |\langle n | j_{\pm}(0) | p \rangle|^2 \delta(M - E_n + \omega)$$

arises from the whole range $0 < \omega < \mu$ while the term

$$(16) \quad |\langle n | j_{\mp}(0) | p \rangle|^2 \delta(M - E_n - \omega)$$

contributes only when

$$0 < \omega < \mu^2/2M.$$

We will calculate the correction due to the electromagnetic interactions

in the approximation $M \rightarrow \infty$. Since the correction is expected to be small this approximation is certainly permissible.

Then the term (16) does not contribute at all, and the term (15) gives a contribution $A_-^{(0)}(\omega)$ only to $A_-(\omega)$ since $|n\rangle$ must be a neutron plus photon state.

Therefore, from eq. (10), we have in the unphysical range

$$(17) \quad A_+(\omega) = A_+^{(0)}(\omega); \quad A_-(\omega) = A_-^{(0)}(\omega).$$

3. - Numerical results.

We come now to the explicit evaluation of the corrections.

To obtain an expression for $A_-^{(0)}(\omega)$ in the unphysical range we make an analytic continuation from the values of ω immediately above threshold where

$$(18) \quad A_-^{(0)}(\omega) = \frac{q}{4\pi} \sigma(\pi^- + p \rightarrow n + \gamma).$$

Since at threshold the radiative capture cross-section is proportional to the inverse of the meson velocity q/ω eq. (18) shows that

$$(19) \quad A_-^{(0)}(\omega) = K\omega,$$

where the constant K will be determined from experiment. Clearly the expression (19) for $A_-^{(0)}(\omega)$ can be safely used in the whole unphysical range $0 < \omega < \mu$ without introducing a considerable error. This will be checked by means of the Kroll-Ruderman theorem which allows a determination of K at $\omega = 0$.

At threshold one has ⁽⁶⁾

$$(20) \quad \sigma(\pi^- + p \rightarrow n + \pi^0) = (1.52 \pm 0.27) \sigma(\pi^- + p \rightarrow n + \gamma)$$

and since

$$(21) \quad \lim_{\omega \rightarrow 0} \frac{q}{\omega} \sigma(\pi^- + p \rightarrow n + \pi^0) = \frac{8\pi}{9} A^2 \sqrt{2\varepsilon},$$

where

$$(22) \quad \left\{ \begin{array}{l} \varepsilon = 1 - \mu_0/\mu_c \approx 0.04 \\ A = \frac{\alpha_3 - \alpha_1}{q} \approx \frac{0.27}{\mu}, \end{array} \right.$$

⁽⁶⁾ CASSELS: *Proceedings 6-th Annual Rochester Conference*, 1956, Chap. I, p. 15.

one has easily from (19), (20) and (21)

$$(23) \quad K = \frac{1}{1.52} \frac{2}{9} A^2 \sqrt{2\varepsilon} \approx \frac{0.003}{\mu^2}.$$

From the Kroll-Ruderman theorem one has

$$(24) \quad A_{-}^{(c)} = 4e^2 \frac{f^2}{\mu^2} \omega, \quad \omega \rightarrow 0$$

or

$$(25) \quad K^{(KR)} = \frac{0.003}{\mu^2} \quad \text{with } f^2 \approx 0.10.$$

The agreement between (23) and (25) is quite good.

Dispersion relations now have the form

$$(26) \quad D_{\pm}(\omega) - \frac{1}{2} \left(1 + \frac{\omega}{\mu} \right) D_{\pm}(\mu) - \frac{1}{2} \left(1 - \frac{\omega}{\mu} \right) D_{\mp}(\mu) = \\ = \pm \frac{2f^2}{\mu^2} \frac{q^2}{\omega \mp \mu^2/2M} + \frac{q^2}{4\pi^2} \int_{\mu}^{\infty} d\omega' \left[\frac{\sigma_+(\omega')}{\omega' \mp \omega} + \frac{\sigma_-(\omega')}{\omega' \pm \omega} \right] + K \frac{q^2}{\pi} \int_0^{\mu} \frac{d\omega'}{q'^2} \frac{\omega'}{\omega' \pm \omega}.$$

The last term, however, is not the whole correction we are looking for (it is easily seen in fact that it diverges logarithmically at the upper limit), because one must take into account that the total cross-section σ_-^c introduced in the conventional dispersion relations is not identical to the total cross-section σ_- that appears in the integrals on the r.h.s. of (26). In fact the total cross-section σ_-^c in the conventional case is assumed to remain constant from, say, $\omega = \omega_0$ ($\omega_0 \approx \mu + 30$ MeV) down to $\omega = \mu$, while actually the radiative capture part of σ_- increases approaching threshold according to eqs. (8) and (19).

Therefore comparison with the conventional expressions can be made by writing, in the range $\mu < \omega < \omega_0$

$$(27) \quad \sigma_-(\omega) = \sigma_-^c(\omega) - 4\pi K \frac{\omega_0}{q_0} + 4\pi K \frac{\omega}{q}.$$

The final expression for the electromagnetic correction turns out therefore to be

$$(28) \quad C_{\pm}^{(c)}(\omega) = K \frac{q^2}{\pi} \int_0^{\omega_0} \frac{d\omega'}{q'^2} \frac{\omega'}{\omega' \pm \omega} - K \frac{\omega_0 q^2}{q_0 \pi} \int_{\mu}^{\omega_0} \frac{d\omega'}{q'} \frac{1}{\omega' \pm \omega},$$

which is now obviously finite. The first integral is easily performed and the second one, when $\omega \ll \omega_0$, which is the generally interesting case, can be approximated by taking out of the integral the factor

$$\frac{1}{\bar{\omega} \pm \omega},$$

where $\mu < \bar{\omega} < \omega_0$. In this case one has

$$(29) \quad C_{\mp}^{(\gamma)}(\omega) = \frac{Kq^2}{2\pi} \left\{ \frac{1}{\pm \omega - \mu} \ln \frac{(\omega_0 + \mu)\omega}{|\omega_0 \pm \omega|} + \frac{1}{\pm \omega + \mu} \ln \frac{(\omega_0 - \mu)\omega}{|\omega_0 \pm \omega|} - \frac{2\omega_0}{q_0} \frac{1}{\bar{\omega} \pm \omega} \ln \left(\frac{\omega_0}{\mu} + \sqrt{\left(\frac{\omega_0}{\mu} \right)^2 - 1} \right) \right\}$$

Numerical results are the following

$$\omega = \sqrt{2}\mu : \mu C_{-}^{(\gamma)} = 0.0057; \quad \mu C_{+}^{(\gamma)} = -0.0015,$$

$$\omega = 2\mu : \mu C_{-}^{(\gamma)} = 0.0084; \quad \mu C_{+}^{(\gamma)} = -0.0041.$$

These corrections give rise to a difference, in the conventional dispersion relations, between the coupling constants for positive and negative mesons of the order of 5%, in the energy range between 50 and 150 MeV.

The effect is therefore by far too small to account for the experimental results of the Bologna group.

RASSUNTO

Viene studiato l'effetto delle interazioni elettromagnetiche sulle relazioni di dispersione per lo scattering di pioni da protoni. La correzione, che può essere interpretata come una differenza tra le costanti di accoppiamento per mesoni positivi e negativi, raggiunge un valore minimo del 5% per energia compresa tra i 50 e i 150 MeV, e perciò è di gran lunga troppo piccola per rendere conto di recenti indicazioni sperimentali.

Approximate Methods in *S* Wave Pion Nucleon Scattering.

B. H. BRANSDEN and R. G. MOORHOUSE

Department of Natural Philosophy, The University, Glasgow

(ricevuto il 12 Giugno 1957)

Summary. — This note examines the reliability of the Tamm-Dancoff and Cini-Fubini methods for *S*-wave pion scattering, by applying these approximations to an example for which the exact solution is known. It is shown that under certain conditions the Tamm-Dancoff method in its lowest orders is quite accurate, the Cini-Fubini method being unreliable.

Following the success of the static ps(ps) theory of *p* wave pion nucleon scattering, developed by CHEW ⁽¹⁾ and his collaborators, attempts have been made to extend the theory by adding terms to the interaction Hamiltonian that give rise to the scattering of *S* waves. Recently LOMON ⁽²⁾ has found an exact solution for a static non-local theory with an interaction

$$(1) \quad H_I = g \int \varrho(x) \varrho(x') \varphi(x) \cdot \varphi(x') dx dx' + \lambda \int \varrho(x) \varrho(x') \tau \cdot (\varphi(x) \times \pi(x')) dx dx',$$

where $\varrho(x)$ is a nucleon form factor and τ , φ , π are the nucleon isotopic spin and pion field operators respectively. The results of this theory agree qualitatively with the observed pion nucleon *S* wave scattering data, but to obtain quantitative agreement it will be necessary to add further terms to H_I ; for example, the Foldy-Dyson transformation of the relativistic ps(ps) interaction suggest that other important terms will be the gradient interaction (virtual *p* wave effect) and the Galilean terms (recoil effects). In these circumstances

⁽¹⁾ G. F. CHEW: *Phys. Rev.*, **94**, 1748, 1755 (1954).

⁽²⁾ E. L. LOMON: *Nuovo Cimento*, **4**, 106 (1956).

it is no longer possible to give an exact expression for the phase shifts and approximate methods have to be employed. It is the intention of this note to examine the reliability of two such methods—the Tamm-Dancoff and Cini-Fubini (3)—by applying them to the interaction (1) and comparing the results with the exact solution.

1. – The exact solution.

The isotopic triplet and singlet S wave phase shifts δ_3 , δ_1 , given by the interaction (1), are (2)

$$(2) \quad k \cot \delta_j = -\frac{4\pi}{v^2(k)} \left[\frac{1 + S(k)(g - 2\lambda_j \omega(k) - \lambda_j^2 V)}{g - 2\lambda_j \omega(k) - \lambda_j^2 V} \right],$$

where

$$\lambda_1 = 2\lambda,$$

$$\lambda_3 = -\lambda,$$

and where k is the pion momentum (*), $v(k)$ is the momentum transform of $\varrho(x)$, and $v(0) = 1$,

$$(3) \quad \begin{cases} V &= \frac{1}{2\pi^2} \int_0^\infty v^2(k') k'^2 dk', \\ S(k) &= \frac{1}{2\pi^2} \int_0^\infty \frac{v^2(k') k'^2}{k'^2 - k^2} dk'. \end{cases}$$

At incident energies below 58 MeV, the experimental scattering data are well represented by (4)

$$(4) \quad \delta_j = \alpha_j k, \quad \text{with} \quad \alpha_1 = 0.167, \quad \alpha_3 = -0.105,$$

and λ , g may be fixed, for a given source function, so that the calculated phases are correct at a particular energy. It may be noted that as (2) is a quadratic expression in λ , there will be two sets of coupling constants obtained by this procedure. For one of these $\delta_1 > 0$ and $\delta_3 < 0$ at all energies (set A), but for the other (set B) δ_1 changes sign at some energy below the cut-off. The variation with momentum of the phase shifts given by (2) is illustrated in Fig. 1, for a square cut-off $v(k) = 1$, $0 \leq k \leq k_m$; $v(k) = 0$, $k > k_m$; $k_m = 5.51$

(*) Natural units $\hbar = c = \mu = 1$ are used throughout.

(3) M. CINI and S. FUBINI: *Nuovo Cimento*, **11**, 142 (1954).

($\omega_m = 5.6$), and where the coupling constants have been chosen to give the correct phases at $k = 1$, so that (set *A*),

$$g = 1.537,$$

$$\lambda = 0.311.$$

A corresponding graph for coupling constants *B* is not shown as in this case the calculated value of $\lim_{k \rightarrow 0} ((\delta_1 - \delta_3)/k)$ is 10.1, in definite disagreement with the experimental value ⁽⁴⁾ of 0.26.

In his paper LOMON ⁽²⁾, using cut-offs of 1.5 *M* and 3.5 *M* (*M* being the nucleon mass), exhibited the energy dependence of phases obtained with coupling constants *B*. He found that it was impossible to obtain large enough values for δ_1 , when the zero energy slopes of the calculated phases were made to agree with the experimental values. At a higher cut off of $\omega_m = 11.2$, phases determined with coupling constants *A*, show a similar energy dependence to those shown in Fig. 1 and those determined with set *B* agree with Lomon's result.

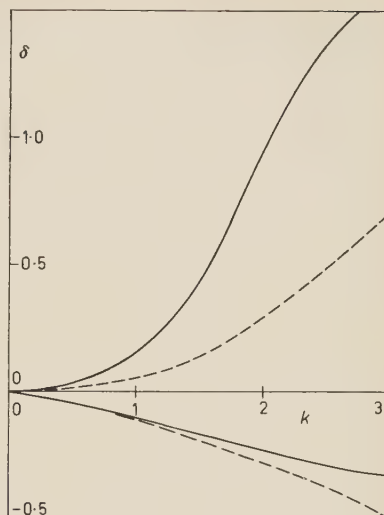


Fig. 1. — Variation of *S* wave phase shifts with energy. — Calculated from the Lomon solution (2) with $\lambda = 0.311$, $g = 1.537$, $\omega_m = 5.6$ (see text). ----- Calculated from the Tamm-Dancoff approximation with the same parameters.

2. — The Tamm-Dancoff method.

The first order (retaining one virtual pion in intermediate states) Tamm-Dancoff approximation, applied to interaction (1), results in an integral equation for the scattering amplitude $a_j(k)$

$$(5) \quad (\omega(k_0) - \omega(k))a_j(k) =$$

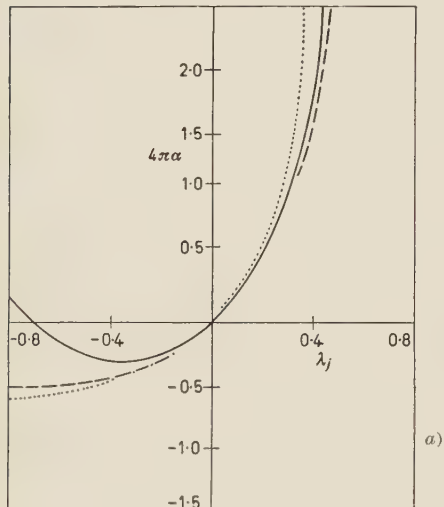
$$= \frac{v(k)}{4\pi^2} \int_0^\infty \frac{v(k')}{\sqrt{\omega(k)} \sqrt{\omega(k')}} \{g - \lambda_j(\omega(k) + \omega(k'))\} a_j(k') k'^2 dk'.$$

⁽⁴⁾ J. OREAR: *Nuovo Cimento*, **4**, 856 (1956).

This equation may be solved *exactly*, and the resulting phase shifts are given by

$$(6) \quad k \cot \delta_j = -$$

$$-\frac{4\pi}{v^2(k)} \left[\frac{1 + \frac{1}{2}gL_{-1}(k) - \frac{1}{2}\lambda_j(\omega(k)L_{-1}(k) + L_0(k) - V) - (\lambda_j/2)^2(VL_{-1}(k) - \bar{V}L_0(k))}{g - 2\lambda_j\omega(k) - \frac{1}{2}\lambda_j^2(V - \omega(k)\bar{V})} \right],$$



where

$$L_n(k) = \frac{1}{2\pi^2} \int_0^\infty \frac{v^2(k') k'^2 \omega^n(k')}{\omega(k') - \omega(k)} dk',$$

and

$$\bar{V} = \frac{1}{2\pi^2} \int_0^\infty \frac{v^2(k') k'^2}{\omega(k')} dk'.$$

This result is similar in form to the exact result (2), but the coefficients of g , λ_j , and λ_j^2 differ.

The scattering length $\alpha = \lim_{k \rightarrow 0} (\delta/k)$, given by (6), is compared with that

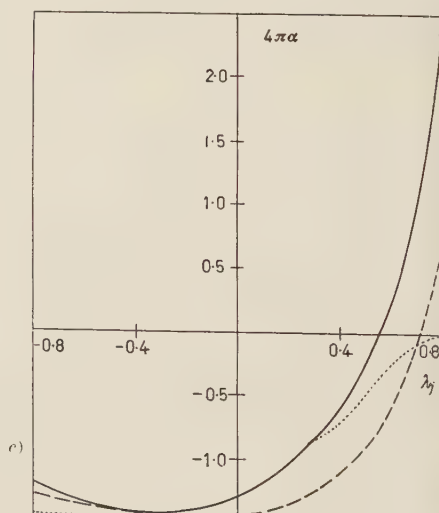
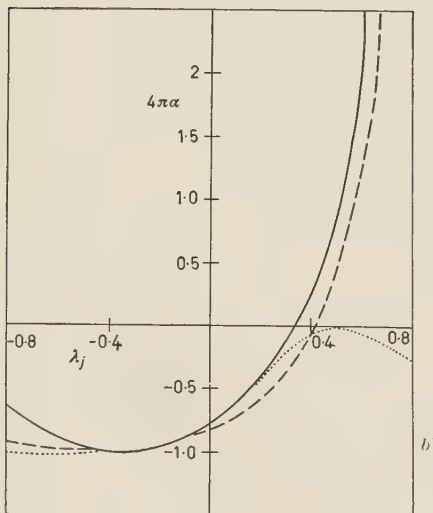
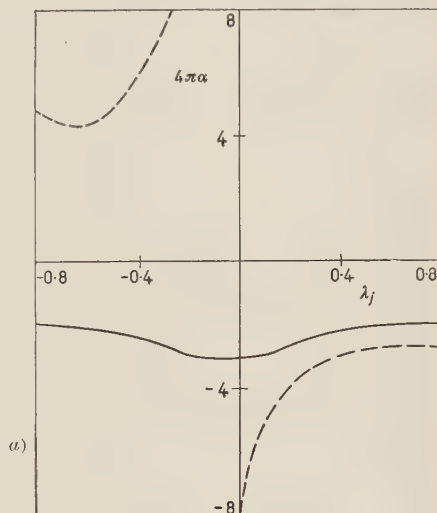


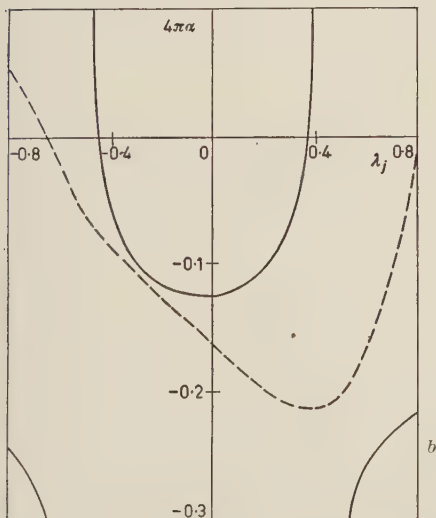
Fig. 2. – Variation of the scattering length with λ_j for $\omega_m = 5.6$; a) $g = 0$; b) $g = 1$; c) $g = 2$. — Lomon solution, equation (2); - - - Tamm-Dancoff approximation, equation (6); ····· Cini-Fubini approximation equation (12).

obtained from the exact expression (2), for cut-offs $\omega_m = 5.6$ and $\omega_m = 11.2$, in Fig. 2 and 3 respectively. The variation of α with λ_j is shown for a number of values of g . It is seen that at the lower cut-off of $\omega_m = 5.6$, for negative values of λ_j (from which region the triplet phase shifts are derived with coupling constants A) agreement is very close. For positive λ_j , the Tamm-Dancoff scattering length varies in a similar manner to the exact solution, but where the scattering amplitude becomes positive (set A singlet phase shifts) the error may become large. At the higher cut-off ($\omega_m = 11.2$), the Tamm-Dancoff and exact solutions differ widely. This is not unexpected as the constant V for example that occurs in (2) and (6) depends on ω_m^3 and therefore the error in the Tamm-Dancoff solution will increase rapidly with increasing ω_m .

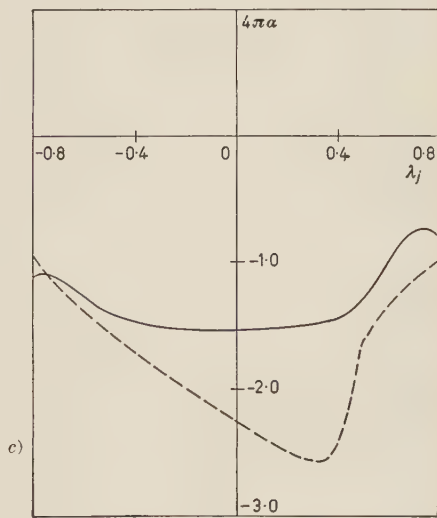
The variation with energy of the Tamm-Dancoff phases are compared with the exact solution, with coupling constants $\lambda = 0.311$, $g = 1.537$, $\omega_m = 5.6$ in Fig. 1. The triplet phases shift



a)



b)



c)

Fig. 3. – Variation of the scattering length with λ_j for $\omega_m = 11.2$; a) $g = -4$; b) $g = 4$; c) $g = 12$. — Lomon solution, equation (2); - - - Tamm-Dancoff approximation; equation (6).

agrees closely, but the singlet calculated phase shift falls considerably below the exact phase shift.

The special case $\lambda = 0$ leads to the « Wentzel example ». In this case, the exact solution for the scattering length may be written, for an exponential nucleon form factor, with momentum cut-off at M the nucleon mass⁽⁵⁾

$$(7) \quad 4\pi\alpha_E = \frac{g}{1 + (2.65/\pi^2)g},$$

and the first Tamm-Dancoff approximation gives

$$(8) \quad 4\pi\alpha = \frac{g}{1 + (1.86/\pi^2)g},$$

a good approximation, provided g is not close to $-\pi^2/1.86$. This result differs from an earlier investigation by TOUSCHEK and MORPURGO⁽⁵⁾, who omitted terms in μ^2/M^2 from their final evaluation.

Using a Levy-Klein expansion of the kernel and retaining terms of order g^2 , the integral equation for the second Tamm-Dancoff approximation is readily obtained for the $\lambda = 0$ case

$$(9) \quad (\omega(k_0) - \omega(k)) a(k) = \\ = g \frac{v(k)}{4\pi^2} \int_0^\infty \frac{v(k')}{\sqrt{\omega(k)} \sqrt{\omega(k')}} \left[1 + \frac{g}{4\pi^2} \int_0^\infty \frac{v^2(k'') k''^2 dk''}{\omega(k'') (\omega(k_0) - \omega(k) - \omega(k') - \omega(k''))} \right] a(k') k'^2 dk' .$$

This equation cannot be solved exactly, but CHEW's⁽⁶⁾ form of the Lippmann-Schwinger variational method may be used to provide an approximate solution for the scattering length

$$(10) \quad 4\pi\alpha = \frac{g \left(1 - \frac{0.791}{\pi^2} g \right)}{1 + 1.860 \left(\frac{g}{\pi^2} \right) - 2.171 \left(\frac{g}{\pi^2} \right)^2 + 0.681 \left(\frac{g}{\pi^2} \right)^3},$$

and this agrees closely with the exact result provided

$$-1 < 2.65 \frac{g}{\pi^2} < 1 .$$

(5) G. MORPURGO and B. F. X. TOUSCHEK: *Nuovo Cimento*, **10**, 1681 (1953).

(6) G. F. CHEW: *Phys. Rev.*, **43**, 341 (1954).

It may be concluded, that the Tamm-Danoff method provides a powerful method of approximation to problems containing interactions similar to (1), if the momentum cut-off is not greater than M , the nucleon mass, but that the first approximation will not be adequate to deal with the singlet case quantitatively.

When further terms are added to the interaction (1) in the majority of cases the resulting Tamm-Danoff equation cannot be solved exactly other than by numerical methods (7). It is therefore desirable to evaluate the effectiveness of simple approximations to the Tamm-Danoff solution (6). The first Fredholm approximation and Chew's form of the Lippman-Schwinger variational method have been applied to equation (5), and the results, for

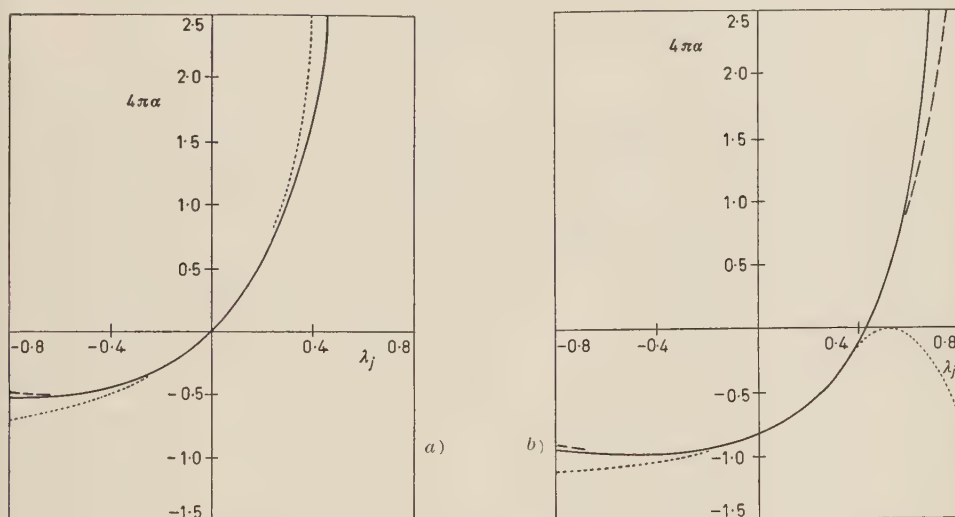


Fig. 4. – The scattering length determined from the Tamm-Danoff equation as a function of λ_j for $\omega_m = 5.6$; a) $g=0$; b) $g=1$. — Exact solution, equation (6); - - - First Fredholm approximation; ····· Chew variational approximation.

zero momentum and cut-off $\omega_m = 5.6$ are summarized in Fig. 4. The Fredholm approximation is very close to the exact solution of the Tamm-Danoff equation for $g = 0$, and for $g = 1$ the approximation is excellent for $|\lambda| < 0.6$ but for $|\lambda| > 0.6$ becomes rather poor. The variational method, although reasonable for $g = 0$, fails completely when $g \neq 0$ and $\lambda > 0$, not exhibiting the characteristic sign change of the exact solution.

(7) For example L. FONDA and I. REINA: *Nuovo Cimento*, **4**, 1399 (1956), have investigated the addition of recoil terms to interaction (1).

3. – The Cini-Fubini variational method.

The Cini-Fubini variational method⁽³⁾ has been applied in the lowest approximation to the interaction (1). It is found that

$$(11) \quad k \cot \delta_j = -\frac{4\pi}{v^2(k)(g - 2\lambda_j \omega(k))} \left[1 + \frac{\omega(k)}{2(g - 2\lambda_j \omega(k))} \cdot \right. \\ \left. \cdot \left\{ \frac{g^2}{\omega(k)} (L_{-1}(k) + M_{-1}(k)) - 2\lambda_j g \left(\frac{1}{\omega(k)} L_0(k) + L_{-1}(k) + \frac{1}{\omega(k)} M_0(k) + M_{-1}(k) \right) + \right. \right. \\ \left. \left. + \lambda_j^2 \left(\frac{1}{\omega(k)} L_1(k) + \frac{1}{\omega(k)} M_1(k) + \omega(k) L_{-1}(k) + \omega(k) M_{-1}(k) - 2L_0(k) - 2M_0(k) \right) \right\} \right],$$

where L_n is given in (6) and

$$M_n(k) = \frac{1}{2\pi^2} \int \frac{v^2(k') k'^2 \omega_n(k') dk'}{\omega(k') + \omega(k)}.$$

For $\lambda = 0$, this reduces to the « Wentzel example » and gives the exact result, as shown by CINI *et al.*⁽⁸⁾. The variation of the scattering length with λ_j is illustrated in Fig. 2 for $\omega_m = 5.6$, and compared with exact and Tamm-Dancoff solutions. It is seen that this method fails in the same way as the Chew variational method applied to the Tamm-Dancoff equations, namely the scattering length does not change sign in positive λ_j region ($g \neq 0$). This may be attributed mainly to the absence of terms λ^2 in the denominator of the approximate solution (11). These terms reduce the effective value of g , which suggests that in complicated problems where approximations beyond the lower variational method may be impracticable, insight into the behaviour of the solution may be obtained by reducing g in the manner indicated by the exact solution of (1). It is also worth noting that, contrary to often expressed opinion, an approximation not satisfying the crossing theorem (the Tamm-Dancoff) may be better than one that does (the Cini-Fubini method).

⁽⁸⁾ M. CINI, G. MORPURGO and B. F. TOUSCHEK: *Nuovo Cimento*, **11**, 316 (1954).

RIASSUNTO (*)

La nota esamina l'attendibilità dei metodi di Tamm-Dancoff e Cini-Fubini per lo scattering di pioni dell'onda S , applicando queste approssimazioni a un esempio di cui si conosce la soluzione esatta. Si dimostra che in certe condizioni il metodo di Tamm-Dancoff negli ordini minimi è assai esatto, mentre il metodo di Cini e Fubini è inattendibile.

(*) Traduzione a cura della Redazione.

A Čerenkov Counter as High Energy Photon Spectrometer (*).

I. FILOSOFO (**)

Physics Research Laboratory, University of Illinois - Urbana, Ill.

(ricevuto il 12 Giugno 1957)

Summary. — A Čerenkov counter designed as high energy γ spectrometer is described. Lead glass is used as a medium in which the shower from a γ is both produced and absorbed. The incident energy is measured by means of the Čerenkov light produced in the medium by the electrons of the shower. The counter has been calibrated with electrons of energies up to 275 MeV and has shown high efficiency, linear response with the energy and energy resolution from $\pm 28\%$ at 80 MeV to $\pm 17\%$ at 275 MeV. Possible improvements of this type of instrument are discussed.

1. — Introduction.

Present day techniques can furnish accurate and exhaustive information about charged particles for a very broad interval of energies, by means of measurements of momenta, range and ionization. As is well known, the situation is quite different for the detection and measurement of the energy of neutral particles and quanta. Of particular importance is the case of high energy γ -rays, since these are frequently associated with the interactions now being investigated with high energy accelerators.

The pair spectrometer has been used to measure the energy and flux of γ -radiation, but it is often of limited usefulness because of its low efficiency, and is therefore inadequate for the study of phenomena characterized by a low value of the cross-section.

(*) This work was performed while the author was holding a O.E.E.C. fellowship granted by the Foreign Operations Administration, Washington D.C.

(**) Now at the University of Padua, Institute of Physics, Padua, Italy.

An efficiency approaching 100% with a reasonable resolution in energy can be obtained by the use of the principle of the total absorption of γ -rays in a medium, through the detection of a signal proportional to the total energy released in the development of the electrophotonic shower. The absorption is complete if the medium has sufficiently large dimensions with respect to the radiation length. A signal correlated with the energy carried by the γ can be obtained in one of the following ways: a scintillator can be used as an absorber, or one can produce the total absorption of the shower in a transparent medium and detect the Čerenkov light produced therein by the electrons.

The applicability of total absorption to high energy γ spectrometry was suggested by KANTZ and HOFSTADTER (¹), who also investigated experimentally the development and absorption of showers in different radiators.

Calculations have been made in recent years by R. STERNHEIMER (²) and R. WILSON (³) in order to predict the pattern of a shower in a radiator. In addition, mention should be made of the calculations of YAMAGATA and YOSHIMINE (⁴), of particular interest for the purposes of this report. These authors, using the Monte Carlo method to study the development of the shower in various materials, express their results as distributions of the number of visible quanta of Čerenkov light produced in the medium by the shower. Different thicknesses of radiators were considered; one of these could be considered as infinite, as far as the showers were concerned, while others were limited, and from these latter an appreciable part of the shower escaped from the medium. The calculations were performed in great detail by use of the ILLIAC digital computer; the results clearly demonstrate what the thickness of the radiator should be in order to make negligible the fluctuations due to the pattern of the shower with respect to those inevitably introduced through the transformation of the optical signal into an electric signal.

At present, different types of total absorption spectrometers are in use in various laboratories, and detailed reports of some of these have already appeared (^{5,6}).

Certain advantages make advisable the use of the Čerenkov effect in the designing of a spectrometer for high energy γ -rays, although the light output of a Čerenkov counter is much smaller than that of a scintillation counter. The principal advantage of the Čerenkov is, perhaps, the fact that its back-

(¹) A. KANTZ and R. HOFSTADTER: *Nucleonics*, n. **12**, 3, 36 (1954).

(²) R. STERNHEIMER: AECU Reports, 2982, 2983, 2984, BNS Internal Report, RS-5.

(³) R. WILSON: *Phys. Rev.*, **86**, 261 (1952).

(⁴) T. YAMAGATA and M. YOSHIMINE: private communication.

(⁵) G. PUGH, D. FRISH and R. GOMEZ: *Rev. Sci. Instr.*, **25**, 1124 (1954).

(⁶) C. SWARTZ and J. DE WIRE: *Phys. Rev.*, **98**, 1164 (1955).

(⁷) M. JESTER: UCRL 2990 (1955).

(⁸) W. B. JONES, H. R. KRATZ and J. ROUVINA: *Rev. Sci. Instr.*, **28**, 167 (1957).

ground is very low, since it is practically insensitive to low energy neutrons and protons. Furthermore, since the light is not generated by an intermediate process, the output signal is the most rapid and sharpest obtainable; this is important in cases where the counter is needed for experiments requiring very fast electronics. In addition, there is the practical advantage of a wider choice of radiators among various substances of high Z and of fine optical properties; this permits the construction of γ counters that are very compact in comparison with those using scintillators, which usually have a relatively low density and Z .

Compromise solutions have been adopted and are being studied in an attempt to obtain compact γ counters. Here, the light signal is produced by scintillation either by means of sandwiches formed by alternate strata of substances of high Z and of liquid scintillators, or by means of mixtures of liquid scintillators and beads or fragments of glass of high average Z . So far, no definite answer has been given as to the effectiveness of these methods. However, it seems clear that the resolution in energy of such counters is greatly affected by statistical fluctuations in the partition into the two parts (absorbed respectively by the scintillator and by the absorber) of the total energy absorbed by the system.

2. – Design of counter.

The facts and considerations given above led to the decision to use a Čerenkov counter for a group of experiments now in progress at the University of Illinois, Physics Research Laboratory. The first two experiments, completed last year, were a study of the Compton effect by protons, and an investigation of the photoproduction of π^0 in hydrogen (⁹).

The counter used was designed to permit measurements in the range of energies up to the maximum energy (300 MeV) of the University of Illinois Betatron and to give a fast output signal. This made possible the use of fast electronics, particularly necessary for the study of the Compton effect, for which a low value of the cross-section was predictable.

Notwithstanding the fact that the need to obtain a fast output led to a design that could not be ideal for the collection of a maximum amount of Čerenkov light, the behaviour of the counter in two experiments carried out last year, and the resolution in energy shown in the calibration with fast electrons were good, even better than expected.

This performance justifies a detailed description at this stage of the de-

(⁹) L. B. AUERBACH, G. BERNARDINI, I. FILOSOFO, A. O. HANSON, A. C. ODIAN and T. YAMAGATA: *CERN Symposium*, 2 (1956).

velopment of the instrument, which on the other hand, is in process of being improved.

Fig. 1 shows a sketch of the set-up of the counter. The radiator is made up of two cylindrical blocks of lead glass acquired from the Corning Glass Works (Code Number 8392). Each piece is 12 in. in diameter and 7 in. long,

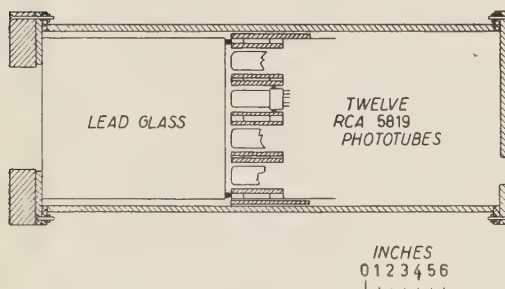


Fig. 1.

with density 3.89, the refractive index being 1.65 for the sodium D line. The composition of this glass is approximately 55% lead oxide and 45% silica, and computation showed that one radiation length is very close to 1 in. The two pieces of glass were cemented together with Canada balsam to form a medium of 14 radiation lengths in thickness and 12 radiation lengths in diameter.

To define the effective entrance, and hence to avoid the development of showers too close to the cylindrical side wall of the glass, a lead diaphragm, 2 in. thick (corresponding to 10 radiation lengths in lead), with a 7.5 in. diameter hole in its center, was placed in front of the glass.

As regards the phototubes, a preliminary study was made to decide between the use of a certain number of small ones and the use of a single large one. The counter was set up and tested, first, with a phototube, eleven inches in diameter, manufactured by A.I.F. of Zurich and next with twelve RCA 5819 phototubes uniformly distributed on the back surface of the radiator. Tests carried out with light sources and with cosmic rays showed that the large phototube would not offer any practical advantages over the twelve small phototubes as far as the resolution in energy of the counter was concerned. This was probably due to the smaller and non-uniform photocathode sensitivity of the large phototube. On the other hand, the twelve small phototubes had the advantage of furnishing a more rapid signal. With the large phototube the counter gave an output signal with a spread in time of about 50 m μ s; with the small ones, it gave a signal with about 20 m μ s. The spread in time being defined as the extrapolated width at the base of the pulse.

The counter was therefore set up with the small phototubes. They were divided into four groups of three each; the anodes of the three phototubes of each group were connected in parallel, so that four outputs were formed which were then sent to the adder-integrator circuit. Integration was made over a time of $3 \cdot 10^{-8}$ s, which was also the length of the output signal.

In order to increase the light collection efficiency, the side wall of the glass cylinder was silver-coated and the front surface was painted with a white

paint of a high reflectance (DuPont Company, No. 29-915). Paraffine oil was used for the optical contact between the radiator and the phototubes.

The entire assembly was contained within a soft iron cylinder, $\frac{1}{2}$ in. thick and 34 in. long, which acted as a magnetic shield. An additional shield of soft iron, $\frac{1}{4}$ in. thick, was placed around each phototube. The shielding proved to be quite effective, even when working in a stronger magnetic field than that present during the actual runs of the experiments mentioned above.

To check the stability of response, a simple device was permanently attached to the counter (¹⁰). A small flash bulb, located at the bottom of the front surface of the counter, conveyed light flashes of a few millimicroseconds into the counter by means of a thin lucite rod. Since the light signal was available 60 times per second, the counter output could be observed on the oscilloscope screen. Another check was made occasionally by means of the distribution in amplitude of the signals due to cosmic rays which crossed the counter in an almost vertical direction. One scintillation counter was mounted above and another beneath the radiator. The double coincidence pulse of these two counters triggered the oscilloscope; only the Čerenkov pulses due to cosmic rays which crossed all three counters were observed and photographed.

3. – Calibration and tests.

The counter was calibrated with fast electrons produced in a lead target by γ -rays from the 300 MeV Betatron. An analyzing magnet was used to select the energy of electrons which were produced in the target. A calibration of this magnet had already been made previously by the hot-wire technique. Nevertheless, a careful check of this calibration by means of fast electrons was considered advisable before proceeding with the Čerenkov calibration.

Two small scintillation counters 1 in \times 1.5 in \times 0.5 in. were placed one on the image point of the magnet and the other 20 in. further along the central trajectory of the magnet. Fig. 2 shows the layout of this test. Given the dimensions of the target and counters and the particular geometry used in this test, the spread in energy was calculated as $\pm 3\%$.

Activation curves of the coincidence outputs of the counters were taken for several magnet currents. Keeping the magnet current constant at a certain value, the energy of the betatron was gradually stepped up. At energies below the energy defined by the magnet current in accordance with the hot-wire calibration, a negligible counting rate was observed. With a rise in the energy of the betatron to a certain value, a quick rise in the counting rate

(¹⁰) The device was developed by J. H. MALMBERG. A report will soon appear in print.

occurred. The energy-current relationship defined by this method agreed very well with the hot-wire calibration.

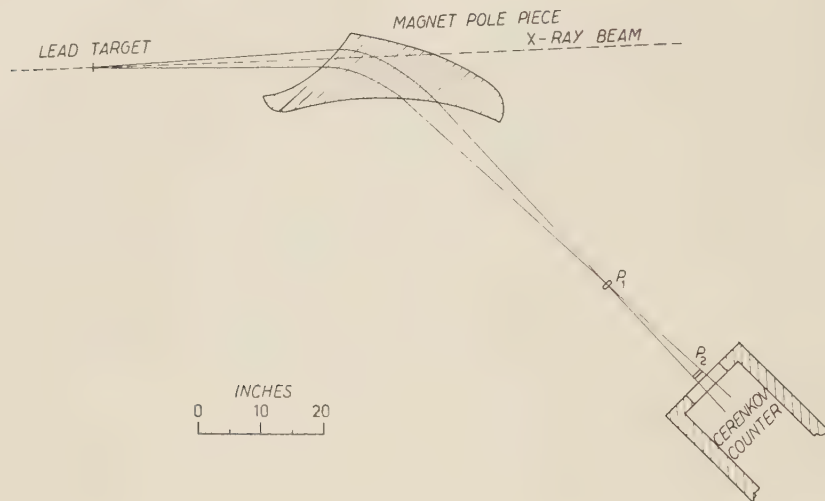


Fig. 2.

The Čerenkov counter was then aligned with the two scintillation counters, as shown in Fig. 2. The coincidence outputs of the two counters were used to trigger the oscilloscope by means of which the Čerenkov pulses were observed and photographed. Fig. 3 shows the pulse-height distribution curves obtained for several electron energies.

The table summarizes the results of the calibration. The resolution in energy is defined, both here and below, as the total width at half height of the pulse-height distribution curve, with respect to the pulse-height at the maximum.

Energy in MeV	80	150	200	240	275
Pulse-height at the maximum (arbitrary units)	1.5	2.9	4.0	4.7	5.4
Resolution in energy	56%	44%	40%	38%	34%

The calibration was made with electrons satisfying particularly stringent conditions: they were incident in the counter parallel to the axis and in a small area around the center of the front surface. When the counter is used to detect and measure γ -rays entering through a larger area and contained in a wider solid angle, poorer resolution in energy is to be expected as a

result of the side-wall effect, that is, as a result of the loss of part of the shower through the lateral walls.

During the calibration of an earlier version of the counter, two tests were made to determine the influence of the side wall effect upon the resolution in energy. The first test used electrons entering the medium off-axis by 3 in.; in the second the electrons were off-axis by 2 in. and made an angle of 10° with respect to the axis. The resolution in energy for 170 MeV electrons, which had been 46% for electrons along the axis, became 48% in both of these tests.

The most complete and consistent test of the counter was, however, its behavior during the three months run of the two experiments described above. In these, the Čerenkov counter detected and measured the energies of γ entering the counter through the large diaphragm shown in Fig. 1, and coming from a target placed 10 in. in front of the counter and on its axis. Fig. 4 shows the resolution of the counter, based on measurements made at different periods of time.

During these experiments the counter showed only a small effect at the lateral lead shielding, and no shielding against the neutron background was necessary. The stability in response was excellent and was always known throughout the period of measurement by means of the flashlight and cosmic ray checks described above.

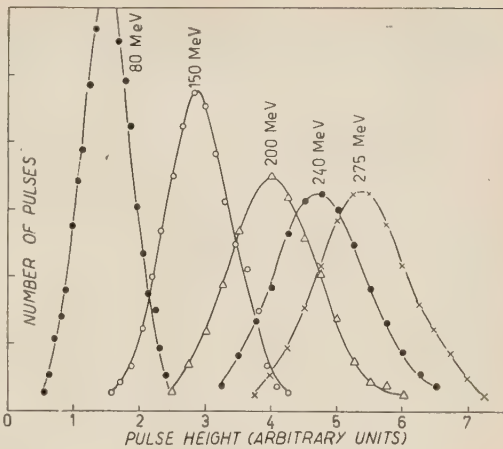


Fig. 3.

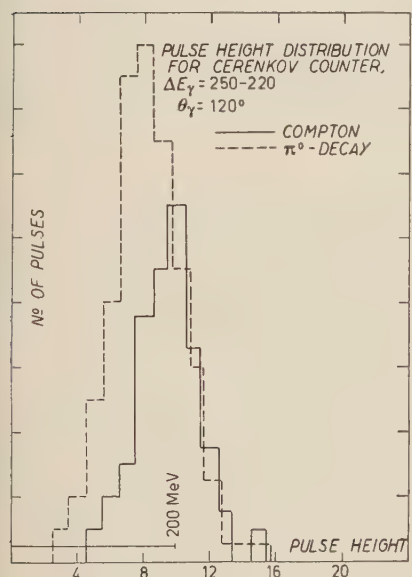


Fig. 4.

4. - Discussion and conclusions.

While the efficiency of the counter is 100% and the response is fairly linear with respect to the incident energy, the resolution in energy is not as good

as that predicted by the evaluation of YAMAGATA and YOSHIMINE (see Fig. 5) for an absorber equivalent to the radiator used in this counter (11).

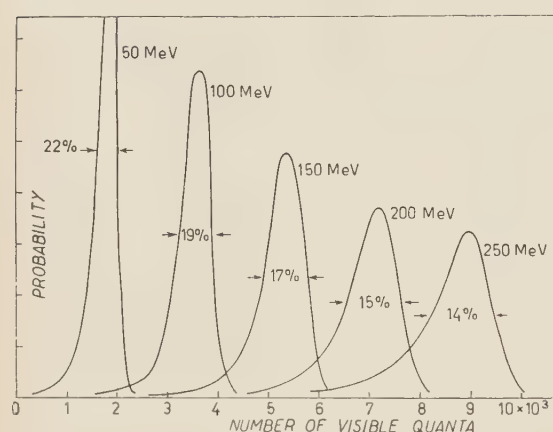


Fig. 5.

covered only about 25% of the area of the back face of the radiator;

3) several mismatchings were present between the indices of refraction of the various transparent materials (lead glass, Canada balsam, oil and phototube bulbs) of the system. Consequently, an appreciable fraction of the Čerenkov light was reflected back and then lost almost completely owing to the poor transmission of the lead glass.

As a consequence, only a small fraction of the Čerenkov radiation has been collected by the photocathodes. Furthermore, a photocathode conversion efficiency of the order of 5% led to the production of only a small number of photoelectrons, and the fluctuation in number of these then became preponderant in defining the resolution in energy.

Probably other factors, such as the discontinuity of the photosensitive surface on the back face of the counter and the particular pattern of the shower with respect to the phototubes, affect somewhat the resolution in energy obtained. One may, conclude, however, that inefficiency in light collection and the small conversion factor of the phototubes are the principal causes of a poor resolution in energy. This, therefore, needs to be taken into account in any attempt to improve this type of γ detector.

This behaviour is not surprising, however, in view of the following unfavorable factors in the light collection:

1) the transmission of the light is poor in this type of lead glass, especially in the region of highest frequencies, to which the phototubes are more sensitive, and of which the Čerenkov radiation is characteristically rich;

2) the active cathode surface of the phototubes co-

(11) Fig. 5 represents the results of calculations made for an absorber 10 inches thick with infinite lateral size. The experiments of Hofstadter show that this case is equivalent to the radiator used in this Čerenkov counter, as far as the fraction of the shower that escapes the medium is concerned.

Improved performance from a Čerenkov counter can be expected with the use of:

- 1) a radiator with high Z , endowed with a good light transmission, particularly in the high frequency region;
- 2) larger phototubes, which will permit a better value in the ratio between the photosensitive surface and that of the radiator;
- 3) phototubes with photocathodes of greater efficiency than those now available; and
- 4) special substances or methods that will reduce internal reflection among the various components of the system.

The rapid development in techniques and devices which is now under way gives promise of a greatly improved situation in the near future. It may soon be possible to have much smaller fluctuations in the number of photoelectrons than those shown in Fig. 5 for the number of Čerenkov quanta.

If such an improvement comes about, the fluctuations due to the shower, which are at present hidden by the much greater one mentioned above, can in turn become preponderant in determining the resolution of the counter. In that case, greater care will be needed in establishing the dimensions of the radiator for a γ spectrometer planned for use in a certain interval of energy.

* * *

The writer wishes to express his sincere gratitude to Professors G. BERNARDINI and A. O. HANSON, and to Dr. T. YAMAGATA, all of the University of Illinois, for many helpful discussions during the design and study of this counter.

R I A S S U N T O

Viene descritto un contatore di Čerenkov progettato come spettrometro per raggi γ di alta energia. Del vetro al piombo viene usato come materiale nel quale si sviluppa e viene assorbito lo sciamo generato da un γ . L'energia incidente viene misurata per mezzo della luce Čerenkov prodotta nel vetro dagli elettroni dello sciamo. Il contatore è stato tarato con elettroni di energie fino a 275 MeV ed ha mostrato una elevata efficienza, una risposta proporzionale all'energia e una risoluzione in energia che va da $\pm 28\%$ a 80 MeV a $\pm 17\%$ a 275 MeV. Vengono discusse le possibilità di un perfezionamento di questo tipo di apparecchio.

Sull'operatore hamiltoniano delle teorie beta.

P. BOCCIERI (*) e E. MONTALDI (†)

(*) Istituto di Fisica dell'Università - Pavia

(†) Istituto di Scienze Fisiche dell'Università - Milano

(*) (†) Istituto Nazionale di Fisica Nucleare - Sezione di Milano

(ricevuto il 26 Luglio 1957)

Riassunto. — Dopo aver definito lo spazio hilbertiano \mathcal{H}^* in cui agisce l'operatore hamiltoniano H delle teorie beta si considerano le proprietà di quest'ultimo in vari sottospazi di \mathcal{H}^* . Si dimostra che in uno di tali sottospazi le proprietà di H coincidono essenzialmente con quelle dell'hamiltoniano del modello di Lee. In un altro sottospazio si ha un modello di teoria dei campi senza rinormalizzazioni. Si fa inoltre vedere che gli auto-vettori di H non costituiscono un insieme completo in \mathcal{H}^* .

1. — È noto che l'operatore hamiltoniano H di una qualsiasi teoria quantistica dei campi è definito in uno spazio hilbertiano \mathcal{H}^* che è più ampio dello spazio \mathcal{H}_p , composto dagli stati ad energia positiva di particelle non interagenti. Per chiarire meglio la situazione esaminiamo in dettaglio la struttura di questi spazi hilbertiani.

Un campo quantizzato, che supporremo racchiuso in una scatola di volume finito V , si può sempre pensare come l'insieme di un numero infinito di oscillatori fermionici o bosonici, gli stati dei quali

$$\varphi_{n_i}; \quad n_i = \begin{cases} 0, 1 & \text{se l'oscillatore è fermionico} \\ 0, 1, 2, \dots & \text{se l'oscillatore è bosonico} \end{cases}$$

hanno sede in opportuni spazi hilbertiani $\mathcal{H}_1, \dots, \mathcal{H}_i, \dots$.

Seguendo von NEUMANN⁽¹⁾ si può definire uno spazio hilbertiano

$$\mathcal{H}^* = \prod_i \otimes \mathcal{H}_i,$$

detto prodotto infinito diretto degli \mathcal{H}_i nel seguente modo. Considerato il prodotto $\prod_i z_i$ (z_i numeri complessi qualsiasi) è facile provare che se $\prod_i z_i$ è convergente lo è pure $\prod_i |z_i|$, ma che non è in generale vero il viceversa.

Diremo allora che $\prod_i z_i$ è quasi convergente se il prodotto $\prod_i |z_i|$ è convergente. Nel caso che $\prod_i z_i$ sia quasi convergente, ma non convergente, si assume come suo valore lo zero.

Indi, sempre in fase preliminare, si introducono le nozioni di C -sequenza e di C^0 -sequenza.

Un insieme $\{\varphi_{n_i}\}$ si dirà essere una C -sequenza se

$$\prod_i (\|\varphi_i\|) < \infty$$

e una C^0 -sequenza se

$$\sum_i (\|\varphi_i\| - 1) < \infty.$$

Si dimostra facilmente che una C -sequenza è anche una C^0 -sequenza, ma che in generale non vale l'inverso.

Inoltre due C^0 -sequenze $\{\varphi_{n_i}\}, \{\varphi_{m_i}\}$ si dicono equivalenti se

$$\sum_i (|\langle \varphi_{n_i}, \varphi_{m_i} \rangle| - 1) < \infty$$

e si scrive

$$\{\varphi_{n_i}\} \asymp \{\varphi_{m_i}\}.$$

Tutte le C^0 -sequenze si potranno dividere in classi $\sigma_1, \dots, \sigma_n, \dots$ ponendo nella stessa classe tutte le C^0 -sequenze che sono tra di loro equivalenti. Sia Γ l'insieme di queste classi.

A questo punto si può iniziare la definizione assiomatica dello spazio \mathcal{H}^* . Ad ogni C^0 -sequenza facciamo corrispondere in \mathcal{H}^* un elemento simbolico $\prod_i \otimes \varphi_{n_i}$ tale che

$$(\prod_i \otimes \varphi_{n_i}, \prod_j \otimes \varphi_{m_j}) = \prod_i (\varphi_{n_i}, \varphi_{m_i}).$$

⁽¹⁾ J. von NEUMANN: *Compositio Mathematica*, 6, 1 (1939).

L'insieme dei $\prod_i \otimes \varphi_{n_i}$ e dei loro punti di accumulazione in una conveniente metrica, costituisce lo spazio hilbertiano \mathcal{H}^* che identifieremo con lo spazio $\prod_i \otimes \mathcal{H}_i$.

In modo analogo si costruisca lo spazio $\prod_i^\sigma \otimes \mathcal{H}_i \equiv \mathcal{H}^\sigma$ prendendo come C^0 -sequenze generatrici tutte le C^0 -sequenze tra di loro equivalenti appartenenti ad una classe σ .

Noi chiameremo (introducendo una dizione più approssimata) tale sottospazio di \mathcal{H}^* una *fibra* di \mathcal{H}^* .

Si può allora dimostrare facilmente che $\mathcal{H}^\sigma \subset \prod_i^\sigma \otimes \mathcal{H}_i$ coincide con la chiusura dei $\prod_i \otimes \varphi_{n_i}$ ove $\{\varphi_{n_i}\}$ sono le C^0 -sequenze che differiscono per un numero finito di termini da una C^0 -sequenza fissata.

Nelle teorie fisiche soltanto una fibra \mathcal{H}_p gioca un ruolo essenziale. Ad esempio, nella teoria del positone essa è quella generata dalle C^0 -sequenze che sono equivalenti alla C^0 -sequenza corrispondente allo stato di vuoto costruito considerando occupati gli stati ad energia negativa e liberi gli stati ad energia positiva.

Non è però privo di interesse lo studio delle proprietà di H nelle altre fibre.

Per esempio, nell'elettrodinamica quantistica H dà origine nella fibra di interesse fisico alla teoria del positone, in un'altra ⁽²⁾, generata dalle C^0 -sequenze equivalenti alla C^0 -sequenza in cui tutti gli n_i sono nulli, alla teoria di Dirac-Fock-Podolsky ⁽³⁾ che, sebbene non fisica per la difficoltà delle energie negative, presenta però delle caratteristiche interessanti. Molti effetti calcolati secondo le due teorie danno risultati identici all'ordine più basso de la teoria delle perturbazioni (effetto Compton, scattering di Møller ed altri).

In altri casi si ottengono però risultati completamente diversi. Tipica è la polarizzazione del vuoto che risulta in un caso infinita e nell'altro zero.

In questo lavoro ci si propone di studiare alcune proprietà dello hamiltoniano delle teorie beta in alcune fibre scelte tra le più significative dello spazio hilbertiano in cui tale operatore è definito. Noi faremo vedere che il modo di operare di H è di gran lunga più complesso nella fibra che ha interesse fisico. In altre, invece, il suo modo di operare è abbastanza semplice potendosene anzi determinare degli autostati.

Noi noteremo che in uno di questi sottospazi l'hamiltoniano delle teorie beta ha proprietà sostanzialmente coincidenti con quelle dell'hamiltoniano del mo-

⁽²⁾ P. BOCCIERI e A. LOINGER: *Nuovo Cimento*, **2**, 314 (1955).

⁽³⁾ Vedi per esempio, P. A. M. DIRAC: *The Principles of Quantum Mechanics*, 2nd ed. (Oxford, 1935), p. 286 e segg.

dello di Lee⁽⁴⁾, a parte la comparsa nel nostro caso delle energie negative che non modificano però l'essenza matematica del modello stesso.

In un'altra fibra H dà origine ad un modello di teoria dei campi in cui non intervengono rinormalizzazioni né di carica né di massa, cioè a dire le quantità massa matematica e costante di accoppiamento matematica coincidono con le corrispondenti quantità fisiche.

Noi faremo inoltre vedere che in questi due ultimi sottospazi si possono trovare autovettori di H non formanti però un insieme completo. Nella fibra di interesse fisico H non ha invece autovettori.

2. – L'operatore hamiltoniano della teoria beta nel caso di accoppiamento scalare è dato da: $H = H_0 + H_{\text{int.}}$;

$$H_0 = \int d^3x \left\{ \bar{\psi}_N(\mathbf{x}) \left(\gamma^k \frac{\partial}{\partial x^k} + m_N \right) \psi_N(\mathbf{x}) + \bar{\psi}_P(\mathbf{x}) \left(\gamma^k \frac{\partial}{\partial x^k} + m_P \right) \psi_P(\mathbf{x}) + \bar{\psi}_e(\mathbf{x}) \left(\gamma^k \frac{\partial}{\partial x^k} + m_e \right) \psi_e(\mathbf{x}) + \bar{\psi}_v(\mathbf{x}) \left(\gamma^k \frac{\partial}{\partial x^k} + m_v \right) \psi_v(\mathbf{x}) \right\},$$

$$H_{\text{int.}} = g \int d^3x \left\{ \bar{\psi}_N(\mathbf{x}) \psi_P(\mathbf{x}) \bar{\psi}_v(\mathbf{x}) \psi_e(\mathbf{x}) + \bar{\psi}_P(\mathbf{x}) \psi_N(\mathbf{x}) \bar{\psi}_v(\mathbf{x}) \psi_e(\mathbf{x}) \right\},$$

che nello spazio degli impulsi diventa:

$$(1) \quad H_0 = \sum_{\mathbf{k}, \varepsilon, \sigma} \left\{ \sqrt{\bar{k}^2 + m_N^2} \eta(\varepsilon) a_{\mathbf{k}, \varepsilon, \sigma}^{(N)*} a_{\mathbf{k}, \varepsilon, \sigma}^{(N)} + \sqrt{\bar{k}^2 + m_P^2} \eta(\varepsilon) a_{\mathbf{k}, \varepsilon, \sigma}^{(P)*} a_{\mathbf{k}, \varepsilon, \sigma}^{(P)} + \sqrt{\bar{k}^2 + m_e^2} \eta(\varepsilon) a_{\mathbf{k}, \varepsilon, \sigma}^{(e)*} a_{\mathbf{k}, \varepsilon, \sigma}^{(e)} + |k| \eta(\varepsilon) a_{\mathbf{k}, \varepsilon, \sigma}^{(v)*} a_{\mathbf{k}, \varepsilon, \sigma}^{(v)} \right\};$$

$$(2) \quad H_{\text{int.}} = g \sum_{\substack{\mathbf{k}_1, \mathbf{k}_2, \mathbf{k}_3 \\ \varepsilon_1, \varepsilon_2, \varepsilon_3, \varepsilon_4 \\ \sigma_1, \sigma_2, \sigma_3, \sigma_4}} \left\{ a_{\mathbf{k}_1 + \mathbf{k}_2 - \mathbf{k}_3, \varepsilon_1, \sigma_1}^{(N)*} a_{\mathbf{k}_3, \varepsilon_3, \sigma_3}^{(v)*} a_{\mathbf{k}_1, \varepsilon_2, \sigma_2}^{(P)} a_{\mathbf{k}_2, \varepsilon_4, \sigma_4}^{(e)} + \text{h. c.} \right\};$$

$$\eta(\varepsilon) = \begin{cases} +1 & \text{se } \varepsilon > 0, \\ -1 & \text{se } \varepsilon < 0. \end{cases}$$

Abbiamo considerato il caso del decadimento del neutrone, ma le considerazioni che seguono valgono anche per tutti gli altri tipi di accoppiamento e per gli altri decadimenti.

$\psi^{(A)}(\mathbf{x})$ e $\psi^{(B)}(\mathbf{x})$ sono operatori che soddisfano alle seguenti regole di anticommutazione:

$$\bar{\psi}_{\lambda}^{(B)}(\mathbf{x}) \psi_{\mu}^{(A)}(\mathbf{x}') + \psi_{\mu}^{(A)}(\mathbf{x}') \bar{\psi}_{\lambda}^{(B)}(\mathbf{x}) = \delta^{(A), (B)} \delta_{\lambda \mu} \delta(\mathbf{x} - \mathbf{x}'),$$

(4) T. D. LEE: *Phys. Rev.*, **95**, 1329 (1954).

dove A e B possono essere N, P, e, \bar{e} , e

$$\delta^{(A), (B)} = \begin{cases} 1 & \text{se } A = B, \\ 0 & \text{es } A \neq B. \end{cases}$$

Consideriamo dapprima la fibra \mathcal{H}^{σ_1} generata dalle C^0 -sequenze che sono equivalenti alla C^0 -sequenza in cui tutti gli n_i relativi ai protoni, neutroni, elettroni sono nulli, mentre quelli relativi ai neutrini coincidono con l'unità.

Se si tiene presente che C^0 -sequenze che differiscono tra di loro per un numero finito di n_i sono equivalenti, si vede che come vettori fondamentali di \mathcal{H}^{σ_1} possono essere scelti quegli autostati di H_0 che contengono un numero finito di protoni, neutroni, elettroni e un numero finito di stati non occupati dal neutrino.

Se si pone $a_{\nu}^* = b_{\nu}$, $a_{\nu} = b_{\nu}^*$ (b_{ν}^* creatore di buchi di neutrino o antineutrini) e si sostituisce in H_0 e $H_{\text{int.}}$ trascurando il termine $\sum \eta(\varepsilon) \omega_{k\sigma}$, che è un c -numero indeterminato e pertanto inessenziale, si ottengono le espressioni:

$$(1') \quad H_0 = \sum_{k, \varepsilon, \sigma} \left\{ \sqrt{k^2 + m_N^2} \eta(\varepsilon) a_{k, \varepsilon, \sigma}^{(N)*} a_{k, \varepsilon, \sigma}^{(N)} + \sqrt{k^2 + m_P^2} \eta(\varepsilon) a_{k, \varepsilon, \sigma}^{(P)*} a_{k, \varepsilon, \sigma}^{(P)} + \right. \\ \left. + \sqrt{k^2 + m_e^2} \eta(\varepsilon) a_{k, \varepsilon, \sigma}^{(e)*} a_{k, \varepsilon, \sigma}^{(e)} - |k| \eta(\varepsilon) b_{k, \varepsilon, \sigma}^{(\nu)*} b_{k, \varepsilon, \sigma}^{(\nu)} \right\};$$

$$(2') \quad H_{\text{int.}} = g \sum_{\substack{k_1, k_2, k_3 \\ \varepsilon_1, \varepsilon_2, \varepsilon_3, \varepsilon_4 \\ \sigma_1, \sigma_2, \sigma_3, \sigma_4}} \left\{ a_{k_1+k_2-k_3, \varepsilon_1, \sigma_1}^{(N)*} b_{k_3, \varepsilon_3, \sigma_3}^{(\nu)} a_{k_1, \varepsilon_2, \sigma_2}^{(P)} a_{k_2, \varepsilon_4, \sigma_4}^{(e)} + \text{h. c.} \right\}.$$

$H_{\text{int.}}$ dà luogo in questa fibra alla reazione:



Matematicamente, prescindendo cioè dalla presenza degli stati ad energia negativa che compaiono in questa fibra, le proprietà di $H_0 + H_{\text{int.}}$ coincidono con quelle dell'hamiltoniano del modello di Lee. Infatti gli stati di particella nuda di protone, elettrone e antineutrino sono anche autostati dell'hamiltoniano totale e possono perciò identificarsi con i corrispondenti stati di particella fisica. Ulteriori autostati dell'hamiltoniano totale sono anche tutti quegli stati che non contengono né un neutrone né le tre particelle P, e, \bar{e} . È anche facile vedere, se si procede in modo analogo a quanto esposto in (), che se si introduce un fattore di taglio sulle energie, ad esempio, di P ed e, è possibile trovare anche gli stati fisici di N e la rinormalizzazione della massa del neutrone.

(5) G. KÄLLÉN e W. PAULI: *Dan. Mat. Fys. Medd.*, **30**, no. 7 (1955).

Le energie negative che compaiono in \mathcal{H}^{σ_1} non danno luogo a difficoltà matematiche.

Noi faremo ora vedere che, se nessun fattore di convergenza viene introdotto, H non ha autostati in \mathcal{H}^{σ_1} oltre a quelli che abbiamo ora menzionato. Noi useremo di un procedimento dimostrativo usato per la prima volta da VAN HOVE⁽⁶⁾ per studiare proprietà analoghe nel caso dell'elettrodinamica quantistica.

Considerato $\varphi = \sum_{\{n_i\} \in \mathcal{H}^{\sigma_1}} c^{\{n_i\}} \varphi_{\{n_i\}}$ e preso $\varphi_{\{n_i^0\}}$ che contenga almeno una particella N, si definisca con A_k l'insieme dei vettori di stato $\varphi_{\{n_i\}}$ ottenuti da $\varphi_{\{n_i^0\}}$ togliendo una particella N e aggiungendo una terza P, e, \bar{v} con impulsi \mathbf{k}_1 , \mathbf{k}_2 , \mathbf{k}_3 che siano tutti in modulo maggiori di k e che soddisfino con la particella N al teorema della conservazione della quantità di moto. Definiamo inoltre con D_k l'insieme dei vettori di stato che contengono almeno una particella con impulso in modulo maggiore di k . Sia ora φ_{A_k} un generico vettore appartenente al primo insieme e φ_{D_k} quella parte di φ che è sovrapposizione di vettori appartenenti al secondo insieme.

Indicando allora con $H_{\text{int.}}^K$ l'operatore ottenuto da $H_{\text{int.}}$ limitando in esso la somma a termini appartenenti ad impulsi in modulo minori di K , è facile vedere che:

$$(\varphi_{A_k} H_{\text{int.}}^K, \{\varphi - c^{\{n_i^0\}} \varphi_{\{n_i^0\}} - \varphi_{D_k}\}) = 0.$$

Applicando ora la disuguaglianza triangolare e la disuguaglianza di Bessel, dopo alcuni semplici calcoli si perviene a:

$$(3) \quad \sqrt{\sum_{\{n_i\} \in A_k} |(\varphi_{\{n_i\}} H_{\text{int.}}^K, \varphi)|^2} \geq \sqrt{\sum_{\{n_i\} \in A_k} |c_{\{n_i\}} (\varphi_{\{n_i\}} H_{\text{int.}}^K, \varphi_{\{n_i^0\}})|^2} - \text{cost}_1 \|\varphi_{D_k}\| \cdot \text{Max} \|H_{\text{int.}}^K \varphi_{\{n_i\}}\|.$$

Considerando la struttura di $H_{\text{int.}}^K$ si può vedere che per le espressioni a secondo membro della (3) valgono le disuguaglianze

$$\begin{aligned} \sum_{\{n_i\} \in A_k} |c_{\{n_i\}}|^2 \cdot |(\varphi_{\{n_i\}} H_{\text{int.}}^K, \varphi_{\{n_i^0\}})|^2 &\geq \text{cost}_1^2 \cdot K^6; \\ \text{Max} \|H_{\text{int.}}^K \varphi_{\{n_i\}}\| &\leq \text{cost}_2 \cdot K^3. \end{aligned}$$

Pertanto la (3) diventa

$$(4) \quad \sqrt{\sum_{\{n_i\} \in A_k} |(\varphi_{\{n_i\}} H_{\text{int.}}^K, \varphi)|^2} \geq [\text{cost}_1 - \text{cost}_2 \cdot \text{cost}_2 \|\varphi_{D_k}\|] \cdot K^3.$$

Ma siccome $\|\varphi_{D_k}\| \rightarrow 0$ per $k \rightarrow \infty$, sarà sempre possibile scegliere k in modo

(6) L. VAN HOVE: *Bull. Ac. Roy. Belg., Cl. Sci.*, **27**, 1055 (1951).

che il secondo membro della (4) sia della forma $A \cdot K^2$ con $A = \text{cost} > 0$.

Si conclude pertanto che nel limite per K tendente all'infinito è

$$\lim_{K \rightarrow \infty} \|H_{\text{int.}}^K \varphi\| = \infty.$$

Lo stesso vale per H . Infatti usando la disugualianza triangolare si ha:

$$\|H^K \varphi\| \geq \sqrt{\sum_{\{n_i\} \in A_K} |(\varphi_{\{n_i\}} H^K, \varphi)|^2} \geq |g| \cdot \sqrt{\sum_{\{n_i\} \in A_K} |(\varphi_{\{n_i\}} H_{\text{int.}}^K, \varphi)|^2} - \sqrt{\sum_{\{n_i\} \in A_K} |(\varphi_{\{n_i\}} H_0^K, \varphi)|^2}.$$

Ma il secondo termine a secondo membro, per $K \rightarrow \infty$, diverge al più come

$$\sqrt{K^2 + m_N^2} + \sqrt{K^2 + m_P^2} + \sqrt{K^2 + m_e^2} + |K|$$

e non può pertanto compensare l'infinità dovuta al primo termine.

Resta così provato, potendosi ripetere il ragionamento di cui sopra nel caso che $\varphi_{\{n_i\}}$ contenta le tre particelle P, e, v, che H non ha in questo sottospazio altri autostati oltre a quelli particolari che abbiamo precedentemente considerato.

3. — Consideriamo ora il sottospazio \mathcal{H}^{σ_2} dello spazio hilbertiano totale \mathcal{H}^* generato dalle C^0 -sequenze che sono equivalenti alla C^0 -sequenza in cui tutti gli n_i sono nulli.

Gli autovettori di H_0 che corrispondono ad un numero finito di particelle costituiscono una base in \mathcal{H}^{σ_2} .

La reazione permessa in questa fibra è:



In questo sottospazio esistono autostati di H . Tra questi abbiamo anzitutto gli stati ad una particella poiché particelle nude e particelle fisiche vengono a coincidere (non c'è rinormalizzazione di massa). Altri autostati sono quelli che non contengono una delle coppie N, v e P, e.

Anche qui, definendo opportunamente degli insiemi A_k e D_k si riesce a far vedere che l'hamiltoniano totale non possiede altri autostati all'infuori di quelli ora detti.

In questa fibra non si ha inoltre rinormalizzazione di carica come sarebbe facile mostrare seguendo gli usuali metodi di calcolo.

4. — Nella usuale formulazione della teoria beta lo stato di vuoto è definito in modo che tutti gli stati ad energia negativa risultino occupati e lo spazio

hilbertiano \mathcal{H}^{σ_3} di questa teoria è generato dalle C^0 -sequenze che sono equivalenti alla C^0 -sequenza corrispondente allo stato di vuoto.

Ponendo, per tutti gli stati ad energia negativa: $a = b^*$, $a^* = b$ (b^* creatore di antiparticelle; stato di vuoto: zero particelle e antiparticelle), si avrà:

$$H_0 = \sum_{\mathbf{k}, \sigma} \left\{ \sqrt{k^2 + m_N^2} a_{\mathbf{k}, \sigma}^{(N)*} a_{\mathbf{k}, \sigma}^{(N)} + \sqrt{k^2 + m_N^2} b_{\mathbf{k}, \sigma}^{(N)*} b_{\mathbf{k}, \sigma}^{(N)} \right\} + \\ + \text{termini analoghi per } P, e, v;$$

$$H_{\text{int.}} = g \sum_{\substack{\mathbf{k}_1, \mathbf{k}_2, \mathbf{k}_3, \mathbf{k}_4 \\ \sigma_1, \sigma_2, \sigma_3, \sigma_4}} \left\{ [a_{-\mathbf{k}_1 + \mathbf{k}_2 - \mathbf{k}_3, \sigma_1}^{(N)*} + b_{\mathbf{k}_1 - \mathbf{k}_2 + \mathbf{k}_3, \sigma_1}] \cdot [a_{\mathbf{k}_1, \sigma_2}^{(P)} + b_{\mathbf{k}_1, \sigma_2}^{(P)*}] \cdot \right. \\ \cdot [a_{-\mathbf{k}_2, \sigma_3}^{(v)*} + b_{\mathbf{k}_2, \sigma_3}^{(v)}] \cdot [a_{\mathbf{k}_3, \sigma_4}^{(e)} + b_{-\mathbf{k}_3, \sigma_4}^{(e)*}] + \text{h. c.} \left. \right\};$$

(anche qui si prescinde da c -numeri inessenziali). Le transizioni permesse, che sono quelle generalmente note (e non saranno qui elencate), sono molto più numerose di quelle delle fibre precedenti.

In questa fibra non esistono affatto autostati di H .

Questo si può far vedere ragionando come prima, considerando cioè un vettore qualsiasi della fibra, un altro autovettore dell'hamiltoniano imperturbato che abbia proiezione non nulla su di esso e definendo con A_k l'insieme degli stati $\varphi_{\{n_i\}}$ ottenuti aggiungendo a $\varphi_{\{n_i\}}$ le quattro particelle P, \bar{e}, v, N tutte con impulso maggiore di k e soddisfacenti al teorema delle conservazioni della quantità di moto, e con D_k l'insieme degli stati che contengono almeno una particella con impulso in modulo maggiore di k .

5. – I risultati ottenuti mostrano: 1) che nel sottospazio \mathcal{H}^{σ_1} di \mathcal{H}^* le proprietà dell'hamiltoniano delle teorie beta coincidono essenzialmente con quelle dell'hamiltoniano del modello di Lee; 2) che un modello di teoria dei campi in cui non si hanno rinormalizzazioni né di carica né di massa si può ottenere considerando le proprietà di H in \mathcal{H}^{σ_2} .

Il fatto che in nessuna delle tre fibre considerate H non abbia altri autostati all'infuori di quelli che si determinano direttamente mostra che non è in linea di principio giustificato l'uso del calcolo delle perturbazioni.

Il modo più naturale per ovviare a questa difficoltà e far sì che H abbia altri autostati è di introdurre un fattore di convergenza. Ciò può essere fatto essenzialmente in due modi. Si può limitare la somma sugli impulsi nell'hamiltoniano di interazione a termini cui corrispondono impulsi di modulo inferiore ad un numero K prefissato; oppure mantenere la somma su tutti gli impulsi ma introdurre un fattore di taglio. Nel primo caso ogni difficoltà scompare perché il numero dei gradi di libertà del sistema diventa essenzialmente finito.

È allora possibile l'uso del calcolo perturbativo nell'ambito di ciascuna fibra purchè la costante di accoppiamento sia opportunamente piccola.

Nel secondo caso non è detto che $\|H\varphi\|$ risulti sempre finito. La condizione affinchè ciò avvenga varia in generale da sottospazio a sottospazio.

Nelle prime due fibre che abbiamo considerato una condizione sufficiente è che il fattore di taglio dipenda dagli impulsi di due particelle e faccia convergere l'integrale:

$$\int_0^\infty k_1^2 dk_1 \int_0^\infty k_2^2 dk_2 f^2(k_1, k_2) .$$

Nella fibra di interesse fisico il fattore di taglio deve invece dipendere dagli impulsi di tre particelle in modo da far convergere l'integrale:

$$\int_0^\infty k_1^2 dk_1 \int_0^\infty k_2^2 dk_2 \int_0^\infty k_3^2 dk_3 f^3(k_1, k_2, k_3) .$$

In ogni caso, oltre alle condizioni dette si può mostrare che deve essere soddisfatta anche la condizione:

$$\sum_{\{n_i\}} |e^{\{n_i\}}| < \infty .$$

Che il fattore di taglio debba essere più « forte » nel sottospazio di interesse fisico è intuitivo, in quanto il modo di operare di H risulta ivi molto più complesso che nelle altre fibre a causa del « mare » dei fermioni ad energia negativa.

* * *

Ringraziamo cordialmente gli amici A. LOINGER per le proficue discussioni e S. ALBERTONI per utili schiarimenti sulla teoria degli spazi prodotti infiniti diretti di von Neumann da lui forniti in una serie di seminari.

S U M M A R Y

The mathematical behaviour of the Hamiltonian H of the beta-theories when acting on some subspaces of the von Neumann infinite direct product space \mathcal{H}^* is considered. It is shown that the properties of H in one of these subspaces coincide from a mathematical point of view with those of the Hamiltonian in the Lee model. In another subspace one finds a model of field theory without renormalizations. It is also shown that the eigenvectors of H do not form a complete set in \mathcal{H}^* .

NOTE TECNICA

Counting Rate Curves for Geiger Counters and their Geometry.

P. J. GROUSE and H. D. RATHGEBER

The F.B.S. Falkiner Nuclear Research Laboratory (),
School of Physics, The University of Sydney - Sydney (N.S.W.)*

(ricevuto il 5 Febbraio 1957)

Summary. — The shape of the counting rate curve for a particular type of Geiger counter has been computed from purely geometrical considerations. Experiments designed to minimize non-geometrical effects support these calculations. General observations are made concerning the effect of design parameters upon counting curves for counters of all designs.

The starting voltage of counters has been investigated from the point of view of the mechanism of gas discharge ⁽¹⁾. It has also been shown that the shape of the counting curve between starting voltage and plateau depends on the number of primary ions ⁽²⁾. Several investigations have been concerned with the influence of the gas filling and cathode materials on the slope of the plateau and its upper end ⁽³⁾. However it is common experience that even under the best conditions both as to materials and number of primary ions the shape of the counting curve differs for counters of different designs.

Our investigation of the variation of effective length with applied voltage ⁽¹⁾ (referred to in this as I) makes it clear that the potentials of all surfaces inside a counter determine its effective length, and consequently influences its counting curve.

As end effects will be more pronounced the shorter the counter, we have investigated counters of widely different lengths. The calculations in I have

(*) Also supported by the Nuclear Research Foundation within the University of Sydney.

(¹) S. C. CURRAN and J. D. CRAGGS: *Counting Tubes* (London, 1949).

(²) D. H. WILKINSON: *Phys. Rev.*, **74**, 1417 (1948).

(³) D. H. WILKINSON: *Ionisation Chambers and Counters*.

(⁴) P. J. GROUSE and H. D. RATHGEBER: *Nuovo Cimento* **5**, 707 (1957).

been extended to cover all practical cathode lengths. The results of numerical calculations, performed with Silliac, the electronic digital computer within the School of Physics, University of Sydney, for counters of the design used in I, are shown in Fig. 1, k being the ratio of the length of the effective cathode to inside diameter, and s the ratio of effective gap length to inside diameter. When $k > 2$ the results obtained differ by less than 1% from those obtained in I for an infinitely long cathode.

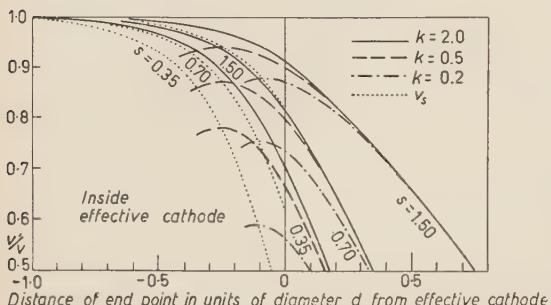


Fig. 1. — Calculated end of effective volume on axis of Geiger counter. V' starting voltage of infinitely long counter. For starting voltage V_s real: x -axis: $k/2$; y -axis: V'/V_s

The experimental conditions were chosen such as to minimize the influence of the non-geometrical factors mentioned above. The calculated curves were fitted to the experimental results for $k = 14.1$. There is agreement as to the general features of the increasing slope in the plateau and of the increasing rounding off of the rise to the plateau with decreasing k .

Since the effective surface of a counter consists of the cylinder and the two end surfaces, the shorter the counter the larger the relative contribution of these end surfaces. As the calculations above neglect the end areas it is to be expected that the observed counting rate curves should exceed the calculated curves by the same amount for all cathode lengths. In fact for the two curves for which the difference lies outside the experimental errors, i.e. $k = 2$ and 0.2, the absolute difference just above the starting voltage is the same, namely 7 ± 1 .

For the same counters the observed slope of the plateau is smaller than calculated. The main factor is that the end surface is not a plane normal to the axis as was assumed for the calculations but an approximate cone which becomes sharper as the end point moves into the gap; the effective area increases slower than the effective length. Thus using the

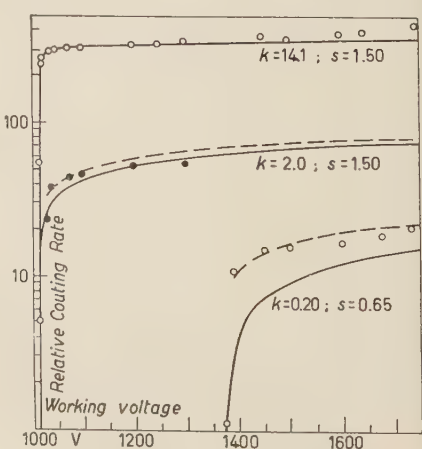


Fig. 2. — Counting rate curves. Plain curves: calculated. Dashed curves: calculated and corrected for contribution by end surfaces. Standard deviation equal diameter of dots.

length of cone measured in I we calculate that for $k = 2$ a difference of 6 between the calculated curve corrected for the contribution of the end surfaces and the measurements is to be expected at 1180 V. From geometrical considerations about the length of the cone we further deduce differences of between 12 and 15 at 1500 V for the same k and of between 4 and 6 at 1600 V for $k = 0.2$. These differences agree with those of 7, 14, and 3 respectively which have been obtained from the experimental data in Fig. 2.

It has thus been proved that in the absence of the disturbing factors mentioned at the beginning the shape of counting rate curves is uniquely determined by geometrical factors. This conclusion applies not only to one design but to all types of counters.

The slope of any of the measured curves does not exceed that of the calculated and corrected ones. There occur thus no spurious or multiple pulses up to an applied voltage of 1600 V. The counter was filled with argon of the quality used for welding with 10% Ethylformiate. Contrary to the usual prescriptions for Maze type counters this one was baked out at 350 °C and the wire heated to cherry red whilst under vacuum.

Since the relative contribution of the end surfaces and of the cylinder will depend upon the spatial distribution of the radiation, its specific ionization, its δ -rays and its scattering, the shape of the counting curve will not be the same for all radiations.

The curves of Fig. 1 show further that for $k < 2$ at the centre of the counters $V'/V < 1$, i.e. the actual starting voltage V_s is measurable, higher than the starting voltage V' for the infinitely long cathodes (see I). This effect has been observed previously (5). Assuming that the Geiger discharge spreads along the wire only as far as the end points it is evident that for very short counters the observed starting voltage will depend strongly on the sensitivity of the scaler. For the same cathode the starting voltage V_s increases with decreasing gap length. Starting voltages measured with the high sensitivity scaler for

$$\begin{array}{ll} k = 0.25 & s = 0.35, 0.45, 0.65 \text{ and } 0.85 \\ k = 0.45 & s = 0.85 \\ k = 1.40 & s = 0.85 \end{array}$$

agree with those predicted within 20 V.

Reference to Fig. 1 also explains the observation that the plateau slope increases with increasing gap length (6) because the increase in effective length is the larger the longer the gap.

The above considerations apply generally to all counter designs with suitable alterations allowing for different geometries. Thus it appears that the well known fact of bad plateaux for short counters is due to poor geometry.

In investigations on the influence of gas fillings the effect of geometry on starting voltage, on rise, and on plateau slope will have to be taken into account (7). In many counter designs the geometrical effect cannot be cal-

(5) D. BLANC and M. SCHERER: *Compt. Rend.*, **228**, 2018 (1949).

(6) D. BLANC: *Nuovo Cimento*, **1**, 1280 (1955).

(7) H. L. DE VRIES and G. W. BARENSEN: *Physica*, **18**, 927 (1952).

culated and therefore except for gross effects the comparison of measurements made with different counter designs is not possible.

RIASSUNTO (*)

La forma della curva del tasso di conteggio di un particolare tipo di contatore Geiger è stata calcolata in base a considerazioni puramente geometriche. Esperimenti ideati allo scopo di render minimi gli effetti non geometrici corroborano questi calcoli. Seguono osservazioni generali concernenti l'effetto dei parametri di progetto sulle curve di conteggio per contatori di ogni specie.

(*) Traduzione a cura della Redazione.

Experiments in the use of Thermistors for Low Pressure-Measurements.

M. VARIČAK

*The Institute of Physics, Faculty of Science
and the Rudjer Bošković Institute - Zagreb, Yugoslavia*

(ricevuto il 20 Giugno 1957)

Summary. — Experiments investigating the use of thermistors for low pressure-measurements were carried out. It is shown that bead thermistors may be used only in the pressure range from $1 \div 10^{-3}$ mm Hg. On the contrary thermistor-systems consisting of bead thermistors fixed to thin metallic foils take advantage not only of the high temperature coefficient of thermistors but also of the low radiation emissivity and heat capacity of metals. These samples allow precise measurements down to 10^{-6} mm Hg.

1. — Introduction.

1.1. *The principle of resistance gauges.* — Let us consider a metal filament in a tube at temperature T_1 , filled with gas at pressure p . It is evident that the temperature T_2 of the filament, heated by an electric current of intensity I , depends on the equilibrium between the input energy and the energy dissipated by thermal conduction through the gas, radiation and thermal conduction through the supports of the filament. In the molecular or Knudsen region, the thermal conductivity of the gas is dependent upon the pressure of the gas. Hence, neglecting the loss of energy through the supports, the stationary state of the filament is attained when

$$(1) \quad RI^2 = \beta p S(T_2 - T_1)T_1^{-\frac{1}{2}} + \sigma S(\varepsilon_2 T_2^4 - T_1^4).$$

R is the resistance and S the surface of the filament, β a constant depending on the nature of the gas, σ the radiation constant and ε_2 the radiation emissivity of the filament. Equation (1) is the base of resistance-gauges in which

the change of temperature T_2 is determined by measuring the change in resistance of the filament.

It is readily seen that the sensitivity of pressure measuring depends on the temperature coefficient of the filament. In recent years several gauges have been constructed using instead of filaments thermistors whose temperature coefficient is about ten times that of metals. In our opinion the results are disappointing as the pressure range of these gauges does not exceed pressures below 10^{-3} mm Hg.

To find the cause of this discrepancy and to investigate the possibility of the use of thermistors for measurements of low pressures, experiments with various samples of thermistors were carried out.

1·2. Discussion on the possibility of extending the pressure range of the gauge.

In order to extend the pressure range of the gauges, the loss of heat by conduction of gas

$$(2) \quad Q_1 = \beta p S(T_2 - T_1) T_1^{-\frac{1}{2}},$$

must be increased, and at the same time the loss of heat by radiation,

$$(3) \quad Q_2 = \sigma S(\varepsilon_2 T_2^4 - T_1^4),$$

must be reduced.

As is seen by (2), Q_1 may be increased, by increasing the temperature factor $(T_2 - T_1) T_1^{-\frac{1}{2}}$ and the surface S of the thermistor. The increase of the temperature factor by lowering the temperature of the tube walls T_1 is followed by a great inertia of the thermistor system so that pressure measurements under such conditions are practically impossible ⁽¹⁾.

The experiments described in this paper have the purpose of proving the influence of the dimensions of the surface of the thermistor on its sensitivity to pressure measurements.

1·3. Definition of sensitivity and inertia of thermistors to pressure change. — The sensitivity and inertia of a thermistor to pressure change are defined as follows.

The sensitivity σ is the change in the voltage drop on the thermistor, for a given current I and pressure change Δp . This may be written

$$(4) \quad \sigma = \left[\frac{\Delta V}{\Delta p} \right] I \text{ (mA)} \quad \text{volts.}$$

The inertia τ is the time during which the thermistor, for a given current I and pressure change Δp , attains 90% of its change in resistance. This gives

$$(5) \quad \tau = \left[\frac{t}{\Delta p} \right] I \text{ (mA)} \quad \text{seconds.}$$

The curves giving the change in resistance of a thermistor for current I and pressure change Δp as a function of time are called the σ - τ diagrams ⁽²⁾.

⁽¹⁾ M. VARIČAK: *Compt. Rend. Paris*, **245**, 853 (1956) and *J. Phys. et Rad.*, **18**, 70 A (1957).

⁽²⁾ M. VARIČAK: *Thesis* (Zagreb, 1957).

2. – Experimental work.

2.1. Experimental procedure. – The experiments were carried out by measuring the V - I and σ - τ diagrams of various samples by means of an oscilloscope. From the V - I diagrams the resistances R of the thermistor for every value of the current were determined. Wilson's resistance-temperature equation

$$(6) \quad R = a \exp [b/T],$$

gave the corresponding temperatures. The sensitivity and inertia of every sample were measured by the σ - τ oscillograms.

The experiments can be divided into two series. The first series consists of experiments with thermistors of various surface dimensions. The second series was carried out with thermistor-systems, that is, with bead thermistors attached to metallic foils.

2.2. Experiments with thermistors of various surface dimensions. – The samples chosen for these experiments were hematite bead thermistors and thermistors in the form of plates of various dimensions. Figure 1 shows the σ - τ diagram of a bead thermistor (N_1) and a thermistor in the form of a plate (N_2). N_1 has a surface of about $S \sim 0.01 \text{ cm}^2$, resistance $R_{20^\circ\text{C}} \sim 100000 \Omega$ and heat capacity $K = 0.0002 \text{ cal g}^{-1}$.

N_2 has a surface $S \sim 0.6 \text{ cm}^2$, $R_{20^\circ\text{C}} \sim 5000 \Omega$ and $K = 0.0285 \text{ cal g}^{-1}$. The currents through the samples were chosen according to their V - I diagrams.

In our notation the sensitivity and inertia of these samples may be written:

$$(7) \quad \left\{ \begin{array}{l} N_1: \quad \sigma_1 = \left[\begin{matrix} 0.3 \\ 10^{-2} \div 10^{-3} \end{matrix} \right] \text{volts}, \\ \quad \tau_1 = \left[\begin{matrix} 5 \\ 10^{-2} \div 10^{-3} \end{matrix} \right] \text{seconds}, \\ \\ N_2: \quad \sigma_2 = \left[\begin{matrix} 0.84 \\ 10^{-2} \div 10^{-3} \end{matrix} \right] \text{volts}, \\ \quad \tau_2 = \left[\begin{matrix} 68 \\ 10^{-3} \div 10^{-2} \end{matrix} \right] \text{seconds}. \end{array} \right.$$

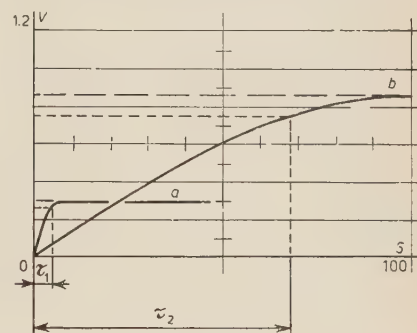


Fig. 1. – The σ - τ diagrams of the samples N_1 and N_2

- a) N_1 : $I = 1 \text{ mA}$,
 $\Delta p = (10^{-2} \div 10^{-3}) \text{ mm Hg}$,
- b) N_2 : $I = 10 \text{ mA}$,
 $\Delta p = (10^{-2} \div 10^{-3}) \text{ mm Hg}$.

The ratio of the loss of heat by gas-conduction and by radiation, cal-

culated from the equations (2), (3) and (6) is at a pressure of $p = 10^{-3}$ mm Hg:

$$(8) \quad \begin{cases} N_1: & Q_1/Q_2 = 0.01, \\ N_2: & Q_1/Q_2 = 0.03. \end{cases}$$

In these calculations the radiation emissivity of the thermistors is assumed to be $\varepsilon_2 = 1$.

It is evident that the size of the surface dimensions influences the sensitivity of the thermistor, but as may be seen by (8) the loss of heat by radiation is relatively very great.

In addition, the increase of surface of the thermistor plates, followed by increase of their mass and heat capacity, prevents these samples from indicating momentaneous pressure changes (Fig. 1).

2·3. Experiments with thermistor-systems. — From the described experiments, it could be concluded that it is necessary to reduce the effect of radiation as well as the heat capacity of the samples. This experience led to the construction of thermistor systems, consisting of a bead thermistor fixed to a metal foil. These systems take advantage not only of the high temperature coefficient of thermistors but also of the small radiation emissivity and heat capacity of metals.

Experiments were carried out with a thermistor N_1 and metal foils of silver, copper, aluminium and tin. Symbolically the thermistor-systems with various metals are denoted Sn- r , Cu- r etc., where r is the radius given in centimeters of the metal discs. It was found that tin is the most adequate material, as it has not only a very small heat capacity but is also inert to the influence of the atmosphere and to corrosive vapours.

The thermistor-systems Sn - 0.5 to Sn - 3, were examined. It was found that the sensitivity of the samples practically did not change for all dimensions of the foil between 1.5 cm and 3 cm.

Fig. 2 and Fig. 3 give the σ - τ diagrams of Sn - 1.5 and Sn - 2.5. These oscillograms obviously indicate the improvement in sensitivity attained by the construction of thermistor-systems. While bead thermistors cannot be

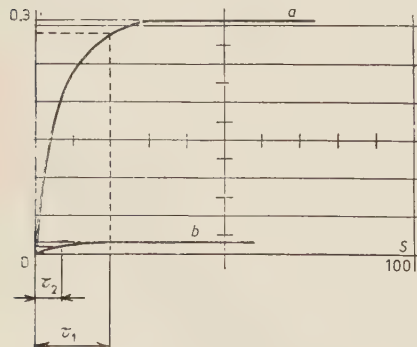


Fig. 2. — The σ - τ diagrams of Sn - 1.5

- a) $I = 1$ mA, $\Delta p = (10^{-4} \div 5 \cdot 10^{-6})$ mm Hg,
- b) $I = 1$ mA, $\Delta p = (10^{-5} \div 5 \cdot 10^{-6})$ mm Hg.

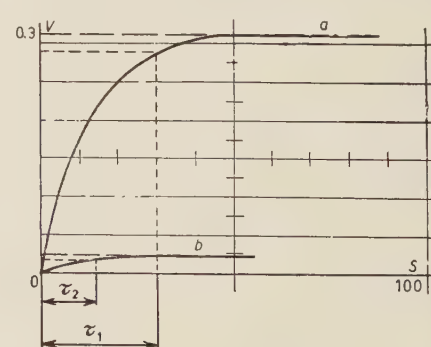


Fig. 3. — The σ - τ diagrams of Sn - 2.5

- a) $I = 1$ mA, $\Delta p = (10^{-4} \div 5 \cdot 10^{-6})$ mm Hg,
- b) $I = 1$ mA, $\Delta p = (10^{-5} \div 5 \cdot 10^{-6})$ mm Hg.

used for pressure changes below $p = 10^{-3}$ mm Hg, the thermistor system Sn - 1.5 for example provokes a change of voltage of 18 mV, even for a pressure change $\Delta p = 10^{-5} \div 5 \cdot 10^{-6}$ mm Hg and this change occurs in 7 s. The results of sensitivity and inertia, written in our notation are

$$(9) \quad \left\{ \begin{array}{l} \text{Sn - 1.5:} \quad \sigma = \left[0.31 \right] \frac{1}{10^{-1} \div 5 \cdot 10^{-6}} \quad \text{volts,} \\ \tau_1 = \left[20 \right] \frac{1}{10^{-1} \div 5 \cdot 10^{-6}} \quad \text{seconds,} \\ \sigma_2 = \left[0.018 \right] \frac{1}{10^{-5} \div 5 \cdot 10^{-6}} \quad \text{volts,} \\ \tau_2 = \left[7 \right] \frac{1}{10^{-5} \div 5 \cdot 10^{-6}} \quad \text{seconds,} \end{array} \right.$$

$$(10) \quad \left\{ \begin{array}{l} \text{Sn - 2.5:} \quad \sigma_1 = \left[0.32 \right] \frac{1}{10^{-1} \div 5 \cdot 10^{-6}} \quad \text{volts,} \\ \tau_1 = \left[30 \right] \frac{1}{10^{-1} \div 5 \cdot 10^{-6}} \quad \text{seconds,} \\ \sigma_2 = \left[0.02 \right] \frac{1}{10^{-5} \div 5 \cdot 10^{-6}} \quad \text{volts,} \\ \tau_2 = \left[14 \right] \frac{1}{10^{-5} \div 5 \cdot 10^{-6}} \quad \text{seconds.} \end{array} \right.$$

Fig. 4 shows the temperature distribution $T = f(r)$ on the thermistor system Sn - 0.5 and Sn - 3, measured by means of thermo-couples soldered to the metal foils. It can be seen that the temperature of the margin of Sn - 3, is nearly identical with the temperature of the surroundings, so that the loss of heat from this part of the system is negligible. This explains the fact that the sensitivity of systems Sn - 1.5 until Sn - 3 practically did not change.

3. – Conclusion.

From the experiment described above the following conclusions may be drawn:

The bead thermistors, produced by various factories for vacuum-measurements, can be used only for pressures between (1 and 10^{-3}) mm Hg. Increasing the dimensions of thermistors leads to samples that cannot follow pressure changes quickly enough to allow precise measurements.

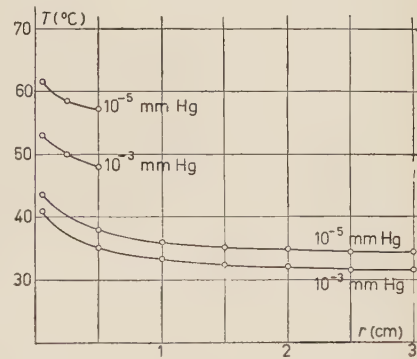


Fig. 4. – The experimental curves $T = f(r)$ for Sn-0.5 and Sn-3.

Thermistor-systems, on the contrary though their surface is several hundred times greater, have a heat capacity approximately only ten times that of bead thermistors. Therefore they respond nearly instantaneously to pressure changes. In addition, the low radiation emissivity of the metal foils considerably increases the sensitivity of these samples, so that they can be used for low pressure measurements down to 10^{-6} mm Hg.

* * *

The author wishes to thank Professor M. PAIĆ for his interest and encouragement in this work.

RIASSUNTO (*)

Si sono eseguiti esperimenti per indagare sull'uso dei termistori nella misura delle basse pressioni. Si dimostra che i termistori a perle si possono usare solo nel campo di pressioni da 1 a 10^{-3} mm Hg. Viceversa sistemi di termistori a perle fissati a sottili fogli metallici beneficiano non solo dell'elevato coefficiente termico dei termistori ma anche del debole potere radiante e della capacità termica dei metalli. Essi consentono misure esatte fino a 10^{-6} mm Hg.

(*) Traduzione a cura della Redazione.

Information on a 2.5 MeV Microtron.

A. CARRELLI and F. PORRECA

Istituto di Fisica Sperimentale dell'Università - Napoli

(ricevuto il 21 Luglio 1957)

Summary (*). — An electron microtron of the $a = 3$, $b = 1$ model has been built and his essential parts are described. 10 orbits have been obtained and the final energy of the particles is 2.5 MeV. The machine is at present without an extractor and therefore only γ -rays are available. The average intensity on the last orbits is some 10^{-7} A.

(*) *Editor's translation.*

1. — Introduction.

Herewith some information on the construction and the first results of the operation of an electron accelerator of a relatively simple make up, of the microtron type.

The principle of its operation was explained for the first time by VEKSLER⁽¹⁾ in 1945, while the first machine was built by REDHEAD *et al.*⁽²⁾ in 1950. The extraction of electrons was obtained by HENDERSON *et al.*⁽³⁾ in London, in the 4.5 MeV microtron.

The intensity H of the constant magnetic field, the potential ΔV and the frequency f of the accelerating electromagnetic field must satisfy the following equations:

$$H = \frac{1}{a-b} \frac{2\pi f cm_0}{e}, \quad \Delta V = \frac{b}{a-b} \frac{m_0 c^2}{e},$$

(¹) V. VEKSLER: *Journ. Phys. USSR*, **9**, 153 (1945).

(²) P. A. REDHEAD, H. LE CAINE and W. J. HENDERSON: *Canad. Journ. Res., A* **28**, 73 (1950).

(³) C. HENDERSON, F. F. HEYMANN and R. S. JENNINGS: *Proc. Phys. Soc., B* **66**, 654 (1953).

where m_0 is the electron rest mass, and a and b are the parameters which determine the operation type of the machine.

For the time being our microton works at $a = 3$; $b = 1$, $H = 520$ Oe, $f = 2930$ MHz and therefore ΔV results equal to ~ 250 kV.

The energy increment per orbit is about 0.25 MeV. Since the 0.25 MeV electrons are already highly relativistic particles (their speed being about $4/5$ of that of light), the first orbit, completed within a period equal to three times that of the rf., has fairly accurately 3λ length (λ being equal to 10 cm). The diameter of the first orbit is therefore corresponding to approximately $3\lambda/\pi \sim 9.55$ cm, while that of the successive ones increases per each orbit by $\lambda/\pi \approx 3.18$ cm.

2. - Construction particulars.

The diameter of the magnetic poles corresponds to 60 cm, but the dimensions required for the acceleration of the electrons on stable orbits are limited to a central area of about 44 cm diameter, whose intensity H is strictly constant

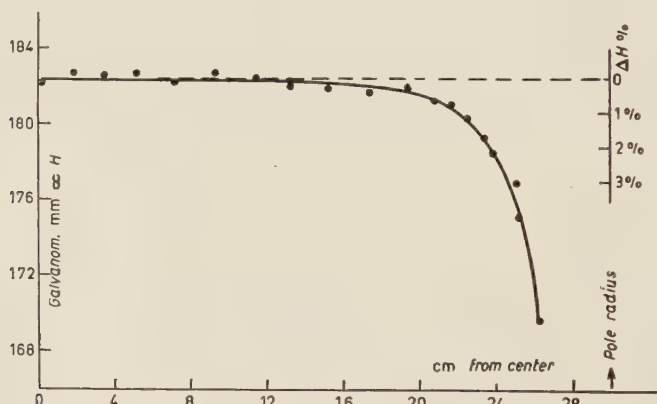


Fig. 1.

within 1%. The intensity of the field is shown by Fig. 1. Between the poles of the magnet is located the box in which vacuum is obtained. The box has a certain number of lateral openings, as shown by Fig. 2, to which are attached a vacuum pump, a vacuum meter, the termination of the wave guide with the acceleration cavity and two windows for the observation of the interior.

Diametrically opposite to the opening of the wave guide is located another opening through which runs a metal rod carrying the target.

At the beginning the machine worked without any relevant variations, with a vacuum of $5 \cdot 10^{-4} \div 10^{-4}$ mm Hg, obtained by the combination of a rotating pump with another Pfeffer diffusion pump. The wave guide with the cavity is also placed in the vacuum, by means of a special window, as vacuum seal which allows for the passage of electromagnetic waves.

Fig. 3 shows the design of the transmission line from the magnetron M to the cavity C . The window is placed in OO' . The rf. energy is supplied by the 2 J29 Magnetron (Raytheon), which gives, under the established con-

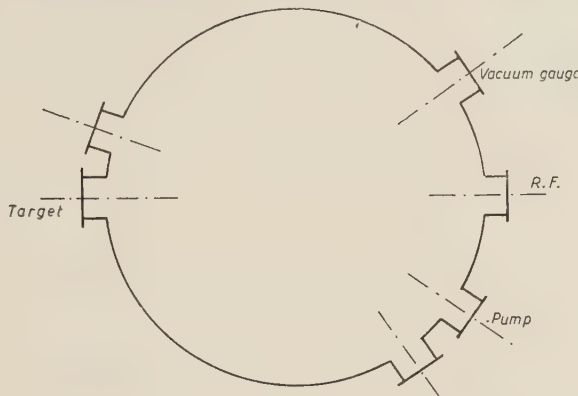


Fig. 2.

ditions, a peak power of about 200 kW, with a repetition frequency of 200 Hz with a $1.6 \cdot 10^{-6}$ s duration. The line consists of a standard wave guide, 3 in. \times 1.5 in., operating in the mode H_{01} , with the E vector in the plane of the orbits. First, the guide carries the magnetron probe, while tract 2 bears a plexiglass phase shifter of suitable size and shape, micrometrically manageable, so that inside the cavity best possible resonance conditions can be obtained, by means of modification of the actual length of the electric transmission line.

A T joint 3 provides a series connection of the guide terminal branch, carrying the cavity with a high power load, which stabilizes the operation frequency. Special devices have been applied in the designing of the resonant cavity, which must be small, in order not to hinder the passage of the electrons of the first orbit, and should furthermore possess a high Q . The shape and the size of the cavity have been established on the basis of previous experience (⁴) and information kindly provided by Dr. R. E. JENNINGS of the U.C. London. The resonant cavity consists chiefly of a cylindric cavity whose bases have conic recesses, symmetrical with regard to the cylinder axis, which is the direction of the electron acceleration. Inside the cavity the working

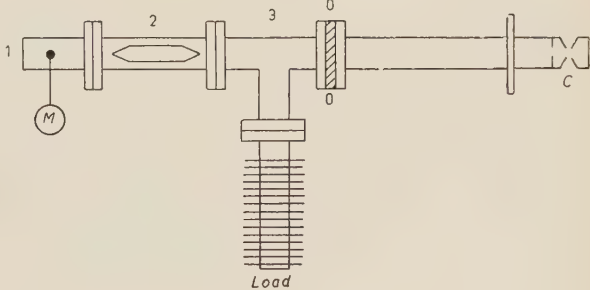


Fig. 3.

(⁴) W. H. HANSEN and R. D. RICHTERMAYER: *Journ. Appl. Phys.*, **10**, 189 (1949).

power lines generate a very high field E of an average of 300 kV/cm, concentrated along the gap crossed by the electrons.

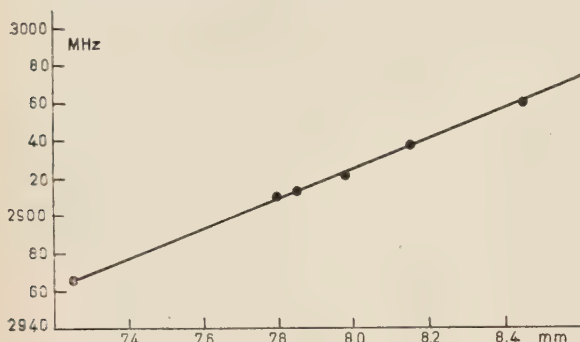


Fig. 4.

Small resonance frequency variations of the cavity can be obtained through modification of gap length by some tenth of mm, by means of a sensitive thermal device which can be adjusted from outside. Fig. 4 shows a plot of the calibration curve of the resonance frequency, depending on the length of the gap. The operation frequency of the magnetron corresponds to (2930 ± 10) MHz and the length

allowed for the cavity gap is $(7.95 \pm 5) \cdot 10^{-2}$ mm, while the cavity resonance factor, without the electronic load, amounts to about 8000. The highly intense electromagnetic field between the tops of the conic recesses of the cavity extracts the electrons to be accelerated, the cavity thus working also as a particles injector.

3. - The results.

Efficient operation of the machine can already be seen from the first results regarding the number of visible orbits and the current intensity of the electronic beam. In order to provide the possibility of checking on the number of orbits and their dislocation, the movable target carries a small electroluminous screen, so as to observe the traces of the intercepted beam.

An index, fixed on the target, running along a firm graduated ruler, allows for the reading of the orbital position. An excellent agreement has been observed between the theoretical values of the orbital diameters and those which have been measured, taking into account the uncertainty, due to the limited dimensions of the luminous trace produced by impact on the screen. The first orbits in particular are very wide and intense: the mark of the first has a section of $2 \div 3$ cm diameter, as has also been proved by JENNINGS *et al.*, while only a particle fraction remains in resonance with the accelerating field.

We have observed 10 orbits with $a = 3$ and $b = 1$. Table I shows the computed values as well as the measured ones of the observed orbits.

By well-times reduction of the intensity H , the microtron can work also under the conditions of $a > 3$ and $b = 1$. For $H \cong 354$ Oe 9 orbits were in fact observed, corresponding to the case $a = 4$, $b = 1$; with $H = 260$ Oe, 5 orbits relative to the case $a = 5$, $b = 1$; with $H = 210$ Oe 3 orbits for $a = 6$ and $b = 1$. As was foreseen, it has been observed that the diameter of the first orbit (orbit n), of one of these superior ways ($a = i$) corresponds to that of the second orbit (orbit $n+1$), of the previous way ($a = i-1$).

Ing. S. & Dr. GUIDO BELOTTI

Telegrammi:
INGBELOTTI - MILANO

MILANO
Piazza Trento, 8

Telef.: 54.20.51 - 54.20.52
54.20.53 - 54.20.20

GENOVA

Via G. D'Annunzio, 1-7 - Tel. 52.309

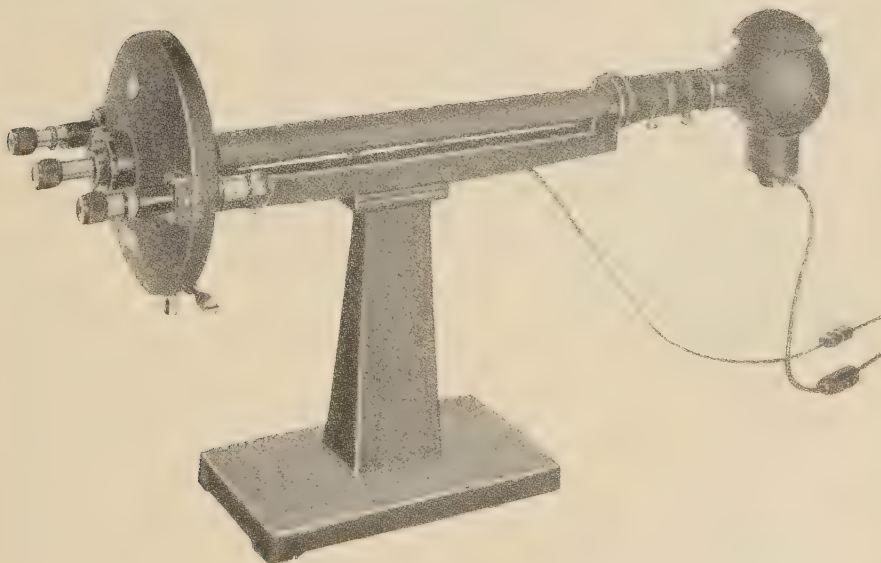
ROMA

Via del Tritone, 201 - Tel. 61.709

NAPOLI

Via Medina, 61 - Tel. 23.279

Polarimetro di Lippich SCHMIDT & HAENSCH



A lettura diretta su scala graduata - Precisione 0,005°

Agenti generali per l'Italia della

SCHMIDT & HAENSCH

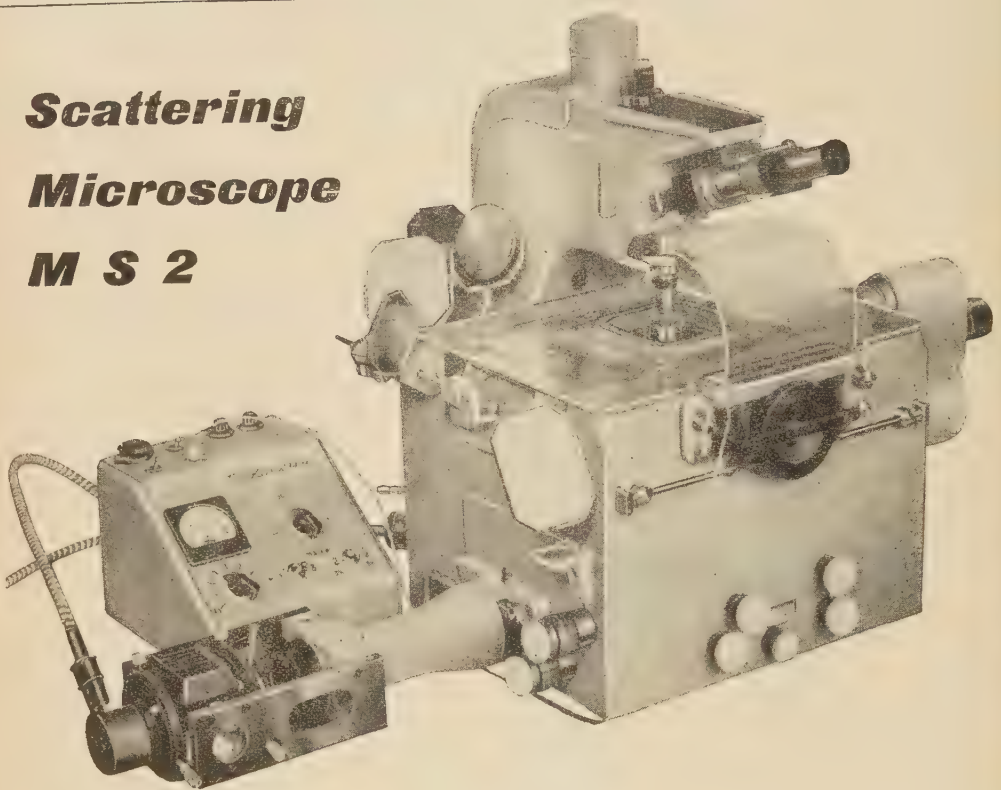
COLORIMETRI - SACCARIMETRI - REFRAZIONIMETRI (0-80° Brix) - FOTOMETRI - DENSITOMETRI -
TENSIOSCOPI - ANOMALOSCOPI - SPETTROSCOPICI - SPETTROGRAFI - MONOCROMATORI -
SPETTROFOTOMETRI - PIROMETRI - SPETTROMETRI - APPARECCHI DI CONTROLLO OTTICO.

DEPOSITO - SERVIZIO RIPARAZIONI

Fratelli *Koristka s.p.a.*

MILANO, Italy
VIA AMPÈRE 43

**Scattering
Microscope
M S 2**



Stage movements:

X axis = 50 mm - noise level < 100 Å/2 mm - reading to 1 μ

Y " = 50 mm - " " < 500 Å/2 mm - " " 10 μ

Z " = 30 + 3 mm - " " < 50 Å/2 mm - " " 1 μ

Long working distance oil immersion objectives:

3 mm; f = 5.7 mm achromatic N.A. = 1.05

1.35 mm; f = 3.5 mm " = 0.90

0.70 mm; f = 3 mm apochromatic " = 1.25

0.53 mm; f = 1.8 mm semi apochromatic " = 1.25

Ocular tubes:

binocular head;

monocular goniometer eyepiece 360°/1' or 360°/10';

eyepiece drum micrometer;

eyepiece blade micrometer (Poohstrolino).

Field enlarger.

Plate coordinate reader.

Repeater for lengthening X and Y movements.

Magnetic plate fixers.

Vacuum device for the rotation of small plates on the Z axis through 180°.

• Magnification to 3600.

Max plate size 7" x 7".

Weight 52 Kg.

TABLE I.

Orbit	1	2	3	4	5	6	7	8	9	10
Theoretical diameter cm	9.6	12.7	16.0	19.1	22.3	25.5	28.6	31.8	35.0	38.2
Experimental diameter cm	9.3	12.5	15.5	19.7	23.3	27.0	29.5	32.5	35.5	38.0
Energy (MeV)	0.25	0.5	0.75	1.0	1.25	1.5	1.75	2.0	2.25	2.5

For the measuring of the electronic beam the average current intensity was evaluated, by intercepting the particles with a Pb target instead of the screen, of a thickness of about 2 mm, sufficient to absorb totally the electrons till about 3 MeV (range 1.5 g/cm^2).

A long period galvanometer connected directly with the target and with the box, allows for the measuring of the average current intensity of the electron beam. The latter consists of electron convoys, which occur at every peak period of the rf. accelerator potential, during the 200 impulses per second of the magnetron, each lasting $1.6 \cdot 10^{-3} \text{ s}$. The distribution intensity is shown

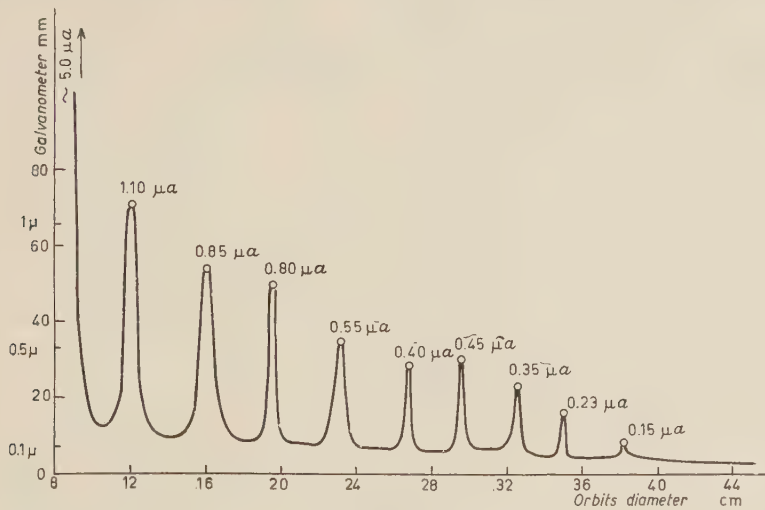


Fig. 5.

by Fig. 5. The average values are not inferior to those obtained by the machines of the same type of an earlier make. By multiplying the values obtained by $(5 \cdot 10^{-3})/(1.6 \cdot 10^{-6}) \sim 3 \cdot 10^3$ we shall obtain the average value of the intensity during each impulse, resulting in about $\gtrsim 1 \text{ mA}$ on the orbits of highest energy.

In order to stabilize best the intensity value along the orbits, it is neces-

sary to improve the resonance conditions, which are strongly influenced by the position of the phase shifter, by the resonance of the cavity with the frequency emitted by the magnetron, and by the value of H for obtaining resonance.

We are now proposing to design the electron extractor and to increase the produced energy to 6 MeV.

RIASSUNTO

È stato realizzato un microtrone per elettroni, di tipo $a = 3$ e $b = 1$ e si descrivono le sue parti essenziali. Sono state ottenute 10 orbite e l'energia finale delle particelle è di 2.5 MeV. La macchina attualmente non è munita di estrattore e quindi sono utilizzabili solo raggi γ . L'intensità media sulle ultime orbite è di qualche 10^{-7} A.

LETTERE ALLA REDAZIONE

(La responsabilità scientifica degli scritti inseriti in questa rubrica è completamente lasciata dalla Direzione del periodico ai singoli autori)

Counting Rate of Cosmic Ray Counter Telescopes in Inclined Directions.

D. A. TIDMAN and K. W. OGILVIE

School of Physics - The University of Sydney - Sydney

(ricevuto il 12 Marzo 1957)

Counter telescopes, consisting essentially of two uniformly sensitive plane rectangular areas, are often used to study the zenith angular dependence of an incoming flux of radiation. If the cross-sectional area of the telescope is not small compared with its length, a correction factor f , depending upon the geometry of the telescope, must be included in the formula

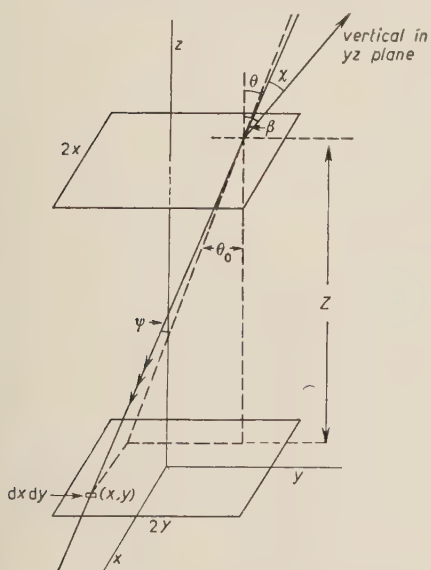


Fig. 1.

$$(1) \quad \varphi = I_v \cos^n \beta \cdot \frac{4XY}{Z^2} \cdot 4XY \cdot f.$$

Here the directional intensity of the incoming radiation varies as the n -th power of the angle β between the vertical and the telescope axis in the Y direction. The telescope trays are of dimension $2X$ by $2Y$, separated by a distance Z .

Referring to Fig. 1, we have

$$\cos \theta = \cos \theta_0 \cos \psi,$$

$$\cos \chi = \cos (\beta - \theta_0) \cos \psi,$$

$$d\omega = \cos \psi d\psi d\theta_0.$$

Also, the resolved element of area in the direction of the ray is $dA = dxdy \cos \theta_0$, and I_v is the vertical flux of particles per cm^2 per s per sr.

⁽¹⁾ A. LOVATI, A. MURA, G. SUCCI and G. TAGLIAFERRI: *Nuovo Cimento*, **12**, 526 (1954).

Then the total flux is

$$(2) \quad \varphi \left(n, \beta, \frac{2Y}{Z}, \frac{2X}{Z} \right) = I_\nu \int_{-Y}^Y dy \int_{\theta_1}^{\theta_2} \cos^n (\beta - \theta_0) \cos \theta_0 d\theta_0 \int_{-x}^x dx \int_{\psi_1}^{\psi_2} \cos^{n+2} \psi d\psi$$

with

$$\theta_1 = -\operatorname{tg}^{-1} \left(\frac{Y+y}{Z} \right), \quad \psi_1 = -\operatorname{tg}^{-1} \left(\frac{X+x}{Z} \right) \cos \theta_0,$$

$$\theta_2 = \operatorname{tg}^{-1} \left(\frac{Y-y}{Z} \right), \quad \psi_2 = \operatorname{tg}^{-1} \left(\frac{X-x}{Z} \right) \cos \theta_0.$$

This expression has in general to be integrated numerically. We give curves of f in equation (1) above in Fig. 2, corresponding to the case of a square section telescope, $X = Y$, for various values of $2X/Z$, and $n = 2, 3, 4, 5, 6$. These were obtained by numerical integration, using the electronic computer « Silliac ».

To cover cases where $X \neq Y$, and for other values of n , we also give an expansion of expression (2) above.

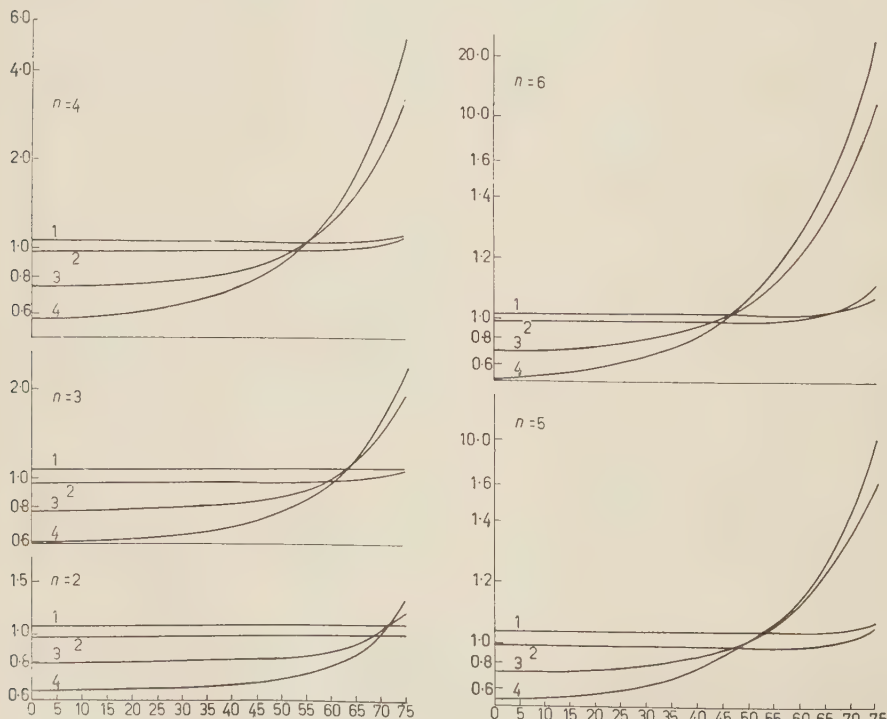


Fig. 2. — Curve 1 refers to $(2X/Z) = 0.05$; Curve 2 refers to $(2X/Z) = 0.1$;
 3 " " $(2X/Z) = 0.5$; 4 " " $(2X/Z) = 0.75$;

If we invert the first and second pairs of integrals, and assume $\operatorname{tg} \beta < Z/2Y$, so that $\operatorname{tg} \theta_0 \operatorname{tg} \beta < 1$ over our range of integration, we find,

$$\varphi = 2I_\nu \cos^n \beta \sum A_r \operatorname{tg}^{2r} \beta ,$$

where

$$A_r = \frac{2n!}{(2r)!(n-2r)!} \int_0^{\operatorname{tg}^{-1}(2Y/Z)} d\theta_0 (2Y - Z \operatorname{tg} \theta_0) \cos^{n+1} \theta_0 \operatorname{tg}^{2r} \theta_0 \int_0^{\operatorname{tg}^{-1}(2X \cos \theta_0/Z)} d\psi \cos^{n+2} \psi \left(2X - \frac{Z \operatorname{tg} \psi}{\cos \theta_0} \right) .$$

We now approximate the ψ integral by writing $\cos \theta_0 \operatorname{tg} \psi' = \operatorname{tg} \psi$, so that it becomes

$$2X \cos \theta_0 \int_0^{\operatorname{tg}^{-1}(2X/Z)} d\psi' \frac{\sec^2 \psi' [1 - (Z/2X) \operatorname{tg} \psi']}{(1 + \cos^2 \theta_0 \operatorname{tg}^2 \psi')^{(n+4)/2}} .$$

Since $\operatorname{tg}^2 \psi' < 4X^2/Z^2$, and the maximum value of $\cos^2 \theta_0 \operatorname{tg}^2 \psi'$ is when

$$1 - \frac{Z}{2X} \operatorname{tg} \psi' = 0 ,$$

we can expand the denominator of the above integrand, obtaining finally

$$(3) \quad \varphi_n = 8I_\nu \cos^n \beta X Y \sum_{rj} A_{rj} \operatorname{tg}^{2r} \beta ,$$

where

$$A_{rj} = \binom{n}{2r} \binom{-(n+4)/2}{j} \frac{(2X/Z)^{2j+1}}{(2j+1)(j+1)} \int_0^{\operatorname{tg}^{-1}(2Y/Z)} d\theta_0 \left(1 - \frac{Z}{2Y} \operatorname{tg} \theta_0 \right) \cos^{2j-n-2} \theta_0 \operatorname{tg}^{2r} \theta_0 .$$

All the A_{rj} 's are simple integrals, which can be evaluated for any likely value of n . Exact evaluation of the expression 2 for $2X/Z = 0.465$, $2Y/Z = 0.744$ and $n = 2$, gives

$$\varphi_2(\beta) = \varphi(0)(1 + 0.069 \operatorname{tg}^2 \beta) ,$$

while three terms of the expansion 3 lead to

$$\varphi_2(\beta) = \varphi(0)(1 + 0.07 \operatorname{tg}^2 \beta) .$$

These formulae allow the geometrical correction to be evaluated rapidly to sufficient accuracy for most experimental purposes. Corrections for efficiency, effective length etc. are easily introduced by variation of the area of the trays.

Another use for this approximation is to compute projected angular distributions, such as those given by the photographic records of cloud chamber operation, with a $\cos^n \theta$ law of zenith angular distribution. This problem has been studied by

LOVATI *et al.* (2) who show that $N_n(\theta_0)$, the orthogonal projection on the vertical plane yz , of the zenith angular distribution function, is given by the relation

$$\frac{\partial \varphi_n}{\partial \theta_0} = N_n(\theta_0) .$$

Thus putting $\beta = 0$ we have

$$N_n(\theta_0) = 16XY \left(1 - \frac{Z}{2Y} \operatorname{tg} \theta_0 \right) \cos^{n+2} \theta_0 \sum F_k ,$$

where

$$F_r = 2^{2r} \left[\frac{1}{2(2r-1)} - \frac{1}{4r} \right] \binom{X}{Z} .$$

Measurement of Ionization on Dipping Tracks in Nuclear Emulsion.

R. C. KUMAR

Physics Department - University College, London

(ricevuto il 10 Maggio 1957)

Introduction.

The distribution in observed gap length on tracks of ionizing particles in nuclear emulsions has been shown to be exponential over the entire range of ionization (O'CEALLAIGH⁽¹⁾; P. H. FOWLER and D. H. PERKINS⁽²⁾, to be referred to as FP hereafter). The coefficient of exponent of this distribution, g , is found to be a useful measure of the ionization in a track. Knowing B , the number of blobs (or gaps) per unit length on a track and H , the number of gaps per unit length that exceed a certain length l , g can be determined from the equation

$$(1) \quad H = B \exp [-gl].$$

Another relation between B and g also exists, given by the equation

$$(2) \quad B = g \exp [-g\alpha].$$

In the models, given by FP, of distribution of crystals over tracks in emulsions, α is identified with the mean separation of the centres of two crystals, which are just resolved upon develop-

ment. Thus the value of α is determined largely by the developed grain size. Experimentally it is best determined by measuring B and H on a flat track of about six times minimum ionization with the help of equations (1) and (2). α is found to be approximately constant for one particular stack of plates developed under identical conditions and for different stacks it usually varies between 0.60 μm and 0.90 μm . It is also found (e.g. in the present work) that the value of α does not depend appreciably on dip angle up to 60 degrees in unprocessed emulsion. Once α is known, the value of g for any track that is not too heavily ionizing can be determined by measuring B alone.

The case of lightly ionizing dipping tracks.

Comparatively little attention has been paid previously to the measurement of ionization for steep tracks although measurements on relativistic α -tracks of dip up to about 50° in unprocessed emulsion have been described by WINZELER⁽³⁾.

⁽¹⁾ C. O'CEALLAIGH: *CERN Report*, B. S. 11. (1954)

⁽²⁾ P. H. FOWLER and D. H. PERKINS: *Phil. Mag.*, **46**, 587 (1955)

⁽³⁾ H. WINZELER: *Suppl. Nuovo Cimento*,

4, 259 (1956).

For dipping tracks, equations (1) and (2) need modification. In equation (2) α has to be replaced by $\alpha \sec \theta$ where θ is the angle of dip of the track in unprocessed emulsion. This is because the centres of two grains separated by a length $\alpha \sec \theta$ on the actual trajectory of the particle would appear to be separated only by a length α on projection and the two grains would be only just resolved. Therefore, equation (2) becomes, for dipping tracks

$$(3) \quad B^l = g \exp [-g\alpha^l],$$

where $B^l = N_B/L_B \sec \theta$, N_B being the number of blobs counted on a projected length L_B of the track and $\alpha^l = \alpha \sec \theta$. Using equation (3), measurements of g^x ($= g/g_0$) were made on some π -meson tracks of known range having angles of dip between 0° and 62° in unprocessed emulsion. From the experimental curve of FP connecting g^x with range the expected values of g^x for those tracks were estimated. The results are given in Fig. 1.

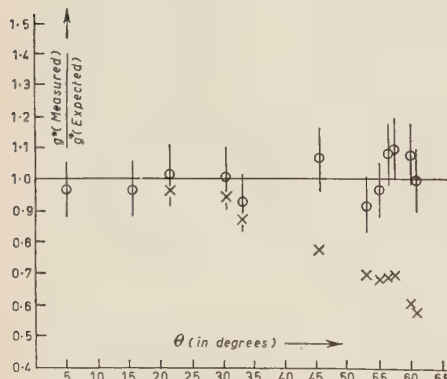


Fig. 1. — Shows the ratio $g^x(\text{meas.})/g^x(\text{exp.})$ for π -mesons of different dips. The points marked with x result from the use of the formula $B^l = g \cdot \exp [-g\alpha^l]$ which corrects for the length of the dipping track alone. Points marked with \odot result from the use of equation (3) which in addition corrects for the effect of the obscuration of grains due to inclinations of trajectory. The measured g^x values lie between 1.5 and 3.0. The vertical bars indicate statistical errors for the points marked with \odot .

It is seen that the agreement between g^x determined using equation (3) and that expected from the FP relation between g^x and range is quite good up to angles of dip of about 60° in unprocessed emulsion. An equation which is not corrected for dip in α gives inaccurate values of g for tracks having $\theta > 30^\circ$ (see Fig. 1) (*).

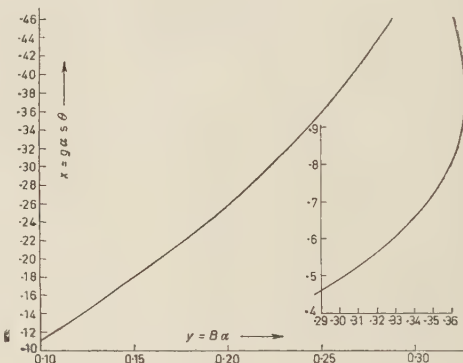


Fig. 2.

Multiplication of both sides of equation (3) by α^l gives

$$(4) \quad B^l \alpha^l = g \alpha^l \exp [-g \alpha^l],$$

or

$$(5) \quad y = x \exp [-x],$$

putting $B^l \alpha^l = y$ and $g \alpha^l = x$. Fig. 2 shows a curve of this nature. For a known value of α , this curve gives the value of g corresponding to a measured value of B . It is seen from the nature of this curve (Fig. 2) that after a certain

(*) It has been pointed out by Birge (4) that for minimum tracks the apparent blob density (the number of blobs observed/true length) is equal to the true blob density (the number of blobs per unit length as would be observed at right angles to the track) to within about 1% for $\theta \leqslant 20^\circ$.

(4) R. W. BIRGE, D. H. PERKINS, J. R. PETERSON, D. H. STERK and M. N. WHITEHEAD: *Nuovo Cimento* **4**, 834. (1956)

point B is not very sensitive to variation in g . Hence the method of counting blobs alone can give accurate results only for values of g and θ satisfying the condition $gx \sec \theta \leq 0.40$. But reasonably accurate results may be expected even up to $gx \sec \theta = 0.50$.

The case of heavily ionizing dipping tracks ($gx \sec \theta > 0.40$).

To determine g on tracks of higher ionization, both the total number of blobs and the number of holes greater than a certain length must be counted.

In equation (1) corrections for dip have to be made to l , H and B :

1) l - The projected gap-length l is related to the true gap-length l_t (O'CEAL-LAIGH⁽¹⁾) by the equation

$$(6) \quad l_t = l \sec \theta + \alpha (\sec \theta - 1).$$

The apparent grain size α in fact exceeds the actual mean grain diameter of d but equation (6) assumes that this difference can be neglected.

2) H - If N_H is the number of holes greater than the projected length l counted on a total projected length L_H of the track, then the correct quantity to use in equation (1) for a dipping track is

$$(7) \quad H^l = \frac{N_H}{L_H \sec \theta}.$$

3) B - Similarly B becomes

$$(8) \quad B^l = \frac{N_B}{L_B \sec \theta}.$$

Here, however, the need for an additional correction arises since small gaps on a dipping track are obscured in the projected plane; this decreases the number of blobs counted per unit length. The correction due to this factor can be evaluated as follows. The previous measurements on lightly ionizing dipping tracks, have shown that B^l (equation (8))

is related to the true value of g on the track by equation (3). Also, the true blob density B_t (i.e., the true number of blobs per unit length on the track as observed at right angles to its direction) is related to g by the equation

$$B_t = g \exp [-gx].$$

From this and equation (3) we get

$$(9) \quad B_t = B^l \exp [gx(\sec \theta - 1)].$$

For dipping tracks then

$$(10) \quad \begin{aligned} H^l &= B_t \exp [-gl_t] \\ &= B^l \exp [-gl \sec \theta], \end{aligned}$$

substituting for B_t and l_t from equations (6) and (9).

This equation turns out to be the same as that given by FP, for dipping tracks, derived using simpler considerations. To test the correctness of equation (10) measurements of gx were made

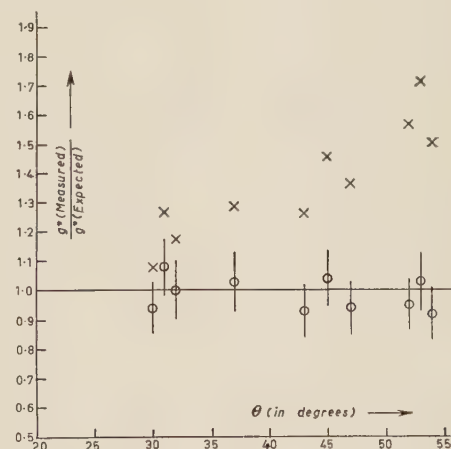


Fig. 3. - Shows the ratio $g_x^{(meas.)}/g_x^{(exp.)}$ for π -mesons of different dips. The points marked with x result from the use of the formula $H^l = B^l \exp [(-gl)]$ which corrects for the length of the dipping track alone. Points marked with \odot result from the use of equation (10) which in addition corrects for the effect of the obscuration of grains and change in the apparent gap lengths due to inclination of trajectory. The measured g_x values lie between 2.4 and 5.1. The vertical bars indicate statistical errors for the points marked with \odot .

on steeply dipping pion tracks at various residual ranges. They were compared with the values of g^x expected from the g^x -range curve of FP. The results are shown in Fig. 3. It is seen that the $\sec \theta$ correction to l , as given in equation (10), is quite important for angles of dip of 30° and above.

The results given above show that for a dipping track, whether it is lightly or heavily ionizing, the relation (*)

$$(11) \quad g_{\text{true}} = g_{\text{apparent}} \cos \theta,$$

holds for values of θ up to 60° where g_{true} is the reciprocal of the «true mean gap-length» and g_{apparent} is the actual value of g measured on the steep track, taking no account of its dip in the emulsion.

(*) This follows from equations (3) and (10).

On lightly ionizing dipping tracks, it is more convenient and perhaps more accurate to measure g by blob count alone since for dipping tracks, in general, the track length available for measurement may be quite short and hence the value of N_H that is expected is quite small. This will increase the statistical error in g . However, in many cases it is possible to follow the steep track through a few plates and so obtain an adequate number of gaps to be counted.

* * *

I should like to thank Dr. W. B. LASICH for many helpful discussions. I am greatly indebted to Dr. E. H. S. BURHOP for his constant encouragement and advice. My thanks are due to other members of the group for their co-operation.

Backscattering dei positroni del ^{22}Na .

A. CAMBIERI e R. PAPPALARDO

Istituto di Fisica dell'Università - Pavia

(ricevuto l'8 Giugno 1957)

Un recente articolo di DANGUY e QUIVY⁽¹⁾ dà notizia di una interessante relazione cui sembrano soddisfare le particelle β^- quando subiscono riflessioni da parte di sostanze di diverso numero atomico.

Le proprietà di questa diffusione totale (backscattering) sono, secondo gli autori citati, le seguenti:

a) Esiste una semplice proporzionalità tra il quadrato del numero di particelle diffuse in un determinato angolo solido e il numero atomico dell'elemento diffondente.

b) Nel caso di un composto chimico, di leghe binarie e di soluzioni acquose di sali binari e ternari, la relazione precedente è verificata purchè si sostituisca al numero atomico un numero atomico fittizio Z_f , definito da:

$$(1) \quad Z_f = \sum_i P_i Z_i$$

essendo P_i la percentuale in peso dell'elemento i -esimo e Z_i il numero atomico dell'elemento i -esimo.

In questa nota riportiamo i risultati

⁽¹⁾ L. DANGUY and R. QUIVY: *Journ. Phys. et Rad.*, **17**, 320 (1956).

ottenuti in base alle a) e b) nel caso dei positroni del ^{22}Na .

Lo schema del dispositivo sperimentale è rappresentato in Fig. 1. La so-

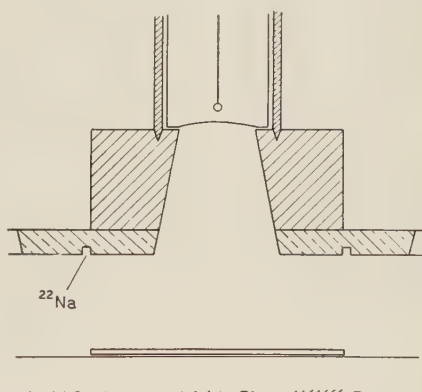


Fig. 1.

stanza radioattiva è stata depositata, per evaporazione di una sua soluzione in acqua, in una gola circolare praticata lungo la faccia inferiore di un disco di plexiglas. Tale disco è forato nella parte centrale, e attraverso questa apertura le particelle diffuse raggiungono il contatore, sostenuto da uno schermo in piombo opportunamente sagomato.

L'esigenza di schermare il contatore dai quanti γ emessi dalla sostanza radioattiva costituisce un non lieve inconveniente per una buona geometria del dispositivo.

Le sostanze riflettenti sono sostenute, a distanza ottimale dal contatore, mediante fili tesi, allo scopo di ridurre al minimo le riflessioni dovute al dispositivo.

I risultati ottenuti sono riportati in Fig. 2 (in ascisse Z o Z_f , ricavato me-

Si tratta di valori relativi a lamine di metalli puri e di leghe, sette delle quali sono a contenuto variabile di Cd e Pb. Lo spessore delle sostanze riflettenti è superiore al percorso massimo delle particelle β^+ nel mezzo stesso.

I punti sperimentali si dispongono in modo soddisfacente lungo una retta. Nelle misure effettuate la probabilità di annichilazione dei positroni è trascurabile; e poichè, per il resto, il comportamento delle β^+ e β^- è equivalente, i risultati di DANGUY e QUIVY risultano così confermati.

R. H. MÜLLER⁽²⁾ aveva trovato, nel caso delle particelle del ^{90}Y , che il backscattering relativo, e quindi il numero di particelle riflesse dai vari elementi, varia come $Z^{\frac{1}{2}}$.

Riportando in ascisse Z_f ed in ordinate N^2 si ottengono, nel caso delle nostre misure, punti che non s'inseriscono su una retta, quantunque le deviazioni dall'andamento rettilineo non siano molto grandi.

Invece, come è stato accennato, la relazione quadratica corrisponde meglio ai risultati sperimentali, e perciò potrebbe eventualmente essere utilizzata per l'analisi di leghe.

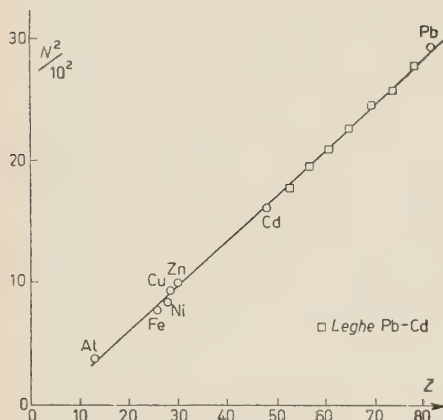


Fig. 2.

diente la (1); in ordinate il quadrato del numero delle particelle diffuse).

⁽²⁾ R. H. MÜLLER: *Phys. Rev.*, **93**, 195 (1954).

Correlation between Circularly Polarized γ -Rays and β -Particles.

A. LUNDBY, A. P. PATRO and J. P. STROOT

CERN - Geneva

(ricevuto il 24 Giugno 1957)

As suggested by LEE and YANG (¹) one can demonstrate the non-conservation of parity in β -decay by measuring the circular polarization of γ -rays following β -transitions as a function of the angle between the momenta of β and γ . We have performed such an experiment by measuring the transmission of γ -rays through magnetized iron. The experimental arrangements are shown in the following diagrams. We favoured the measurement of the transmission (²) to differential scattering (³) of γ -rays by magnetized iron due to the ease with which energy discrimination can be achieved in the former case. One thereby eliminates effects due to scattering from the surroundings. The magnetic flux density in the iron could also easily be controlled, and was kept sufficiently high always to saturate the iron.

If we denote the $\beta\gamma$ coincidence rate with the magnetic field pointing towards and away from the source by C_{down} and

C_{up} respectively we have

$$R = \frac{C_{\text{down}} - C_{\text{up}}}{\frac{1}{2}(C_{\text{down}} + C_{\text{up}})} = P \cdot 2 \cdot \tanh(N\nu\sigma T),$$

where $P = (N_r - N_l)/(N_r + N_l)$, N_r and N_l being the number of right circularly polarized and left circularly polarized (angular momentum of photon in direction of propagation) γ -rays respectively. N is the number of atoms per unit volume in the iron, ν is the number of polarized electrons per iron atom and is equal to 2.06, σ is the part of the total Compton cross-section dependent on polarization and T is the thickness of the iron. According to SKYRME (⁴)

$$P = -\alpha\lambda\bar{\beta} \cos\theta,$$

where θ is the angle between β and γ , $\bar{\beta}$ is the average velocity of the electrons (about 0.6 in our case), λ is a function of the β -interaction coupling constants and α is a quantity dependent on the spin sequence of the nucleus and the multipole order of the γ -rays (⁴) ($\alpha = \frac{1}{3}$ in our case). According to the two-component neutrino theory of Lee and

(¹) T. D. LEE and C. N. YANG: *Phys. Rev.*, **104**, 254 (1956).

(²) S. B. GUNST and L. A. PAGE: *Phys. Rev.*, **92**, 970 (1953).

(³) F. P. CLAY and F. L. HEREFORD: *Phys. Rev.*, **85**, 675 (1952); J. C. WHEATLEY, W. J. HUISKAMP, A. N. DIDDENS, M. J. STEENLAND and H. A. TOLHOEK: *Physica*, **21**, 841 (1955).

(⁴) T. H. R. SKYRME: private communication of calculations by him and F. MANDL.

Yang (5), admitting only tensor interaction, $\lambda = -1$ for electrons emitted in allowed transitions according to Gamow-Teller selection rules.

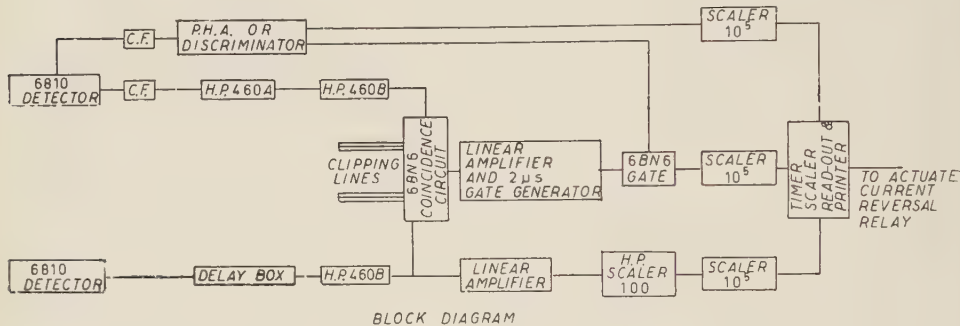


Fig. 1.

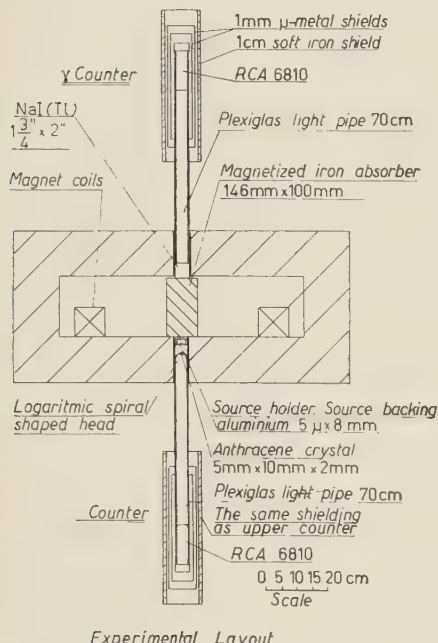


Fig. 2.

We have used ^{60}Co so far in our experiments. The source strength was about 200 μC , the β -counter registered

about $8 \cdot 10^{-3}$ and the γ -counter about $4 \cdot 10^{-6}$ of the disintegrations of the source. Only the highest energy photo-peak of the γ -spectrum in the NaI(Tl)-crystal

was selected. The effect of the magnetic field on the individual counting rates was within statistical error ($\sim 10^{-4}$). The resolution of the coincidence circuit was 10^{-8} s.

The sequence of the experiment was as follows. The gated coincidence rate and individual counting rates were accumulated over 200 s with magnetic field in one direction. The sealers were then stopped for 10 s during which time the accumulated counts were printed, the sealers reset and the direction of the magnetic field reversed. The counting was then started again. The sequence was completely automatized.

The effect obtained for ^{60}Co was

$$R = (1.75 \pm 0.37) \%$$

corresponding to

$$\lambda\alpha = -0.32 \pm 0.07.$$

When the distance between source and β -counter was diminished, or the discrimination level for γ -rays lowered appreciably, the effect disappeared.

The experiments were commenced in February this year and had to be discontinued at the end of May. Mean-

(5) T. D. LEE and C. N. YANG: *Phys. Rev.*, **105**, 1671 (1957).

while, experiments by SCHOPPER (⁶) and by BOEHM and WAPSTRA (⁷), both of whom measured the differential scattering of γ -rays in a magnetized iron cylinder, gave the following results for ^{60}Co :

SCHOPPER

$$\lambda\alpha = -0.41 \pm 0.07,$$

BOEHM and WAPSTRA

$$\lambda\alpha = -0.40 \pm 0.09.$$

Forming an average of the three values

- (⁶) H. SCHOPPER: *Phil. Mag.*, **2**, 710 (1957).
 (⁷) F. BOEHM and A. H. WAPSTRA: in press.

one obtains

$$\lambda\alpha = -0.377 \pm 0.046.$$

Besides the statistical error one should bear in mind that the β 's may differ somewhat in the different experiments. The results do not contradict the two-component neutrino theory of Lee and Yang.

Note added in proof.

We have recently measured for ^{22}Na $\alpha\lambda = +34 \pm 0.14$, in agreement with (⁸) and (⁹); and the circular polarization of Bremsstrahlung from ^{90}Y and ^{32}P , in agreement with M. GOLDHABER *et al.* and K. W. McVOY: *Phys. Rev.*, **106**, 826 (1957).

A Correction to Previously Quoted Cosmic Ray Flux Values.

C. J. WADDINGTON

H. H. Wills Physical Laboratory - Bristol

(ricevuto il 2 Luglio 1957)

During the past few years a considerable number of reports have been made of determinations of the fluxes of the various components of the multiply charged nuclei in the primary cosmic radiation. The majority of these, particularly those on the heavier nuclei, have been made using nuclear emulsions to detect these particles. These flux values have customarily had statistical errors of somewhat more than 10%, and it is, therefore, perhaps worth while to point out that a proportion of these measurements have a systematic error which is also somewhat more than 10%. This error arises from the failure to allow for the particles that enter the emulsions while they are rising to ceiling altitude during the exposure, and cause the fluxes to be overestimated.

The magnitude of the correction that should be applied depends on the rate at which the emulsions rise, the time spent at ceiling altitude, and the height attained. Because of the non-exponential rate of decrease of the fluxes of the nuclei as they pass down the atmosphere it is difficult to give an analytical form to this correction. Instead it has been calculated numerically for a number of specific cases, in order to correct α -particle flux values reported previously from this laboratory.

Fig. 1 shows the variation of flux with depth in the atmosphere for α -particles, L -nuclei ($3 < Z < 5$), M -nuclei ($6 < Z < 9$) and H -nuclei ($Z \geq 10$). These curves are based on the following considerations:

(i) It is assumed that the fluxes at the top of the atmosphere, $J_n 0$, of α -particles, L -nuclei, M -nuclei and H -nuclei are in the ratios 70:2:5:2 respectively.

(ii) The flux of the n -th component at a depth of x g/cm² in the atmosphere, $J_n x$, is assumed to be given by:

$$(1) \quad J_n x = J_n 0 \cdot \exp [-x/\lambda_n] + \sum_{m > n} J_m 0 \frac{\lambda_n P'_{mn}}{\lambda_n - \lambda_m} (\exp [-x/\lambda_n] - \exp [-x/\lambda_m])$$

where

$$P'_{mn} = \frac{P_{mn}}{(1 - P_{mm})}.$$

AESSE

APPARECCHI ELETTRONICI DI MISURA

VIA RUGABELLA 9 - TEL. 896334 - 891896

MILANO

DECADI DI FREQUENZA

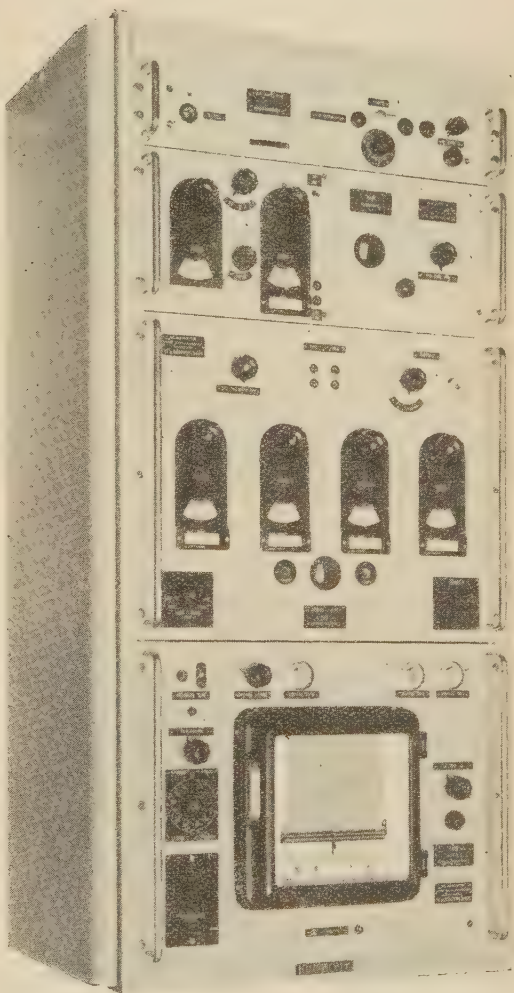
Complessi per misure di frequenze da: 0 a 30 000 MHz

Di uso facile
e semplice

Regolazione comple-
tamente decadica

Massima precisione
fino a $1 \cdot 10^{-8}$

Di impiego
universale



SCHOMANDL K. G. - Monaco (Germania)

Problemi per chi guida



E' o non è valido il segnale di "Stop"?

A chi spettava la precedenza in un caso come questo? All'automobilista proveniente da destra - come prescrive il Codice della strada - o a quello proveniente da sinistra, protetto dal segnale di "Stop"?

Le strade "Stop" non sono previste dall'attuale Codice della strada e, quindi, la questione è controversa. I Pretori hanno emesso sentenze contrastanti, tuttavia un giudizio definitivo dovrebbe essere quello della Suprema Corte di Cassazione che, con sentenza del 7 giugno 1956, sancisce la legittimità delle strade "Stop". Ma intanto, come deve regolarsi il guidatore?

Il nostro consiglio è questo: meglio fermarsi in

due che non fermarsi né l'uno né l'altro. Siate perciò sempre pronti a bloccare la macchina in pochi metri! A questo scopo i famosi **Ceat DR** vi forniscono un aiuto provvidenziale: sul battistrada di questi pneumatici che "centuplicano la frenata" migliaia di piccole ancorizzazioni circolari, che agiscono come ventose, sono pronte ad abbarbicarsi al terreno non appena la macchina minaccia di slittare.

I **Ceat DR**, frutto di 5 anni di ricerche con la collaborazione della Casa americana "General Tire and Rubber Co.", per la *sicurezza*, la *confortevolezza di guida*, la *silenziosità* e la *durata* rappresentano un progresso di moltissimi anni.



CE
go

LARGO REGIO 1



D

λ_n was the absorption mean free path of the n -th component and P_{mn} was the probability of a m -type nucleus producing an n -type secondary nucleus in a disintegration. This relation is a simplified version of that used by KAPLON *et al.* (1), and neglects the influence of consecutive fragmentations. This simplification has little effect on any of the components except the L -nuclei, and even for these it results in only a 4% underestimation at a depth of 50 g/cm².

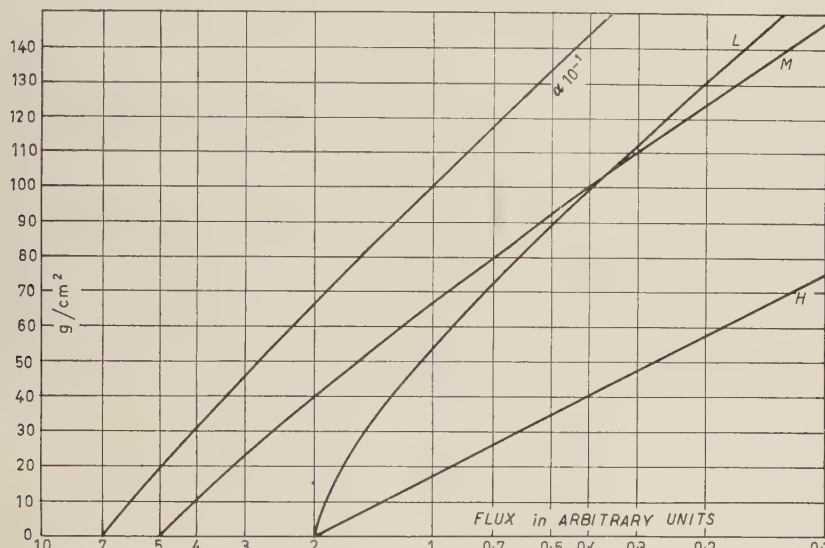


Fig. 1. — The variation of flux with depth in the atmosphere for α -particles—times 10^{-1} — h -nuclei, M -nuclei and H -nuclei.

(iii) The fragmentation probabilities used were those reported by FOWLER *et al.* (2), and the values taken for the absorption mean free paths were, $\lambda_\alpha = 46$ g/cm²; $\lambda_L = 38$ g/cm²; $\lambda_M = 33$ g/cm² and $\lambda_H = 25$ g/cm².

Using the curves of Fig. 1 and the known flight characteristics of any exposure, it is possible to calculate the ratio of the number of particles which entered during the ascent to the number which entered at ceiling. In what follows, this calculation has been made by determining the relative number of particles that entered in every 10 minute interval during the ascent, and comparing the sum of these numbers with the total relative number that entered at ceiling. These corrections have been expressed as percentages of the total number of entering particles, so that the true flux in the emulsions is given by subtracting this percentage from the flux value determined before the correction.

This procedure is only valid for stacks exposed at localities where there is a high cut-off energy, since Eq. (1) does not allow for those particles brought to rest by ionization loss. For the H , M and L -nuclei the resulting reduction in the number of particles entering during the ascent can be considerable, but the calculation

(1) M. F. KAPLON, J. H. NOON and G. W. RACETTE: *Phys. Rev.*, **96**, 1408 (1954).

(2) P. H. FOWLER, R. R. HILLIER and C. J. WADDINGTON: *Phil. Mag.*, **2**, 293 (1957).

of this reduction is complex, particularly for the *L*-nuclei, and has not been considered here. For the α -particles the effect is small, and may be allowed for by considering only the reduction in the number of primary particles, since secondary particles make up only some 10% of the total number observed at any depth.

These corrections have been made on four α -particle flux values reported previously (³⁻⁵). The details are shown in the Table. At the same time the opportunity has been taken to make the extrapolation to the top of the atmosphere with the latest values of the fragmentation probabilities (²), and the effect of this is to compensate partially for the reduction produced by applying the correction. It should be noticed that this correction amounts to as much as an 18% reduction in the flux at the top of the atmosphere for the determination over Southern England and cannot, therefore, be regarded as negligible. It should also be noted that these alterations in the flux values do not alter any of the conclusions as to the energy spectra or cut-off energies derived from the old flux values.

TABLE I.

Effect of correction for particles entering emulsions during rise to ceiling altitude.

Place	Cut-off energy GeV/nucl.	Flight characteristics		
		Altitude feet	Time hours	Rate of ascent ft/min
Minnesota (³)	≤ 0.14	96 000	4.0	800
Southern England (³)	~ 0.65	101 000	4.13	700
Northern Italy (⁴) . .	1.55 ± 0.06	106 000	5.75	1 000
Sardinia (⁵)	~ 2.3	85 000	7.17	1 000

Flux in plates parts/m ² ·s·sec	Correction %	Flux at top of atmosphere	
		Uncorrected (parts./m ² ·s·sec)	Corrected (parts./m ² ·s·sec)
207 ± 23	— 10.8	292 ± 32	272 ± 30
138 ± 16	— 13.5	182 ± 21	162 ± 17
76 ± 7	— 8.7	93 ± 8	89 ± 8
38 ± 5	— 4.1	72 ± 9	70 ± 9

The corrections for heavier nuclei have been calculated for the emulsions flown over Northern Italy, neglecting ionization losses, and turn out to be 6%, 8% and 10% for the *H*, *M* and *L*-nuclei respectively. Thus they represent corrections of 11% on each group at the top of the atmosphere, and again are not negligible.

(³) C. J. WADDINGTON: *Nuovo Cimento*, **3**, 930 (1955).

(⁴) P. H. FOWLER and C. J. WADDINGTON: *Phil. Mag.*, **1**, 637 (1956).

(⁵) H. H. ALY and C. J. WADDINGTON: *Nuovo Cimento*, **5**, 1679 (1957).

On the Ruijgrok-Van Hove Model.

G. DELL'ANTONIO (*)

Institute for Theoretical Physics, University of Copenhagen

F. DUIMIO (*)

CERN Theoretical Study Division

at the Institute for Theoretical Physics, University of Copenhagen

(ricevuto il 26 Luglio 1957)

In a recent paper RUIJGROK and VAN HOVE ⁽¹⁾ propose a model of renormalizable field theory, which can be considered as a generalization of the Lee-model.

It consists of a field of spin zero neutral bosons (θ -particles) coupled with fixed nucleons, which can be in n different states N_i , through interactions causing the transitions:

$$N_0 \rightleftharpoons N_1 + \theta$$

$$N_1 \rightleftharpoons N_2 + \theta$$

$$N_n \rightleftharpoons N_0 + \theta$$

.

The strength of each interaction is determined by the (unrenormalized) coupling constant $g_i^{(0)}$; $i = 0, 1, \dots, n$.

It follows that an unrestricted number of θ -particles can be emitted and absorbed by a nucleon and, in contrast to the Lee-model, that a mass renormalization for every nucleon state and a non-trivial charge-renormalization are needed. The renormalization constants can be calculated explicitly.

A very interesting feature of this model is that the renormalized coupling constants g_i , which are in general different from each other for finite cut-off, become equal in the limit of point-source.

In this letter we examine, following the method which has been developed by PAULI and KÄLLÉN ⁽²⁾ in their analysis of the mathematical structure of the Lee-

(*) On leave of absence from the Institute of Physics of the University of Milan, Italy.

(¹) TH. W. RUIJGROK and L. VAN HOVE: *Physica*, **22**, 880 (1956).

(²) G. KÄLLÉN and W. PAULI: *Dan. Mat. Fys. Medd.*, **30**, No. 7 (1955).

model (3), the dependence of the renormalized coupling constants on the cut-off function and the limitations to be imposed on them to avoid the appearance of unphysical (« ghost ») states.

The Hamiltonian of the system (for simplicity we consider the case $n = 2$) is given, with the same notations as in (1), by

$$(1) \quad \left\{ \begin{array}{l} H = H_0 + H_1 \\ H_0 = (\mathcal{M} - \delta M_0) \sum_p \psi_0^*(p) \psi_0(p) + (\mathcal{M} - \delta M_1) \sum_p \psi_1^*(p) \psi_1(p) + \sum_k \omega(k) a^*(k) a(k), \\ H_1 = -(2v)^{-\frac{1}{2}} \sum_{p'=p+k} f(k) \omega^{-\frac{1}{2}}(k) [g_0^{(0)} \psi_1^*(p) \psi_0(p') a^*(k) + g_1^{(0)} \psi_0^*(p) \psi_1(p') a^*(k) + \text{h. c.}] . \end{array} \right.$$

For the renormalization constants one obtains:

$$(2) \quad \left\{ \begin{array}{l} \delta M_0 = -(2v)^{-1} (g_0^{(0)})^2 \sum_k f^2(k) / \omega^2 \\ \delta M_1 = -(2v)^{-1} (g_1^{(0)})^2 \sum_k f^2(k) / \omega^2 \quad (\text{mass renorm.}) \end{array} \right.$$

$$(3) \quad \left\{ \begin{array}{l} Z_2^{-1}(0) = \cosh(g_0^{(0)} g_1^{(0)} L) + \frac{g_0^{(0)}}{g_1^{(0)}} \sinh(g_0^{(0)} g_1^{(0)} L) \\ Z_2^{-1}(1) = \cosh(g_0^{(0)} g_1^{(0)} L) + \frac{g_1^{(0)}}{g_0^{(0)}} \sinh(g_0^{(0)} g_1^{(0)} L) \quad (\text{nucleon amplitude renorm.}) \\ L = (2v)^{-1} \sum_k f^2(k) / \omega^3 , \end{array} \right.$$

$$(4) \quad \left\{ \begin{array}{l} Z_1(0) = Z_2(1) \\ Z_1(1) = Z_2(0) . \end{array} \right. \quad (\text{charge renorm.})$$

The connection between renormalized and unrenormalized coupling constants is given by

$$(5) \quad \left\{ \begin{array}{l} g_0 = Z_2^{\frac{1}{2}}(0) Z_2^{-\frac{1}{2}}(1) g_0^{(0)} , \\ g_1 = Z_2^{\frac{1}{2}}(1) Z_2^{-\frac{1}{2}}(0) g_1^{(0)} . \end{array} \right.$$

From (3) and (5) we can obtain $Z_2(0)$ and $Z_2(1)$ as functions of g_0 and g_1 :

$$(6) \quad \left\{ \begin{array}{l} Z_2(0) = \cosh(g_0 g_1 L) - \frac{g_0}{g_1} \sinh(g_0 g_1 L) , \\ Z_2(1) = \cosh(g_0 g_1 L) - \frac{g_1}{g_0} \sinh(g_0 g_1 L) . \end{array} \right.$$

(3) T. D. LEE: *Phys. Rev.*, **95**, 1329 (1954).

These expressions can assume negative values. As they cannot be simultaneously negative, when one of them is < 0 , the unrenormalized $g_0^{(0)}$ and $g_1^{(0)}$ have to be imaginary with the consequence that the Hamiltonian is non-hermitian.

If we impose the conditions

$$(7) \quad \begin{cases} Z_2(0) \geq 0 \\ Z_2(1) \geq 0 \end{cases}$$

it is easy to see that g_0 and g_1 must satisfy the inequalities

$$(8) \quad \operatorname{tgh}(g_0 g_1 L) \leq \frac{g_0}{g_1} \leq \operatorname{cotgh}(g_0 g_1 L),$$

i. e. for any given g_0 (L is kept fixed), g_1 can assume only the values contained in an interval around g_0 , which is the more narrow, the more the product $g_0 L$ becomes large.

Where (8) is satisfied, it follows from (6) that

$$(9) \quad Z_2(0), Z_2(1) \leq \frac{1}{\cosh(g_0 g_1 L)} \leq 1.$$

Therefore the general theorem ⁽⁴⁾, stating that the constants Z_2 must lie between 0 and 1, is valid here. When the conditions (8) are violated, the theory gives unphysical results, i.e. «ghost» states with negative probabilities appear.

This can be simply shown, as indicated by KÄLLÉN ⁽⁵⁾, evaluating the expectation value in the vacuum of the anticommutator of the renormalized operators $\psi'_0(p) = \psi_0(p) \cdot Z^{-\frac{1}{2}}(0)$ and $\psi'^{*}_0(p)$. We obtain

$$(10) \quad \langle 0 | \{\psi'^*_z(p), \psi'_0(p)\} | 0 \rangle = \sum_z |\langle z | \psi'^*_0(p) | 0 \rangle|^2 = Z_2^{-1}(0),$$

where the sum is extended over all the complete set of eigenstates of H . Obviously, when $Z_2(0)$ is < 0 , the sum has to contain some terms with negative norm.

Another indication of the pathological behaviour of the theory when the conditions (8) do not hold, comes out from the evaluation of the expectation value in the physical N_0 -state

$$(11) \quad |N_0\rangle = Z_2^{\frac{1}{2}}(0) \left\{ |N_0\{0\}_0\rangle + \sum_{n=0}^{\infty} \sum \alpha_0^{(2n+1)}(\{l_k\}_{2n+1}) |N_1\{l_k\}_{2n+1}\rangle + \right. \\ \left. + \sum_{n=1}^{\infty} \sum \alpha_0^{(2n)}(\{l_k\}_{2n}) \cdot |N_0\{l_k\}_{2n}\rangle \right\},$$

⁽⁴⁾ See for ex. H. UMEZAWA and S. KAMEFUCHI: *Progr. Theor. Phys.*, **6**, 543 (1951).

⁽⁵⁾ G. KÄLLÉN: unpublished.

of the operators number of N_0 and N_1 (bare) particles:

$$(12) \quad \left\{ \begin{array}{l} \mathcal{N}_0 = \langle N_0 | \sum_p \psi_0^*(p) \psi_0(p) | N_0 \rangle = Z_2(0) \cosh(g_0^{(0)} g_1^{(0)} L) = \\ \qquad \qquad \qquad = \cosh^2(g_0 g_1 L) - \frac{g_0}{g_1} \sinh(g_0 g_1 L) \cosh(g_0 g_1 L), \\ \mathcal{N}_1 = \langle N_0 | \sum_p \psi_1^*(p) \psi_1(p) | N_0 \rangle = Z_2(0) \frac{g_0^{(0)}}{g_1^{(0)}} \sinh(g_0^{(0)} g_1^{(0)} L) = \\ \qquad \qquad \qquad = \frac{g_0}{g_1} \sinh(g_0 g_1 L) \cosh(g_0 g_1 L) - \sinh^2(g_0 g_1 L). \end{array} \right.$$

The sum of \mathcal{N}_0 and \mathcal{N}_1 gives obviously 1 (law of conservation of nucleons). But, when (8) is violated, one of them turns out to be negative and the other >1 .

Finally, let us consider the case $L \rightarrow \infty$, i.e. the point-source limit: g_0 and g_1 tend to the common value ⁽¹⁾ $(g_0^{(0)} g_1^{(0)})^{\frac{1}{2}}$.

It is evident that the Lee-model is a particular case of the Ruijgrok-Van Hove model with $g_1^{(0)}$ (or $g_0^{(0)}$) equal to zero. It follows that in the Lee-model the renormalized coupling constant has to be equal to zero in the point-source limit. It is now apparent that this result is a consequence of the very special structure of the Lee-model, and no conclusion can be drawn for a more general model.

In fact, in the model discussed here, even in the point-source limit it is possible to obtain physically meaningful results, which are essentially the results of a neutral scalar theory with fixed sources.

* * *

We want to thank Professors NIELS BOHR and C. MØLLER for their kind hospitality and Dr. G. KÄLLÉN for useful comments and suggestions.

A Remark on the Paper «Gravitational Motion and Hamilton's Principle»⁽¹⁾.

B. BERTOTTI

Istituto di Fisica dell'Università - Pavia

(ricevuto il 27 Luglio 1957)

The following criticism has been raised by Prof. A. H. TAUB to the result of the paper mentioned in the title⁽²⁾: since a test-particle is supposed to have no influence on the gravitational field, how can the latter be a solution of the equations

$$(1) \quad G_{\mu\nu} + 4\pi T_{\mu\nu} = 0 \quad [T^{\mu\nu} = q\dot{y}^\mu\dot{y}^\nu],$$

which is required for setting up the variational principle (8 H)⁽³⁾? On the other hand, if the g 's are affected by the particle, how can they be regular on l ?

We think it useful to supplement here the understated deduction contained in Sec. 2 of (H) with a fuller explanation. We do assume that a *test-particle has an influence on the gravitational field, but we let it tend to zero*. The procedure, often adopted in general relativity⁽⁴⁾, can be

⁽¹⁾ B. BERTOTTI: *Nuovo Cimento*, **3**, 655 (1956), here quoted as (H).

⁽²⁾ A. H. TAUB: *Mat. Rev.*, **18**, 177 (1957).

⁽³⁾ Please, note in equation (8 H) the omission, by a misprint, of $= 0$.

⁽⁴⁾ See, e.g., L. INFELD and A. SCHILD: *Phys. Rev.*, **21**, 408 (1949).

clarified as follows. Instead of (11 H), write for the matter tensor:

$$(2) \quad T^{\mu\nu} = \lambda q\dot{y}^\mu\dot{y}^\nu$$

(λ being a dimensionless constant); and assume that both $g_{\mu\nu}(\lambda)$ and $T^{\mu\nu}(\lambda)$ are analytical in the neighbourhood of $\lambda=0$. Then one can write

$$(3) \quad g_{\mu\nu} = \underset{0}{g}_{\mu\nu} + \underset{1}{\lambda} g_{\mu\nu} + \underset{2}{\lambda} g_{\mu\nu} + \dots$$

and

$$(4) \quad T^{\mu\nu} = \underset{1}{\lambda} T^{\mu\nu} + \underset{2}{\lambda} T^{\mu\nu} + \dots;$$

here $\underset{0}{g}_{\mu\nu}$ is, of course, a solution of

$$(5) \quad R_{\mu\nu}(\underset{0}{g}) = 0.$$

The series (3) and (4), inserted in (8 H) yield a series in λ , starting with a term of the first degree which contains the g 's only, regular functions of the

co-ordinates. Since this vanishes separately, we conclude that our theorem holds, in the limit $\lambda \rightarrow 0$, with respect to the g -field.

One can picture the situation by considering an empty space-time, corresponding to $\lambda=0$, and «switching on» gradually energy and momentum by increasing λ . The essential fact is that one can not «switch on» *any* distribution of matter, lest the conservation laws be violated. The reason why at the very beginning of the process—corresponding to the case of a test-particle—

the latter involve $\overset{0}{g}_{\mu\nu}$ only, is because at this stage the T -tensor is very small, while $g_{\mu\nu}$ is finite; one can therefore neglect in the metric field the perturbation induced by $T_{\mu\nu}$.

* * *

A correspondence with Prof. A. H. TAUB is acknowledged.

PROPRIETÀ LETTERARIA RISERVATA
